

ADVISORY BOARD

A. H. Cowley

*University of Texas
Austin, Texas*

H. B. Gray

*California Institute of Technology
Pasadena, California*

O. Kahn

*Université de Paris-Sud
Orsay, France*

A. Ludi

*Universität Bern
Bern, Switzerland*

J. Reedijk

*Leiden University
Leiden, The Netherlands*

A. M. Sargeson

*Australian National University
Canberra, Australia*

D. F. Shriver

*Northwestern University
Evanston, Illinois*

K. Wieghardt

*Ruhr Universität Bochum
Bochum, Germany*

Advances in **INORGANIC CHEMISTRY**

Iron—Sulfur Proteins

EDITED BY

Richard Cammack

*Division of Biomolecular Sciences
King's College
London, England*

SERIES EDITOR

A. G. Sykes

*Department of Chemistry
The University
Newcastle upon Tyne, England*

VOLUME 38



ACADEMIC PRESS, INC.
Harcourt Brace Jovanovich, Publishers

San Diego New York Boston
London Sydney Tokyo Toronto

Illustration on page viii by P. Leslie Dutton.

This book is printed on acid-free paper. (∞)

Copyright © 1992 by ACADEMIC PRESS, INC.

All Rights Reserved.

No part of this publication may be reproduced or transmitted in any form or by any means, electronic or mechanical, including photocopy, recording, or any information storage and retrieval system, without permission in writing from the publisher.

Academic Press, Inc.

1250 Sixth Avenue, San Diego, California 92101-4311

United Kingdom Edition published by

Academic Press Limited

24-28 Oval Road, London NW1 7DX

Library of Congress Catalog Number: 59-7692

International Standard Book Number: 0-12-023638-9

PRINTED IN THE UNITED STATES OF AMERICA

92 93 94 95 96 97 EB 9 8 7 6 5 4 3 2 1

HELMUT BEINERT

This volume is dedicated to Professor Helmut Beinert, who, over the years, has made unique contributions to the area of iron-sulfur proteins. Although he has been involved in many aspects of bioinorganic chemistry, his work is perhaps best known for the discovery of mitochondrial iron-sulfur proteins, first those of the respiratory chain, and later aconitase.

Helmut Beinert can recall the time, as a student in Germany in the 1930s, when "bioinorganic" chemistry was not even remotely recognized. The sheer name would probably have been considered by most to be a bad joke. If anything, organic chemistry laid claim to what is called biochemistry today; biochemistry had gained little recognition in Germany. While it was true there was "physiological chemistry," this was part of the medical curriculum and was not for chemists. Inorganic chemistry was taught in the university in a largely descriptive fashion, sometimes interspersed with thrilling experiments. Thus it would have been rather farfetched to think of a career in bioinorganic chemistry. Yet, in retrospect, it was the time when bioinorganic chemistry was developing its roots, as for example, in the pioneering work on heme and copper proteins by David Keilin, Otto Warburg, and their schools. However, since the understanding of metal-ligand interactions was in its infancy, interest in the heme proteins was more concerned with the porphyrin ring than with the metal ligand.

Helmut Beinert attributes the choice of his research field to a number of fortunate circumstances. Almost at his doorstep, the Kaiser-Wilhelm-Institut (now the Max-Planck-Institut) had been erected in Heidelberg on the sportsfield rented by the high school (the classical Gymnasium). There Otto Meyerhof was directing pioneering research on muscle contraction, glycolysis, adenine nucleotides, and phosphorylation, and Richard Kuhn on flavins and carotenoids. Meyerhof's children were contemporaries (though younger) of Helmut Beinert at the Gymnasium. Steeped as he was for 9 years in ancient history, Latin, and Greek, with only a year each of chemistry and physics, he was somewhat ill prepared to engage in the frontline research that was going on at the Kaiser-Wilhelm-Institut. Luckily, a young "Docent," formerly an assistant of Wilhelm Klemm (a pioneer in magnetochemis-

try) brought to his university new thinking in inorganic chemistry—approaches that were inspired by the influence of Linus Pauling and other contemporary physical chemists. Helmut Beinert was attracted more to inorganic and physical chemistry than to organic chemistry, for which a theoretical basis was still largely lacking.

In the war years that followed, with all their turmoil, pressures, and restrictions, Beinert recalls there were few, if any, choices and one had to seize opportunities whenever they emerged. On the whole, though, he had the good fortune to survive this difficult period.

During work for his Ph.D. thesis at the Kaiser-Wilhelm-Institut, Helmut Beinert had his first encounter with an enzyme when Richard Kuhn suggested that he should study the inhibition of yeast pyruvate carboxylase by free radicals. The enormous activity of this enzyme, even in dilute rinsings from his glassware, made such an impression on him that he thought of pursuing research in the emerging field of enzyme chemistry.

The 1930s and 1940s had seen a rise of biochemistry and enzymology in the United Kingdom and the United States, and Helmut Beinert followed the literature avidly, whenever he could. At an opportune time he applied to David E. Green for a fellowship at the then newly founded Institute for Enzyme Research at the University of Wisconsin at Madison.

In studying flavins and flavoproteins, he became particularly intrigued by the formation of semiquinones and was looking for nondestructive approaches to determine these species. This led him into the field of electron paramagnetic resonance (EPR), where he encountered the physicist Richard H. Sands, beginning a collaboration that had a profound influence on his future career. It now appeared possible to study not only semiquinones but also metals such as iron, copper, and molybdenum in proteins by EPR and to resolve the question of whether these metals were participating in electron transfer.

At that time very few people were seriously pursuing biological EPR spectroscopy. With the supply of interesting materials at the Enzyme Institute, with the dedicated assistance of his long-time associate Raymond E. Hansen, a largely self-taught electronics and instrument expert, and with Dick Sands in the background, Beinert set up one of the most active and best-equipped laboratories for biological low-temperature EPR in the United States. Soon, samples at equilibrium states were no longer sufficient to satisfy their curiosity, and they built apparatus for rapid reaction studies, anaerobic work, and for reflectance and absorption spectroscopy on samples in EPR tubes. Their expectations were indeed fulfilled in that they observed iron and copper in many

proteins and occasionally molybdenum, manganese, and cobalt. In pioneering experiments they studied the behavior of these metals in oxidation–reduction processes. The hallmark of Beinert’s work has been the striving for precise and quantitative measurements. Of all his work, nonheme iron, which turned out to be largely present in iron–sulfur proteins, was the most challenging and ultimately promising subject, because the proteins occur ubiquitously and in so many different forms.

Since the proteins were first identified about 40 years ago, Helmut Beinert has contributed much to the iron–sulfur field. The subject continues to expand, as this volume shows. Recent years have seen the discovery of [3Fe–4S] clusters, 3Fe- to 4Fe-cluster interconversions, the formation of mixed-metal clusters, and direct participation of iron–sulfur clusters in catalysis. Studies of molecular evolution of the proteins have revealed unexpected sequence homologies, and, most recently, the apparent involvement of iron–sulfur proteins in post-transcriptional regulatory mechanisms.

The final word is from Helmut Beinert himself. He writes, “My career developed in a rather haphazardous way, as is probably the case for many careers. I did not set out to become a bioinorganic chemist, I just followed some sense for opportunities and ended up there.” Beinert continues, “In his 1956 Harvey lecture, D. E. Green said: ‘I have not been endowed with great talents, but I have been blessed with gifted colleagues. . . .’ I like to think that I was among those to whom Green referred and it is my pleasure now to be in a position where I can share the credit for the work attributed to *me* with all those junior and senior colleagues whose names appear on our joint publications. It certainly does not seem yet the time to quit, if such a time ever arises as long as the mind stays alert.”

Richard Cammack

TRINUCLEAR CUBOIDAL AND HETEROMETALLIC CUBANE-TYPE IRON-SULFUR CLUSTERS: NEW STRUCTURAL AND REACTIVITY THEMES IN CHEMISTRY AND BIOLOGY

R. H. HOLM

Department of Chemistry, Harvard University, Cambridge, Massachusetts 02138

- I. Introduction
- II. Homometallic Cubane-Type Clusters
 - A. Protein-Bound Clusters with Unconventional Terminal Ligation
 - B. Subsite-Differentiated Synthetic Clusters
- III. Trinuclear Cuboidal Clusters
 - A. Protein-Bound Fe_3S_4 Clusters
 - B. Clusters of Related Structure
 - C. Inverted (M_4S_3) Clusters
- IV. Heterometallic MFe_3S_4 Cubane-Type Clusters
 - A. Clusters of Synthetic Origin
 - B. Protein-Bound Clusters
 - C. The Fe_3S_4 Cluster as a Ligand and Cluster Spin
 - D. Biological Implications
 - E. Nonbiological $\text{M}'\text{M}_3\text{S}_4$ Clusters
 - F. Prospectus
- References

I. Introduction

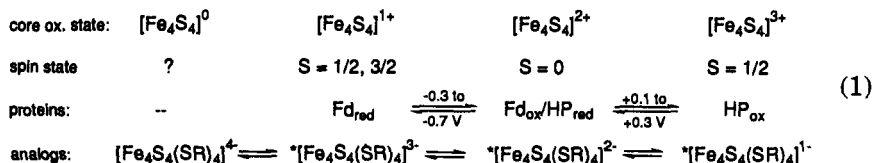
More than ever, it is now apparent that protein-bound Fe_4S_4 clusters must be accorded significance as prosthetic groups at a level that has historically been reserved for hemes and flavins. Although we have observed that iron-sulfur proteins, "having passed from scientific near-obscurity to prosperity in the last 15 [now ~20] years, represent one of the major stories in contemporary metallobiochemistry" (1), knowledge of their structure and function certainly has not reached maturity. This contention is well supported by consideration of just four of the major

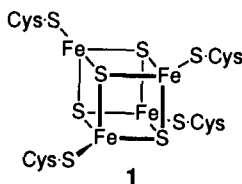
discoveries in the field in the last decade: (1) not all reduced ($[\text{Fe}_4\text{S}_4]^{1+}$) clusters have the classical " $g = 1.94$ -type" $S = \frac{1}{2}$ ground state with otherwise standard electronic properties; (2) an Fe_4S_4 cluster is covalently bound to a catalytic site (in sulfite reductase), to which it electronically couples and functions as an electron donor; (3) Fe_4S_4 and (probably) Fe_2S_2 clusters are implicated in the catalysis of nonredox enzymatic reactions (as in aconitase); (4) protein-bound Fe_4S_4 clusters may be converted adventitiously or deliberately by oxidation to the previously unknown and unanticipated cuboidal cluster Fe_3S_4 , which has an unprecedented electronic structure and supports reconstitution with metal ions to afford the heterometal cubane-type clusters MFe_3S_4 .

It may be noted that the foregoing developments involve nearly exclusively Fe_4S_4 clusters, indicating that these species (with occasionally modified terminal ligation) possess the more diverse structural and functional roles. In this article, some of the most significant recent findings and unusual properties of native and synthetic Fe_4S_4 clusters are first examined. Certain of these properties lead to newer types of clusters, viz., the cuboidal and heterometal cubane-type species mentioned above. As will be shown, these afford new structural and reactivity themes in both inorganic chemistry and biology.

II. Homometallic Cubane-Type Clusters

The cluster 1 is one of the most pervasive electron transfer centers in biology. Accessible Fe_4S_4 core oxidation states, presented in vertical alignment with isoelectronic protein and synthetic analog clusters, are set out in Eq. (1). The indicated potential ranges are approximate. The cubane-type structure and tetracysteinate ligation of 1 have been demonstrated most directly by the protein crystallography of *Peptococcus aerogenes* ferredoxin (Fd) (2), *Chromatium* "high-potential" (HP) protein (3, 4), trimethylamine dehydrogenase (5), *Azotobacter vinelandii* Fd I (6, 7), *Bacillus thermoproteolyticus* Fd (8, 9), the active form of pig heart aconitase (10), and a mutated form of *A. vinelandii* Fd I (11). In addition, the structures of over 35 synthetic clusters containing the





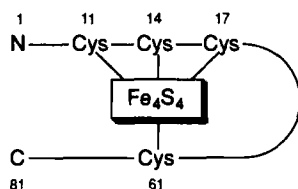
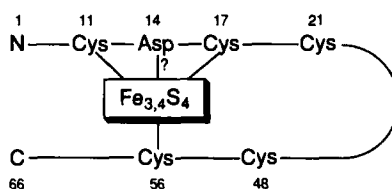
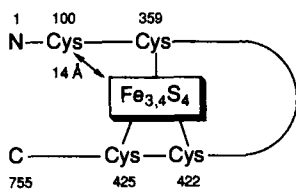
Fe_4Q_4 core ($\text{Q} = \text{S}, \text{Se}, \text{or Te}$) in different oxidation states have been determined by X-ray analysis. The great majority of these contain the $[\text{Fe}_4\text{S}_4]^{2+/1+}$ cores, usually with four terminal thiolate ligands (1, 12–14). A smaller body of structural data is available for $[\text{Fe}_4\text{Se}_4]^{2+/1+}$ clusters (1, 13, 15), and the structures of two $[\text{Fe}_4\text{Te}_4]^{1+}$ clusters have been determined (16, 17). Consequently, native and synthetic Fe_4Q_4 cubane-type species constitute the most extensive structurally defined cluster type. With the former clusters, structural definition has advanced to the point where the relative stabilities of oxidation states of conventional Fd versus HP proteins can be sensibly interpreted in terms of the influence of the immediate protein environment; viz., the different numbers of protein–cluster $\text{N—H} \cdots \text{S}$ hydrogen bonds (18). As will become evident, however, considerably more is known about structure than about structure/property relationships and the reactivity of terminal and core ligands. Many of the recent developments in the chemistry and biology of Fe_4S_4 clusters have been summarized (19–23). The majority of topics presented here have not been comparably treated in these sources.

A. PROTEIN-BOUND CLUSTERS WITH UNCONVENTIONAL TERMINAL LIGATION

The tetracysteinate binding of cluster 1 is the conventional terminal ligation mode of protein-bound Fe_4S_4 clusters. It has been established by protein crystallography in some cases, which serve as points of reference for the many other proteins in which terminal coordination has been deduced from spectroscopic and amino acid sequence data. Proved and probable cluster binding patterns for representative proteins of interest are illustrated schematically in Table I.

In the case of *B. thermoproteolyticus* Fd (8, 9), three of the residues that bind the cluster occur in the prototypical Cys-triplet run Cys-X-X-Cys-X-X-Cys near the N terminus of the polypeptide chain. The fourth Cys residue occurs near the C terminus and is often part of a Cys-Pro-Val fragment. In the 8Fe protein *P. aerogenes* Fd (2, 18), there are two triplet runs and two “distant” Cys residues that bind the two

TABLE I

CLUSTER BINDING PATTERNS IN PROTEINS WITH $[\text{Fe}_4\text{S}_4]$ AND $[\text{Fe}_3\text{S}_4]$ CLUSTERS*B. thermoproteolyticus* Fd*P. furiosus* Fd

Pig Heart Aconitase (11-12 Cys)

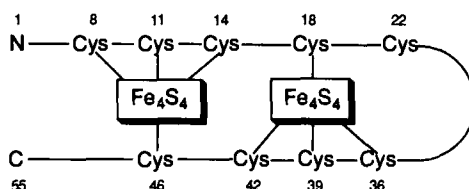
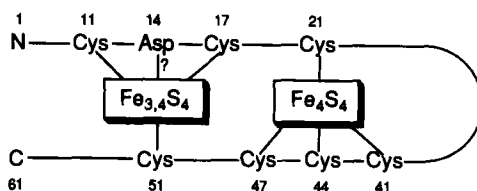
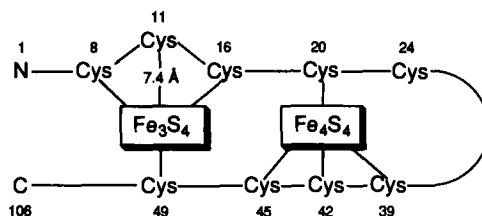
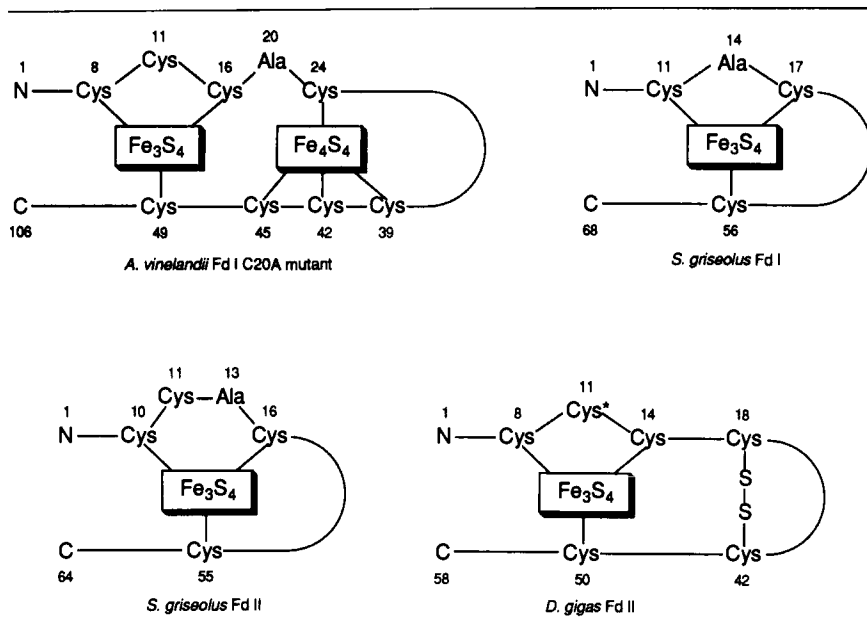
*P. aerogenes* Fd*D. vulgaris* Fd I*D. africanus* Fd III*S. acidocaldarius* Fd (7 Cys, 103 residues)*T. acidophilum* Fd (9 Cys, 142 residues)*A. vinelandii* Fd I

TABLE I (Continued)



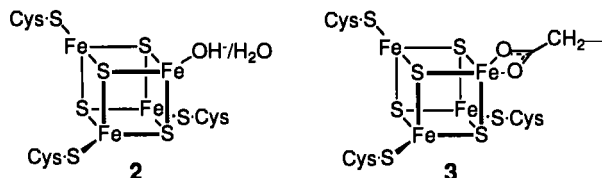
clusters. Consequently, the protein is disposed in a cross-threaded structure of near twofold symmetry. [Note that the original X-ray structure has recently been amended to include Cys 22 and increase the number of residues by one (18).] In the 7Fe protein *A. vinelandii* Fd (6, 7), the fold of the N-terminal half of the polypeptide chain is very similar to that of *P. aerogenes* Fd, and Fe_4S_4 cluster binding also occurs by means of a Cys triplet and a distant residue. In the C20A mutant protein, Cys 20 has been replaced by Ala using site-directed mutagenesis. The tendency to achieve the binding pattern of 1 results in a “cluster-driven protein rearrangement” (11) whereby Cys 24, uncoordinated in the native form, is positioned to bind to the cluster.

Proteins of comparable sizes that observe these sequence patterns (24) are expected to bind Fe_4S_4 clusters similarly. The HP proteins represent an exception. They contain a single cluster 1 that is not bound to residues in a Cys-triplet run. Because these proteins exhibit only electron transfer reactivity thus far, they are not directly pertinent to this report.

Sequence departures from the patterns in the foregoing proteins signal potentially unconventional terminal binding modes. Thus, *Pyro-*

coccus furiosus Fd (25) carries Asp 14 in the central Cys position in the triplet run of other proteins. Similarly, one of the triplets in the sequences of the 8Fe proteins *Desulfovibrio vulgaris* Fd I (26, 27) and *Desulfovibrio africanus* Fd III (28–30) is broken by a central Cys/Asp replacement. Similar situations are found with the ferredoxins from *Sulfolobus acidocaldarius* (7 Cys, 103 residues) (31, 32) and *Thermoplasma acidophilum* (9 Cys, 142 residues) (31, 33). Two 3Fe ferredoxins have been isolated from *Streptomyces griseolus* (34). Both contain an Ala residue at the central position of what would be a Cys triplet near the N terminus. Fd I has only three Cys residues, whereas Fd II has four Cys, but one of these (Cys 11) is located in a nonstandard position for cluster binding. *Desulfovibrio gigas* Fd II, whose structure has been crystallographically determined (35, 36), has six Cys residues, three of which are involved in a triplet near the N terminus, and an Fe_3S_4 cluster. However, the side chain of Cys 11 is rotated away from the Fe_3S_4 cluster and the sulfur atom appears to be substituted, possibly with a thiomethyl group, leading to a modified (Cys*) residue that may be incapable of cluster binding. The binding pattern of the 3Fe cluster of *A. vinelandii* Fd I is somewhat different, owing to the presence of a Cys- X_4 -Cys run involving one of the cluster ligands (Cys 16). The sulfur atom of uncoordinated Cys 11 is placed 7.37 Å from the nearest Fe atom, possibly due to interactions with other residues.

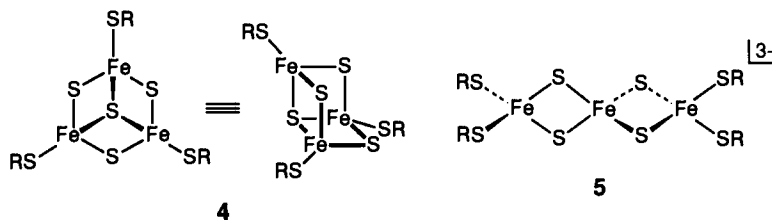
The information in Table I presents three circumstances leading to unconventional Fe_4S_4 cluster binding patterns: (1) occurrence of fewer than four Cys residues per cluster; (2) displacement of Cys residues from, or their replacement in, conventional sequence positions in chain segments where they are known to bind in other proteins; and, correlatively, (3) placement of Cys residues outside of binding distances as dictated by the exigencies of protein structure. In these events, proteins contain clusters whose Fe subsites are differentiated in a 3:1 ratio by the terminal ligands, and the binding modes of clusters 2 and 3 become



possible. Some evidence has been adduced for binding of the carboxylate group of Asp (shown arbitrarily in a chelate form in 3) in *D. africanus* Fd III (30). Among other observations is the small or nil pH dependence of redox potentials, a behavior inconsistent with a coordinated $\text{H}_2\text{O}/\text{OH}^-$ equilibrium. Alternatively, only hydroxide may be ligated over

the pH range investigated. Cluster 2 has been crystallographically established in the active form of pig heart aconitase, in which the unique subsite of 2 is coordinated by water or hydroxide and the sulfur atom of the nearest Cys residue is 14.3 Å from the center of the cluster (10). Inasmuch as the homology of the Cys sequence of the beef heart enzyme (37) with the DNA-derived pig heart enzyme sequence is greater than 98% (10), it is likely that all properties associated with the clusters in the two enzymes will be nearly identical. Indeed, electron-nuclear double-resonance (ENDOR) studies of active, substrate-free beef heart aconitase reveal the presence of $\text{H}_2\text{O}/\text{OH}^-$ ligation (38). In view of the large size of these molecules ($M_r \approx 80,000$), it is unlikely that circumstance (2) given above is pertinent to cluster binding patterns in these enzymes.

The foregoing circumstances could conceivably destabilize Fe_4S_4 clusters to the extent that they cannot be readily maintained, or formed at all, in a protein structure. In this event, with three Cys ligands available, the only known alternative is the cuboidal Fe_3S_4 cluster 4 ($\text{RS} = \text{Cys} \cdot \text{S}$), which is considered in some detail later. In addition to the foregoing cases, this cluster has been crystallographically demonstrated in the inactive form of aconitase (10). On the basis of an electron paramagnetic resonance (EPR) criterion (a broad asymmetric signal centered at $g \approx 2.01$ and observable below ~ 15 K), it is present in the *S. griseolus* proteins wherein Fd I has only three Cys residues and Fd II lacks the standard Cys-triplet binding sequence (Table I). The Fe_3S_4 cluster in *A. vinelandii* Fd I is not readily converted to an Fe_4S_4 cluster, presumably because of the unfavorable location of Cys 11 as a fourth ligand. There is a further structural alternative, the linear cluster 5, which requires four Cys ligands. It has been detected thus far only in an unfolded form of inactive aconitase (39), where ligands in the Cys-X-X-Cys segment apparently are retained (40). Linear cluster 5 has been synthesized and fully characterized (41), but cuboidal cluster 4 has not been obtained in isolable form.



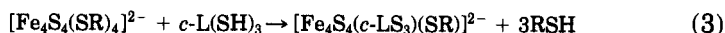
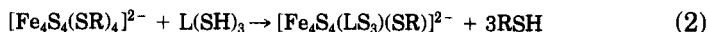
Having established the existence of unconventional ligation in protein-bound clusters, we shall examine the consequences of the resultant

subsite differentiation and its relation to Fe_3S_4 cluster formation and reactivity. As will be seen, protein-bound **4** and synthetic **5**, although of much interest in their own right, are precursors to new clusters.

B. SUBSITE-DIFFERENTIATED SYNTHETIC CLUSTERS

1. 3 : 1 Subsite Differentiation

Stimulated by the recognition of such clusters in proteins, research was undertaken in this laboratory to prepare clusters whose subsites are differentiated in a 3 : 1 ratio. We have obtained two solutions to this problem by use of trithiol ligands **6** and **7**. These are shown in Fig. 1 together with their subsite-differentiated clusters **8** and **9**. The design aspects of **6** [$\text{L}(\text{SH})_3$] and its successful use in the binding of cubane-type clusters have been summarized (22). Molecular mechanics and dynamics analysis of this ligand reveals majority conformations in which central ring substituents alternate in position above and below the central ring (42). The coordinating "arms" with their thiol groups are buttressed in positions on the same side of the ring by the *p*-tolylthio "legs" on the opposite side. Further, the 6Me substituents on the arms tend to direct rotation of the phenyl rings such that their thiol groups are pointed inward over the central ring. This arrangement is sterically preferred to one that places one or more methyl groups over this ring. The existence of configurations of this type is experimentally recognized by the substantial nuclear magnetic resonance (NMR) shielding of the 2H protons. Thus, ligand **6** is largely predisposed to capture a cubane cluster in ligand substitution reactions such as Eq. (2) [R = alkyl and LS_3 = 1,3,5-tris((4,6-dimethyl-3-mercaptophenyl)thio)-2,4,6-tris(*p*-tolylthio)benzene(3-), or triply deprotonated **6**] and to suppress polymer formation. *In situ* cluster capture is quantitative in this reaction and isolated yields of product cluster **8** ($\text{L}' = \text{SR}$) are high (42–44). When 6H rather than 6Me is present, the directing influence on the rotation of the arms is lost, and the amount of insoluble oligomeric product in Eq. (2) substantially increases (42). Cyclic ligand **7** [$c\text{-L}(\text{SH})_3$] is of a different design, with the 3-3-2 pattern of methylene groups selected in order that the ligand bind snugly to three subsites of the cluster. The substitution reaction given by Eq. (3) proceeds smoothly to afford the subsite-differentiated cluster **9** ($\text{L}' = \text{SR}$) (45).



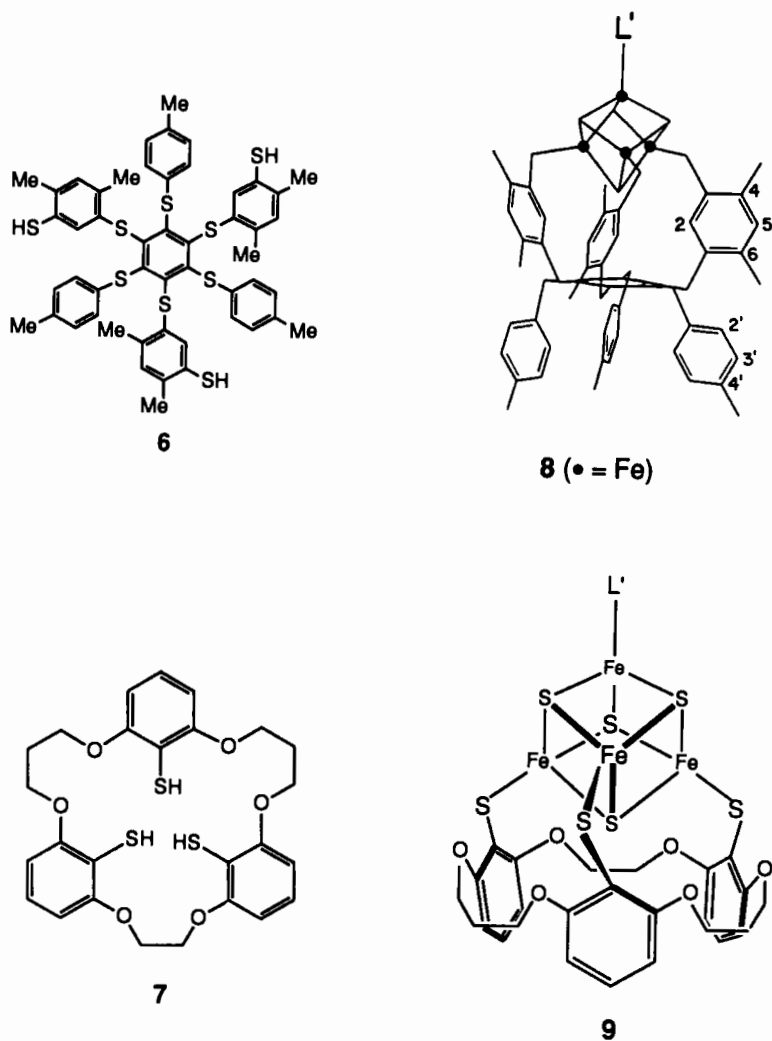


FIG. 1. Formulas of the trithiol ligand $L(SH)_3$ (**6**) and cyclic trithiol ligand $c-L(SH)_3$ (**7**) and schematic depictions of their 3 : 1 subsite-differentiated clusters $[Fe_4S_4(LS_3)L']^{2-}$ (**8**) and $[Fe_4S_4(c-LS_3)L']^{2-}$ (**9**), respectively.

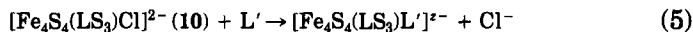
The cluster binding mode of **8** has been verified by X-ray structure determinations (42, 43) and the trigonally symmetric configuration is consistent with the 1H NMR spectra of over 40 clusters. The ligand resembles a cavitand whose floor is the central benzene ring and whose "walls" are the closest edge regions of the three coordinating phenyl

rings. The $[\text{Fe}_4\text{S}_4]^{2+}$ core partially occupies this cavity, the perpendicular distance from the unique sulfur atom of the core to the central ring being 3.74 Å in $[\text{Fe}_4\text{S}_4(\text{LS}_3)\text{Cl}]^{2-}$ (43). The ligand is sufficiently flexible that it binds the $[\text{Fe}_4\text{Se}_4]^{2+}$ core, whose van der Waals volume is ~25% larger than that of $[\text{Fe}_4\text{S}_4]^{2+}$. In the Ph_4P^+ salt of $[\text{Fe}_4\text{Se}_4(\text{LS}_3)\text{Cl}]^{2-}$, there are three inequivalent clusters, each with crystallographically imposed trigonal symmetry and different extents of cavity occupancy (42). The corresponding distances from the unique selenium atom to the ring centroid are 3.68, 3.69, and 4.09 Å. These observations afford the description of the deprotonated form of **6** as a semirigid cavitand ligand. Diffraction-quality crystals of salts of **9** have not been obtained, but the indicated structure with mirror symmetry is fully supported by ^1H NMR spectra (45). The ligand in this cluster is not of the cavitand type.

The principal advantage of subsite-differentiated clusters **8** and **9**—indeed, the reason they were prepared—is that they undergo subsite-specific substitution reactions at the unique subsite, thereby opening a new dimension in the chemistry of Fe_4S_4 clusters. Although clusters of the general type $[\text{Fe}_4\text{S}_4\text{L}_4]^{2-}$ ($\text{L} = \text{RS}^-$, halide) readily undergo substitution reactions, any mixed ligand products that are formed occur in near-statistical mixtures and are in labile equilibrium in solutions of polar solvents (22). This is not the case with **8** and **9** and their derivatives, most importantly the chloride clusters ($\text{L}' = \text{Cl}^-$). These clusters are obtained as exemplified with **8** ($\text{L}' = \text{RS}^-$) in the reaction given by Eq. (4) (43).



As anticipated by earlier work (46), chloride is an excellent leaving group. Thus the reactions of cluster **10**, represented generally by Eq. (5) and illustrated in Fig. 2, lead to a diverse set of products (47, 48). Most of these species were not isolated but were generated in solution



and unambiguously detected by ^1H NMR. The isotropically shifted resonances of the 4Me, 5H, and 6Me substituents of the phenyl rings in the coordinating arms of the ligand are exquisitely sensitive to the nature of ligand(s) L' at the unique subsite. In most cases, substitution could also be detected by potential shifts of the $[\text{Fe}_4\text{S}_4]^{2+/1+}$ couple of Eq. (1). The reactions of **9** ($\text{L}' = \text{Cl}^-$) have been less thoroughly examined, but reactivity, where tested with the same ligand, is analogous (45). The ligand structural features of **8** do not appear to have any special effects on reactivity at the unique subsite.

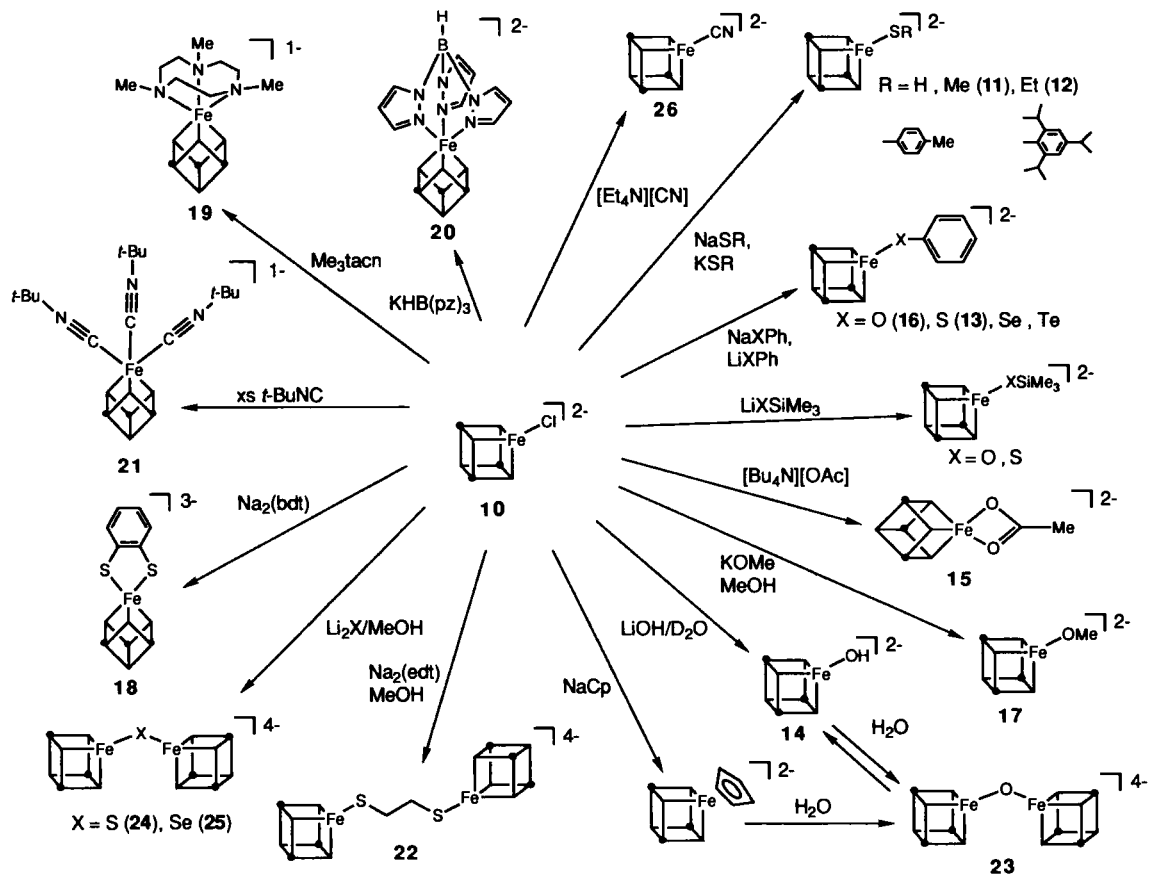
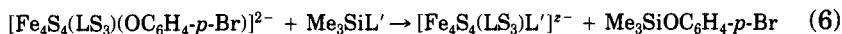


FIG. 2. Summary of subsite-specific substitution reactions of $[\text{Fe}_4\text{S}_4(\text{LS}_3)\text{Cl}]^{2-}$ (10) in Me_2SO solution (47). The cube symbol represents the $\text{Fe}_4\text{S}_4(\text{LS}_3)$ portion of generalized cluster 8. A related summary involving other ligands is given elsewhere (48).

In the event that displacement of chloride from **10** is not successful, Eq. (6) offers an alternative means of substitution. Advantage is taken



of the higher strength of a Si—O versus a Si—L' bond. The *p*-bromophenolate ligand has been utilized because it facilitates isolation of the initial cluster. In this way, clusters with $\text{L} = \text{N}_3^-$ and MeSO_3^- , ligands that do not displace chloride, were obtained as well as certain other clusters that have also been prepared by the reaction given in Eq. (5) (47).

Among the clusters obtained are those whose ligands L' simulate known or potential cysteinate (**11–13**, as in **1**), hydroxide (**14**, as in **2**), and carboxylate (**15**, as in **3**) ligation of protein-bound clusters. Note also phenolate binding (**16**), which had been established earlier with $[\text{Fe}_4\text{S}_4(\text{OPh})_4]^{2-}$ (49) and indicates the feasibility of Tyr as a cluster ligand. Cluster **17** simulates alkoxide binding; however, no deprotonated Ser residue has been detected as a ligand in any metalloprotein. Somewhat less exactly, **18** presents the possibility of a five-coordinate subsite with two Cys ligands, and **19** and **20** that of six-coordinate subsites with neutral weak-field ligands. At the same time, **20** and $[\text{Fe}_4\text{S}_4(\text{LS}_3)(\text{H}_2\text{B}(\text{pz})_2)]^{2-}$ [not shown; $\text{H}_2\text{B}(\text{pz})_2$ is dihydrobis(pyrazolyl)-borate(1–)] suggest that imidazole groups of His residues may have cluster binding affinity.

Subsite-differentiated synthetic clusters lend themselves to many applications, which have been summarized (22). These include modulations of redox potentials, electron distributions, and interactions between subclusters in bridged double cubanes, all dependent on the ligand at the unique subsite. Although detailed consideration of these matters is beyond the purview of this article, certain leading results are noted. Introduction of a dianionic electron-rich ligand such as benzene-1,2-dithiolate in **18** causes very large (~500–600 mV) negative shifts of the $[\text{Fe}_4\text{S}_4]^{3+/2+}$ potential (48), thereby stabilizing the +3 core to reduction. Alteration of core electron distribution reaches an extreme upon the binding of three strong-field isonitrile ligands, as in **21**. The unique subsite becomes low-spin Fe(II), thereby generating the $[\text{Fe}_3\text{S}_4]^0$ cluster fragment with the same ground state spin ($S = 2$) and electronic structure as protein-bound cuboidal cluster **4** in the same oxidation state (50, 51). Clusters may be covalently linked by dithiolate bridges, as in **22**, or by oxide (**23**), sulfide (**24**), or selenide (**25**). When centroids of subclusters bridged by dithiolates are separated by less than ~11 Å, the two redox steps of the double cubanes are detectably coupled when examined by differential pulse polarography (52). The largest coupling,

in terms of a potential difference (220–230 mV), is found with oxide and sulfide bridges, which reduce subcluster separation to a minimum. The sulfide bridge has been structurally demonstrated in $[(\text{Fe}_4\text{S}_4\text{Cl}_3)_2\text{S}]^{4-}$ ($\text{Fe}-\text{S}-\text{Fe} = 102^\circ$, $\Delta E_{1/2} = 300$ mV), which was prepared without using a subsite-differentiated cluster (53). In a further application, sulfur-bound pyridine-3/4-thiolate groups have been placed at the unique site. These bind Fe(II) complexes in covalently bridged assemblies, which provide an initial approach to the bridged Fe_4S_4 -siroheme active site of *Escherichia coli* sulfite reductase (54).

The reactions of cluster 10, which were conducted in Me_2SO solutions, represent the first extensive examination of the reactivity of an Fe_4S_4 cluster toward terminal ligand substitution.¹ Nearly all reactions are stoichiometric and, under the constant conditions employed, demonstrate that an iron subsite has an intrinsic affinity for a large range of ligands. Inasmuch as no nonthiolate ligand is known to displace alkylthiolate, it is improbable that other protein ligands can compete with cysteinate when four Cys residues are within bonding distance of a single-cubane core. However, it is now clear that, if not blocked by cysteinate, a subsite may accept other terminal ligands, including those in clusters 2 and 3.

The reactions in Fig. 2 provide a guide to possible reactions of subsite-differentiated native clusters with exogenous ligands, at least in the $[\text{Fe}_4\text{S}_4]^{2+}$ oxidation state. In the only detailed study thus far, certain spectroscopic evidence has been interpreted in terms of cyanide binding to the cluster of *P. furiosus* Fd_{red} (56). ENDOR results indicate the presence of a type 2 cluster, which, from EPR spectra, exists as a ground spin state mixture of 20% $S = \frac{1}{2}$ and 80% $S = \frac{3}{2}$. Incubation of the protein with a 250-fold excess of cyanide resulted in conversion to a single EPR species with $S = \frac{1}{2}$ and a magnetic circular dichroism (MCD) spectrum consistent with the $[\text{Fe}_4\text{S}_4]^{1+}$ state but different from that of the initial cluster. Removal of cyanide by gel filtration restored the original EPR spectrum. Cyanide-induced perturbations of the EPR and MCD spectra were not observed with *Clostridium pasteurianum* Fd_{red} , which contains two standard clusters 1, or with the 3Fe form of *P. furiosus* Fd. These results are consistent with reversible cyanide binding to the unique subsite of the cluster, similar to formation of oxidized cluster 26 (Fig. 2). The number of cyanide ligands bound to the protein cluster has not been established. Experience with synthetic clusters

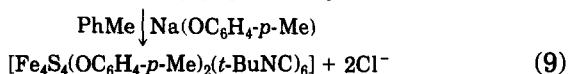
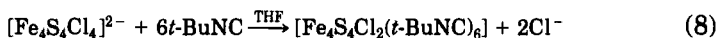
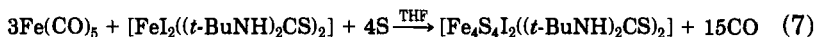
¹ Core ligand substitution in the form of chalcogenide atom (Q) exchange reactions in the clusters $[\text{Fe}_4\text{Q}_4(\text{SR})_4]^{2-}$ and $[\text{Fe}_4\text{Q}_4(\text{SR})_4]^{3-}$ (Q = S, Se) had been demonstrated earlier (55).

such as **8** indicates that only one anionic monodentate ligand binds at a given subsite, a behavior that derives in part from ligand–ligand repulsion; two such ligands have been bound in a stable cluster only by chelation as, e.g., in **18**. In these experiments, bound cyanide has not been directly detected. It is unclear whether the observed spectral perturbations could arise from cyanide interactions with the protein but without specific cluster binding. Despite this uncertainty, it appears likely that a substantial reaction chemistry of protein-bound clusters having one labile subsite will be developed with *P. furiosus* Fd or other proteins, provided that protein structure allows access to the cluster by a variety of potential ligands.

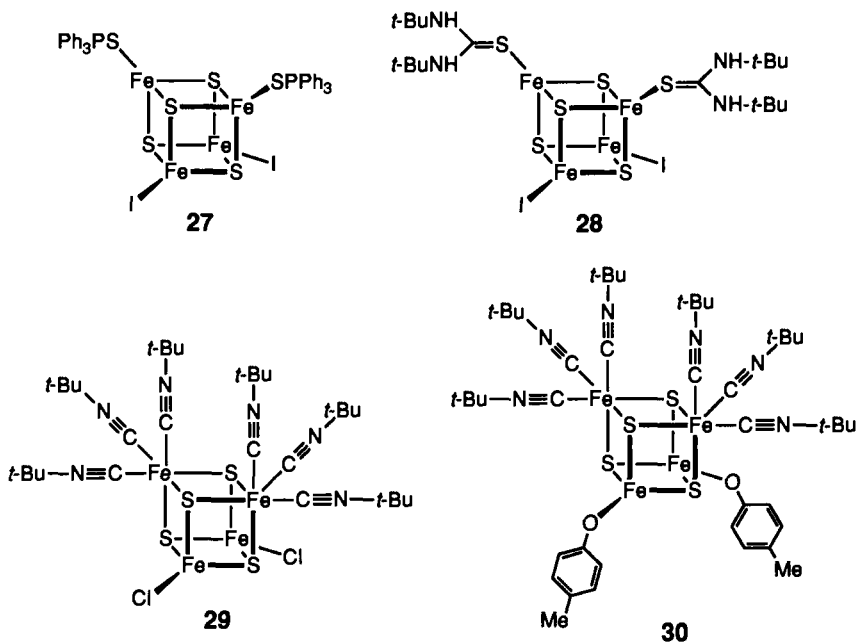
2. 2:2 Subsite Differentiation

Although no protein-bound clusters with two non-Cys ligands have been recognized, we note, in the context of subsite differentiation, the existence of synthetic clusters with two different ligands. Anionic clusters of the general type $[\text{Fe}_4\text{S}_4\text{L}_2\text{L}'_2]^{2-}$ in polar solvents tend to exist in disproportion equilibria with other clusters. Several such clusters, among them $[\text{Fe}_4\text{S}_4\text{Cl}_2(\text{OPh})_2]^{2-}$ and $[\text{Fe}_4\text{S}_4\text{Cl}_2(\text{SPh})_2]^{2-}$, have been crystallized and their structures established by X-ray analysis (57, 58).

Somewhat more interesting are the neutral clusters $[\text{Fe}_4\text{S}_4\text{L}_2\text{L}'_n]$, examples of which have only recently been prepared. These species contain anionic (L) and neutral (L') ligands. Cluster **27** has been obtained from the reaction of $[\text{Fe}(\text{THF})_6][\text{Fe}_4\text{S}_4\text{I}_4]$, Ph_3PS , and sulfur in toluene/dichloromethane (59). The related cluster **28** was synthesized in the cluster assembly system, Eq. (7) (60). Cluster **29** was prepared by ligand substitution reaction, Eq. (8) (51), similar to the method for **21**, and **30** was readily produced by the subsequent substitution reaction, Eq. (9), in the presence of excess *t*-BuNC to suppress ligand dissociation (61). Under these conditions in the indicated solvents, neutral rather than charged products are formed.

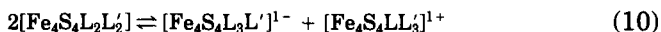


The structures of **27** and **28** contain the familiar $[\text{Fe}_4\text{S}_4]^{2+}$ cubane-type cores with unexceptional dimensions except for the relatively short Fe–Fe distance [2.687(4) Å] between atoms bound to the thiourea ligands of **28**. The structures of **29** and **30** are nearly isodimensional and



are conspicuously different from those of any other $[\text{Fe}_4\text{S}_4]^{2+}$ species. The cores exhibit six long and six short Fe–S distances. In **30** the mean values are 2.38(2) and 2.26(1) Å. The short distances are normal and involve the four-coordinate subsites, which are separated by 2.74–2.77 Å. The long distances are found at the six-coordinate subsites, and, together with the long Fe . . . Fe separation of 3.45 Å, demonstrate the presence of two low-spin Fe(II) subsites and their effective electronic isolation from each other and from the Fe_2S_2 cluster portion with tetrahedral subsites. The structures at the six-coordinate subsites undoubtedly represent that of the corresponding subsite in cluster **21**, whose electronic structure has been elucidated (50, 51).

In low-polarity solvents such as toluene, tetrahydrofuran (THF), and dichloromethane, neutral clusters should prove stable to disproportionation inasmuch as the reaction given by Eq. (10) generates ionic prod-



ucts. The occurrence of these reactions, Eqs. (7)–(9), in such media is an obvious reflection of stability of the product clusters.² The solution

² There is no implication that only neutral clusters will be formed in low-polarity solvents; for example, $[\text{Fe}_4\text{S}_4\text{I}_3((\text{Me}_2\text{N})_2\text{CS})]^{1-}$ [as the $[\text{FeI}((\text{Me}_2\text{N})_2\text{CS})_3]^{1+}$ salt] is formed by two different reactions in THF (60).

properties of **27** and **28** have not been reported other than the note that the former decomposes (to unspecified products) in THF and acetonitrile (59). Clusters **29** and **30** are stable in toluene, THF, and dichloromethane; the occurrence of the (heterogeneous) reaction, Eq. (9), demonstrates the feasibility of anion/anion ligand substitution in toluene to generate another neutral cluster. Neutral ligands, especially those at tetrahedral high-spin subsites, are potentially susceptible to replacement by other neutral ligands. Neutral/anion substitution appears most likely when the other two subsites carry strongly bound thiolate ligands, but the formation of charged clusters implies the possibility of disproportionation even in a low-polarity medium. Among Fe_4S_4 clusters, the unique potential reactivity of $[\text{Fe}_4\text{S}_4\text{L}_2\text{L}'_n]$ is that of neutral/neutral ligand substitution in low-polarity media to afford stable 2:2 subsite-differentiated products. At present, there is practically no information on the affinity of Fe_4S_4 clusters in any oxidation state for neutral ligands. Clusters **19–21** and **27–30**, $[\text{Fe}_4\text{S}_4(\text{LS}_3)(\text{tacn})]^{1-}$ (**48**), and $[\text{Fe}_4\text{S}_4(\text{CO})_{12}]$ (**62**), with the fully reduced $[\text{Fe}_4\text{S}_4]^0$ core, are the only examples with neutral ligand donors (tacn is 1,4,7-triazacyclononane).

III. Trinuclear Cuboidal Clusters

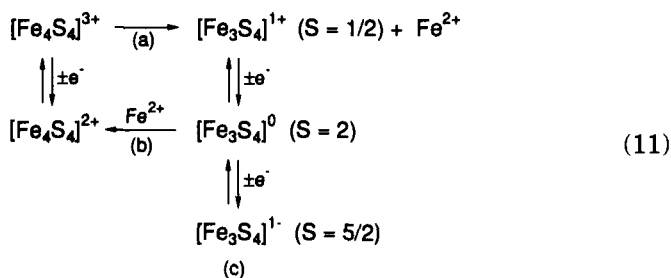
A. PROTEIN-BOUND Fe_3S_4 CLUSTERS

Whereas the synthesis of new clusters is an everyday occurrence in chemistry, the discovery of a new metal cluster in biology is a signal event. The pleasure of watching the chemistry and biochemistry of the cuboidal Fe_3S_4 cluster **4** and its derivatives unfold is enhanced by the realization that its occurrence was totally unpredicted. Although not a new structural motif (*vide infra*), it joins Fe_4S_4 and Fe_2S_2 (**63–66**) units in the set of structurally defined biological iron–sulfur clusters and is among the very few structurally characterized (**67**) polynuclear metal units in proteins. An account of the discovery of Fe_3S_4 clusters has been provided by Beinert and Thomson (**68**). In brief, aerobically purified ferredoxins often show a nearly isotropic EPR signal at $g \approx 2.01$, which was first thought by some investigators in the 1970s to arise from a minor impurity of “superoxidized” ($[\text{Fe}_4\text{S}_4]^{3+}$) clusters. Subsequent spectroscopic and crystallographic studies of *D. gigas* Fd II and *A. vinelandii* Fd I, originally believed to be an 8Fe protein, led to the conclusion that both proteins accommodated the same cluster that contained *three* iron atoms. This conflicted with the orthodox view at the time that low-molecular-weight ferredoxins contained only two cluster

types, Fe_2S_2 and Fe_4S_4 . The definitive identification of the cluster as cuboidal Fe_3S_4 was forthcoming from protein crystallography in 1988 (6, 7, 35).

1. Formation, Oxidation States, and Spin States

Consideration of the occurrence and formation of Fe_3S_4 clusters in proteins necessarily involves those factors that destabilize, or prevent the formation of, the far more widely distributed Fe_4S_4 clusters. Two factors are of prime importance: protein compositional and structural features that lead to unconventional terminal ligation, and cluster oxidation level. Except for the standard cases of *B. thermoproteolyticus* Fd and *P. aerogenes* Fd, the cluster binding patterns in Table I reveal that known or putative Fe_4S_4 clusters in these proteins display the unconventional terminal ligation in 2 and, perhaps, 3. The lack of a strongly bound Cys ligand promotes lability at the unique subsite. For at least aconitase (38) and *P. furiosus* Fd (69), the ligand at that subsite is $\text{OH}^-/\text{H}_2\text{O}$. In those cases wherein an iron atom has been removed from a tetranuclear cluster, the atom is released from the $[\text{Fe}_4\text{S}_4]^{3+}$ oxidation level in reaction (a) of the scheme given by Eq. (11). Spontaneous iron atom uptake to rebuild an Fe_4S_4 cluster occurs with $[\text{Fe}_3\text{S}_4]^0$ in reaction (b). Neither reaction is known to be reversible.



Protein cluster conversion reactions are summarized in Table II (70–84). Those of aconitase and *D. gigas* Fd II have been the most carefully studied, and afford different results. With use of Mössbauer spectroscopy and ^{57}Fe -enriched samples, it has been demonstrated that the subsite voided in reaction (a) of aconitase is that occupied in reaction (b) (70). In the case of *D. gigas* Fd II, the addition of external $^{57}\text{Fe}^{2+}$ to the $[\text{Fe}_3\text{S}_4]^0$ form of the protein results in the occupation of one of three subsites that are indistinguishable by Mössbauer spectroscopy (76). It was also shown that exchange between the two Mössbauer-detectable subsites of the Fe_4S_4 cluster, present in a 3 : 1 ratio, does not occur over a time sufficient for cluster conversion. This indicates that the (final)

TABLE II
CLUSTER CONVERSION REACTIONS

Reaction	Protein	Ref.
$[\text{Fe}_3\text{S}_4] \rightleftharpoons [\text{Fe}_4\text{S}_4]$	Aconitase (beef heart)	70-74
	<i>Desulfovibrio gigas</i> Fd II	75-77
	<i>Pyrococcus furiosus</i> Fd	25
$[\text{Fe}_3\text{S}_4] \rightarrow [\text{Fe}_4\text{S}_4]$	<i>Desulfovibrio africanus</i> Fd III	30
	<i>Thermodesulfobacterium commune</i> Fd	78
$[\text{Fe}_4\text{S}_4] \rightarrow [\text{Fe}_3\text{S}_4]$	<i>Azotobacter chroococcum</i> Fd	79
	<i>Bacillus stearothermophilus</i> Fd	80, 81
	<i>Clostridium pasteurianum</i> Fd	82, 83
	<i>Mycobacterium smegmatis</i> Fd	84
	<i>Pseudomonas ovalis</i> Fd	84
	<i>Thermus thermophilus</i> Fd	84

subsite assumed is one of the three that are Cys ligated rather than the initially vacant subsite, in contrast to the behavior of aconitase. In proteins such as *B. stearothermophilus* Fd and *C. pasteurianum* Fd, which contain only type 1 clusters, conversion to the Fe_3S_4 form has been accomplished by treatment with an excess of a chemical oxidant such as ferricyanide. Assuming that the iron atoms retain four coordination, one or more Cys ligands must be removed from the cluster in the process, either by displacement and protonation or by oxidation, possibly to the sulfonate. Treatment of *A. vinelandii* Fd I with excess ferricyanide results in selective destruction of the Fe_4S_4 cluster, leaving the Fe_3S_4 cluster intact (85).

Although few details of reactions (a) and (b) of Eq. (11) are known, it is now quite clear that the electrophilic demands of the three Fe(III) atoms in $[\text{Fe}_3\text{S}_4]^{1+}$ render the sulfur atoms insufficiently nucleophilic to bind relatively hard (divalent) metal ions. Reduction by one electron redresses this problem. We shall return to the concept of the cuboidal Fe_3S_4 cluster as a ligand.

Also shown in Eq. (11) is the electron transfer series (c) of Fe_3S_4 clusters and the ground spin state of each oxidation level. The latter has been established for $[\text{Fe}_3\text{S}_4]^{1+/0}$ by analysis of low-temperature MCD spectra (25, 82, 86-90) and by direct measurement of magnetization (91). In the oxidized state $[\text{Fe}_3\text{S}_4]^{1+}$, the three $S = \frac{1}{2}$ Fe(III) atoms, indistinguishable by Mössbauer spectroscopy, are antiferromagnetically coupled to give an $S = \frac{1}{2}$ ground state with a nearly isotropic EPR

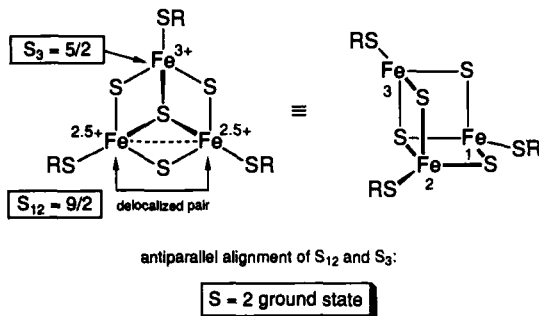


FIG. 3. Schematic representation of the geometric and electronic structure of the $[\text{Fe}_3\text{S}_4]^0$ oxidation level showing the high-spin Fe^{3+} site and the $\text{Fe}^{3+/2+}$ delocalized pair, which account for doublets A and B,B', respectively, in the Mössbauer spectra (Table III).

signal near $g \approx 2.01$ (68). Potentials for the $[\text{Fe}_3\text{S}_4]^{1+/0}$ couple span the range -130 to -420 mV (29, 92–95).³

The most unusual electronic structure of $[\text{Fe}_3\text{S}_4]^0$ is schematically represented in Fig. 3; isomer shifts (δ) and quadrupole splittings (ΔE_Q) of representative proteins are listed in Table III. The cluster contains a high-spin Fe(III) subsite with normal Mössbauer parameters (doublet A), which are nearly the same as those for $[\text{Fe}_3\text{S}_4]^{1+}$. Also present is an electronically delocalized pair of Fe(II,III) atoms (doublets B,B') that are effectively identical on the Mössbauer time scale; a small inequivalence has been detected in aconitase. The average isomer shift is in the range of $[\text{Fe}_4\text{S}_4]^{2+}$ clusters, indicating the mean oxidation state $\text{Fe}^{2.5+}$. The spins at these subsites ($S = 2, \frac{5}{2}$) are ferromagnetically coupled to afford the resultant $S = \frac{9}{2}$. This spin is in turn antiferromagnetically coupled to the Fe(III) spin to yield the system spin $S = 2$. A spin-coupling mechanism with electron delocalization over two subsites has been proposed to account for the observed electronic structure (99, 100), which shall be of subsequent interest in connection with the ligand properties of $[\text{Fe}_3\text{S}_4]^0$. In selenide-reconstituted aconitase, the $[\text{Fe}_4\text{S}_4]^{2+}$ cluster can be converted with ferricyanide to $[\text{Fe}_3\text{Se}_4]^{1+}$. This cluster is reducible to $[\text{Fe}_3\text{Se}_4]^0$, which has the same electronic structure as its sulfide congener (96).

³ In accordance with the way in which they are typically reported, protein potentials are referenced to the normal hydrogen electrode (NHE) and those of synthetic compounds (usually in nonaqueous solvents) are versus the SCE ($E_{\text{NHE}} = E_{\text{SCE}} + 0.24$ V). When applied to redox reactions, the term "reversible" refers to chemical reversibility ($i_{\text{pa}}/i_{\text{pc}} \approx 1$ in cyclic voltammetry).

TABLE III

MÖSSBAUER PARAMETERS AND OXIDATION AND SPIN STATES FOR CUBOIDAL $[\text{Fe}_3\text{S}_4]$ AND HETEROMETAL CUBANE $[\text{MFe}_3\text{S}_4]$ CLUSTERS

Cluster/protein	Oxidation state	$\delta^{a,b}$ (mm/sec)	ΔE_Q^b (mm/sec)	Spin state (S)	Fragments	Ref.
$[\text{Fe}_3\text{S}_4]$						
Aconitase (beef heart)	$[\text{Fe}_3\text{S}_4]^{1+}$	0.27	0.71	$\frac{1}{2}$	—	70
<i>A. vinelandii</i> Fd I	$[\text{Fe}_3\text{S}_4]^{1+}$	0.27	0.63	$\frac{1}{2}$	—	97
<i>D. gigas</i> Fd II	$[\text{Fe}_3\text{S}_4]^{1+}$	0.27	0.54	$\frac{1}{2}$	—	98
Aconitase (beef heart)	$[\text{Fe}_3\text{S}_4]^0$	A 0.31	0.56	2	—	96
		B 0.46	1.15		—	
		B' 0.49	1.46		—	
<i>A. vinelandii</i> Fd I	$[\text{Fe}_3\text{S}_4]^0$	A 0.29	0.40	2	—	97
		B 0.47	1.45		—	
<i>D. gigas</i> Fd II	$[\text{Fe}_3\text{S}_4]^0$	A 0.30	0.47	2	—	98
		B 0.46	1.47		—	
Mean (three proteins)		0.42	—			
$[\text{MFe}_3\text{S}_4]$						
M = Fe, Co, Ni, Zn, Cd (Set I)						
$[\text{Fe}_4\text{S}_4(\text{LS}_2)(t\text{-BuNC})_3]^{1-}$ (21)	$[\text{Fe}_4\text{S}_4]^{2+}$	A 0.34	0.59	2	$[\text{Fe}_3\text{S}_4]^0 + \text{Fe}^{2+}$ (S = 0)	50, 51
		B 0.46	1.21			
		B' 0.47	1.49			
<i>D. gigas</i> Fd II/Co	$[\text{CoFe}_3\text{S}_4]^{2+}$	A 0.35	1.1	$\frac{1}{2}$ }		199
		B 0.44	1.35			
$[\text{CoFe}_3\text{S}_4(\text{tibt})_4]^{2-}$ (70)	$[\text{CoFe}_3\text{S}_4]^{2+}$	A 0.33	0.78	$\frac{1}{2}$ }	$[\text{Fe}_3\text{S}_4]^0 + \text{Co}^{2+}$ (S = $\frac{3}{2}$)	197
		B 0.43	1.32			
		B' 0.46	0.93			

TABLE III (continued)

Cluster/protein	Oxidation state	$\delta^{a,b}$ (mm/sec)	ΔE_Q^b (mm/sec)	Spin state (<i>S</i>)	Fragments	Ref.
<i>D. gigas</i> Fd II/Co	[CoFe ₃ S ₄] ¹⁺	0.53	1.28	>0 (1) ^d	[Fe ₃ S ₄] ¹⁻ + Co ²⁺ (<i>S</i> = 3/2)	199
<i>P. furiosus</i> Fd/Ni	[NiFe ₃ S ₄] ¹⁺	— ^c	— ^c	$\left. \begin{array}{c} \text{Fe}_3 \\ \text{Fe}_2 \\ \text{Fe}_2 \end{array} \right\}$	[Fe ₃ S ₄] ¹⁻ + Ni ²⁺ (<i>S</i> = 1)	201
[NiFe ₃ S ₄ (SEt) ₃ (PPh ₃) ²⁻ (68)	[NiFe ₃ S ₄] ¹⁺	0.47	0.90			195
<i>D. gigas</i> Fd II/Cd	[CdFe ₃ S ₄] ¹⁺	— ^c	— ^c			200
<i>D. gigas</i> Fd II/Zn	[ZnFe ₃ S ₄] ¹⁺	A 0.62 B 0.51 B' 0.54	2.7 1.6 1.6	$\left. \begin{array}{c} \text{Fe}_3 \\ \text{Fe}_2 \\ \text{Fe}_2 \end{array} \right\}$	[Fe ₃ S ₄] ¹⁻ + Cd ²⁺ [Fe ₃ S ₄] ¹⁻ + Zn ²⁺	102
Mean		0.56	—			
M = V, Mo, W, Re (Set II)						
[VFe ₃ S ₄ (<i>S-p</i> -tol) ₃ (DMF) ₃] ¹⁻ (56)	[VFe ₃ S ₄] ²⁺	0.46	1.08	$\left. \begin{array}{c} \text{Fe}_3 \\ \text{Fe}_2 \\ \text{Fe}_2 \end{array} \right\}$	[Fe ₃ S ₄] ^{0/1-} + V ^{2+/3+}	189
[Mo ₂ Fe ₆ S ₈ (SPh) ₃] ³⁻ (43)	[MoFe ₃ S ₄] ³⁺	0.40	1.01			176
		0.44	1.41			
[MoFe ₃ S ₄ (<i>S-p</i> -C ₆ H ₄ Cl) ₄ (cat)] ³⁻ (48)	[MoFe ₃ S ₄] ³⁺	0.40 0.43	1.76 1.14	$\left. \begin{array}{c} \text{Fe}_3 \\ \text{Fe}_2 \\ \text{Fe}_2 \end{array} \right\}$	[Fe ₃ S ₄] ⁰ + Mo ³⁺	202
[Mo ₂ Fe ₆ S ₈ (SPh) ₃] ⁵⁻ (45)	[MoFe ₃ S ₄] ²⁺	0.53	2.21			176
		0.54	0.84			
[MoFe ₃ S ₄ (<i>S-p</i> -C ₆ H ₄ Cl) ₄ (EtCN)] ³⁻ (48)	[MoFe ₃ S ₄] ²⁺	0.52 0.54	2.25 0.91	2	[Fe ₃ S ₄] ¹⁻ + Mo ³⁺	202
[W ₂ Fe ₆ S ₈ (SEt) ₉] ³⁻	[WFe ₃ S ₄] ³⁺	0.45 ^e	1.41 ^e			203
[Re ₂ Fe ₇ S ₈ (SEt) ₁₂] ²⁻ (66)	[ReFe ₃ S ₄] ⁴⁺	0.37	0.86			191
[Re ₂ Fe ₆ S ₈ (SEt) ₉] ³⁻ (63)	[ReFe ₃ S ₄] ³⁺	0.44	0.87	$\left. \begin{array}{c} \text{Fe}_3 \\ \text{Fe}_2 \\ \text{Fe}_2 \end{array} \right\}$	[Fe ₃ S ₄] ⁰ + Re ⁴⁺	204
		0.46	1.17			
[ReFe ₃ S ₄ (SEt) ₄ (dmpe)] ¹⁻ (67)	[ReFe ₃ S ₄] ³⁺	0.49 ^e	1.37 ^e			2

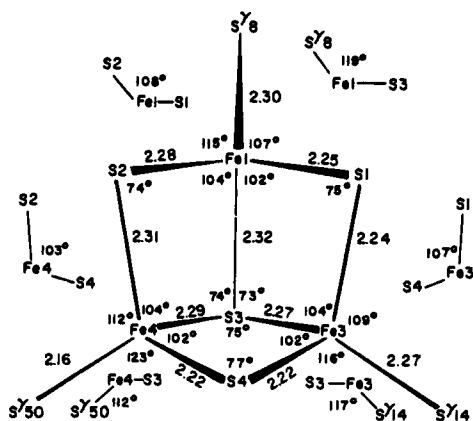
^a Referenced to Fe metal at room temperature.^b Measured at 4.2 or 80 K.^c Not reported.^d Predicted value.^e Average values.

The terminal reduced member of series (c) has not yet been detected in the unmodified $[\text{Fe}_3\text{S}_4]^{1-}$ form. However, this oxidation level has been stabilized as $[\text{ZnFe}_3\text{S}_4]^{1+}$ (101), from which the $S = \frac{5}{2}$ ground state has been determined. This cluster will be considered later in connection with heterometallic MFe_3S_4 clusters. An electrochemical study of *D. africanus* Fd III has shown that a reduction step at near -720 mV is coupled to the $[\text{Fe}_3\text{S}_4]^{1+/0}$ reaction at -140 mV (95). The pH dependence of the potential together with the approximately twofold greater current passed than in the -140 -mV process implies the proton-coupled reaction $[\text{Fe}_3\text{S}_4]^0 + 2e^- + 2\text{H}^+ \rightarrow [\text{Fe}_3\text{S}_4\text{H}_2]^0$. The product, which without protonation would be a dianionic 3Fe(II) cluster, could conceivably be sufficiently basic to be stabilized by sulfide protonation in the 6.2–7.8 pH range studied. The reason why the potentials of two successive one-electron reductions are not resolved is unclear, and it has been suggested that a chemical step of structural rearrangement may intervene (95).

2. Structures

Similarities in the MCD and Mössbauer spectra of $[\text{Fe}_3\text{S}_4]^{1+/0}$ clusters in various proteins make it virtually certain that all such clusters have the cuboidal structure 4. This structure has been crystallographically established for the $[\text{Fe}_3\text{S}_4]^{1+}$ clusters in inactive aconitase (10), *A. vinelandii* Fd I (6, 7), the C20A mutant of this protein (11), and *D. gigas* Fd II (35, 36). The most detailed metric data have been reported for *D. gigas* Fd II, whose cluster structure at 1.7 Å resolution is presented in Fig. 4. Two principal points emerge from the structural results, although exact comparisons among structures are not possible owing to different states of refinement.

First, clusters are dimensionally similar and bond distances and angles are unexceptional in relation to those of protein-bound and synthetic Fe_4S_4 clusters. For example, when the clusters of aconitase (2.1 Å refinement) and *A. vinelandii* Fd I (1.9 Å refinement) are compared, the positions of the seven iron and sulfur atoms agree on average to 0.09 Å (10). Second, Fe_3S_4 portions of trinuclear and tetranuclear clusters are structurally nearly the same. To demonstrate this point, Kissinger *et al.* (35) have provided a comparative tabulation of cluster bond distances and angles of *D. gigas* Fd II, *P. aerogenes* Fd_{ox}, and *Chromatium vinosum* HP_{red}. Consider the case of inactive and active aconitase, which are isomorphous and whose cluster structures are shown in Fig. 4. The seven iron and sulfur atoms common to the two clusters differ in position on average by only 0.11 Å, and the three common Cys sulfur atoms vary by 0.25 Å (10). It seems highly probable

D. gigas Fd II

Aconitase (pig heart)

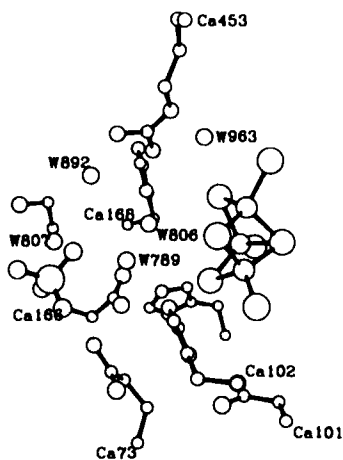
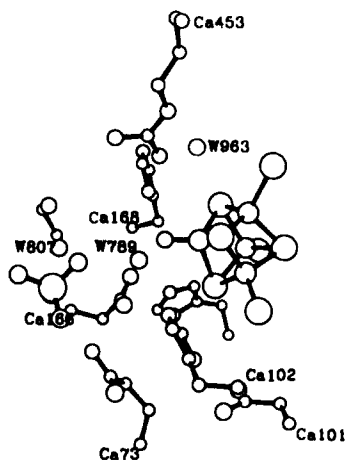
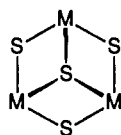
inactive: $[\text{Fe}_3\text{S}_4]^{1+}$ active: $[\text{Fe}_4\text{S}_4]^{2+}$

FIG. 4. Structures of the $[\text{Fe}_3\text{S}_4]^{1+}$ cluster in *D. gigas* Fd II (35) and the $[\text{Fe}_3\text{S}_4]^{1+}$ and $[\text{Fe}_4\text{S}_4]^{2+}$ clusters in inactive and active aconitase (10), respectively.

that such a condition would hold also for the $[\text{Fe}_3\text{S}_4]^0$ oxidation state, which in *D. gigas* Fd II is fully delocalized at ambient temperature (99). It remains to be learned whether the lack of structural relaxation, say to a more open or flattened structure along the (idealized) threefold axis of 4, upon removal of an iron atom is an intrinsic cluster property or is enforced by protein structure. In any event, the Fe_3S_4 cluster is effectively configured to bind a metal atom with very little structural rearrangement required of the product cluster core.

B. CLUSTERS OF RELATED STRUCTURE

Cluster 4 is one member of a larger series of molecules containing the generalized cuboidal core 31. While such a structure might appear



31

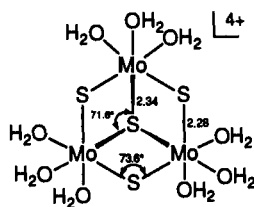
relatively ordinary, there was, in fact, only a single proved molecular example in metal–chalcogenide chemistry prior to 1980 (102). In 1971, Dahl and co-workers (103) prepared and determined the structure of $[\text{Cp}_3\text{Mo}_3\text{S}_4]^{1+}$ [Cp is cyclopentadienide(1–)]. They noted about this molecule, somewhat prophetically in a biological context (despite the difference in metals), that it “can be visualized as arising from a cubane-like $[\text{Cp}_4\text{Mo}_4\text{S}_4]$ architecture by formal removal of one $[\text{MoCp}]$ group.” The compound $[\text{Cp}_3\text{Mo}_3\text{S}_4]$ was prepared in 1973 (104), but its structure was not determined. No further activity on cuboidal M_3S_4 compounds was evident until the report in 1980 of $[\text{Mo}_3\text{S}_4(\text{CN})_9]^{5-}$ (105). In that same year, Müller *et al.* (106) reviewed the state of trinuclear clusters and noted the existence of “incomplete cube” structures in oxo- and halide-bridged compounds of niobium, molybdenum, and tungsten. An explosive growth of the chemistry of synthetic cuboidal clusters occurred in the 1980s, somewhat coincidentally with the recognition of the related cluster 4 in proteins. The accomplishments of Cotton, Shibahara, Sykes, and their co-workers, in particular, have done much to open and define this area of cluster chemistry.

There are now over 30 synthetic cuboidal clusters 31 whose structures have been demonstrated by X-ray analysis. These are of the types $\text{M}_3\text{S}_4\text{L}_n$, with $n = 6, 8, \text{ or } 9$, examples of which are collected in Table IV. There is a notably large group $[\text{Mo}_3\text{S}_4(\text{dtp})_4\text{L}]$, in which L is a loosely

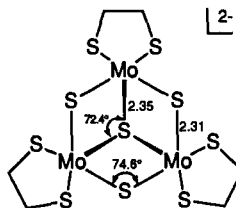
held neutral ligand (129) [dtp is *O,O*-diethyldithiophosphate(1-)]. All molybdenum and tungsten compounds contain the metal in the IV oxidation state. Differences in coordination numbers and ligand types notwithstanding, the core structures of the molybdenum and tungsten clusters are very similar, as illustrated for cationic six-coordinate $[\text{Mo}_3\text{S}_4(\text{OH}_2)_{12}]^{4+}$ (32) (110) and anionic five-coordinate $[\text{Mo}_3\text{S}_4(\text{edt})_3]^{2-}$ (33) (120), whose dimensions are typical [edt is ethane-1,2-dithio-

TABLE IV
SYNTHETIC CLUSTERS WITH THE CUBOIDAL M_3S_4
CORE (31)

Cluster	Ref.
$[\text{V}_3\text{S}_4(\text{edt})_3]^{3-}$	112
$[\text{Mo}_3\text{S}_4(\text{OH}_2)_9]^{4+}$	107–111, 250
$[\text{Mo}_3\text{S}_4(\text{CN})_9]^{5-}$	105, 113
$[\text{Mo}_3\text{S}_4(\text{C}_2\text{O}_4)_3(\text{OH}_2)_3]^{2-}$	107
$[\text{Mo}_3\text{S}_4(\text{tacn})_3]^{4+}$	114
$[\text{Cp}_3\text{Mo}_3\text{S}_4]^{1+}$	103
$[\text{Mo}_3\text{S}_4(\text{ida})_3]^{12}$	115
$[\text{Mo}_3\text{S}_4(\text{Hnta})_3]^{2-}$	250
$[\text{Mo}_3\text{S}_4(\text{nta})(\text{Hnta})_2]^{3-}$	116
$[\text{Mo}_3\text{S}_4(\text{S}_2\text{PET}_2)_4]$	117–119
$[\text{Mo}_3\text{S}_4(\text{edt})_3]^{2-}$	120
$[\text{Mo}_3\text{S}_4\text{Cl}_3(\text{dmpe})_3]^{1+}$	121–123
$[\text{Mo}_3\text{S}_4\text{Cl}_4(\text{PET}_3)_3(\text{MeOH})_2]$	124
$[\text{Mo}_3\text{S}_4\text{Cl}_4(\text{PET}_3)_4(\text{MeOH})]$	124
$[\text{Mo}_3\text{S}_4\text{Cl}_4(\text{PPh}_3)_3(\text{OH}_2)_2]$	122, 128
$[\text{Mo}_3\text{S}_4\text{Cl}_4(\text{PET}_3)_3(\text{OH}_2)_2]$	252
$[\text{Mo}_3\text{S}_4\text{Br}_4(\text{PET}_3)_3(\text{OPet}_2\text{H})(\text{OH}_2)]$	252
$[\text{Mo}_3\text{S}_4(\text{dtp})_4(\text{OH}_2)]$	125, 129
$[\text{Mo}_3\text{S}_4(\text{dtp})_4(\text{PhCH}_2\text{CN})]$	126
$[\text{Mo}_3\text{S}_4(\text{dtp})_3(\text{OAc})(\text{MeCN})]$	127
$[\text{Mo}_2\text{WS}_4(\text{OH}_2)_9]^{4+}$	134
$[\text{MoW}_2\text{S}_4(\text{OH}_2)_9]^{4+}$	134
$[\text{W}_3\text{S}_4(\text{OH}_2)_9]^{4+}$	130, 131, 250, 251
$[\text{W}_3\text{S}_4(\text{S}_4)_3(\text{OH}_2)_3]^{2-}$	135
$[\text{W}_3\text{S}_4(\text{S}_4)_3(\text{NH}_3)_3]^{2-}$	251
$[\text{W}_3\text{S}_4(\text{NCS})_9]^{5-}$	132, 250, 251
$[\text{W}_3\text{S}_4(\text{Hnta})_3]^{2-}$	250
$[\text{W}_3\text{S}_4\text{Cl}_3(\text{dmpe})_3]^{1+}$	123, 133
$[\text{W}_3\text{S}_4\text{Cl}_3(\text{depe})_3]^{1+}$	123
$[\text{W}_3\text{S}_4\text{H}_3(\text{dmpe})_3]^{1+}$	123
$[\text{W}_3\text{S}_4\text{Br}_4(\text{PET}_3)_3(\text{OPet}_2\text{H})(\text{OH}_2)]$	252
$[\text{W}_3\text{S}_4(\text{dtp})_3(\text{OAc})(\text{py})]$	136, 137, 253



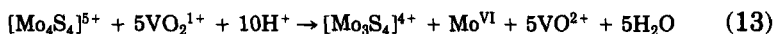
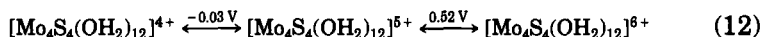
32 (Mo-Mo, 2.74)



33 (Mo-Mo, 2.78)

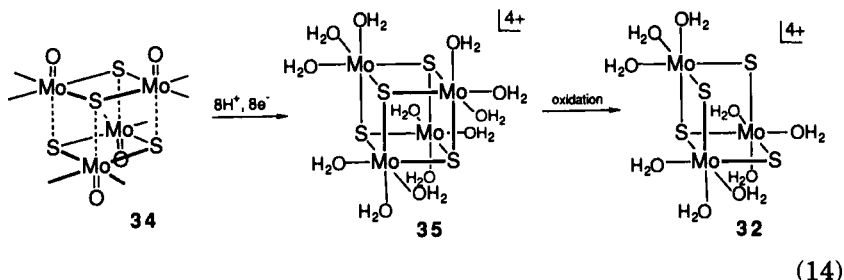
late(2-)]. The clusters are electron precise inasmuch as they contain the six electrons necessary for M—M single bonds. In addition, there are subsets of cuboidal clusters $M_3O_{4-n}S_n$ displaying permutations of oxygen and sulfur atoms in the μ_2 and μ_3 positions. The complete set of eight molybdenum clusters ($n = 0-4$) has been obtained, primarily by the chemical ($NaBH_4$) or electrochemical reduction of $[Mo_2O_{4-n}S_n(S \cdot Cys)_2]^{2-}$ in aqueous solution followed by aerial oxidation (108, 109, 138–144).

Reduction of $Mo_2^VO_{4-n}S_n$ complexes affords both trinuclear and tetranuclear clusters, and has been the most frequently utilized method for the preparation of Mo_4S_4 clusters (108, 109, 111, 115, 145–148). It was recognized in the early work on these species that exposure to air resulted in the formation of some trinuclear clusters (107, 108, 114, 145). Under the usual workup conditions, the acidic aqueous reaction mixture after reduction is handled in the air and the cluster products are separated by ion-exchange chromatography. With controlled exposure to oxidizing conditions, the green +5 cubane-type aqua ion can be obtained, which is part of the three-membered electron transfer series of Eq. (12) (144). An analogous series [Eq. (13)] of ethylenediaminetetraacetate(4-) (EDTA) complexes has been prepared (149, 150). Both series



can be traversed chemically and electrochemically. When stored under dinitrogen, acid solutions of the +5 aqua ion are stable indefinitely. For this ion in air, $t_{1/2} \approx 4$ days at 50°C (1 M HCl); heating at 95°C for 2–3 hr gives $[Mo_3S_4(OH_2)_9]^{4+}$ in essentially quantitative yield (148). Further, the reaction given by Eq. (13) with excess oxidant has been demonstrated; with a restricted amount of V(V) oxidant, the +6 cubane cluster is obtained (148).

These observations, summarized in the scheme shown in Eq. (14), show that when sufficiently oxidized, the aqua cubane cluster will



release a molybdenum atom. The initial cluster is likely formed by the interaction of two $\text{Mo}_2\text{O}_2\text{S}_2$ fragments (34). Essentially concomitant reduction and protonation would transform oxo to aqua ligands, thereby removing an oxo trans effect unfavorable to dimerization. Under reducing conditions the $+4$ aqua cubane 35 is first generated, but is subsequently oxidized to a level, presumably past the $+6$ aqua ion, where the affinity for one molybdenum atom has decreased to the point of spontaneous release of that atom. The reaction shown in Eq. (15), with NaBH_4 as the reductant, occurs to a limited extent (111). It suggests



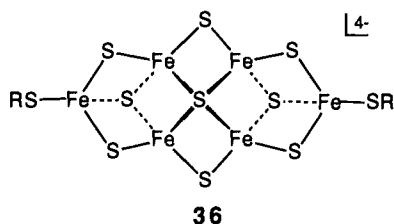
that the cuboidal cluster requires reduction by two electrons to bind a (tripositive) cation. In the preparation of $[\text{Mo}_4\text{S}_4(\text{EDTA})_2]^{3-}$, a solution was maintained at 90°C for 24 hr in the air just prior to chromatographic separation of the ion (150). The chelating ligand does not stabilize the cluster against oxidation because the potentials are ~ 0.2 V more negative than those in Eq. (12). Apparently, the ligand impedes spontaneous loss of a molybdenum atom, which would require the rupture of three terminal $\text{Mo}-\text{O}/\text{N}$ bonds. An unforeseen parallel behavior of Fe_4S_4 and Mo_4S_4 clusters is evident. When sufficiently oxidized, the M_3S_4 fragment of each loses binding affinity for the remaining M atom of the cluster, which then dissociates. Protein cysteinate and edta ligands may perhaps be likened in the sense that their strong coordination slows or altogether prevents M atom loss. As will be seen, cuboidal Mo_3S_4 binds metal ions. The formation of heterometal cubanes MMo_3S_4 often requires the use of reducing conditions, and the nature of the product is such as to suggest a two-electron reduction of the cuboidal cluster in most cases.

Certain preparative routes to M_3S_4 clusters either do not, or are not known to require, the intermediacy of a cubane cluster. No such cluster intervenes in the desulfurization of coordinated persulfide in the trinuclear core $[\text{M}_3(\eta^4\text{-}\mu_2\text{-S}_2)_3(\mu_3\text{-S})]^{4+}$ ($\text{M} = \text{Mo}, \text{W}$) by thiophilic reagents

such as cyanide (105, 113) and tertiary phosphines (118, 122, 135). The reaction of MoCl_3 or WCl_4 with NaSH in the presence of chelating diphosphines (121, 123) and the reduction of $[\text{WS}_4]^{2-}$ with NaBH_4 (130–132) are other cases in which tetranuclear species are evidently not necessary to product formation. Reduction of a mixture of $[\text{WS}_4]^{2-}$ and $[\text{Mo}_2\text{O}_2\text{S}_2(\text{S} \cdot \text{Cys})_2]^{2-}$ affords mixed-metal aqua ions, which were separated by cation exchange (134). Their identification completes the series of cuboidal nonaqua ions.



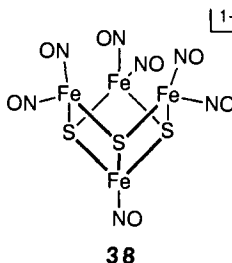
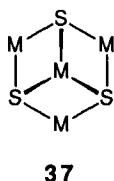
Before leaving the subject of trinuclear cuboidal clusters, we observe that cuboidal units occur in clusters of higher nuclearity. In the context of iron–sulfur chemistry, several examples may be cited. The clusters $[\text{Fe}_6\text{S}_9(\text{SR})_2]^{4-}$ (36) contain two $[\text{Fe}_3(\mu_2\text{-S})_2(\mu_3\text{-S})(\mu_4\text{-S})]$ units (41, 151,



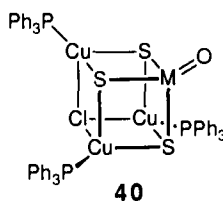
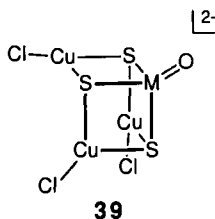
152); these also occur in the cyclic cluster $[\text{Na}_2\text{Fe}_{18}\text{S}_{30}]^{8-}$ (153). In the discrete double cluster $[\text{Na}_2(\text{Fe}_6\text{S}_9(\text{SMe})_2)_2]^{6-}$, crystallized as its Et_4N^+ salt (152), the two Fe_6S_9 clusters are bridged by two sodium ions, each of which forms six Na-S interactions to two Fe_3S_4 units. In an approximate sense, the sodium ions occupy the voids in these incomplete cubes, but the long bond lengths (2.88–3.11 Å) suggest that the interactions are mainly ionic in character. No transition element ion has been placed in these voids, where it may be expected that interactions with the $\mu_4\text{-S}$ atoms in the intact cluster will be weak.

C. INVERTED (M_4S_3) CLUSTERS

Although tetranuclear rather than trinuclear, these clusters are considered briefly here in the context of cuboidal structures. In relation to 31, cuboidal core $\text{M}_4(\mu_3\text{-S})_3$ (37) has an inverted population of metal and sulfur subsites; it is represented by very few compounds. Cluster 38 is the classical black Roussin monoanion. It may be conceived as a derivative of the cubane $\text{Fe}_4\text{S}_4(\text{NO})_4$ by removal of one sulfur atom and the addition of three nitrosyl ligands and one electron. The structures of two salts (154, 155) establish that the Fe_4S_3 core is a virtually congruent



fragment of the cubane core. The cluster has been obtained by reduction (Na/Hg) of $\text{Fe}_4\text{S}_4(\text{NO})_4$ in THF (154). The course of this reaction is unknown. One might speculate that the process is the inverse of Fe_3S_4 cluster formation; viz., a sufficiently reduced cluster releases sulfide (to a suitable acceptor). The clusters $[\text{MCu}_3\text{OS}_3\text{Cl}_3]^{2-}$ (39, M = Mo, W) also have a voided core ligand position (156–158). Occupation of this subsite, as by chloride in $[\text{MCu}_3\text{OS}_3\text{Cl}(\text{PPh}_3)_3]$ (40, M = Mo, W) (159),

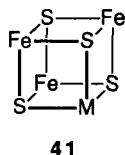


completes a distorted cubane framework. The Fe_4S_3 cluster core, with the fourth ligand subsite occupied by an element other than sulfur or selenium (55), has not been encountered.

IV. Heterometallic MFe_3S_4 Cubane-Type Clusters

A. CLUSTERS OF SYNTHETIC ORIGIN

The first clusters containing the cubane-type MFe_3S_4 core unit 41 were prepared in 1978. Double cubanes composed of two MoFe_3S_4 groups bridged through the molybdenum atoms by a sulfide atom and two thiolates, and by three thiolates, were obtained by my group (160) and by Christou *et al.* (161, 162), respectively. An extensive research



effort followed, which in this laboratory has resulted in the synthesis of bridged double cubanes and single cubanes with $M = \text{Mo}, \text{W}, \text{V}$, and Re , and, most recently, Co, Ni , and Nb . In the early development of the chemistry of these clusters, all examples contained either molybdenum or tungsten as the heterometal. The motivation for much of this work remains unchanged: clarification of the structure and other properties of the Fe-Mo cofactor of nitrogenase by the synthesis and characterization of suitable model clusters or, in the limit of unqualified success, the cofactor itself. With the recent demonstrations of vanadium-containing nitrogenases, pursuit of the Fe-V cofactor has become an equivalent challenge. Much of the extensive research through 1985 has been reviewed (163–165), at which time only the $M = \text{Mo}$ and W clusters had been prepared. In the sections that follow, attention is restricted to recent developments, especially as related to synthesis, reactivity, and biological relevance. The considerable scope of the chemistry of synthetic MFe_3S_4 clusters is evident from Table V, which reveals that seven heterometals have thus far been incorporated in the cubane-type core units, each of which may exist in several oxidation levels.

1. Tetrathiometalates

The intensely colored tetrahedral d^0 species $[\text{MS}_4]^{2-}$ (166) are obligatory precursors to all heterometal cubanes with $M = \text{V}, \text{Nb}, \text{Mo}, \text{W}$, and Re synthesized by cluster self-assembly. Of these, $[\text{VS}_4]^{3-}$, $[\text{MoS}_4]^{2-}$, and $[\text{WS}_4]^{2-}$ were prepared before 1900 by the reaction of hydrogen sulfide with oxoanions in strongly alkaline solutions and were isolated as alkali metal or ammonium salts. $[\text{ReS}_4]^{1-}$ has been obtained similarly (167). Known tetrathiometalates and the dates of their initial preparations are summarized in Fig. 5. The foregoing salts of $[\text{MoS}_4]^{2-}$ and $[\text{WS}_4]^{2-}$ are water soluble; quaternary ammonium salts soluble in organic solvents are also available (168). The recently prepared compound $\text{Li}_3[\text{VS}_4] \cdot 2\text{DMF}$ (DMF is *N,N*-dimethylformamide) has the advantage in reaction chemistry of solubility in water and in dry anaerobic polar solvents such as DMF and Me_2SO (169).

The newest additions to the set of soluble tetrathiometalates are $[\text{NbS}_4]^{3-}$ and $[\text{TaS}_4]^{3-}$. These ions had been earlier recognized as components of certain intractable solids prepared by high-temperature methods (170). Low-temperature preparations have been hampered by the lack of suitable oxometalate precursors. Recently, the reaction given by Eq. (16) ($M = \text{Nb}, \text{Ta}$) in acetonitrile has been devised in this laboratory (171).



TABLE V

SCOPE OF $[\text{MFe}_3\text{S}_4]$ CLUSTER FORMATION^a

Electron number ^b /spin S	Cluster
49 $e^-/S = ?$	$[\text{MoFe}_3\text{S}_4]^{5+}$ $[\text{WFe}_3\text{S}_4]^{5+}$
50 $e^-/S = ?$	$[\text{VFe}_3\text{S}_4]^{3+}$ $[\text{NbFe}_3\text{S}_4]^{3+}$ $[\text{MoFe}_3\text{S}_4]^{4+}$ $[\text{WFe}_3\text{S}_4]^{4+}$
51 $e^-/S = \frac{3}{2}$	$[\text{VFe}_3\text{S}_4]^{2+}$ $[\text{NbFe}_3\text{S}_4]^{2+}$ $[\text{MoFe}_3\text{S}_4]^{3+}$ $[\text{WFe}_3\text{S}_4]^{3+}$ $[\text{ReFe}_3\text{S}_4]^{4+}$
52 $e^-/S = 2$	$[\text{VFe}_3\text{S}_4]^{1+}$ $[\text{Fe}_4\text{S}_4]^{4+}$ $[\text{MoFe}_3\text{S}_4]^{2+}$ $[\text{WFe}_3\text{S}_4]^{2+}$ $[\text{ReFe}_3\text{S}_4]^{3+}$
53 $e^-/S = \frac{1}{2}$	$[\text{Fe}_4\text{S}_4]^{3+}$ $[\text{ReFe}_3\text{S}_4]^{2+}$
54 $e^-/S = 0$	$[\text{Fe}_4\text{S}_4]^{2+}$
55 $e^-/S = \frac{1}{2}, \frac{3}{2}$	$[\text{Fe}_4\text{S}_4]^{1+}$ $[\text{CoFe}_3\text{S}_4]^{2+}$
56 $e^-/S = ?$	$[\text{Fe}_4\text{S}_4]^0$ $[\text{CoFe}_3\text{S}_4]^{1+}$ $[\text{NiFe}_3\text{S}_4]^{2+}$ $[\text{NiFe}_3\text{S}_4]^{1+}$
57 $e^-/S = \frac{3}{2}$	$[\text{ZnFe}_3\text{S}_4]^{1+}$
58 $e^-/S = ?$	$[\text{CdFe}_3\text{S}_4]^{1+}$
59 $e^-/S = \frac{3}{2}$	$[\text{ZnFe}_3\text{S}_4]^{1+}$ $[\text{CdFe}_3\text{S}_4]^{1+}$

^a Boldface denotes an isolated cluster; p, protein-bound cluster; other clusters have been detected electrochemically.

^b S, Six-electron donor.

After workup, the compounds $\text{Li}_3[\text{MS}_4] \cdot 2\text{TMEDA}$ (TMEDA is N,N,N',N' -tetramethylethylenediamine) were isolated in ~60% yield. The compounds are isostructural and contain discrete tetrahedral $[\text{MS}_4]^{3-}$ ions. They are soluble and stable in polar solvents; the light yellow color of these solutions results from the occurrence of ligand to metal charge transfer (LMCT) bands below 400 nm rather than in the visible region as for the other tetrathiometalates. With the likely exceptions of chromium and manganese, it is possible that tetrathio-

SOLUBLE TETRATHIOMETALATES: $[\text{M}^z\text{S}_4]^{(8-z)-}$

Ti ^{IV}	V ^V 1890	Cr ²	Mn ²	
Zr ^{IV}	Nb ^V 1990	Mo ^{VI} 1884	Tc ^{VII}	Ru ²
Hf ^{IV}	Ta ^V 1990	W ^{VI} 1886	Re ^{VII} 1970	Os ²

FIG. 5. Elements of Groups IV–VIII that form tetrathiometalates and the dates of their original syntheses (white boxes); nearby elements, some of which might form $[\text{MS}_4]^{2-}$ species, are shown in shaded boxes. The case of Fe(III) is discussed in the text.

metalates of the other elements in Fig. 5 may be obtainable as soluble salts. Of these, $[\text{TcS}_4]^{2-/1-}$ appear to be the most readily achievable. Last, we take note of the compound Na_5FeS_4 , synthesized from Na_2S , Fe, and S at 970 K (172). It contains discrete tetrahedral $[\text{FeS}_4]^{5-}$ ions, each of which is immersed in an environment of sodium ions, effectively reducing anion–anion repulsion and stabilizing the small, very highly charged anions. Although a tetrathiometalate by definition, $[\text{FeS}_4]^{5-}$ lacks the short bond distances associated with multiple bonding in d^0 $[\text{MS}_4]^{2-}$ species. It is too intensely nucleophilic to have any solution stability unless this property is modulated by association with cations such as Li^+ or Mg^{2+} . Li^+ –anion interactions occur in the structures of $\text{Li}_3[\text{MS}_4] \cdot 2\text{TMEDA}$ and very probably in solutions of these compounds. Interactions of this sort would presumably be necessary to obtain stable solution species of the Group IV anions $[\text{MS}_4]^{4-}$. Any new $[\text{MS}_4]^{2-}$ species is a potential cluster precursor in the types of self-assembly systems to be considered next.

2. $[\text{MoFe}_3\text{S}_4]$ and $[\text{WFe}_3\text{S}_4]$ Clusters

Because the preparations and properties of these two cluster types are in general similar, with the main differences being more negative redox potentials and somewhat stronger terminal ligand binding of the tungsten clusters, we shall deal only with the molybdenum clusters.

In the original cluster self-assembly system in methanol shown in Fig. 6, three double-cubane clusters **42–44** were obtained (163, 165, 173–175). Cluster **42** is our original contribution to this field; because it is not easy to purify, its chemistry has been little developed. Triply thiolate-bridged cluster **43** can be readily obtained in high yield. It has been converted to the doubly reduced species **45**, which has been isolated and exists in the $[\text{MoFe}_3\text{S}_4]^{2+}$ state (176). The easily accessible

Fe(II,III)-bridged clusters **44** are principally important as forerunners of single cubanes. Reaction of the Fe(III) form with catecholates affords the doubly thiolate-bridged clusters **46** whose Mo-S-Fe links are readily cleaved in coordinating solvents to produce the solvated single

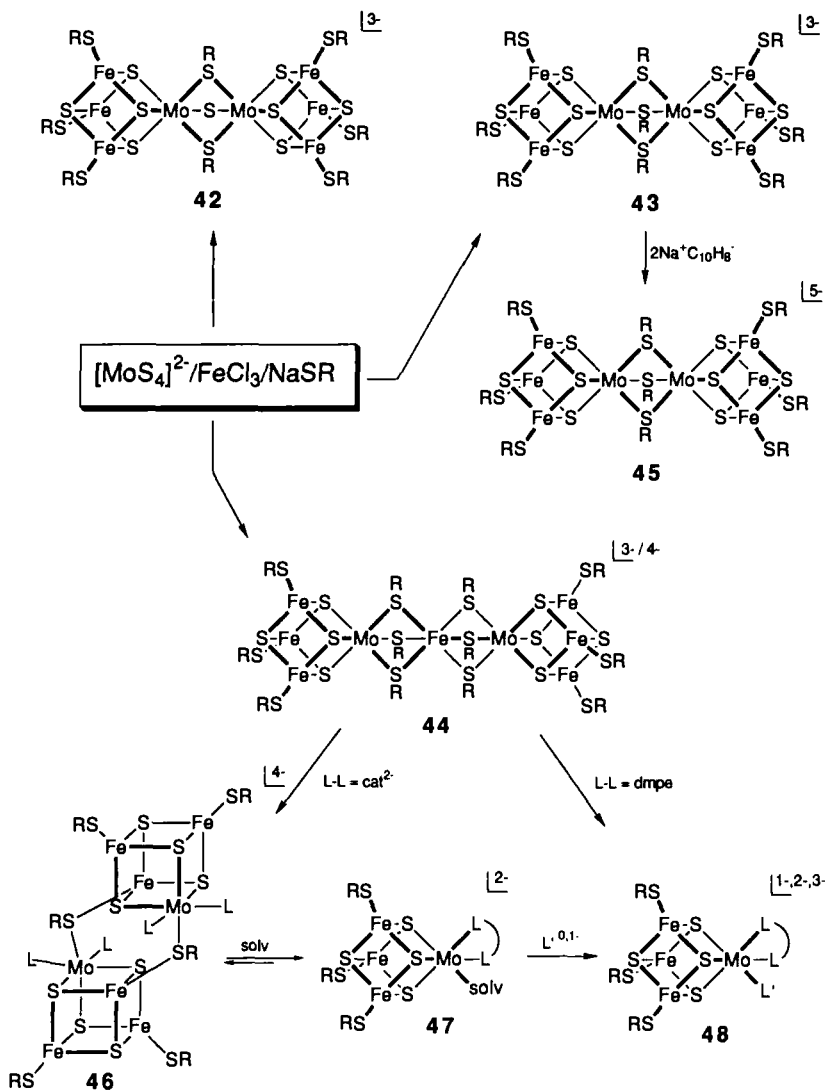
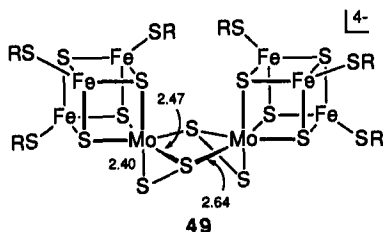


FIG. 6. The original MoFe_3S_4 cluster self-assembly system yielding triply bridged double cubanes **42** and **43** and the Fe(II,III)-bridged clusters **44** (160, 173–175). Also shown is the two-electron reduction of **43** to yield **45** and the reactions of **44** to give the doubly bridged double cubane **46** and the single cubanes **47** and **48** (165).

cubanes **47**. These react with neutral or anionic monodentate ligands to afford **48**, examples of which have been isolated (165). Single cubanes are also obtainable by cleavage of **44** with 1,2-bis(dimethylphosphino)ethane (dmpe); product clusters **48** retain one thiolate ligand ($L' = RS^-$) at the molybdenum site (177). Inclusion of Na_2S_2 in the assembly system results in the reaction given by Eq. (17), which produces the

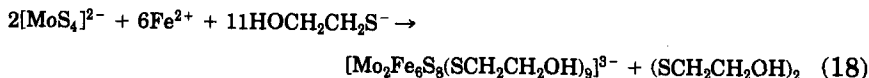


persulfide-bridged double cubane **49** ($R = p\text{-C}_6\text{H}_5\text{Cl}$) in low yield together with an appreciable quantity of $[Fe_4S_4(S\text{-}p\text{-C}_6\text{H}_4\text{Cl})_4]^{2-}$, which is separated by fractional crystallization (178).⁴ The unsymmetrical $Mo_2(\eta^4\text{-}\mu_2\text{-}S_2)_2$ bridge structure is preceded. Cluster **49** offers a num-



ber of intriguing reaction possibilities, including reductive cleavage of the persulfide bridges with low-valent metal compounds to afford modified single cubanes with external metal bridges $Mo(\mu_2\text{-}S)_2M$. These cluster assembly systems are conducted with exact stoichiometries (or with nonstoichiometric mole ratios constituting a redox buffer) that afford the $[MoFe_3S_4]^{3+}$ oxidation state. Bridged clusters and single cubanes can be reduced [usually at <1 V versus a saturated calomel electrode (SCE)] and several have been oxidized, thereby encompassing the $[MoFe_3S_4]^{4+/3+/2+}$ oxidation levels in Table V.

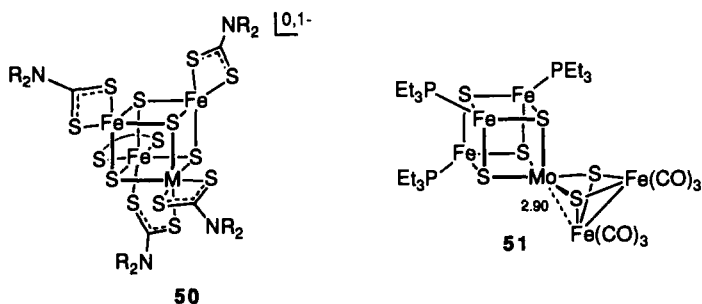
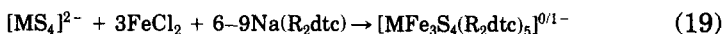
Since the foregoing developments, several other valuable results in cluster synthesis have been reported. One double cubane (**43**) has been assembled in aqueous solution by means of the reaction given by Eq. (18); the *in situ* yield exceeds 80% (179). The same cluster can also be



⁴ In more recent work in this laboratory, the yield of $(Et_4N)_4$ [**49**] in Eq. (17) has been increased from 11 to 35%.

formed from $[\text{MoO}_4]^{2-}$ and FeCl_2 in the presence of a dithiol, $\text{S}_2\text{O}_3^{2-}$, and the enzyme rhodanese. The latter three components separately generate hydrosulfide, which may react with molybdate to produce thiomolybdates prior to cluster formation; however, the immediate source of the sulfide incorporated into the cluster has not been identified.

The anaerobic reaction system given by Eq. (19) in DMF affords in one operation the single cubanes **50** ($\text{M} = \text{Mo}, \text{W}$) in moderate yields

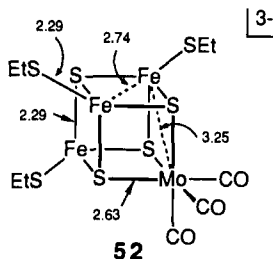


(180–183). Although the system subsumes the stoichiometry required for formation of $[\text{MFe}_3\text{S}_4(\text{R}_2\text{dtc})_5]^{1-}$ (dtc is dithiocarbamate), this is not the case for the neutral cluster, whose $[\text{MFe}_3\text{S}_4]^{5+}$ state is one electron more oxidized than the apparent stoichiometry permits. The source of the additional oxidizing equivalent is unclear. Owing to very similar six-coordinate geometries at the iron and heterometal subsites on the same core face, clusters exhibit a twofold disorder in the crystalline state. Consequently, a precise metric comparison in the two oxidation states is lacking. However, it is clear that the reduced cluster has slightly increased dimensions and, from Mössbauer spectroscopic data, the larger ^{57}Fe isomer shift indicates that the added electron is associated mainly with the iron atoms (183). The clusters **50** have several notable properties. Their single-cubane structure is assembled directly, without the necessity of prior cleavage of a double cubane. The tendency of dithiocarbamates to stabilize higher oxidation states is reflected in the occurrence of the $[\text{MFe}_3\text{S}_4]^{4+/5+}$ states in isolated compounds. These have not been stabilized in isolated MFe_3S_4 clusters ($\text{M} = \text{Mo}, \text{W}$) with any other terminal ligands; their ground state spins have not been reported and would be of much interest. A cluster formulated as $[\text{MoFe}_3\text{S}_4(\text{Me}_2\text{dtc})_6]$ has been claimed (183). Because its structure has not been demonstrated, its apparent core oxidation state is not included

in Table V. The ease of synthesis of these single cubanes may be offset, in reactivity studies at the heterometal subsite, by the potential difficulty of removing dithiocarbamate ligands with retention of the core structure.

Cluster **51** contains the features, unique to MoFe_3S_4 clusters, of terminal phosphine ligands at the iron subsites and bidentate coordination of $[\text{Fe}_2\text{S}_2(\text{CO})_6]^{2-}$ at the molybdenum subsite with an accompanying weak Mo–Fe interaction at 2.90 Å (184). It was prepared by the reaction of $[\text{MoFe}_5\text{S}_6(\text{CO})_6\text{I}_3]^{2-}$ with three equivalents of triethyl phosphine (PEt_3) in acetonitrile solution. The structure of the precursor may be inferred from that of **51**, but in the process of ligand substitution its $[\text{MoFe}_3\text{S}_4]^{3+}$ oxidation state was reduced by one electron. These species are members of a set of Mo–Fe–S–CO clusters prepared by Averill and co-workers as “potential precursors to models for the FeMo-cofactor of nitrogenase” (185).

Last, we note the occurrence of the reaction given by Eq. (20) (186). Here, linear trinuclear **5** is caused to rearrange to cuboidal **4**, ligating the $\text{Mo}(\text{CO})_3$ fragment to form the product **52**, whose average bond



lengths are indicated. Although disulfide formation was not proved,



isomer shifts and the terminal Fe–SR bond distance are entirely consistent with a one-electron reduction of the Fe_3S_4 fragment. Compared to $[\text{Fe}_4\text{S}_4(\text{SR})_4]^{2-}$ clusters (1), bond distances within this fragment are normal. However, the cluster displays a trigonal elongation that is evident in the very long Mo–S and Mo–Fe distances; in the $[\text{MoFe}_3\text{S}_4]^{3+}$ clusters of Fig. 6, these occur in the ranges 2.3–2.4 and 2.7–2.8 Å, respectively (165). These ranges largely apply to more oxidized and reduced clusters as well. Consequently, the molybdenum atom is not tightly integrated into the MoFe_3S_4 “core,” and **52** is appropriately considered as a complex between the cuboidal $[\text{Fe}_3\text{S}_4]^0$ fragment and the Lewis acidic $\text{Mo}(\text{CO})_3$ group. As will be seen, Eq. (20) is

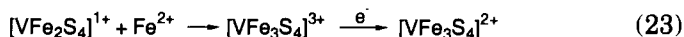
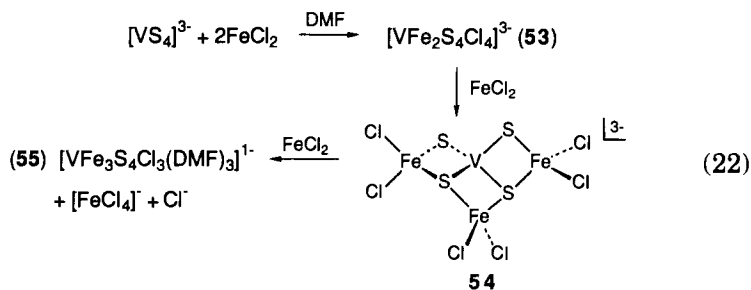
representative of a transformation of more general consequence wherein **5** is induced to rearrange to cuboidal **4**, which captures a heterometal. The first indication of this rearrangement was found with the homometallic reaction given by Eq. (21), which resulted in a 63% isolated yield of the tetranuclear product (**41**). Although rupture



of the Fe_3S_4 fragment of **5** has not been eliminated, the implication of both reactions is that fragment reduction in the presence of a suitable metal drives the rearrangement to the cuboidal form, which is immediately stabilized by metal binding.

3. $[\text{VFe}_3\text{S}_4]$ and $[\text{NbFe}_3\text{S}_4]$ Clusters

The first vanadium-containing cluster, $[\text{VFe}_3\text{S}_4\text{Cl}_3(\text{DMF})_3]^{1-}$ (**55**), was reported in 1986 (187). It and related clusters are set out in Fig. 7. The cluster formation reaction given by Eq. (22) in DMF solution proceeds in two detectable stages. In the first, the linear trinuclear cluster **53** is formed; this has been isolated (188). This species then reacts with an additional equivalent of FeCl_2 to produce an as-yet undetected intermediate with the proposed structure **54** [Eq. (22)]. The second stage likely involves intermolecular electron transfer, causing reduction below the V(V) state and electron redistribution within the core. Core conversion steps are summarized in the sequence given in Eq. (23). The six-coordinate stereochemical preference of reduced vanadium is considered to drive the rearrangement of **54** to the cubane-type structure **55**. This is an exceptional means of closing a metal cluster polyhedron. Isomer shifts and structural results for **55** imply that the hetero-



metal oxidation state does not exceed V^{3+} and that the iron oxidation state is near $\text{Fe}^{2.5+}$ (189). The latter allows the formalisms $\text{V}^{3+} +$

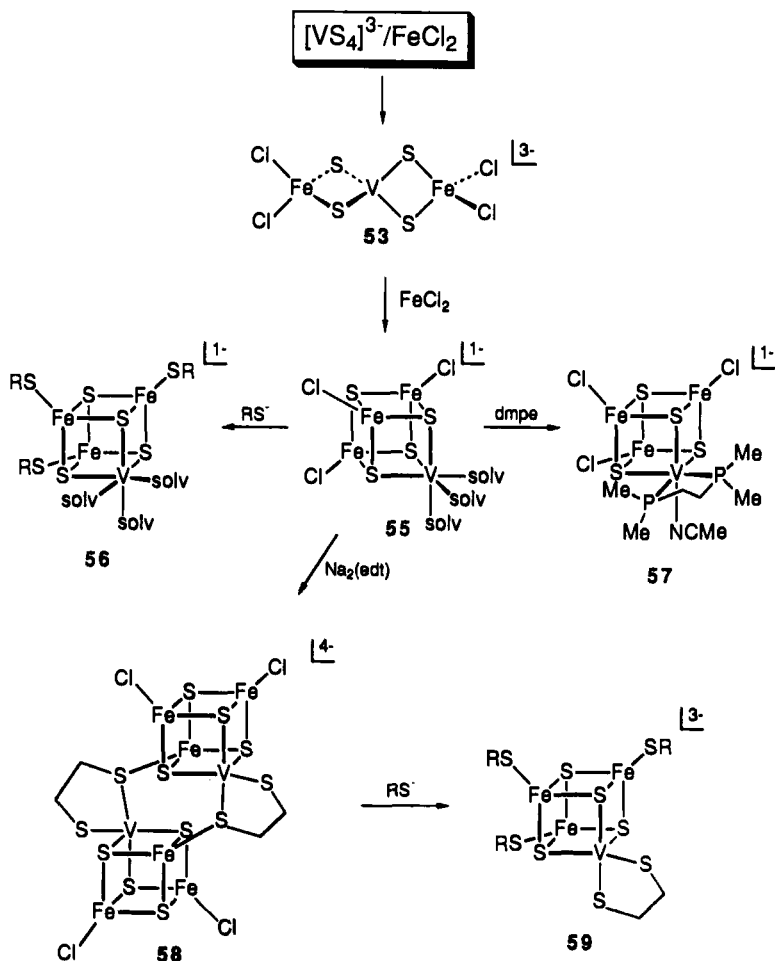
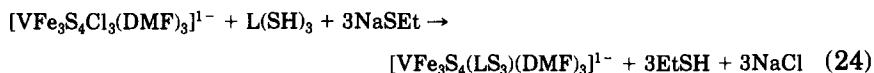


FIG. 7. The VFe_3S_4 cluster self-assembly system showing the trinuclear intermediate **53**, its conversion to cubane cluster **55**, and ligand substitution reactions of **55** at the vanadium and iron subsites (190).

$[Fe_3S_4]^{1-}$ and $V^{2+} + [Fe_3S_4]^0$. In the reactivity studies summarized next, a variety of clusters in the $[VFe_3S_4]^{2+}$ oxidation state have been prepared. There is only one example of a chemically reversible reduction to the $[VFe_3S_4]^{1+}$ state, but several clusters are reversibly oxidized to the $[VFe_3S_4]^{3+}$ state. Clusters in these two oxidation states have not been isolated. The three states are included in Table V, but the cluster spin state has been proved only for $[VFe_3S_4]^{2+}$ (189).

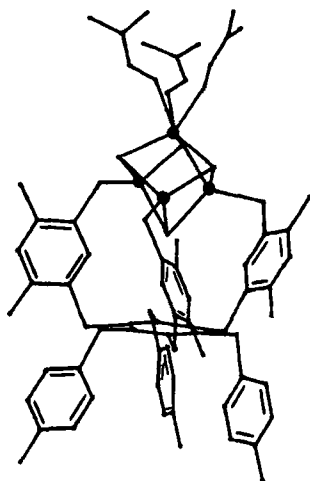
The key species in the reaction chemistry of VFe_3S_4 clusters is **55**. The original preparation of the Me_4N^+ salt (190) has been improved, and the compound is readily obtainable in ~60% yield (44). It is stable in the coordinating solvents DMF and Me_2SO , and acetonitrile, although in Me_2SO a very slow conversion to **53** has been observed (190). The order of binding affinity at the vanadium subsite is $\text{MeCN} < \text{DMF} < \text{Me}_2\text{SO}$. Owing to labile ligands at both the vanadium and iron subsites, the cluster undergoes a variety of substitution reactions and offers an opportunity to examine relative reactivities at the two subsites. Some of these reactions (190) are summarized in Fig. 7. Thiolate reacts preferentially at the iron subsites to afford **56**; an excess causes core breakdown. *p*-Cresolate also binds preferentially at the iron subsites. Phosphines, including dmpe (**57**), react at the vanadium subsite; 2,2-bipyridyl (bpy) behaves similarly. In acetonitrile solution, edt binds at both the vanadium and iron subsites to yield the double cubane **58**, whose V–S–Fe doubly bridged structure is analogous to **46** (Fig. 6). Unlike the latter, **58** is not cleaved by solvent in Me_2SO solution, but chloride substitution by *p*-tolylthiolate results in the generation of **59**. Similarly, reaction with *p*-tolylthiol in Me_2SO gave the solvated cluster with mixed chloride/thiolate terminal ligation. The structures of **53**, **55**, **57**, **58**, and $[\text{VFe}_3\text{S}_4\text{Cl}_3(\text{bpy})(\text{DMF})]^{1-}$ have been proved by X-ray diffraction (190).

Competitive reactivity at the two types of subsites can be altered by cluster insertion into the semirigid cavatand ligand **6** (Fig. 1). The reaction given by Eq. (24) affords cluster **60** in 87% isolated yield (44).



The intrinsic subsite differentiation by the heterometal is reinforced by the ligand, which directs substrate reactivity to the vanadium subsite. One cluster prepared in this way is $[\text{VFe}_3\text{S}_4(\text{LS}_3)(\text{HB}(\text{pz})_3)]^{2-}$ [$\text{HB}(\text{pz})_3$ is hydrotris(pyrazolyl)borate(1–)], which undergoes chemically reversible oxidation and reduction at $E_{1/2} = -0.37$ and -1.52 V, respectively, thereby demonstrating the existence of the three oxidation levels in Table V with a single cluster. In another application, **60** in Me_2SO solution reacts with cyanide in stepwise equilibria, forming as the final product the stable cluster $[\text{VFe}_3\text{S}_4(\text{LS}_3)(\text{CN})_3]^{4-}$. In contrast, **55** and **56** are decomposed by three equivalents of cyanide.

Despite its trisolvated condition, the vanadium subsites in **55** and **60** are not especially reactive. Of other ligands tested, cresolate and azide bind weakly and incompletely when present in excess. A variety of

**60**

anionic and neutral ligands such as halide, SCN^- , pyridine, imidazole, aliphatic amines, and NH_3 , when present in large excess, are bound slightly or not at all. In comparison, the monosolvated molybdenum site in cluster **47** binds a much wider variety of ligands, including R_3P , RS^- , RO^- , CN^- , N_3^- , hydrazines, amines, and ammonia (165). The corresponding tungsten cluster behaves similarly. None of these clusters has been shown to bind dinitrogen. However, as seen later, they are meaningful structural models of the vanadium and molybdenum sites in nitrogenases.

With the recent access to $[\text{NbS}_4]^{3-}$ and $[\text{TaS}_4]^{3-}$, the chemistry of the corresponding MFe_3S_4 clusters can now be explored. At this writing, experimentation is in an early stage. Several results are summarized in Fig. 8. Cluster **61** and $[\text{TaFe}_2\text{S}_4\text{Cl}_4]^{3-}$ have been prepared from $[\text{MS}_4]^{3-}$ and FeCl_2 in acetonitrile and were shown to be isostructural with the vanadium cluster **53** by X-ray analysis (171). In a self-assembly system, **61** and the strong reductant $[\text{Fe}(\text{SEt})_4]^{2-}$ yield the triply thiolate-bridged double cubane **62**, which is isostructural with the MoFe_3S_4 cluster **43** ($\text{R} = \text{Et}$). Cluster **62** is reducible in two chemically reversible one-electron steps, thereby demonstrating the existence of the two oxidation levels in Table V. It remains to be seen if $[\text{TaS}_4]^{3-}$ is reducible and analogously reactive in a cluster self-assembly system.

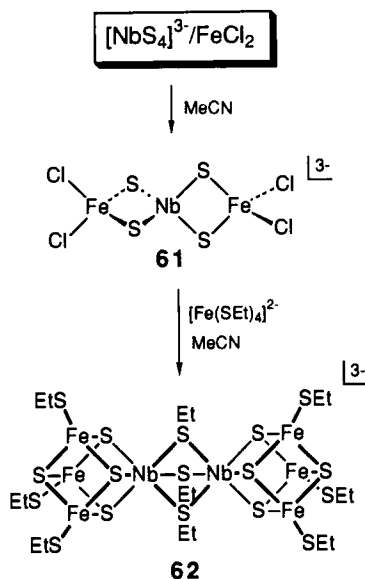


FIG. 8. The NbFe_3S_4 cluster self-assembly system showing the trinuclear cluster **61** (171) and the formation of the triply bridged double cubane **62**.

4. $[\text{ReFe}_3\text{S}_4]$ Clusters

The self-assembly system in Fig. 9 produces the triply thiolate-bridged double-cubane trianion **63** and a mixture of the Fe(II)-bridged double cubanes **65** and **66** (191, 192). The outcome of the assembly reaction is sensitive to temperature and reactant mole ratios. Manipulation of these factors has led to the preparation of the individual clusters in yields in excess of $\sim 70\%$. Cluster **63**, containing two $[\text{ReFe}_3\text{S}_4]^{3+}$ cores, undergoes a two-electron oxidation to **64**, with two $[\text{ReFe}_3\text{S}_4]^{4+}$ cores. Structural, magnetic, and spectroscopic evidence establishes the presence of Fe(II) in the bridge units of **65** and **66**, which therefore contain the +3 and +4 cores, respectively. Reaction of **66** with dmpe effects bridge cleavage and apparent core reduction by thiolate to form the single cubane **67** with the $[\text{ReFe}_3\text{S}_4]^{3+}$ oxidation state (193). This cluster undergoes reversible one-electron oxidation and reduction at -0.31 and -1.18 V, respectively. This result and the redox reactions of the double cubanes demonstrate the three oxidation states

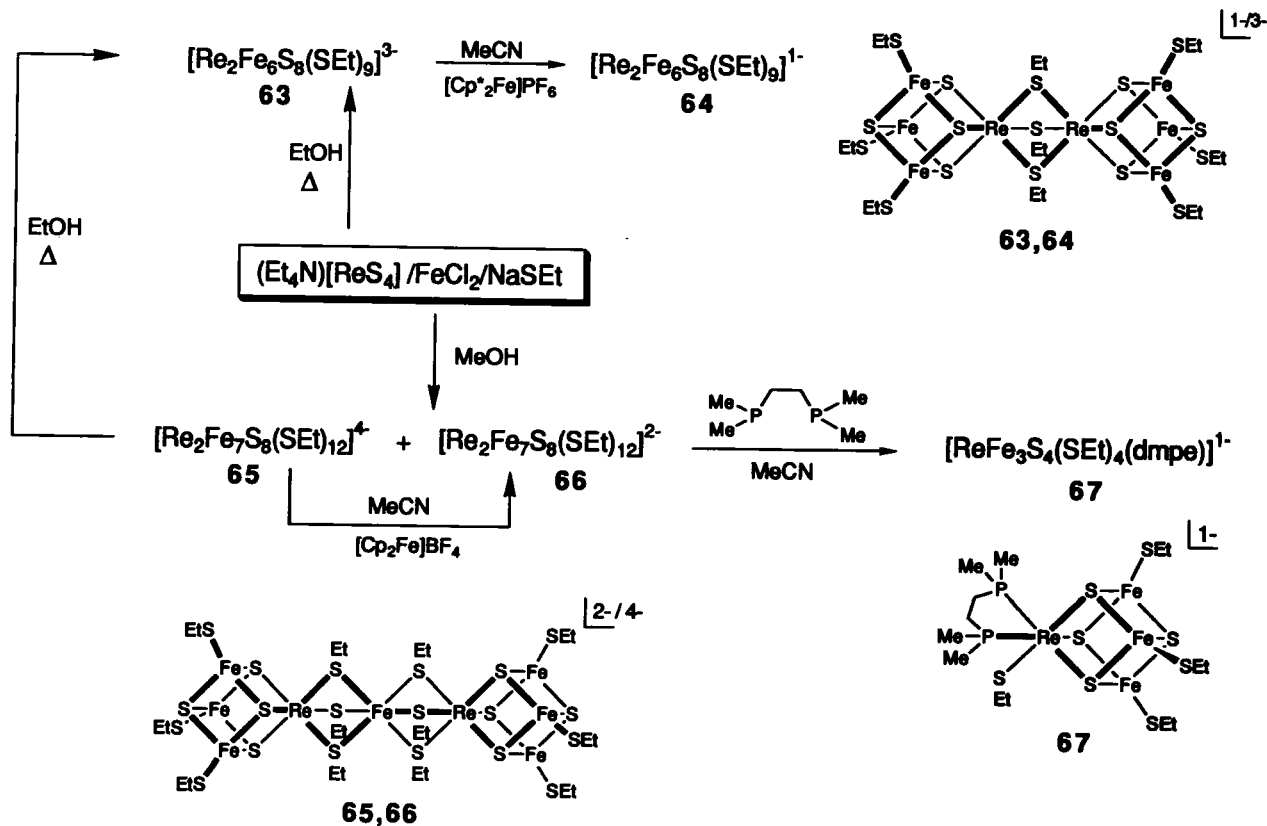
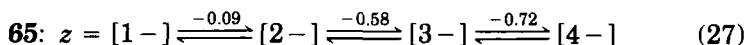
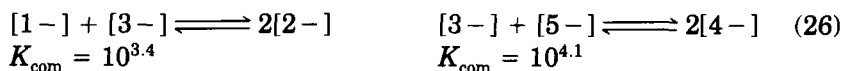
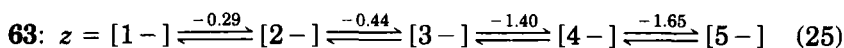


FIG. 9. The ReFe_3S_4 cluster self-assembly system showing the triply bridged double cubane **63** and the Fe(II)-bridged double cubanes **65** and **66**. Also shown is the two-electron oxidation of **63** to **64** and cleavage of **66** to give the single cubane **67** (191–193).

entered in Table V; the ground state spin has not been demonstrated for $[\text{ReFe}_3\text{S}_4]^{2+}$.

Cluster **63** exhibits the five-member electron transfer series, Eq. (25), with overall charge $z = -1$ to -5 and the indicated $E_{1/2}$ values. It encompasses the $[\text{ReFe}_3\text{S}_4]^{4+/3+/2+}$ oxidation levels with 51–53 e^- . Species of intermediate charge can be generated by comproportion reactions (26). With attainment of the 52- e^- level in $[3-]$, the individual cubanes become much more difficult to reduce and the potentials are shifted in the negative direction by 1 V or more. Clusters **65** and **66** are part of the four-member series [Eq. (27)]. These series are analogous to



those for $[\text{M}_2\text{Fe}_6\text{S}_8(\text{SET})_9]^{3-}$ and $[\text{M}_2\text{Fe}_7\text{S}_8(\text{SET})_{12}]^{3-}$ ($\text{M} = \text{Mo}, \text{W}$) (163, 165, 174). Potential differences of successive steps are essentially independent of M , and are relatively large (200–250 mV), showing that electron transfer reactions of individual cubanes are coupled. Potentials for the reduction of isoelectronic clusters with $\text{M} = \text{Mo}$ and W generally differ by ≤ 100 mV, but those for the reductions of the 51- e^- cores in $[\text{Mo}_2\text{Fe}_6\text{S}_8(\text{SET})_9]^{3-/4-}$ are ~ 1 V more negative than those for $[\text{Re}_2\text{Fe}_6\text{S}_8(\text{SET})_9]^{1-/2-}$, primarily because of the larger negative charge of the molybdenum clusters. In the series given by Eq. (27), the first step, at -0.09 V, is reduction of bridge Fe(III) to Fe(II) . However, the potential for this step is sufficiently close to that of an irreversible multielectron process near 0 V that it is doubtful if the Fe(III) -bridged cluster can be prepared. Succeeding steps result in subcluster reductions, for which the potential difference (140 mV) is smaller than in the series given by Eq. (25) because of the greater separation of subclusters. However, this difference is considerably larger than that (< 100 mV) in the $[\text{M}_2^{\text{II}}\text{Fe}_7\text{S}_8(\text{SET})_{12}]^{4-/5-/6-}$ ($\text{M} = \text{Mo}, \text{W}$) series, presumably because of the larger incremental increase in cluster negative charge upon reduction.

5. Stability Patterns

Because all other MFe_3S_4 clusters are not prepared by assembly methods based on $[\text{MS}_4]^{2-}$ and involve the later transition metals, it

is useful at this point to summarize the scope of cluster formation and stability thus far. From the results of four self-assembly systems containing $[\text{MS}_4]^{2-}$, FeCl_3 or FeCl_2 , and RS^- , the pattern of stable heterometal cubanes has emerged. Systems with $\text{M} = \text{Nb}$, Mo , W , and Re form the triply thiolate-bridged double cubanes $[\text{M}_2\text{Fe}_6\text{S}_8(\text{SR})_9]^{3-}$ (**42**, **62**, and **63**), the most widely distributed cluster structural type. Systems with $\text{M} = \text{Mo}$, W , and Re form the Fe(II) -bridged double cubanes $[\text{M}_2\text{Fe}_7\text{S}_8(\text{SR})_{12}]^{4-}$ (**44** and **65**) and the Fe(III) -bridged species $[\text{M}_2\text{Fe}_7\text{S}_8(\text{SR})_{12}]^{3-}$ (**44**). The latter has not been isolated with $\text{M} = \text{Re}$. The lack of vanadium double cubanes of these types may simply be a consequence of the absence of thiolate in the assembly system (Fig. 7). However, solvated clusters such as **56** have shown little affinity for binding monofunctional thiolates at the vanadium subsite. Double cubanes with two M-S(R)-Fe bridges have been obtained with $\text{M} = \text{V}$, Mo , and W (**46** and **58**) and may be cleaved to single cubanes (**47**, **48**, and **59**). Similarly, Fe(II,III) bridges of double cubanes may be severed with *dmpe* to afford single cubanes in which the metal retains a thiolate ligand (**48** and **67**). Single cubanes (MFe_3S_4) can be assembled directly with $\text{M} = \text{V}$ (**55**), but thus far with $\text{M} = \text{Mo}$ and W only in the presence of dithiocarbamates (**50**).

Clusters with the foregoing heterometals exhibit a stability plateau at $49\text{--}53 e^-$, especially at $51 e^-$ (Table V). Based on the broken symmetry $\text{MS-X}\alpha$ calculation of $[\text{MoFe}_3\text{S}_4(\text{SH})_6]^{3-}$ by Cook and Karplus (194), the highest occupied orbitals, at least for $[\text{MoFe}_3\text{S}_4]^{3+/2+}$ species, are mainly antibonding core Fe-S in character. It may be anticipated that the cluster types encountered with $\text{M} = \text{Mo}$, W , and Re can be prepared with $\text{M} = \text{Nb}$ and, possibly, Ta . The present results certainly imply stability of TcFe_3S_4 clusters. In view of the unlikely existence of tetra-thiometalates of chromium and manganese, their heterometal clusters will have to be obtained by different routes. For the same reason, this is the case for the synthetic nickel and cobalt clusters, which are considered next. Research on these cluster types is at an early stage.

6. $[\text{NiFe}_3\text{S}_4]$ Clusters

The reaction given by Eq. (28) in Fig. 10 affords in the same system the two clusters **68** and **69** in $\sim 40\%$ yield each as Et_4N^+ salts (195). The corresponding clusters $[\text{NiFe}_3\text{Se}_4(\text{SEt})_3(\text{PPh}_3)]^{2-}$ and $[\text{NiFe}_3\text{Se}_4(\text{SEt})_4]^{3-}$ have been prepared in an analogous manner. The reactions involve reductive rearrangement of the linear cluster precursors by interaction with Ni(0) , which may be considered to form a persistent inner sphere complex concomitant with the formal electron transfer $[\text{Fe}_3\text{S}_4]^{1+} + \text{Ni(0)} \rightarrow [\text{Fe}_3\text{S}_4]^{1-}$ and Ni^{2+} . Thus these processes bear a relation to Eq. (20), but there the apparent reducing equivalent derives

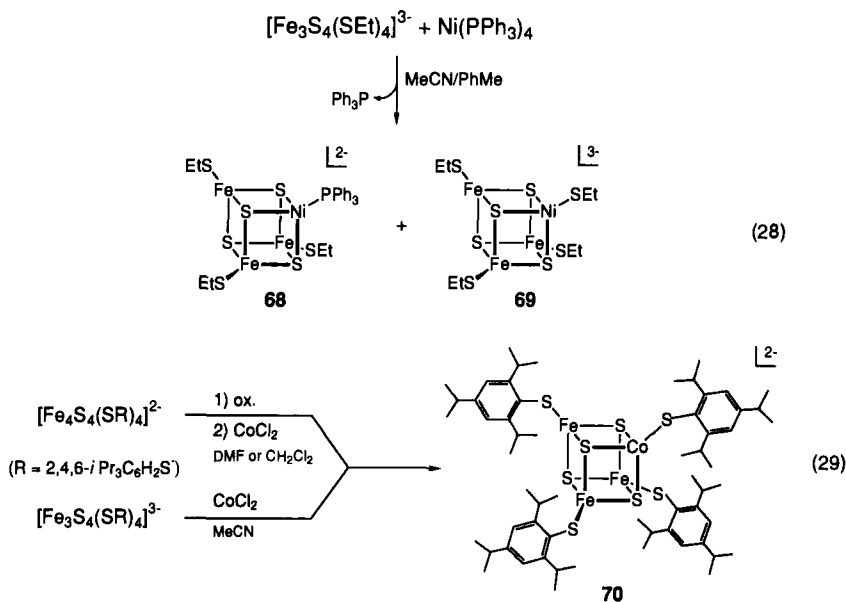


FIG. 10. Reactions [Eqs. (28) and (29)] resulting in the formation of the $[\text{NiFe}_3\text{S}_4]$ clusters **68** and **69** (195) and the $[\text{CoFe}_3\text{S}_4]$ cluster **70** (197).

from a coordinated ligand and not a low-valent metal. In the reaction workup, **69** is obtained as an inseparable mixture with $[\text{Fe}_4\text{S}_4(\text{SEt})_4]^{3-}$. The cubane-type structure of **68** has been demonstrated by X-ray diffraction, as has that of **69** in a disordered single crystal also containing $[\text{Fe}_4\text{S}_4(\text{SEt})_4]^{3-}$. Pure cluster **69** may be prepared by treatment of **68** with excess thiolate, and is likely formed in the reaction mixture by the same process.

The core unit in **68** and **69** is $[\text{NiFe}_3\text{S}_4]^{1+}$, whose $S = \frac{3}{2}$ ground state has been demonstrated from its low-temperature Curie paramagnetism and EPR spectrum. Magnetically perturbed Mössbauer spectra can be satisfactorily fit with this spin (195). Access to **69** permits the first comparison of redox potentials of (nonisoelectronic) Fe_4S_4 and MFe_3S_4 clusters with identical overall charges and terminal ligands. The effect of nickel as a heterometal is considerable, and provides a relative stability to the reduced form; thus, for the $[\text{NiFe}_3\text{S}_4]^{2+/1+}$ couple of **69**, $E_{1/2} = -0.95$ V, whereas $E_{1/2} = -1.26$ V for the $[\text{Fe}_4\text{S}_4]^{2+/1+}$ couple of $[\text{Fe}_4\text{S}_4(\text{SEt})_4]^{2-/3-}$. These oxidation states are included in Table V. The phosphine ligand in **68** is replaceable in substitution reactions that usually afford some $[\text{Fe}_4\text{S}_4(\text{SEt})_4]^{2-/3-}$ by-product, which is readily detected when reactions are monitored by ^1H NMR. Clusters containing CN^- , RNC , and RS^- ligands at the unique site have been detected

in this way. The reaction chemistry of **68** and **69** is currently under investigation in this laboratory.

7. [CoFe₃S₄] Clusters

The first indication that cobalt could be integrated into a cubane cluster of the Fe₄S₄ type was obtained when a small amount of CoCl₂ was added to the cluster assembly reaction mixture that forms [Fe₄S₄(SPh)₄]²⁻ (196). This resulted in a cobalt-doped preparation of (Bu₄N)₂[Fe₄S₄(SPh)₄], whose EPR spectrum is indicative of the [CoFe₃S₄]²⁺ core with $S = \frac{1}{2}$. More recently, this cluster type has been directly prepared by Jordanov and co-workers (197) using the two reactions of Eq. (29) in Fig. 10. One method is based on controlled aerobic oxidation of [Fe₄S₄(tibt)₄]²⁻ [tibt is 2,4,6-tris(isopropyl)benzenethiolate(1-)]. Presumably the first event is oxidation to the known species [Fe₄S₄(tibt)₄]¹⁻, which is the only [Fe₄S₄]³⁺ cluster as yet isolated and is of known structure (198). This is followed by appearance of Fe³⁺ (detected by EPR and possibly arising from Fe²⁺ that dissociated from the cluster) and another species with $g = 2.022$, a value similar to those of protein-bound [Fe₃S₄]¹⁺ clusters (68). Treatment of this solution with anhydrous CoCl₂ followed by the admission of air affords a species with an EPR spectrum, including eight hyperfine lines from ⁵⁹Co ($I = \frac{7}{2}$), described as strikingly similar to the cobalt-doped cluster above. Although the sequence of redox events is not clear, the formation of [CoFe₃S₄]²⁺ in the form of cluster **70** is apparent.

A second preparative route utilizes the linear cluster [Fe₃S₄(tibt)₄]³⁻ and Co(II) under anaerobic conditions and results in same product, isolated as black (Et₄N)₂[CoFe₃S₄(tibt)₄] (197). This reaction, described as quantitative, is easily rationalized if one thiolate ligand functions as a reductant. In this case, the transformation is closely analogous to the reactions given by Eqs. (20) and (21). As yet, the cubane structure of **70** has not been verified by X-ray diffraction. Magnetization measurements indicate an $S = \frac{1}{2}$ ground state for [CoFe₃S₄]²⁺. Potentials for the [CoFe₃S₄(tibt)₄]^{2-/3-} and [Fe₄S₄(tibt)₄]^{2-/3-} couples are -1.09 and -1.21 V, respectively, again indicating that the heterometal provides a relative stabilization of the reduced form, here [CoFeS₄]¹⁺. Cluster oxidation states are listed in Table V.

B. PROTEIN BOUND CLUSTERS

With the [Fe₃S₄] → [Fe₄S₄] cluster conversion reaction (Table II) having been demonstrated, Moura *et al.* (199) recognized the possibility

of introducing a heterometal atom into protein-bound cluster 4. This was accomplished in 1986 by the formation of the CoFe_3S_4 unit in *D. gigas* Fd II. Subsequently, the clusters MFe_3S_4 with $\text{M} = \text{Zn}$ and Cd have been formed in this protein (100, 200) and in *D. africanus* Fd III (255). Typically, these clusters are formed by incubating the dithionite-reduced protein in aqueous buffer with a large excess of an M^{2+} salt in the presence of dithiothreitol. After purification, the proteins have been inspected by Mössbauer and EPR spectroscopies, by which means ground spin states and effective oxidation states of the Fe_3S_4 portions of the clusters have been determined. Formation of protein-bound clusters is described schematically in Fig. 11. As was anticipated in Eq. (11), the protein must be reduced to the $[\text{Fe}_3\text{S}_4]^0$ state before binding of M^{2+} can occur. However, the relatively soft ion Tl^+ will bind to both oxidation states $[\text{Fe}_3\text{S}_4]^{1+/0}$ (256), and is the only ion thus far shown to do so. Binding of Tl^+ to $[\text{Fe}_3\text{S}_4]^{1+}$ is described as weak; it is substantially stronger with $[\text{Fe}_3\text{S}_4]^0$ inasmuch as Fe^{2+} coordination to this oxidation state is inhibited. It may be anticipated that in proteins or synthetic

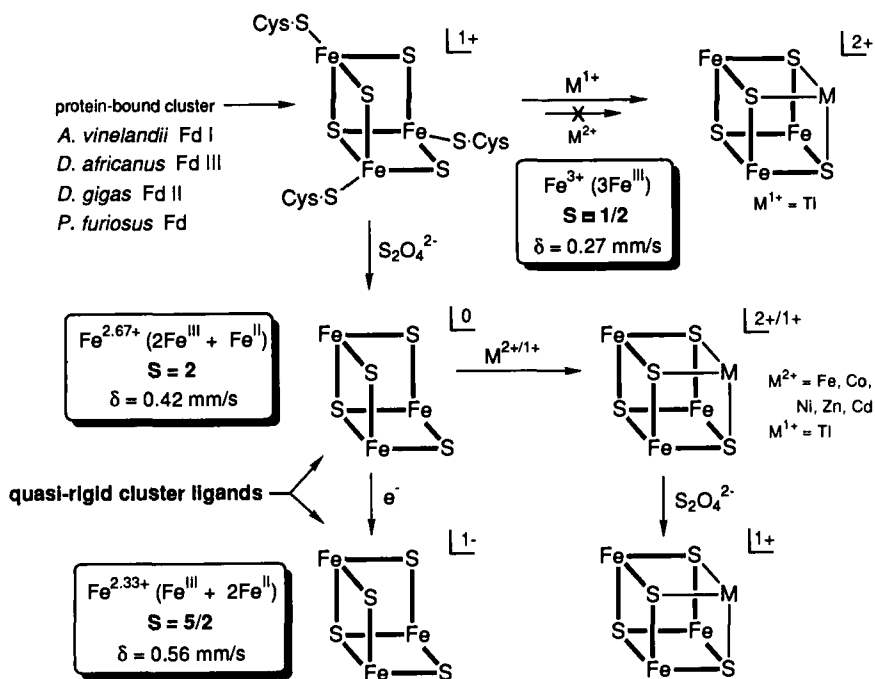


FIG. 11. Schematic depiction of protein-bound $[\text{Fe}_3\text{S}_4]$ cluster oxidation levels and the formation of heterometal $[\text{MFe}_3\text{S}_4]$ clusters by the reactions of the indicated Fd proteins with Co^{2+} , Ni^{2+} , Zn^{2+} , Cd^{2+} , and Tl^{1+} under reducing conditions (101, 199–201, 255, 256).

clusters, soft thiophilic metals such as Cu^+ , Ag^+ , and $\text{Hg}^{2+,+}$ will also bind to $[\text{Fe}_3\text{S}_4]^{1+}$.

Mössbauer parameters and oxidation and spin states for protein-bound Fe_3S_4 and MFe_3S_4 clusters are presented in Table III. It is immediately evident that the isomer shifts of $[\text{Fe}_3\text{S}_4]^{1+,0}$ clusters are practically independent of protein, and therefore are intrinsic values. The cobalt cluster was obtained in two oxidation states, while the zinc and cadmium clusters were detected in the fully reduced condition. Given these results, it is reasonable to assume that in these and other cases the $[\text{MFe}_3\text{S}_4]^{2+}$ cluster was formed first and then reduced to $[\text{MFe}_3\text{S}_4]^{1+}$ by excess dithionite (Fig. 11).

In protein-bound $[\text{CoFe}_3\text{S}_4]^{2+}$ and cluster **70**, the Fe^{3+} subsite (doublet A) and the delocalized pair (doublets B,B') of the $[\text{Fe}_3\text{S}_4]^0$ fragment (Fig. 3) are preserved. Upon reduction, the added charge mainly reduces the Fe^{3+} subsite, such that the three iron atoms become virtually indistinguishable. In the zinc cluster the subsite with $\delta = 0.62$ mm/sec and the large quadrupole splitting (doublet A) contains Fe^{2+} , and the two smaller isomer shifts are associated with the delocalized pair. The same applies to the cadmium cluster, but details have not been published (200). Cluster **21**, although not heterometallic, is included in Table III because its low-spin $\text{Fe}^{\text{II}}(\text{RNC})_3$ subsite is spin isolated from the $[\text{Fe}_3\text{S}_4]^0$ fragment and thus it behaves like Zn^{2+} . Here also the Fe^{3+} subsite and the delocalized pair are preserved. This is not the case with nickel cluster **68**, whose Mössbauer spectra can be fit by assuming delocalization over all three iron subsites. The reason for the difference in delocalization properties between $[\text{CoFe}_3\text{S}_4]^{2+}$ and $[\text{NiFe}_3\text{S}_4]^{1+}$ clusters is presently unclear.

The structure of no protein-bound MFe_3S_4 cluster has been determined by X-ray methods. However, the similarities in EPR spectra and the same ground spin state ensure that the protein-bound nickel cluster and **68** are isoelectronic, and that the nickel atom is tightly integrated into essentially isostructural cubane-type clusters. An agreeable assumption is that this structure applies to the other protein-bound clusters in Table III.

C. THE Fe_3S_4 CLUSTER AS A LIGAND AND CLUSTER SPIN

Whether functioning as such in the metal-binding reaction in Fig. 11 or being built up around a metal atom in cluster self-assembly, the Fe_3S_4 fragment of an MFe_3S_4 cluster is a conceptual ligand of heterometal M. Collected in Table VI are the main structural features of single-cubane clusters with $\text{M} = \text{V}, \text{Mo}, \text{Re}, \text{and Ni}$. The Fe-Fe and

TABLE VI

COMPARATIVE STRUCTURAL PROPERTIES OF MFe_3S_4 ($M = V, Mo, Re, Ni$) SYNTHETIC SINGLE CUBANES AND PROTEIN-BOUND $[Fe_3S_4]^{1+}$ CUBOIDAL CLUSTERS^a

Cluster	M . . . Fe	M-S	Fe . . . Fe	Fe-S	M-P	M-SR	Fe-SR	Ref.
$[VFe_3S_4Cl_3(dmpe)(MeCN)]^{1-}$ (57)	2.72(2)	2.32(6)	2.72(5)	2.28(2)	2.500(6)	—	—	190
$[MoFe_3S_4(SET)_4(dmpe)]^{1-}$ ^b (48)	2.75(3) 2.72(1)	2.37(2)	2.71(1) 2.726(8)	2.26(2) 2.27(2)	2.502(5) 2.59(3)	2.486(8) 2.566(8)	2.25(1) 2.25(2)	177
$[ReFe_3S_4(SET)_4(dmpe)]^{1-}$ ^b (67)	2.79(1) 2.758(7)	2.389(6) 2.36(2)	2.72(3) 2.72(1)	2.26(3) 2.27(1)	2.413(7) 2.492(3)	2.418(1) 2.536(1)	2.254(2) 2.24(1)	193
$[NiFe_3S_4(SET)_3(PPh_3)]^{2-}$ (68)	2.69(2)	2.262(6)	2.75(2)	2.29(2)	2.174(6)	—	2.283(6)	195
$[Fe_3S_4]^{1+}$ <i>D. gigas</i> Fd II ^c	—	—	2.75 2.72–2.77 ^d	2.27 2.22–2.32 ^d	—	—	2.24 2.16–2.30 ^d	35
$[Fe_3S_4]^{1+}$ aconitase ^e	—	—	2.69 2.64–2.73 ^d	2.30 2.25–2.35 ^d	—	—	2.32 2.28–2.34 ^d	10

^a Mean distances (Å). The standard deviation of the mean was estimated from $\sigma \cong s = [(\sum x_i^2 - nx^2)/(n-1)]^{1/2}$.

^b The two sets of distances refer to two independent anions.

^c Structure solved at 1.7 Å resolution; cf. Fig. 4.

^d Range of observed distances.

^e Structure solved at 2.5 Å resolution.

Fe-S distances depend only slightly on M and are within the ranges of the corresponding but less accurately known distances in the protein-bound cuboidal clusters **4**. The M-S, M-Fe, and terminal Fe-SR distances are somewhat more dependent on M. A tabulation showing these same features for double-cubane structures is available (192). From this brief but typical comparison, we conclude that the Fe_3S_4 fragment as a tridentate ligand can accommodate metals of different sizes with only small changes in its internal dimensions.

The isomer shift data in Table III permit assignment of, or an approximation of, effective oxidation states of the cluster fragments Fe_3S_4 and M when compared against protein values as standards. Weighted mean values are used as appropriate. A formal decomposition of clusters into fragments leads to a zero-order description of charge distribution. Series (30) sets out the isomer shift/oxidation state correlation provided

$$\begin{array}{lll} [\text{Fe}_3\text{S}_4]^{1+} & [\text{Fe}_3\text{S}_4]^0 & [\text{Fe}_3\text{S}_4]^{1-} \\ 0.27 (\text{Fe}^{3+}) & 0.42 (\text{Fe}^{2.67+}) & 0.56 (\text{Fe}^{2.33+}) \end{array} \quad \text{mm/sec} \quad (30)$$

by presently available data; small ranges around these values are to be expected as more data become available. It is immediately evident that the shifts of all clusters with M = Fe, Co, Ni, and Zn (Set I) require that the effective oxidation levels of the iron-sulfur fragments be in the $[\text{Fe}_3\text{S}_4]^{0/1-}$ range. Thus, protein-bound $[\text{CoFe}_3\text{S}_4]^{2+}$, with $\delta_{\text{av}} = 0.41$ mm/sec, may be formalized into the indicated fragments even in the absence of knowledge of the 2+ oxidation state. Cluster **70**, with its known charge, confirms this state for the protein. A description such as $[\text{Fe}_3\text{S}_4]^{1-} + \text{Co}^{3+}$ is inconsistent with the isomer shifts as well as the tetrahedral stereochemistry of the cobalt subsite as inferred from the cluster composition. Protein-bound $[\text{ZnFe}_3\text{S}_4]^{1+}$, whose odd spin requires the indicated fragments, currently provides the only available isomer shift of the $[\text{Fe}_3\text{S}_4]^{1-}$ state. The δ value of the $[\text{NiFe}_3\text{S}_4]^{1+}$ core of **68** is biased toward, but does not reach, the value for this state. The indicated fragments are the preferred description, but this cluster, which does not preserve any subsite differentiation within the Fe_3S_4 fragment, may be more delocalized than other clusters with the Set I metals. Under the fragment formulation, the spins of clusters containing these metals can be derived from antiferromagnetic coupling of the $S = 2$ or $\frac{3}{2}$ spin of the Fe_3S_4 fragment with that of the tetrahedral M^{2+} ion. The value of $S = 1$ is predicted for $[\text{CoFe}_3\text{S}_4]^{1+}$; the experimental value has not been reported.

We next inquire if the same Fe_3S_4 fragment oxidation states and spin coupling apply to the early transition metal clusters in which the heterometal is in a higher oxidation state and occurs in each of the three transition series. Representative isomer shift data for clusters

with $M = V, Mo, W,$ and Re (Set II) are included in Table III. All species have terminal thiolate ligands at the iron subsites, a requirement for internal comparison of isomer shifts. Variation of ligands at the heterometal subsites has an effect on isomer shifts that is slight compared to that of changing cluster oxidation state. Isomer shifts are decisively larger than those of the $[Fe_3S_4]^{1+}$ clusters, indicating, as for the Set I metals, the effective oxidation states $[Fe_3S_4]^{0/1-}$. Fragment formulations follow from isomer shifts, which in some cases match closely with those in series (30). Cluster spins can be rationalized in terms of antiparallel spin coupling as for the Set I cases, but with the additional assumption that d^3 and $d^4 M^{2+}$ fragments have $S = \frac{1}{2}$ and 0, respectively. These spins can be achieved by, say, a strong trigonal distortion resulting in the order $e < a$ for orbitals of octahedral t_{2g} parentage. At the low temperatures of measurement (usually 4.2 K), only the e orbitals are populated. For example, in the $[MoFe_3S_4]^{3+}$ case the coupling is between fragments with $S = 2$ and $S = \frac{1}{2}$, resulting in the observed cluster spin $S = \frac{3}{2}$. Reduction of this core to $[MoFe_3S_4]^{2+}$ primarily affects the Fe_3S_4 fragment, and the experimental cluster spin $S = 2$ is considered to arise from coupling of $S = \frac{3}{2}$ and $\frac{1}{2}$ fragments.

In the $M = Re$ and V cases, for which there is a limited data base of isomer shifts, the fragment formulation seems clear for $[ReFe_3S_4]^{4+}$. But for $[ReFe_3S_4]^{3+}$ the shifts do not allow, as indicated, a clear distinction between two formulations, either of which is consistent with $S = 2$. The situation with $[VFe_3S_4]^{2+}$ is similar. However, in this case, the $0/2+$ formulation, under the spin-coupling model, requires a large distortion of V^{2+} (d^3 , $S = \frac{1}{2}$), which may be unreasonable for a first transition series ion. The fragment formulations for clusters of known structures are entirely consistent with bond distances involving core and terminal ligand atoms (163, 165, 176, 189–193).

Although the fragment formulation and the spin-coupling model are simplistic and the latter lacks a theoretical foundation, they do offer an approximation to the actual charge distribution and provide a ready means of rationalizing and predicting cluster spins. For example, the unknown species $[MnFe_3S_4]^{2+/1+}$ would be expected to have spins of $S = \frac{1}{2}$ and 0, respectively. No diamagnetic MFe_3S_4 cluster has yet been prepared! Some may favor other formulations, such as $[Fe_3S_4]^{1-}$ and Mo^{4+} for $[MoFe_3S_4]^{3+}$. However, provided the heterometal does not significantly perturb fragment isomer shifts, the $[Fe_3S_4]^0 + Mo^{3+}$ formalism is preferred. Others may understandably resist the fragment concept applied to a tightly bound cluster, yet account must be taken of the effort required to obtain a theoretical electronic structural description of an open-shell cluster at the $X\alpha$ calculational level (194).

Summarized in Table V is the scope of heterometal cluster formation

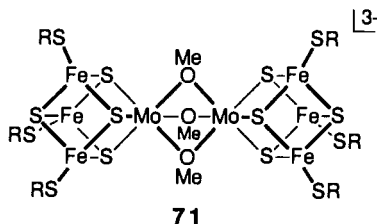
and known spin states. It is extensive and may be expected to expand considerably. We propose that the Fe_3S_4 unit be considered a *quasi-rigid cluster ligand*, whose effective oxidation state lies at or between 0 and -1 when bound to a fourth metal and whose internal structural features and electronic distribution are largely unchanged upon binding a heterometal atom (193). The indicated oxidation states are sufficient for binding but may not always be necessary, for as noted above $[\text{Fe}_3\text{S}_4]^{1+}$ may have latent binding affinity for the especially thiophilic (soft) metals. Also included for reference in Table III are $[\text{Fe}_3\text{S}_4]^{z+}$ clusters. Those of the types $[\text{Fe}_4\text{S}_4]^{3+/2+/1+}$ have been very thoroughly examined as synthetic analogs of biological clusters. The terminal members of the series, $[\text{Fe}_4\text{S}_4]^{4+}$ as $[\text{Fe}_4\text{S}_4(\text{R}_2\text{dtc})_4]$ (183, 205) and $[\text{Fe}_4\text{S}_4]^0$ as $[\text{Fe}_4\text{S}_4(\text{CO})_{12}]$ (62), have oxidation states not yet detected in native clusters. We next inquire into the biological relevance of heterometal cubane-type clusters.

D. BIOLOGICAL IMPLICATIONS

Although MFe_3S_4 clusters can be prepared in proteins (Fig. 11), no such cluster has yet been detected in a native protein. Indeed, there is as yet no clearly defined biological function of the precursor Fe_3S_4 cluster. In one case, aconitase, the Fe_3S_4 form of the enzyme is inactive but can be converted to the active form by cluster reconstitution with Fe(II) (Fig. 4). Consequently, we turn our attention to synthetic clusters.

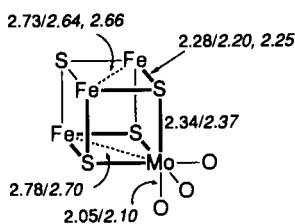
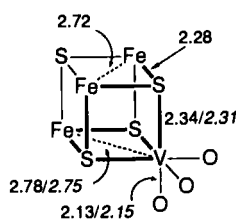
1. Structural Models

It is uncommon that the development of a distinct area of chemistry can be traced to a single event, but this is the case with MFe_3S_4 clusters. The event was the Mo K-edge extended X-ray absorption fine structure (EXAFS) analysis of the Fe–Mo protein and Fe–Mo cofactor of nitrogenase by Hodgson and co-workers in 1978 (206, 207). It was concluded that molybdenum in both samples is implicated in a Mo–Fe–S cluster with similar environments of probable near-neighbor composition MoFe_3S_3 . This work impelled development of the cluster assembly systems in Fig. 6 as well as later advancements (165). Subsequent Mo X-ray absorption near-edge structure (XANES) experiments ruled out tetrahedral MoS_4 and octahedral MoS_6 coordination, and pointed to the inclusion of low- Z atoms in the coordination sphere (208). Protein and cofactor second-derivative XANES indicated that the first coordination shells were similar but not identical and that the cofactor spectra closely resembled the edge spectra of $[\text{MoFe}_3\text{S}_4(\text{SET})_3\text{Fe}(\text{cat})_3]^{3-}$ [cat is catecholate(2-)] (209) and $[\text{Mo}_2\text{Fe}_6\text{S}_8(\text{SET})_6(\text{OMe})_3]^{3-}$ (71) (175, 210).



The preparation and properties of the Fe–Mo cofactor have been incisively summarized by Burgess (211), who has included an account of the X-ray absorption spectroscopic results, providing all of the concrete structural information on the native cluster. Descriptions of the Fe–V cofactor and Fe–V proteins are also available (211, 212). The composition of the Fe–Mo cofactor is in the range $\text{MoFe}_{6-8}\text{S}_{8-10}$. Properties of the Fe–V cofactor suggest that it is an analogous species, but this cannot be decided at present from analytical data. We confine attention to structural properties only. Average bond distances from the most recent EXAFS studies on the Fe–Mo cofactor and Fe–Mo protein (213), and the Fe–V protein (214–216), are presented in Table VII. The three species are in the semireduced oxidation state, with $S = \frac{3}{2}$, and in that sense are related to $[\text{MoFe}_3\text{S}_4]^{3+}$ and $[\text{VFe}_3\text{S}_4]^{2+}$ clusters (Table V). The sum of O + S atom numbers indicates six-coordinate molybdenum.

In formula **72**, bond distances of the Fe–Mo cofactor (*italics*) are compared with those of $[\text{MoFe}_3\text{S}_4\text{Cl}_3(\text{cat})(\text{THF})]^{2-}$ (217); a similar comparison between $[\text{VFe}_3\text{S}_4\text{Cl}_3(\text{DMF})_3]^{1-}$ (**55**) (190) and the Fe–V protein is provided in formula **73**. Also included are Fe–Fe and Fe–S distances

**72****73**

obtained from Fe EXAFS (211). In **72**, the Mo–Fe and Fe–Fe distances of the cofactor appear to be somewhat shorter, but mean values in synthetic clusters span the ranges 2.68–2.73 and 2.70–2.79 Å, respectively (165). The Mo–O bond length of 2.10 Å in the cofactor is in good agreement with the Mo–O(cat) distance of 2.05 Å in the synthetic cluster. When compared with the Mo–O(THF) value of 2.35 Å, the cofactor bond length is further seen to be consistent with an anionic ligand, perhaps homocitrate, which has been shown to be an endoge-

TABLE VII

THE M = Mo/V SITES IN THE Fe–Mo COFACTOR AND Fe–Mo/V PROTEINS OF NITROGENASE FROM EXAFS RESULTS

Sample	Distance (Å)			No. of atoms		
	M–S	M–Fe	M–O	S	Fe	O
Fe–Mo cofactor (as isolated) ^a	2.37(2)	2.70(2)	2.10(2)	3.1	2.6	3.1
Fe–Mo protein (semireduced) ^a	2.37(1)	2.68(1)	2.12(1)	4.5	3.5	1.7
Fe–V protein (semireduced) ^b	2.31	2.75	2.15	3(1)	3(1)	3(1)

^a *Clostridium pasteurianum* and *A. vinelandii* nitrogenase (213).

^b *Azotobacter chroococcum* nitrogenase (214, 215); very similar results have been obtained for the *A. vinelandii* Fe–V protein (216).

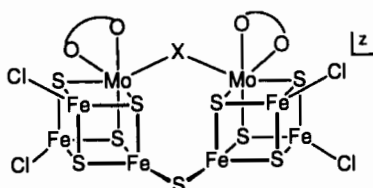
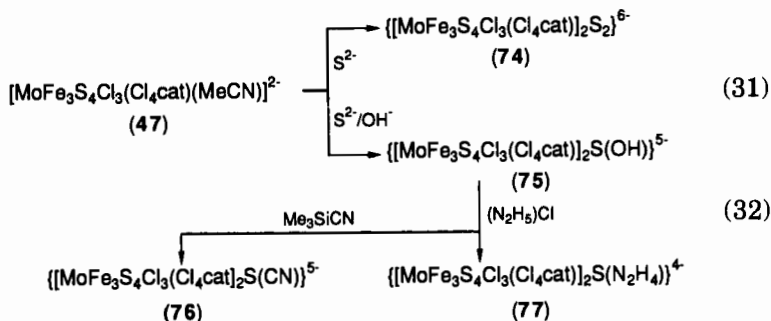
nous component of the cofactor (211). The apparent bond distance concordance in **73** is even better. Here the V–O distance involves a neutral ligand (DMF). From a Mo EXAFS intensity analysis of single crystals of the Fe–Mo protein, it has been concluded that a linear Fe–Mo–Fe arrangement is unlikely and that the Fe–Mo–Fe angle lies within the limits 50–130° (218). This angle in the cluster summarized by **72** is 59°, a typical value for such species, in which the MoFe₃ unit is a distorted tetrahedron.

All evidence sustains the conclusion that the cubane-type cluster **72** still provides the best structural model for the molybdenum site in the cofactor. This conclusion is less satisfactory for the protein-bound cofactor. It follows from the results of Table VII that the (minimum) coordination number of the molybdenum atom is the same in the free cofactor and in the protein, but the atom composition changes pursuant to protein binding. One iron and one sulfur atom appear in the molybdenum environment, indicating that a change in core structure cannot be discounted. Cluster **73** is clearly an excellent model for the vanadium site in the Fe–V protein, in which cofactor binding apparently differs to some extent from that in the Fe–Mo protein. The boldface portions of **72** and **73** imply fragments of radially averaged structural similarity to the native clusters. The cubane structure cannot be proved because the nonbonded M . . . S intracluster distance of ~4 Å is too long to be observed by EXAFS. Last, no structure such as **72** can generate second shell scattering and Fe–Fe separations near 3.7 Å deduced from the Fe EXAFS of the Fe–Mo cofactor (211). The native cluster has a more elaborate structure, as required by its composition.

2. Linked Cubane Clusters

There is no shortage of models, all synthetically unfulfilled, for the Fe–Mo cofactor (164, 165). One of these, containing the MoFe_7S_6 noncubane polyhedron and originating in this laboratory (163, 219), could account for the long-range Fe–Fe scattering observed by EXAFS. In the quest for the synthesis of the Fe–Mo cofactor, clusters within the core compositional limits have been difficult to achieve. The species $[\text{MoFe}_6\text{S}_6(\text{CO})_{16}]^{2-}$ (185), which does not contain a heterometal cubane unit, is the closest approximation to the composition. Although it is a possible precursor to a model, it is not one.

Given the considerable thermodynamic stabilities of Fe_4S_4 and MoFe_3S_4 clusters as judged from their rapid, high-yield formation in assembly systems, a rational cofactor structure concept follows. That structure may consist of a linked combination of these two cubane-type units. The highly significant crystallographic work of Bolin *et al.* (220) on the Fe–Mo protein of *C. pasteurianum* places the two cofactor clusters 70 Å from each other, thereby eliminating as directly pertinent to the nitrogenase problem any unit containing two molybdenum atoms and substrate reductions based on binuclear activation by molybdenum. Nonetheless, the problem at hand requires, at the outset, learning how to link clusters of these types, whether the same or different. One method, employing subsite-differentiated clusters and affording the singly bridged double cubanes **23–25**, is outlined in Fig. 2. The double cubane $[(\text{Fe}_4\text{S}_4\text{Cl}_3)_2\text{S}]^{4-}$ has been isolated and the Fe–S–Fe bridge was proved by an X-ray structure determination (53). Very recently, Coucouvanis and co-workers (221–223) demonstrated means of linking two MoFe_3S_4 clusters. The reactions given by Eq. (31) lead to the doubly bridged clusters **74** and **75**. Unlike the double cubane, **46**, the bridges connect the same metal atom. In **74**, the bridges are unsymmetrical, especially at the molybdenum atom where $\text{Mo–S} = 2.60$ and 2.69 Å. The mean Fe–S bridge distance (2.20 Å) is shorter than the average of core Fe–S distances [$2.27(3)$ Å], presumably because of the lesser bridging multiplicity in the former bond. In contrast, the mean Mo–S bridge distance (2.65 Å) is substantially longer than the average of core Mo–S distances [$2.35(2)$ Å]. A somewhat related feature is the long terminal Mo–S distance of 2.60 Å found in the single cubane $[\text{MoFe}_3\text{S}_4(\text{S-}p\text{-C}_6\text{H}_4\text{Cl})_4(\text{cat})]^{3-}$ (**48**) (224). In **74** and **75**, $\text{Fe–S–Fe} = 98\text{--}99^\circ$ [5° less than in $[(\text{Fe}_4\text{S}_4\text{Cl}_3)_2\text{S}]^{4-}$], and $\text{Mo–X–Mo} = 137^\circ$ and 158° , respectively. With limited data, it would appear that these double cubanes are constructed with bridges of unexceptional bond distances and Mo–X–Mo angles that vary as required for structural stability.



- 74: $\text{X} = \text{S}^{2-}$, $z = 6$ -
 75: $\text{X} = \text{OH}^-$, $z = 5$ -
 76: $\text{X} = \text{CN}^-$, $z = 5$ -
 77: $\text{X} = \text{N}_2\text{H}_4$, $z = 4$ -

In the reactions given by Eq. (32), the Mo—(OH)—Mo bridge is cleaved and the potentially reducible substrates cyanide and hydrazine are inserted between two units capable of one-electron reduction. A low-resolution X-ray study is said to support structure **77** (222). No substrate transformations have yet been reported. Coucouvanis (223) has hypothesized a pathway for the reduction of dinitrogen in which the substrate is bridged between molybdenum and iron subsites of different cubanes in an otherwise singly bridged (Mo—S—Fe) double cubane of the type $\text{MoFe}_3\text{S}_4\text{—S—Fe}_3\text{S}_4$. Isolation of such a cluster has been mentioned but structural proof is lacking (221).

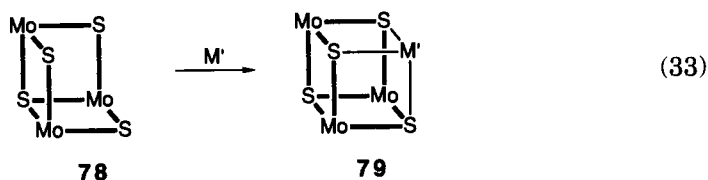
E. NONBIOLOGICAL $\text{M}'\text{M}_3\text{S}_4$ CLUSTERS

The existence of the cuboidal M_3S_4 unit **31** (Table IV) raises the possibility of $\text{M}_3\text{S}_4 \rightarrow \text{M}'\text{M}_3\text{S}_4$ cluster conversion reactions when **31** is in a suitable oxidation state. The Mo_3S_4 core **78** is available in a variety of clusters and is potentially susceptible to closure to cubanes. A rather extensive group of clusters with the cubane-type $\text{M}'\text{M}_3\text{S}_4$ cores ($\text{M} = \text{Mo}, \text{W}$, and Cr) in fact has been synthesized, all since 1981; these clusters are collected in Table VIII. The large majority have been characterized by X-ray structural determinations. Representative structures are depicted in Fig. 12. Only the species with $\text{M} = \text{Cr}$ were *not* synthesized by a cluster conversion reaction. These clusters are termed "nonbiological" inasmuch as neither the M_3S_4 portion nor the $\text{M}'\text{M}_3\text{S}_4$ core has been found in a natural molecule.

TABLE VIII
HETEROMETALLIC $M'M_3S_4$ CUBANE-TYPE CLUSTERS

Cluster	Ref.
[M'Mo₃S₄]	
Group I	
[Fe ^{II} Mo ₃ S ₄ (OH ₂) ₁₀] ⁴⁺	225, 226
[Fe ^{II} Mo ₃ S ₄ (NH ₃) ₉ (OH ₂) ₁] ⁴⁺	225
[Ni ^{II} Mo ₃ S ₄ (OH ₂) ₁₀] ⁴⁺ (80)	227, 228
[Ni ^{II} Mo ₃ S ₄ (nta) ₂ (Hnta)Cl] ⁵⁻ (81)	227
[Sn ^{IV} Mo ₃ S ₄ (OH ₂) _x] ⁶⁺	229
[Sn ^{IV} Mo ₃ S ₄ (Hnta) ₃ Cl ₃] ³⁻	229
[Sn ^{IV} (Mo ₃ S ₄ (OH ₂) ₉) ₂] ⁸⁺ (82)	229
[Mo(Mo ₃ S ₄ (OH ₂) ₉) ₂] ⁸⁺	230
[Hg(Mo ₃ S ₄ (OH ₂) ₉) ₂] ⁸⁺	231
[Sb(Mo ₃ S ₄ (OH ₂) ₉) ₂] ⁸⁺	254
[Co ₂ ^{II} (Mo ₃ S ₄ (OH ₂) ₉) ₂] ⁸⁺	231
[Cu ₂ ^I (Mo ₃ S ₄ (OH ₂) ₉) ₂] ⁸⁺ (83)	232
Group II	
[Sn ^{IV} Mo ₃ S ₄ (S ₂ PEt ₂) ₆] (84)	233
[WMo ₃ S ₄ (S ₂ PEt ₂) ₆]	234
[Cu ^I Mo ₃ S ₄ (dtp) ₃ I(Cl ₃ CO ₂)(MeCN)]	235
[Cu ^I Mo ₃ S ₄ (dtp) ₃ I(OAc)L] (L = DMF, H ₂ O) (85)	236
[Sb ^{III} Mo ₃ S ₄ (dtp) ₄ Cl ₃ L] (L = EtOH, oxazole)	237
[M'WS₄]	
[Cu ^I W ₃ S ₄ (dtp) ₃ I(OAc)(py)]	238
[M'Fe₃S₄]	
[Cp ₄ VFe ₃ S ₄]	239
[Cp ₄ NbFe ₃ S ₄]	239
[M'Cr₃S₄]	
[Cp ₃ Fe(O ₂ C- <i>t</i> -Bu)Cr ₃ S ₄] (86)	240
[Cp ₃ Fe(SPh)Cr ₃ S ₄] (87)	241
[Cp ₃ Co(CO)Cr ₃ S ₄], [(MeCp) ₃ Co(CO)Cr ₃ S ₄]	242, 243

Because of differences in preparation, it is convenient to subdivide $M'Mo_3S_4$ clusters into two groups, as indicated in Table VIII. All clusters in Group I are prepared by the core conversion reaction, Eq. (33),



(M = Fe, Co, Ni, Cu, Mo, Hg, Sn, Sb)

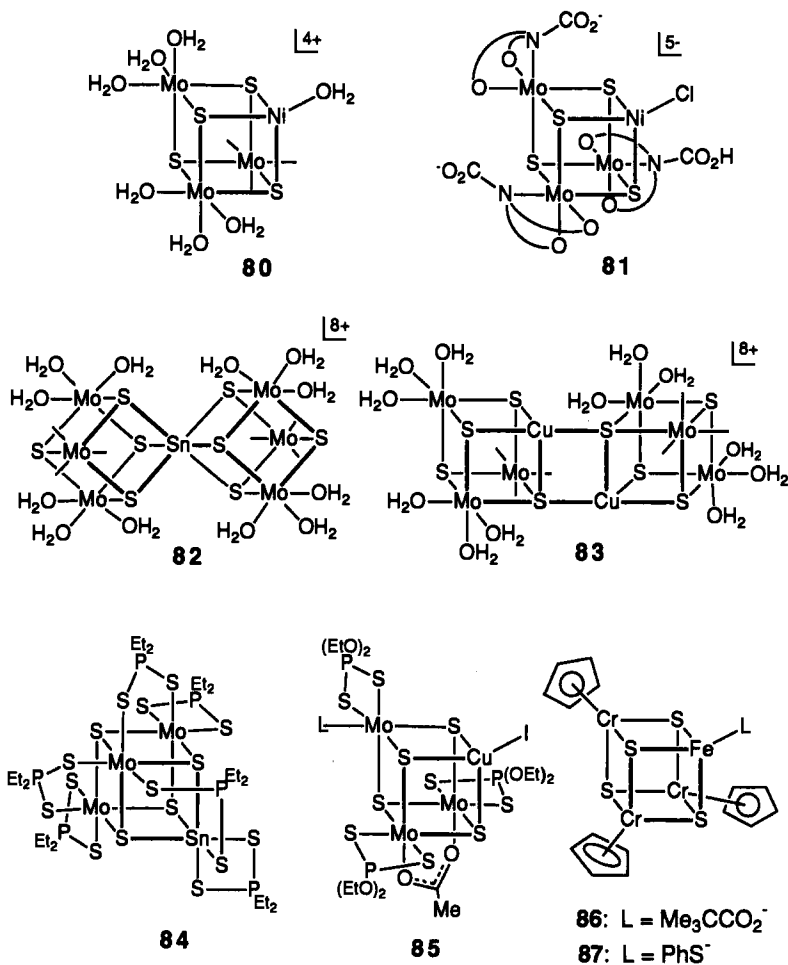
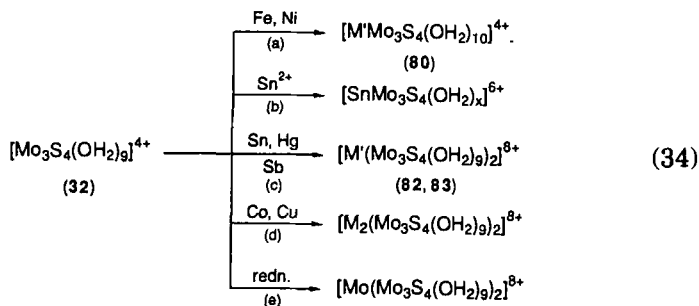


FIG. 12. Schematic structures of the $M'M_3S_4$ cubane-type clusters 80–87 (Table VIII).

in which the boldface portion of product cluster 79 emphasizes the ligand nature of 78. In an elegantly simple experiment reported in 1986, Shibahara *et al.* (225) performed the redox reaction (a) given by Eq. (34) ($M' = \text{Fe}$) in aqueous acid solution. This reaction not only afforded the indicated product but has been generalized for the preparation of the aqua clusters shown in Eq. (34).

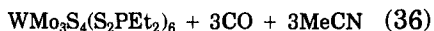
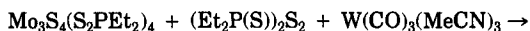


In this experiment, iron wire was placed in a 2 M HCl solution of **32**; a color change from green to red-purple ensued in a few hours. The product aqua ion was separated by cation exchange. Treatment of the reaction mixture with concentrated ammonia led to the formation of $[\text{FeMo}_3\text{S}_4(\text{NH}_3)_9(\text{OH}_2)]^{4+}$, which was isolated as the chloride salt. An analogous reaction afforded the NiMo_3S_4 cluster **80**, which was readily converted to the chelated cluster **81** with nitrilotriacetate(3-) (NTA). The structures of these species confirm the cubane cores, tetrahedral M' subsites, and six-coordinate molybdenum subsites; the latter is an invariant feature of the clusters in Table VIII. Reaction (b) in Eq. (34) gives the tin cluster; it has not been isolated and the exact number of aqua ligands is not known. With the metals in reactions (c) and (d) in Eq. (34) double cubanes are obtained. Clusters containing tin, antimony, or mercury are bridged by a six-coordinate metal atom as in **82**, whereas the copper and cobalt clusters are bridged by two M' —S bonds involving distorted tetrahedral heterometal subsites as in **83**. In reaction (e) in Eq. (34), cuboidal **32** is fragmented by reduction and the product cluster, whose structure is analogous to **82**, is obtained in low (15%) yield.

The processes involved in reactions (a)–(d) in Eq. (34), excluding that with copper and possibly mercury, are satisfactorily interpreted in terms of a two-electron reduction of **32** by the M' reactant (227). This results in formation of the $[\text{Mo}_3\text{S}_4]^{2+}$ core, which, because of the reduced oxidation state ($\text{Mo}^{3.33+}$) and consequent attenuated electrophilic demand of the molybdenum atoms, is a much more effective ligand. In an equivalent reaction, cluster **80** has been obtained by the reduction of **32** with NaBH_4 in the presence of NiCl_2 in aqueous acid solution (228). Tetrahedral stereochemistry at the copper subsites in **83** implies Cu(I) and a one-electron reduction of **32**, a plausible situation given the affinity of Cu(I) for sulfur ligands. In the case of $\text{M}' = \text{Hg}$, Shibahara *et al.* (231) conclude that the Hg—S bonds are too long to indicate

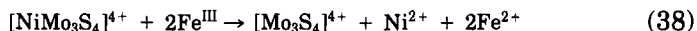
oxidation to Hg(II), but bond distances were not given. On the basis of E_0 values, mercury, of all metals M' in Eq. (34), is the most difficult to oxidize in acid solution. Shibahara has summarized his work in this field (257).

Among Group II clusters, the approximately octahedral coordination at the tin subsite of **84** implies Sn(IV) and a two-electron oxidation of Sn(II) in Eq. (35). The presence of Cu(I) is quite obvious in clusters typified by **85**, whose copper subsite is tetrahedrally coordinated. The product cluster of Eq. (36) is isostructural with **84** and the $[\text{WMo}_3\text{S}_4]^{6+}$



core is generated with two oxidizing equivalents from the ligand disulfide. Although the preferred formulation in terms of W(IV) and $[\text{Mo}_3\text{S}_4]^{2+}$ (234) may be meaningful, this compound points out the difficulty in deducing simple charge distributions in this class of compounds. Inasmuch as molybdenum does not provide a Mössbauer nucleus, charge distributions will have to be deduced from the isomer shifts of the heterometal (when applicable) and ^{95}Mo chemical shifts (when observable). Either method will require a data base for interpretations of cluster properties. It remains to be seen if other techniques such as XANES or X-ray photoelectron spectroscopy can be applied to these clusters, whose polarizable sulfide ligands can be expected to attenuate differences arising from changes in metal oxidation state.

From the array of $M'\text{Mo}_3\text{S}_4$ clusters in Table VIII and their means of formation, it is evident that two features in particular contribute to stability: (1) the oxidation state of the Mo_3S_4 fragment and (2) the intrinsic affinity of heterometal M' for anionic sulfur ligands. Overall, Eqs. (37) and (38) (aqua ligands omitted) (226, 228), whereby hetero-



metal cores are disrupted by oxidation, underscore the necessity for a reduced Mo_3S_4 fragment as a ligand to Fe(II) and Ni(II). The $[\text{Mo}_3\text{S}_4]^{3+,2+}$ states have not been demonstrated for the aqua ion but have been detected electrochemically in $[\text{Mo}_3\text{S}_4(\text{ida})_3]^{3-,4-}$ [ida is imidodiacetate(2-)] (115). When reactions are carried out without an exogenous reductant as in scheme (34), a requirement equivalent to feature (1) mentioned above is that the M' reactant be a sufficient reductant. Standard potentials for the two-electron reductants in Eq. (34) occur in

the range -0.44 (Fe) to $+0.15$ V (Sn^{2+}). With Cu ($+0.52$ V) as a reactant, a one-electron reduction suffices. It would appear that a substantial number of other clusters should be accessible by the methods of this scheme or by the addition of a reductant in the presence of **32** and an M' source. It remains to be seen if $[\text{W}_3\text{S}_4(\text{OH}_2)_9]^{4+}$ can be reduced to a level that will support cluster formation. In the cuboidal series of ions on p. 28, the ease of reducibility is expected to decrease in proceeding to the right. No reductant is necessary for the formation of the $[\text{CuMo}_3\text{S}_4]^{5+}$ cores in clusters such as **85**, which are formed directly from $[\text{Mo}_3\text{S}_4(\text{dtp})_4(\text{OH}_2)]$ and a Cu(I) source. Given the existence of cuboidal species such as $[\text{Mo}_2\text{MS}_4(\text{edt})_2(\text{PPh}_3)]^{1-}$ ($\text{M} = \text{Cu}, \text{Ag}$) (**244**, **245**), it would appear that heterotrimetallic clusters are within easy reach.

The final set of heterometal clusters in Table VIII contains the $\text{M}'\text{Cr}_3\text{S}_4$ core unit; these clusters have been prepared by Pasynskii and co-workers. The synthetic methods for these compounds utilize the common starting material $[\text{Cp}_2\text{Cr}_2(\mu\text{-St-Bu})_2(\mu\text{-S})]$ and proceed by oxidative decarbonylation of M' carbonyl precursors under thermal or photolytic conditions. The steps in the formation of the clusters are decidedly obscure. Clusters **86** and **87** are of potential interest in the manipulation of one labile subsite in molecules whose three other subsites are irreversibly blocked.

F. PROSPECTUS

It has now been 20 years since the Fe_4S_4 cubane-type structure was proved by protein crystallography, in a landmark contribution by Sieker, Adman, and Jensen (**246**), and since the first synthetic analog of the native cluster was prepared (**247**). In the intervening period, the compositions and structures of only two other native iron-sulfur clusters, of the types Fe_2S_2 and Fe_3S_4 and in that order, have yielded to experimentation. One need only contemplate the P-clusters and cofactors of nitrogenase (**22**, **211**, **220**, **248**) and the H-clusters of hydrogenase (**21**) to recognize that there remain formidable challenges in protein-bound cluster structural, electronic, and reactivity characterization and in the synthesis of meaningful analogs of these clusters. What role, if any, Fe_3S_4 and MFe_3S_4 clusters will play in a fuller exposition of iron-sulfur biochemistry remains to be learned. What is evident is that one cluster affords the other in a protein and in the laboratory, but we must progress further before knowing if nature executes cluster conversion and regards heterometal cubanes as salutary to any biological function. In the context of inorganic clusters, these are the most

rapidly growing type. Only lack of ingenuity will prevent the synthesis of MFe_3S_4 clusters containing nearly all metals and metalloids. That this report has concentrated mainly on synthesis and structure is one indication that, with the exception of $[VFe_3S_4]^{2+}$ and $[MoFe_3S_4]^{3+}$ clusters, the understanding of electronic structures and reactivities at all metal subsites is presently quite elementary. Harris (249) has presented a useful survey of cubane-type clusters and qualitative core bonding models. Nonetheless, developments in iron-sulfur chemistry and biochemistry have proceeded apace. It is desired that their treatment here vindicates the title of this article.

ACKNOWLEDGMENTS

It is a personal privilege of high order to contribute to this volume, which honors the scientific works of Helmut Beinert. His collective contributions to iron-sulfur biochemistry over three decades, well known to veteran investigators in the field, stand second to none. For those who have been attracted only recently to the subject, examination of the work of Beinert and his colleagues on the aconitase problem will reveal a modern chemical/biochemical classic.

The research of the author in iron-sulfur and heterometal cluster chemistry has, since its inception (247), been supported by the National Institutes of Health and the National Science Foundation. I thank C. K. Ryder for preparation of figures and formulas and S. C. Lee for useful discussions.

REFERENCES

1. Berg, J. M., and Holm, R. H., in "Iron-Sulfur Proteins" (T. G. Spiro, ed.), Chap. 1. Wiley (Interscience), New York, 1982.
2. Adman, E. T., Sieker, L. C., and Jensen, L. H., *J. Biol. Chem.* **248**, 3987 (1973); Adman, E. T., Sieker, L. C., and Jensen, L. H., *J. Biol. Chem.* **251**, 3806 (1976).
3. Carter, C. W., Jr., Kraut, J., Freer, S. T., Xuong, N., Alden, R. A., and Bartsch, R. G., *J. Biol. Chem.* **249**, 4212 (1974).
4. Carter, C. W., Jr., Kraut, J., Freer, S. T., and Alden, R. A., *J. Biol. Chem.* **249**, 6339 (1974).
5. Lim, L. W., Shamala, N., Mathews, F. S., Steenkamp, D. J., Hamlin, R., and Xuong, N., *J. Biol. Chem.* **261**, 15140 (1986).
6. Stout, G. H., Turley, S., Sieker, L. C., and Jensen, L. H., *Proc. Natl. Acad. Sci. U.S.A.* **85**, 1020 (1988).
7. Stout, C. D., *J. Biol. Chem.* **263**, 9256 (1988); Stout, C. D., *J. Mol. Biol.* **205**, 545 (1989).
8. Fukuyama, K., Nagahara, Y., Tsukihara, T., Katsube, Y., Hase, T., and Matsubara, H., *J. Mol. Biol.* **199**, 183 (1988).
9. Fukuyama, K., Matsubara, H., Tsukihara, T., and Katsube, Y., *J. Mol. Biol.* **210**, 383 (1989).

10. Robbins, A. H., and Stout, C. D., *Proc. Natl. Acad. Sci. U.S.A.* **86**, 3639 (1989); Robbins, A. H., and Stout, C. D., *Proteins* **5**, 289 (1989).
11. Martin, A. E., Burgess, B. K., Stout, C. D., Cash, V. L., Dean, D. R., Jensen, G. M., and Stephens, P. J., *Proc. Natl. Acad. Sci. U.S.A.* **87**, 598 (1990).
12. Carney, M. J., Papaefthymiou, G. C., Spartalian, K., Frankel, R. B., and Holm, R. H., *J. Am. Chem. Soc.* **110**, 6084 (1988); and references therein.
13. Carney, M. J., Papaefthymiou, G. C., Whitener, M. A., Spartalian, K., Frankel, R. B., and Holm, R. H., *Inorg. Chem.* **27**, 346 (1988).
14. Carney, M. J., Papaefthymiou, G. C., Frankel, R. B., and Holm, R. H., *Inorg. Chem.* **28**, 1497 (1989).
15. Yu, S., Papaefthymiou, G. C., and Holm, R. H., *Inorg. Chem.* **30**, 3476 (1991); and references therein.
16. Simon, W., Wilk, A., Krebs, B., and Henkel, G., *Angew. Chem., Int. Ed. Engl.* **26**, 1009 (1987).
17. Barbaro, P., Bencini, A., Bertini, I., Briganti, F., and Midollini, S., *J. Am. Chem. Soc.* **112**, 7238 (1990).
18. Backes, G., Mino, Y., Loehr, T. M., Meyer, T. E., Cusanovich, M. A., Sweeney, W. V., Adman, E. T., and Sanders-Loehr, J., *J. Am. Chem. Soc.* **113**, 2055 (1991).
19. Beinert, H., and Kennedy, M. C., *Eur. J. Biochem.* **186**, 5 (1989).
20. Beinert, H., *FASEB J.* **4**, 2483 (1990).
21. Adams, M. W. W., *Biochim. Biophys. Acta* **1020**, 115 (1990).
22. Holm, R. H., Ciurli, S., and Weigel, J. A., *Prog. Inorg. Chem.* **38**, 1 (1990).
23. Lindahl, P. A., and Kovacs, J. A., *J. Cluster Sci.* **1**, 29 (1990).
24. Bruschi, M., and Guerlesquin, F., *FEMS Microbiol. Rev.* **54**, 155 (1988).
25. Conover, R. C., Kowal, A. T., Fu, W., Park, J.-B., Aono, S., Adams, M. W. W., and Johnson, M. K., *J. Biol. Chem.* **265**, 8533 (1990).
26. Okawara, N., Ogata, M., Yagi, T., Wakabayashi, S., and Matsubara, H., *J. Biochem. (Tokyo)* **104**, 196 (1988).
27. Ogata, M., Kondo, S., Okawara, N., and Yagi, T., *J. Biochem. (Tokyo)* **103**, 121 (1988).
28. Bovier-Lapierre, G., Bruschi, M., Bonicel, J., and Hatchikian, E. C., *Biochim. Biophys. Acta* **913**, 20 (1987).
29. Armstrong, F. A., George, S. J., Cammack, R., Hatchikian, E. C., and Thomson, A. J., *Biochem. J.* **264**, 265 (1989).
30. George, S. J., Armstrong, F. A., Hatchikian, E. C., and Thomson, A. J., *Biochem. J.* **264**, 275 (1989).
31. Kerscher, L., Nowitzki, S., and Oesterhelt, D., *Eur. J. Biochem.* **128**, 223 (1982).
32. Minami, Y., Wakabayashi, S., Wada, K., Matsubara, H., Kerscher, L., and Oesterhelt, D., *J. Biochem. (Tokyo)* **97**, 745 (1983).
33. Wakabayashi, S., Fujimoto, N., Wada, K., Matsubara, H., Kerscher, L., and Oesterhelt, D., *FEBS Lett.* **162**, 21 (1983).
34. O'Keefe, D. P., Gibson, K. J., Emptage, M. H., Lenstra, R., Romesser, J. A., Litle, P. J., and Omer, C. A., *Biochemistry* **30**, 447 (1991).
35. Kissinger, C. R., Adman, E. T., Sieker, L. C., and Jensen, L. H., *J. Am. Chem. Soc.* **110**, 8721 (1988).
36. Kissinger, C. R., Sieker, L. C., Adman, E. T., and Jensen, L. H., *J. Mol. Biol.* **219**, 693 (1991).
37. Plank, D. W., and Howard, J. B., *J. Biol. Chem.* **263**, 8184 (1988).
38. Werst, M. M., Kennedy, M. C., Beinert, H., and Hoffman, B. M., *Biochemistry* **29**, 10526 (1990).

39. Kennedy, M. C., Kent, T. A., Emptage, M. H., Merkle, H., Beinert, H., and Münck, E., *J. Biol. Chem.* **259**, 14463 (1984).
40. Plank, D. W., Kennedy, M. C., Beinert, H., and Howard, J. B., *J. Biol. Chem.* **264**, 20385 (1989).
41. Hagen, K. S., Watson, A. D., and Holm, R. H., *J. Am. Chem. Soc.* **105**, 3905 (1983).
42. Stack, T. D. P., Weigel, J. A., and Holm, R. H., *Inorg. Chem.* **29**, 3745 (1990).
43. Stack, T. D. P., and Holm, R. H., *J. Am. Chem. Soc.* **110**, 2484 (1988).
44. Ciurli, S., and Holm, R. H., *Inorg. Chem.* **28**, 1685 (1989).
45. Whitener, M. A., Peng, G., and Holm, R. H., *Inorg. Chem.* **30**, 2411 (1991).
46. Wong, G. B., Bobrik, M. A., and Holm, R. H., *Inorg. Chem.* **17**, 578 (1978).
47. Wiegel, J. A., and Holm, R. H., *J. Am. Chem. Soc.* **113**, 4184 (1991).
48. Ciurli, S., Carrié, M., Weigel, J. A., Carney, M. J., Stack, T. D. P., Papaefthymiou, G. C., and Holm, R. H., *J. Am. Chem. Soc.* **112**, 2654 (1990).
49. Cleland, W. E., Holtzman, D. A., Ibers, J. A., DeFotis, G. C., and Averill, B. A., *J. Am. Chem. Soc.* **105**, 6021 (1983).
50. Weigel, J. A., Holm, R. H., Surerus, K. K., and Münck, E., *J. Am. Chem. Soc.* **111**, 9246 (1989).
51. Weigel, J. A., Srivastava, K. K. P., Day, E. P., Münck, E., and Holm, R. H., *J. Am. Chem. Soc.* **112**, 8015 (1990).
52. Stack, T. D. P., Carney, M. J., and Holm, R. H., *J. Am. Chem. Soc.* **111**, 1670 (1989).
53. Challen, P. R., Koo, S.-M., Dunham, W. R., and Coucouvanis, D., *J. Am. Chem. Soc.* **112**, 2455 (1990).
54. Liu, H. Y., Scharbert, B., Holm, R. H., *J. Am. Chem. Soc.* **113**, 9529 (1991).
55. Reynolds, J. G., and Holm, R. H., *Inorg. Chem.* **20**, 1873 (1981).
56. Conover, R. C., Park, J.-B., Adams, M. W. W., and Johnson, M. K., *J. Am. Chem. Soc.* **113**, 2791 (1991).
57. Kanatzidis, M. G., Baenziger, N. C., Coucouvanis, D., Simopoulos, A., and Kostikas, A., *J. Am. Chem. Soc.* **106**, 4500 (1984).
58. Kanatzidis, M. G., Coucouvanis, D., Simopoulos, A., Kostikas, A., and Papaefthymiou, V., *J. Am. Chem. Soc.* **107**, 4925 (1985).
59. Saak, W., and Pohl, S., *Z. Naturforsch., B: Chem. Sci.* **43B**, 813 (1988).
60. Pohl, S., and Bierbach, U., *Z. Naturforsch., B: Chem. Sci.* **46B**, 68 (1991).
61. Weigel, J. A., and Holm, R. H., unpublished results (1991).
62. Nelson, L. L., Lo, F. Y.-K., Rae, A. D., and Dahl, L. F., *J. Organomet. Chem.* **225**, 309 (1982).
63. Tsukihara, T., Fukuyama, K., Nakamura, M., Katsube, Y., Tanaka, N., Kakudo, M., Wada, K., Hase, T., and Matsubara, H., *J. Biochem (Tokyo)* **90**, 1763 (1981).
64. Sussman, J. L., Brown, J. H., and Shoham, M., in "Iron-Sulfur Protein Research" (H. Matsubara, Y. Katsube, and K. Wada, eds.), p. 68. Japan Sci. Soc. Press, Tokyo/Springer-Verlag, Berlin, 1987.
65. Tsukihara, T., Fukuyama, K., Mizushima, M., Harioka, T., Kusunoki, M., Katsube, Y., Hase, T., and Matsubara, H., *J. Mol. Biol.* **216**, 399 (1990).
66. Rypniewski, W. R., Breiter, D. R., Benning, M. M., Wesenberg, G., Oh, B.-H., Markley, J. L., Rayment, I., and Holden, H. M., *Biochemistry* **30**, 4126 (1991).
67. Armstrong, W. H., in "Metal Clusters in Proteins" (L. Que, Jr., ed.), ACS Symp. Ser. No. 372, Chap. 1. American Chemical Society, Washington, D.C., 1988.
68. Beinert, H., and Thomson, A. J., *Arch. Biochem. Biophys.* **222**, 333 (1983).
69. Park, J.-B., Fan, C., Hoffman, B. M., and Adams, M. W. W., *J. Biol. Chem.* **266**, 19351 (1991).
70. Kent, T. A., Dreyer, J.-L., Kennedy, M. C., Huynh, B. H., Emptage, M. H., Beinert, H., and Münck, E., *Proc. Natl. Acad. Sci. U.S.A.* **79**, 1096 (1982).

71. Beinert, H., Emptage, M. H., Dreyer, J.-L., Scott, R. A., Hahn, J. E., Hodgson, K. O., and Thomson, A. J., *Proc. Natl. Acad. Sci. U.S.A.* **80**, 393 (1983).
72. Kennedy, M. C., Emptage, M. H., Dreyer, J.-L., and Beinert, H., *J. Biol. Chem.* **258**, 11098 (1983).
73. Emptage, M. H., Dreyer, J.-L., Kennedy, M. C., and Beinert, H., *J. Biol. Chem.* **258**, 11106 (1983).
74. Kent, T. A., Emptage, M. H., Merkle, H., Kennedy, M. C., Beinert, H., and Münck, E., *J. Biol. Chem.* **260**, 6871 (1985).
75. Kent, T. A., Moura, I., Moura, J. J. G., Lipscomb, J. D., Huynh, B. H., LeGall, J., Xavier, A. V., and Münck, E., *FEBS Lett.* **138**, 55 (1982).
76. Moura, J. J. G., Moura, I., Kent, T. A., Lipscomb, J. D., Huynh, B. H., LeGall, J., Xavier, A. V., and Münck, E., *J. Biol. Chem.* **257**, 6259 (1982).
77. Moura, J. J. G., LeGall, J., and Xavier, A. V., *Eur. J. Biochem.* **141**, 319 (1983).
78. Guigliarelli, B., Bertrand, P., More, C., Papavassiliou, P., Hatchikian, E. C., and Gayda, J. P., *Biochim. Biophys. Acta* **810**, 319 (1985).
79. George, S. J., Richards, A. J. M., Thomson, A. J., and Yates, M. G., *Biochem. J.* **224**, 247 (1984).
80. Bell, S. H., Dickson, D. P. E., Robinson, C. E., Cammack, R., Hall, D. O., and Rao, K. K., *FEBS Lett.* **142**, 143 (1982).
81. Nagayama, K., Ozaki, Y., Kyogoku, Y., Hase, T., and Matsubara, H., *J. Biochem. (Tokyo)* **94**, 893 (1983).
82. Thomson, A. J., Robinson, A. E., Johnson, M. K., Cammack, R., Rao, K. K., and Hall, D. O., *Biochim. Biophys. Acta* **637**, 423 (1981).
83. Johnson, M. K., Spiro, T. G., and Mortenson, L. E., *J. Biol. Chem.* **257**, 2447 (1982).
84. Nagayama, K., Imai, T., Ohmori, D., and Oshima, T., *FEBS Lett.* **169**, 79 (1984).
85. Stephens, P. J., Morgan, T. V., Devlin, F., Penner-Hahn, J. E., Hodgson, K. O., Scott, R. A., Stout, C. D., Burgess, B. K., *Proc. Natl. Acad. Sci. U.S.A.* **82**, 5661 (1985).
86. Thomson, A. J., Robinson, A. E., Johnson, M. K., Moura, J. J. G., Moura, I., Xavier, A. V., and LeGall, J., *Biochim. Biophys. Acta* **670**, 93 (1981).
87. Johnson, M. K., Morningstar, J. E., Bennett, D. E., Ackrell, B. A. C., and Kearney, E. B., *J. Biol. Chem.* **260**, 7368 (1985).
88. Morningstar, J. E., Johnson, M. K., Cecchini, G., Ackrell, B. A. C., and Kearney, E. B., *J. Biol. Chem.* **260**, 13631 (1985).
89. Johnson, M. K., Bennett, D. E., Fee, J. A., and Sweeney, W. V., *Biochim. Biophys. Acta* **911**, 81 (1987).
90. Johnson, M. K., Thomson, A. J., Richards, A. J. M., Peterson, J., Robinson, A. E., Ramsay, R. R., and Singer, T. P., *J. Biol. Chem.* **259**, 2274 (1984).
91. Day, E. P., Peterson, J., Bonvoisin, J. J., Moura, I., and Moura, J. J. G., *J. Biol. Chem.* **263**, 3684 (1988).
92. Sweeney, W. V., Rabinowitz, J. C., and Yoch, D. C., *J. Biol. Chem.* **250**, 7842 (1975).
93. Cammack, R., Rao, K. K., Hall, D. O., Moura, J. J. G., Xavier, A. V., Bruschi, M., LeGall, J., Deville, A., and Gayda, J.-P., *Biochim. Biophys. Acta* **490**, 311 (1977).
94. Ohnishi, T., Blum, H., Sato, S., Nakazawa, K., Hon-nami, K., and Oshima, T., *J. Biol. Chem.* **255**, 345 (1980).
95. Armstrong, F. A., Butt, J. N., George, S. J., Hatchikian, E. C., and Thomson, A. J., *FEBS Lett.* **259**, 15 (1989).
96. Surerus, K. K., Kennedy, M. C., Beinert, H., and Münck, E., *Proc. Natl. Acad. Sci. U.S.A.* **86**, 9846 (1989).
97. Emptage, M. H., Kent, T. A., Huynh, B. H., Rawlings, J., Orme-Johnson, W. H., and Münck, E., *J. Biol. Chem.* **255**, 1793 (1980).

98. Huynh, B. H., Moura, J. J. G., Moura, I., Kent, T. A., LeGall, J., Xavier, A. V., and Münck, E. *J. Biol. Chem.* **255**, 3242 (1980).
99. Papaefthymiou, V., Girerd, J.-J., Moura, I., Moura, J. J. G., and Münck, E., *J. Am. Chem. Soc.* **109**, 4703 (1987).
100. Girerd, J.-J., Papaefthymiou, V., Surerus, K. K., and Münck, E., *Pure Appl. Chem.* **61**, 805 (1989).
101. Surerus, K. K., Münck, E., Moura, I., Moura, J. J. G., and LeGall, J., *J. Am. Chem. Soc.* **109**, 3805 (1987).
102. This statement excludes compounds containing the $M_3S_7 = [M_3(\eta^4-\mu_2-S_2)_3(\mu_3-S)]^{4+}$ unit, examples of which were known somewhat earlier [Lee, S. C., and Holm, R. H., *Angew. Chem., Int. Ed. Engl.* **29**, 840 (1990)].
103. Vergamini, P. J., Vahrenkamp, H., and Dahl, L. F., *J. Am. Chem. Soc.* **93**, 6327 (1971).
104. Beck, W., Danzer, W., and Thiel, G., *Angew. Chem., Int. Ed. Engl.* **12**, 582 (1973).
105. Müller, A., and Reinsch, U., *Angew. Chem., Int. Ed. Engl.* **19**, 72 (1980).
106. Müller, A., Jostes, R., and Cotton, F. A., *Angew. Chem., Int. Ed. Engl.* **19**, 875 (1980).
107. Cotton, F. A., Dori, Z., Llusar, R., and Schwotzer, W., *J. Am. Chem. Soc.* **107**, 6734 (1985).
108. Kathirgamanathan, P., Martinez, M., and Sykes, A. G., *J. Chem. Soc., Chem. Commun.* **953**, 1437 (1985).
109. Martinez, M., Ooi, B.-L., and Sykes, A. G., *J. Am. Chem. Soc.* **109**, 4615 (1987).
110. Akashi, H., Shibahara, T., and Kuroya, H., *Polyhedron* **9**, 1671 (1990).
111. Ooi, B.-L., and Sykes, A. G., *Inorg. Chem.* **28**, 3799 (1989).
112. Money, J. K., Huffman, J. C., and Christou, G., *Inorg. Chem.* **27**, 507 (1988).
113. Howlader, N. C., Haight, G. P., Jr., Hambley, T. W., Lawrance, G. A., Rahmoeller, K. M., and Snow, M. R., *Aust. J. Chem.* **36**, 377 (1983).
114. Cotton, F. A., Dori, Z., Llusar, R., and Schwotzer, W., *Inorg. Chem.* **25**, 3654 (1986).
115. Shibahara, T., and Kuroya, H., *Polyhedron* **5**, 357 (1986).
116. Cotton, F. A., Llusar, R., Marler, D. O., and Schwotzer, W., *Inorg. Chim. Acta* **102**, L25 (1985).
117. Wunderlich, H., *Acta Crystallogr., Sect. C: Cryst. Struct. Commun.* **C43**, 24 (1987).
118. Keck, H., Kuchen, W., and Mathow, J., *Z. Anorg. Allg. Chem.* **537**, 123 (1986).
119. Keck, H., Kuchen, W., Mathow, J., and Wunderlich, J., *Angew. Chem., Int. Ed. Engl.* **21**, 929 (1982).
120. Halbert, T. R., McGauley, K., Pan, W.-H., Czernuszewicz, R. S., and Stiefel, E. I., *J. Am. Chem. Soc.* **106**, 1849 (1984).
121. Cotton, F. A., and Llusar, R., *Polyhedron* **9**, 1741 (1987).
122. Cotton, F. A., Kibala, P. A., Matusz, M., McCaleb, C. S., and Sandor, R. B. W., *Inorg. Chem.* **28**, 2623 (1989).
123. Cotton, F. A., Llusar, R., and Eagle, C. T., *J. Am. Chem. Soc.* **111**, 4332 (1989).
124. Saito, T., Yamamoto, N., Yamagata, T., and Imoto, H., *Chem. Lett.*, 2025 (1987).
125. Lin, X., Lin, Y., Huang, J., and Huang, J., *Kexue Tongbao* **32**, 810 (1987).
126. Lu, S., Huang, J., Lin, Y., and Huang, J., *Jiegou Huaxue* **6**, 154 (1987).
127. Zheng, U., Zhu, N., Zhan, H., and Wu, X., *Acta Crystallogr., Sect. C: Cryst. Struct. Commun.* **C45**, 1632 (1989).
128. Fedin, V. P., Sokolov, M. N., Mironov, Yu. V., Kolesov, B. A., Tkachev, S. V., and Federov, V. Ye., *Inorg. Chim. Acta* **167**, 39 (1990).

129. Huang, J. Q., Huang, J. L., Shang, M. Y., Lu, S. F., Lin, X. T., Lin, Y. H., Huang, M. D., Zhuang, H. H., and Lu, J. X., *Pure Appl. Chem.* **60**, 1185 (1988).
130. Shibahara, T., Takeuchi, A., Ohtsuji, A., Kohda, K., and Kuroya, H., *Inorg. Chim. Acta* **127**, L45 (1987).
131. Nasreldin, M., Olatunji, A., Dimmock, P. W., and Sykes, A. G., *J. Chem. Soc., Dalton Trans.*, 1765 (1990).
132. Shibahara, T., Kohda, K., Ohtsuji, A., Yasuda, K., and Kuroya, H., *J. Am. Chem. Soc.* **108**, 2757 (1986).
133. Cotton, F. A., and Llusar, R., *Inorg. Chem.* **27**, 1303 (1988).
134. Shibahara, T., and Yamasaki, M., *Inorg. Chem.* **30**, 1687 (1991).
135. Fedin, V. P., Sokolov, M. N., Geras'ko, O. A., Sheer, M., Federov, V. Ye., Mironov, A. V., Slovokhotov, Yu. L., and Strutchkov, Yu. T., *Inorg. Chim. Acta* **165**, 25 (1989).
136. Zheng, Y., Zhan, H., and Wu, X., *Acta Crystallogr., Sect. C: Cryst. Struct. Commun.* **C45**, 1424 (1989).
137. Zhan, H., Zheng, Y., Wu, X., and Lu, J., *J. Cryst. Mol. Struct.* **196**, 241 (1989).
138. Shibahara, T., Hattori, H., and Kuroya, H., *J. Am. Chem. Soc.* **106**, 2710 (1984).
139. Shibahara, T., Miyake, H., Kobayashi, K., and Kuroya, H., *Chem. Lett.*, 139 (1986).
140. Dori, Z., Cotton, F. A., Llusar, R., and Schwotzer, W., *Polyhedron* **5**, 907 (1986).
141. Shibahara, T., Miyake, H., Kobayashi, K., and Kuroya, H., *Chem. Lett.*, 139 (1986).
142. Shibahara, T., Takeuchi, A., and Kuroya, H., *Inorg. Chim. Acta* **127**, L39 (1987).
143. Shibahara, T., Takeuchi, A., Nakajima, M., and Kuroya, H., *Inorg. Chim. Acta* **143**, 147 (1988).
144. Shibahara, T., Akashi, H., Nagahata, S., Hattori, H., and Kuroya, H., *Inorg. Chem.* **28**, 362 (1989).
145. Cotton, F. A., Diebold, M. P., Dori, Z., Llusar, R., and Schwotzer, W., *J. Am. Chem. Soc.* **107**, 6735 (1985).
146. Shibahara, T., Yamada, T., Kuroya, H., Hills, E. F., Kathirgamanathan, P., and Sykes, A. G., *Inorg. Chim. Acta* **113**, L19 (1986).
147. Akashi, H., Shibahara, T., Narahara, T., Tsuru, H., and Kuroya, H., *Chem. Lett.*, 129 (1989).
148. Ooi, B.-L., Sharp, C., and Sykes, A. G., *J. Am. Chem. Soc.* **111**, 125 (1989).
149. Shibahara, T., Kuroya, H., Matsumoto, K., and Ooi, S., *J. Am. Chem. Soc.* **106**, 789 (1984); Shibahara, T., Kuroya, H., Matsumoto, K., and Ooi, S., *Inorg. Chim. Acta* **116**, L25 (1986).
150. Dimmock, P. W., McGinnis, J., Ooi, B.-L., and Sykes, A. G., *Inorg. Chem.* **29**, 1085 (1990).
151. Christou, G., Sabat, M., Ibers, J. A., and Holm, R. H., *Inorg. Chem.* **21**, 3518 (1982).
152. Strasselt, H., Krebs, B., and Henkel, G., *Inorg. Chem.* **23**, 1816 (1984).
153. You, J.-F., Snyder, B. S., Papaefthymiou, G. C., and Holm, R. H., *J. Am. Chem. Soc.* **112**, 1067 (1990).
154. Chu, C. T.-W., and Dahl, L. F., *Inorg. Chem.* **16**, 3245 (1977).
155. Glidewell, C., Lambert, R. J., Harman, M. E., and Hursthouse, M. B., *J. Chem. Soc., Dalton Trans.*, 2685 (1990).
156. Müller, A., Schimanski, U., and Schimanski, J., *Inorg. Chim. Acta* **76**, L245 (1983).
157. Clegg, W., Garner, C. D., Nicholson, J. R., and Raithby, P. R., *Acta Crystallogr., Sect. C: Cryst. Struct. Commun.* **C39**, 1007 (1983).
158. Clegg, W., Scattergood, D., and Garner, C. D., *Acta Crystallogr., Sect. C: Cryst. Struct. Commun.* **C44**, 29 (1988).
159. Müller, A., Bögge, H., and Schimanski, U., *Inorg. Chim. Acta* **69**, 5 (1983).

160. Wolff, T. E., Berg, J. M., Warrick, C., Hodgson, K. O., Holm, R. H., and Frankel, R. B., *J. Am. Chem. Soc.* **100**, 4630 (1978).
161. Christou, G., Garner, C. D., and Mabbs, F. E., *Inorg. Chim. Acta* **28**, L189 (1978).
162. Christou, G., Garner, C. D., Mabbs, F. E., and King, T. J., *J. Chem. Soc., Chem. Commun.*, 740 (1978).
163. Holm, R. H., *Chem. Soc. Rev.* **10**, 455 (1981).
164. Averill, B. A., *Struct. Bonding* **53**, 59 (1983).
165. Holm, R. H., and Simhon, E. D., in "Molybdenum Enzymes" (T. G. Spiro, ed.), Chap. 2. Wiley (Interscience), New York, 1985.
166. Müller, A., Diemann, E., Jostes, R., and Bögge, H., *Angew. Chem., Int. Ed. Engl.* **20**, 934 (1981).
167. Müller, A., Krickemeyer, E., and Bögge, H., *Z. Anorg. Allg. Chem.* **554**, 61 (1987).
168. McDonald, J. W., Freisen, G. D., Rosenhein, L. D., and Newton, W. E., *Inorg. Chim. Acta* **72**, 205 (1983).
169. Zhang, Y., and Holm, R. H., *Inorg. Chem.* **27**, 3875 (1988).
170. Latroche, M., and Ibers, J. A., *Inorg. Chem.* **29**, 1503 (1990); and references therein.
171. Lee, S. C., and Holm, R. H., *J. Am. Chem. Soc.* **112**, 9654 (1990).
172. Klepp, K. O., and Bronger, W., *Z. Anorg. Allg. Chem.* **532**, 23 (1986).
173. Wolff, T. E., Berg, J. M., Hodgson, K. O., Frankel, R. B., and Holm, R. H., *J. Am. Chem. Soc.* **101**, 4140 (1979).
174. Wolff, T. E., Power, P. P., Frankel, R. B., and Holm, R. H., *J. Am. Chem. Soc.* **102**, 4694 (1980).
175. Christou, G., and Garner, C. D., *J. Chem. Soc., Dalton Trans.*, 2354 (1980).
176. Christou, G., Mascharak, P. K., Armstrong, W. H., Papaefthymiou, G. C., Frankel, R. B., and Holm, R. H., *J. Am. Chem. Soc.* **104**, 2820 (1982).
177. Zhang, Y., Bashkin, J. K., and Holm, R. H., *Inorg. Chem.* **26**, 694 (1987).
178. Kovacs, J. A., Bashkin, J. K., and Holm, R. H., *J. Am. Chem. Soc.* **107**, 1784 (1985); Kovacs, J. A., Bashkin, J. K., and Holm, R. H., *Polyhedron* **6**, 1445 (1987).
179. Anglin, R. J., Bonomi, F., and Kurtz, D. M., Jr. *Inorg. Chem.* **27**, 3434 (1988).
180. Liu, Q., Huang, L., Kang, B., Liu, C., Wang, L., and Lu, J., *Acta Chim. Sin.*, 107 (1986).
181. Liu, Q., Huang, L., Kang, B., Yang, Y., and Lu, J., *Kexue Tongbao* **32**, 898 (1987).
182. Lei, X., Huang, Z., Hong, M., Liu, Q., and Liu, H., *Jiegou Huaxue* **8**, 152 (1989).
183. Liu, Q., Huang, L., Liu, H., Lei, X., Wu, D., Kang, B., and Lu, J., *Inorg. Chem.* **29**, 4131 (1990).
184. Bose, K. S., Chmielewski, S. A., Eldredge, P. A., Sinn, E., and Averill, B. A., *J. Am. Chem. Soc.* **111**, 8953 (1989).
185. Eldredge, P. A., Bose, K. S., Barber, D. E., Bryan, R. F., Sinn, E., Rheingold, A., and Averill, B. A., *Inorg. Chem.* **30**, 2365 (1991).
186. Coucouvanis, D., Al-Ahmad, S., Salifoglou, A., Dunham, W. R., and Sands, R. H., *Angew. Chem., Int. Ed. Engl.* **27**, 1353 (1988).
187. Kovacs, J. A., and Holm, R. H., *J. Am. Chem. Soc.* **108**, 340 (1986).
188. Do, Y., Simhon, E. D., and Holm, R. H., *Inorg. Chem.* **24**, 4635 (1985).
189. Carney, M. J., Kovacs, J. K., Zhang, Y.-P., Papaefthymiou, G. C., Spartalian, K., Frankel, R. B., and Holm, R. H., *Inorg. Chem.* **26**, 719 (1987).
190. Kovacs, J. A., and Holm, R. H., *Inorg. Chem.* **26**, 702, 711 (1987).
191. Ciurli, S., Carney, M. J., Holm, R. H., and Papaefthymiou, G. C., *Inorg. Chem.* **28**, 2696 (1989).
192. Ciurli, S., Carrié, M., and Holm, R. H., *Inorg. Chem.* **29**, 3493 (1990).
193. Ciurli, S., and Holm, R. H., *Inorg. Chem.* **30**, 743 (1991).

194. Cook, M., and Karplus, M., *J. Chem. Phys.* **83**, 6344 (1985).
195. Ciurli, S., Yu, S.-B., Holm, R. H., Srivastava, K. K. P., and Münck, E., *J. Am. Chem. Soc.* **112**, 8169 (1990).
196. Gloux, J., Gloux, P., and Rius, P., *J. Am. Chem. Soc.* **108**, 3541 (1986).
197. Roth, E. K. H., Greneche, J. M., and Jordanov, J., *J. Chem. Soc., Chem. Commun.*, 105 (1991).
198. O'Sullivan, T., and Millar, M. M., *J. Am. Chem. Soc.* **107**, 4096 (1985).
199. Moura, I., Moura, J. J. G., Münck, E., Papaefthymiou, V., and LeGall, J., *J. Am. Chem. Soc.* **108**, 349 (1986).
200. Münck, E., Papaefthymiou, V., Surerus, K. K., and Girerd, J.-J., in "Metal Clusters in Proteins" (L. Que, Jr., ed.), ACS Symp. Ser. 372, Chap. 15. American Chemical Society, Washington, D.C., 1988.
201. Conover, R. C., Park, J.-B., Adams, M. W. W., and Johnson, M. K., *J. Am. Chem. Soc.* **112**, 4562 (1990).
202. Mascharak, P. K., Papaefthymiou, G. C., Armstrong, W. H., Foner, S., Frankel, R. B., and Holm, R. H., *Inorg. Chem.* **22**, 2851 (1983).
203. Christou, G., Garner, C. D., Miller, R. M., Johnson, C. E., and Rush, J. D., *J. Chem. Soc., Dalton Trans.*, 2363 (1980).
204. Ciurli, S., Ph.D. Thesis, Harvard University, Cambridge, Massachusetts (1990).
205. Liu, Q. T., Huang, L. R., Yang, Y., and Lu, J. X., *Kexue Tongbao* **33**, 1633 (1988).
206. Cramer, S. P., Hodgson, K. O., Gillum, W. O., and Mortenson, L. E., *J. Am. Chem. Soc.* **100**, 3398 (1978).
207. Cramer, S. P., Gillum, W. O., Hodgson, K. O., Mortenson, L. E., Stiefel, E. I., Chisnell, J. R., Brill, W. J., and Shah, V. K., *J. Am. Chem. Soc.* **100**, 3814 (1978).
208. Conradson, S. D., Burgess, B. K., Newton, W. E., Hodgson, K. O., McDonald, J. W., Robinson, J. F., Gheller, S. F., Mortenson, L. E., Adams, M. W. W., Mascharak, P. K., Armstrong, W. H., Holm, R. H., *J. Am. Chem. Soc.* **107**, 7935 (1985).
209. Wolff, T. E., Berg, J. M., and Holm, R. H., *Inorg. Chem.* **20**, 174 (1981).
210. Huang, L., and Lin, S., *Jiegou Huaxue* **3**, 25 (1984).
211. Burgess, B. K., *Chem. Rev.* **90**, 1377 (1990).
212. Eady, R. R., *Polyhedron* **8**, 1695 (1989); Eady, R. R., *Adv. Inorg. Chem.* **36**, 77 (1991).
213. Conradson, S. D., Burgess, B. K., Newton, W. E., Mortenson, L. E., and Hodgson, K. O., *J. Am. Chem. Soc.* **109**, 7507 (1987).
214. Arber, J. M., Dobson, B. R., Eady, R. R., Stevens, P., Hasnain, S. S., Garner, C. D., and Smith, B. E., *Nature (London)* **325**, 372 (1987).
215. Arber, J. M., Dobson, B. R., Eady, R. R., Hasnain, S. S., Garner, C. D., Matsushita, T., Nomura, M., and Smith, B. E., *Biochem. J.* **258**, 733 (1989).
216. George, G. N., Coyle, C. L., Hales, B. J., and Cramer, S. P., *J. Am. Chem. Soc.* **110**, 4057 (1988).
217. Palermo, R. E., and Holm, R. H., *J. Am. Chem. Soc.* **105**, 4310 (1983).
218. Flank, A. M., Weininger, M., Mortenson, L. E., and Cramer, S. P., *J. Am. Chem. Soc.* **108**, 1050 (1986).
219. Christou, G., Hagen, K. S., and Holm, R. H., *J. Am. Chem. Soc.* **104**, 1744 (1982).
220. Bolin, J. T., Ronco, A. E., Mortenson, L. E., Morgan, T. V., Williamson, M., and Xuong, N.-H., in "Nitrogen Fixation: Achievements and Objectives" (R. Gresshoff, J. Stacey, and W. E. Newton, eds.), Chapman & Hall, New York, 1990.
221. Coucouvanis, D., Challen, P. R., Koo, S.-M., Davis, W. M., Butler, W., and Dunham, W. R., *Inorg. Chem.* **28**, 4183 (1989).
222. Challen, P. R., Koo, S.-M., Kim, C. G., Dunham, W. R., and Coucouvanis, D., *J. Am. Chem. Soc.* **112**, 8606 (1990).

223. Coucouvanis, D., *Acc. Chem. Res.* **24**, 1 (1991).
224. Mascharak, P. K., Armstrong, W. H., Mizobe, Y., and Holm, R. H., *J. Am. Chem. Soc.* **105**, 475 (1983).
225. Shibahara, T., Akashi, H., and Kuroya, H., *J. Am. Chem. Soc.* **108**, 1342 (1986).
226. Dimmock, P. W., and Sykes, A. G., *J. Chem. Soc., Dalton Trans.*, 3101 (1990).
227. Shibahara, T., Yamasaki, M., Akashi, H., and Katayama, T., *Inorg. Chem.* **30**, 2693 (1991).
228. Dimmock, P. W., Lamprecht, G. J., and Sykes, A. G., *J. Chem. Soc., Dalton Trans.*, 955 (1991).
229. Akashi, H., and Shibahara, T., *Inorg. Chem.* **28**, 2906 (1989).
230. Shibahara, T., Yamamoto, T., Kanadani, H., and Kuroya, H., *J. Am. Chem. Soc.* **109**, 3495 (1987).
231. Shibahara, T., Akashi, H., Yamasaki, M., and Hashimoto, K., *Chem. Lett.*, 689 (1991).
232. Shibahara, T., Akashi, H., and Kuroya, H., *J. Am. Chem. Soc.* **110**, 3313 (1988).
233. Keck, H., Kruse, A., Kuchen, W., Mootz, D., Wiskemann, R., and Wunderlich, H., *Z. Naturforsch., B: Chem. Sci.* **45B**, 461 (1990).
234. Deeg, A., Keck, H., Kruse, A., Kuchen, W., and Wunderlich, H., *Z. Naturforsch., B: Chem. Sci.* **43B**, 1541 (1988).
235. Wu, X., Zheng, Y., Zhu, N., and Lu, J., *Jiegou Huaxue* **7**, 137 (1988).
236. Wu, X., Lu, S., Zu, L., Wu, Q., and Lu, J., *Inorg. Chim. Acta* **133**, 39 (1987).
237. Lu, S., Huang, J., Lin, Y., and Huang, J., *Huaxue Xuebao* **45**, 666 (1987).
238. Zhan, J., Zheng, Y., Wu, X., and Lu, J., *Jiegou Huaxue* **7**, 157 (1988).
239. Pasynskii, A. A., Eremenko, I. L., Orazsakhov, B., Kalinnikov, V. T., Aleksandrov, G. G., and Struchkov, Yu. T., *J. Organomet. Chem.* **216**, 211 (1981).
240. Eremenko, I. L., Pasynskii, A. A., Orazsakhov, B., Ellert, V. M., Novotortsev, V. M., Kalinnikov, V. T., Porai-Koshits, M. A., Antsyshkina, A. S., Dikareva, L. M., Ostrikova, V. N., Struchkov, Yu. T., and Gerr, R. G., *Inorg. Chim. Acta* **73**, 225 (1983).
241. Nefedov, S. E., Pasynskii, A. A., Eremenko, I. L., Stomakhina, E. E., Yanovsky, A. I., and Struchkov, Yu. T., *J. Organomet. Chem.* **405**, 287 (1991).
242. Pasynskii, A. A., Eremenko, I. L., Orazsakhov, B., Kalinnikov, V. T., Aleksandrov, G. G., and Struchkov, Yu. T., *J. Organomet. Chem.* **214**, 367 (1981).
243. Pasynskii, A. A., Eremenko, I. L., Katugin, A. S., Gasanov, G. Sh., Turchanova, E. A., Ellert, O. G., Struchkov, Yu. T., Shklover, V. E., Berberova, N. T., Sogomnova, A. G., and Okhlobystin, O. Yu., *J. Organomet. Chem.* **344**, 195 (1988).
244. Zhu, N., Zheng, Y., and Wu, X., *Inorg. Chem.* **29**, 2707 (1990).
245. Zhu, N., Wu, X., and Lu, J., *J. Chem. Soc., Chem. Commun.*, 235 (1991).
246. Sieker, L. C., Adman, E., and Jensen, L. H., *Nature (London)* **235**, 40 (1972).
247. Herskovitz, T., Averill, B. A., Holm, R. H., Ibers, J. A., Phillips, W. D., and Weiher, J. F., *Proc. Natl. Acad. Sci. U.S.A.* **69**, 2437 (1972).
248. Orme-Johnson, W. H., *Annu. Rev. Biophys. Biophys. Chem.* **14**, 419 (1985).
249. Harris, S., *Polyhedron* **8**, 2843 (1989).
250. Shibahara, T., Yamasaki, M., Sakane, G., Minami, K., Yabuki, T., and Ichimura, A., *Inorg. Chem.* **31**, 640 (1992).
251. Fedin, V. P., Sokolov, M. N., Geras'ko, O. A., Kolesov, B. A., Fedorov, V. Ye., Mironov, A. V., Yufit, D. S., Slovohotov, Yu. L., and Struchkov, Yu. T., *Inorg. Chim. Acta* **175**, 217 (1990).
252. Cotton, F. A., Kibala, P. A., and Miertschin, C. S., *Inorg. Chem.* **30**, 548 (1991).

- 253. Zheng, Y., Zhan, H., and Wu, X., *Acta Crystallogr., Sect. C: Cryst. Struct. Commun.* **C45**, 1424 (1989).
- 254. Shibahara, T., Hashimoto, K., Sakano, G. Abstract, Fifth International Conference on Bioinorganic Chemistry, Oxford, 1991; Shibahara, T., Hashimoto, K., and Sakano, G., *J. Inorg. Biochem.* **43**, 280 (1991).
- 255. Butt, J. N., Armstrong, F. A., Breton, J., George, S. J., Thomson, A. J., and Hatchikian, E. C., *J. Am. Chem. Soc.* **113**, 6663 (1991).
- 256. Butt, J. N., Sucheta, A., Armstrong, F. A., Breton, J., Thomson, A. J., and Hatchikian, E. C., *J. Am. Chem. Soc.* **113**, 8948 (1991).
- 257. Shibahara, T., *Adv. Inorg. Chem.* **37**, 143 (1991).

REPLACEMENT OF SULFUR BY SELENIUM IN IRON-SULFUR PROTEINS

JACQUES MEYER,* JEAN-MARC MOULIS,* JACQUES GAILLARD,† and
MARC LUTZ‡

* DBMS-Métalloprotéines, CENG 85X 38041 Grenoble, France

† DRFMC-SCPM, CENG 85X, 38041 Grenoble, France

‡ DBCM Biophysique des Protéines et des Membranes, CE-Saclay,
91191 Gif-sur-Yvette, France

- I. Introduction
- II. Selenium in Biology
 - A. Selenium: A Toxic though Essential Element
 - B. Selenium-Containing Biomolecules
 - C. Artificial Incorporation of Selenium into Proteins
 - D. Selenium as a Probe
- III. Preparation of Selenium-Substituted Iron-Sulfur Proteins
 - A. Historical Background
 - B. Preparation of Apoproteins
 - C. Assembly of Iron-Selenium Active Sites
 - D. Assembly of Iron-Tellurium Active Sites
- IV. Mechanisms of Iron-Sulfur Cluster Assembly *in Vitro* and *in Vivo*
- V. Biochemical Properties of Iron-Selenium Proteins
 - A. Stability
 - B. UV-Visible Absorption Spectra
 - C. Redox Potentials
 - D. Enzymatic Activity
- VI. Magnetic Properties of Iron-Selenium Clusters
 - A. [2Fe-2S(e)] Proteins
 - B. [4Fe-4S(e)] Proteins
 - C. [3Fe-4S(e)] Proteins
- VII. Ground Spin State Variability in [4Fe-4S(e)]⁺ Clusters
 - A. Clostridial 2[4Fe-4Se]⁺ Ferredoxins
 - B. Nitrogenase Iron Protein
 - C. Synthetic Analogs
 - D. Other Proteins
 - E. Room Temperature Data Obtained from Proton NMR
 - F. Significance of the Ground Spin State Variability
- VIII. Vibrational Spectroscopy of Iron-Selenium Clusters
 - A. [2Fe-2Se] Proteins
 - B. [4Fe-4Se] Proteins
- IX. Prospects
- References

I. Introduction

Selenium is a Group VIA element; it is in a bridging position in its column, lying between two nonmetals, oxygen and sulfur, and the increasingly metallic tellurium and polonium. In its period it lies between the metalloid arsenic and the halogen bromine. Se has six naturally occurring stable isotopes, ^{74}Se (0.87%), ^{76}Se (9.02%), ^{77}Se (7.58%), ^{78}Se (23.52%), ^{80}Se (49.82%), and ^{82}Se (9.19%), and several radioactive ones, including the γ emitter ^{75}Se ($t_{1/2} = 120$ days), which is widely used as a tracer. ^{77}Se has a nuclear spin ($I = \frac{1}{2}$) and is increasingly used in nuclear magnetic resonance (NMR) studies (1, 2).

By its chemical properties, selenium is most similar to sulfur, and occurs in the same valence states, -2 , 0 , $+2$, $+4$, and $+6$. However, the two elements display noteworthy differences relevant to the biochemistry of selenium. Selenium tends to be more stable than sulfur in its intermediate oxidation states, and less stable in the extreme ones. Accordingly, selenate and selenite are relatively easy to reduce to the element, and selenides are more reactive (reducing) than sulfides. Selenium is most often found in biological systems in compounds such as selenols, diselenides, and selenoethers, which are usually more reactive than their sulfur counterparts, because of the greater polarity and lower strength of the C-Se, N-Se and O-Se bonds. Selenols are more acidic (usually ionized at neutral pH), are better nucleophiles, better leaving groups, and are more reducing than the corresponding thiols (1, 2).

The average concentration of selenium is ~ 0.1 ppm in the earth's crust, and three orders of magnitude lower in the oceans (3, 4). The biogeochemical cycle of selenium is similar to, but not coincident with, that of sulfur (3, 4). Selenium is used in electronics and metallurgy; in the glass and ceramics industry; in rubber, pigment, and explosive manufacture; and in some pharmaceuticals (reviewed in Ref. 2).

II. Selenium in Biology

A. SELENIUM: A TOXIC THOUGH ESSENTIAL ELEMENT

Fatal horse and cattle diseases known as "blind staggers" and "alkali disease" were described in the Dakota Territory and neighboring states and territories in the 1850s, and were ascribed to selenium poisoning some 80 years later. Based on his description of 1295, Marco Polo came across similar diseases in his travels to China. Selenium has also been

labeled as carcinogenic, thus increasing the general feeling that it is a highly toxic and undesirable element (5). The subsequent demonstration of its essentiality (6), of human diseases associated with selenium deficiency (7), and of the presence of selenium in a number of biomolecules (8) has failed to reverse the mostly negative image of this element.

B. SELENIUM-CONTAINING BIOMOLECULES

Unlike animals, plants do not seem to require selenium and are less sensitive to the toxic effects of this element. In fact, some species of plants growing on selenium-rich soils accumulate considerable amounts (up to 0.5% of their dry weight) of this chalcogenide. In these plants selenium is stored in compounds that are metabolic dead ends, and is thus prevented from poisoning important processes (9).

Several enzymes have been demonstrated to contain selenium in the form of selenocysteine: formate dehydrogenases from *Escherichia coli*, glycine reductase from amino acid-fermenting clostridia, hydrogenases from *Methanococcus vannielii* and from *Desulfovibrio baculatus*, and mammalian glutathione peroxidase (8). Recent additions to this list are type I iodothyronine 5'-deiodinase from rat thyroid (10, 11) and a rat selenoprotein containing 10 UGA-encoded selenocysteines (12). Major advances have recently been made toward elucidation of the molecular mechanism by which selenocysteine incorporation takes place (8). This amino acid is encoded by UGA in all cases investigated so far (8, 13, 14). Selenocysteinyl-tRNA is formed by phosphorylation and subsequent selenylation of serine bound to a specific suppressor seryl-tRNA. Four genes, whose products are required for the incorporation of selenocysteine into proteins, have been identified in *E. coli*. These findings truly establish selenocysteine as the twenty-first amino acid (8).

A number of other selenoproteins, in which the status of selenium is still uncertain, have been reported. In most of these, neither the chemical form nor the specificity of selenium incorporation has been established (15). In the case of the thiolase from *Clostridium kluyveri*, selenomethionine is incorporated cotranslationally into the enzyme, in competition with methionine (8).

Selenium specifically occurs in tRNAs of some bacteria, plant cells, and mammalian cell lines. Bacterial seleno-tRNAs having glutamate- or lysine-accepting specificity contain 5-methylaminomethyl-2-selenouridine in the wobble position of the anticodons. The incorporation of selenium takes place by an ATP-dependent replacement of the sulfur atom of the corresponding thionucleoside (8).

In view of the numerous specific and well-characterized occurrences

of selenium in biomolecules, the essentiality of this element is obvious. Other possible beneficial effects of selenium are its working as an antioxidant or as a complexing agent of toxic heavy metals (7). In contrast, the well-known toxicity of selenium is less straightforwardly explained on a molecular basis. In fact, the replacement of sulfur by selenium is known to have little bearing on some coenzymes (16), and on the activity of the β -galactokinase from *E. coli* when substitution occurs on the methionine residues (17). The cysteine residues of proteins are a more critical target for selenium substitution, as they become more reactive and less stable. The toxic effect of selenium, which is often ingested as selenite, can also be exerted by the oxidative properties of the latter compound toward thiols: formation of disulfides or selenotrisulfides may result in the blocking of functionally essential cysteine residues (4, 18, 19).

C. ARTIFICIAL INCORPORATION OF SELENIUM INTO PROTEINS

As outlined above, selenium occurs in various biomolecules as a substitute for sulfur for the fulfillment of particular functions. Following this rationale, attempts have been made to artificially incorporate selenium into specific sites of proteins in order to modify their properties: the targets of these modifications have been cysteine or methionine residues, and the inorganic sulfur atoms of iron-sulfur proteins.

Selenocysteine has been introduced into the protease subtilisin by chemical modification of serine 221. The latter reaction was carried out by activating the hydroxyl group of the target residue with phenylmethylsulfonyl fluoride and subsequently treating the sulfonylated enzyme with a large excess of hydrogen selenide (20). Interestingly, the modification converted subtilisin into an acyltransferase with selectivity properties suitable for a peptide ligase (20), and into a glutathione peroxidase mimic (20a). A different approach, namely chemical synthesis of the whole polypeptide, was used to prepare several selenium analogs of small peptides or proteins, namely glutathione, oxytocin (21), somatostatin (22), and metallothionein (23). In the latter case, the substitution was aimed at obtaining structural information on the copper-chalcogenide cluster present in the protein.

Quantitative substitutions of methionine by selenomethionine in the copper protein azurin (24) and in ribonuclease H (25) were performed by growing methionine auxotrophic strains on selenomethionine.

Replacement of sulfide by selenide in the inorganic cores of iron-sulfur proteins will be treated in detail in the main body of this

review (see Table I for a summary on artificial replacement of sulfur by selenium in peptides and proteins).

D. SELENIUM AS A PROBE

As was discussed previously, the chemical properties of selenium are sufficiently similar to those of sulfur to allow replacement of the latter by the former in many biomolecules. However, the two elements differ significantly from each other by some of their physical characteristics, and for several methods of investigation selenium has proved to be a more efficient probe than sulfur.

The two chalcogens differ considerably in their atomic mass number A , selenium ($A = 79$) being more than twice as heavy as sulfur ($A = 32$). Accordingly, the replacement of S by Se is expected to considerably modify the vibrational properties of the substituted molecule. These selenium-induced changes have been instrumental in the analysis of resonance Raman spectra of iron-sulfur proteins (Section VIII).

Furthermore, the atomic mass of selenium qualifies it as a target for techniques that are impossible or difficult to perform with sulfur. In particular, selenium can be used as the absorbing atom for X-ray absorption spectroscopy; measurements on iron-selenium synthetic compounds have demonstrated the feasibility of the method (26), and recently it has been used to show that the coordination sphere of selenium in a hydrogenase from *D. baculatus* includes nickel and carbon (27). Selenium has also been used as an anomalous scatterer for phasing the X-ray diffraction data of ribonuclease H (28).

Another advantage of selenium is its possessing an isotope (^{77}Se) with nuclear spin $S = \frac{1}{2}$. When selenium atoms are involved in or near a paramagnetic center, enrichment with ^{77}Se results in electron paramagnetic resonance (EPR) spectra displaying hyperfine structures that can be resolved in some cases. This property has been implemented for several iron-sulfur proteins (Sections VI and VII), and has recently been used to confirm the involvement of selenocysteine in the nickel-containing active site of a hydrogenase from *D. baculatus* (29). Moreover, electron-nuclear double resonance (ENDOR) should in principle be possible with ^{77}Se , although no success has yet been reported. Finally, a probably even more promising application of ^{77}Se is its use in NMR: it provides adequate sensitivity (7×10^{-3} and 3 with respect to the proton and to ^{13}C , respectively) and a very wide chemical shift range (3000 ppm) (2). A considerable body of ^{77}Se NMR data has been gathered on a variety of synthetic compounds (2). The feasibility of NMR studies on selenium covalently or noncovalently attached to proteins

TABLE I

ARTIFICIAL INCORPORATION OF SELENIUM INTO PEPTIDES AND PROTEINS

	Peptide or protein	Number of amino acids	Function	Site of selenium incorporation	Method	Reported results	Ref.
78	Subtilisin (<i>Bacillus subtilis</i>)	275	Protease	Conversion of Ser 221 into SeCys	Chemical modification	Conversion of enzyme into an acyltransferase and into a glutathione peroxidase mimic	20, 20a
	Oxytocin	9	Hypophyseal hormone	Replacement of Cys 1 or Cys 6 by SeCys	Chemical synthesis	Subtle modifications of biological activity	21
	Somatostatin	14	Inhibition of insulin secretion	Replacement of Cys 3 and Cys 14 by SeCys	Chemical synthesis	Functionally similar to native peptide	22
	Metallothionein (<i>Neurospora crassa</i>)	25	Metal accumulation	Replacement of the seven Cys residues by SeCys	Chemical synthesis	UV-vis, CD, fluorescence	23
	Azurin (<i>Pseudomonas aerogenes</i>)	128	Electron transfer	Replacement of the six methionine residues by SeMet	Growth of a methionine auxotroph on Se-methionine	Reduction potential, EPR, UV-vis spectra	24
	Ribonuclease H (<i>E. coli</i>)	155	Degradation of RNA on DNA:RNA hybrids	Replacement of the four Met residues by SeMet	Growth of a methionine auxotroph on Se-methionine	Phasing of X-ray diffraction data	25, 28

Putidaredoxin (<i>Pseudomonas putida</i>)	106	Electron transfer in camphor oxidation	Inorganic sulfur atoms of [2Fe-2S] cluster	<i>In vitro</i> removal and reconstitution of Fe-Se cluster	Reduction potential, activity, UV-vis, EPR, Mössbauer	35, 36, 81, 94, 96
Adrenodoxin (beef adrenal glands)	114	Electron transfer in hormone hydrox- ylation	Inorganic sulfur atoms of [2Fe-2S] cluster	<i>In vitro</i> removal of native Fe-S and reconstitution of Fe-Se cluster	Reduction potential, activity, UV-vis, EPR, ENDOR, resonance Raman	36, 38, 67, 82, 95, 96, 147
Parsley ferredoxin	96	Electron transfer in photosynthesis	Inorganic sulfur atoms of [2Fe-2S] cluster	<i>In vitro</i> removal of native Fe-S and reconstitution of Fe-Se cluster	Reduction potential, UV-vis, CD, EPR	37, 57, 96
Spinach ferredoxin	97	Electron transfer in photosynthesis	Inorganic sulfur atoms of [2Fe-2S] cluster	<i>In vitro</i> removal of native Fe-S and reconstitution of Fe-Se cluster	UV-vis, resonance Raman	48, 154
Clostridial ferredoxins (<i>C. pasteurianum</i> and two other species)	55	Electron transfer in anaerobic metabolism	Inorganic sulfur atoms of [4Fe-4S] clusters	<i>In vitro</i> removal of native Fe-S and reconstitution of Fe-Se cluster	Reduction potential, activity, UV-vis, EPR, Mössbauer, MCD, resonance Raman, ¹ H NMR	39, 43, 49, 58, 59, 98-101, 153
HiPIP (<i>Chromatium vinosum</i>)	85	Unknown	Inorganic sulfur atoms of [4Fe-4S] cluster	<i>In vitro</i> removal of native Fe-S and reconstitution of Fe-Se cluster	Reduction potential, UV-vis, EPR, resonance Raman, ¹ H NMR	40, 103
Aconitase (beef heart mitochondria)	755	Isomerization of citrate	Inorganic sulfur atoms of [4Fe-4S] or of [3Fe-4S] cluster	<i>In vitro</i> removal of native Fe-S and reconstitution of Fe-Se cluster	Activity, EPR, Mössbauer	41

has been demonstrated (30) and recently confirmed with glutathione peroxidase containing ^{77}Se -enriched selenocysteine (31).

III. Preparation of Selenium-Substituted Iron-Sulfur Proteins

A. HISTORICAL BACKGROUND

Soon after the discovery of ferredoxins (32, 33), it was shown that their active sites could be destroyed by acid and reconstituted *in vitro* (34, 34a). Several investigations were then carried out with selenide as a substitute for sulfide. The first studies were performed with the [2Fe-2S] proteins putidaredoxin (35), adrenodoxin (36), and parsley ferredoxin (37). A cobalt-selenium cluster has also been assembled in adrenodoxin (38). Successful substitutions have since been reported for [4Fe-4S] proteins: *Clostridium pasteurianum* ferredoxin (39), *Chromatium vinosum* high-potential ferredoxin (HiPIP) (40), and beef heart aconitase (41).

It had been observed early on that active site sulfide of *C. pasteurianum* ferredoxin could exchange with free sulfide at alkaline pH in the presence of urea, without complete denaturation of the protein (42). A similar exchange reaction with free selenide was later found in the same protein (43). It has also been demonstrated that iron and chalcogenide atoms are shuffled among synthetic analog molecules in solution (44). These reactions result in a random distribution of the chalcogenides in the metal clusters, and therefore cannot be used for the preparation of homogeneous selenium-substituted proteins. All such substitutions have so far invariably involved two steps: first, complete removal of the inorganic core of the active site, and then assembly of a new active site into the apoprotein.

B. PREPARATION OF APOPROTEINS

For the preparation of a totally substituted protein in good yield, a prerequisite is the isolation of apoprotein completely devoid of iron and inorganic sulfur. When the conditions of iron-sulfur removal are not carefully controlled, zero-valent sulfur (mainly present as trisulfide bridges involving cysteine residues) remains attached to the apoprotein (45) and is subsequently reincorporated into the active site during the reconstitution reaction, together with the added chalcogenide. The resulting contamination is a serious problem when sulfur isotopes or

selenide are wanted in the active site (Section VIII). Although sulfur (0) can be removed from the apoprotein (45, 46), it is more convenient to set up conditions that yield S(0)-free apoprotein during the denaturation reaction.

1. Acid Denaturation

From our experience with several types of ferredoxins, we have deduced an experimental procedure applicable to most such proteins. The ferredoxin solution has to be brought to a concentration not exceeding 1 mg/ml and kept at $\sim 0^{\circ}\text{C}$ under a flow of inert gas prior to the addition of acid. During and after the addition of acid, stirring and inert gas flow should not be interrupted, thus allowing inorganic sulfur to escape as H_2S before it is oxidized. The reaction time is 30–60 min. Optimal conditions for the acid treatment are not the same for all proteins, and are therefore outlined below.

The preparation of apoproteins from plant [2Fe–2S] ferredoxins (37, 47) has been reexamined in detail (48), and the use of HCl (0.5–1 *M*) has been found to be essential for the isolation of clean apoprotein; trichloroacetic acid, which is often used in order to obtain other apoferreredoxins, is not suitable here.

Sulfide-free apoproteins are usually easier to obtain with [4Fe–4S] than with [2Fe–2S] ferredoxins. The experimental conditions used for *C. pasteurianum* ferredoxin (43), namely treatment with 0.5 *M* trichloroacetic acid, can be extended to other ferredoxins of this family (49).

The isolation of apoproteins of high-potential [4Fe–4S] ferredoxins has proved more difficult than for the low-potential ones, most probably because of the larger size of the proteins and the limited accessibility of the cluster to reactants; complete removal of the inorganic core requires all the reactants to be kept in solution. This is achieved by bringing the protein solution to 5 *M* in guanidinium chloride before adding HCl to a final concentration of 0.5 *M*. After neutralization and dialysis, the apoprotein is precipitated with 0.5 *M* trichloroacetic acid (40).

2. Other Methods

For iron–sulfur proteins significantly larger than ferredoxins ($M_r > 20,000$), the treatment with acid often yields irreversibly denatured apoprotein. A possible way out, which has only been implemented with ferredoxins (34a), would be to dissolve the precipitated protein in a chaotropic solvent (5–7 *M* guanidinium chloride, for instance), carry

out the reconstitution reaction in this solvent, and slowly eliminate guanidine by dialysis in oxygen-free conditions.

A different procedure, which has been used in the case of aconitase, consists in avoiding the acid denaturation altogether. The enzyme was treated with EDTA and ferricyanide until the chromophore was completely lost, and the apoprotein was subsequently separated from the other reactants by gel filtration (50).

Another possibility has been opened by the development of extrusion reactions (51) and by the separation of apoproteins from these reaction mixtures (52). However, the method is limited by the poor solubility of many of the larger iron-sulfur proteins in the mixed aqueous-organic solvents used for the extrusion reactions (51, 53). Thus, for proteins other than ferredoxins, the preparation of reversibly denatured apoproteins remains to be worked out in each particular case.

C. ASSEMBLY OF IRON-SELENIUM ACTIVE SITES

The incorporation of iron-selenide active sites has been carried out by very similar procedures in all proteins, under experimental conditions based on those described for iron-sulfide clusters (34). Minor adjustments have been made in the pH and stoichiometry of the reagents (43, 48). The only difficulty arises from the low stability of selenide, as compared with sulfide: whereas the latter can be added as a commercial reagent (sodium sulfide, for example), selenide has to be prepared *in situ*.

Several ways of producing selenide have been elaborated: elemental selenium can be reduced by heating in a hydrogen atmosphere (54), by aluminum powder in aqueous ammonia (55), or by borohydride (56). An alternative consists in the straightforward reduction of selenite by thiols (18, 19). The latter procedure is convenient and is used most often (37, 39, 40, 48). We have observed that allowing selenite to react with the thiol (dithiothreitol is more effective than 2-mercaptoethanol) before adding the apoprotein resulted in higher yields (48) than adding selenite to the thiol-apoprotein mixture (37).

Stable selenium isotopes are often available only in the elemental state. They may be either first converted into selenite with nitric acid and then allowed to react with thiols (37), or reduced directly to selenide. The latter reaction was carried out with aluminum (55) in early studies (35, 36), but heating in a hydrogen atmosphere (54) has subsequently been preferred (36, 48, 57, 58). The same procedure has been implemented to reduce elemental sulfur to sulfide (48, 58). With both

chalcogenides, the best reconstitution yields have been obtained when the hydrogen-chalcogen reaction products were solubilized with a stoichiometric amount of dithiothreitol solution prior to the injection of the protein (48, 58).

Following the assembly of the Fe-S or Fe-Se active sites, a combination of anion-exchange chromatography (on DE-52 cellulose) and gel filtration (on Sephadex G-25) removes the excesses of inorganic reactants and of apoprotein (48, 58).

D. ASSEMBLY OF IRON-TELLURIUM ACTIVE SITES

Because tellurium follows sulfur and selenium in the VIA group, one may expect it to be a potential substitute for these elements in iron-sulfur proteins, despite its increased metallic character. Following the successful incorporation of selenium, we attempted to prepare $2[4\text{Fe}-4\text{Te}]$ *C. pasteurianum* ferredoxin (59). A number of means were used to prepare telluride: reduction of tellurite with dithiothreitol and reduction of elemental tellurium with borohydride, with heated dihydrogen, or with sodium in liquid ammonia (60). No chromophore-containing protein could be isolated, either due to the lack of active site assembly or to the instability of the product. At that time, only one synthetic $[4\text{Fe}-4\text{Te}]$ -containing compound ($\text{Cs}_7\text{Fe}_4\text{Te}_8$) had been synthesized in the solid state at a high (1050 K) temperature (61), and nothing was known about the stability of these species in solution. Incorporation of iron-tellurium clusters into bovine serum albumin had been claimed previously, but the experimental support was not compelling (62). Later, $[4\text{Fe}-4\text{Te}]$ clusters with tellurolate (63, 63a) or thiolate (64) ligands were synthesized in solution, and the possibility of assembling such sites in proteins might be reevaluated. In any case, a low stability of the tellurated ferredoxin is to be expected, due to the high reactivity of telluride and to the larger size of the $[4\text{Fe}-4\text{Te}]$ core (63a, 64), as compared to the native one. The decrease in active site stability observed upon Se/S substitution (43) is likely to be even larger upon Te substitution. In addition, all $[4\text{Fe}-4\text{Te}]$ synthetic clusters reported so far have been isolated in the $[4\text{Fe}-4\text{Te}]^+$ oxidation state (61, 63, 64), and no evidence for reversible redox behavior has been provided. Extrapolation of these features to the active sites of proteins would constitute an additional destabilizing factor. Nevertheless, in view of the results obtained with the selenium-substituted ferredoxin, efforts aimed at the preparation of the tellurium analog would probably be rewarding.

IV. Mechanisms of Iron–Sulfur Cluster Assembly *in Vitro* and *in Vivo*

The mechanisms of metallocenter biosynthesis are currently under intense scrutiny (65). In comparison with other electron transfer proteins, cytochromes being a case in point, ferredoxins are remarkable in that their prosthetic groups do not, in principle, require complicated enzyme-catalyzed pathways for their biosynthesis. This property, together with particular features in their sequences, has led to the still widely accepted proposal that ferredoxins are probably the most primitive electron transfer proteins (66). The observation that the active sites of [4Fe–4S] ferredoxins assemble spontaneously when the reduced apoprotein is reacted with iron and sulfide (34) has been confirmed in numerous instances with many different ferredoxins, using selenide as well as sulfur (Section III,C). In addition, a given polypeptide chain strongly directs assembly toward its indigenous active site: attempts to incorporate alien centers into iron–sulfur apoproteins have only yielded very unstable products (67, 68). These data have suggested that, in ferredoxins at least, iron–sulfur centers might assemble *in vivo* by nonenzymatic reactions (48, 66).

The physiological significance of *in vitro* reconstitution reactions has been questioned upon finding that rhodanese would facilitate the assembly of [2Fe–2S] and [4Fe–4S] clusters in plant and *C. pasteurianum* ferredoxins, respectively (69, 70). However, the absence of rhodanese activity in *C. pasteurianum* appears to forbid any function of this enzyme in iron–sulfur cluster synthesis (71). Concerning plant ferredoxin, the improvement afforded by rhodanese was most likely due to the use of apoferredoxin containing significant amounts of sulfide, as witnessed by its UV-visible absorption in the 300- to 400-nm region (69). In our hands, the implementation of apoferredoxin deprived of any inorganic material allowed reconstitution reactions (48) at least as satisfactory as those reported with rhodanese (69).

A breakthrough in the understanding of iron–sulfur cluster assembly *in vivo* was apparently achieved with the discovery that chloroplasts contain an enzymatic activity allowing the use of cysteine sulfur as a source of sulfide for the [2Fe–2S] cluster of ferredoxin (72). More recently, however, the same group has reported that no more than a few percent of the labeled sulfide entered the ferredoxin [2Fe–2S] cluster, and that this incorporation was inhibited by the addition of nonradioactive sulfide (73). They have nevertheless found the Fe–S cluster formation to be ATP dependent, which might suggest an enzymatic process (73). In the present state of knowledge, no strong experimental evidence allows the rejection of a nonenzymatic process for the *in vivo* assembly of

at least some of the ferredoxin active sites: the main unsolved problem is the provision of sulfide (presumably in low concentrations) in the vicinity of the nascent or freshly synthesized polypeptide.

In the case of larger iron-sulfur proteins, which often contain more elaborate active sites than the ferredoxin ones, the involvement of ancillary proteins for the production of active enzymes is well established. One of the best known cases is nitrogenase, which catalyzes the reduction of dinitrogen to ammonia at the expense of ATP, and comprises two proteins, the Fe protein and the Mo-Fe (or V-Fe in some cases) protein (74). The molybdenum-iron cofactor of the Mo-Fe protein requires several proteins for its synthesis. The Fe protein, which contains a [4Fe-4S] cluster, also requires an additional protein (NifM) for its conversion into an active state, but it is not known whether NifM participates directly in the formation of the iron-sulfur cluster (74). Indirect evidence for enzymatic assembly of an Fe-S cluster has also been produced for the iron-only hydrogenase from *Desulfovibrio vulgaris*; upon expression in *E. coli*, this protein possesses its full complement of [4Fe-4S] clusters, but lacks its putative hydrogen-activating site, an iron-sulfur cluster of unknown structure. The latter can therefore be assumed to require for its biosynthesis an enzymatic system proper to the organisms producing this kind of enzyme (75).

Some proteins appear to stand on the borderline between those that can be reconstituted *in vitro* (most ferredoxins and aconitase; Section III,C) and those that definitely require additional enzymes for their conversion into active species (preceding paragraph). A case in point is the [2Fe-2S] ferredoxin from *C. pasteurianum* (76), which, upon reconstitution, yields a brown protein (the native one is red) having UV-visible (Fig. 1) and resonance Raman (Fig. 2) spectra different from those of the native one. The reconstituted protein does contain a conventional [2Fe-2S] cluster, but its iron content is twice as high as that of the native protein, in line with its larger absorbance in the UV-visible region (Fig. 1). Additional iron is thus present in other structures, the instability of which has so far impeded their full characterization (J. Meyer, J.-M. Moulis, J. Gaillard, and M. Lutz, unpublished results, 1984). Considering that the protein contains, in addition to the four cysteine ligands of the [2Fe-2S] cluster, one cysteine and three histidine residues, an additional cluster is possibly assembled during the reconstitution process, provided these potential ligands are appropriately positioned in the three-dimensional space. This, however, does not imply the operation *in vivo* of an enzymatic system for cluster assembly: the difference between the native and the reconstituted ferredoxin may result from different folding mechanisms occurring *in vivo* and *in vitro*.

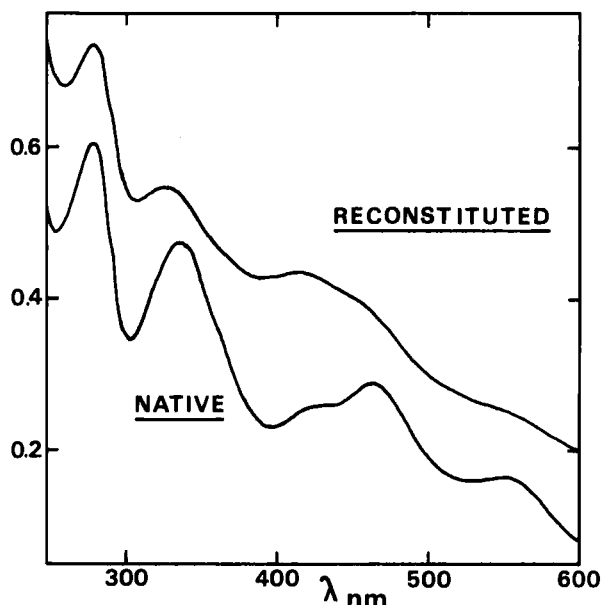


FIG. 1. UV-visible absorption spectra of native and reconstituted [2Fe-2S] *C. pasteurianum* ferredoxin. The native protein was purified as described (76). The reconstituted protein was prepared by the method (48) worked out for spinach ferredoxin. The path length was 1 mm and the protein concentrations were 7 mg/ml for the native one and 5 mg/ml for the reconstituted one. The difference spectrum (not shown) displays maxima at 300, 400, and 510 nm.

V. Biochemical Properties of Iron-Selenium Proteins

A. STABILITY

Selenium-substituted ferredoxins have consistently been found to be less stable than their native counterparts (36, 37, 43), in line with the intrinsically lower stability of the synthetic [4Fe-4Se] clusters, as compared to the [4Fe-4S] ones (77). A possible additional factor of instability in proteins is the larger size (77, 77a) of the [4Fe-4Se] cluster, which may therefore be less efficiently accommodated and protected by the polypeptide (43). We have measured the kinetics of solvolysis (78) of [4Fe-4S] and [4Fe-4Se] clusters in *C. pasteurianum* ferredoxin under oxygen-free conditions. The native protein was found not only to be more stable at neutral pH, but also to be stable over a much broader pH range than the selenium-substituted one (43). In addition, the selenium-substituted ferredoxins are more sensitive to oxidative

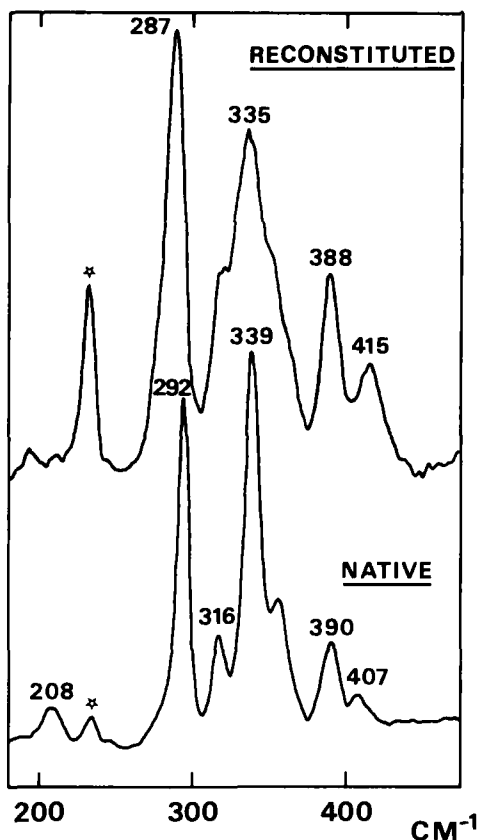


FIG. 2. Resonance Raman (RR) spectra, obtained with a 457.9-nm excitation wavelength, of native and of reconstituted [2Fe-2S] *C. pasteurianum* ferredoxin. The protein samples, which were those used in Fig. 1, were processed for RR data collection as described (48, 153). Other experimental conditions have been detailed elsewhere (148, 153). The starred bands at $\sim 230 \text{ cm}^{-1}$ arise from the Raman scattering of ice.

denaturation than the native ones (43), and should therefore systematically be handled under inert atmosphere.

B. UV-VISIBLE ABSORPTION SPECTRA

Replacement of sulfur by selenium in otherwise identical complexes has the general effect of decreasing ligand \rightarrow metal charge transfer energy (77, 77a). Indeed, in selenium-substituted [2Fe-2S] proteins, the absorption bands at ~ 420 and 460 nm undergo red shifts of ~ 20

nm. In contrast, the ~ 330 -nm band remains unchanged, which suggests that it arises mainly from (Cys)S \rightarrow Fe charge transfer (35, 36, 37, 48). Similar shifts have been reported for synthetic analogs of binuclear active sites (77a, 79).

In [4Fe-4S] proteins the bathochromic shifts of the broad absorption bands at ~ 300 and 400 nm upon selenium substitution are hardly detectable (43) or are ill-defined (40). The main cause of this small effect is that these transitions involve overlapping S(e)* \rightarrow Fe and (cys)S \rightarrow Fe charge transfers. Similar observations have been reported for synthetic water-soluble clusters having aliphatic thiolate ligands (43). Well-characterized red shifts have only been observed in [4Fe-4S(e)] clusters having aromatic ligands: in this case, the shifts were larger when the substitution was carried out on the terminal organic ligands (20 nm) than when carried out on the bridging inorganic ones (8–13 nm) (77, 80), as expected for clusters having predominantly RS \rightarrow Fe transitions near their visible absorption maxima at ~ 450 nm (58).

C. REDOX POTENTIALS

The replacement of sulfur by selenium in homologous coordination complexes most often results in positive reduction potential shifts (77, 77a). The same holds true for synthetic analogs of [2Fe-2S] (79) and [4Fe-4S] active sites (77), with positive shifts in the 0- to 60-mV range. In proteins, the reduction potential shifts have similar magnitudes, but are more variable in sign: shifts of +38 mV (parsley ferredoxin) (Ref. 57), -10 mV (putidaredoxin) (Ref. 81), and -14 mV (adrenodoxin) (Ref. 82) have been reported for [2Fe-2S] proteins, and shifts of +6 mV (*C. pasteurianum* ferredoxin) (Ref. 43) and -65 mV (*C. vinosum* HiPIP) (Ref. 40) have been reported for [4Fe-4S] proteins. These apparent inconsistencies may arise in part from the lack of accuracy of the measurements, but the effect of the polypeptide chain, which is different in each case, probably plays a role as well. It should be kept in mind that the [4Fe-4S]^{2+/+} active sites, for example, cover an ~ 300 -mV range of reduction potentials, depending on the protein in which they are accommodated (83). A number of parameters, including solvent accessibility and networks of hydrogen bonds surrounding the active sites, are likely contributors to the adjustment of the redox properties of the iron-sulfur clusters in proteins. The balance between these effects remains ill-defined and is likely to vary from one protein to another. For instance, the hydrogen bonds involving chalcogenide atoms proba-

bly differ in various proteins, but are also likely to be modified in different ways upon Se/S substitution.

D. ENZYMATIC ACTIVITY

The only true iron-sulfur enzyme in which sulfide has been replaced by selenide is aconitase. Its activity with isocitrate as the substrate is enhanced upon selenium substitution (41). In ferredoxins of known function, the selenium-substituted proteins are only marginally different from their native counterparts in their ability to exchange electrons with their redox partners (35-37, 43). In the case of the electron transfer from the $2[4\text{Fe}-4\text{S}(\text{e})]$ ferredoxin to hydrogenase I from *C. pasteuriana*, the selenium-substituted ferredoxin has a lower maximum velocity and a lower K_m than its native counterpart (43).

VI. Magnetic Properties of Iron-Selenium Clusters

Ferredoxins and other iron-sulfur proteins containing simple clusters are characterized, in their paramagnetic states, by a fast-relaxing EPR signal observed at low temperatures (usually between 4 and 100 K) in the $g = 2$ region. This property led to the discovery of these proteins (84) and to the deduction of the essential structural elements of the $[2\text{Fe}-2\text{S}]$ site (85, 86). Besides EPR, the techniques used most often for monitoring the magnetic properties of iron-sulfur clusters are Mössbauer spectroscopy (87) and magnetic circular dichroism (MCD) (88). A unique position is held by ^1H NMR, which can use the protons neighboring the metal centers as probes of their magnetic state in liquid solution (89).

A. $[2\text{Fe}-2\text{S}(\text{e})]$ PROTEINS

In the $[2\text{Fe}-2\text{S}(\text{e})]^{2+}$ redox level, these proteins are diamagnetic due to the strong antiferromagnetic coupling between the two $\text{Fe}(\text{III})$ ions. Upon reduction, the added electron is localized on one of the iron atoms, and the ground spin state of the antiferromagnetically coupled system has invariably been found to be $S = \frac{1}{2}$ (90, 91), even in those cases in which partial nonsulfur ligation is believed to occur (92).

The replacement of sulfide by selenide in adrenodoxin has allowed an unequivocal demonstration that two inorganic chalcogenide atoms are involved in the binuclear iron-sulfur sites. This has been inferred from the hyperfine structure appearing in the low-field component of

the EPR spectrum of samples enriched with ^{77}Se ($I = \frac{1}{2}$) (36). In contrast, ^{33}S ($I = \frac{3}{2}$) produced only line broadening and could not be used for a quantitative evaluation.

In all cases investigated so far, including a number of synthetic analogs (93), the replacement of sulfide by selenide has resulted in a general shift of the EPR spectra to a lower field (35–37). Concerning the symmetry of the g tensor, the effects of selenium substitution are more variable: in the case of putidaredoxin, the axial spectrum of the native protein is converted into a rhombic one (35), whereas in the case of parsley ferredoxin, the rhombic spectrum of the native protein is converted into one nearer to axial symmetry (37). Comparison of native and $[\text{2Fe-2Se}]$ putidaredoxin by Mössbauer spectroscopy has shown that the hyperfine coupling constants and the isomer shifts of the iron atoms are slightly decreased in the Se-substituted protein (94). Similar results and conclusions have been reached by ^{57}Fe and proton ENDOR spectroscopy of native and Se-substituted adrenodoxin, with different effects, however, on the Fe(III) and on the Fe(II) sites (95). These variations have been interpreted as being similar to those observed among native $[\text{2Fe-2S}]$ proteins (96).

In ^1H NMR spectra of synthetic binuclear iron–sulfur clusters, the isotropic shifts of the protons of the thiolate ligands increase slightly when sulfide is replaced by selenide, in both the oxidized (77a, 79) and the reduced (44) state. No data of this kind are available for $[\text{2Fe-2S(e)}]$ proteins.

B. $[\text{4Fe-4S(e)}]$ PROTEINS

Tetranuclear iron–sulfur clusters are diamagnetic at low temperature in the $[\text{4Fe-4S}]^{2+}$ redox level, and are paramagnetic ($S = \frac{1}{2}$; but see Section VII) either in the $[\text{4Fe-4S}]^+$ (reduced low-potential ferredoxins) or $[\text{4Fe-4S}]^{3+}$ (oxidized HiPIP) redox levels (87). The replacement of sulfide by selenide in $[\text{4Fe-4S}]^{2+}$ centers results in changes qualitatively similar to those described above for $[\text{2Fe-2S}]$ clusters. The resonances of the protons neighboring the iron–sulfur cluster are consistently shifted to lower field upon replacement of sulfide by selenide, in synthetic analogs (44, 97) as well as in proteins (98). The intensity of the MCD spectra is greater for Se-substituted *C. pasteurianum* ferredoxin than for its native counterpart (99). The Mössbauer isomer shifts of the Se-substituted protein are slightly larger than those of the native protein (100, 101). A similar change has been observed in aconitase (41).

Similar variations in MCD (99), and ^1H NMR (44, 97) spectra have

been observed for $[4\text{Fe}-4\text{S}(\text{e})]^+$ clusters upon replacement of sulfide by selenide, in those cases in which the ground spin state is $S = \frac{1}{2}$. The EPR spectra in the $g = 2$ region are slightly shifted to lower field (49, 77, 100), as observed for $[2\text{Fe}-2\text{S}(\text{e})]^+$ clusters (Section VI,A). The ^1H NMR spectra of $[4\text{Fe}-4\text{S}]^+$ synthetic clusters with $\text{C}_6\text{H}_5\text{XH}$ ($\text{X} = \text{S}, \text{Se}, \text{Te}$) terminal ligands display increasingly shifted proton NMR resonances when going downward in the row of the VIA elements (64).

For the $[4\text{Fe}-4\text{Se}]^{3+}$ redox level, the only available data are those concerning the oxidized HiPIP from *C. vinosum*. The EPR spectra are shifted to lower field in this case as well and are more anisotropic than those of the native protein (40). Whereas no low-field signals suggestive of $S > \frac{1}{2}$ ground spin states have been detected, the occurrence of several signals in the $g = 2$ region may arise from the existence of more than one $S = \frac{1}{2}$ ground spin state (40, 102). The shifted proton resonances occur at slightly lower field in NMR spectra of the Se-substituted protein than in those of the native one (103; J.-M. Moulis and J. Gaillard, unpublished results, 1987). Some of the latter results have been obtained with the HiPIP of a most interesting chimeric organism, combining, if not the properties, at least the names of anaerobic heterotrophs and purple sulfur bacteria, "*Clostridium vinosum*" (103).

C. $[3\text{Fe}-4\text{S}(\text{e})]$ PROTEINS

The only reported case of selenium incorporation into a trinuclear cluster is that of inactive aconitase (41). The EPR spectrum of the $[3\text{Fe}-4\text{Se}]^+$ protein ($S = \frac{1}{2}$) is not shifted to low field, but displays a significant increase in g tensor anisotropy, as compared to the $[3\text{Fe}-4\text{S}]^+$ protein (41). The Mössbauer spectra of the two species in this redox level witness slight differences in hyperfine parameters and larger anisotropies in the Se-substituted protein than in the native one. Upon reduction to $[3\text{Fe}-4\text{S}(\text{e})]^0$, the Mössbauer spectra of the two proteins are nearly identical (41).

VII. Ground Spin State Variability in $[4\text{Fe}-4\text{S}(\text{e})]^+$ Clusters

The spin-coupling model resulting in a $S = \frac{1}{2}$ ground state (87) has long been considered to be valid for all $[4\text{Fe}-4\text{S}(\text{e})]^+$ clusters. Exceptions to the normally expected spectroscopic signature were few: the low-field EPR features of some synthetic analogs in the solid state (104, 104a) (Section VII,C), the so-called P-clusters of the nitrogenase Mo-Fe

protein (105) (Section VII,D,1), and the phosphoribosylpyrophosphate amidotransferase from *Bacillus subtilis* (106) (Section VII,D,2). These observations became more meaningful upon analysis of the unusual features displayed by the EPR and Mössbauer spectra of reduced Se-substituted clostridial ferredoxins, and the subsequent unveiling of analogous spin states in a number of other proteins.

A. CLOSTRIDIAL $2[4\text{Fe}-4\text{Se}]^+$ FERREDOXINS

Reduced Se-substituted clostridial ferredoxins display EPR features in the $g = 2$ region that are not unlike those observed for their native counterparts. Upon partial (<20%) reduction, the proportion of molecules containing two reduced clusters is negligible, and $S = \frac{1}{2}$ spectral features are observed (Section VI,B), with a slight shift to lower field in the case of the Se-substituted proteins (100). Upon full reduction, the native ferredoxins have long been known to display a seven-line spectrum arising from the interaction of two $S = \frac{1}{2}$ systems (107). In contrast, in $2[4\text{Fe}-4\text{Se}]^+$ proteins, the interaction is reflected in a mere broadening of the spectra (49, 100). Whether this is due to specific properties of the $S = \frac{1}{2}$ spin states in $[4\text{Fe}-4\text{Se}]^+$ clusters or to the superimposition of spectral components involving interactions among various spin states (see below) remains to be determined.

Downfield of the $S = \frac{1}{2}$ signals, $2[4\text{Fe}-4\text{Se}]^+$ clostridial ferredoxins display unusual features that have counterparts in the Mössbauer spectra (100); these have been assigned to $S = \frac{3}{2}$ and $S = \frac{7}{2}$ ground spin states (49, 100, 101). Low-temperature MCD spectra of these proteins are much more intense than those of their native counterparts, and their magnetization curves confirm the coexistence of $S > \frac{1}{2}$ ground spin states (99).

1. $S = \frac{3}{2}$ Spin State

Besides the signal corresponding to the $S = \frac{1}{2}$ species, the EPR spectra of $2[4\text{Fe}-4\text{Se}]^+$ clostridial ferredoxins are dominated by a broad, fast-relaxing feature around $g = 4$. It is sensitive to cluster-cluster magnetic interaction, since, in the partially reduced proteins, it is resolved into two lines with g values of 4.5 and 3.5 (100). As it spreads into the $g = 2$ region, it has been described by a rhombic g tensor with principal values, 4.5, 3.5, and 2, and attributed to the $\pm\frac{1}{2}$ fundamental doublet of a spin quartet state with $|E/D| = 0.08$ (100), D being the zero-field splitting constant and E the rhombic distortion parameter. Additional information has been gathered from the Mössbauer spectra; after subtracting the contributions from the $S = \frac{1}{2}$ and $S = \frac{7}{2}$ (Section VII,A,2)

spin systems, the low-temperature spectra of $2[4\text{Fe-4Se}]^+$ *C. pasteurianum* ferredoxin recorded under very strong applied fields (5–10 T) reveal that the iron sites experience a quasi-isotropic hyperfine tensor of small negative principal values. Moreover, the iron sites appear to be identical, although some inequivalence may be hidden under the breadth of the lines (101). From the shape of the Mössbauer spectra at intermediate applied fields, D has tentatively been estimated to be smaller than $+3\text{ cm}^{-1}$. All of these characteristics clearly distinguish the species giving rise to the $S = \frac{3}{2}$ state from those generating $S = \frac{1}{2}$ spin systems. Spin states closely resembling the one described above have been identified in a number of $[4\text{Fe-4S}]^+$ clusters, including those occurring in natural proteins (Sections VII,B–VII,D).

2. $S = \frac{1}{2}$ Spin State

The $\frac{1}{2}$ spin state, which has not yet been observed in any *bona fide* $[4\text{Fe-4S(e)}]^+$ clusters other than those of clostridial ferredoxins (77a), has been detected in the EPR and Mössbauer spectra of the latter proteins as very characteristic features (49, 100, 101). In fact, all sublevels of this octet spin system have been observed by a combination of these two spectroscopic techniques. The fundamental Kramers' doublet is very anisotropic, as indicated by its calculated g values (14.3, ~ 0 , ~ 0), and can only be observed in the low-temperature (below $\sim 15\text{ K}$) Mössbauer spectra, even without applied magnetic fields (100). It is observed, on both sides of the central doublet, as a doublet of lines arising from two antiferromagnetically coupled species in a 3:1 intensity ratio. It can be described, to a first approximation, by a very simple model involving three ferromagnetically coupled Fe(II) ions, antiferromagnetically coupled with a single Fe(III) ion (101). At least one component of each of the excited levels has been observed by EPR (49); signals at $g = 10.08$, $g = 5.17$, and $g = 12.88$ have been assigned to the $\pm\frac{3}{2}$, $\pm\frac{5}{2}$, and $\pm\frac{7}{2}$ Kramers' doublets, respectively, of the $S = \frac{1}{2}$ state, with $D = -2\text{ cm}^{-1}$ and $|E/D| = 0.12$. These characteristics suggest that the species giving rise to the $S = \frac{1}{2}$ spin state experiences forces that strongly tend to localize the electrons on the iron sites, a rather uncommon feature for $[4\text{Fe-4S(e)}]^+$ clusters.

3. Comments

At the time of their initial characterization in $[4\text{Fe-4Se}]^+$ clostridial ferredoxins (100), the novelty of the $S = \frac{3}{2}$ and $S = \frac{1}{2}$ spin states might have raised some doubts as to their being associated with tetranuclear Fe-S(e) clusters. A comprehensive set of chemical, biochemical (43), and spectroscopic (resonance Raman and Mössbauer) (58, 100) data was

therefore collected, providing ample evidence that all the iron in these proteins is present in $[4\text{Fe}-4\text{Se}]^{2+/+}$ clusters.

The coexistence of three ground spin states in proteins containing only two $[4\text{Fe}-4\text{Se}]$ clusters forbids the assignment of a given spin state to a specific cluster. By combining integration of EPR spectra and fitting of Mössbauer spectra, we have been able to show that the proportion of $[4\text{Fe}-4\text{Se}]^+$ clusters assuming a given spin state is invariable in different preparations of the same protein, but variable as a function of the ferredoxin used (*C. pasteurianum*, *Clostridium acidurici*, and *Clostridium thermosaccharolyticum*) (49). These results point to the essential role, in the present case, of the polypeptide chain in determining the forces giving rise to the ground spin state variability, and to the minor role, if any, of extrinsic factors such as sample processing or solvent composition. Further evidence of the paramount importance of the protein is provided by the observation that in Se-substituted *Bacillus stearothermophilus* ferredoxin only the $S = \frac{1}{2}$ ground spin state has been observed (49). The fact that the latter protein contains only one $[4\text{Fe}-4\text{Se}]^+$ cluster might suggest that the ground spin state variability in clostridial ferredoxins arises from magnetic interactions between the two clusters present in these proteins. This possibility is excluded by the observation that the high-spin multiplets occur in partially reduced clostridial ferredoxins as well (100). In fact, the magnetic interaction between the two clusters can be observed, not only on the EPR signal of the $S = \frac{1}{2}$ spin state, but also on that of the $S = \frac{3}{2}$ spin state (Section VII,A). In contrast, the $g = 5.17$ EPR line (attributed to the $\pm\frac{3}{2}$ Kramers' doublet of the $S = \frac{7}{2}$ state) appears to be insensitive to the interaction between the two clusters (100).

The ground spin state variability of tetranuclear iron-sulfur clusters has been analyzed in detail in two other cases, the nitrogenase iron protein (Section VII,B) and a series of synthetic analogs (Section VII,C). These studies have prompted a number of searches for similar properties (Section VII,D), and the general occurrence of ground spin state variability in $[4\text{Fe}-4\text{S(e)}]^+$ clusters is now widely recognized (Sections VII,B-VII,D; see Table II).

B. NITROGENASE IRON PROTEIN

The Fe protein is the smaller (~ 60 kDa) component of nitrogenase, and is a dimer of two identical subunits (74). It contains a $[4\text{Fe}-4\text{S}]$ cluster, which in the reduced state displays an $S = \frac{1}{2}$ -type EPR spectrum (74, 108). Integration of the latter, however, has without exception yielded less than 0.5 spin/molecule, which has led to various hypotheses

on the active site structure (reviewed in Ref. 109). The early observation of low-field EPR features in the $g = 4-5$ region (110) has long been overlooked. It has eventually been demonstrated, upon analysis of a comprehensive set of EPR, Mössbauer, and magnetic susceptibility data, that the $[4\text{Fe}-4\text{S}]^+$ cluster of the Fe protein exhibits a mixture of $S = \frac{1}{2}$ and $S = \frac{3}{2}$ spin states (109). The $S = \frac{3}{2}$ state is characterized by $D = -2.5 \text{ cm}^{-1}$, $|E/D| = 0.22$, and by weak and negative magnetic hyperfine interactions (109). The latter property has been observed for the $S = \frac{3}{2}$ state of $2[4\text{Fe}-4\text{Se}]^+$ ferredoxins as well (Section VII,A,1). Interconversions between the two spin states occur upon changes in solvent composition: in 50% ethylene glycol most of the clusters are in the $S = \frac{1}{2}$ state, whereas in 0.4 *M* urea the $S = \frac{3}{2}$ state predominates (109). The complexity of the electronic structure of the $[4\text{Fe}-4\text{S}]^+$ cluster in nitrogenase Fe protein is further illustrated by the effects of adenine nucleotide binding; the EPR and Mössbauer data again indicate the coexistence of $S = \frac{1}{2}$ and $S = \frac{3}{2}$ states, but they are not identical with those of the native protein. In addition, minor features in the spectra suggest the occurrence of an $S = \frac{5}{2}$ spin state in the ATP-bound Fe protein (111). Although the main characteristics of the Fe protein electronic structure have been worked out with the protein from *Azotobacter vinelandii* (109, 111, 112), equivalent features have been reported for the Fe proteins purified from *Klebsiella pneumoniae*, *Azotobacter chroococcum* (113), and *C. pasteurianum* (114, 115).

C. SYNTHETIC ANALOGS

Synthetic analogs are structural and electronic representations of isoelectronic protein sites, where thiolate ligands simulate cysteinate binding in proteins (116). One of the significant advantages of these compounds, as compared with proteins, is the potential to obtain highly accurate tridimensional structures.

Initial observations of low-field features in EPR spectra of $[4\text{Fe}-4\text{S}]^+$ in the solid state (104, 104a) have subsequently been extended to show that $S = \frac{3}{2}$ ground spin states are exhibited by some of these clusters either in the solid state or in frozen solution (117). A wide survey of many $[4\text{Fe}-4\text{S(e)}]^+$ compounds in the polycrystalline state has revealed that those possessing a pure $S = \frac{1}{2}$ or $\frac{3}{2}$ spin state are a minority, and that most of them exhibit mixtures of these two spin states, or even spin admixed states. The latter are distinct from physical mixtures of $S = \frac{1}{2}$ and $S = \frac{3}{2}$ states, and possess properties intermediate between those of the pure states (118). When dissolved and frozen in acetonitrile or in *N,N*-dimethylformamide (DMF), however, all of these clusters

TABLE II
GROUND SPIN STATES OF $[4\text{Fe}-4\text{S(e)}]^+$ CLUSTERS

Compound	Ground spin state properties	Ref.
Synthetic $[\text{Fe}_4\text{S(e)}_4(\text{SR})_4]^{3-}$ clusters	<p><i>In crystalline state</i>, three categories: pure $S = \frac{1}{2}$ or $S = \frac{3}{2}$, physical mixture of $S = \frac{1}{2}$ and $S = \frac{3}{2}$, spin admixed ($S = \frac{1}{2} + \frac{3}{2}$)</p> <p><i>In frozen solution</i>, always a physical mixture of $S = \frac{1}{2}$ and $S = \frac{3}{2}$; relative proportion of $S = \frac{3}{2}$ state tends to increase with bulkiness of ligand</p>	77a, 104a, 104, 117–120
$2[4\text{Fe}-4\text{Se}]^+$ clostridial ferredoxins	<p>Three coexistent ground spin states: $S = \frac{1}{2}$, $S = \frac{3}{2}$, $S = \frac{5}{2}$; their relative proportions depend only on polypeptide chain, not on extrinsic parameters (solvent composition, freezing conditions)</p> <p>High-spin states contribute to the magnetic properties in solution at room temperature</p>	49, 59, 98–101
Nitrogenase iron protein	<p>Two coexistent spin states: $S = \frac{1}{2}$, $S = \frac{3}{2}$; their relative proportions depend on extrinsic parameters (solvent composition, freezing conditions (Fig. 3). Upon ATP or ADP binding, a different type of $S = \frac{3}{2}$ state appears; ATP binding causes the appearance of an $S = \frac{5}{2}$ state</p> <p>No contribution of the $S > \frac{1}{2}$ states is observed in solution at room temperature</p>	109, 111–115

Nitrogenase Mo-Fe protein (P-clusters)	An $S = \frac{7}{2}$ ground spin state is observed, but only upon addition of solid thionine in large excess Note: the P-clusters have not been conclusively demonstrated to assume a [4Fe-4S] structure	121-125
Glutamine phosphorybosyl- pyrophosphate amidotransferase	$S = \frac{3}{2}$ is the predominant ground state, $S = \frac{1}{2}$ and $S = \frac{5}{2}$ are also observed; $S = \frac{5}{2}$ becomes dominant at high protein concentrations	106, 126-129
<i>Pyrococcus furiosus</i> ferredoxin	$S = \frac{1}{2}$ and $S = \frac{3}{2}$ states, the latter one being predominant; relative proportions nearly independent of solvent composition The [4Fe-4S] cluster has only three cysteine ligands; upon cyanide binding, only $S = \frac{1}{2}$ is observed	130, 131
<i>Desulfovibrio africanus</i> ferredoxin III	$S = \frac{1}{2}$ and $S = \frac{3}{2}$	132, 133
<i>C. pasteurianum</i> hydrogenase I (F-clusters)	$S = \frac{1}{2}$ and $S = \frac{3}{2}$	134
<i>Clostridium thermoaceticum</i> CO dehydrogenase	$S = \frac{1}{2}$ and $S = \frac{3}{2}$	135

display physical mixtures of $S = \frac{1}{2}$ and $\frac{3}{2}$ states (118). In frozen solution, the proportion of $S = \frac{3}{2}$ state increases roughly with the steric size of the thiolate ligand (118). Extensive crystallographic work has been carried out on these compounds, in an attempt to correlate structure and spin state. Several kinds of distortions have been evidenced in these studies performed at ambient temperature, but no unique core distortion or thiolate ligand conformation can be associated with any of the spin states observed at cryogenic temperature (77a, 119, 120).

D. OTHER PROTEINS

1. Nitrogenase Mo-Fe Protein

This protein is the larger component of nitrogenase. It contains 30–32 Fe and 2 Mo atoms per $\alpha_2\beta_2$ tetramer ($M_r \sim 230,000$). The Mo-Fe protein possesses two identical cofactors of approximate composition $\text{MoFe}_{6-8}\text{S}_{8-10}$, which are the probable catalytic centers. The remaining iron atoms belong to structures, referred to as "P-clusters," which have long been considered, but not proved, to be $[\text{4Fe-4S}]$ centers (74, 108, 116). According to recent X-ray diffraction data, the P-clusters would appear to consist of two closely associated $[\text{4Fe-4S}]$ clusters, or of a larger type of iron-sulfur cluster (120a). Most of the current knowledge on the P-clusters has been obtained from Mössbauer experiments that revealed coupled iron sites compatible with $[\text{4Fe-4S}]$ structures (105, 108, 116). A particularly interesting study has been carried out on a protein having P-clusters specifically enriched in ^{57}Fe , and which did therefore not require subtraction of the contributions of the Mo-Fe cofactors (121).

In the Mo-Fe protein as isolated, the P-clusters (P^{N}) are diamagnetic in their ground state. Upon one-electron oxidation (P^{OX}), they are split into two subpopulations (each consisting of antiferromagnetically coupled iron sites in a 3 : 1 ratio) that differ only in the parameters of their minor component. Despite this difference, both subsets have $S > \frac{1}{2}$ noninteger spin states (121), in agreement with previous low-temperature MCD (122) and room temperature magnetic susceptibility (123) measurements. However, the spin multiplet could not be identified unambiguously, since only the ground doublet had been detected in the Mössbauer spectra (121). In another study, large excesses of solid thionine have been found to generate EPR signals at $g = 10.4, 5.8$, and 5.5 ; these have been attributed to the excited sublevels of a $S = \frac{7}{2}$ spin state with $D = -4 \text{ cm}^{-1}$ and $E = 0.16 \text{ cm}^{-1}$ (124). These spectra have arbitrarily been assigned to the P^{OX} state, and two speculative models

have been proposed to represent the redox reactions of the P-clusters (124). Subsequent Mössbauer studies of samples oxidized with solid thionine have proved that a P^{OX} ($S = \frac{1}{2}$) state is generated, but that it is different, though isoelectronic, from the previously studied P^{OX} state (125). The former lacks the trapped-valence Fe(II) site characteristic of the latter. Upon removal of the solid dye, the P^{OX} ($S = \frac{1}{2}$) state disappears and reverts to the classical P^{OX} state (125). The evidence presented strongly suggests that the $S = \frac{1}{2}$ state results from the interaction of the protein with the solid dye and that this state does not satisfactorily describe the spin states of the oxidized P-clusters in solution, in particular during the catalytic cycle (125). Concerning the latter point, it remains to be established that the P^{OX} state bears any relevance to the catalytic cycle of nitrogenase, since the available evidence rather suggests that the Mo-Fe protein requires reduction of the "as-isolated" level before passing on electrons to the substrates (74, 108).

Definite problems remain unresolved concerning the P-clusters, mainly due to their differing in many properties from well-characterized [4Fe-4S] clusters. If they are demonstrated to possess the latter structural framework, their terminal ligation pattern may have to differ from the classical one (one cysteine per iron), in order to simultaneously accommodate all of their known properties (116).

2. Glutamine Phosphoribosylpyrophosphate Amidotransferase (GPRPAT)

This enzyme catalyzes the replacement of the pyrophosphate group of 5-phosphoribosyl-1-pyrophosphate by the amide amino group of glutamine, the first step in purine nucleotide biosynthesis. The enzyme purified from *B. subtilis* contains a [4Fe-4S] cluster essential for activity, and is one among an increasing number of iron-sulfur enzymes that are not involved in redox reactions (126). The cluster has been suggested to work as an oxygen sensor, but whether it undergoes redox transitions *in vivo* remains undetermined (127). The enzyme can be partially reduced *in vitro* to the $[4Fe-4S]^+$ level, quantitative reduction being difficult because of its unusually low (-600 mV) reduction potential (106). Mössbauer spectra of the reduced enzyme have pointed to a half-integer ground spin state with a very anisotropic fundamental doublet, resulting in almost undetectable EPR spectra (106). MCD data have suggested an $S = \frac{3}{2}$ ground spin state with axial symmetry and $D > 3 \text{ cm}^{-1}$ (128). Furthermore, EPR signals consistent with transitions within the $\pm\frac{1}{2}$ Kramers' doublet of the $S = \frac{3}{2}$ spin state have been detected at low field, together with additional signals attributable to

$S = \frac{1}{2}$ and $S = \frac{5}{2}$ spin states (128). If these species are truly associated with $[4\text{Fe-4S}]^+$ clusters, which remains to be demonstrated, it is interesting that the $S = \frac{5}{2}$ spin state increases in abundance with protein concentration (128). Since GPRPAT has been shown to be a mixture of monomers, dimers, and tetramers in solution (129), the spin state variability of the cluster has tentatively been correlated with the quaternary structure of the protein (128).

3. Miscellaneous

Pyrococcus furiosus ferredoxin, which contains a single $[4\text{Fe-4S}]$ cluster having noncysteinyl ligation on one of its metals, displays in its reduced form a mixture of $S = \frac{1}{2}$ (20%) and $S = \frac{3}{2}$ (80%, with $D = +3.3 \text{ cm}^{-1}$, $|E/D| = 0.22$) ground spin states (130). Upon binding of cyanide, they are both converted into a new, pure $S = \frac{1}{2}$ state (131).

Desulfovibrio africanus ferredoxin III contains one classical $[4\text{Fe-4S}]$ cluster and one $[3\text{Fe-4S}]$ cluster that can be converted into a $[4\text{Fe-4S}]$ cluster having one noncysteinyl ligated metal (132). The $S = \frac{3}{2}$ spin state observed in the 8Fe ferredoxin has been attributed to the cluster having one noncysteinyl ligand (133).

EPR signals consistent with $S = \frac{3}{2}$ spin states have also been obtained with reduced *C. pasteurianum* hydrogenase I (134) and *Clostridium thermoaceticum* CO dehydrogenase (135).

E. ROOM TEMPERATURE DATA OBTAINED FROM PROTON NMR

Protons neighboring paramagnetic centers are considerably perturbed by the strong local electronic spin and it is therefore generally easy to distinguish their nuclear magnetic resonances from those of the bulk of the molecule (89, 136). These perturbations result in large chemical shifts with strong temperature dependences and short relaxation times, properties that are useful to obtain information on the electronic spin of the paramagnetic center.

This has proved particularly true in the case of the $2[4\text{Fe-4Se}]^+$ clostridial ferredoxins (98). A set of ~ 20 resonances, which all integrate to the intensity of one proton, occur outside of the 0- to 10-ppm diamagnetic range. These shifted resonances can be divided into two subsets, each comprising ~ 8 protons, on the basis of their chemical shifts and temperature dependences. One subset has temperature dependences ($\sim 0.2 \text{ ppm/K}$) and chemical shifts very similar to those measured for reduced native ferredoxins. The chemical shifts are slightly larger in the former than in the latter proteins, which is a general effect of the replacement of sulfur by selenium (Section VI). The second set

of resonances displays very different characteristics: the temperature dependence is much larger (up to 1 ppm/K in some cases), and the chemical shifts span a considerably wider range (from -50 to $+160$ ppm). Such features are unprecedented for $[4\text{Fe}-4\text{S}(\text{e})]^+$ clusters, and most probably reflect the occurrence in the conditions of the NMR experiments, i.e., at room temperature in liquid solution, of electronic spins arising from at least one of the high ground spin states observed in frozen solutions by EPR, Mössbauer, or MCD spectroscopies (Section VII,A). This conclusion has been borne out by measuring the bulk magnetic susceptibility of ferredoxin solutions, which can be derived from the induced chemical shift of a reference proton. The value obtained is related to the effective magnetic moment of the protein and enables a direct comparison between samples (137). In the case of reduced *C. pasteurianum* ferredoxin, the seleno derivative exhibits an effective magnetic moment of $6.3 \mu_{\text{B}}$ (Bohr magneton), 50% higher than that ($4.2 \mu_{\text{B}}$) of the native molecule. The large difference observed between the two reduced ferredoxins clearly confirms that the protein containing selenium has an effective spin quantum number at ambient temperature higher than the native one. Thus, the ^1H NMR data demonstrate that at least some of the high-spin states observed at low temperature (<20 K) for reduced $2[4\text{Fe}-4\text{Se}]^+$ clostridial ferredoxins are still relevant at room temperature, i.e., under conditions in which the protein is functioning.

A completely different situation is encountered in the case of the nitrogenase Fe protein, for which a mixture of $S = \frac{1}{2}$ and $S = \frac{3}{2}$ ground spin states has been evidenced (Section VII,B). The shifted proton resonances of the reduced protein are very similar, with regard to chemical shifts and temperature dependences, to those, among the reduced ferredoxins, which display only $S = \frac{1}{2}$ ground spin states (115). Furthermore, the significant spectroscopic features, as well as the solution magnetic susceptibility, are insensitive to variations in solvent compositions, which, at low temperature, considerably modify the relative ratios of the two ground spin states. Binding of adenine nucleotides (ADP, ATP, and some analogs) to the Fe protein induces small changes in the shifted proton resonances (115); further discussion of this is outside the scope of this review. Here again, however, the spectroscopic features indicate similar electronic properties of the $[4\text{Fe}-4\text{S}]^+$ cluster (115). It has therefrom been deduced that a single spin manifold of the latter cluster contributes to the paramagnetic shifts of the protons neighboring the active site. This suggests that the ground spin state heterogeneity may arise from constraints appearing upon freezing. Indeed, of the two solvent compositions that induce the most divergent relative abun-

dances of the $S = \frac{1}{2}$ and $S = \frac{3}{2}$ ground spin states, one (50% ethylene glycol) freezes as a glass whereas the other (0.4 *M* urea) is more crystalline. It is relevant to mention here that the EPR spectra of $[2\text{Fe}-2\text{S}(\text{e})]^+$ synthetic analogs display variations in the main values of their g tensors, depending on the solvents in which they are frozen (93). Samples of Fe protein prepared with rapid freeze techniques (~ 5 msec) have been reported to display the spectroscopic signatures of the two ground spin states, but possible changes in the relative proportions of the latter, depending on the rapidity of freezing, have not been indicated (109). An experiment has been carried out (115) that points to the importance of the freezing process with respect to the ground spin state variability of the Fe protein. EPR samples in several solvent compositions favoring either the $S = \frac{1}{2}$ or the $S = \frac{3}{2}$ spin state were frozen in liquid nitrogen and displayed the expected signals in the expected ratios. The samples were subsequently equilibrated in an acetone-dry ice bath (~ 230 K), and then taken back to liquid nitrogen temperature (77 K). At no stage in this procedure were the solutions allowed to thaw. The EPR spectra recorded thereafter showed that the relative ratios of the two spin states had changed; for instance, in 0.4 *M* urea, the $S = \frac{1}{2}$ to $S = \frac{3}{2}$ ratio was 1 : 10 before the temperature cycling and 1 : 3 afterward (Fig. 3, spectra a and b). Furthermore, when the samples were thawed and refrozen in liquid nitrogen after the temperature cycling, the ratio returned to the initial 1 : 10 value (Fig. 3, spectrum c). These experiments leave little doubt that the freezing process is of prime importance, in this case at least, for the appearance of the spin state variability and for the modulation of the relative contribution of each of the spin states.

So far, room temperature data are available only for the two protein types discussed above. In the case of the nitrogenase iron protein, facile ground spin state interconversion at cryogenic temperatures correlates with the coalescence at room temperature into a single species, which includes no contribution from the $S = \frac{3}{2}$ ground spin state. In contrast, in the $2[4\text{Fe}-4\text{Se}]^+$ ferredoxins, the ground spin states are not, despite numerous attempts, interconvertible at low temperature. Moreover, some of these high ground spin states still contribute to the magnetic properties of the reduced Se-substituted ferredoxins in solution. Thus, the active site of the Fe protein appears to be more sensitive to the solvent (directly, or through the polypeptide chain) than those of the clostridial ferredoxins. This inference may be rationalized by the crystal structure of the former protein (138), which shows the $[4\text{Fe}-4\text{S}]$ cluster to be held between the two subunits, in a highly exposed region.

Useful proton NMR spectra are unlikely to be retrieved easily from most of the other proteins discussed in this review, due to their con-

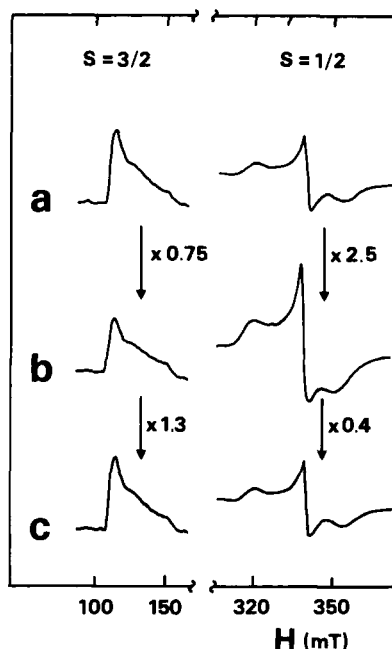


FIG. 3. EPR spectra of *C. pasteurianum* nitrogenase iron protein showing the dependence of the relative amounts of $S = \frac{1}{2}$ and $S = \frac{3}{2}$ spin ground states on the freezing procedure. The protein (30 mg/ml), dissolved in 0.4 M urea, 0.05 M potassium phosphate, pH 8.0, and 2 mM dithionite, was handled and transferred into EPR tubes in an anaerobic glove box (<2 ppm O_2). The tubes were frozen in liquid nitrogen and the spectra were recorded at 5 K for the low-field region and 12 K for the high-field region. Other experimental conditions are given elsewhere (115). (a) Spectrum recorded subsequent to initial freezing in liquid nitrogen. (b) Sample (a) brought to acetone/dry ice temperature (230 K) for 15 min. (c) Sample (b) after thawing and subsequent freezing in liquid nitrogen. The numbers next to the arrows are the changes in the integrated intensity of the EPR signals observed after each step in the thermal cycling.

taining paramagnetic centers in addition to those of interest here. *Pyrococcus furiosus* ferredoxin, in view of its small size and single [4Fe-4S] cluster (130), might be an exception. A more promising field of investigation is afforded by the synthetic analogs (117-120). 1H NMR studies on the host of compounds that have been analyzed in great detail by X-ray crystallography and by low-temperature magnetic techniques might contribute significant data. Previously published NMR spectra, however, including those of some compounds now known to exhibit spin quartet states in frozen solution, consistently display the same features

as those of synthetic clusters and proteins assuming a pure $S = \frac{1}{2}$ ground spin state (44, 77a, 97, 139).

F. SIGNIFICANCE OF THE GROUND SPIN STATE VARIABILITY

The functional relevance of the ground spin state variability of $[4\text{Fe}-4\text{S}(\text{e})]^+$ clusters may appear doubtful, since 2 $[4\text{Fe}-4\text{Se}]$ ferredoxins are the only case in which they seem to have any bearing on the room temperature electronic properties (Section VII,E). However, these proteins are providing a unique means to explore the rate dependence for electron transfer on electronic structure (and in particular on the spin state) in iron-sulfur proteins. According to current theories (reviewed in Ref. 140), an electronic factor representing the interactions between the initial and final states of the redox system contributes to the rate of electron transfer. From a detailed comparative survey of the redox reactivity of clostridial ferredoxins with either $[4\text{Fe}-4\text{S}]$ or $[4\text{Fe}-4\text{Se}]$ clusters, and for which high-resolution X-ray structures are available (141, 142), it should be possible to determine the influence of the initial and final spin states on the redox process.

An additional feature of the ground spin state variability of $[4\text{Fe}-4\text{S}(\text{e})]^+$ clusters has been the stimulation of intense theoretical work aimed at understanding the electronic structure of the clusters, and in particular the conditions leading to the occurrence of high-spin states. The most recent efforts (143, 144) have succeeded, using an appropriate balance of exchange (J) and resonance (B) parameters between the iron atoms, and are able to account for most of the spin states observed and discussed above. Depending on the relative values of the Heisenberg parameters for the Fe(II) pair on one hand, and for the mixed-valence pair on the other hand, the $S = \frac{1}{2}$, $\frac{3}{2}$, $\frac{5}{2}$, and $\frac{7}{2}$ (but in no case $\frac{3}{2}$) spin states can occur at lowest energy. Interestingly, the valence localization observed for the $S = \frac{7}{2}$ state (101) has been nicely reproduced by the model (143).

VIII. Vibrational Spectroscopy of Iron-Selenium Clusters

The properties of metal-containing active sites in proteins indicate small variations that are difficult to detect in X-ray crystal structures. Vibrational spectroscopy has been widely used to characterize these minute changes, as it has the potential to provide a wealth of information on the symmetry and bond strengths of a molecule. Resonance

Raman (RR) spectroscopy, in which laser excitation within an electronic absorption band produces selective enhancement of Raman lines arising from vibrations of the chromophore, is able to reveal specific vibrational features of the active site (145).

In the case of iron-sulfur proteins, the instability of the active sites and their poor Raman scattering efficiencies limited information obtainable from early spectra of rubredoxin (146) and [2Fe-2S] (147) and [4Fe-4S] ferredoxins (148). Significant progress has been made by analyzing light scattered by frozen droplets of concentrated solutions of protein (149). Application of this experimental approach to iron-sulfur proteins and to synthetic analogs of their active sites has allowed the collection of high-quality spectra (58, 150-153) and the measurement of reliable isotopic shifts and depolarization ratios (58, 154). A few examples are given below, and these illustrate the wealth of experimental data that can be obtained from the S \rightarrow Se substitution in iron-sulfur active sites.

A. [2Fe-2Se] PROTEINS

The first RR study on this type of protein has been carried out on adrenodoxin and on its selenium-substituted analog (147). Only three bands assignable to Fe-S(e) stretching frequencies have been detected for the native protein, and two for the selenium-substituted protein. Tentative assignments of the observed bands to Fe-S(cys) and to Fe-S(e)* stretching modes have been derived from the comparison of the spectra (147). Later, largely improved RR spectra of another [2Fe-2Se] protein have been obtained: a comprehensive set of data has been collected for spinach ferredoxin, for its Se-substituted analog, and for the [2Fe-2S] ferredoxin from *C. pasteurianum*, including measurements of depolarization ratios, isotopic substitutions on the core chalcogenides (for the spinach ferredoxins), and excitation with several different wavelengths (154). The number of bands observed in the Fe-Se stretching frequency range (at least seven in each spectrum), and the high number of totally symmetric modes, have shown that in all of these proteins the chromophores experience distortions lowering their symmetry (154) from the D_{2h} point group observed in synthetic analogs (155). All bands in the region of 250-450 cm^{-1} , in which the Fe-S stretching modes are expected to occur, display relatively uniform isotopic shifts upon $^{32}\text{S} \rightarrow ^{34}\text{S}$ substitution at the core. This suggests an extensive mixing of bridging and terminal motions, hence forbidding assignment of any of the observed bands to simple, normal modes.

In contrast, $^{76}\text{Se} \rightarrow ^{82}\text{Se}$ isotopic substitution allows discrimination between the bridging and terminal stretching modes, showing that in this case the coupling between the two types of modes is weaker. In a previous study on spinach ferredoxin and adrenodoxin, inaccurate measurements of $^{32}\text{S} \rightarrow ^{34}\text{S}$ isotopic shifts had led to erroneous normal mode calculations and assignments (155). Subsequent revisitation of the subject by the same group has yielded data and interpretation (156) supporting and extending our former conclusions (154).

Analysis of the RR spectra of spinach ferredoxin reconstituted with mixtures of sulfide and selenide has revealed that not only $[\text{2Fe-2S}]$ and $[\text{2Fe-2Se}]$ clusters but also $[\text{2Fe-S-Se}]$ hybrid clusters are present in the reaction products (48). Similar occurrences have previously been demonstrated by EPR in the case of adrenodoxin (82), and by ^1H NMR for $[\text{Fe}_2\text{X}_2(\text{SR})_4]^{2-}$ synthetic analogs (44).

An extensive set of RR spectra of $[\text{Fe}_2\text{X}_2(\text{YR})_4]^{2-}$ ($\text{X}, \text{Y} = \text{S}, \text{Se}$) synthetic analogs has been reported, and tentative assignments of the observed bands to bridging or terminal normal modes have been derived from the observed shifts upon $\text{S} \rightarrow \text{Se}$ substitution in either one or both positions (157). These spectra are valuable in that they display low-frequency bands (in the range of $100\text{--}200\text{ cm}^{-1}$) assignable to bending modes of the Fe-S(e) chromophore. Such bands have also been observed in some spectra of $[\text{2Fe-2X}]$ proteins (152, 154).

B. $[\text{4Fe-4Se}]$ PROTEINS

RR spectra of Se-substituted *C. pasteurianum* ferredoxin have initially been recorded to analyze the active sites of ferredoxin preparations reconstituted with mixtures of sulfide and selenide. By comparing their spectra with those of proteins containing either chalcogenide alone, they have been shown to contain hybrid clusters of the $[\text{4Fe-(4-nS-nSe)}]$ series (153), similar to those identified in synthetic analogs by ^1H NMR spectroscopy (44). Thus, no discrimination between sulfide and selenide occurs when $[\text{4Fe-4S(e)}]$ or $[\text{2Fe-2S(e)}]$ active sites are inserted into apoferredoxins (see Section III,C). Detailed studies on the synthesis of iron-sulfur clusters have shown that the reaction proceeds in two main steps, the first one being the binding of iron and the second one being the reaction with chalcogenide (158, 159). If this reaction scheme holds true for the assembly of active sites in *C. pasteurianum* ferredoxin, our results would suggest that the overall reaction is limited by the binding of iron rather than by the binding of chalcogenide (43, 153).

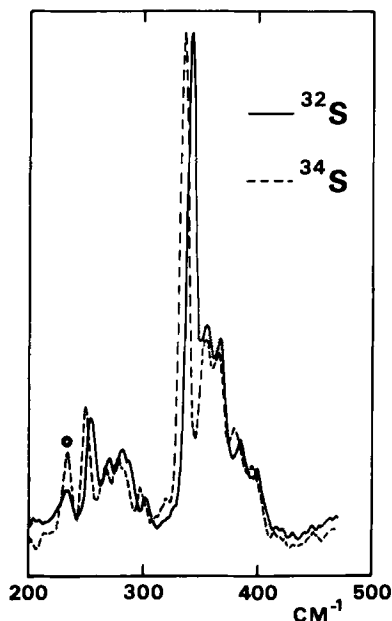


FIG. 4. Resonance Raman spectra of the native (^{32}S) and of the ^{34}S -substituted (on the inorganic sulfur atoms only) $2[4\text{Fe}-4\text{S}]$ ferredoxins from *C. pasteurianum*. The preparation of the samples and the experimental conditions have been described (58). The excitation wavelength was 457.9 nm. Two bands at 353 and 365 cm^{-1} are practically unshifted, whereas all other bands undergo conspicuous shifts to lower frequency upon ^{34}S substitution. These data have allowed a clear discrimination between the $\text{Fe}-\text{S}^*$ and the $\text{Fe}-\text{S}(\text{cys})$ stretching modes (58). The starred bands arise from the Raman scattering of ice.

RR spectra of $2[4\text{Fe}-4\text{S}]$ and $2[4\text{Fe}-4\text{Se}]$ *C. pasteurianum* ferredoxins have been analyzed in detail, using isotopic shift measurements upon $^{32}\text{S} \rightarrow ^{34}\text{S}$ (Fig. 4) and $^{76}\text{Se} \rightarrow ^{82}\text{Se}$ substitutions on the bridging chalcogenides, and determination of the depolarization ratios of most of the observed bands (58). Unlike the case of the binuclear clusters (Section VIII,A), the bridging and terminal stretching motions are largely uncoupled whether S or Se is the bridging ligand, thus enabling discrimination between the two types of modes in both cases. Additional data have been obtained with synthetic analogs possessing either aliphatic or aromatic thiolate ligands. This comprehensive set of data has allowed complete assignments to be made for the $\text{Fe}_4\text{X}_4(\text{Scys})_4$ chromophores in the framework of the D_{2d} point group (58), as an extension of previous assignments assuming T_d symmetry (151). The subsequent analysis of additional data and normal mode calculations (160) confirmed D_{2d} as

the relevant point group for $[4\text{Fe}-4\text{S}(\text{e})]$ centers in proteins, but challenged some of the previous assignments (58).

The comparative analysis of native and Se-substituted active sites has been particularly fruitful in the case of the HiPIP from *C. vinosum*. The $[4\text{Fe}-4\text{S}(\text{e})]^{2+}$ active sites of the reduced proteins have been demonstrated to display almost the same spectra and thus to assume the same D_{2d} local symmetry as in oxidized *C. pasteurianum* ferredoxin (40), in contradiction with a previous report suggesting that the active site of HiPIP experiences smaller distortions than those of low-potential ferredoxins (160). These conclusions (40) have recently been confirmed by a thorough investigation, including RR data on several ferredoxins and HiPIPs, which has unequivocally shown that the $[4\text{Fe}-4\text{S}]^{2+}$ clusters in all of the examined proteins display the same distortion from T_d symmetry (161). The availability of Se-substituted *C. vinosum* HiPIP has also allowed the vibrational properties of the oxidized $[4\text{Fe}-4\text{S}(\text{e})]^{3+}$ clusters to be analyzed: the bridging modes are only marginally affected by electron removal, whereas the Fe-S(cys) stretching modes occur at higher frequency than in the reduced protein, and with larger splittings. It has therefore been inferred that the major effect of electron exchange bears on the Fe-S(cys) bonds. One or two of the latter bonds are likely to play a crucial role in the function of these proteins (40).

IX. Prospects

Once the feasibility of exchanging the inorganic atoms in the active sites of ferredoxins was established (34), it appeared rather trivial to replace sulfide by its close analog selenide. Indeed, the first $[2\text{Fe}-2\text{Se}]$ ferredoxins were prepared soon thereafter (25, 36, 37), although more than a decade elapsed before similar substitutions were carried out in $[4\text{Fe}-4\text{S}]$ proteins (39). Generally, the substitution reactions are rather straightforward, with, in general, hardly any greater experimental difficulties for the assembly of Fe-Se active sites than for Fe-S active sites (Section III,C). It has also turned out that the Se-substituted proteins have most of their properties only marginally modified, as compared to their native counterparts (Sections V and VI).

However, the study of Se-substituted proteins has led to interesting findings. Some of these were targeted; in particular, ^{77}Se ($I = \frac{1}{2}$) was used to demonstrate that the $[2\text{Fe}-2\text{S}(\text{e})]$ active sites contain two inorganic chalcogenide atoms (36), and selenium was implemented as a vibrational band-shifting probe (Section VIII). Other findings have been serendipitous, such as the discovery in clostridial $2[4\text{Fe}-4\text{Se}]^+$ ferredoxins of high ground spin states, which have subsequently been found

to be of widespread occurrence in natural and synthetic $[4\text{Fe}-4\text{S}(\text{e})]^+$ clusters (Section VII).

These results should encourage further work on chalcogenide substitutions in iron-sulfur proteins. A promising and yet unexplored path is the replacement of sulfur by tellurium, which, if such species can be stabilized, may be expected to yield some further surprises. The successful synthesis of soluble iron-tellurium clusters (Section III,D) suggests the feasibility of their assembly in proteins.

All Se/S substitutions carried out so far have consistently shown an absence of discrimination between the two chalcogenides. This would seem to preclude the selective incorporation of selenide into a subset of atomic positions within an inorganic core. Such site-directed substitutions might nevertheless become possible upon isolation and characterization of enzymatic systems catalyzing the assembly of iron-sulfur clusters into proteins. If such reactions are stepwise, conditions might be found under which a given chalcogenide could be incorporated in predetermined positions, and another one (or an isotope) in the remaining positions. This would allow experimental approaches analogous to those implemented for the iron atoms of aconitase (162).

The replacement of sulfur by selenium has been carried out in a number of inorganic cores within iron-sulfur proteins, but not yet on the cysteinyl ligands of these active sites. Selenocysteine has now been incorporated into synthetic peptides having half the size of the smallest ferredoxins (23). Since *C. pasteurianum* ferredoxin has been chemically synthesized (163), analogs of such proteins with one or several selenocysteinyl ligands to their active sites are likely to be produced in the near future. Another possible way of incorporating selenocysteine into proteins is by chemical modification of serine residues (20), although this procedure is likely to raise some problems in the case of ferredoxins, due to their high cysteine content. A major recent advance in the biochemistry of selenium has been the discovery and characterization of an elaborate natural system incorporating selenocysteine in some proteins (Section II,B). Once this reaction mechanism is fully understood, its application to iron-sulfur proteins, by site-directed mutagenesis, could provide an elegant experimental procedure for those proteins that cannot be obtained by total synthesis or chemical modification.

REFERENCES

1. Cotton, F. A., and Wilkinson, G., "Advanced Inorganic Chemistry." Wiley, New York, 1980.
2. Odom, J. D., *Struct. Bonding* **54**, 1 (1983).

3. Frost, D. V., and Ingvaldstad, D., *Chem. Scripta* **8A**, 96 (1975).
4. Doran, J. W., in "Advances in Microbial Ecology" (K. C. Marshall, ed.), Vol. 6, p. 1. Plenum, New York, 1982.
5. Spallholz, J. E., Martin, J. L., and Ganther, H. E., eds., in "Selenium in Biology and Medicine." Avi Publ., Westport, Connecticut, 1981.
6. Schwarz, K., and Foltz, C. M., *J. Am. Chem. Soc.* **79**, 3292 (1957).
7. Diplock, A. T., *Philos. Trans. R. Soc. London, Ser. B* **294**, 105 (1981).
8. Stadtman, T. C., *Annu. Rev. Biochem.* **59**, 111 (1990).
9. Brown, T. A., and Schrifft, A., *Biol. Rev.* **57**, 59 (1982).
10. Behne, D., Kyriakopoulos, A., Meinhold, H., and Köhrle, J., *Biochem. Biophys. Res. Commun.* **173**, 1143 (1990).
11. Berry, M. J., Banu, L., and Larsen, P. R., *Nature (London)* **349**, 438 (1991).
12. Hill, K. E., Lloyd, R. S., Yang, J.-G., Read, R., and Burk, R. F. *J. Biol. Chem.* **266**, 10050 (1991).
13. Chambers, I., Frampton, J., Goldfarb, P., Affara, N., McBain, W., and Harrison, P. R., *EMBO J.* **5**, 1221 (1986).
14. Zinoni, F., Birkmann, A., Stadtman, T. C., and Böck, A., *Proc. Natl. Acad. Sci. U.S.A.* **83**, 4650 (1986).
15. Sunde, R. A., *Annu. Rev. Nutr.* **10**, 451 (1990).
16. Stadtman, T. C., *Science* **183**, 915 (1974).
17. Huber, R. E., and Criddle, R. S., *Biochim. Biophys. Acta* **141**, 587 (1967).
18. Tsen, C. C., and Tappel, A. L., *J. Biol. Chem.* **233**, 1230 (1958).
19. Kice, J. L., Lee, T. W. S., and Pan, S.-T., *J. Am. Chem. Soc.* **102**, 4448 (1980).
20. Wu, Z.-P., and Hilvert, D., *J. Am. Chem. Soc.* **111**, 4513 (1989).
- 20a. Wu, Z.-P., and Hilvert, D., *J. Am. Chem. Soc.* **112**, 5647 (1990).
21. Walter, R., and Chan, W. Y., *J. Am. Chem. Soc.* **89**, 3892 (1967).
22. Hartrodt, B., Neubert, K., Bierwolf, B., Blech, W., and Jakubke, H.-D., *Tetrahedron Lett.* **21**, 2393 (1980).
23. Oikawa, T., Esaki, N., Tanaka, H., and Soda, K., *Proc. Natl. Acad. Sci. U.S.A.* **88**, 3057 (1991).
24. Frank, P., Licht, A., Tullius, T. D., Hodgson, K. O., and Pecht, I., *J. Biol. Chem.* **260**, 5518 (1985).
25. Yang, W., Hendrickson, W. A., Kalman, E. T., and Crouch, R. J., *J. Biol. Chem.* **265**, 13553 (1990).
26. Weatherill, T. D., Rauchfuss, T. B., and Scott, R. A., *Inorg. Chem.* **25**, 1466 (1986).
27. Eidsness, M. K., Scott, R. A., Prickril, B. C., DerVartanian, D. V., LeGall, J., Moura, I., Moura, J. J. G., and Peck, H. D., Jr., *Proc. Natl. Acad. Sci. U.S.A.* **86**, 147 (1989).
28. Yang, W., Hendrickson, W. A., Crouch, R. J., and Satow, Y., *Science* **249**, 1398 (1990).
29. He, S. H., Teixeira, M., LeGall, J., Patil, D. S., Moura, I., Moura, J. J. G., DerVartanian, D. V., Huynh, B. H., and Peck, H. D., Jr., *J. Biol. Chem.* **264**, 2678 (1989).
30. Mullen, G. P., Dunlap, R. B., and Odom, J. D., *J. Am. Chem. Soc.* **107**, 7187 (1985).
31. Gettins, P., and Crews, B. C., *J. Biol. Chem.* **266**, 4804 (1991).
32. Mortenson, L. E., Valentine, R. C., and Carnahan, J. E., *Biochem. Biophys. Res. Commun.* **7**, 448 (1962).
33. Tagawa, K., and Arnon, D. I., *Nature (London)* **195**, 537 (1962).
34. Malkin, R., and Rabinowitz, J. C., *Biochem. Biophys. Res. Commun.* **23**, 822 (1966).
- 34a. Hong, J.-S., and Rabinowitz, J. C., *Biochem. Biophys. Res. Commun.* **29**, 246 (1967).

35. Tsibris, J. C. M., Namtvedt, M. J., and Gunsalus, I. C., *Biochem. Biophys. Res. Commun.* **30**, 323 (1968).
36. Orme-Johnson, W. H., Hansen, R. E., Beinert, H., Tsibris, J. C. M., Bartholomaeus, R. C., and Gunsalus, I. C., *Proc. Natl. Acad. Sci. U.S.A.* **60**, 368 (1968).
37. Fee, J. A., and Palmer, G., *Biochim. Biophys. Acta* **245**, 175 (1971).
38. Sugiura, Y., Ishizu, K., and Kimura, T., *Biochemistry* **14**, 97 (1975).
39. Meyer, J., and Moulis, J.-M., *Biochem. Biophys. Res. Commun.* **103**, 667 (1981).
40. Moulis, J.-M., Lutz, M., Gaillard, J., and Noodleman, L., *Biochemistry* **27**, 8712 (1988).
41. Surerus, K. K., Kennedy, M. C., Beinert, H., and Münck, E., *Proc. Natl. Acad. Sci. U.S.A.* **86**, 9846 (1989).
42. Hong, J.-S., and Rabinowitz, J. C., *J. Biol. Chem.* **245**, 6582 (1970).
43. Moulis, J.-M., and Meyer, J., *Biochemistry* **21**, 4762 (1982).
44. Reynolds, J. G., and Holm, R. H., *Inorg. Chem.* **20**, 1873 (1981).
45. Petering, D., Fee, J. A., and Palmer, G., *J. Biol. Chem.* **246**, 643 (1971).
46. Wood, J. L., in "Methods in Enzymology" (W. B. Jakoby and O. Griffith) Vol. 143, p. 25. Academic Press, New York, 1987.
47. Rao, K. K., Cammack, R., Hall, D. O., and Johnson, C. E., *Biochem. J.* **122**, 257 (1971).
48. Meyer, J., Moulis, J.-M., and Lutz, M., *Biochim. Biophys. Acta* **871**, 243 (1986).
49. Gaillard, J., Moulis, J.-M., Auric, P., and Meyer, J., *Biochemistry* **25**, 464 (1986).
50. Kennedy, M. C., and Beinert, H., *J. Biol. Chem.* **263**, 8194 (1988).
51. Que, L., Jr., Holm, R. H., and Mortenson, L. E., *J. Am. Chem. Soc.* **97**, 463 (1975).
52. Bonomi, F., and Kurtz, D. M., Jr., *Anal. Biochem.* **142**, 226 (1984).
53. Orme-Johnson, W. H., and Holm, R. H., in "Methods in Enzymology" (S. Fleischer and L. Packer, eds.), Vol. 53, p. 268. Academic Press, New York, 1978.
54. Waitkins, G. R., and Shutt, R., *Inorg. Synth.* **2**, 183 (1946).
55. Nitsche, R., *Angew. Chem.* **69**, 333 (1957).
56. Klayman, D. L., and Griffin, T. S., *J. Am. Chem. Soc.* **95**, 197 (1973).
57. Fee, J. A., Mayhew, S. G., and Palmer, G., *Biochim. Biophys. Acta* **245**, 196 (1971).
58. Moulis, J.-M., Meyer, J., and Lutz, M., *Biochemistry* **23**, 6605 (1984).
59. Moulis, J.-M., *Ph.D. Thesis*, University of Grenoble, Grenoble, France (1985).
60. Klemm, W., Sodomann, H., and Langmesser, P., *Z. Anorg. Allg. Chem.* **241**, 281 (1939).
61. Bronger, W., Kimpel, M., and Schmitz, D., *Angew. Chem., Int. Ed. Engl.* **21**, 544 (1982).
62. Arakawa, S., and Kimura, T., *Biochim. Biophys. Acta* **580**, 382 (1979).
63. Simon, W., Wilk, A., Krebs, B., and Henkel, G., *Angew. Chem., Int. Ed. Engl.* **26**, 1009 (1987).
- 63a. Krebs, B., and Henkel, G., *Angew. Chem., Int. Ed. Engl.* **30**, 769 (1991).
64. Barbaro, P., Bencini, A., Bertini, I., Briganti, F., and Midollini, S., *J. Am. Chem. Soc.* **112**, 7238 (1990).
65. Hausinger, R. P., *BioFactors* **2**, 179 (1990).
66. Hall, D. O., Cammack, R., and Rao, K. K., *Nature (London)* **233**, 136 (1971).
67. Sugiura, Y., Ishizu, K., and Kimura, T., *Biochem. Biophys. Res. Commun.* **60**, 334 (1974).
68. Christou, G., Ridge, B., and Rydon, H. N., *J. Chem. Soc., Chem. Commun.* p. 20 (1979).
69. Pagani, S., Bonomi, F., and Cerletti, P., *Eur. J. Biochem.* **142**, 361 (1984).
70. Bonomi, F., Pagani, S., and Kurtz, D. M., Jr., *Eur. J. Biochem.* **148**, 67 (1985).

71. Sandberg, W., Graves, M. C., and Rabinowitz, J. C., *Trends Biochem. Sci.* **12**, 56 (1987).
72. Takahashi, Y., Mitsui, A., Hase, T., and Matsubara, H., *Proc. Natl. Acad. Sci. U.S.A.* **83**, 2434 (1986).
73. Takahashi, Y., Mitsui, A., Fujita, Y., and Matsubara, H., *Plant Physiol.* **95**, 104 (1991).
74. Dean, D. R., and Jacobson, M. R., in "Nitrogen Fixation" (G. Stacey, R. H. Burris, and H. J. Evans, eds.), p. 759. Chapman & Hall, London, 1991.
75. Voordouw, G., Hagen, W. R., Krüse-Wolters, K. M., van Berkel-Arts, A., and Veeger, C., *Eur. J. Biochem.* **162**, 31 (1987).
76. Meyer, J., Bruschi, M. H., Bonicel, J. J., and Bovier-Lapierre, G. E., *Biochemistry* **25**, 6054 (1986).
77. Bobrik, M. A., Laskowski, E. J., Johnson, R. W., Gillum, W. O., Berg, J. M., Hodgson, K. O., and Holm, R. H., *Inorg. Chem.* **17**, 1402 (1978).
- 77a. Yu, S.-B., Papaefthymiou, G. C., and Holm, R. H., *Inorg. Chem.* **30**, 3476 (1991).
78. Maskiewicz, R., and Bruce, T. C., *Biochemistry* **16**, 3024 (1977).
79. Reynolds, J. G., and Holm, R. H., *Inorg. Chem.* **19**, 3257 (1980).
80. Christou, G., Ridge, B., and Rydon, H. N., *J. Chem. Soc., Chem. Commun.*, 1423 (1978).
81. Wilson, G. S., Tsibris, J. C. M., and Gunsalus, I. C., *J. Biol. Chem.* **248**, 6059 (1973).
82. Mukai, K., Huang, J. J., and Kimura, T., *Biochim. Biophys. Acta* **336**, 427 (1974).
83. Cammack, R., in "Charge and Field Effects in Biosystems" (M. J. Allen and P. N. R. Usherwood, eds.), p. 41. Abacus Press, Tunbridge Wells, U.K., 1984.
84. Beinert, H., and Sands, R. H., *Biochem. Biophys. Res. Commun.* **3**, 41 (1960).
85. Brintzinger, H., Palmer, G., and Sands, R. H., *Proc. Natl. Acad. Sci. U.S.A.* **55**, 397 (1966).
86. Gibson, J. F., Hall, D. O., Thornley, J. H. M., and Whatley, F. R., *Proc. Natl. Acad. Sci. U.S.A.* **56**, 987 (1966).
87. Cammack, R., Dickson, D. P. E., and Johnson, C. E., in "Iron-Sulfur Proteins" (W. Lovenberg, ed.), Vol. 3, p. 283. Academic Press, New York, 1977.
88. Johnson, M. K., Robinson, A. E., and Thomson, A. J., in "Iron-Sulfur Proteins" (T. G. Spiro, ed.), p. 367. Wiley (Interscience), New York, 1982.
89. Phillips, W. D., and Poe, M., in "Iron-Sulfur Proteins" (W. Lovenberg, ed.), Vol. 2, p. 255. Academic Press, New York, 1973.
90. Sands, R. H., and Dunham, W. R., *Q. Rev. Biophys.* **7**, 443 (1975).
91. Bertrand, P., and Gayda, J.-P., *Biochim. Biophys. Acta* **579**, 107 (1979).
92. Fee, J. A., Findling, K. L., Yoshida, T., Hille, R., Tarr, G. E., Hearshen, D. O., Dunham, W. R., Day, E. P., Kent, T. A., and Münck, E., *J. Biol. Chem.* **259**, 124 (1984).
93. Beardwood, P., and Gibson, J. F., *J. Chem. Soc., Dalton Trans.*, 737 (1983).
94. Münck, E., Debrunner, P. G., Tsibris, J. C. M., and Gunsalus, I. C., *Biochemistry* **11**, 855 (1972).
95. Bowman, M., Kevan, L., Mukai, K., and Kimura, T., *Biochim. Biophys. Acta* **328**, 244 (1973).
96. Bertrand, P., and Gayda, J.-P., *Biochim. Biophys. Acta* **625**, 337 (1980).
97. Reynolds, J. G., Coyle, C. L., and Holm, R. H., *J. Am. Chem. Soc.* **102**, 4350 (1980).
98. Gaillard, J., Moulis, J.-M., and Meyer, J., *Inorg. Chem.* **26**, 320 (1987).
99. George, S. J., Thomson, A. J., Crabtree, D. E., Meyer, J., and Moulis, J.-M., *New J. Chem.* **15**, 455 (1991).

100. Moulis, J.-M., Auric, P., Gaillard, J., and Meyer, J., *J. Biol. Chem.* **259**, 11396 (1984).
101. Auric, P., Gaillard, J., Meyer, J., and Moulis, J.-M., *Biochem. J.* **242**, 525 (1987).
102. Rius, G., and Lamotte, B., *J. Am. Chem. Soc.* **111**, 2464 (1989).
103. Sola, M., Cowan, J. A., and Gray, H. B., *J. Am. Chem. Soc.* **111**, 6627 (1989).
104. Laskowski, E. J., Reynolds, J. G., Frankel, R. B., Foner, S., Papaefthymiou, G. C., and Holm, R. H., *J. Am. Chem. Soc.* **101**, 6562 (1978).
- 104a. Collison, D., and Mabbs, F. E., *J. Chem. Soc., Dalton Trans.*, 1565 (1982).
105. Zimmermann, R., Münck, E., Brill, W. J., Shah, V. K., Henzl, M. T., Rawlings, J., and Orme-Johnson, W. H., *Biochim. Biophys. Acta* **537**, 185 (1978).
106. Vollmer, S. J., Switzer, R. L., and Debrunner, P. G., *J. Biol. Chem.* **258**, 14284 (1983).
107. Mathews, R., Charlton, S., Sands, R. H., and Palmer, G., *J. Biol. Chem.* **249**, 4326 (1974).
108. Orme-Johnson, W. H., *Annu. Rev. Biophys. Biophys. Chem.* **14**, 419 (1985).
109. Lindahl, P. A., Day, E. P., Kent, T. A., Orme-Johnson, W. H., and Münck, E., *J. Biol. Chem.* **260**, 11160 (1985).
110. Zumft, W. G., Palmer, G., and Mortenson, L. E., *Biochim. Biophys. Acta* **292**, 413 (1973).
111. Lindahl, P. A., Gorelick, N. J., Münck, E., and Orme-Johnson, W. H., *J. Biol. Chem.* **262**, 14945 (1987).
112. Watt, G. D., and McDonald, J. W., *Biochemistry* **24**, 7226 (1985).
113. Hagen, W. R., Eady, R. R., Dunham, W. R., and Haaker, H., *FEBS Lett.* **189**, 250 (1985).
114. Morgan, T. V., Prince, R. C., and Mortenson, L. E., *FEBS Lett.* **206**, 4 (1986).
115. Meyer, J., Gaillard, J., and Moulis, J.-M., *Biochemistry* **27**, 6150 (1988).
116. Holm, R. H., Ciurli, S., and Weigel, J. A., *Prog. Inorg. Chem.* **38**, 1 (1990).
117. Carney, M. J., Holm, R. H., Papaefthymiou, G. C., and Frankel, R. B., *J. Am. Chem. Soc.* **108**, 3519 (1986).
118. Carney, M. J., Papaefthymiou, G. C., Spartalian, K., Frankel, R. B., and Holm, R. H., *J. Am. Chem. Soc.* **110**, 6084 (1988).
119. Carney, M. J., Papaefthymiou, G. C., Whitener, M. A., Spartalian, K., Frankel, R. B., and Holm, R. H., *Inorg. Chem.* **27**, 346 (1988).
120. Carney, M. J., Papaefthymiou, G. C., Frankel, R. B., and Holm, R. H., *Inorg. Chem.* **28**, 1497 (1989).
- 120a. Bolin, J. T., Campobasso, N., Muchmore, S. W., Minor, W., Mortenson, L. E., and Morgan, T. V., Abstract K004, Fifth International Conference on Bioinorganic Chemistry, Oxford, 1991.
121. McLean, P. A., Papaefthymiou, V., Orme-Johnson, W. H., and Münck, E., *J. Biol. Chem.* **262**, 12900 (1987).
122. Johnson, M. K., Thomson, A. J., Robinson, A. E., and Smith, B. E., *Biochim. Biophys. Acta* **671**, 61 (1981).
123. Smith, J. P., Emptage, M. H., and Orme-Johnson, W. H., *J. Biol. Chem.* **257**, 2310 (1982).
124. Hagen, W. R., Wassink, H., Eady, R. R., Smith, B. E., and Haaker, H., *Eur. J. Biochem.* **169**, 457 (1987).
125. Lindahl, P. A., Papaefthymiou, V., Orme-Johnson, W. H., and Münck, E., *J. Biol. Chem.* **263**, 19412 (1988).
126. Switzer, R. L., *BioFactors* **2**, 77 (1989).
127. Grandoni, J. A., Switzer, R. L., Makaroff, C. A., and Zalkin, H., *J. Biol. Chem.* **264**, 6058 (1989).

128. Oñate, Y. A., Vollmer, S. J., Switzer, R. L., and Johnson, M. K., *J. Biol. Chem.* **264**, 18386 (1989).
129. Wong, J. Y., Meyer, E., and Switzer, R. L., *J. Biol. Chem.* **252**, 7424 (1977).
130. Conover, R. C., Kowal, A. T., Fu, W., Park, J.-B., Aono, S., Adams, M. W. W., and Johnson, M. K., *J. Biol. Chem.* **265**, 8533 (1990).
131. Conover, R. C., Park, J.-B., Adams, M. W. W., and Johnson, M. K., *J. Am. Chem. Soc.* **113**, 2799 (1991).
132. Armstrong, F. A., George, S. J., Cammack, R., Hatchikian, E. C., Thomson, A. J., *Biochem. J.* **264**, 265 (1989).
133. George, S. J., Armstrong, F. A., Hatchikian, E. C., and Thomson, A. J., *Biochem. J.* **264**, 275 (1989).
134. Zambrano, I. C., Kowal, A. T., Mortenson, L. E., Adams, M. W. W., and Johnson, M. K., *J. Biol. Chem.* **264**, 20974 (1989).
135. Lindahl, P. A., Münck, E., and Ragsdale, S. W., *J. Biol. Chem.* **265**, 3873 (1990).
136. La Mar, G. N., in "Biological Applications of Magnetic Resonance" (R. G. Shulman, ed.), p. 305. Academic Press, New York, 1979.
137. Phillips, W. D., and Poe, M., in "Methods in Enzymology" (A. S. Pietro, ed.), Vol. 24, p. 304. Academic Press, New York, 1972.
138. Georgiadis, M. M., Chakrabarti, P., and Rees, D. C., in "Nitrogen Fixation: Achievements and Objectives" (P. M. Gresshoff, L. E. Roth, G. Stacey, and W. E. Newton, eds.), p. 111. Chapman & Hall, New York, 1990.
139. Reynolds, J. G., Laskowski, E. J., and Holm, R. H., *J. Am. Chem. Soc.* **100**, 5315 (1978).
140. Bertrand, P., *Struct. Bonding* **75**, 1 (1991).
141. Adman, E. T., Sieker, L. C., and Jensen, L. H., *J. Biol. Chem.* **251**, 3801 (1976).
142. Tranqui, D., Fanchon, E., Vicat, J., Sieker, L. C., Meyer, J., Moulis, J.-M., Gagnon, J., and Duée, E. D., Abstract D049, Fifth International Conference on Bioinorganic Chemistry, Oxford, 1991.
143. Noodleman, L., *Inorg. Chem.* **30**, 246 (1991).
144. Noodleman, L., *Inorg. Chem.* **30**, 256 (1991).
145. Meyer, J., Moulis, M., and Lutz, M., in "Frontiers in Bioinorganic Chemistry" (A. V. Xavier, ed.), p. 537. VCH Verlag, Weinheim, 1986.
146. Long II, T. V., and Loehr, T. M., *J. Am. Chem. Soc.* **92**, 6384 (1970).
147. Tang, S.-P. W., Spiro, T. G., Mukai, K., and Kimura, T., *Biochem. Biophys. Res. Commun.* **53**, 869 (1973).
148. Tang, S.-P. W., Spiro, T. G., Antanaitis, C., Moss, T. H., Holm, R. H., Herskovitz, T., and Mortenson, L. E., *Biochem. Biophys. Res. Commun.* **62**, 1 (1975).
149. Lutz, M., *Biochim. Biophys. Acta* **460**, 408 (1977).
150. Lutz, M., Moulis, J.-M., and Meyer, J., *FEBS Lett.* **163**, 212 (1983).
151. Johnson, M. K., Czernuszewicz, R. S., Spiro, T. G., Fee, J. A., and Sweeney, W. V., *J. Am. Chem. Soc.* **105**, 6671 (1983).
152. Meyer, J., Moulis, J.-M., and Lutz, M., *Biochem. Biophys. Res. Commun.* **119**, 828 (1984).
153. Moulis, J.-M., Meyer, J., and Lutz, M., *Biochem. J.* **219**, 829 (1984).
154. Meyer, J., Moulis, J.-M., and Lutz, M., *Biochim. Biophys. Acta* **873**, 108 (1986).
155. Yachandra, V. K., Hare, J., Gewirth, A., Czernuszewicz, R. S., Kimura, T., Holm, R. H., and Spiro, T. G., *J. Am. Chem. Soc.* **105**, 6462 (1983).
156. Han, S., Czernuszewicz, R. S., Kimura, T., Adams, M. W. W., and Spiro, T. G., *J. Am. Chem. Soc.* **111**, 3505 (1989).
157. Beardwood, P., and Gibson, J. F., *J. Chem. Soc., Dalton Trans.*, 1507 (1984).

- 158. Christou, G., Ridge, B., and Rydon, H. N., *J. Chem. Soc., Chem. Commun.*, 908 (1977).
- 159. Hagen, K. S., Reynolds, J. G., and Holm, R. H., *J. Am. Chem. Soc.* **103**, 4054 (1981).
- 160. Czernuszewicz, R. S., Macor, K. A., Johnson, M. K., Gewirth, A., and Spiro, T. G., *J. Am. Chem. Soc.* **109**, 7178 (1987).
- 161. Backes, G., Mino, Y., Loehr, T. M., Meyer, T. E., Cusanovich, M. A., Sweeney, W. V., Adman, E. T., and Sanders-Loehr, J., *J. Am. Chem. Soc.* **113**, 2055 (1991).
- 162. Beinert, H., and Kennedy, M. C., *Eur. J. Biochem.* **186**, 5 (1989).
- 163. Smith, E. T., Feinberg, B. A., Richards, J. H., and Tomich, J. M., *J. Am. Chem. Soc.* **113**, 688 (1991).

DYNAMIC ELECTROCHEMISTRY OF IRON-SULFUR PROTEINS

FRASER A. ARMSTRONG

Department of Chemistry, University of California, Irvine, Irvine, California 92717

- I. Introduction
- II. Background
 - A. Some Recent Developments with Fe-S Clusters
 - B. Problems Encountered in Studying Reactions of Fe-S Clusters in Proteins
 - C. Useful Features of Direct (Unmediated) Dynamic Electrochemistry
 - D. Achieving Direct Electrochemistry of Ferredoxins
- III. Applications
 - A. Redox Properties of *Azotobacter* Ferredoxin I and Site-Directed Mutant Forms
 - B. Characterizing the Fe-S Clusters in *Desulfovibrio africanus* Ferredoxin III, a Protein Containing a Reactive [3Fe-4S] Cluster
 - C. Investigating Cluster Reactivities in Adsorbed Protein Films
- IV. Conclusions
- References

I. Introduction

Modern dynamic electrochemical methods¹ offer a powerful yet relatively inexpensive means for studying a variety of redox-active chemical systems. It is widely recognized that in addition to providing detailed thermodynamic and kinetic information, their use can yield valuable qualitative insight into aspects of complicated reactivities. Yet, while dynamic electrochemical techniques have made important contributions to coordination chemistry, even such now-standard meth-

¹ My use of the term "dynamic electrochemistry" refers to experiments in which one monitors a reaction via measurement of current (in this case a net flow of electrons) at the working electrode. There is a clear and important distinction to be made with "static electrochemistry," notably potentiometry, which is concerned with measurement of the position of equilibrium (i.e., the potential of zero net current) at the electrode.

ods as cyclic voltammetry have remained largely unexploited for the investigation of metal centers in proteins. Why? As I now hope to convey in this article, electrochemical methods afford interesting possibilities for exploring and quantitatively examining reactions of Fe-S clusters in both the time domain and the potential domain.

A major view that may account for the underuse of dynamic electrochemical methods for studying proteins reflects the experimental difficulties that are encountered. It is important to obtain a *direct* electrochemical response—that is, without the need for a mediator (typically a small, stable molecule displaying clean and reversible electrochemistry) to relay electrons between the protein's active site and the electrode. Generally speaking, the achievement of direct (i.e., unmediated) electrochemistry of various proteins has not proved straightforward. Two problems in particular have to be overcome (1–3). First, since redox centers in proteins tend to be shielded from the solvent by a variable intervening medium, electron exchange with an external redox agent depends upon the formation of a precursor assembly within which the two molecules are positioned so as to optimize electronic coupling (interaction between donor and acceptor wavefunctions). This requirement is serviced through noncovalent interactions involving a number of surface groups, and provides kinetic specificity in biological electron transfer (4–6). Clearly, in order to engage such selective macromolecules productively at an electrode, similar kinds of interactions need to be generated. Second, any such intimate association between electrode surface and protein must not cause denaturation, particularly if the denatured product remains adsorbed. This may occur, particularly if the protein is conformationally labile (7).

An alternative view is that the underuse of dynamic electrochemical methods for characterizing redox proteins reflects what is in my view an unfortunate misconception, namely, that such techniques provide the same information as may be obtained by mediated redox potentiometry. Naturally, so long as this notion persists, there exists little stimulus for the efforts necessary to achieve and interpret a direct, dynamic electrochemical response from a protein system. Indeed, for determining reduction potentials of uncomplicated redox couples, potentiometric methods are certainly more widely applicable (8).

In this article, I wish to provide some perception of the contribution that can be made by dynamic electrochemical methods toward the often difficult task of defining reactions of Fe-S clusters in a protein molecule. Despite the relatively modest amount of material published to date, these reports do show that such an approach, when combined with appropriate spectroscopic techniques, can yield valuable insight

that is not obtained readily or in acceptable detail by other means. Most of the work described has taken place in my own laboratory and in collaboration with other scientists. My emphasis is upon the detection and study of unusual or subtle features of reactivity, and I have not dwelled heavily upon studies that have focused upon voltammetry as an alternative to potentiometry. Although electrochemistry is both a broad and mathematically sophisticated field, it is covered in several excellent textbooks that provide clear descriptions of theory and experimental procedures (9–12). Thus only supplementary concepts and necessary clarification will be presented throughout the text.

II. Background

A. SOME RECENT DEVELOPMENTS WITH Fe-S CLUSTERS

Several significant developments have occurred during the past decade. Stemming from endeavors in various disciplines—molecular biology, spectroscopy, crystallography, and synthetic “model” chemistry—they are described in detail by other authors in this volume and only a brief summary is presented here.

1. A wide-reaching biological aspect is the realization that Fe-S clusters have important functions outside the established realm of electron transport (13). More specific catalytic roles are being established—most significantly in the area of nonredox enzymes. Due to the efforts of Beinert and his co-workers, much is now known about the structure and mechanism of aconitase, a dehydratase of the citric acid cycle, in which the active site [4Fe-4S] cluster catalyzes the interconversion between citrate and isocitrate (14). Most recently, evidence has been presented that suggests that Fe-S clusters may be involved directly in the genetic regulation of Fe levels in eukaryotic cells (15, 16).

2. The formulation of a class of clusters as [3Fe-4S] (essentially a [4Fe-4S] cubane with one Fe missing) is now established, following a decade of disagreement between the conclusions stemming from spectroscopy and crystallography (17–24).

3. There has been growing awareness of diversity in the modes of coordination of Fe-S clusters. In addition to cysteine thiolate, it is now clear that other protein donor groups can be ligands to Fe. For example, the “Rieske”-type [2Fe-2S] cluster is coordinated by two cysteine thiolate S atoms to one Fe and by two imidazole N atoms (histidine) to

the other (25). Exogenous (nonprotein) ligands may be coordinated. Aconitase provides such an example; here, one Fe of the [4Fe-4S] cluster is not bound to a protein donor but to OH⁻ (26, 27). This "subsite-differentiated" Fe atom is also the site of substrate binding.

4. The ability of Fe-S clusters to alter their structure within certain protein hosts is now recognized. Specifically, several examples are established in which [3Fe-4S] and [4Fe-4S] clusters interconvert readily (13, 14, 28-30). In the case of aconitase, isolation under aerobic conditions induces release of the labile, subsite-differentiated Fe atom and loss of catalytic activity (14). Activation of the inactive enzyme involves addition of Fe(II) to the reduced [3Fe-4S]⁰ cluster. Taking this theme further, it has recently been reported that the amino acid sequence of human iron-responsive element binding protein (IRE-BP), which regulates the expression of ferritin and of transferrin receptor, bears marked homology with sequence of aconitase (pig heart mitochondria) (15, 16). This has raised some speculation that interconversion between [3Fe-4S] and [4Fe-4S] clusters may provide a basis for sensing the Fe activity in the cytoplasm or an organelle.

5. There is spectroscopic evidence for the existence of Fe-S clusters having more than four Fe atoms (31).

6. Addition of metals other than Fe to [3Fe-4S] clusters has been demonstrated *in vitro* for certain proteins (32-36). Studies with such heterometal clusters are leading to a greater understanding of complex magnetic properties. There is also the possibility that heterometal clusters may be more widespread in nature than is currently recognized (we are already aware, for example, of the existence of Fe-Mo-S or Fe-V-S clusters as cofactors of nitrogenase) (37, 38).

7. Synthesis and characterization of "model" complexes has continued to be a powerful strategy for understanding the fundamental chemical and spectroscopic properties of Fe-S clusters. Efforts by Holm and others are now directed at achieving discrete, subtle variants of Fe-S clusters, creating what they have termed "subsite specific" systems, and examining their chemical and spectroscopic properties (39-46).

B. PROBLEMS ENCOUNTERED IN STUDYING REACTIONS OF Fe-S CLUSTERS IN PROTEINS

These developments highlight the importance of *dynamic* properties that must be relevant to the *in vivo* functioning of clusters, particularly in catalysis or regulation. To gain a greater understanding of these aspects it is necessary to examine equilibria and kinetics of metal and ligand interchange, and to determine how these reactivities vary with

the cluster oxidation level (and, consequently, upon the electrochemical potential of the surrounding environment). Sensitive, quantitative measurements need to be made. Current strategies for studying reactions of Fe-S clusters in proteins are dominated by a general theme—that is, the preparation and spectroscopic examination of a sample in some stationary homogeneous state. Such a strategy focuses upon the characterization of structural, electronic, and magnetic properties of the isolated species. However, certain limitations are apparent. First, the most widely used spectroscopic methods for studying Fe-S clusters—electron paramagnetic resonance (EPR), electron-nuclear double resonance (ENDOR), Mössbauer, magnetic circular dichroism (MCD) and resonance Raman—each require the sample to be in the frozen state. To monitor reactions in the time domain at ambient temperature it is necessary to use nuclear magnetic resonance (NMR) or circular dichroism (CD), since absorption spectra of Fe-S species are typically broad and devoid of characteristic features. Second, in order to probe tight-binding equilibria (dissociation constants in the micromolar range or lower) it is necessary to make measurements with low concentrations of protein. However, most spectroscopic techniques require cluster concentrations that are higher than $50\ \mu M$. Third, sample preparation is often slow and is usually complicated by the need to manipulate sensitive materials under critical conditions of controlled potential.

C. USEFUL FEATURES OF DIRECT (UNMEDIATED) DYNAMIC ELECTROCHEMISTRY

Dynamic electrochemical methods have several useful features for studies of redox proteins.

1. In appropriate cases, the voltammetric response (i.e., the voltage-current profile) constitutes a "signal" that can be assigned to a specific species (redox couple). For Fe-S clusters this is particularly useful since a convenient label is now provided. The usefulness continues for proteins that contain several clusters, provided their reduction potentials are sufficiently separated.

2. In the absence of a requirement for artificial redox mediators, electrochemistry is dynamically interactive and enables quantitative studies to be undertaken in the time domain. It is possible to transform and monitor states simultaneously under potential control, and to maneuver reversibly with respect to potential on short time scales. New species formed as a result of redox activity may be studied as coupled equilibria or "trapped," depending upon the electrochemical time scale.

3. The useful potential range is wide and continuous, being restricted only by the limits for electrical breakdown of the solvent or electrode surface and not by the properties of mediators or titrants. Voltammetry of neutral aqueous solutions at carbon electrodes is feasible at potentials more negative than -1 V and more positive than 0.8 V (all potentials given are versus the standard hydrogen electrode). By contrast, the useful lower limit for sodium dithionite, the most widely used biochemical reductant, is around -550 mV at pH 7 (47). As described later, voltammetry has been used to study chemically reversible redox transitions occurring at electrode potentials of -0.75 V or lower.

The above-mentioned features are generally applicable and have been exploited in several studies of Fe-S proteins. Even so, much more can be gained in terms of experimental refinement by restricting our observation to protein molecules that are immobilized at the electrode surface, i.e., not diffusing rapidly between the electrode and bulk solution. Since electron transfer is dependent upon specific protein-electrode interactions, an electrode surface that is not homogeneous may appear to an approaching protein molecule as an array of microelectrodes—that is, some areas being active (sites at which interaction leads to very fast electron transfer, i.e., reversible electrochemistry) and others being inactive (sites at which the protein does not interact in such a way, i.e., giving extremely irreversible electrochemistry) (48–50). In the limit of the entire electrode surface being active, the situation becomes that of linear diffusion to a planar macroelectrode and the voltammetric response conforms to the theory described by Nicholson and Shain (51). If, however, the fraction of active areas is small, the situation becomes that of radial diffusion to a microelectrode, and a steady-state voltammetric response (a sigmoidal wave) is obtained (48). The broad, poorly defined waveforms that are observed commonly for cyclic voltammetry of protein solutions may therefore be a combination of peaklike (linear diffusion) and sigmoidal (radial diffusion) waveforms.

Exploited with caution, the voltammetry of adsorbed protein molecules offers many important and useful features. The schematic shown in Fig. 1 illustrates what we can regard as an idealized situation. The concept is described as follows:

1. Redox-active protein molecules are adsorbed at an electrode surface. Electron transfer between the electrode and the protein's redox-active site(s) occurs reversibly.

2. Adsorption occurs with minimal conformational disruption and native functional properties are retained throughout the experimental

range of applied electrode potential. (While a large electric field can significantly alter the properties of a protein molecule, it should be borne in mind that fields of varying strength exist also at biological membranes.)

3. The coverage is monolayer or lower, and active sites in each protein molecule behave independently (but identically) to those in neighboring molecules.

Formation of such an array can depend critically upon conditions such as electrode surface preparation and modification, solution ionic composition and pH, and coadsorption of other complex molecules, as indicated by the triangular shapes in Fig. 1. Since the protein molecules are absent from the electrolyte solution and none effectively leaves the electrode surface, all the charge that passes across the protein-electrode interface is accounted for in what may be regarded as a closed system. Analysis of the observed voltammetric response yields quantitative information on reactivities of specific active sites—information that for very reactive systems may be difficult to obtain by more conventional methods.

Some specific advantages of studying protein molecules adsorbed as an electroactive monolayer/submonolayer are as follows:

1. The status of each redox-active site may be addressed on a rapid time scale. Unlike the situation in which the electrode contacts a “thick” solution of freely diffusing protein molecules, the voltammetric (linear sweep or cyclic) response that is observed for a well-behaved

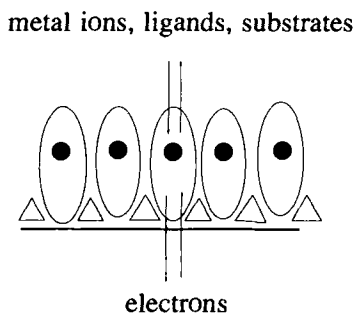


FIG. 1. Schematic illustrating a layer of protein and coadsorbate molecules strongly adsorbed at an electrode surface. In an ideal situation, redox-active sites behave independently of each other, exhibit reversible electrochemistry, and interact freely with reagents in the contacting electrolyte.

surface-confined system is compact and finite. Figure 2 illustrates the limiting (ideal) case described by Laviron, in which a reversible, diffusionless electron transfer reaction occurs uncomplicated by species heterogeneity, intersite interaction, or coupled chemistry (52–54). Peak potentials correspond to the formal reduction potential $E^{0'}$, the separation between reduction and oxidation peaks (ΔE_p) is 0 mV, and the theoretical peak width at half-height (δ) is $91/n$ mV at 25°C, where n is the number of electrons required to be transferred in the process.

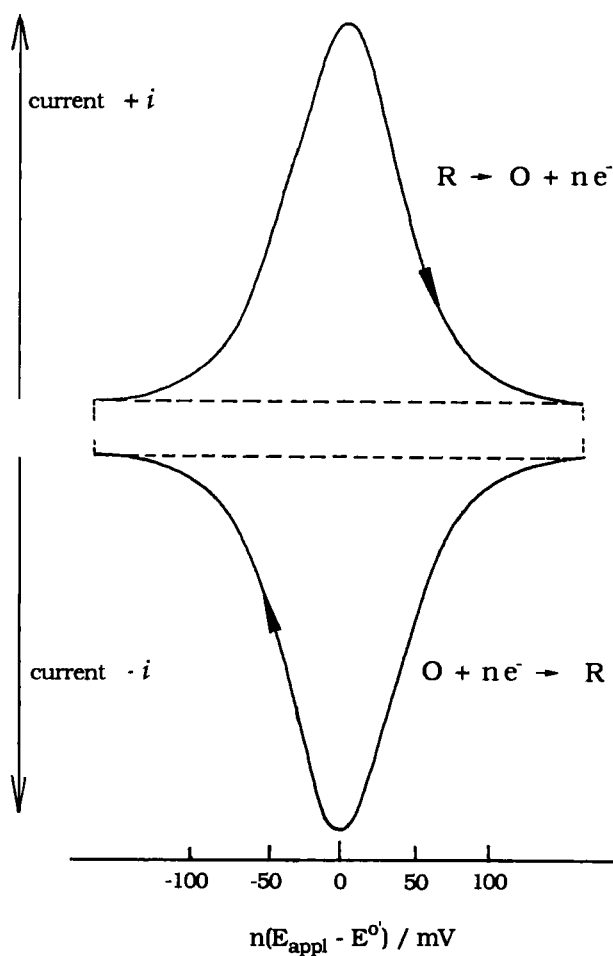


FIG. 2. Theoretical cyclic voltammogram for an ideal, reversible, electrode reaction of an adsorbed redox couple (see Refs. 52–54).

2. For each redox couple, the following readily measured parameters are analytically useful: the area under the wave yields the total charge exchanged between the electrode and the active site (for multicentered proteins, ratios of areas of separate waves can yield the relative site stoichiometries); the parameter δ gives information on species heterogeneity and intersite interactions; and the standard rate constant (k^0) for electron exchange (if this falls short of being reversible) can be estimated from ΔE_p (53, 54). Complex waveforms arise if two or more redox couples have similar reduction potentials; however, these are more readily resolved than for the case of diffusing redox couples.

3. The amount of material required to form a monolayer at a typical electrode surface (0.2 cm²) corresponds to a picomole or less. Thus a large number of experiments can be conducted with a limited supply of precious sample.

4. Sensitivity for determination of tight-binding equilibria is good. The small number of molecules under examination makes it possible to study and quantify reactions that occur between the protein active sites and reagents that are contained in the electrolyte at high dilution. In terms of this sensitivity to trace reagents, the philosophy bears resemblance to that of stripping voltammetry (9–12). Effects of solvents (such as glassing agents required for MCD spectroscopy) can also be screened, without risking sacrifice of a significant amount of precious material.

5. By analysis of the voltammetric response, it is possible to obtain kinetic information; this includes the rates of entry and release of reagents at specific centers.

6. If the adsorbed protein is an enzyme, the capability for precisely imposing a continuously variable electrode potential enables detailed examination of the potential dependence of catalytic function. Such an ability to fine tune the electrode potential (and thus vary the driving force for the electrode–protein electron transfer step) can lead to the detection of gating effects and the identification of redox-active groups that may regulate electron flow, depending upon their redox status.

Which techniques are most useful? Electrochemistry offers a wide selection. To date, direct current (DC) cyclic voltammetry has been the most widely used method, but as mentioned earlier, the linear sweep response obtained with a protein solution often consists of just a weak sigmoidal-like wave. Where greater current sensitivity and potential resolution are required, potential-step techniques, particularly square-wave voltammetry, offer considerable advantages since the response is greatly amplified by digital modulation of the potential sweep (55).

Recent examples of the application of square-wave voltammetry can be found in studies reported by Smith and co-workers, who have investigated reduction potentials for the $[4\text{Fe}-4\text{S}]^{2+/1+}$ couple in several bacterial ferredoxins (56, 57). For more refined kinetic measurements, techniques such as chronocoulometry, chronoabsorptometry, and rotating disk voltammetry are widely used by electrochemists and have been applied to protein electrochemistry (58, 59).

How reliable are direct, dynamic electrochemical techniques for determining reduction potentials? For a diffusion-controlled electrode reaction, agreement should be good provided reagents (promoters) that may be required to enable the protein to interact with the electrode do not bind to the protein in a way that either causes a conformational change or favors one redox state over another. Discrepancy is expected to be more significant for studies on adsorbed proteins. Feinberg and co-workers have compiled reduction potential data for *Clostridium pasteurianum* 2[4Fe-4S] ferredoxin as reported by a number of groups using different methods, including voltammetry, at various electrodes (56, 57). A spread of ~ 50 mV is observed, but this does not indicate any trend that distinguishes between equilibrium and dynamic electrochemistry.

D. ACHIEVING DIRECT ELECTROCHEMISTRY OF FERREDOXINS

Several early reports described polarography of ferredoxins and observations of waves in the regions of applied electrode potential expected on the basis of equilibrium potentiometric measurements (60-66). The question of whether these waves reflected properties of adsorbed or diffusing molecules was debated. In their studies on the effects of solvent on the redox properties of *C. pasteurianum* 2[4Fe-4S] ferredoxin, Holm and co-workers concluded that the polarographic response was reversible; plots of $\log i/(i_d - i)$ against the applied potential E_{appl} gave gradients of -59 mV and half-widths of pulse polarographic waves were 90 mV, each as expected for a one-electron process (in this case two noninteracting redox sites) (63). The reduction (half-wave) potential thus obtained was -430 mV at pH 8.4, at the negative end of the range of values determined by potentiometry. Polarography is a technique in which the electrochemical response is recorded at short contact time; consequently extended time processes and the stability of the response are not addressed (9-12). The effect of extended contact with a mercury electrode was investigated by Ikeda and co-workers, who carried out cyclic voltammetry experiments on *Clostridium* ferredoxin at a hanging mercury drop electrode (65). The results showed

that the ferredoxin is adsorbed strongly and that the Fe-S clusters are rapidly degraded, giving rise to signals attributable to cysteine thiolate redox activity. This is not unexpected, given the well-known affinity of Hg for sulfur ligands (67).

In 1977, Hawkrigde and co-workers discovered that quasi-reversible electrochemistry of a solution of spinach [2Fe-2S] ferredoxin could be achieved with a gold electrode that had been coated with an electrochemically polymerized form of methyl viologen (58, 68). Ferredoxins generally have pI values below 4 and carry significant negative charges at neutral pH. One likely rationale is therefore that the layer functions by providing a noninsulating positively charged surface that is suited for interaction with the protein surface. Bianco and co-workers and, more recently, Smith and Feinberg have employed this type of modified electrode to study ferredoxins; however, a small concentration of methyl viologen (10% of the protein) was required in solution (56, 69). Van Dijk and co-workers have also described results with a glassy carbon electrode modified by polymeric viologen (70).

In 1982, Hill and co-workers reported that quasi-reversible electrochemistry of *C. pasteurianum* 2[4Fe-4S] ferredoxin (Fd) could be obtained at pyrolytic graphite electrodes in the presence of Mg^{2+} ions (71). In a subsequent paper it was shown that the electrochemical response depended upon the electrode surface oxide density (polished edge > polished basal \gg cleaved basal) and was promoted by metal aquo ions and a variety of complex cations, none of which are redox active in the potential range of the experiment (72). Many other proteins, including spinach [2Fe-2S] ferredoxin, were found to be similarly active, giving cyclic voltammetry that could be described as diffusion controlled. It was proposed that the cationic promoters function by forming salt-bridge-like cross-linkages between residues on the protein surface and the weakly acidic C-O groups of the electrode surface. By such interactions, the protein molecule can be held and oriented at the electrode in the manner of a precursor electron transfer complex. Such reagents may be thought of as greatly increasing the number of protein interaction sites on the electrode surface. Without promoters, the electrochemistry may still be reversible, but occur at few sites, thus resulting in a weak sigmoidal-like response as viewed by linear-sweep methods (49). Using square-wave voltammetry, Feinberg and co-workers have obtained an electrochemical response for a solution of *C. pasteurianum* Fd at a pyrolytic graphite edge (PGE) electrode without the addition of any ionic species apart from Tris/HCl and NaCl (57).

In 1988, it was reported that aminocyclitols such as neomycin or

tobramycin were much more effective than metal ions and complexes for promoting electrochemistry of ferredoxins (73). This was evident from a study of the cyclic voltammetry of *Azotobacter chroococcum* 7Fe ferredoxin at edge-oriented graphite (PGE). Aminocyclitols (also known as aminoglycosides) are a class of molecules that have useful antibiotic properties (74). A key feature undermining their effectiveness is that they contain a number of basic ($-\text{NH}_3^+$, $-\text{NH}_2\text{R}^+$) groups positioned at locations on a complex oligosaccharide. This spatial complexity probably suits them particularly well for interaction with residues on the protein surface and with irregular C—O sites on the electrode. They have since proved to be very effective with other ferredoxins (29, 75, 76). In addition to being redox inactive, they are also colorless and diamagnetic and thus do not interfere with spectroscopic examination of electrochemically transformed samples. A further development has been the discovery that they induce the formation of an electroactive film of protein molecules, effectively monolayer/submonolayer thickness, that can be transferred upon the electrode between various electrolyte solutions (35, 36, 77).

III. Applications

A. REDOX PROPERTIES OF *Azotobacter* FERREDOXIN I AND SITE-DIRECTED MUTANT FORMS

Studies with this protein serve to demonstrate the most obvious application of direct electrochemical methods, that is, the investigation of basic redox properties. Voltammetry provides advantages of rapidity, sample economy, and the ability to measure reduction potentials of redox couples that involve unstable species, either by virtue of intrinsic lability or oxygen sensitivity. Direct electrochemical methods are valuable for determining reduction potentials that are too negative to be addressed effectively by chemical titrants and mediators, and for preparing samples of highly reducing products for spectroscopic examination. They are also suited for extensive investigations, for example, in the measurement of $E^{0'}$ under a range of conditions of temperature or pH.

We have been interested in the redox properties of 7Fe ferredoxins from the N_2 -fixing aerobe *Azotobacter*. The so-called ferredoxins I (Fd I) isolated from *Azotobacter vinelandii* or *A. chroococcum* each contain one [3Fe—4S] and one [4Fe—4S] cluster (24). The protein from *A. vinelandii* (polypeptide $M_r \sim 12,700$) has been particularly well

studied. The crystal structure of the oxidized form shows that the two clusters are ligated by seven out of a total of nine cysteine residues, according to the scheme shown in Fig. 3A (21, 22). At the present time, the amino acid sequence of *A. chroococcum* ferredoxin is not known.

Spectroscopic studies with Fd I isolated from *A. vinelandii* and *A. chroococcum* have shown that the two proteins possess very similar, unusual properties. In either case, the $[3\text{Fe}-4\text{S}]^0$ cluster generated upon one-electron reduction exists in two pH-interconvertible forms, each having a spin state $S = 2$, but exhibiting different low-temperature MCD spectra (24, 78, 79). The alkaline form (pH > 7) shows a spectrum that is very similar to that exhibited by $[3\text{Fe}-4\text{S}]^0$ clusters

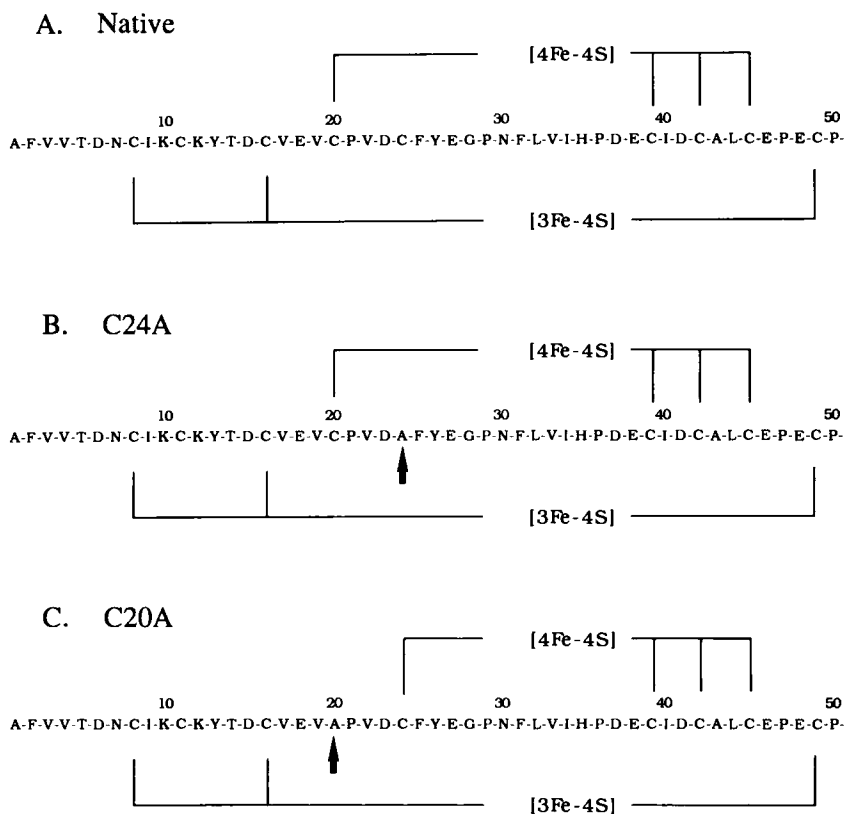


FIG. 3. Amino acid sequences of native *A. vinelandii* Fd I and the site-directed mutants C24A and C20A. Only amino acids 1–50 are shown since the second half of the polypeptide chain does not coordinate the clusters. Altered residues are indicated by arrows.

in other proteins, including inactive beef heart aconitase and the (so-called) ferredoxin II from *Desulfovibrio gigas* (80, 81). By contrast, the acid form shows an MCD spectrum which is unlike that observed for other proteins. By use of CD spectroscopy it has been shown (for *A. vinelandii* Fd I) that this difference persists at ambient temperature and in the absence of glassing agents (24).

It was known also that the [4Fe-4S] cluster in *A. vinelandii* or *A. chroococcum* Fd I is unusual in being nonreducible by dithionite at neutral pH. An earlier proposal that this was a high-potential iron-sulfur protein (HiPIP)-type cluster, i.e., operating between +3 and +2 oxidation levels, was shown to be in error (82). It was suggested instead that this was an unusual [4Fe-4S]^{2+/1+} system for which $E^{0'}$ is more negative than -600 mV.

Direct electrochemical studies have provided a more detailed quantitative description of these anomalies. In the first such study, solutions of *A. chroococcum* Fd I at various pH values were examined by cyclic voltammetry at a PGE electrode (73). To promote the electrochemical response, millimolar levels of the aminocyclitols neomycin or tobramycin were included in the buffer electrolyte. Three redox couples, labeled A, B, and C, were observed, as shown in Fig. 4. At pH 8.3, the dominant wave pairs A and B appear of similar size. Couple A was shown to be quasi-reversible and to behave in the manner expected for an electrochemical process in which the current is limited by diffusion of molecules to a planar electrode surface; for example, a plot of peak current against (scan rate)^{1/2} was linear up to a scan rate of 100 mV/sec. Couple B was also observed to be electrochemically well-behaved. At pH values >7, where there is no interference from couple C, the electrode reaction appeared diffusion controlled up to at least 1 V/sec, while the peak separation remained <80 mV.

Assignments of couples A and B were made following spectroscopic examination of samples prepared by bulk electrolysis under controlled potential conditions. Small volumes (0.3–0.4 ml) of ferredoxin solutions can be electrochemically transformed conveniently using cells in which (in order to obtain a large surface area) the PGE electrode forms both the base and walls. Exhaustive reduction at an applied potential of -550 mV consumed one electron per molecule of protein and produced a product showing complete bleaching of the $g = 2.01$ EPR spectrum due to [3Fe-4S]¹⁺. A similar product, giving rise to the pH-dependent MCD spectra assigned as [3Fe-4S]⁰, could be prepared by reduction with sodium dithionite. In this way, couple A was established to be due to the [3Fe-4S]^{1+/0} cluster. Observed reduction potentials $E_{\text{obs}}^{0'}$ (deter-

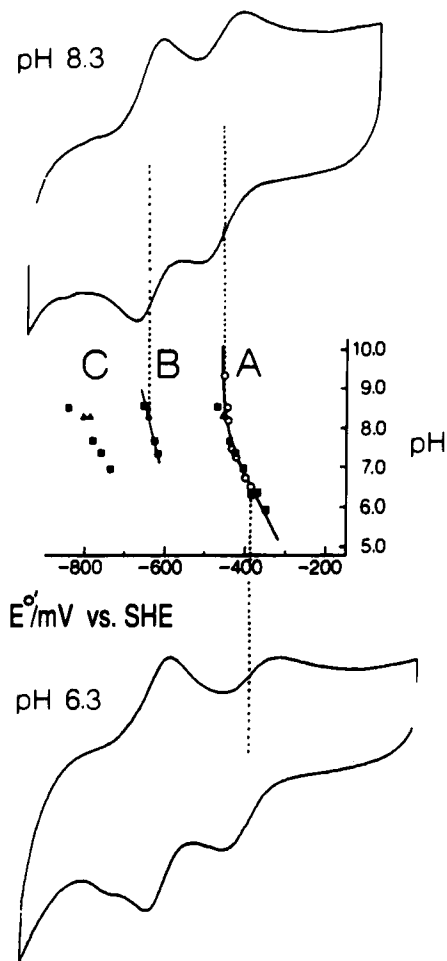
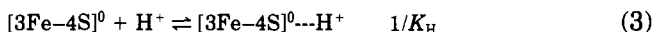
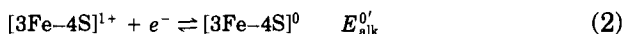


FIG. 4. Cyclic voltammetry of *A. chroococcum* Fd I at pH 8.3 {84 μM protein in 20 mM 3-[tris(hydroxymethyl)methylamino]-1-propanesulfonic acid, 0.1 M NaCl, 1.5 mM neomycin} and pH 6.3 [85 μM protein in 20 mM 1,4-piperazinebis(ethanesulfonic acid), 0.1 M NaCl, 1 mM tobramycin]. Temperature 3°C, scan rate 10 mV/sec. Electrode is PGE. Shown at the center is the pH dependence of E'° values. [Adapted from Armstrong, F. A., George, S. J., Thomson, A. J., and Yates, M. G., *FEBS Lett.* **234**, 107 (1988), with permission].

mined from the average peak potentials for reduction and oxidation waves) were pH dependent and data gave a good fit to Eq. (1),

$$E_{\text{obs}}^{0'} = E_{\text{alk}}^{0'} + (2.3RT/F) \log\{1 + [\text{H}^+]/K_{\text{H}}\} \quad (1)$$

which describes a system comprising the reactions given by Eqs. (2) and (3)) in which electron transfer is coupled to net addition of one H^+ to the reduced form, equilibrium being established rapidly and within the voltammetric scan time.



Under the conditions of the voltammetric measurements (temperature 3°C , 0.1 M NaCl as supporting electrolyte, 5 mM mixed-buffer system) the $\text{p}K$ ($-\log K_{\text{H}}$) was determined to be 7.8 ± 0.1 , with $E_{\text{alk}}^{0'} = -460\text{ mV}$ and $\Delta E_{\text{obs}}^{0'}/d(\text{pH}) = -55\text{ mV}$ (i.e., consistent with net addition of one bound H^+ per protein molecule. Such direct coupling to a proton transfer process is unusual for Fe-S clusters.

Anaerobic controlled potential electrolysis at -835 mV of a pH 8.3 solution consumed two electrons per protein molecule. Cyclic voltammetry of this product confirmed full retention of couples A and B, thus showing that no significant irreversible changes had occurred to the sample upon electrolysis. The EPR spectrum was complicated, being of the " $g = 1.94$ " type with additional features and arising from 0.8 spin per molecule. It was similar to that of the two-electron reduced 7Fe ferredoxin from *Thermus thermophilus*, which contains a $[\text{4Fe-4S}]^{1+}$ cluster that is spin coupled to $[\text{3Fe-4S}]^0$ (83). Couple B could thus be assigned to the $[\text{4Fe-4S}]^{2+/1+}$ cluster. The mild pH dependence [$dE^{0'}/d(\text{pH}) = -25\text{ mV}$] suggested weak coupling to a protonation equilibrium. At pH 8.3, $E^{0'}$ was determined to be -645 mV , thus explaining why the reduced form could not be obtained by reduction with dithionite and confirming the earlier suggestion by Morgan *et al.* (82). It is worth noting that the bulk electrolysis approaches being quantitative even at the very low potentials used, and that the reduced $[\text{4Fe-4S}]^{1+}$ cluster does not react with water at any significant rate.

Couple C, a relatively minor feature in this case, has appeared to be a typical feature of ferredoxins that contain a $[\text{3Fe-4S}]$ cluster. For most proteins (see below) we have found it to be a chemically complex process that occurs readily only for protein molecules that are confined to the electrode surface. As outlined later, some clarification of the nature of this redox couple has arisen from voltammetry of protein films in the absence of freely diffusing molecules.

A long-standing question, highlighted by the results obtained with *A. chroococcum* Fd I, is the origin of the large variation in reduction potentials of [4Fe-4S] clusters among different proteins (84). Most vividly of course, there exist two distinct classes of protein that display redox couples involving different pairs of oxidation levels. For the [4Fe-4S]^{2+/1+} couple (as exhibited by ferredoxins), $E^{0'}$ values cover the range -250 to -650 mV, whereas for HiPIPs ([4Fe-4S]^{3+/2+}), $E^{0'}$ values range between +50 and +450 mV. It is found that ferredoxins do not exhibit the +3 oxidation level. A search for oxidation processes occurring at *C. pasteurianum* 2[4Fe-4S] ferredoxin using differential pulse and square-wave voltammetry revealed only reactions generating rapidly decomposing species (85). The first of these reactions, suggested to be the couple [4Fe-4S]^{3+/2+} (product lifetime <2 msec) is associated with a reduction potential estimated at 850 mV. Conversely, there is no evidence to show that HiPIPs can attain the +1 oxidation level under physiologically feasible conditions. In what has been a much-cited experiment, Cammack showed that the [4Fe-4S]²⁺ cluster in *Chromatium vinosum* HiPIP becomes reducible by dithionite (i.e., "ferredoxin-like") if the protein is unfolded in 80% dimethyl sulfoxide (DMSO) (86). Cyclic voltammetry of *C. vinosum* HiPIP under normal conditions failed to find any evidence for the [4Fe-4S]^{2+/2+} couple at electrode potentials as negative as -1.2 V (87).

On the basis of detailed comparisons of the resonance Raman and crystallographic structures of several ferredoxins and several HiPIPs, it has been concluded that the two classes of proteins are distinguished by major differences in the local environment of the [4Fe-4S] cluster (84). These differences are the number of N-H...S hydrogen bonds (five in HiPIP against eight in Fds—the greater number stabilizing the electron-rich +1 oxidation level), the cysteine torsional angles (larger in HiPIP), the positions of cysteine residues in the sequence, and the degree of solvent accessibility of the cluster (much less in HiPIP). However, it has also been concluded that *within* each class there is remarkably little difference in these parameters. The question of the extent to which reduction potentials are modulated electrostatically by the presence of charged residues is an obvious one. Consider the +1 oxidation level, which with tetrathiolate ligation has a local charge of -3; this should be destabilized by the close proximity of a negative charge but should be stabilized by a nearby positive charge. It was suggested that while the nature of the amino acids close to the cluster must be influential in modulating the reduction potential, the *charge* on these groups should be unimportant since charged residues tend to be located on the protein surface (84). It is well known that reduction

potentials are modulated by protonation, although marked effects are rare for Fe-S clusters. For *A. chroococcum*/*A. vinelandii* Fd I, the combined voltammetric/MCD evidence provides strong evidence that site of protonation is very near or indeed at the $[3\text{Fe}-4\text{S}]^0$ cluster (24, 73, 78, 79). Another demonstration of the influence of a proton is given in a report by Smith and Feinberg (56). From voltammetric studies on several $2[4\text{Fe}-4\text{S}]$ ferredoxins, it was noted that one example (*Clostridium thermosaccharolyticum* Fd) showed a sigmoidal relationship between E^0' and pH. The perturbation, approximately 40 mV in total, was attributed to redox-linked protonation of an adjacent histidine residue that is absent from the sequence of other bacterial ferredoxins. Systematic studies of subsite-differentiated cluster analogs have shed light upon the influence of intrinsic factors. Valence localization [Fe(III) character versus Fe(II)-type character] and ligand type (electron donor strength, monodentate versus bidentate) have each been shown to modulate the reduction potential (40-42).

To gain a more systematic understanding of how the redox properties and stabilities of Fe-S centers are influenced by the protein structure, Burgess and co-workers have used site-directed mutagenesis to alter specific amino acid residues in ferredoxin I from *A. vinelandii* (76). Mutant forms of this Fd I were expressed and isolated, then crystals were examined by X-ray diffraction in order to compare their structures with that of the native protein. In the two examples to be described, cysteine residues close to the $[4\text{Fe}-4\text{S}]$ cluster were replaced by Ala, as shown in Fig. 3 (B and C). In the case of the C24A mutant, a nonligating Cys that is in van der Waals contact with the $[4\text{Fe}-4\text{S}]$ cluster is replaced by alanine, but the resulting environment in the vicinity of the cluster is otherwise very similar to that of the native form (88). For the C20A mutant a ligating Cys is replaced; the cluster instead adopts Cys 24 and there is a large rearrangement of the local structure (89).

Electrochemistry was performed with ~ 0.1 mM ferredoxin solutions over a range of conditions of pH, using tobramycin or neomycin to promote interaction of the protein with the PGE electrode. Square-wave voltammograms of native, C20A, and C24A forms at pH 7.8 are shown in Fig. 5. As evidenced by the excellent alignment of couples A and C, the $[3\text{Fe}-4\text{S}]$ cluster appears unperturbed. By contrast, the position of couple B, assigned as $[4\text{Fe}-4\text{S}]^{2+/1+}$ by analogy with *A. chroococcum* Fd I, varies over a range of ~ 150 mV. Collective data are given in Table I.

Further refinement stemmed from measurements of the pH dependence of E^0' values for each couple. As shown in Fig. 6, data for couple A ($[3\text{Fe}-4\text{S}]^{1+/0}$) overlay and yield essentially indistinguishable values

TABLE I

REDUCTION POTENTIALS $E_{\text{obs}}^{0'}$ FOR THE Fe-S CLUSTERS OF NATIVE, C20A, AND C24A FORMS OF *Azotobacter vinelandii* FERREDOXIN I AS DETERMINED BY SQUARE-WAVE VOLTAMMETRY^a

Couple	Protein	$E_{\text{obs}}^{0'}$ (pH 7.8) (mV)	$-d(E)/d(\text{pH})_{\text{obs}}$ (mV)	$-d(E)/d(\text{pH})_{\text{lim}}$ (mV)	pK	$E_{\text{alk}}^{0'}$ (mV)
[3Fe-4S] ¹⁺ 0 (= A)	Native	-425 (±5)	—	43 (+4)	7.8 (+0.2)	-445 (+15)
	C20A	-429 (±5)	—	42 (+3)	7.6 (+0.2)	-440 (+15)
	C24A	-427 (±5)	—	43 (+4)	7.9 (+0.2)	-449 (+15)
[4Fe-4S] ²⁺ 1- (= B)	Native	-647 (±5)	16	—	—	—
	C20A	-746 (±10)	15	—	—	—
	C24A	-600 (±5)	18	—	—	—
C	Native	-772 (±15)	—	—	—	—
	C24A	-782 (±5)	52	—	—	—

^a All measurements made at 3°C. Data taken from Ref. 76.

of pK , $dE_{\text{obs}}^{0'}/d(\text{pH})$, and $E_{\text{alk}}^{0'}$ as analyzed according to Eq. (1). The result is consistent with the conclusion, drawn from the crystallography studies, that the alterations caused in the [4Fe-4S] cluster binding domain induce no significant structural changes close to the [3Fe-4S] cluster (88, 89). The center-to-center distance between clusters is 11 Å.

Data for couple B yield a set of essentially parallel straight lines having slopes $dE_{\text{obs}}^{0'}/d(\text{pH})$ of approximately -16 mV. The increase in $E^{0'}$ of ~50 mV upon replacement of Cys 24 by alanine, in comparing what are otherwise very similar cluster environments, suggests that the noncoordinating cysteine in native *A. vinelandii* Fd I might be ionized (i.e., exist as the thiolate anion) throughout this pH range. While this may be considered unlikely, removal of a unit negative charge from a distance of van der Waals contact would certainly be expected to stabilize the reduced form of the cluster. On the other hand, the ~100-mV decrease in $E^{0'}$ observed upon replacement of Cys 20 by alanine shows that the advantage of removing the neighboring cysteine is outweighed considerably by effects due to the structural changes thus induced. Several factors are clearly involved. What is interesting, however, is that the C20A mutation produces no change in the exposure of the [4Fe-4S] cluster to solvent molecules, and that the number, type, and distances of NH...S hydrogen bonds are unchanged (although there are significant changes elsewhere).

The physiological function of Fd I is not known. The finding by Burgess' group that double-mutant strains C20A/Fld⁻ and C24A/Fld⁻ (Fld⁻ strains do not synthesize flavodoxin) grow at the same rate as wild-type cells is interesting, since it raises the question of the physio-

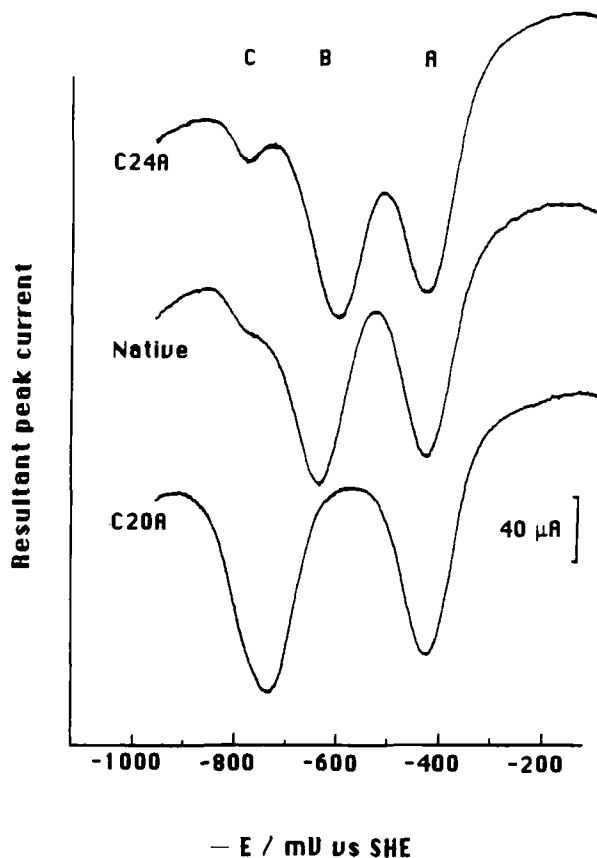
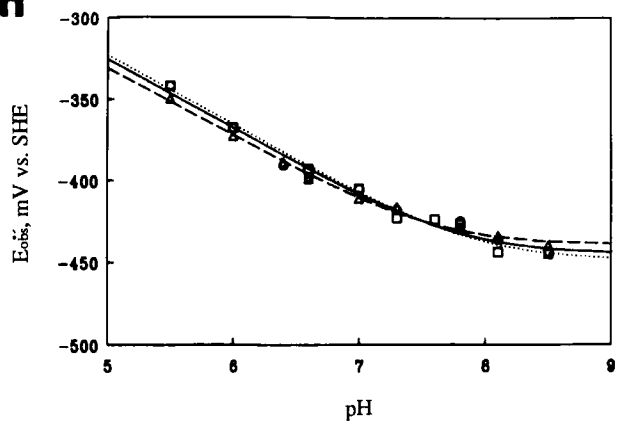
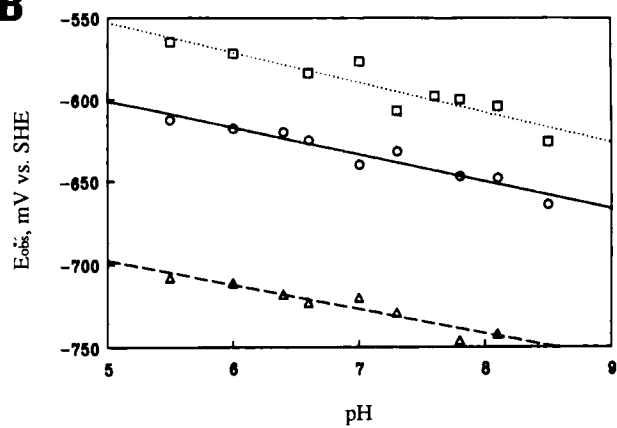
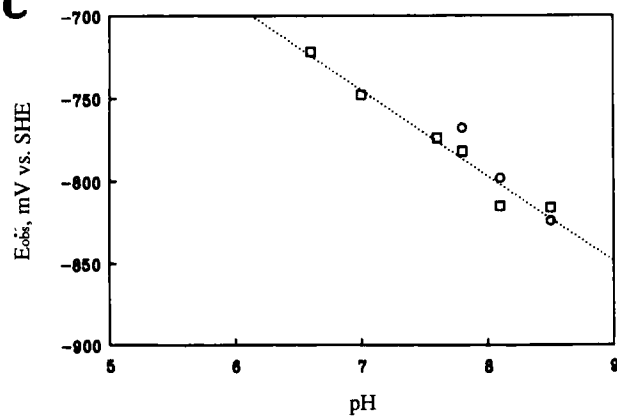


FIG. 5. Square-wave voltammetry of native *A. vinelandii* Fd I and site-directed mutants at a PGE electrode. Shown are resultant peak currents for scans made in the direction of increasing negative potential. Protein concentrations are $100\ \mu\text{M}$ each in $0.1\ \text{M}$ NaCl, $20\ \text{mM}$ mixed buffer, pH 7.8. Temperature 3°C . Square-wave frequency is 60 Hz, pulse amplitude is 40 mV, potential step size is 1 mV. [Adapted from Iismaa, S. E., Vázquez, A. E., Jensen, G. M., Stephens, P. J., Butt, J. N., Armstrong, F. A., and Burgess, B. K., *J. Biol. Chem.* **266**, 21563 (1991), with permission.]

FIG. 6. Graph of $E_{\text{obs}}^{0'}$ against pH for redox couples A, B, and C of native *A. vinelandii* Fd I (\circ) and site-directed mutants C20A (\triangle) and C24A (\square). All data obtained at 3°C , $0.1\ \text{M}$ NaCl, $20\ \text{mM}$ mixed buffer, $1\text{--}2\ \text{mM}$ neomycin or tobramycin. Graph A shows nonlinear regression fit to Eq. (1). Graphs B and C show best linear fits. [Adapted from Iismaa, S. E., Vázquez, A. E., Jensen, G. M., Stephens, P. J., Butt, J. N., Armstrong, F. A., and Burgess, B. K., *J. Biol. Chem.* **266**, 21563 (1991), with permission.]

A**B****C**

logical relevance of the very low-potential $[4\text{Fe}-4\text{S}]^{2+/1+}$ cluster (76). If it does indeed function as a redox center, its reduction *in vivo* requires that the natural electron donor has a reduction potential lower than -750 mV or that the process is coupled to an exergonic process such as ATP hydrolysis.

B. CHARACTERIZING THE Fe-S CLUSTERS IN *Desulfovibrio africanus* FERREDOXIN III, A PROTEIN CONTAINING A REACTIVE $[3\text{Fe}-4\text{S}]$ CLUSTER

Ferredoxin III from *Desulfovibrio africanus* has proved to be an interesting subject for studying facile metal ion and ligand exchange reactions at clusters. As isolated, this small protein (polypeptide $M_r \sim 6600$) was found to contain seven or eight Fe atoms and seven or eight labile sulfides per molecule and to possess a total of seven cysteines occupying positions in the amino acid sequence as shown in Fig. 7 (90). In this schematic, the two clusters have been included in positions that we now believe to be correct, although support from crystal structure determination has yet to be obtained. Early attempts to characterize the clusters in *D. africanus* Fd III had met with limited success. From EPR spectroscopy it was known that the oxidized protein, as isolated, contains a $[3\text{Fe}-4\text{S}]^{1+}$ cluster, while spectra measured for a dithionite-reduced sample revealed the presence of $[4\text{Fe}-4\text{S}]^{1+}$. However, a satisfactory quantitative analysis was not obtained. Inspection of spectra obtained during conventional potentiometric titrations at various degrees of reduction revealed complex changes in spectral appearance and indicated that irreversible transformations were occurring.

As with *Azotobacter* ferredoxins, direct electrochemistry of a solution of *D. africanus* Fd III could be achieved readily with a PGE electrode

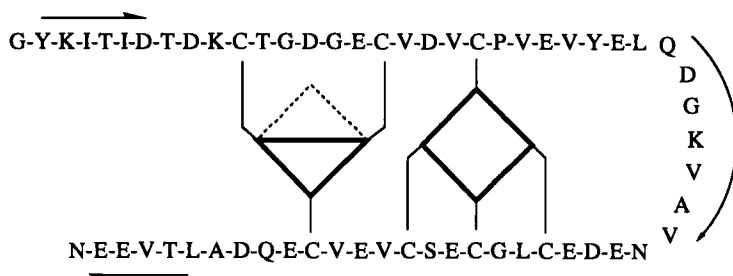


FIG. 7. Amino acid sequence of *D. africanus* Fd III showing proposed coordination of $[3\text{Fe}-4\text{S}]$ and $[4\text{Fe}-4\text{S}]$ clusters in the isolated 7Fe form.

in the presence of neomycin (75). Cyclic voltammetry under slow scan rate conditions (<20 mV/sec) showed two prominent pairs of waves (A and B) and a third weaker feature (C). This is displayed in Fig. 8. Couples A and B are of similar magnitude, provided (1) the scan rate is not increased (in which case waves A collapse to become a weak sigmoidal feature, eventually revealing an underlying adsorption wave at scan rates >160 mV/sec) and (2) provided a metal chelator such as EGTA is present in solution (in this case, EGTA is used instead of EDTA since the voltammetric response of FeEDTA interferes with

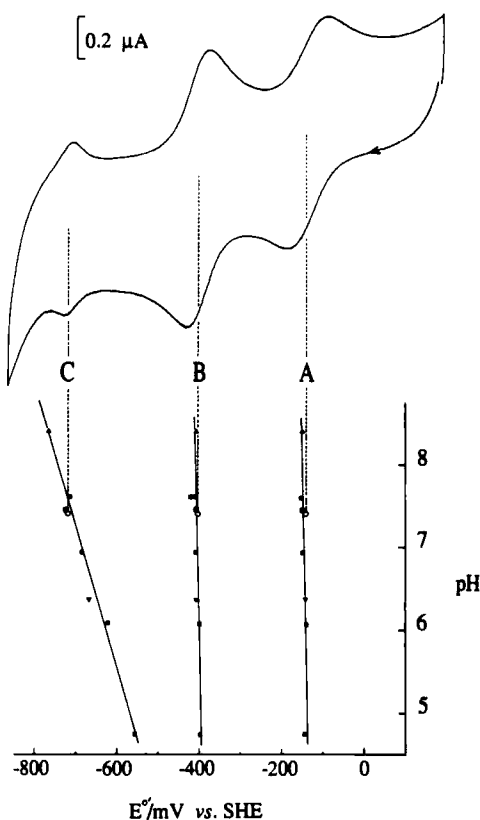


FIG. 8. Top: cyclic voltammetry of a solution of *D. africanus* Fd III at a PGE electrode showing couples A, B, and C. Protein concentration is $110 \mu\text{M}$ in 0.1 M NaClO_4 , 20 mM HEPES buffer, 0.1 mM EGTA, 1.1 mM neomycin, at pH 7.4. Temperature 2°C , scan rate 8 mV/sec . Bottom: pH dependence of E^0 values, various buffer electrolytes used. Lines are least-squares fits to data. [Adapted from Armstrong, F. A., George, S. J., Cammack, R., Hatchikian, E. C., and Thomson, A. J., *Biochem. J.* **264**, 265 (1989), with permission.]

couple A). The first observation is still unanswered [by contrast, couple B behaves much more classically in terms of exhibiting a linear relation between peak current and (scan rate)^{1/2} up to 800 mV/sec, and ΔE_p values of 55–60 mV]. Further experiments (see below) have provided an explanation for the second observation in terms of a rapid reaction of the reduced ($[3\text{Fe}-4\text{S}]^0$) cluster with traces of Fe(II) liberated by slow, continual protein decomposition.

Couples A ($E^{0'} = -140$ mV) and B ($E^{0'} = -410$ mV) were each assigned by performing bulk electrolyses at controlled potential, and then examining the products by EPR and MCD. Exhaustive reduction at -260 mV in the presence of an equivalent of EGTA consumed one (0.9) electron per molecule. The resulting sample showed almost complete loss of the EPR signal at $g = 2.01$ and the appearance of a broad feature at $g = 12$. The MCD of the one-electron reduced protein is very similar to that of $[3\text{Fe}-4\text{S}]^0$ clusters in other proteins (91). Exhaustive reduction at a potential of -605 mV consumed two electrons per molecule and samples thus prepared showed (in addition to the $g = 12$ feature) an axial EPR spectrum with g values $g_{\perp} = 1.93$, $g_{\parallel} = 2.05$. Double integration of the high-field signal yielded values averaging 1.0 ± 0.1 spins. Couples A and B were thus assigned as $[3\text{Fe}-4\text{S}]^{1+/0}$ and $[4\text{Fe}-4\text{S}]^{2+/1+}$, respectively. Experiments carried out over the pH range 5–8 showed that neither couple exhibits a significant pH dependence (cf. the $[3\text{Fe}-4\text{S}]^{1+/0}$ cluster of *A. chroococcum*/*A. vinelandii* Fd I). Couple C appeared to be a kinetically complex pH-dependent redox couple, resembling the observation made for *A. chroococcum*/*A. vinelandii* Fd I.

From their respective spectroscopic similarities to $[3\text{Fe}-4\text{S}]$ and $[4\text{Fe}-4\text{S}]$ clusters in other proteins, positions in the protein were assigned as indicated in Fig. 7. The partial sequences -C-Xaa-Xaa-C-Xaa-Xaa-C- and remote -C-P- form a characteristic binding motif for $[4\text{Fe}-4\text{S}]$ clusters in ferredoxins (92). The remaining three cysteine residues, located in the partial sequences -C-Xaa-Xaa-D-Xaa-Xaa-C and remote -C-E- were assigned to the $[3\text{Fe}-4\text{S}]$ cluster. The resulting binding domain resembles that of a $[4\text{Fe}-4\text{S}]$ domain except that an aspartate occupies the normal central cysteine position, and the remote cysteine that is normally followed by the kink former proline is followed instead by glutamate. Marked changes in the cyclic voltammetry are observed upon addition of two equivalents of Fe(II), i.e., sufficient to complex with the EGTA and react 1:1 with the ferredoxin (29). As shown in Fig. 9, reduction of the $[3\text{Fe}-4\text{S}]^{1+}$ cluster initiates its transformation into another species. Continued cycling results in complete disappearance of couples A and C and an apparent twofold increase in

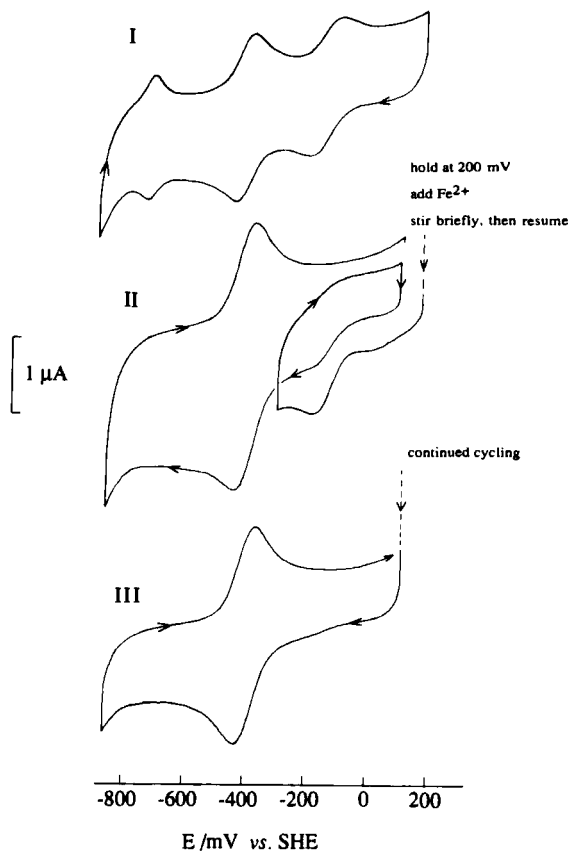


FIG. 9. Cyclic voltammetry of a solution of *D. africanus* Fd III showing the effect of adding Fe(II) to the electrolyte. Protein concentration was $110\ \mu\text{M}$ in electrolyte composed of $0.1\ \text{M}$ NaClO_4 , $20\ \text{mM}$ HEPES, $0.1\ \text{mM}$ EGTA, $1.1\ \text{mM}$ neomycin. At stage II, Fe(II) was added to give a total concentration of $0.21\ \text{mM}$. Scan rate $16\ \text{mV/sec}$. Temperature 2°C . [Adapted from George, S. J., Armstrong, F. A., Hatchikian, E. C., and Thomson, A. J., *Biochem. J.* **264**, 275 (1989), with permission.]

the amplitude of couple B. For the resulting product, peak currents were observed to be proportional to scan rate up to at least $160\ \text{mV/sec}$ and the peak-to-peak separation was $60\ \text{mV}$ at $16\ \text{mV/sec}$. The waveshape conforms closely to that expected for a single one-electron couple with $E^0 = -400\ \text{mV}$, or more than one such couple having reduction potentials very close in value. Similar results were obtained in different electrolyte media, for example $0.1\ \text{M}$ NaClO_4 instead of NaCl , and $\text{pH } 6.3$ [4-(2-hydroxyethyl)-1-piperazineethanesulfonic acid

(HEPES)] or pH 8.3 {3-[tris(hydroxymethyl)methylamino]-1-propanesulfonic acid (TAPS)}.

A quantitative analysis of this transformation was undertaken by performing bulk electrolysis prior to, during, and following addition of Fe(II) to the sample solution. The course of one such determination is shown in Fig. 10. A solution of *D. africanus* Fd III containing one equivalent of EGTA was exhaustively reduced at -610 mV. This consumed two electrons per molecule. Then aliquots of Fe(II) [each corresponding to approximately 0.25 Fe(II) per protein molecule] were injected into the stirred cell while the electrode potential was maintained at -610 mV. The first two additions produced little change because the Fe(II) is complexed preferentially by the remaining EGTA, but several subsequent additions resulted in large increases in current until a

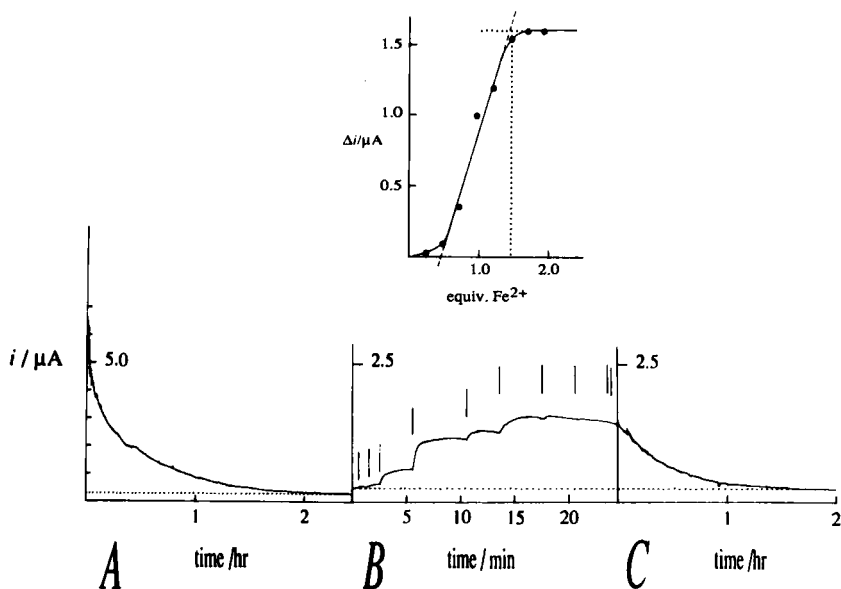
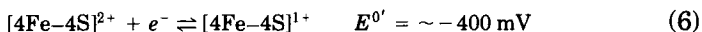
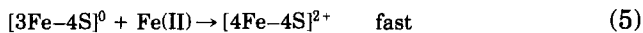
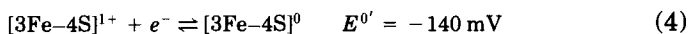


FIG. 10. Bulk electrolytic reduction of *D. africanus* Fd III and titration with Fe(II). (A) Bulk reduction at -610 mV in stirred cell. Solution is 0.4 ml containing $110 \mu\text{M}$ protein in 0.1 M NaCl, 20 mM HEPES, 0.1 mM EGTA, 1.5 mM neomycin, pH 7.4. Temperature 3°C . (B) Additions of 0.25 equivalents of Fe(II) to the two-electron-reduced protein while holding applied potential at -610 mV. Graph shows the increase in current observed as a function of the number of equivalents of Fe(II) added. The line drawn through the central points corresponds to a predicted uptake of 1.0 equivalent Fe(II) per protein molecule, following the initial lag due to complexation by EGTA. (C) Further bulk reduction at -610 mV, following from B. [Adapted from George, S. J., Armstrong, F. A., Hatchikian, E. C., and Thomson, A. J., *Biochem. J.* **264**, 275 (1989), with permission.]

limiting value was reached. Analysis of the Fe(II) titration showed that one Fe(II) was taken up per protein molecule. The solution was then electrolyzed further to equilibrium. Determination of the charge passed in this second phase was consistent with addition of one further electron per protein molecule.

The products of this reaction [and of chemically transformed samples prepared by addition of Fe(II) and variable amounts of dithionite to the 7Fe protein] were examined by EPR and MCD spectroscopy. The spectrum of the oxidized product [formed by reducing with one electron equivalent of dithionite, then adding Fe(II)] showed no significant EPR signals. In the UV-visible spectrum, the 408-nm shoulder exhibited by the 7Fe protein was replaced by a rounded peak at 390 nm, similar to that observed for ferredoxins containing only [4Fe-4S] clusters. MCD spectroscopy showed that this product was diamagnetic. The EPR spectra of the partial and fully reduced products were interesting. A rhombic signal with g values 2.05, 1.93, and 1.89 was observed upon reduction by <0.5 electron equivalents. Upon complete reduction (i.e., by two electron equivalents) the spectrum appeared more complicated, indicative of spin coupling to a nearby paramagnet. However, double integration of the low-field signals yielded only a single spin per molecule, leaving one spin unaccounted for. The other clearly distinguished feature in the spectrum was a signal at $g = 5.27$, and this was assigned to a major species with spin $S = \frac{3}{2}$. The MCD spectrum was very different from that of the [3Fe-4S]⁰ cluster, but similar in feature to those of other [4Fe-4S]¹⁺ cluster-containing proteins. Its intensity was greater than expected for two $S = \frac{1}{2}$ [4Fe-4S]¹⁺ clusters, and the form of the resulting magnetization curve indicated the presence of species having $S > \frac{1}{2}$.

Together, the results from these experiments suggested a sequence of reactions [Eqs. (4)–(6)] in which Fe(II) enters the reduced [3Fe-4S]⁰ cluster rapidly to complete a cubane-type [4Fe-4S]²⁺ structure, which can undergo further one-electron reduction. No reaction occurs with the oxidized [3Fe-4S]¹⁺ cluster. Such a scheme resembles the *in vitro* activation of aconitase (14). The reactivity also explained the problems involved in characterizing the 7Fe protein, which is subject to slow degradation accompanied by loss of Fe.



The resulting product is an 8Fe ferredoxin containing two [4Fe-4S] clusters. However, unlike *C. pasteurianum* Fd, one of the clusters must lack a cysteine thiolate donor. The question of the nature of the nonthiolate ligand is not yet answered, although a water molecule ($\text{H}_2\text{O}/\text{OH}^-$) and the carboxylate function of Asp 14 are the primary possibilities. Several other ferredoxins containing a [3Fe-4S] cluster are known to have a partial sequence -C-Xaa-Xaa-D-Xaa-Xaa-C- similar to that of *D. africanus* Fd III. The most notable of these is the unusual ferredoxin isolated from the hyperthermophile *Pyrococcus furiosus* (30). This protein is a monomer (polypeptide $M_r \sim 7500$), containing a single [4Fe-4S] cluster that is readily degraded to a [3Fe-4S] cluster if isolated under aerobic conditions. Like *D. africanus* Fd III, the reduced [3Fe-4S] 0 cluster takes up Fe(II), but in this case the reduced [4Fe-4S] $^{1+}$ cluster exists as a mixture of $S = \frac{1}{2}$ (20%) and $S = \frac{3}{2}$ (80%) ground states. From the presence of a strongly coupled ^1H ENDOR resonance in each case, it has been proposed that the noncysteine ligand is H_2O or OH^- , although the absence of a variation in $E^{0'}$ over the pH range 6.8–10.5 argues in favor of OH^- (93).

C. INVESTIGATING CLUSTER REACTIVITIES IN ADSORBED PROTEIN FILMS

In the experiments described in Section III,B, application of two electrochemical methods, cyclic voltammetry and bulk electrolytic titration, facilitated the task of characterizing an unstable protein containing a labile Fe-S cluster. Even so, a considerable improvement in the exploratory and analytical capabilities of voltammetry may be achieved by addressing protein molecules that are confined to the electrode surface. Certain advantages of this approach have been outlined in the previous section.

The voltammograms in Fig. 11 show how an electroactive film of *D. africanus* Fd III (in this case the 7Fe form, as isolated) can be formed and stabilized at a PGE electrode in the presence of neomycin. In the first case, a freshly polished electrode is smeared with an ice-cold solution of protein (100 μM) from a capillary tube, then transferred to electrolyte in an electrochemical cell and voltammetrically scanned. Only an initial weak response is observed. If neomycin (2 mM) is included in the coating solution (but still absent from the cell electrolyte), a voltammetric response is observed that dies away rapidly upon repeated cycling. However, if neomycin is present also in the cell electrolyte, the response is considerably stabilized after several cycles, thereafter undergoing only slow attenuation with time. The observa-

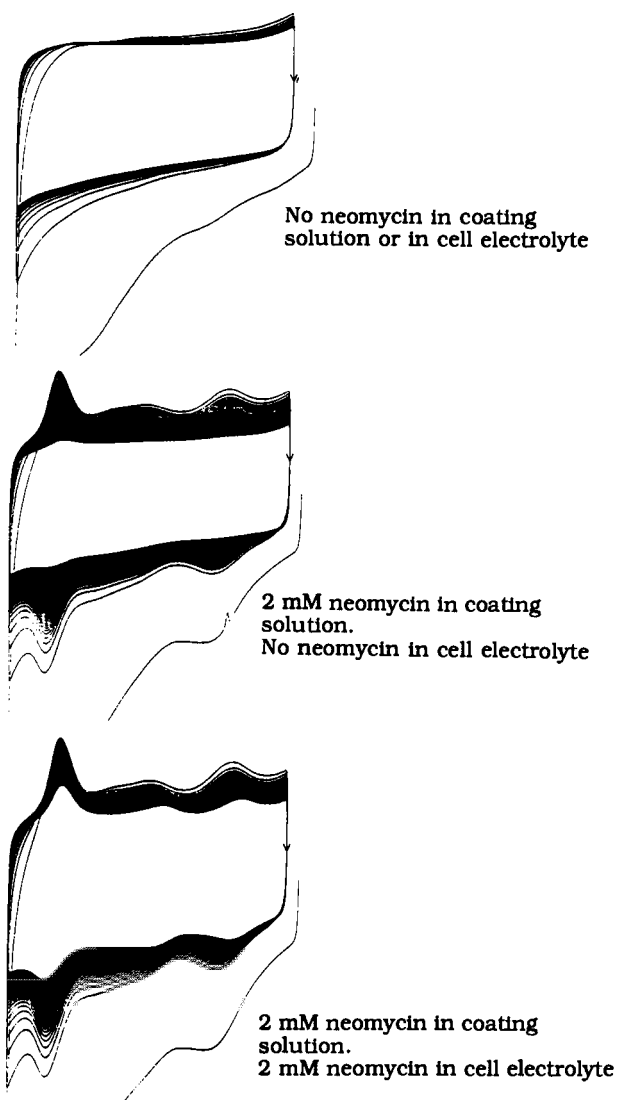


FIG. 11. Top: cyclic voltammograms (successive cycles) of a freshly polished PGE electrode coated with a drop ($\sim 1 \mu\text{l}$) of a solution of *D. africanus* Fd III ($100 \mu\text{M}$ in $0.1 M$ NaCl, $20 mM$ mixed buffer, $0.1 mM$ EGTA, pH 7) and scanned in the same electrolyte solution. Scan rate 190 mV/sec . Center: as for top voltammogram but $2 mM$ neomycin present in coating solution. Bottom: as for center but $2 mM$ neomycin present in cell solution.

tion is consistent with the formation of a protein layer in which the molecules are stabilized by the coadsorption of neomycin. Other ferredoxins, including *A. chroococcum*/*A. vinelandii* Fd I, exhibit similar behavior, and other aminocyclitols have been found to be active to varying extents (87). The structure of such films is clearly a complicated issue, but we have been able to exploit the situation to define several interesting reactions of [3Fe-4S] clusters and their derivatives.

After several cycles, the voltammetry of a film of 7Fe *D. africanus* Fd III appears as shown in Fig. 12. Based upon the close correspondence with the voltammetric waves A and B observed for solutions of the protein, the wave pairs A' and B' were assigned to the couples [3Fe-4S]^{1+/0} and [4Fe-4S]^{2+/1+}, respectively (35, 77). It may be noted that ΔE_p values are small, (e.g., <30 mV at 190 mV/sec), thus indicating that electron transfer between the electrode and clusters approaches reversibility. Half-height widths (typically 100 and 120 mV, respectively) are close to theoretically expected values for a homogeneous population of noninteracting one-electron systems (see discussion in Section II,C). Furthermore, integration of these waves yields a value for the transferred charge that is consistent with the formation of approximately a one-protein monolayer. The third and most prominent wave pair C' coincides with the appearance of C, a minor feature in the solution electrochemistry. This suggested that the redox process responsible for C' occurs readily only in adsorbed protein molecules.

From a number of studies with other ferredoxins, it has become apparent that the low-potential couple C' is associated closely with the presence of a [3Fe-4S] cluster. For example, a similar feature is evident for *A. chroococcum*/*A. vinelandii* Fd I and for the 7Fe proteins from *Sulfolobus acidocaldarius* and *Thermoplasma acidophilum* (73, 76, 87). For *D. africanus* Fd III, this proposal was supported further by the observation that both couples A and C vanish if the [3Fe-4S]⁰ cluster is transformed by uptake of Fe(II), and by the absence of cysteine residues, additional to those required for cluster binding, that might constitute a redox-active cysteine/cystine redox couple. The positions and shapes of the reduction and oxidation waves were found to be dependent upon scan rate and upon pH (77). As the pH is lowered (e.g., below pH 7) and at slower scan rates, it was observed that ΔE_p decreases and the two waves become similar in shape with half-height widths less than 60 mV. The two-electron nature of this reaction has been confirmed by a series of comparisons of the integrated areas of oxidation waves A' and C' (77). Within experimental error, the charge passed for C' is twice that for couple A'.

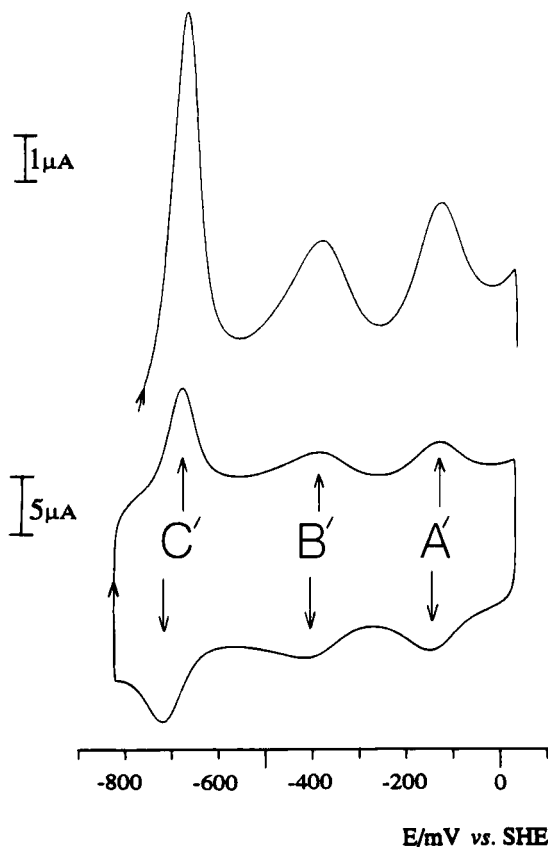
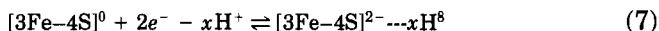


FIG. 12. Steady-state cyclic voltammogram of a film of *D. africanus* Fd III scanned in 0.1 M NaCl, 20 mM mixed buffer, pH 7, containing 2 mM neomycin and 10 mM EGTA. Temperature 0°C; scan rate 190 mV/sec. Upper trace is an oxidative scan measured at higher gain. [Reproduced from Butt, J. N., Armstrong, F. A., Breton, J., George, S. J., Thomson, A. J., and Hatchikian, E. C., *J. Am. Chem. Soc.* 113, 6663 (1991), with permission.]

The nature of the reduced product of C' remains unclear up to the time of preparing this manuscript. It is reasonably stable, as evident from the appearance of the oxidation wave even after holding the potential of the film-coated electrode below -850 mV for several minutes. Furthermore, it does not undergo turnover with evolution of H_2 (which should be thermodynamically favored under these conditions of very low potential). The most likely (yet still remarkable) rationale is that

the species $[3\text{Fe-4S}]^0$ itself is reducible by a further two electrons, as described by Eq. (7). This would give a cluster that is composed formally of three Fe(II).



In recent studies, the reduction potential for Reaction (7) (as gauged from the average position of anodic and cathodic peaks) has been found to vary with pH (range 4.5–8.3) in an almost linear manner with a gradient corresponding to $x = 3$, i.e., suggesting that couple C' as observed for *D. africanus* Fd III is a $2e^-/3\text{H}^+$ process (87).

As outlined earlier, it is widely recognized that the redox chemistry of $[2\text{Fe-2S}]$ and $[4\text{Fe-4S}]$ clusters in proteins is controlled tightly by the environment and is restricted to one-electron transitions between two adjacent oxidation levels (84). It now appears possible that $[3\text{Fe-4S}]$ clusters are not so restricted. An important factor must be the accompanying binding of H^+ (possibly to bridging sulfides?) that compensates for the change in charge. However, the reason(s) why this reactivity appears confined to adsorbed protein molecules (at least in the case of *D. africanus* Fd III and *A. chroococcum/A. vinelandii*) is not clear. Adsorption may assist complicated electrode reactions that involve successive electron transfers separated by a chemical rearrangement. Another possibility is that a rapid and reversible alteration of the cluster environment is induced under the condition of very low applied potential.

The adsorbed-film approach has provided a good way to explore the reactivity of the $[3\text{Fe-4S}]$ cluster of *D. africanus* Fd III toward uptake of Fe(II) and other metals ions, under finely controlled conditions of applied potential (35, 36, 87). In a typical experiment, following film preparation and precycling in an EGTA-containing electrolyte solution, the electrode is transferred to another cell containing a known concentration of the metal ion to be tested. Reactivity may be controlled by varying the potential range or by applying routines in which the potential is held at certain values for periods of time. Cluster transformations are monitored and analyzed through changes in the appearance of the voltammogram. Following transfers of an electrode coated with a film of 7Fe *D. africanus* Fd III to solutions of Fe(II), Zn(II), and Cd(II), dramatic changes are observed over several rapid cycles (35). Some results are shown in Fig. 13, in which only the oxidative sweeps are displayed.

Couples A' and C' disappear to be replaced in each case by a single new couple D', the reduction potential of which depends markedly upon the identity of the metal ion. Correspondence between the disappear-

ance of waves A' and C' and the appearance of waves D' was established by comparing differential current amplitudes (expressed logarithmically) as an arbitrary function of time (cycle number). The reactions were found to proceed in a first-order manner, to an equilibrium position that is dependent upon the concentration of the particular metal ion. Estimated integrated areas of waves D' and widths at half-height were similar to values observed for the original waves A'. Waves B' were found to be unaffected. The semilog plots and resulting final voltammograms obtained under conditions of high metal ion concentration are also shown in Fig. 13. Interestingly, it was observed that the reactions with Cd and Zn were complete at much lower metal ion concentrations than was the case with Fe. This will be discussed further below.

As with the incorporation of Fe(II) described earlier, it was confirmed that reactions of *D. africanus* Fd III with Zn(II) or Cd(II) occurred with "free," i.e., unadsorbed, protein molecules (35). Bulk electrolytic titrations analogous to the type carried out to quantify Fe(II) incorporation showed that one equivalent of Zn(II) or Cd(II) was taken up by the $[3\text{Fe}-4\text{S}]^0$ form of the protein. Comparisons of $E^{0'}$ measured for films and for stoichiometrically transformed solutions are given in Table II. The close correspondence between reduction potentials determined for solution and film indicates that *D. africanus* Fd III molecules adsorbed at the electrode surface, under conditions of applied potential down to at least -600 mV, maintain cluster environments that are little perturbed from the native state. On the basis of EPR and MCD spectroscopic examination, it was proposed that the reaction products are $[\text{Zn}3\text{Fe}-4\text{S}]^{2+/1+}$ and $[\text{Cd}3\text{Fe}-4\text{S}]^{2+/1+}$ clusters. Two-electron reduced protein samples electrolysed at potentials of -535 and -650 mV, respectively, gave EPR spectra with signals around $g = 2$ (double integration giving ≤ 1 spin per molecule) and at $g = 4-5$. The former signals were assigned to the indigenous $[4\text{Fe}-4\text{S}]^{1+}$ cluster, i.e., couple B (B'), whereas the latter signals were assigned to the transformed product $[\text{M}3\text{Fe}-4\text{S}]^{1+}$, specifically the $M_s = \pm \frac{3}{2}$ middle Kramers' doublet of an $S = \frac{5}{2}$ state. In support of this, two weaker signals could be observed at low field ($g = 9.6$ and ~ 8.8) as predicted for the $M_s = \pm \frac{5}{2}$ and $\pm \frac{1}{2}$ doublets. The new spectral features resembled those assigned to the $[\text{Zn}3\text{Fe}-4\text{S}]^{1+}$ cluster that can be formed in *D. gigas* ferredoxin II (33). As shown by MCD spectroscopy, the oxidized species $[\text{Zn}3\text{Fe}-4\text{S}]^{2+}$ and $[\text{Cd}3\text{Fe}-4\text{S}]^{2+}$ each have the ground state $S = 2$. Spectra of each species are similar in the visible region (which is dominated by transitions due to the $[3\text{Fe}-4\text{S}]^0$ core) but differ in the region below 400 nm, where localized transitions, for example, $d^{10} \rightarrow s(p)$ or $\text{S}^{2-} \rightarrow \text{Cd(II)}$, are expected.

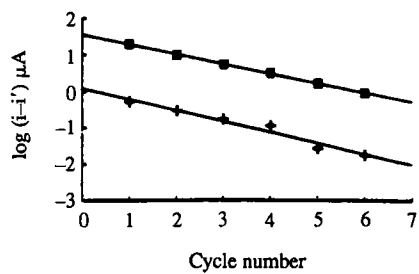
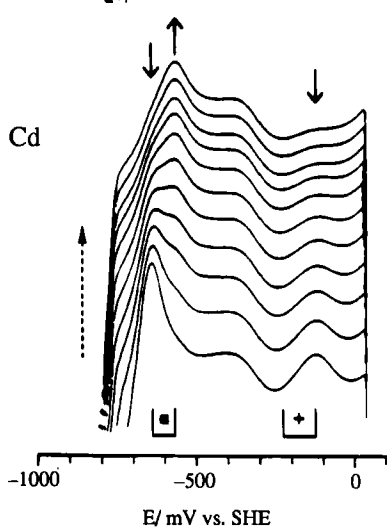
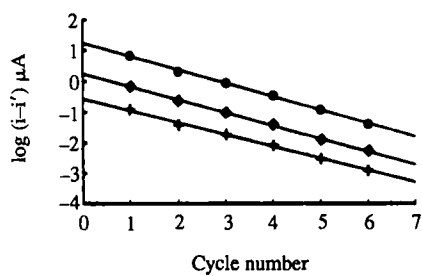
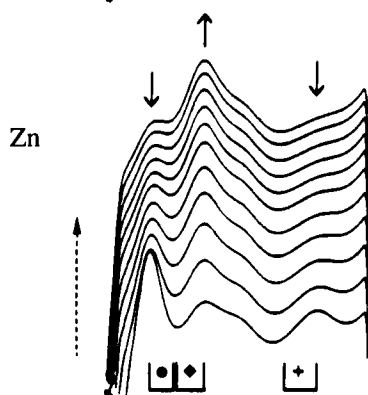
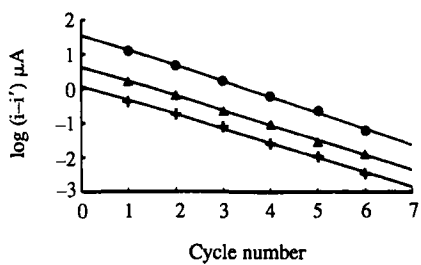
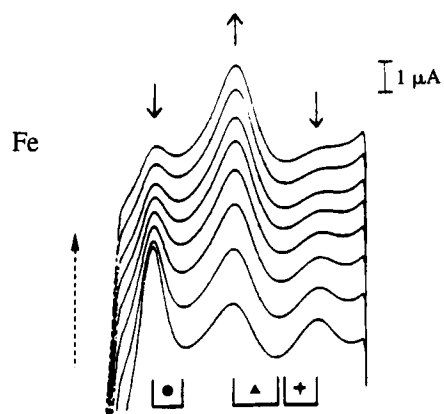


TABLE II
 $E^{0'}$ VALUES FOR FILMS AND TRANSFORMED
 SOLUTIONS^a

[M3Fe-4S]	K_d (μM)	$E^{0'}$ (mV vs. SHE)	
		Film	Bulk
[4Fe-4S] ²⁺	30 \pm 15	-393	-400
[Zn3Fe-4S] ²⁺	1.6 \pm 1.0	-492	-480
[Cd3Fe-4S] ²⁺	0.8 \pm 0.5	-569	-580
[Tl3Fe-4S] ¹⁺	1.5 \pm 1.0	—	—
[Tl3Fe-4S] ²⁺	34 mM	+81	—

^a Upper set: values of voltammetrically determined dissociation constants K_d for Eq. (8) and comparison of reduction potentials $E^{0'}$ for the corresponding couple D' ([M3Fe-4S]^{2+/1+}) as measured from film and bulk solution voltammetry of *D. africanus* Fd III. Conditions: 0.1 M NaCl, 20 mM mixed buffer as electrolyte; pH 7-7.4; temperature 0°C (film), 3-4°C (bulk). Data taken from Ref. 35. Lower set: values of dissociation constants K_d for equilibrium of Tl(I) with the [3Fe-4S] cluster in a film of *D. africanus* Fd III. Conditions: 0.5 M Na/Tl acetate as electrolyte; pH 7; temperature 7°C. Data taken from Ref. 36.

These reactions were shown to be reversible by transferring electrodes coated with transformed films back to electrolyte solutions containing no metal ion (87). As shown in Fig. 14, upon repeated cycling, the voltammogram of the original 7Fe ferredoxin reappears upon repeated cycling in the potential region favoring the presence of the

FIG. 13. Left: oxidative scans (successive cycles) of a film of 7Fe *D. africanus* Fd III upon transfer to M²⁺ solutions. Conditions otherwise as given for Fig. 12. Right: corresponding semilog plots showing time correspondence of appearance of waves D' and disappearance of waves A'. The potential was held briefly at $\sim +50$ mV prior to commencement of scanning at 470 mV/sec. Each determination involved measurement of the difference in current at two potentials as indicated. Fe²⁺ (300 μM): +, $i_{-129 \text{ mV}} - i_{-229 \text{ mV}}$, couple A'; \blacktriangle , $i_{-393 \text{ mV}} - i_{-250 \text{ mV}}$, couple D'; \bullet , $i_{-651 \text{ mV}} - i_{-554 \text{ mV}}$, couple C'. Zn²⁺ (10 μM): +, $i_{-129 \text{ mV}} - i_{-229 \text{ mV}}$, couple A'; \blacktriangle , $i_{-484 \text{ mV}} - i_{-570 \text{ mV}}$, couple D'; \bullet , $i_{-655 \text{ mV}} - i_{-579 \text{ mV}}$, couple C'. Cd²⁺ (10 μM): +, $i_{-129 \text{ mV}} - i_{-229 \text{ mV}}$, couple A'; \blacksquare , $i_{-641 \text{ mV}} - i_{-568 \text{ mV}}$, combination of couples C' and D'. [Reproduced from Butt, J. N., Armstrong, F. A., Breton, J., George, S. J., Thomson, A. J., and Hatchikian, E. C., *J. Am. Chem. Soc.* **113**, 6663 (1991), with permission].

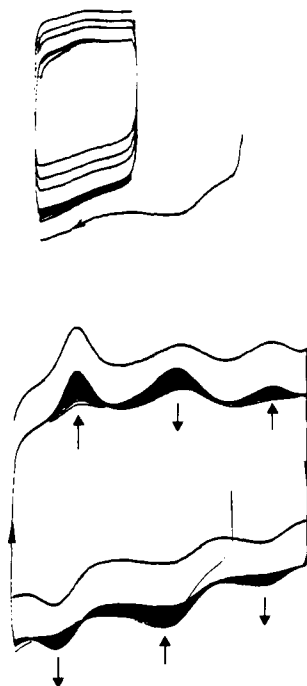


FIG. 14. Cyclic voltammograms showing release of Fe(II) from the transformed $[4\text{Fe}-4\text{S}]$ cluster of *D. africanus* Fd III. Conditions as given for Fig. 13 but electrolyte contains no divalent metal ion. Top: cycling at 470 mV/sec restricted to potential region below -500 mV. There is no reappearance of couple C' over a period of 10 min. Bottom: cycling at 470 mV/sec now including potential region in which transformed $[4\text{Fe}-4\text{S}]$ cluster is oxidized. Couples A' and C' reappear within a minute.

oxidized cluster $[\text{M3Fe}-4\text{S}]^{2+}$. Metal ion release is not observed if cycling is restricted to the potential region in which $[\text{M3Fe}-4\text{S}]$ remains in the $+1$ oxidation level. This shows that the reduced tetrametal cluster is more stable than the oxidized cluster with respect to release of the exchangeable metal ion. One way of viewing this is in terms of the immediate product $[\text{3Fe}-4\text{S}]^{1-}$ for which there is no evidence for stability. The observation emphasizes the importance of the environmental electrochemical potential in controlling such cluster transformations as they may occur *in vivo*.

At this juncture, it is appropriate to summarize the chemistry established to date for the two Fe-S clusters of *D. africanus* Fd III. The reactions are outlined in Fig. 15. The $[\text{3Fe}-4\text{S}]$ cluster exhibits a wide and interesting reactivity, showing unusual capabilities for extensive electron/proton transfer and, in addition, undergoing facile, reversible

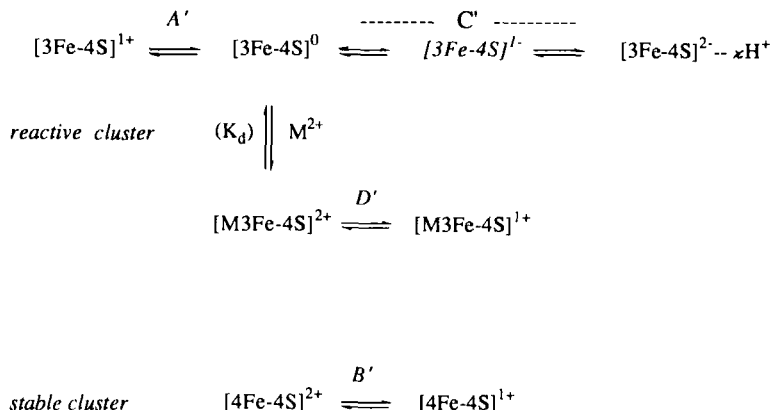
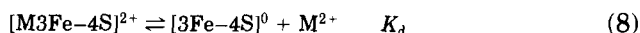


FIG. 15. Scheme showing the identities of couples A', B', C', and D' as observed in voltammetry of films of *D. africanus* Fd III.

incorporation of certain divalent and monovalent (see below) metal ions.

Reversible binding of divalent metal ions M^{2+} to the $[3\text{Fe-4S}]^0$ cluster is described by Eq. (8),



for which the dissociation constant K_d is given by

$$K_d = \{[3\text{Fe-4S}]^0\}\{M^{2+}\}/\{[M3\text{Fe-4S}]^{2+}\} \quad (9)$$

and

$$\{[M3\text{Fe-4S}]^{2+}\}/\{[3\text{Fe-4S}]^0\} = \{M^{2+}\}/K_d \quad (10)$$

in which $\{[M3\text{Fe-4S}]^{2+}\}$ and $\{[3\text{Fe-4S}]^0\}$ are surface populations (typically picomole or lower) and $\{M^{2+}\}$ is the solution concentration of metal ion. Equilibrium (dissociation) constants for these reactions were determined by measuring voltammetric signal amplitudes observed in a rapid cycle following equilibration of the film at a fixed potential in electrolyte solutions containing various concentrations of M^{2+} . Such a method is applicable if the rates of entry and release of Fe(II), Zn(II), and Cd(II) are slow compared to the voltammetric scan rates used. By carrying out such a determination under conditions of controlled potential, it could be ensured that the oxidation levels of each cluster species are as required by Eq. (9). From Eq. (10), a plot of the observed ratio $\{[M3\text{Fe-4S}]\}/\{[3\text{Fe-4S}]\}$ (oxidation levels omitted) against $\{M^{2+}\}$ is expected to yield a straight line with slope $1/K$.

Some results are illustrated in Fig. 16. A clearer distinction between the similar affinities displayed for Zn and Cd was made by direct competition experiments in which a film was transferred to solutions containing 1:1 and 2:1 (micromolar) ratios of the two ions. In the former case, the voltammogram was dominated by the appearance of the couple $[\text{Cd}3\text{Fe}-4\text{S}]^{2+/1+}$; in the latter case the couple $[\text{Zn}3\text{Fe}-4\text{S}]^{2+/1+}$ appeared at equal magnitude. The $[\text{3Fe}-4\text{S}]^0$ cluster in *D. africanus* Fd III thus displays the affinity order $\text{Cd} \geq \text{Zn} \gg \text{Fe}$. This comes as no surprise, since it is indeed the result that we expect from consideration of the Irving-Williams order (94). While it must be stressed that the nature of the noncluster ligand is not established [water ($\text{H}_2\text{O}/\text{OH}^-$) and aspartate are most likely], the identification of one example in which a $[\text{3Fe}-4\text{S}]^0$ cluster favors $\text{Zn}(\text{II})$ over $\text{Fe}(\text{II})$ by more than one order of magnitude implies an interesting and important viability of $[\text{Zn}3\text{Fe}-4\text{S}]$ clusters in biological systems, for which Zn levels may approach (or even exceed) levels of Fe (95, 96). This possibility certainly requires further investigation, particularly since the EPR spectra reported for $[\text{Zn}3\text{Fe}-4\text{S}]^{1+}$ clusters differ so much from those normally observed for $[\text{4Fe}-4\text{S}]^{1+}$. Such heterometal species might readily escape

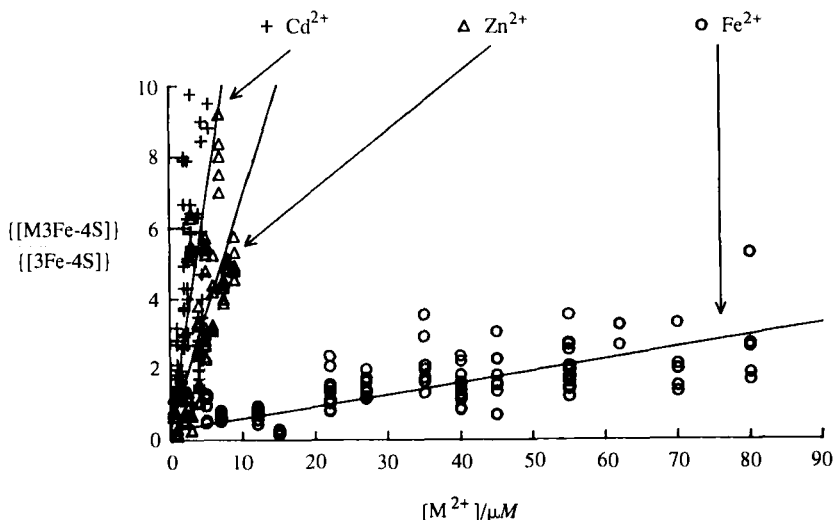


FIG. 16. Graph showing the dependence of the cluster population ratio $\{[\text{M}3\text{Fe}-4\text{S}]\}/\{[\text{3Fe}-4\text{S}]\}$ for a film of *D. africanus* Fd III upon the concentration of metal ions in the electrolyte $\{\text{M}^{2+}\}$. [Adapted from Butt, J. N., Armstrong, F. A., Breton, J., George, S. J., Thomson, A. J., and Hatchikian, E. C., *J. Am. Chem. Soc.* 113, 6663 (1991), with permission.]

attention. Without further structural information to reveal the nature of the noncluster ligation in each case, it is difficult to rationalize the large variation in reduction potentials that is observed. Such a variation, however, requires that the environmental electrochemical potential should be an important factor for controlling speciation in the presence of different metal ions.

An interesting extension of this theme is provided by the reaction of the [3Fe-4S] cluster of *D. africanus* Fd III with Tl(I) ions (36). This is an interesting example in which metal ion uptake and release is very fast, and occurs measurably for [3Fe-4S]¹⁺ in addition to [3Fe-4S]⁰. Figure 17 shows how the position of couple A' varies with the concentration of Tl(I) in the cell electrolyte. Waves B' are unaffected, although Tl(0) deposition interferes with observation of waves C'. No such shifts were observed if 0.1 M K⁺ (radius 138 pm) or 0.1 M Rb⁺ (radius 152 pm) was substituted for Tl⁺ (radius 150 pm). Competition experiments showed further that Tl(I) inhibits the coordination of Fe(II) at [3Fe-4S]⁰.

Since the tri- μ -sulfido cluster face provides the only polarizable ligand group on the protein likely to be so selective for Tl⁺ over similarly sized alkali metal ions, it was proposed that Tl(I) coordinates to the [3Fe-4S] core. The sigmoidal dependence of $E^{0'}$ upon Tl(I) concentra-

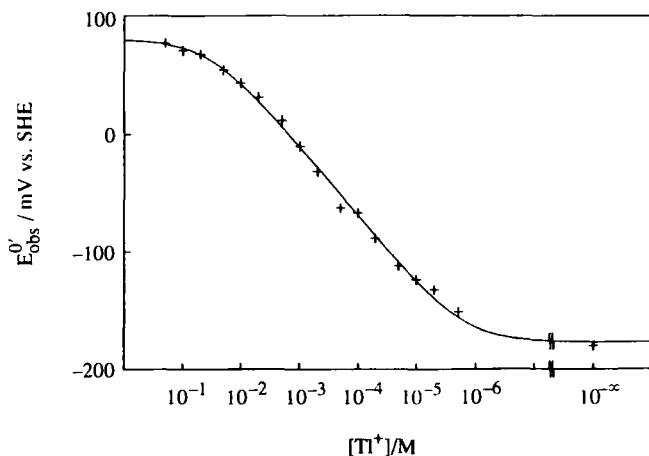


FIG. 17. Graph of observed reduction potentials for couple A' (*D. africanus* Fd III) as a function of the concentration of Tl(I) in the electrolyte. The curve is the computed nonlinear regression fit to Eq. (11). [Reproduced from Butt, J. N., Sucheta, A., Armstrong, F. A., Breton, J., Thomson, A. J., and Hatchikian, E. C., *J. Am. Chem. Soc.* **113**, 8948 (1991), with permission.]

tion was rationalized in terms of the cyclic reaction scheme shown in Fig. 18, in which electron transfer is coupled to very rapid uptake and release of Tl(I). This type of situation, in which species equilibrate rapidly within the voltammetric scan time, is analogous to a potentiometric experiment. Values of K_d^{ox} , K_d^{red} , and $E_{\text{Tl}}^{0'}$ are obtained from application of Eqs. (11) and (12). Results are included in Table II.

$$E_{\text{obs}}^{0'} = E^{0'} + (2.303 RT/F) \log\{(1 + [\text{Tl}^+]/K_d^{\text{red}})/(1 + [\text{Tl}^+]/K_d^{\text{ox}})\} \quad (11)$$

$$E_{\text{Tl}}^{0'} = E^{0'} + (2.303 RT/F) \log(K_d^{\text{ox}}/K_d^{\text{red}}) \quad (12)$$

The proposal that Tl(I) enters the [3Fe-4S] core was supported by spectroscopic studies (36). With a $[\text{Tl}^+]$ concentration of 133 mM (i.e., a fourfold excess over the determined value of K_d^{ox}), the characteristic $g = 2.01$ signal of $[\text{3Fe-4S}]^{1+}$ was replaced by a rhombic spectrum having g values 2.04, 1.99, and 1.95. Intermediate concentrations of Tl(I) produced spectra that were superpositions of the new species and of $[\text{3Fe-4S}]^{1+}$. The K_d^{ox} value estimated from these spectra was in good agreement with that determined from the film voltammetry. As with other transformation products, the identity of the noncluster ligand(s) to the Tl site has not been established at the time of preparing this manuscript.

The results highlight several new features. First, they demonstrate the existence of a possible biological target for Tl(I), a known toxic element (97); indeed the affinity of Tl(I) for $[\text{3Fe-4S}]^0$ is much stronger than reported affinities for Tl(I) occupancy of K^+ sites (98). Second, they demonstrate the interaction of a monovalent ion with a [3Fe-4S] cluster. Third, by conforming well to a rapid equilibrium model, even

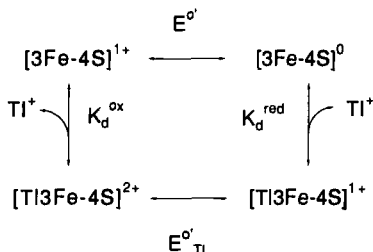


FIG. 18. Scheme showing reversible binding of Tl(I) to +1 and 0 oxidation levels of the [3Fe-4S] cluster of *D. africanus* Fd III. [Reproduced from Butt, J. N., Sucheta, A., Armstrong, F. A., Breton, J., Thomson, A. J., and Hatchikian, E. C., *J. Am. Chem. Soc.* 113, 8948 (1991), with permission.]

at a scan rate of 470 mV/sec, it can be concluded that both "on" and "off" rates for binding of Tl(I) are very fast. This implies that the metal-binding site at the [3Fe-4S] cluster of *D. africanus* Fd III is probably exposed to solvent and that the protein does not resist the transformation. The implication that this access is not restricted significantly (if at all) by the adsorbed state of the protein molecule indicates also that there is considerable fluidity within the protein/aminocyclitol film.

A brief, final illustration of the use of adsorbed film voltammetry is the ability to study rapid interactions of clusters with extraneous ligands (99). From these experiments, as before, new species can be detected and their limits for existence defined to allow isolation and structural characterization. Figure 19 shows the voltammetry that results following transfer of an PGE electrode coated with a Fe-transformed film of *D. africanus* Fd III into a solution containing 0.54 M mercaptoethanol. The observations may be rationalized in terms of the generic scheme shown in Fig. 20, in which rapid and reversible binding of a ligand L occurs to both the 2+ and 1+ oxidation levels of a [M3Fe-4S] cluster [M is a divalent metal, in this case Fe(II)].

Under conditions of rapid scan rate (1 V/sec) waves D', which are normally coincident with waves B' if M = Fe, are replaced by a couple (termed F') for which the reduction potential $E_F^{0'} = -585$ mV. The shift in potential is thus approximately -190 mV. The amplitudes of reduction and oxidation waves F' are similar at this scan rate, but do depend upon pH and mercaptoethanol concentration; under the conditions used for this particular experiment, their amplitude is comparable with waves B'. By contrast, under conditions of slow scan rate (10 mV/sec), D' is replaced by a new couple having an apparent reduction potential $E_{\text{obs}}^{0'}$ that is dependent upon pH and mercaptoethanol concentration. The amplitudes of reduction and oxidation waves are equal, and independent of mercaptoethanol concentration. The two experiments relate to kinetically limiting cases for the scheme shown in Fig. 20. Examination of the effect of pH shows that the active ligand L is ethanol-2-thiolate (the pK of mercaptoethanol under these conditions is 9.8). In the fast scan experiment, ligand binding and release is effectively frozen and the voltammogram displays the isolated couples F' and D' (overlaid on B'; little or no D' is actually observed under the conditions used). In the slow scan limit, equilibrium conditions are established for ligand interaction and the voltammetry becomes analogous to a potentiometric experiment. The observed reduction potential $E_{\text{obs}}^{0'}$ is related to ligand concentration ($[\text{thiolate}] = ([\text{total thiol}])/(1 + [\text{H}^+]/10^{-9.8})$) by equations analogous to those given in Eqs. (11) and (12) for Tl⁺ binding to [3Fe-4S]^{1+/0}. Data analysis shows that the

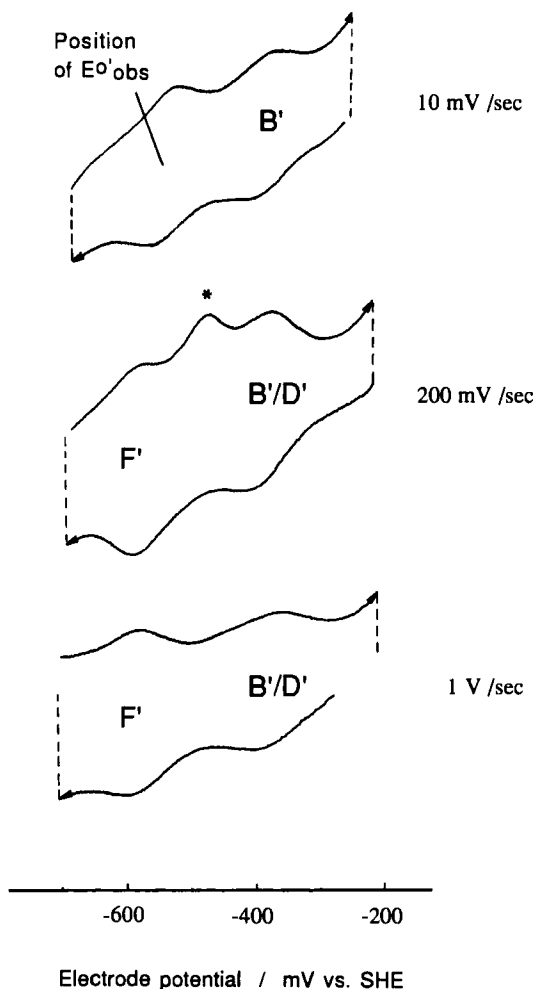


FIG. 19. Cyclic voltammograms at various scan rates, of a pretransformed film of 8Fe *D. africanus* Fd III contacting a solution of Fe(II) (180 μM) and mercaptoethanol (0.54 M). Conditions: electrolyte consists of 0.2 M NaCl, 20 mM Tris HCl, 2 mM neomycin, pH 8; temperature 0°C. In each case the charging current contribution has been trimmed to aid visual comparison. All scans commence from the high-potential limit.

reduced cluster $[4Fe-4S]^{1+}$ displays a much lower affinity for the ligand ($K_{d(L)}^{\text{red}} = 96 \text{ } mM$) than does the oxidized cluster ($K_{d(L)}^{\text{ox}} = 30 \text{ } \mu M$). At the time of writing, it is not established whether L replaces an incumbent ligand or adds to increase the coordination number of the target subsite. The M subsite is implicated since voltammetry of the

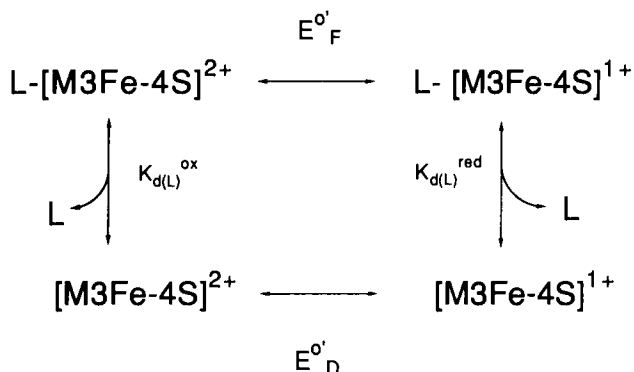


FIG. 20. Scheme showing reversible binding of an extraneous ligand L to 2+ and 1+ oxidation levels of a [M3Fe-4S] cluster (M is a divalent metal ion). All parameters may be determined from the voltammetry.

untransformed 7Fe protein measured in mercaptoethanol is unperturbed. The observations for *D. africanus* Fd III thus provide a further demonstration that incorporation of M into a [3Fe-4S] cluster itself generates new chemical reactivity that may be important in the stabilization of proteins and protein adducts.

Voltammograms measured at intermediate scan rates reveal the kinetics of ligand interaction. Substantial release of L from [4Fe-4S]¹⁺ is evident from inspection of Fig. 19 (center) which shows a much attenuated reoxidation wave for F'. A third oxidation wave (*) is now observed which corresponds to the coupled rapid recombination of the electrode product [4Fe-4S]²⁺ with L. It is noted that the *total* amount of charge passed between the electrode and protein during each scan remains constant. Such voltammograms clearly contain a wealth of information that should be readily extractable using computer simulation methods.

IV. Conclusions

In what is a limited number of experiments described in this Section, I hope to have shown or at least hinted at several useful and interesting aspects of direct electrochemical methods as applied to the problems of Fe-S clusters. The examples given should serve as some demonstration that the techniques can be effective and may have wide application in the area.

It has proved straightforward to detect redox couples at potentials far below the limits of dithionite at neutral pH, to study the stabilities of the reduced species, and to generate samples in specific states of reduction for spectroscopy. Voltammetric signals have been used as signatures of cluster status, appropriate for time domain investigations.

The adsorbed film studies described for *D. africanus* Fd III illustrate a new strategy for studying proteins with very reactive Fe–S clusters. The approach combines high sensitivity, accuracy, and the ability to study reactions under strict conditions of applied potential. Complex, seemingly erratic behavior can be managed and visualized. Equilibrium and kinetic data may be derived with just trace amounts of protein, and verified by preparation of appropriate spectroscopic samples. From the results of spectroscopic studies on the products of parallel transformations carried out in solution, it is indeed demonstrated that the voltammetric interrogation of Fe–S proteins in an adsorbed film can provide an acceptably valid reflection of the chemistry of free molecules. A useful “trailblazing” capability is thus provided to give guidance and to complement the techniques aimed at detailed structural characterization.

ACKNOWLEDGMENTS

The author thanks a number of co-workers who have been closely involved with most of the studies described in this article. These include J. N. Butt, S. J. George, J. Breton, A. Vázquez, A. Sucheta, A. J. Thomson, E. C. Hatchikian, R. Cammack, B. K. Burgess, and P. J. Stephens. Funding from the SERC (UK), The Royal Society, from the Exxon Education Foundation, and the ACS Petroleum Research Fund is gratefully acknowledged.

REFERENCES

1. Armstrong, F. A., Hill, H. A. O., and Walton, N. J., *Acc. Chem. Res.* **21**, 407 (1988).
2. Armstrong, F. A., *Struct. Bonding* **72**, 137 (1990).
3. Guo, L. H., and Hill, H. A. O., in “Advances in Inorganic Chemistry” (A. G. Sykes, ed.), Vol. 36, p. 341. Academic Press, San Diego, California, 1991.
4. Pielak, G. J., Concar, D. W., Moore, G. R., and Williams, R. J. P., *Protein Eng.* **1**, 83 (1987).
5. McLendon, G., *Acc. Chem. Res.* **21**, 160 (1988).
6. Williams, R. J. P., *Biochem. Int.* **18**, 475 (1989).
7. Lyklema, J., *Colloids Surf.* **10**, 33 (1984).

8. Dutton, P. L., in "Methods in Enzymology" (S. Fleischer and L. Packer, eds.), Vol. 54, p. 411. Academic Press, New York, 1978.
9. Bond, A. M., "Modern Polarographic Methods in Analytical Chemistry." Dekker, New York and Basel, 1980.
10. Bard, A. J., and Faulkner, L. R., "Electrochemical Methods, Fundamentals and Applications." Wiley, New York, 1980.
11. Kissinger, P. T., and Heineman, W. R., eds., "Laboratory Techniques in Electroanalytical Chemistry." Dekker, New York and Basel, 1984.
12. Southampton Electrochemistry Group, "Instrumental Methods in Electrochemistry." Ellis Horwood, Chichester, 1985.
13. Beinert, H., *FASEB J.* **4**, 2483 (1990).
14. Beinert, H., and Kennedy, M. C., *Eur. J. Biochem.* **186**, 5 (1989).
15. Rouault, T. A., Stout, C. D., Kaptain, S., Harford, J. B., and Klausner, R. D., *Cell (Cambridge, Mass.)* **64**, 881 (1991).
16. Hentze, M. W., and Argos, P., *Nucl. Acid Res.* **19**, 1739 (1991).
17. Beinert, H., and Thomson, A. J., *Arch. Biochem. Biophys.* **222**, 333 (1983).
18. Beinert, H., Emptage, M. H., Dreyer, J.-L., Scott, R. A., Hahn, J. E., Hodgson, K. O., and Thomson, A. J., *Proc. Natl. Acad. Sci. U.S.A.* **80**, 393 (1983).
19. Stephens, P. J., Morgan, T. V., Devlin, F., Penner-Hahn, J., Hodgson, K. O., Scott, R. A., Stout, C. D., and Burgess, B. K., *Proc. Natl. Acad. Sci. U.S.A.* **83**, 5661 (1985).
20. Antonio, M. R., Averill, B. A., Moura, I., Moura, J. J. G., Orme-Johnson, W. H., Teo, B.-K., and Xavier, A. V., *J. Biol. Chem.* **257**, 6646 (1982).
21. Stout, C. D., *J. Mol. Biol.* **205**, 545 (1989).
22. Stout, G. H., Turley, S., Sieker, L. C., and Jensen, L. H., *Proc. Natl. Acad. Sci. U.S.A.* **85**, 1020 (1988).
23. Kissinger, C. R., Sieker, L. C., Adman, E. T., and Jensen, L. H., *J. Mol. Biol.* **219**, 693 (1991).
24. Stephens, P. J., Jensen, G. M., Devlin, F. J., Morgan, T. V., Stout, C. D., Martin, A. E., and Burgess, B. K., *Biochemistry* **30**, 3200 (1991).
25. Gurbel, R. J., Batie, C. J., Sivaraja, M., True, A. E., Fee, J. A., Hoffman, B. M., and Ballou, D. P., *Biochemistry* **28**, 4861 (1989).
26. Robbins, A. H., and Stout, C. D., *Proc. Natl. Acad. Sci. U.S.A.* **86**, 3639 (1989).
27. Werst, M. M., Kennedy, M. C., Beinert, H., and Hoffman, B. M., *Biochemistry* **29**, 10526 (1990).
28. Moura, J. J. G., Moura, I., Kent, T. A., Lipscomb, J. D., Huynh, B.-H., LeGall, J., Xavier, A. V., and Münck, E., *J. Biol. Chem.* **257**, 6259 (1982).
29. George, S. J., Armstrong, F. A., Hatchikian, E. C., and Thomson, A. J., *Biochem. J.* **264**, 275 (1989).
30. Conover, R. C., Kowal, A. T., Fu, W., Park, J.-B., Aono, S., Adams, M. W. W., and Johnson, M. K., *J. Biol. Chem.* **265**, 8533 (1990).
31. Hagen, W. R., Pierik, A. J., and Veeger, C., *J. Chem. Soc., Faraday Trans. 1*, **85**, 4083 (1989).
32. Moura, I., Moura, J. J. G., Münck, E., Papaefthymiou, V., and LeGall, J., *J. Am. Chem. Soc.* **108**, 349 (1986).
33. Sureus, K. K., Münck, E., Moura, I., Moura, J. J. G., and LeGall, J., *J. Am. Chem. Soc.* **109**, 3805 (1987).
34. Conover, R. C., Park, J.-B., Adams, M. W. W., and Johnson, M. K., *J. Am. Chem. Soc.* **112**, 4562 (1990).
35. Butt, J. N., Armstrong, F. A., Breton, J., George, S. J., Thomson, A. J., and Hatchikian, E. C., *J. Am. Chem. Soc.* **113**, 6663 (1991).

36. Butt, J. N., Sucheta, A., Armstrong, F. A., Breton, J., Thomson, A. J., and Hatchikian, E. C., *J. Am. Chem. Soc.* **113**, 8948 (1991).
37. Burgess, B. K., *Chem. Rev.* **90**, 1377 (1990).
38. Eady, R. R., in "Advances in Inorganic Chemistry" (A. G. Sykes, ed.), Vol. 36, p. 77. Academic Press, San Diego, California, 1991.
39. Stack, T. D. P., and Holm, R. H., *J. Am. Chem. Soc.* **110**, 2484 (1988).
40. Ciurli, S., Carrié, M., Weigel, J. A., Carney, M. J., Stack, T. D. P., Papaefthymiou, G. C., and Holm, R. H., *J. Am. Chem. Soc.* **112**, 2654 (1990).
41. Holm, R. H., Ciurli, S., and Weigel, J. A., *Prog. Inorg. Chem.* **38**, 1 (1990).
42. Weigel, J. A., and Holm, R. H., *J. Am. Chem. Soc.* **113**, 4184 (1991).
43. Kovacs, J. A., and Holm, R. H., *Inorg. Chem.* **26**, 702, 711 (1987).
44. Ciurli, S., Carney, M. J., Holm, R. H., and Papaefthymiou, G. C., *Inorg. Chem.* **28**, 2696 (1989).
45. Ciurli, S., Carrié, M., and Holm, R. H., *Inorg. Chem.* **29**, 3493 (1990).
46. Ciurli, S., Yu, S.-B., Holm, R. H., Srivastava, K. K. P., and Münck, E., *J. Am. Chem. Soc.* **112**, 8169 (1990).
47. Mayhew, S. G., *Eur. J. Biochem.* **85**, 535 (1978).
48. Armstrong, F. A., Bond, A. M., Hill, H. A. O., Psalti, I. S. M., and Zoski, C. G., *J. Phys. Chem.* **93**, 6485 (1989).
49. Armstrong, F. A., Bond, A. M., Hill, H. A. O., Oliver, B. N., and Psalti, I. S. M. J., *J. Am. Chem. Soc.* **111**, 9185 (1989).
50. Buchi, F., and Bond, A. M., *J. Electroanal. Chem.*, in press (1992).
51. Nicholson, R. S., and Shain, I., *Anal. Chem.* **36**, 706 (1964).
52. Laviron, E., *J. Electroanal. Chem.* **52**, 355 (1974).
53. Laviron, E., *J. Electroanal. Chem.* **52**, 395 (1974).
54. Laviron, E., *J. Electroanal. Chem.* **101**, 19 (1979).
55. Osteryoung, J. G., and Osteryoung, R. A., *Anal. Chem.* **57**, 101A (1985).
56. Smith, E. T., and Feinberg, B. A., *J. Biol. Chem.* **265**, 14371 (1990).
57. Smith, E. T., Bennett, D. W., and Feinberg, B. A., *Anal. Chim. Acta* **251**, 27 (1991).
58. Crawley, C. D., and Hawkrigde, F. M., *J. Electroanal. Chem.* **159**, 313 (1983).
59. Alberty, W. J., Eddowes, M. J., Hill, H. A. O., and Hillman, A. R., *J. Am. Chem. Soc.* **103**, 3904 (1981).
60. Weitzman, P. D. J., Kennedy, I. R., and Caldwell, R. A., *FEBS Lett.* **17**, 241 (1971).
61. Dalton, H., and Zubieta, J., *Biochim. Biophys. Acta* **322**, 133 (1973).
62. Zuznetsov, B. A., Mestechkina, N. M., and Shumakovich, G. P., *Bioelectrochem. Bioenerg.* **4**, 1 (1977).
63. Hill, C. L., Renaud, J., Holm, R. H., and Mortenson, L. E., *J. Am. Chem. Soc.* **99**, 2549 (1977).
64. Bianco, P., and Haladjian, J., *Biochem. Biophys. Res. Commun.* **78**, 323 (1977).
65. Ikeda, T., Toriyama, K., and Senda, M., *Bull. Chem. Soc. Jpn.* **52**, 1937 (1979).
66. Van Dijk, C., Van Leeuwen, J. W., Veeger, C., Schreurs, J. P. G. M., and Barendrecht, E., *Bioelectrochem. Bioenerg.* **9**, 743 (1982).
67. Cotton, F. A., and Wilkinson, G., "Advanced Inorganic Chemistry," Wiley (Interscience), 5th Ed., p. 613. New York, 1988.
68. Landrum, H. L., Salmon, R. T., and Hawkrigde, F. M., *J. Am. Chem. Soc.* **99**, 3154 (1977).
69. Bianco, P., Haladjian, J., Tobiana, G., Forget, P., and Bruschi, M., *Bioelectrochem. Bioenerg.* **12**, 509 (1984).
70. Van Dijk, C., Van Eijs, T., Van Leeuwen, J. W., and Veeger, C., *FEBS Lett.* **166**, 76 (1984).

71. Armstrong, F. A., Hill, H. A. O., and Walton, N. J., *FEBS Lett.* **145**, 241 (1982).
72. Armstrong, F. A., Cox, P. A., Hill, H. A. O., Lowe, V. J., and Oliver, B. N., *J. Electroanal. Interfac. Electrochem.* **217**, 331 (1987).
73. Armstrong, F. A., George, S. J., Thomson, A. J., and Yates, M. G., *FEBS Lett.* **234**, 107 (1988).
74. Rinehart, K. L., and Suami, T., eds., "Aminocyclitol Antibiotics," ACS Symp. Ser. Vol. 125, American Chemical Society, Washington, D.C., 1980.
75. Armstrong, F. A., George, S. J., Cammack, R., Hatchikian, E. C., and Thomson, A. J., *Biochem. J.* **264**, 265 (1989).
76. Iismaa, S. E., Vázquez, A. E., Jensen, G. M., Stephens, P. J., Butt, J. N., Armstrong, F. A., and Burgess, B. K., *J. Biol. Chem.* **266**, 21563 (1991).
77. Armstrong, F. A., Butt, J. N., George, S. J., Hatchikian, E. C., and Thomson, A. J., *FEBS Lett.* **259**, 15 (1989).
78. George, S. J., Richards, A. J. M., Thomson, A. J., and Yates, M. G., *Biochem. J.* **224**, 247 (1984).
79. Johnson, M. K., Bennett, D. E., Fee, J. A., and Sweeney, W. V., *Biochim. Biophys. Acta* **911**, 81 (1987).
80. Johnson, M. K., Thomson, A. J., Richards, A. J. M., Peterson, J., Robinson, A. E., Ramsay, R. R., and Singer, T. P., *J. Biol. Chem.* **259**, 2274 (1984).
81. Thomson, A. J., Robinson, A. E., Johnson, M. K., Moura, J. J. G., Moura, I., Xavier, A. V., and LeGall, J., *Biochim. Biophys. Acta* **670**, 93 (1981).
82. Morgan, T. V., Stephens, P. J., Devlin, F., Stout, C. D., Melis, K. A., and Burgess, B. K., *Proc. Natl. Acad. Sci. U.S.A.* **81**, 1931 (1984).
83. Hagen, W. R., Dunham, W. R., Johnson, M. K., and Fee, J. A., *Biochim. Biophys. Acta* **828**, 369 (1985).
84. Backes, G., Mino, Y., Loehr, T. M., Meyer, T. E., Cusanovich, M. A., Sweeney, W. V., Adman, E. T., and Sanders-Loehr, J., *J. Am. Chem. Soc.* **113**, 2055 (1991).
85. Armstrong, F. A., Hill, H. A. O., and Walton, N. J., *FEBS Lett.* **150**, 214 (1982).
86. Cammack, R., *Biochem. Biophys. Res. Commun.* **54**, 548 (1973).
87. Butt, J. N., and Armstrong, F. A., unpublished results (1991).
88. Soman, J., Iismaa, S., and Stout, C. D., *J. Biol. Chem.* **266**, 21558 (1991).
89. Martin, A. E., Burgess, B. K., Stout, C. D., Cash, V. L., Dean, D. R., Jensen, G. M., and Stephens, P. J., *Proc. Natl. Acad. Sci. U.S.A.* **87**, 598 (1990).
90. Bovier-Lapierre, G., Bruschi, M., Bonicel, J., and Hatchikian, E. C., *Biochim. Biophys. Acta* **913**, 20 (1987).
91. Hatchikian, E. C., Cammack, R., Patel, D. S., Robinson, A. E., Richards, A. J. M., George, S. J., and Thomson, A. J., *Biochim. Biophys. Acta* **784**, 40 (1984).
92. Otaka, E., and Ooi, T., *J. Mol. Evol.* **26**, 257 (1987).
93. Park, J.-B., Fan, C., Hoffman, B. M., and Adams, M. W. W., *J. Biol. Chem.* **266**, 19351 (1991).
94. Phillips, C. S. G., and Williams, R. J. P., "Inorganic Chemistry," Vol. 1, p. 630. Oxford Univ. Press, London and New York, 1965.
95. Ochiai, E.-I., "General Principles of Biochemistry of the Elements," Chap. 12. Plenum, New York, 1987.
96. Mills, C. F., ed., "Zinc in Human Biology." Springer-Verlag, Berlin, 1989.
97. Douglas, K. T., Bunni, M. A., and Baidur, S. R., *Int. J. Biochem.* **22**, 429 (1990).
98. Markham, G. D., Hafner, E. W., Tabor, C. W., and Tabor, H., *J. Biol. Chem.* **255**, 9082 (1980).
99. Butt, J. N., and Armstrong, F. A., unpublished results (1992).

EPR SPECTROSCOPY OF IRON-SULFUR PROTEINS

WILFRED R. HAGEN

Department of Biochemistry, Agricultural University, 6703 HA Wageningen,
The Netherlands

- I. Introduction
 - A. EPR Spectroscopy of Metalloproteins
 - B. EPR Spectroscopy of Iron-Sulfur Proteins
 - C. The ELS Classification
- II. Fundamentals of Iron-Sulfur EPR
 - A. The Basic Building Blocks
 - B. Superexchange
 - C. Double Exchange
- III. *g* Strain in Doublet Systems
 - A. Inhomogeneous Broadening of Iron-Sulfur EPR
 - B. The *g*-Strain Equation and Its Implications
- IV. High-Spin Kramers' Systems
 - A. The Weak-Field Regime
 - B. Calculation of Effective *g* Values
 - C. The Reading of Rhombograms
 - D. Practical Aspects of Iron-Sulfur High-Spin EPR
- V. Non-Kramers' Systems
 - A. Principles of Dual-Mode EPR in $S = 2$ Systems
 - B. Iron-Sulfur Non-Kramers' Systems
- VI. Epilogue
- References

I. Introduction

A. EPR SPECTROSCOPY OF METALLOPROTEINS

The phenomenon of electron paramagnetic resonance (EPR) was discovered in 1945 (1) and was developed during the following decade by physicists into a practical method of spectroscopy. Initially, the objects of study were predominantly those of the solid-state physicist, i.e.,

defects in crystals with well-defined symmetry properties. As a consequence, the original experiments and theoretical developments were biased toward single-crystal systems and the optimal use of symmetry arguments and perturbation theory methods. This bias is reflected in the structure of the classical textbooks on EPR (e.g., Ref. 2).

The first EPR experiments on biological systems were carried out very much along the same lines. In the mid-1950s, a group of physicists at Cambridge University, led by D. J. E. Ingram, made a series of single-crystal EPR studies on hemoglobin derivatives (3, 4). They took many spectra as a function of the orientation of the magnetic field with respect to the axes of the hemoglobin crystals frozen in their mother liquor. They were able to determine the orientation of the g -tensor principal axes with respect to crystal axis systems. Later, with the X-ray structures available, the g -tensor axes were found to approximately correspond to the heme plane and heme normal. The authors concluded that, "detailed information on the orientation of the haem plane can be combined with X-ray measurements to calculate the polypeptide chain directions and similar factors" (4).

In spite of the conceptual and experimental beauty of this work, in hindsight we can now assess single-crystal EPR to have proved to be of little value to protein structure determination. In fact, single-crystal EPR studies per se make up an extremely small part of all biological EPR work. This is not only the case because of the obvious practical difficulties of the protein crystallization and of the collection of angular-dependent data. There are also two fundamental difficulties intrinsic to the nature of proteins.

First, a biological metal site formally does not have any symmetry at all, if only because it is ligated by a polypeptide made up of levorotatory amino acid residues. This is especially true when the protein ligation forms a part of the first coordination sphere, as in iron-sulfur proteins. The statement implies that g -tensor axes cannot in general be expected to coincide with molecular bonds. Incidentally, it also explains why biochemists frequently run into problems when they attempt to analyze their EPR spectra using the high-symmetry approaches of the solid-state physicists.

Second, it so happens that the line width in single-crystal protein EPR is similar to (and frequently even significantly larger than) that of the turning-point features in spectra from randomly oriented samples of frozen solutions. There is no increased resolution in protein single-crystal spectra. This fact is related to the phenomenon of g strain that will be discussed later.

Also, in the mid-1950s, R. H. Sands studied transition ions in glasses

and he showed that the principal values of the g tensor and hyperfine tensors can be obtained from a single spectrum of a randomly oriented sample (5). The current widespread application of EPR spectroscopy to metalloproteins traces back to the late 1950s, when biochemist H. Beinert from the University of Wisconsin started to collaborate with physicist Sands at the University of Michigan and to apply the "powder EPR" method to frozen solutions of biological samples. Their first shot was at copper in cytochrome oxidase (6). A year later, in 1960, their second study was on mitochondrial membranes, in which they made the historical detection of what has long become an equivalence to iron-sulfur clusters, "the $g = 1.94$ signal" (7, 8). While the subsequent discussion about the physical and chemical nature of this signal spanned the better part of the ensuing decade, the detection itself is generally—perhaps with the exception of the authors themselves—felt to be the zero point in time of the history of iron-sulfur biochemistry. It is obviously also the first EPR experiment on an iron-sulfur cluster.

B. EPR SPECTROSCOPY OF IRON-SULFUR PROTEINS

The story of the genesis of iron-sulfur biochemistry from the observation of the $g = 1.94$ EPR signal is exemplary for all subsequent major developments in this field. The typical three-phase sequence of events is as follows. The first act is always the detection of an unusual, namely at the time unexplainable, EPR signal. This spurs a free flow of creative thinking, which one then attempts to contain and direct by collecting complementary information. Extensive analytical determinations, e.g., of Fe and acid-labile S content are a mandatory step, although these frequently prove to be rather less conclusive than one would want them to be. Of the other spectroscopies, Mössbauer usually provides a vital piece of the puzzle, notably, in the form of a ratio number of different iron sites, e.g., those with ferric over those with ferrous character. At this point then the time is ripe to formulate "the grand concept" that ties all loose ends together. In the final stage, corroboration is provided by, e.g., X-ray structural determinations, this making the system amenable to structure-function studies on a detailed level.

The assignment of the $g = 1.94$ line to an iron complex was initially controversial when the possibility of clustering of ions was not yet considered. The paramagnet should be high-spin ferric, which was known to exhibit extremely small (in the third decimal), and usually positive, deviations from the free-electron g value of 2.0023, as a consequence of what is known as effective quenching of orbital angular momentum for d^5 systems (2). Attempts to reconcile the incompatible

led to several instants of "creative theorization" (9–12). Also in the same period the idea was formulated of antiferromagnetic Heisenberg exchange coupling between an iron pair of unlike valence, together with the vector coupling model to derive effective g values (the $g = 1.94$ line) and hyperfine coupling values (13, 14). However, it was only several years later that this idea proved to be "the grand concept" for [2Fe–2S] clusters. It had first to be rejected by one of the original proposers (12), and subsequently found sufficient support in magnetic susceptibility (15), electron–nuclear double-resonance (ENDOR) (16), Mössbauer (17), and infrared (18) measurements to deserve reproposing on a sound experimental basis (19) and, later, theoretical elaboration (20–25; see Section II,B,3). This took place well into the 1970s and in the third and final historical phase, in which the concept of exchange coupling was extended to [4Fe–4S] clusters, and in which several X-ray structures were solved. Today these single-electron transferring Fe–S proteins form one of the best characterized classes of metalloproteins. A small caveat: our last statement does not always hold for the assignment of a specific biological role to soluble electron-transferring Fe–S proteins, and generally does not hold for the mechanism(s) of their biosynthesis.

There is a second class of Fe–S proteins whose members do not appear to be involved in net electron transfer at all, but rather act as complex Lewis acids (26–28). The chronicle of this class is very much that of the enzyme aconitase studied by Beinert and collaborators. This in its turn is an outgrowth of the discovery and identification of the 3Fe cluster, a sequence of events that bears remarkable similarity to the $g = 1.94$ story.

The 3Fe story evolves some one and one-half decades out of phase with the 2Fe story. It also starts with an unusual EPR signal, namely a relatively symmetrical and sharp one at $g = 2.01$. It was initially observed in membrane particles (29, 30), and membrane protein complexes (31, 32), and in a soluble protein from mitochondria (33) [which only several years later turned out to be identical to aconitase (34)]. Purification of the latter one allowed for the identification of the $g = 2.01$ signal with iron (33). Also, ^{57}Fe broadening was observed with bacterial membranes (30). For several years the signal was associated with the word HiPIP (high-potential iron protein), although at that time this acronym was already unambiguously assigned to the $[\text{4Fe–4S}]^{3+/2+}$ structure. This mix-up led to amusing misconceptions, such as the "low-potential HiPIP" (35). Although "soluble HiPIP" (i.e., aconitase) contained 3Fe per $S = \frac{1}{2}$ EPR signal, this stoichiometry was initially considered to be "not readily interpretable," because there

were only 2Fe per protein molecule (36). It was only when the Mössbauer spectroscopy of reduced ferredoxin I from *Azotobacter vinelandii* revealed the very characteristic, and not hitherto observed, 2:1 intensity pattern (37) that all pieces once more fell into place and thus allowed for the formulation of the grand concept, namely, of the existence of 3Fe clusters (37). This paved the way for a whole range of derived concepts, e.g., the [3Fe-4S] cluster structure (38, 39), cluster interconversions (39-41), localized valence states (42, 43), and the [4Fe-4S]²⁺ Lewis acid (42). With some hop, step, and jump in the first X-ray analysis of a 3Fe protein (44-46), this story has come to a close. Today we have already entered a new period of detailed studies on the structure-function of both 3Fe proteins and [4Fe-4S]²⁺ enzymes. Yet another caveat: the biological function of the 3Fe cluster remains controversial.

Add another one and one-half decades to the discovery of the "soluble HiPIP" (i.e., aconitase) signal to arrive at approximately the time of this writing. Is there room for yet another renaissance of iron-sulfur biochemistry, and if so, then where to look for it?

Several multicenter iron-sulfur proteins do not seem to fit the patterns outlined thus far. These complex proteins are usually enzymes; however, they are not of the nonredox, Lewis acid type. They are also not of the single-electron transferring type. The catalyzed redox reactions are nonradical wet chemistry, i.e., they involve the transfer of pairs, or multiple pairs, of electrons. The Fe-S content of these proteins is generally quite high.

As every new development in this field starts with an unusual EPR signal, so does this story. In this case a whole collection of unusual signals has been found in recent times: there are those with very high *g* values from very high-spin systems; there are also semiforbidden signals from high-integer spins, and there are the *S* = ½ signals with all three *g* values below the free-electron value.

As this third wave in Fe-S history has only just started to unroll, we cannot perhaps yet be expected to recognize a unifying principle if we see one. Presently, it appears likely [at least to this author (47-59); see also Refs. 60-63] that the "grand concept" for this class of Fe-S proteins will encompass the notion of "larger Fe-S structures," or "superclusters" (i.e., larger than 4Fe-S), and the notion of single-(super)cluster-based multiple-redox transitions. Whatever will crystallize out in its due time, already the current studies of these proteins have provided several novel types of biological EPR spectra ("superspins"; cf. Refs. 49, 51, 52, 54-57, 59, 63), which will be discussed at length below. There is even a first indication of consolidation of the supercluster concept in

the form of x-ray crystallographic data on the P-clusters in nitrogenase (64, 65).

C. THE ELS CLASSIFICATION

Classifications should be an aid in mastering complicated sets of data. In the official classification of iron-sulfur proteins (66), 3Fe clusters as well as mixed-metal clusters are not considered. The major distinction is between simple and complex iron-sulfur proteins. "Complex" is to indicate the presence of additional redox groups, e.g., flavin, molybdenum, and heme. The simple proteins are further subdivided into proteins containing one cluster and two clusters. This approach is not practical in simplifying a discussion of the EPR of iron-sulfur proteins.

In previous general reviews on Fe-S EPR, a common classification was according to the number of iron ions in a cluster, e.g., 1Fe, 2Fe, 3Fe, 4Fe, $2 \times 4\text{Fe}$ (cf. Refs. 67-69). These schemes are similarly less suited for our present purposes as we are in the course of reorienting our spectroscopy to also deal with problems other than the characterization of small Fe-S proteins. This reviewer has found some use in starting from a rather different choice of categories, and this he calls the "ELS classification": class E, *Electron transfer* Fe-S proteins; class L, nonredox Fe-S enzymes that act as *Lewis acids*; and class S, putative Supercluster-containing Fe-S redox enzymes.

This is a classification based on biological function. It also corresponds to the three waves in the history of iron-sulfur proteins outlined above. From the point of view of the EPR spectroscopist, the three classes stand for three dissimilar experimental and theoretical objectives. The proteins of class E are well characterized. EPR is used on them either as a routine analytical measurement, or to support the development of sophisticated theory (cf. *g* strain; double exchange) by test measurements in which the proteins are no more than just model systems. The class L proteins are EPR silent in their active form; however, at least some of them can become paramagnetic upon chemical reduction. In this state they can be scrutinized by EPR—and more effectively by the derived technique of ENDOR—as an indirect way to learn about enzyme mechanisms (27). Class S proteins are the most complicated and the least defined structures. The spectroscopy now means making the first intrusions into an area of novel Fe-S arrangements and of unusual high-spin EPR signals. The concept of the ELS classification is summarized in Table I.

TABLE I

THE ELS CLASSIFICATION: SUMMARY OF THE CURRENT STATUS OF EPR
SPECTROSCOPY OF IRON-SULFUR PROTEINS

Classification	Class E	Class L	Class S
Biological function	Single e^- transfer	Nonredox enzymes	Redox enzymes
First year (Ref.)	1960 (7, 8)	1978 (34)	1987 (49)
EPR theory	Advanced	Irrelevant	Developing
EPR application	Routine analysis	Indirect enzymological tool	Exploring
Typical spectrum	$g \approx 2.1-1.8$	None from native enzyme	Complex ($g \approx 18-1$)

II. Fundamentals of Iron-Sulfur EPR

A. THE BASIC BUILDING BLOCKS

Lemma i: the valency of each iron in Fe-S clusters is always III or II. The iron ion can exist in many valency states; however, the aqueous solution chemistry of iron complexes is essentially limited to the ferric and the ferrous states. The redox behavior of iron in proteins is presumably to a large extent a subset of this chemistry. The occurrence, if only transient, and perhaps even only formally, of higher oxidation states Fe(IV) and Fe(V) has been proposed for a few hemoproteins reactive toward molecular oxygen. Similar proposals have thus far never been put forth in relation with iron-sulfur structures. Considering the iron site in rubredoxins is probably as close as one can get in modeling the individual iron site in iron-sulfur clusters. The FeS_4 sites in rubredoxins (70, 71), desulfuredoxin (72), and desulfoferrodoxin (73) all have a "garden variety" $\text{Fe}^{3+}/\text{Fe}^{2+}$ reduction potential around 0 mV. The putative FeS_4 site in rubrerythrins has $E_m \approx +230$ mV (74).

Lemma ii: the spin state of each iron ion in Fe-S clusters is purely high spin. The d^5 ferric ion is high-spin $S = \frac{5}{2}$ or low-spin $S = \frac{1}{2}$; the d^6 ferrous ion is high-spin $S = 2$ or low-spin $S = 0$. Other possibilities are theoretically unfavorable and experimentally rare (cf. Ref. 75). The six-coordinated iron in hemoproteins experiences a crystal field whose strength is of the order of the high-spin to low-spin cross-over energy. X-Ray crystallography on iron-sulfur proteins has thus far shown that

the crystal field around the iron is deformed tetrahedral. The crystal field splitting for tetrahedral coordination being only four-ninths that of the equivalent octahedral case implies that low-spin configurations are unlikely. Tetrahedrally coordinated mononuclear iron in proteins, e.g., rubredoxin (76), desulfiredoxin (72), desulfoferredoxin (77), rubrerythrin (74), and iron superoxide dismutase (78), is exclusively high spin. It is, therefore, to be expected that Fe-S clusters are made up only of ferric $S = \frac{5}{2}$ and/or ferrous $S = 2$ building blocks.

Note, however, that recent evidence suggests that higher iron coordination numbers are possible. One case is presented by the special iron in the cubane of aconitase, where binding of substrate leads to five, possibly six, coordination (42). Another, presently more remote, possibility is suggested by the structure of capped prismane model compounds, containing one or two six-coordinated metals capping the prismane core (79). In principle, the extension to six-coordinated iron in Fe-S proteins would make low-spin configurations possible. Rather strong-field ligands would, however, be required to add up with the weak-field sulfide contributions. A model system for this phenomenon has recently been synthesized (80).

Lemma iii: the bridging ligand in iron-sulfur clusters is μ -sulfide. This almost tautological statement excludes the Fe-(μ -O)-Fe dinuclear-type clusters (cf. Ref. 81) from our present considerations. The μ -S²⁻ as a ligand to the iron ion is both consistent with the absence of higher Fe oxidation states and the absence of low-spin configurations.

It has been proved possible to do a chemical (i.e., as a treatment of purified protein) global replacement of the μ -S²⁻ in a few Fe-S proteins by μ -Se²⁻ with two interesting consequences for the EPR spectroscopist. First, note that both S²⁻ and Se²⁻ are soft Lewis bases, therefore ligands with potential covalent character. Thus, from the [2Fe-2⁷⁷Se]¹⁺-containing adrenal ferredoxin, ⁷⁷Se ($I = \frac{1}{2}$) splittings in the $S = \frac{1}{2}$ X-band EPR are readily observed as a consequence of delocalization of the spin onto the two bridging ligands. This was early support for the [2Fe-2X] structure (82). Second, the ionic radius of Se²⁻ is significantly greater than that of S²⁻; the S \rightarrow Se substitution means an increased strain on the protein fold. The 2 [4Fe-4Se]¹⁺ configuration in *Clostridium pasteurianum* ferredoxin was the first example of a spin mixture and also of the system spin $S = \frac{1}{2}$ in an iron-"sulfur" protein (83, 84). Note, however, that the acid-labile S/Se substitution has not been shown to be, nor is it expected to be, of any biological relevance.

Lemma iv: the external ligation of iron-sulfur clusters is (predominantly) by the cysteine thiolate side group. This is rather a statement to be questioned. Mixed ligation by sulfur and nitrogen, (Cys)₂(His)₂, of

the [2Fe-2S] cluster in the Rieske protein appears to be well established (85-88). Mixed ligation by sulfur and oxygen, (Cys)₃(Asp), has been proposed for one of the [4Fe-4S] clusters in *Desulfovibrio africanus* ferredoxin III (89, 90) and for the single cubane in *Pyrococcus furiosus* ferredoxin (91). Partial ligation by nitrogen has been inferred from frequency-dependent line broadening in the EPR of a putative prismane [6Fe-6S]-containing protein from *Desulfovibrio vulgaris* (59). However, in most, if not all, cases, the Cys ligation is at least 50%, and for the majority of thus-far scrutinized systems it is, in fact, 100%. In other words, lemma iv is a statement about the relative lack of variation in the external ligation of Fe-S clusters.

Proposition: the building blocks of iron-sulfur structures are very limited in number; therefore, the possible Fe-S structures are limited in number; therefore, the great variation in magnetic and redox properties is imposed by the higher coordination spheres, i.e., the protein and the solvent, and—if there is one—by the substrate.

This statement summarizes the previous four lemmata and points to their implications for the EPR spectroscopist. There are simply four building blocks to construct biological Fe-S clusters from. These are the high-spin ferric ion, the high-spin ferrous ion, the μ -sulfide ion, and the cysteinate side group (with a limited possibility to replace the latter by one or two other amino acid residues). These four elements should provide the structural/chemical basis to explain the basic features of iron-sulfur protein EPR. What remains then are the variations in these EPR features and any additional unexplained properties. These remainders are really the raisins in the pudding, as they represent (bio)chemically relevant information in addition to a simple cluster identification. However, we have only just begun to explore these fields. At this point in time, progress in dealing with the details of Fe-S EPR is still limited even for the best characterized class T electron transfer iron-sulfur proteins. We come back to this theme when we discuss *g* strain.

B. SUPEREXCHANGE

1. Heisenberg Exchange Interaction

When two paramagnetic ions are close to each other they can be subject to direct Heisenberg exchange interaction. This quantum mechanical phenomenon comes about by a finite overlap of the symmetry-adapted molecular orbitals of the individual metal centers. It effectively

results in a decreased energy for the ground state of the coupled complex. The interaction of two local spins S_1 and S_2 is described by the Hamiltonian:

$$H_{\text{exchange}} = JS_1 \cdot S_2 \quad (\text{plus higher order terms}) \quad (1)$$

This direct interaction is *not* operative in Fe-S clusters; there is no direct metal-metal bond. The coupling is via the μ -bridging sulfides, therefore, it is termed indirect exchange or superexchange. This anisotropic interaction is commonly described (cf. Ref. 2, p. 495) with the Hamiltonian:

$$H_{\text{superexchange}} = JS_1 \cdot S_2 + S_1 \cdot K \cdot S_2 + Q \cdot (S_1 \times S_2) \quad (2)$$

The three terms describe the isotropic, the anisotropic, and the asymmetric part of the exchange, respectively. J is a scalar, K is a symmetric tensor, and Q is an antisymmetric tensor. The latter two terms are not easily dealt with especially in noncrystalline material. In relation to Fe-S clusters they have been thus far ignored, and we have presently no choice but to continue to adhere to this—silently made—assumption. Thus, the Heisenberg exchange interaction in Fe-S clusters is described by an effective Hamiltonian:

$$H_{\text{superexchange}} \approx J'S_1 \cdot S_2 \quad (3)$$

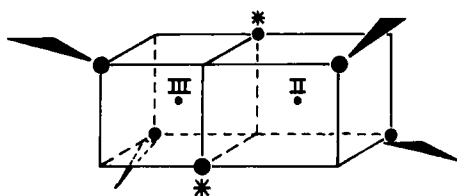
This describes the angular average of Eq. (2). In practice, the prime is dropped from J' .

The far-reaching consequences of the Heisenberg exchange interaction for the EPR of Fe-S clusters is readily illustrated on the simplest possible example, the one-electron reduced $[2\text{Fe}-2\text{S}]^{1+}$ cluster. Mössbauer spectroscopy indicates that the "excess electron" is essentially localized on one of the two iron ions (17), i.e., we have well-defined high-spin ferric and high-spin ferrous entities. This is a simple example for which the epitaph "localized valence" (92) has in recent years become generally accepted. EPR spectroscopy, however, does not show the expected $S = \frac{3}{2}$ and $S = 2$ spin systems, but rather reveals one single $S = \frac{1}{2}$ spectrum per reduced $[2\text{Fe}-2\text{S}]$ cluster. Thus, the two spin systems have been "strongly," antiferromagnetically coupled into a single, new paramagnet with a ground state effectively described as carrying a spin $S = \frac{1}{2}$.

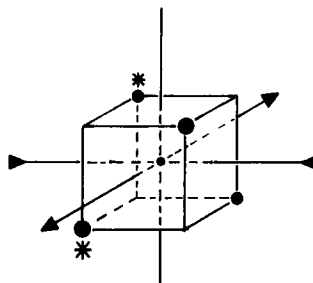
2. The Gibson Model

The first model to successfully describe this situation in a semiquantitative manner is the previously mentioned Gibson model (13, 14). In this antiferromagnetic-coupling model Gibson *et al.* make the following

a. The Gibson model



b. Varret's case 1



c. Varret's case 2

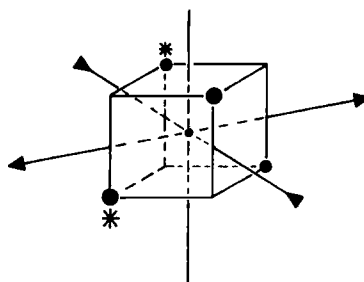


FIG. 1. Distortion of the ferrous site in dinuclear clusters under the Gibson model (a) or the Bertrand-Gayda model (b or c). An asterisk indicates acid-labile sulfide.

assumptions (or symmetry simplifications): (1) the symmetry at the ferric site is tetragonal; (2) the symmetry at the ferrous site is tetrahedral. Graphically this situation can be represented as in Fig. 1a by Fe^{3+} in a cube and Fe^{2+} in an adjacent cube elongated along the Fe-Fe axis. For EPR this means (1) the g tensor of the Fe^{3+} ion is isotropic, its scalar value being slightly greater than g_e ; (2) the Fe^{2+} g tensor has its z axis colinear with the Fe-Fe axis, and $g_z = g_e$.

Making these two assumptions, and assuming the Hamiltonian Eq. (3) to hold, and with the usual procedure of angular momentum projection operators,

$$\mathcal{G}_{\text{dimer}} = c_1 g_1 + c_2 g_2 \quad (4a)$$

$$c_1 = [S(S+1) + S_1(S_1+1) - S_2(S_2+1)]/2S(S+1) \quad (4b)$$

$$c_2 = [S(S+1) + S_2(S_2+1) - S_1(S_1+1)]/2S(S+1) \quad (4c)$$

one readily obtains the Gibson model g -tensor equations for the effective g tensor of the $S = \frac{1}{2}$ ground state:

$$g_{x\text{-dimer}} = (\frac{7}{3})g_{x\text{-ferric}} - (\frac{4}{3})g_{x\text{-ferrous}} \quad (5a)$$

$$g_{y\text{-dimer}} = (\frac{7}{3})g_{y\text{-ferric}} - (\frac{4}{3})g_{y\text{-ferrous}} \quad (5b)$$

$$g_{z\text{-dimer}} = (\frac{7}{3})g_{z\text{-ferric}} - (\frac{4}{3})g_e \quad (5c)$$

For the ferric g tensor, Gibson *et al.* take the isotropic value $g = 2.019$ (from Fe^{3+} in ZnS). The sixth electron of the ferrous ion is taken to be in the $|z^2\rangle$ orbital; therefore, assuming local tetragonal symmetry, the ferrous g tensor is

$$g_{x\text{-ferrous}} = g_e + 6\lambda/\Delta_{yz} \quad (6a)$$

$$g_{y\text{-ferrous}} = g_e + 6\lambda/\Delta_{zx} \quad (6b)$$

$$g_{z\text{-ferrous}} = g_e \quad (6c)$$

The quantity Δ_{ij} is the crystal field splitting between the $|z^2\rangle$ single-electron ground state and the excited state $|ij\rangle$.

The strength of this model is in its prediction that two of the g values are significantly below g_e (i.e., in its explanation of "the" $g = 1.94$ EPR signal) and that the third g value is greater than g_e . All thus far reported EPR spectra on $[\text{2Fe-2S}]^{1+}$ structures are consistent with this model (specifically, cf. Ref. 93).

3. The Bertrand-Gayda Model

The symmetry assumptions of the Gibson model are of course unrealistic for protein Fe-S sites. Bertrand and Gayda have elaborated on the model by relaxing some of the high-symmetry restrictions (20). The crux of the Bertrand-Gayda model is to make the EPR observables (e.g., effective g values) a function of the rhombicity at the ferrous site expressed in terms of a single parameter, Θ . This latter concept comes from the work of Varret on high-spin ferrous ions (94). Varret defines two possible ways of rhombically distorting a tetrahedral site, and these are depicted in Fig. 1.

The Bertrand-Gayda model differs from the Gibson model in two aspects. It allows for rhombicity at the ferrous site, assuming Varret's "case 2" (cf. Fig. 1c) to be operative. It also allows for a rhombic g tensor from the ferric ion, however, without attempting to specify its source

or to model its physics. Furthermore, the two g tensors are assumed to be colinear in order to retain the validity of the coupling Eqs. (4a)–(4c).

Just as the Gibson model is a crystal field approach, so is the Bertrand–Gayda model. It starts from the metal d orbitals in a tetragonal field and then mixes these as a result of rhombic deformation in c_{2v} symmetry. The lowest one-electron orbital (i.e., the one containing the sixth electron) is now

$$|\phi_0\rangle = \cos \Theta |z^2\rangle + \sin \Theta |x^2 - y^2\rangle \quad (7)$$

in which Θ measures the mixing of the $|z^2\rangle$ and $|x^2 - y^2\rangle$ states and also reflects some “degree” of rhombicity. The expressions for the ferrous g -tensor values now become

$$g_{x\text{-ferrous}} = g_e + (8\lambda/\Delta_{yz}) \sin^2(\Theta + \pi/3) \quad (8a)$$

$$g_{y\text{-ferrous}} = g_e + (8\lambda/\Delta_{xz}) \sin^2(\Theta - \pi/3) \quad (8b)$$

$$g_{z\text{-ferrous}} = g_e + (8\lambda/\Delta_{xy}) \sin^2 \Theta \quad (8c)$$

and the effective g values for the cluster are again calculated with Eqs. (5a)–(5c). Note that Eqs. (8a)–(8c) reduce to Eqs. (6a)–(6c) for $\Theta = 0$. A sign error in the original equations was corrected by Hearshen *et al.* (25); the above equations are the corrected ones. Also, they are valid for both types of distortion discerned by Varret (cf. Fig. 1, b and c).

Bertrand *et al.* have used the Bertrand–Gayda model as a means for systematic research on structural variations in dinuclear clusters (20–23). In order to comply to the format used in an early phenomenological study (95), the authors cast their analyses in the form (which they call the Coffman representation) of plots of the three cluster g values, g_x , g_y , and g_z , versus an unnamed, phenomenological parameter χ , defined as

$$\chi = g_y - g_x \quad (9)$$

It should be noted (in the opinion of the present reviewer) that this Coffman representation is only one out of an infinite number of possible ways to graphically analyze the EPR data, and it is not necessarily the most useful one. From Eqs. (5) and (8) it can be seen that the cluster g values are a function of the eight parameters g_{1x} , g_{1y} , g_{1z} , λ , Δ_{yz} , Δ_{xz} , Δ_{xy} , and Θ . By giving the first six of these parameters a fixed value, Bertrand *et al.* force the cluster g values to become a function of the latter two only. This has the practical advantage that two of the g values are a function of χ only, and also that for small values of Θ there is an almost linear relationship between χ and Θ . A disadvantage is that this form of the model is bound to prove its own premise, namely,

that structural variation in $[2\text{Fe}-2\text{S}]$ clusters is a function of χ and Δ_{xy} only.

Some criticism has been ventured by Hearshen *et al.*, notably, on the use of a single set of ferric g values, where there is some evidence that the ferric ion in these systems can have large rhombic components, which are further "amplified" by the factor of (3) in Eqs. (5a)–(5c) (25). The authors also express concern over the fact that their analyses of g strain (see below) in ferredoxins indicate an inherent error in the experimental g values when identified with turning points in the powder spectrum (25). Bertrand *et al.*, however, are not convinced of the relevance of this latter error at the present state of accuracy in testing the model (23).

Finally, we note that even the assumption of C_{2v} symmetry at the ferrous site is a simplification of the real structure determined by X-ray crystallography (96).

C. DOUBLE EXCHANGE

1. Valence Delocalization

When we reduce an $[2\text{Fe}-2\text{S}]^{2+}$ cluster with one electron equivalent, where does this "excess electron" go to? Is it always captured by one and the same iron? In an early attempt to describe the cause of g strain, Hearshen *et al.* played with the idea that there is a comparable chance for the electron to go to Fe_A or to Fe_B , i.e., resulting in a physical mixture of the states $(\text{Fe}_A^{2+}, \text{Fe}_B^{3+})$ and $(\text{Fe}_A^{3+}, \text{Fe}_B^{2+})$ (97). A simple graphical representation of this situation would be a symmetrical, one-dimensional potential well for the excess electron along the Fe–Fe axis with an infinitely high barrier at half-way (Fig. 2a). As this concept found little experimental support, it was later rejected in favor of a g -strain version of the Bertrand–Gayda model (25).

The question was readdressed theoretically from a different angle by Noodleman and Baerends (98), who considered the possibility that the excess electron would be delocalized over the sites Fe_A and Fe_B . We could denote this "resonance" situation, perhaps somewhat simplistically, as $(\text{Fe}_A^{2.5+}, \text{Fe}_B^{2.5+})$. For a quantum mechanical description of the phenomenon of excess electron delocalization, the classical reference is the paper by Anderson and Hasegawa on double-exchange interaction (99). The potential well for the excess electron is now flat, between site A and site B (Fig. 2b). An important generality in this respect was pointed out some years ago by Middleton *et al.* in their Mössbauer studies on the considerably more complicated $[4\text{Fe}-4\text{S}]$ system: "Any

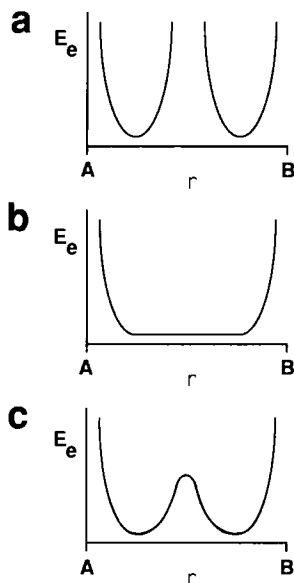


FIG. 2. Schematic representation of the potential of the excess electron (E_e) in an Fe_AFe_B cluster at a distance r from Fe_A when the iron valences (III/II) are fully localized (a), fully delocalized (b), or intermediate (c).

sharing of the electrons between the spin-up and the spin-down iron atoms is inhibited by the Pauli exclusion principle" (100). Noodleman and Baerends have again pointed to this generality, whose importance is not to be underestimated [here, we quote yet a later formulation by Day *et al.* (101)]: "Localized sites couple antiferromagnetically to produce the lowest spin system. On the other hand, sites which share a delocalized electron are coupled ferromagnetically to produce the highest system spin."

For the $[2\text{Fe}-2\text{S}]^{1+}$ cluster this means that, when the excess electron is localized at one of the iron ions, then the system spin for the ground state (i.e., the state observed by EPR at cryogenic temperatures) is $S_{\text{dimer}} = \frac{5}{2} - 2 = \frac{1}{2}$; when the excess electron is delocalized over the two iron sites, then the ground state has $S_{\text{dimer}} = \frac{5}{2} + 2 = \frac{9}{2}$. We have already seen that Mössbauer spectroscopy identifies the excess electron in $[2\text{Fe}-2\text{S}]$ ferredoxins as being localized, and this is consistent with the $S = \frac{1}{2}$ ground state observed in EPR. Therefore, the mechanism of double exchange, or of charge delocalization, is probably not significant for the description of the ground state properties of these proteins

[although it may be relevant to the description of the highest state(s) of the spin ladder (98)]. Interestingly, dinuclear Fe(III/II) model compounds with bridging oxygens have recently been described and have been found to exhibit Mössbauer, EPR, and susceptibility properties consistent with a ground state system spin $S = \frac{3}{2}$ (102–104).

The present interest in double-exchange interactions has been spurred by the observation of valence delocalization in trimeric, cubane, and, possibly, superclusters. Mössbauer data on the $[3\text{Fe}-4\text{S}]^0$ cluster in inactive aconitase and in certain reduced ferredoxins (cf. Ref. 105 and references quoted therein) point to a situation in which one of the irons is localized high-spin ferric while the other two form a fully delocalized pair, i.e., $[(\text{Fe}_\text{A}^{2.5+}, \text{Fe}_\text{B}^{2.5+}), \text{Fe}_\text{C}^{3+}]$. Münck and Kent suggested that the spin of the internal $(\text{Fe}_\text{A}, \text{Fe}_\text{B})$ dimer is $S = \frac{3}{2}$ as a result of double exchange being the dominant interaction (106). The $S = \frac{3}{2}$ spin is then envisioned to couple antiferromagnetically to the $S = \frac{5}{2}$ spin of Fe_C , resulting in a system spin $S_{\text{trimer}} = 2$, consistent with, e.g., EPR data (105, 107).

This conceptually simple scheme was put to the test by Papaefthymiou *et al.*, who calculated ^{57}Fe hyperfine values under this model for the two “sites” $(\text{Fe}_\text{A}, \text{Fe}_\text{B})$ and Fe_C and compared these to their Mössbauer data on *D. gigas* ferredoxin II (105). The sign and magnitude of the predicted and experimental (angular-averaged) A values were found to be in very good agreement. Note, however, that the calculation involved some educated guesses on the starting A values for mononuclear ferric and ferrous sites from available literature data (105). We will not pursue this point here, but rather attempt a qualitative evaluation of the status quo of ongoing attempts to apply the concept of double-exchange interaction to understand the magnetic properties of iron–sulfur proteins. We are particularly interested in their relevance to EPR properties.

2. Spin Ladders

First, we have to point out that there is a mix-up of symbols in the literature for the Heisenberg part of the exchange interaction. Equation (3) can be found under three different forms:

$$H = -2JS_1 \cdot S_2 \quad (10a)$$

$$H = -JS_1 \cdot S_2 \quad (10b)$$

$$H = JS_1 \cdot S_2 \quad (10c)$$

The first form, Eq. (10a), was used in the early work on ferredoxins by Dunham and Sands and co-workers (15, 19, 108). This form has re-

mained in use in the Fe-S field up to today, specifically, in studies on bulk magnetic susceptibility (101). Note that under this form the quantity J has a negative value for $[2\text{Fe}-2\text{S}]^{2+/1+}$ clusters. The second form, Eq. (10b), was recently used by Ding *et al.* in their work on the dinuclear Fe model compound with $S = \frac{3}{2}$ ground state properties (104). The third form, Eq. (10c), has been used in all the recent work on double exchange in iron-sulfur structures, starting with the Noodleman-Baerends paper (98). Not without reluctance I follow here their convention. The reader is urged to check carefully what is the personal preference of each author in order to allow for a meaningful comparison of reported values (and signs!) of J .

With the Heisenberg-type superexchange between two metal sites, site A and site B, written as Eq. (10c), we have a spin ladder of states with absolute energies,

$$E(S_A, S_B, S_{AB}) = (J/2)[S_{AB}(S_{AB} + 1) - S_A(S_A + 1) - S_B(S_B + 1)] \quad (11)$$

in which S_A and S_B are the spin of the individual sites and S_{AB} is the system spin. The last two terms in Eq. (11) are a constant and since one is usually only interested in relative energies, the terms are simply dropped:

$$E(S_{AB}) = (J/2)[S_{AB}(S_{AB} + 1)] \quad (12)$$

With a positive value of J [that is, negative under the format of Eq. (10a) or (10b)] for a high-spin ferric-ferrous pair, we have the spin ladder given in Fig. 3A. When the metal pair is also subject to double-exchange interaction, a second term appears in the spin ladder equation:

$$E(S_{AB}) = (J/2)[S_{AB}(S_{AB} + 1)] \pm B(S_{AB} + \frac{1}{2}) \quad (13)$$

The term results from the double-exchange Hamiltonian (98, 99, 104, 105, 109):

$$H_{\text{double exchange}} = BV_{AB}T_{AB} \quad (14)$$

This operator works on the localized-valence dimer states $|A\rangle$ and $|B\rangle$ (where $|A\rangle$ means that the excess electron is on the A site, i.e., $\text{Fe}_A^{2+}, \text{Fe}_B^{3+}$) according to:

$$V_{AB}T_{AB}|B\rangle = V_{AB}|A\rangle = (S_{AB} + \frac{1}{2})|A\rangle \quad (15)$$

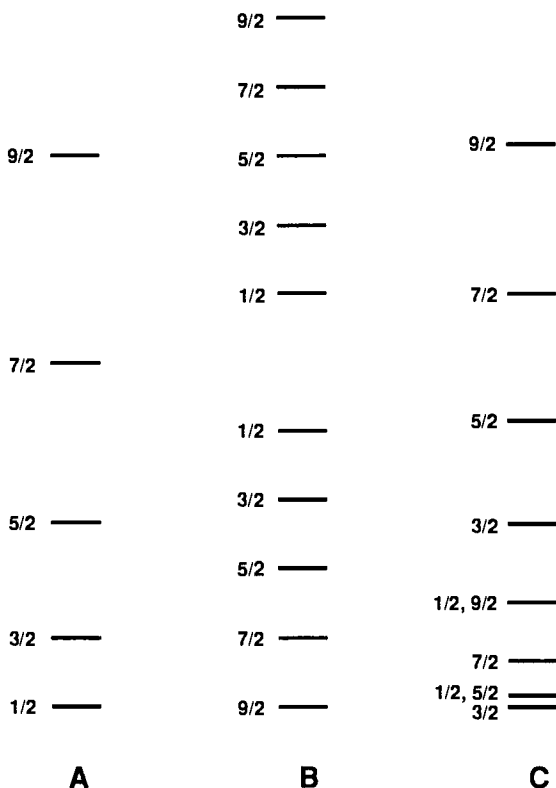


FIG. 3. Spin ladder of the dinuclear Fe(III/II) cluster subject to superexchange and double exchange with $J \gg B$ (ladder A), $J \ll B$ (ladder B), or $J = B/2$ (ladder C). The three ladders are not normalized to the same energy scale.

V_{AB} is a shift operator (sometimes called the double-exchange operator; cf. Ref. 104), T_{AB} is a transfer operator, and the coefficient B in Eq. (14) is a transfer integral.

In simple words these equations have the following meaning: we start from the assumption that there exist two energetically degenerate states, $|A\rangle$ and $|B\rangle$, or $(\text{Fe}_A^{2+}, \text{Fe}_B^{3+})$ and $(\text{Fe}_A^{3+}, \text{Fe}_B^{2+})$. The $|A\rangle$ state is 100% occupied, the $|B\rangle$ state is empty. The effect of the $H_{\text{double exchange}}$ operator is twofold. It delocalizes the electron over the two sites, and it lifts the degeneracy of the two energy states.

Three typical situations can now occur. When $J \gg B$ then the excess electron is essentially localized. The potential well is as in Fig. 2a, and the spin ladder is as in Fig. 3A. The low-temperature EPR is that of an $S = \frac{1}{2}$ system. When $J \ll B$, then the excess electron is essentially fully

delocalized. The potential well is given in Fig. 2b, and the spin ladder is that of Fig. 3B. The low-temperature EPR should be characteristic of an $S = \frac{3}{2}$ system. A third possibility would be $J \approx B$. The energy barrier between the metals has a finite height (Fig. 2c). The spin ladder has an irregular, nested pattern (Fig. 3C). The EPR will be very sensitive to the value of J/B . For example, for the case of $2J = B$ (see Fig. 3C), the ground state is $S = \frac{3}{2}$ and there are two low-lying excited states with $S = \frac{1}{2}$ and $S = \frac{5}{2}$, respectively.

We anticipate that in the coming years the concept of double exchange will be a central theme in the more physically oriented studies on iron-sulfur proteins. The development is presently in its early phase, and this may bring along the risk of zealotry. It is, therefore, important that we realize the limitations as they stand, both in the theory and in the applications, and that we form a clear picture of what we want the ultimate goals of these efforts to be. First we consider the theoretical limitations.

3. Double Exchange Evaluated

The simple form in which we have outlined the theory is approximately the form in which it has thus far been applied to iron-sulfur structures. Under this form the two localized-valence configurations ($\text{Fe}_A^{2+}, \text{Fe}_B^{3+}$) and ($\text{Fe}_A^{3+}, \text{Fe}_B^{2+}$) are assumed to be fully equivalent; however, at the same time, the initial occupancy (i.e., before the application of the double-exchange operator) is assumed to be 100% biased toward the configuration with the ferrous form at the A site. The possibility of a "fractional occupancy" (i.e., a finite number of the molecules have ferrous at the B site) has not been considered since the early proposal by Hearshen *et al.* (97). The possibility of "intermediate cases" ($J \approx B$), resulting in level crossings, has only been touched upon (104). Is our simple picture of a finite, symmetrical barrier in a potential well meaningful? The situation in which the excess electron delocalizes over more than two sites is expected to lead to additional complications (109).

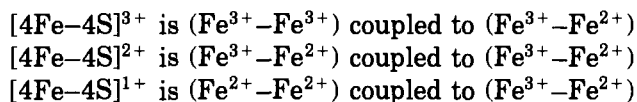
We now consider the applications per cluster type. The calculations of Noodleman and Baerends suggest that double exchange in oxidized and reduced $[2\text{Fe}-2\text{S}]$ clusters is only significant when considering the highest levels of the spin ladder (98), and this is consistent with all EPR results thus far (i.e., $S = 0$, and $S = \frac{1}{2}$, for the ground states) as well as all other magnetic measurements, including those on bulk susceptibility (15).

For the oxidized $[3\text{Fe}-4\text{S}]^{1+}$ cluster, initially a model of isotropic, antiferromagnetic Heisenberg exchange between the three $S = \frac{5}{2}$ spins was proposed (110, 111). Two $S = \frac{5}{2}$ spins are coupled to an intermediate

spin $S' = 2$ (or 3), and this in turn is coupled to the third $S = \frac{5}{2}$ to yield the system spin of the trimer, $S = \frac{1}{2}$. This model appears to have stood the test of time remarkably well (112–116). It is consistent with the $S = \frac{1}{2}$ EPR now observed in innumerable cases as well as with other magnetic measurements, specifically a recent one on susceptibility (101). Double exchange has not been considered, as there is apparently no need to. A similar situation exists in the linear $[3\text{Fe}-4\text{S}]^{1+}$ cluster in “purple” aconitase, except that $S' = 5$ and the system spin is $S = \frac{3}{2}$ (41). Again, double exchange appears to be insignificant.

The reduced $[3\text{Fe}-4\text{S}]^0$ cluster has $S = 2$ EPR, and we have already seen that this is consistent with a model in which a (formally) ferric–ferrous pair forms a delocalized pair by strong double exchange resulting in $S' = \frac{3}{2}$. This in turn is coupled to the $S = \frac{5}{2}$ spin of the third iron to yield the system spin $S = 2$. The model has been tested by comparing calculated iron hyperfine splitting parameters with Mössbauer data on *D. gigas* ferredoxin II (105). There is some indication that the $[3\text{Fe}-4\text{S}]^0$ cluster in this protein has a low-lying excited state in which the electron is delocalized over all three Fe ions (105); however, it is presently not obvious how to interpret this data (101, 109).

The situation for cubane clusters is far less clear. Presently, the point of reference appears to be the idea that the iron in these clusters can be considered to occur in coupled pairs. This concept comes from the early Mössbauer studies of the Liverpool group on *Chromatium vinosum* HiPIP (117–119) and on *Bacillus stearothermophilus* ferredoxin (100). The proposals of these authors are summarized in the following scheme:



Within each pair the spins are coupled parallel, and the resulting dimer spins are coupled antiparallel to yield the cubane cluster spin. For all mixed-valence ($\text{Fe}^{3+}-\text{Fe}^{2+}$) pairs, an ad hoc delocalization is then assumed in order to explain Mössbauer indistinguishability of individual iron atoms. Indeed, this simple addition/subtraction of $S = \frac{5}{2}$ (ferric) and $S = 2$ (ferrous) spins leads to the ground state system spins of $S = \frac{1}{2}$, 0, and $\frac{1}{2}$, respectively, as we observe them, e.g., in EPR. Based on this scheme the authors even proposed a 4Fe version of the Gibson model in order to explain that HiPIP has $g > g_e$ (119), and ferredoxin has $g < g_e$ (100). The authors hasten, however, to state that the system is a complicated one and that the model should be looked upon as an

intermediate in a developing description. We do comply with this and refer the interested reader to the original papers (100, 119).

The relevance of the Liverpool model in the present context is that it has recently been revived by Noodleman in a form in which double exchange is considered explicitly, i.e., as the delocalization mechanism for the $(\text{Fe}^{3+}-\text{Fe}^{2+})$ pair in the $[\text{4Fe-4S}]^{3+}$ HiPIP-type core (120). Jordanov *et al.* have subsequently applied the model to analyze bulk susceptibility data from an $[\text{Fe}_4\text{S}_4(\text{SR})_4]^{1-}$ complex, and they conclude it to be superior to a Heisenberg exchange-only model (121). Very recently, the model has also been considered as a basis to explain paramagnetic shifts in ^1H NMR from cysteine β -protons in HiPIPs (122, 123). The reviewer considers it too early to evaluate these results, and this especially so since he is presently involved in a project to redetermine the magnetic properties of HiPIP proteins. Two significant results of this work thus far are (1) the refutation of the long-standing Antanaitis-Moss model (124) for the EPR from *C. vinosum* HiPIP (and, therefore, a refutation of support from EPR data for the Liverpool model) and (2) the detection of four separate (instead of two pairs of) quadrupole doublets by high-resolution Mössbauer spectroscopy (125).

The relevance of double-exchange interaction to the explanation of the magnetic properties of the other two redox states of the cubane cluster in proteins— $[\text{4Fe-4S}]^{2+}$; $S = 0$, $[\text{4Fe-4S}]^{1+}$; $S = \frac{1}{2}$ —has thus far not been tested experimentally in any way. An interesting aspect is the substrate-induced localized valence in aconitase (42).

In recent times, $S > \frac{3}{2}$ EPR has been reported for several iron-sulfur proteins, and evidence has been put forth to suggest that this is typically associated with clusters containing more than four ions (49–59). A cluster spin with a value larger than that of the high-spin ferric ion implies some sort of parallel spin coupling, i.e., suggestive of double-exchange interaction of significance. Although this possibility has thus far not been discussed, let alone tested experimentally, it is to be expected that the presently evolving research trends in double-exchange interactions and in superclusters/superspins will intertwine in the not too distant future.

In summarizing the previous paragraphs we note that there is reason to believe that the concept of double exchange is an essential element in the description of the magnetic properties of iron-sulfur clusters. Possible exceptions are the reduced 2Fe cluster and the oxidized 2Fe and 3Fe clusters (and perhaps all fully oxidized $n\text{Fe}$ clusters). From an EPR spectroscopist's point of view the concept is especially important for the systems that have a ground state superspin, whose explanation requires some form of parallel spin alignment. At the same time we

should caution that any serious testing has thus far been limited to only one case, now several years ago, of a single protein (105).

Is there any added value for the biochemist in this tedious biophysics? When we know what the basic elements of iron-sulfur clusters are, we can understand the gross features of their EPR spectra. It is then from the fine details of these spectra that we can extract information specific for the protein at hand. Double exchange does not necessarily have *any* direct relevance to biology; however, with elements such as the ($\text{Fe}_A^{2.5+} - \text{Fe}_B^{2.5+}$) delocalized dimer we may be able to extend our list of basic building blocks beyond the four defined previously.

Perhaps a helpful way to look at this problem is to draw an analogy with the definition of structure levels in protein chemistry: the first four building blocks (cf. Section II,A.) are the basis of the primary magnetic structure of the iron-sulfur cluster; there is a secondary level of structure in the delocalized dimers, trimers, etc. within the cluster; a tertiary structural level is imposed on the cluster by the coordinating protein and its environment. All this contributes to the shape of the EPR spectrum. Thus, by a judicious definition of these structural elements and by an establishing of their contributions to the spectrum, we can improve on our capacities to sort out the general from the specific spectral features, i.e., the common from the detailed (bio)chemical information. These details are the subject of the following section.

III. *g* Strain in Doublet Systems

A. INHOMOGENEOUS BROADENING OF IRON-SULFUR EPR

We now turn our attention to an "advanced" topic in the EPR of metalloproteins: *g* strain. The theory has been developed to a large extent with reference to well-characterized iron-sulfur proteins, i.e., to class E systems. I have recently reviewed the complete literature on *g* strain in metalloproteins (126). The present section is an updated summary of Ref. 126.

The EPR of simple $S = \frac{1}{2}$ systems is described by the spin Hamiltonian:

$$H = \beta \mathbf{B} \cdot \mathbf{g} \cdot \mathbf{S} \quad (16)$$

This description should be valid for the low-temperature EPR of many iron-sulfur systems, as they have an $S = \frac{1}{2}$ ground state well separated from the other levels of their spin ladder. We assume here that the cluster under consideration is not subject to dipolar interaction, i.e., it

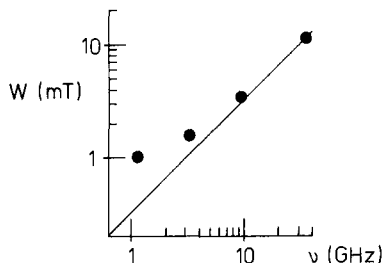


FIG. 4. The EPR line width of $[2\text{Fe}-2\text{S}]^{1+}$ in spinach ferredoxin as a function of the microwave frequency (from Ref. 126).

is magnetically well isolated by the surrounding diamagnetic protein. This is, e.g., a valid assumption for proteins that contain only a single cluster (or only a single paramagnetic cluster). Note, however, that it is very difficult to avoid dipolar broadening in model cluster EPR (cf. Ref. 47). We also assume that the cluster has not been enriched in ^{57}Fe and/or ^{33}S . Thus the only possible interactions, in addition to the Zeeman term of Eq. (16), are superhyperfine interactions with magnetic nuclei in the second and higher coordination sphere, i.e., ^1H , ^{13}C , and ^{14}N from the protein (and, possibly, ^{14}N from coordinating His in the Rieske cluster). In standard continuous wave EPR, these ligand splittings are usually not resolved, but rather contribute to the inhomogeneous line width. In magnetic field units this contribution should be independent of the frequency of the applied microwave. Experimentally, however, one usually finds that the EPR line width from biological $S = \frac{1}{2}$ systems has a major contribution that is linear in the microwave frequency. Figure 4 gives the example of the $[2\text{Fe}-2\text{S}]^{1+}$ cluster in spinach leaf ferredoxin (note: each point is from a different spectrometer). At the common X-band frequency the broadening is essentially dominated by a mechanism linear in the microwave frequency. This observation strongly suggests that the line width reflects a type of Zeeman interaction.

We want to analyze the EPR spectrum by the method of spectral synthesis. This means that we want to faithfully reproduce the experimental spectrum on a computer using a theoretically founded algorithm. There are two good but very different reasons why we want to achieve this goal. In the first place, this simulation technique is the only way in which we can separate in a quantitative manner the fine spectral details (the "tertiary magnetic structure" of the cluster reflecting the specific protein environment) from the more general fea-

tures common to all clusters of a given type. A second objective is the analysis of compound data, i.e., overlapping spectra from different centers in complex systems. A classical example of this latter problem is the determination of the number, type, and stoichiometry of paramagnets in respiratory chain complexes (cf. Refs. 126 and 127).

The technique of simulating "powder" spectra (e.g., spectra from frozen solutions of metalloproteins) is well established (128). The powder pattern is generated by computing individual spectra for many different orientations and adding them all up. This is called integration over the unit sphere:

$$\chi'' = \int \int P(g) S(g, W) d \cos \Theta d\phi \quad (17)$$

$S(g, W)$ is a shape function, usually a Gaussian of width W , whose peak position follows from Eq. (16):

$$B_{\text{resonance}} = (h/\beta)\nu/g \quad (18)$$

in which

$$g = \sqrt{l_x^2 g_x^2 + l_y^2 g_y^2 + l_z^2 g_z^2} \quad (19)$$

The g_i values are the principal values of the g tensor. The l_i values are the direction cosines of the magnetic field vector with respect to the g -tensor axis system. They translate in polar angles as

$$\begin{aligned} l_x &= \sin \Theta \cos \phi \\ l_y &= \sin \Theta \sin \phi \\ l_z &= \cos \Theta \end{aligned} \quad (20)$$

$P(g)$ is the transition probability (129):

$$P(g) = g^{-1} \sum (g_i^2 - g^{-2} l_i^2 g_i^4) \quad (21)$$

This is all standard procedure. However, the line width, W , is experimentally found to be orientation dependent, i.e., a function of the direction cosines. Our problem is that we do not know what the analytical expression of this dependence is.

Two ad hoc solutions have been proposed (and subsequently applied in too many cases to be comprehensively reviewed here). The algorithm of Johnston and Hecht (130),

$$W = \sqrt{l_x^2 W_x^2 + l_y^2 W_y^2 + l_z^2 W_z^2} \quad (22)$$

is simply an analog of the g value, Eq. (19), suggestive of a distribution of the g values themselves. One could call this the simplest possible

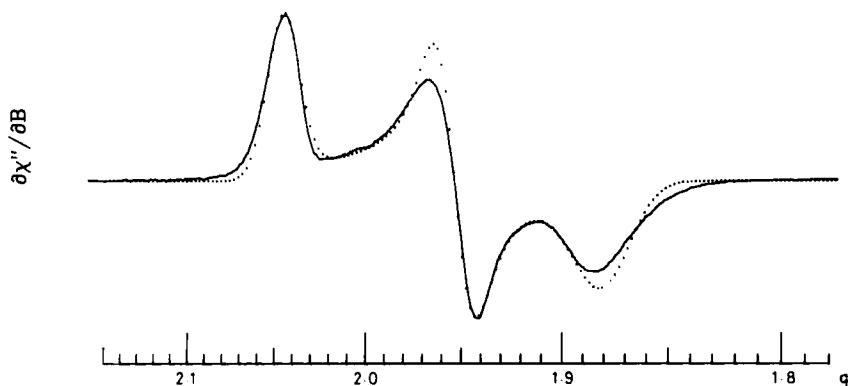


FIG. 5. The X-band spectrum of the reduced [2Fe-2S] cluster in spinach ferredoxin (solid trace) is computer simulated (dots) with a line width anisotropy according to Eq. (23) (132).

form of “*g* strain,” a term that was proposed several years later in the group of Sands and his collaborators (16, 108).

A second proposal, due to Venable (131),

$$W = \sqrt{l_x^2 g_x^4 W_x^2 + l_y^2 g_y^4 W_y^2 + l_z^2 g_z^4 W_z^2} / g^2 \quad (23)$$

is an analog of the expression for the first-order central hyperfine splitting in orthorhombic symmetry:

$$A = \sqrt{l_x^2 g_x^4 A_x^2 + l_y^2 g_y^4 A_y^2 + l_z^2 g_z^4 A_z^2} / g^2 \quad (24)$$

Although Eq. (23) is probably the most frequently used expression in work on iron-sulfur proteins (cf. Ref. 127), it cannot possibly be correct: there is no central (i.e., metal) hyperfine interaction in Fe-S clusters; ligand hyperfine interaction is negligible; the line width is not independent of the microwave frequency.

In practice, the two proposed solutions, Eqs. (22) and (23), give virtually indistinguishable results. This is a consequence of the fact that they both describe an effective line width tensor that is colinear with the *g* tensor. The appearance of the powder spectrum is dominated by the turning points of the *g* value, Eq. (19). What happens off-axis is to a large extent irrelevant to the overall spectral shape. Unfortunately, both solutions give poor results. A typical illustration is given in Fig. 5 (132). The word “typical” here indeed means exemplary for very many simple $S = \frac{1}{2}$ spectra. The low-field peak and the high-field trough in the experimental spectrum are skewed, and this is not reproduced in the fit. Similarly, the asymmetry of the derivative-shaped feature is not

simulated. These asymmetries are the easily recognizable trademark of g -strain broadening.

Over the past 25 years a dozen attempts have been made toward a more sophisticated approach of the line width problem in biological EPR. These studies were mainly concerned with hemoproteins (cf. references quoted in Ref. 126); however, some of the more recent ones address the problem in relation to specific types of iron-sulfur proteins (24, 133). The central idea in all the proposed theories is to have a distributed effective g values by assuming a symmetric distribution in one or more quantities that directly define the effective g value itself. Thus, distributions have been proposed in crystal field splittings, spin-orbit interactions, ground state wave function coefficients, or coefficients in the spin Hamiltonian. All the proposed models approximately simulate the magnitudes of line width anisotropy; however, they *never* generate the skewings and asymmetries of real g strain.

We must, therefore, conclude that the cause of g strain and the cause of the g tensor are two entities of a completely different nature. Somewhere in between these entities is an angular transformation resulting in a noncollinearity of tensor quantities.

B. THE g -STRAIN EQUATION AND ITS IMPLICATIONS

Fritz *et al.*, who first proposed the term " g strain," also suggested a model for its physical nature: microheterogeneity in protein conformation (16). Taking the strain in g strain literally, the present author later proposed to include a strain term in the spin Hamiltonian to describe effects of the matrix surrounding the protein (i.e., the frozen solvent) on the protein and the spin system within (134). The resulting equation for the angular-dependent line width (132, 134) for the first time allowed for a line width tensor to be noncollinear with the g tensor. Its implementation in a spectrum simulation program for the first time closely reproduced the asymmetries of g strain in powder spectra of a low-spin hemoprotein (134) and an iron-sulfur protein (132). The program was also original in calculating spectra in g space with subsequent transformation to field space. This idea was based on the notion, proposed by Strong (135), that the distribution function due to g strain is necessarily nonlinear on a magnetic field scale. However, the line width algorithm (132, 134) was not the result of a rigorous derivation, and in a later study it was shown to contain an error of normalization (136).

Combining the idea of a noncollinear line width tensor (132, 134) with the statistical concept of the g values as random variables (97),

two groups working on the problem of g strain joined forces and developed the statistical theory of g strain (136). This theory was derived from the single premise that the g tensor is a linear function of a three-dimensional random variable:

$$\mathbf{g} = \mathbf{g}_0 + \mathbf{R} \cdot \mathbf{p} \cdot \mathbf{R}^T \quad (25)$$

Here, \mathbf{p} is a tensor whose elements are random variables, \mathbf{g}_0 is a tensor whose elements do not fluctuate, and \mathbf{R} is the three-dimensional rotation that transforms the \mathbf{p} principal axis system to the \mathbf{g}_0 principal axis system. The resulting expression for the angular-dependent line width turned out to be a discouragingly complicated one, both in form and in its amenability to use in numerical analysis (136). It contains, e.g., a five-dimensional rotational transformation.

The problem was saved from intractability by an unexpected finding (136): when the three elements of the \mathbf{p} tensor in Eq. (25) are statistically fully correlated (either positively or negatively), then the complicated five-dimensional expression reduces to a much simpler, three-dimensional expression; this turns out to be a normalized version of the successful (but not rigorously derived) expression in the early work (cf. Refs. 132 and 134).

There is also a plausible physical interpretation of this result. When all the elements of the tensor describing g strain are fully correlated, then their ultimate cause must be a scalar. This scalar can be identified with a hydrostatic pressure exerted on the paramagnetic protein by its surroundings, the matrix of the (frozen) solution (126). Here is a simple picture to envisage the process: the outside of the protein is a globe. Inside is an iron-sulfur cluster, say a cubane, which is connected to the inner surface of the globe by means of a complicated network of strings (the protein structure). A hydrostatic pressure, or uniform stress on the globe is transduced onto the cubane as a strain with directional properties (the \mathbf{p} tensor) *unrelated* to the structure of the cube (the \mathbf{g}_0 tensor).

The unrestricted form of the statistical theory of g strain has been tested on high-quality multifrequency data from $[2\text{Fe}-2\text{S}]^{1+}$ ferredoxins, resulting in (1) very good fits, and (2) proof of full correlation between the \mathbf{p} -tensor elements (25). Figure 6 gives an example of such a fit. In spite of some initial difficulties (137) and concern (138), it now appears that fully correlated g strain is also an adequate model for inhomogeneously broadened EPR from $[4\text{Fe}-4\text{S}]^{3+}$ in HiPIPs (125) as well as from $[4\text{Fe}-4\text{S}]^{1+}$ in ferredoxins (W. R. Dunham, personal communication, 1990) and in complex enzymes (139). It is also operative

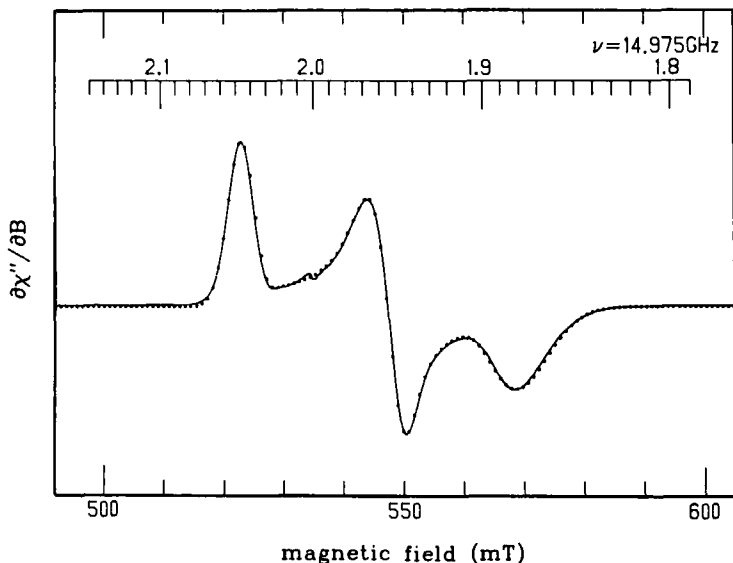


FIG. 6. The P-band spectrum of the reduced $[2\text{Fe}-2\text{S}]$ cluster in *Synechococcus lividus* ferredoxin (solid trace) is computer simulated (dots) with a line width anisotropy according to Eq. (26), the g -strain equation (25, 139).

in biological $[3\text{Fe}-4\text{S}]^{1+}$ clusters (107) and in $[6\text{Fe}-6\text{S}]^{3+}$ prismane cores in model compounds (47).

The g -strain equation is

$$W = |l_x^2 g_x \Delta_{xx} + l_y^2 g_y \Delta_{yy} + l_z^2 g_z \Delta_{zz} + 2l_x l_y \sqrt{g_x g_y} \Delta_{xy} + 2l_x l_z \sqrt{g_x g_z} \Delta_{xz} + 2l_y l_z \sqrt{g_y g_z} \Delta_{yz}|/g \quad (26)$$

Its derivation can be found in Ref. 136 and is not repeated here. Note that in the original work this equation was given in a compact matrix notation [Eq. (34) in Ref. 136; see also Ref. 126]. Equation (26) accurately describes the angular-dependent line width in the above-mentioned iron-sulfur systems. The line width, W , is interpreted as the variance of g in Eq. (25) when the principal g values are functions of fully correlated random variables. Equation (26) follows from a general statistical model that does not assume anything about the physical nature of g strain, other than that the full correlation implies the ultimate cause of g strain to be a scalar quantity. In other words, Eq. (26) provides a practical means to effectively describe line broadening in the EPR of iron-sulfur $S = \frac{1}{2}$ systems while leaving ample room for future theorization on the molecular mechanisms involved.

The Δ values in Eq. (26) are the six independent elements of a 3×3 real, symmetric matrix. This matrix describes the \mathbf{p} tensor of Eq. (25) in the axis system that diagonalizes the \mathbf{g} tensor. The Δ values also have a practical interpretation as g -strain parameters. The absolute values of the diagonal elements Δ_{ii} are to a good approximation equal to the apparent line width on a g -value scale of the three features of the powder spectrum. Their approximate value can be read from the experimental spectrum. The off-diagonal elements, Δ_{ij} , are responsible for the typical asymmetries in g -strain broadened spectra. Their value can not be read from the spectrum, therefore analysis of g -strained spectra always requires computer simulation. Because the Δ values reflect a distribution in effective g values, these simulations have to be made in g space, and the resulting spectrum has to be subsequently transformed to B space for comparison with experimental data (139).

The numerical values of Δ can be positive or negative. This has the implication that the line width from g strain can be zero for some molecules that do not have their \mathbf{g} tensor aligned with the external magnetic field (i.e., for some intermediate orientations). As an important practical consequence the computation time required for simulations based on Eq. (26) increases by some two orders of magnitude compared to simulations based on the ad hoc algorithms of Eq. (22) or (23). A number of tricks on how to handle this problem numerically are detailed elsewhere (139).

It appears to be generally accepted nowadays that g strain is an important determinant for the EPR spectral shape of iron-sulfur proteins. Frequently, however, the concept of g strain is only referred to parenthetically, and quantitative analysis is not attempted. Reluctance to apply Eq. (26) may be related to its complicated mathematical background (136) and to the nontrivial character of its numerical analysis (139). This reviewer hopes for increased efforts in the future, which he advocates as follows. EPR spectral analysis of iron-sulfur proteins using the g -strain concept provides more accurate g values (93); it gives better deconvolutions of complex spectra from multicenter proteins and, therefore, more reliable stoichiometry numbers (139); it should give information—by systematic comparison—on the internal flexibility/rigidity of proteins (25). A direct link has also been suggested between g strain and spin lattice relaxation; a rudimentary theory based on this idea had some success in describing continuous wave saturation of the $[2\text{Fe}-2\text{S}]^{1+}$ EPR from spinach ferredoxin (132). This suggestion has not incited any response in the decade following its proposal.

IV. High-Spin Kramers' Systems

A. THE WEAK-FIELD REGIME

As with g strain, this is another field of biological EPR whose development is presently dominated by examples from iron-sulfur EPR. The biological superspins ($S > \frac{1}{2}$) are unknown outside the Fe-S field. We have already pointed to their association with putative iron-sulfur superclusters. Remarkably, the $S = \frac{1}{2}$ system is a relative rarity for iron-sulfur clusters in contrast to its ubiquity in iron-protein EPR in general. On the other hand, the $S = \frac{3}{2}$ system appears to be limited to the domain of iron-sulfur and mixed-metal iron-sulfur clusters, except for the cases of high-spin ferrous NO (140) and high-spin cobaltous proteins (141).

Half-integer high-spin systems in biology have been analyzed with the spin Hamiltonian:

$$H = \mathbf{S} \cdot \mathbf{D}' \cdot \mathbf{S} + \beta \mathbf{B} \cdot \mathbf{g} \cdot \mathbf{S} \quad (27)$$

For $S > \frac{1}{2}$, higher order terms in S are allowed theoretically (142), but this theme has only rarely been touched in biological EPR (143, 144). There is a practical difficulty in discerning between the effects of higher order terms and the second-order term, $\mathbf{S} \cdot \mathbf{D}' \cdot \mathbf{S}$, in half-integer spin systems (see, e.g., Ref. 145). The subject has thus far been completely ignored in iron-sulfur EPR. We have nothing to add here (but we will have, below, when discussing non-Kramers' systems).

A characteristic aspect of high-spin metalloprotein EPR, including all high-spin iron-sulfur EPR, is the general validity at X-band frequencies of the inequality

$$\mathbf{S} \cdot \mathbf{D}' \cdot \mathbf{S} \gg \beta \mathbf{B} \cdot \mathbf{g} \cdot \mathbf{S} \quad (28)$$

In this "weak-field limit," the $S = n/2$ multiplet forms $(n + 1)/2$ Kramers' doublets, each of which is separated from the others by energies significantly larger than the $\approx 0.3\text{-cm}^{-1}$ microwave quantum. On the other hand, all the doublets within the ground multiplet are at sufficiently low energies to be significantly populated in the temperature range practical for iron-sulfur EPR, typically from 4 to 100 K. In this situation, each doublet of the $S = n/2$ system is expected to give rise to its own resonance, which can be described in terms of an effective $S = \frac{1}{2}$ spectrum with three effective g values. For example, an $S = \frac{3}{2}$ system will have a superposition of five $S_{\text{eff}} = \frac{1}{2}$ spectra with a total of 15 effective g values. However, not all of these g_{eff} values are observables, as will become obvious below. A practical way to analyze these

types of spectra is in terms of a single quantity, the rhombicity parameter, making use of a graphical representation of tabular values, for which I have proposed the name "rhombograms."

B. CALCULATION OF EFFECTIVE g VALUES

Since the zero-field interaction tensor, \mathbf{D}' , is traceless, one usually rewrites the term $\mathbf{S} \cdot \mathbf{D}' \cdot \mathbf{S}$ in the two-parameter form:

$$H_{ZF} = D[S_z^2 - S(S + 1)/3] + E(S_x^2 - S_y^2) \quad (29)$$

and this allows us to define "rhombicity" as a single parameter, E/D , whose value is limited theoretically as (146, 147):

$$0 \leq |E/D| \leq \frac{1}{3} \quad (30)$$

Note that some authors prefer to define a rhombicity parameter, η , in a slightly different manner, namely, $\eta \equiv 3E/D$, as this limits the magnitude of rhombicity between zero and unity.

We assume the \mathbf{D}' and \mathbf{g} tensor to be collinear, and we write out the Zeeman interaction in a shorthand notation as

$$H_{\text{Zeeman}} = G_x S_x + G_y S_y + G_z S_z \quad (31)$$

with

$$G_i = g_i l_i \beta B S_i \quad (i = x, y, z) \quad (32)$$

The direction cosines, l_i , were defined in Eq. (20). With the spin functions for the $S = n/2$ system written as

$$|m_s\rangle = |n/2\rangle; |(n - 1)/2\rangle; \dots; |-n/2\rangle \quad (33)$$

and recalling that

$$\begin{aligned} S_z |m_s\rangle &= m_s |m_s\rangle \\ S_+ |m_s\rangle &= \sqrt{S(S + 1) - m_s(m_s + 1)} |m_s + 1\rangle \\ S_- |m_s + 1\rangle &= \sqrt{S(S + 1) - m_s(m_s + 1)} |m_s\rangle \\ S_x &= (\frac{1}{2})(S_+ + S_-) \\ S_y &= (\frac{1}{2}i)(S_+ - S_-) \end{aligned} \quad (34)$$

we can now construct the energy matrix by calculating all the matrix elements $\langle m_s | H | m'_s \rangle$.

For example, for $S = \frac{3}{2}$ we have

$$|m_s\rangle = |\frac{3}{2}\rangle; |\frac{1}{2}\rangle; |-\frac{1}{2}\rangle; |-\frac{3}{2}\rangle \quad (35)$$

and the energy matrix is

	$ \frac{3}{2}\rangle$	$ \frac{1}{2}\rangle$	$ \frac{1}{2}\rangle$	$ \frac{1}{2}\rangle$
$\langle +\frac{3}{2} $	$D + 3G_z/2$	0	$\sqrt{3}(G_x - iG_y)/2$	$E\sqrt{3}$
$\langle -\frac{3}{2} $	0	$D - 3G_z/2$	$E\sqrt{3}$	$\sqrt{3}(G_x + iG_y)/2$
$\langle +\frac{1}{2} $	$\sqrt{3}(G_x + iG_y)/2$	$E\sqrt{3}$	$-D + G_z/2$	$G_x - iG_y$
$\langle -\frac{1}{2} $	$E\sqrt{3}$	$\sqrt{3}(G_x - iG_y)/2$	$G_x + iG_y$	$-D - G_z/2$

(36)

The equivalent matrices for $S = \frac{5}{2}; \frac{7}{2}; \frac{9}{2}$ and their application to iron-sulfur protein EPR can be found in Refs. 49 and 54. There are two ways to use these matrices for the interpretation of high-spin EPR data: the exact solution and the weak-field approximation. These approaches are similar in conception; however, they differ drastically in their practical applicability.

The exact solution is obtained as follows. Numerical diagonalization of the energy matrix gives the relative energies of the $n + 1$ levels within the $S = n/2$ multiplet. To find the effective g values of the EPR spectrum, we carry out the diagonalization along the principal axes (D' and g are collinear), i.e., for the three possibilities,

$$(l_x, l_y, l_z) = (1, 0, 0); (0, 1, 0); (0, 0, 1) \quad (37)$$

We choose values for the fitting parameters D , E , g_x , g_y , and g_z and subsequently do the diagonalization along each axis for many different values of the external magnetic field, B , in order to find all those B values for which two of the $n + 1$ energy levels differ by an amount, ΔE , equal to the energy of the applied microwave quantum. We then get the effective g values from the resonance condition:

$$g_{\text{effective}} = \Delta E/(\beta B) \quad (38)$$

The amounts of CPU time required by this approach may well be prohibitive in many practical applications.

In the weak-field limit [cf. Eq. (28)] the Zeeman term is only a small perturbation to the zero-field interaction. A significant consequence of this is that the effective g values are frequency independent. In practice, substituting any "large" value for D and any "small" value for B in the energy matrix results in the same set of effective g values. Typical

dummy values can be anywhere within the range $10 < D < 100 \text{ cm}^{-1}$, and $0.01 < B < 1 \text{ T}$. The complexity of the problem is now considerably reduced, because the matrix diagonalization has to be done for a single B value only, and also because the g_{eff} values no longer depend on the values of D and E , but only on their ratio, E/D .

A further simplification ensues from the realization that the g_{eff} values shift much more significantly by changes in the value of E/D than by deviations in the *real* g values from the free-electron value. In other words, we can, as a reasonable starting point, assume that the real g values are

$$g_x = g_y = g_z = 2.00 \quad (39)$$

This should be a good assumption for the $3d^5$ system with quenched orbital angular momentum, e.g., Fe(III) in rubredoxin. It should also be a rather good assumption for iron-sulfur systems, especially for the most oxidized ones. There are few reports on attempts to document deviations from Eq. (39) in high-spin EPR from iron-sulfur proteins. A real $g_z \approx 2.04$ was deduced from the $S = \frac{3}{2}$ EPR from the iron-molybdenum cofactor in dithionite-reduced nitrogenase (148, 149). For the equivalent spectrum from the vanadium-containing nitrogenase, $g \approx 2.06$ has been reported (150). In general, it would appear that the deviations in high-spin iron-sulfur EPR are maximally of the order of a few digits in the second decimal place of the real g values, and this is probably comparable to the uncertainty in the effective g values due to our limited understanding of the details of the line shapes in these spectra.

With the three elements of the real g tensor fixed at 2.00, and the value of the axial zero-field parameter, D , irrelevant, we find that any half-integer high-spin system has an EPR spectrum that is a function of a single parameter only, i.e., the rhombicity E/D . This allows us to analyze these spectra by means of simple, two-dimensional graphs of effective g values versus rhombicity.

C. THE READING OF RHOMBOGRAMS

Rhombograms for the cases $S = \frac{3}{2}, \frac{5}{2}, \frac{7}{2}$, and $\frac{9}{2}$ are given in Fig. 7 (A–D) (54, 69, 147, 151). All possible g values for the subspectrum from a particular Kramers' doublet are represented by the three curves in the individual panels. Spectral analysis means now simply placing a ruler parallel to the vertical axes of Fig. 7 and moving it along the horizontal axes to a rhombicity that produces all the experimentally observed effective g values. Thus graphically determined approximate values

can be checked with more accurate computer calculations. These calculations also allow for trials with real g values deviating from 2.00. A simple, efficient program running on personal computers is available from the author (152). In practice, three types of problems can occur: (1) not all the theoretically predicted effective g values are observed, (2) the system has more than one discrete rhombicity, and (3) the system is a mixture of different spins (the latter two problems will be addressed separately below).

It should be evident from a quick glance at Fig. 7 that in many cases some of the effective g values are simply too low to be detected. The maximum value for the electromagnet of an X-band EPR spectrometer is typically of the order of 1 T. This excludes detection of all $g < 0.6$. The problem can not be solved simply by the application of higher magnetic fields, because this would take us out of the weak-field regime, leading to a breakdown of Eq. (28) and, therefore, of the validity of the

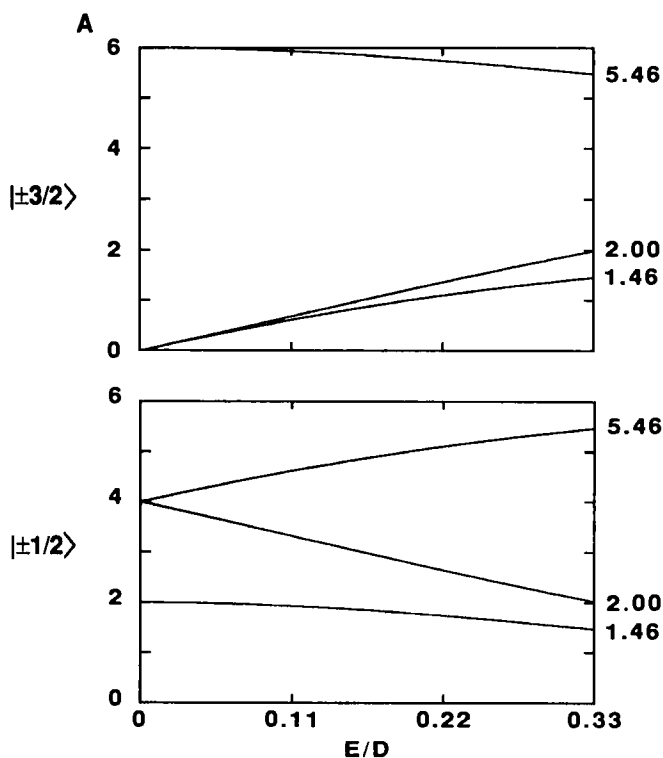


FIG. 7. Rhombograms: (A) $S = \frac{3}{2}$; (B) $S = \frac{5}{2}$; (C) $S = \frac{7}{2}$; (D) $S = \frac{9}{2}$.

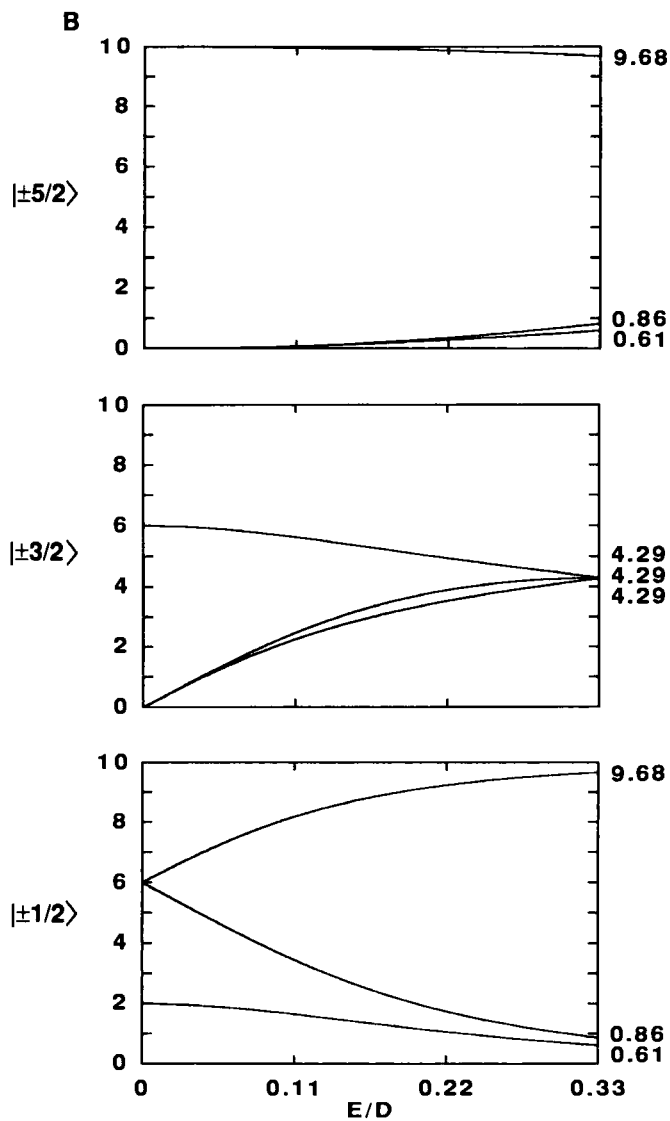


FIG. 7 (continued).

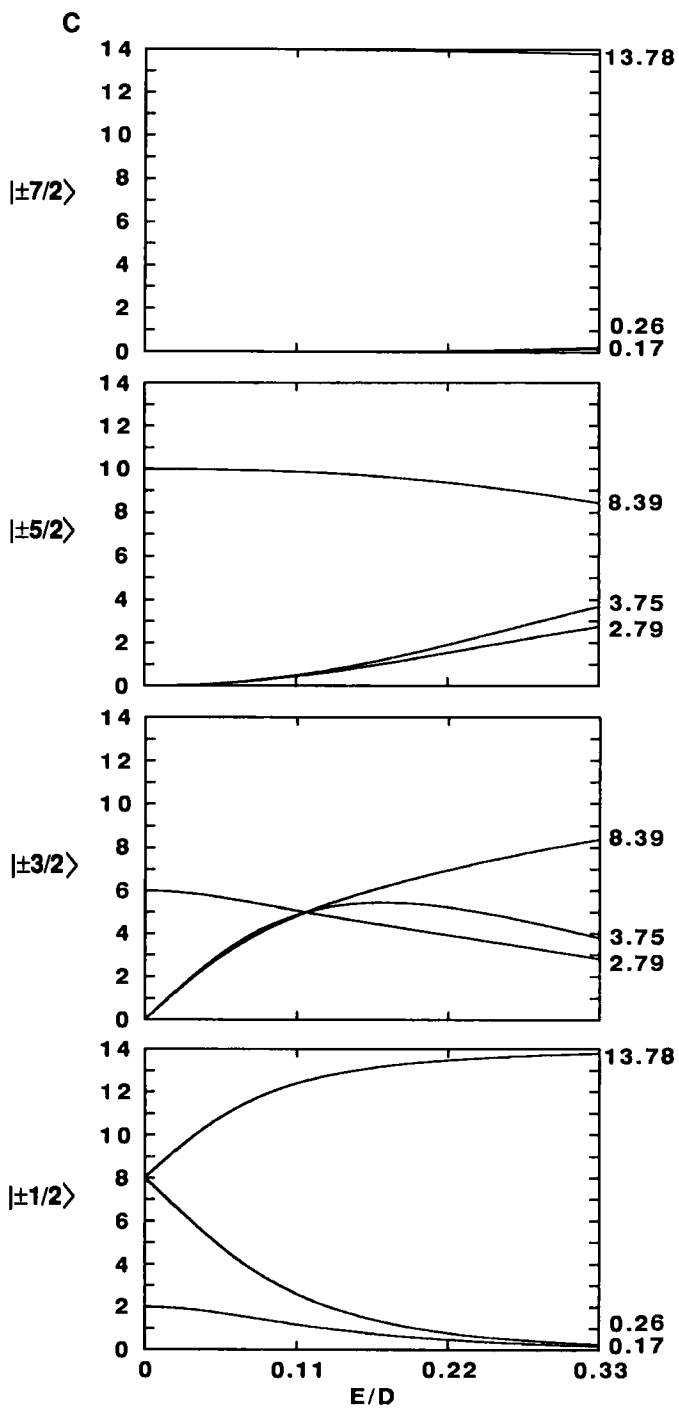


FIG. 7 (continued).

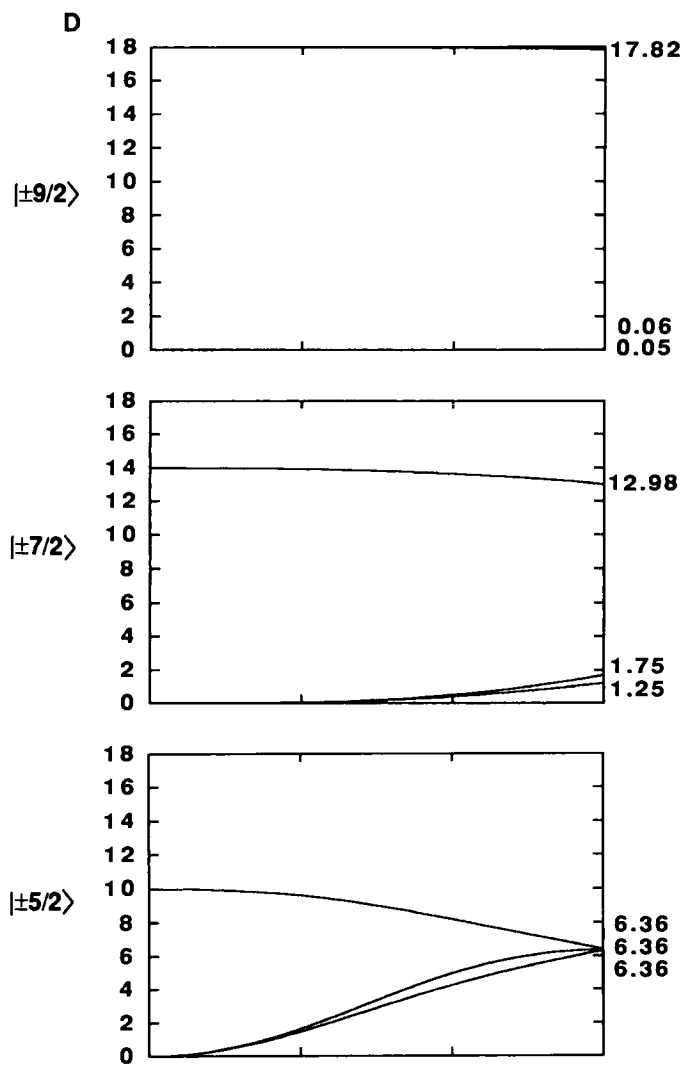


FIG. 7 (continued).

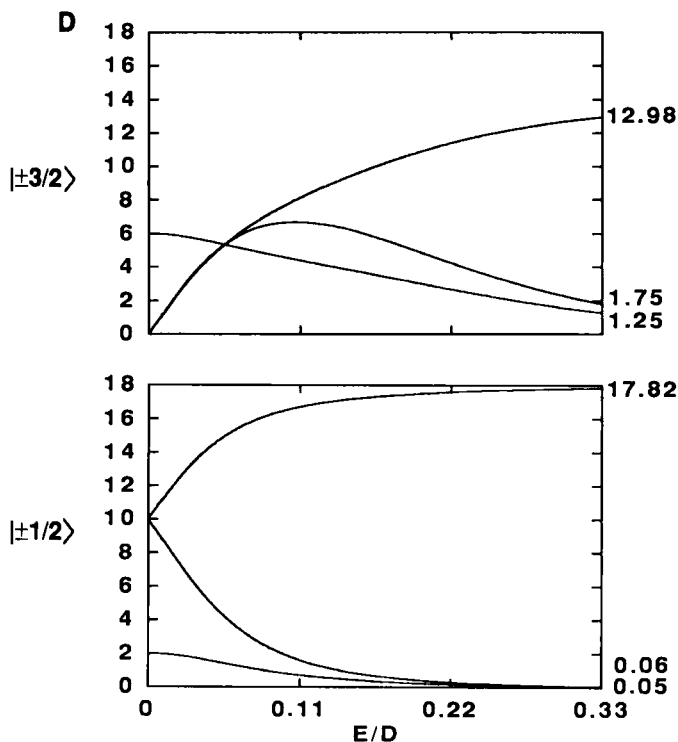


FIG. 7 (continued).

diagrams in Fig. 7. A closely related problem is that of the low intensity of highly anisotropic spectra. In the axial case (i.e., $E = 0$), no spectrum other than that from the $|\pm \frac{1}{2}\rangle$ doublet is observable. All the other doublets have two g values outside the magnetic field range, $g_x = g_y = 0$. The third g value always corresponds to a practical field value; however, it is also not observed because the transition probability is zero [cf. Eq. (21)]. Reworded, an infinitely wide spectrum has infinitely low intensity, or the smaller the g anisotropy the higher the spectral intensity will be. This notion leads to three rules of thumb relating to the intensity of subspectra from half-integer spins:

Rule 1: the likelihood of observing a transition within the higher doublets increases with increasing rhombicity, E/D .

Rule 2: this likelihood decreases with increasing system spin, S .

Rule 3: the likelihood also decreases with increasing projected spin, m_s .

Consider some examples to illustrate these rules. The molybdenum-iron cofactor in nitrogenase is an $S = \frac{3}{2}$ system with a relatively low rhombicity value, $E/D = 0.055$ (148). The spectrum from the $|\pm\frac{3}{2}\rangle$ doublet is extremely weak and is difficult to detect (149). When the cofactor is isolated from the protein, the rhombicity increases ($E/D = 0.11$) and the excited state EPR becomes readily observable (153). In the vanadium-containing nitrogenase the rhombicity has further increased to $E/D = 0.26$, and now the two subspectra have comparable intensity (150). The $S = \frac{5}{2}$ is poorly represented in the iron-sulfur proteins, therefore, we look at other iron proteins. Ferric high-spin hemoproteins are $S = \frac{5}{2}$ systems of low rhombicity. No EPR other than from the $|\pm\frac{1}{2}\rangle$ ground doublet has ever been observed. Highly rhombic $S = \frac{5}{2}$ systems are found in mononuclear ferric centers. In some cases EPR from all three doublets is observable (69, 154). Data on Fe-S (or Fe-Se) $S = \frac{1}{2}$ and $S = \frac{3}{2}$ systems are presently limited to two (49, 84) and four (51, 54, 56, 57) cases, respectively. EPR from the highest doublet has not been observed for any of these systems. EPR from the second highest doublet is, at best, only indicated in one or two cases (49, 57).

A fourth rule of thumb applies to the (lower) intermediate doublets. Again, by inspection of Fig. 7 it is obvious that systems with $S \geq \frac{5}{2}$ have at least one doublet with three coinciding g values for a particular value of the rhombicity parameter. An actual rhombicity close to this value will lead to a near-isotropic subspectrum of relatively high intensity. It is helpful to realize that the rhombograms of Fig. 7 possess a graphical symmetry in the sense that extending the lowest panel along the horizontal axis to the range $\frac{1}{3} \leq E/D \leq 1$ results in the (stretched) mirror image of the upper panel (cf. Ref. 147). The same operation on the next to the lowest panel gives the mirror image of the second highest panel. For those systems that have an odd number of Kramers' doublets (i.e., $S = \frac{3}{2}, \frac{5}{2}, \frac{7}{2}$, etc.), extension of the middle panel should produce its own mirror image. These systems all have an isotropic spectrum at maximal rhombicity, i.e., $E/D = \frac{1}{3}$. For $S = \frac{3}{2}$ this gives rise to the well-known $g = 4.3$ line, whose isotropy allows for the detection of small quantities of adventitiously bound ferric ion in biological preparations. The equivalent of this for $S = \frac{5}{2}$ systems is an isotropic line at $g = 6.4$. The first putative detection of an $S = \frac{5}{2}$ system with $E/D \approx \frac{1}{3}$ has recently been made (57).

In addition, systems with $S \geq \frac{7}{2}$ have another doublet with coinciding g values for intermediate values of E/D . For a real g value of 2.00 we find for the next to the lowest doublet of an $S = \frac{7}{2}$ system an isotropic spectrum with $g = 5.00$ ($E/D = 0.117$). And for an $S = \frac{9}{2}$ system there

is an isotropic spectrum with $g = 5.34$ ($E/D = 0.055$). Actual systems with a rhombicity close to any of the quoted values are likely to have an easily detectable, near-isotropic subspectrum. Examples are found in the $S = \frac{7}{2}$, $g \approx 5.2$ EPR from selenium-substituted ferredoxin (83, 84) and in the recently reported $S = \frac{5}{2}$, $g \approx 5.7$ EPR from the putative prismane protein (52, 55, 59) and from a carbon monoxide dehydrogenase (56). We summarize the previous statements:

Rule 4: near-isotropic, therefore easily detectable, subspectra occur for the middle doublet in maximally rhombic $S = \frac{5}{2}$ or $\frac{3}{2}$ systems and for the $|\pm\frac{3}{2}\rangle$ doublet from $S = \frac{7}{2}$ or $\frac{5}{2}$ systems of intermediate rhombicity.

Finally, we must consider the angular dependency of the line width as well as the dependency on m_g . Since the theoretical description of line width in high-spin systems is undeveloped, we have to rely on a few practical observations plus some very rudimentary theory. From early work on high-spin ferric heme in myoglobin ($S = \frac{5}{2}$, $|\pm\frac{1}{2}\rangle$ EPR, $E/D \approx 0$) it was concluded that the effective g values were distributed as a consequence of the combined effects of g strain in the real g values and a distribution in the parameter E , the latter effect being rather strongly angular dependent (134). Similarly, we have found for other, more rhombic systems, such as for the mononuclear high-spin ferric site in *Escherichia coli* superoxide dismutase with $E/D = 0.24$ (155), that the inhomogeneous line width results from the combined effects of g strain and a distributed rhombicity. Since the real g tensor in the present approach is taken to be (near) isotropic, the line width from g strain is isotropic in magnetic field units. On the other hand, a distributed E value results in line widths that increase very rapidly with increasing magnetic field, i.e., with decreasing effective g value. Considering attempts at further theorization on the subject to be presently premature, I simply summarize a limited set of phenomenological observations:

Rule 5: within a subspectrum the line width in field units usually increases (therefore, the intensity decreases) rather rapidly with decreasing effective g value; lines of different subspectra with similar effective g values have line widths of the same order of magnitude.

When taking all the five rules of thumb together the following picture emerges. Near-axial systems will exhibit the $|\pm\frac{1}{2}\rangle$ subspectrum only. With increasing rhombicity the $|\pm\frac{1}{2}\rangle$ subspectrum becomes more difficult to detect, and subspectra from higher doublets become significant. Sometimes the mathematical coincidence of effective g values causes

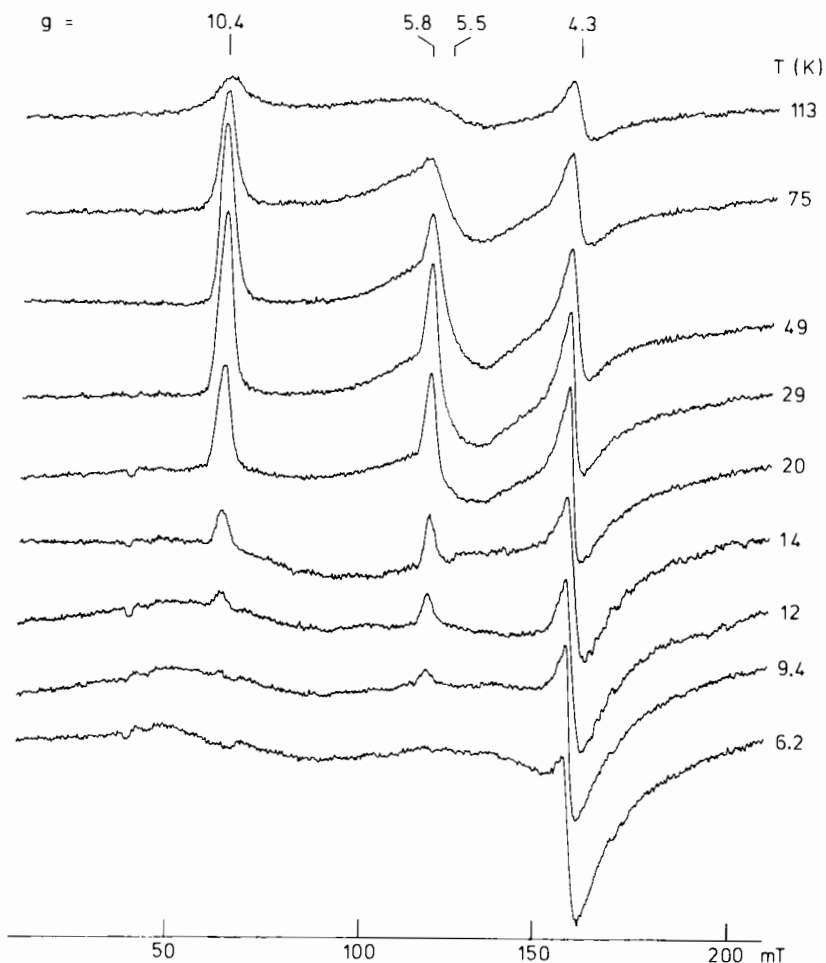


FIG. 8. Temperature dependence of the $S = \frac{1}{2}$ X-band EPR of the P-cluster in thionine-oxidized nitrogenase Mo-Fe protein from *Azotobacter vinelandii* (49).

one of the intermediate subspectra to become dominant. With increasing system spin it is increasingly difficult to detect EPR from the highest doublets.

D. PRACTICAL ASPECTS OF IRON-SULFUR HIGH-SPIN EPR

Figure 8 shows the temperature dependence of part of the X-band spectrum from thionine-oxidized Mo-Fe protein of nitrogenase (49).

The spectrum is from an $S = \frac{7}{2}$ superspin assigned to the P-cluster, a putative iron-sulfur supercluster (49, 63) of otherwise undefined structure. Figure 8 is a convenient example to illustrate the intensity rules derived in the previous section, and to discuss additional practical aspects.

The rhombicity of the $S = \frac{7}{2}$ system is $E/D = 0.043$. This value is consistent with a $|\pm\frac{1}{2}\rangle$ subspectrum with $g = 10.4, 5.4$, and 1.8 (cf. Fig. 7C). We do not observe this subspectrum below $T \approx 10$ K but only at intermediate temperatures (Fig. 8). The $S = \frac{7}{2}$ multiplet is upside down as a result of the D value being negative. This is probably the major reason why the—in principle easily detectable—spectrum of Fig. 8 has escaped detection for a number of years (156–159). In recent times it has become increasingly evident that inverted multiplets are the rule rather than the exception in iron-sulfur $S = \frac{3}{2}$ (150, 151, 160, 161), $S = \frac{5}{2}$ (49, 84), and $S = \frac{7}{2}$ (54–56) systems. This had added importance to extended temperature variation in EPR, thus making the experiment more involved.

Possibly related to the inversion of the spin multiplet is the repeated observation that the EPR is not microwave saturable. All traces in Fig. 8 were recorded with 200 mW microwave power, typically the output of a leveled X-band klystron. Again, this nonsaturability appears to be the rule for high-spin, especially superspin Fe-S, systems. This not only means that current spectrometer performance is suboptimal with respect to the detection of these systems, but it also implies that superspins will probably not readily be studied by pulsed techniques and by double-resonance techniques.

In addition to the $|\pm\frac{1}{2}\rangle$ subspectrum, only the $|\pm\frac{3}{2}\rangle$ subspectrum is positively identified at $g_{\text{eff}} = 5.8$, consistent with out intensity Rules 1–3. The Rule 4-predicted mathematical coincidence of effective g values, resulting in near-isotropic subspectra, is not observed in this particular $S = \frac{7}{2}$ system. However, the isotropic line at $g = 4.3$ from a very small amount of adventitious iron ($S = \frac{5}{2}$) is a case in point. $S = \frac{3}{2}$ examples of this phenomenon may be found in the recently detected EPR spectra from different iron-sulfur proteins (55, 57, 59).

The Rule 5-predicted line width increase with decreasing effective g values is observed for the $g = 10.4$ and 5.5 features from the $|\pm\frac{1}{2}\rangle$ subspectrum.

We have indicated that the broadening described by Rule 5 is related to a distributed rhombicity. This smoothly varying, statistical distribution should be discriminated from a *discrete* distribution of rhombicities reflecting a limited number of discernible conformers. Only the latter results in resolved spectra from different components. For example, it

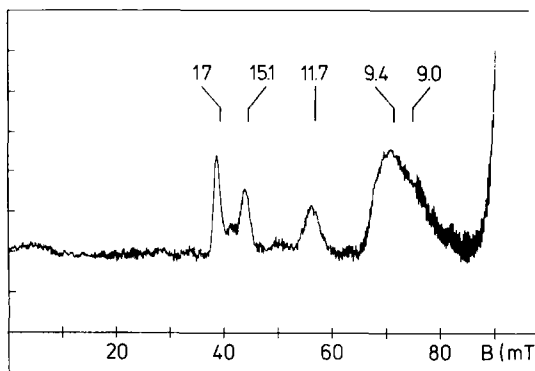


FIG. 9. Multiple rhombicities in the $S = \frac{3}{2}$ X-band EPR of the dissimilatory sulfite reductase from *Desulfovibrio vulgaris* strain Hildenborough (54).

is not at all uncommon to observe up to four different $|\pm\frac{1}{2}\rangle$ subspectra from $S = \frac{3}{2}$ hemoproteins and sirohempoproteins (cf. Refs. 54, 162, and references quoted therein). The limited data presently available on $S = \frac{3}{2}$ systems in iron-sulfur proteins indicate that here discrete distributions in rhombicity are also a common phenomenon. An example is given in Fig. 9. The EPR from *D. vulgaris* sulfite reductase exhibits (at least) three sharp peaks at very high effective g values of 17, 15.1, and 11.7, and these have all been ascribed to the $|\pm\frac{1}{2}\rangle$ subspectrum from an $S = \frac{3}{2}$ system with discretely different rhombicities (54). Similar effects have been observed in the $S = \frac{3}{2}$ EPR from the putative prismane protein (59). These discrete distributions both in hemoproteins and in iron-sulfur proteins have thus far not been explained in (bio)chemical terms; they do present an additional complication in the spectroscopic analysis.

The spectrum of Fig. 9 also illustrates another practical rule for superspin EPR. From the rhombograms in Fig. 7 it can be seen that, in the weak-field limit, there is a maximum to g_{eff} for each particular system spin, namely, $g = 6$ ($S = \frac{3}{2}$), $g = 10$ ($S = \frac{5}{2}$), $g = 14$ ($S = \frac{7}{2}$), and $g = 18$ ($S = \frac{9}{2}$). This can be summarized in the simple rule:

$$g_{\text{max}} \leq S \quad (40)$$

The observation of, e.g., $g = 17$ in spectrum of Fig. 9 identifies the system spin $S \geq \frac{3}{2}$.

The construction of the rhombograms, and every rule deduced from them, is based on the weak-field assumption. At higher magnetic field values, i.e., at lower effective g values, the assumption will increasingly

lose its validity. In attempts to evaluate this problem, rhombogram-predicted g values were compared to g values obtained from exact calculations for $S = \frac{7}{2}$ (49) and $S = \frac{9}{2}$ (54). Even for relatively small values of the zero-field splitting D (twice the X-band microwave quantum), the differences between the two methods became significant only for those lower effective g values that thus far have escaped detection. However, this is not necessarily true for data taken at higher microwave frequencies, as was shown by Aasa for the $S = \frac{5}{2}$ ferric transferrin (163).

At the end of our discussion of high-spin Kramers' systems we briefly consider an important but virtually unexplored theme (see Ref. 164 for a single exception): the validity of spin quantification procedures for high-spin systems. The quantification of $S = \frac{1}{2}$ spectra against that of an $S = \frac{1}{2}$ concentration standard is a well-established procedure (128). It is generally assumed—although nowhere explicitly stated in the vast literature on biological EPR—that this procedure also fully holds for Kramers' high-spin subspectra, provided correction is made for partial population according to Boltzmann statistics. However, no formal mathematical proof of this thesis has been given. There is ad hoc support in the practical finding that quantification of $|\pm\frac{1}{2}\rangle$ subspectra from high-spin systems usually gives a number that is an approximate multiple of the protein concentration. To what extent this "approximate" is a consequence of nonrigorous theory remains to be established. This caveat is emphasized for quantification on other than $|\pm\frac{1}{2}\rangle$ subspectra and on non-weak-field spectra.

V. Non-Kramers' Systems

A. PRINCIPLES OF DUAL-MODE EPR IN $S = 2$ SYSTEMS

We have seen that application of the spin Hamiltonian of Eq. (27) to half-integer spin systems ($S = n/2$) in the weak-field limit results in a grouping of levels within the spin multiplet into $(2n + 1)/2$ doublets. The same Hamiltonian applied to integer spin, or non-Kramers' systems ($S = n$), results in a grouping into n doublets and one singlet (see Fig. 10, left panel). Note, that these doublets are similar to the higher doublets of half-integer systems in that their associated subspectra in axial symmetry have two effective g values equal to zero. However, the two systems are very different with respect to the nature of the transition: Kramers' systems are subject to $|\Delta m| = 1$ transitions; non-Kramers' systems have $|\Delta m| = 0$ transitions. In quantum mechanical lan-

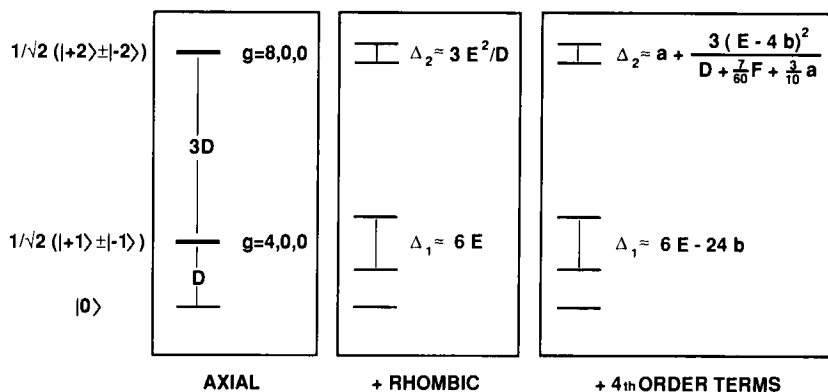


FIG. 10. Level scheme for the $S = 2$ multiplet under different zero-field spin Hamiltonians.

guage the two levels of a non-Kramers' doublet are not interconvertible by the time-reversal operator (2). An important consequence of this statement is that the two levels are not necessarily degenerate in a zero magnetic field. In fact, a finite rhombicity ($E \neq 0$) is sufficient to split the non-Kramers' doublet (Fig. 10). Kramers' doublets can never be split in zero field.

In axial symmetry ($E = 0$) the lowest three levels of Fig. 10 are admixed by the Zeeman interaction; therefore, a $|\Delta m| = 1$ transition within the first doublet is weakly allowed for all orientations except when the magnetic field is along the z axis. This transition is equivalent to the "half-field" transition with $g_{\text{eff}} \approx 4$ observed in many triplet ($S = 1$) systems. However, in the weak field limit this admixture is negligible, and no such subspectrum has ever been positively identified yet for iron-sulfur systems with $S \geq 2$. An additional complication here is that a finite rhombicity splits the doublet by an amount $\Delta_1 \approx 6E$, and this splitting can easily be greater than the energy of practically employed microwave quanta (162).

Rhombicity induces a much smaller splitting in the second doublet, $\Delta_2 \approx 3E^2/D$ for $S = 2$. It also mixes the levels of the doublet through coupling with the $|0\rangle$ singlet, and this creates the possibility to observe $|\Delta m| = 0$ transitions within the doublet (2). This requires a special experimental setup called parallel-mode EPR, in which the magnetic component of the microwave, B_1 , is put parallel to the static magnetic field, B . In standard EPR spectrometers detecting $|\Delta m| = 1$ transitions, the common geometry is to have the vectors B and B_1 perpendicular. A

bimodal cavity is a resonator that can operate in each of the two modes, which are then typically separated in frequency by some 50 MHz (144, 162).

The approximate resonance condition for such non-Kramers' intra-doublets transitions was formulated 40 years ago by Bleaney and Scovil (165) as

$$h\nu = \sqrt{(g_{\text{eff}}\beta B)^2 + \Delta^2} \quad (41)$$

Another simple and useful approximate rule (166) holds for the transition probability, or the intensity of the parallel-mode spectrum I_{\parallel} , at a given microwave frequency:

$$I_{\parallel} \propto \Delta^2 \quad (42)$$

The transition is also observable in a regular spectrometer except for those molecules that have their z axis exactly parallel to the static field B , i.e., $\Theta = 0$. In the neighborhood of the z axis we have (167)

$$I_{\perp}/I_{\parallel} \approx (\frac{1}{2}) \tan^2 \Theta \quad (43)$$

The shape of non-Kramers' resonances is nonstandard in several respects. The inhomogeneous broadening appears to be related to a distribution in the intradoublet splitting Δ , in its turn possibly induced by a distribution in rhombicities (168; see also Refs. 162 and 169 and references quoted therein). As a result of the transition probability being proportional to the splitting Δ , the line shape is asymmetrically tailing toward low field and has a zero intensity at the effective g value for axial symmetry (2, 162, 166). Furthermore, in biological systems the distribution in Δ is frequently such that the resonance line is broadened "into zero field," i.e., $\Delta > h\nu$, with partial loss of intensity (162). Finally, in normal-mode spectra the powder pattern is deformed as a consequence of the zero transition probability along the z axis. All these effects combined have the result that reading effective g values directly from the polycrystal spectrum is usually much less accurate than with Kramers' systems. In many cases g_{eff} determinations are only possible by spectral simulation techniques adapted for integer-spin systems (144, 162). Also, for the quantification of powder spectra from non-Kramers' systems the use of spectral simulations appears to be mandatory; on a more advanced level these simulations become involved and time consuming (144). The bottom line is that there is no quick and easy way to quantitate these spectra.

When discussing high-spin Kramers' systems we noted that for $S > \frac{3}{2}$ higher order terms in the spin operator should be added to the spin

Hamiltonian. We decided that this is very rarely done, possibly because second and higher order terms result in similar effects in the powder spectrum. This is not true for non-Kramers' systems. For example, for a rhombic $S = 2$ system the complete zero-field Hamiltonian is an extension of Eq. (30), namely (2, 145, 170, 171):

$$\begin{aligned}
 H_{\text{ZF}} = & (a/6)[S_x^4 + S_y^4 + S_z^4 - (\frac{1}{5})S(S+1)(3S^2 + 3S - 1)] \\
 & + (F/180)[35S_z^4 - 30S(S+1)S_z^2 \\
 & + 25S_z^2 - 6S(S+1) + 3S^2(S+1)^2] \\
 & + D[S_z^2 - S(S+1)/3] + E[S_x^2 - S_y^2] \\
 & + (b/2)\{[7S_z^2 - S(S+1) - 5](S_x^2 - S_y^2) \\
 & + (S_x^2 - S_y^2)[7S_z^2 - S(S+1) - 5]\}
 \end{aligned} \tag{44}$$

When we calculate the approximate values for the non-Kramers' doublet splittings under this Hamiltonian (they are given in Fig. 10), it can be seen that the effects of the new a , F , and b terms are easily incorporated, by substitution, into the old D and E terms, except for a splitting of the second doublet linear in the quantity a . This has the far-reaching implication that the upper doublet can be split even in cubic symmetry, therefore that no rhombicity is required for a finite transition probability. We have made one attempt at rigorously analyzing a bimodal spectrum ($S = 2$ in cytochrome oxidase) with the Hamiltonian of Eq. (44), and we have found the a term to dominate the splitting of the second doublet (144). It would appear that all studies on biological non-Kramers' doublets ignoring this term are incomplete.

B. IRON-SULFUR NON-KRAMERS' SYSTEMS

EPR on non-Kramers' systems was introduced to the field of iron-sulfur clusters with the detection of an $S = 2$ signal from the $[3\text{Fe}-4\text{S}]^0$ cluster in the 7Fe *Thermus thermophilus* ferredoxin (107). The spectra (see Fig. 11) were very similar to those previously found for $S = 2$ in other biological and model systems (162). Only a single, asymmetric feature is observed extending toward zero field such that the main intensity of the first-derivative spectrum is below the base line. The line is assigned to the transition within the second doublet, subject to a broad distribution in Δ_2 . The transition is $|\Delta m| = 0$, but is generally referred to as " $|\Delta m| = 4$ " (105, 107, 144, 162) to indicate that it originates from the second non-Kramers' doublet, for which the high-field labeling is $|\pm 2\rangle$. Figure 11 also shows the main effect of raising the

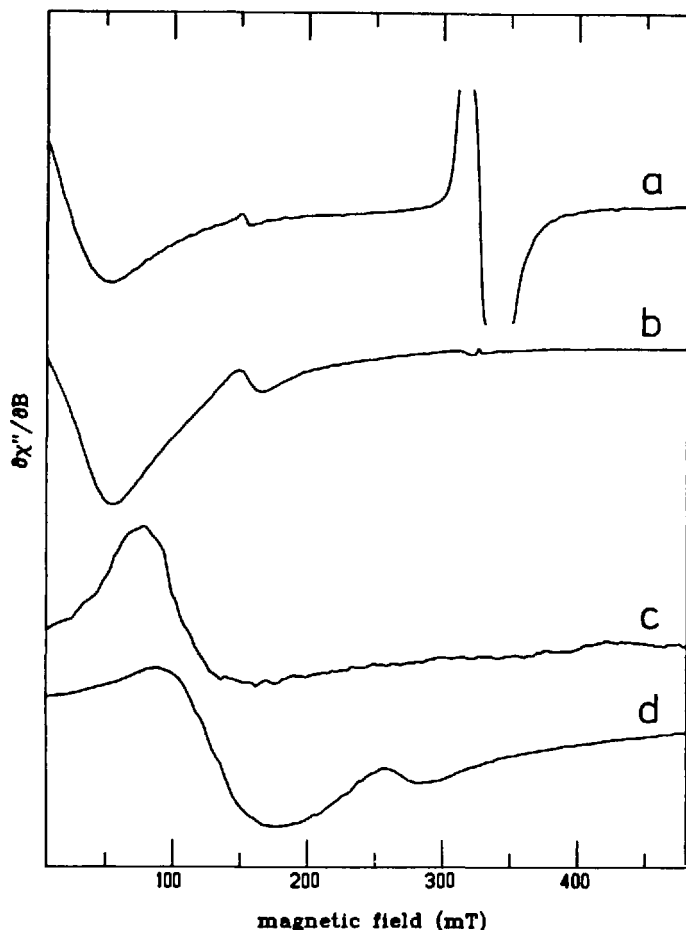


FIG. 11. The $S = 2$ X-band EPR from the $[3\text{Fe-4S}]^0$ cluster in *Thermus thermophilus* ferredoxin (trace a) and ferrous EDTA (trace b), and their respective P-band spectra (traces c and d). The $S = \frac{1}{2}$ signal around $g = 2$ in trace (a) is from the oxidized $[3\text{Fe-4S}]$ cluster (107).

magnitude of the microwave quantum. The spectral feature at higher frequency has a less asymmetric shape due to the fact that a smaller fraction of the distributed Δ values disappears into zero field.

The 7Fe ferredoxin contains a $[3\text{Fe-4S}]$ and a $[4\text{Fe-4S}]$ cluster at a mutual distance of the order of ≈ 1 nm (45, 46). This is the typical distance for which dipole-dipole interactions show up in the EPR spectrum as broadenings, shifts, and/or splittings. The 7Fe ferredoxins have

a protein fold similar to the 8Fe ferredoxins (45, 46). The latter contain two [4Fe-4S] cubanes, and in the reduced state show EPR spectra with dipole-dipole effects between two $S = \frac{1}{2}$ spins (172). The reduced 7Fe ferredoxin is special in that the interaction is between $S = \frac{1}{2}$ (the cubane) and $S = 2$. The $S = 2$ EPR (cf. Fig. 11) is too broad to detect dipolar effects, however, the cubane spectrum is affected in an unusual way: the interaction signal has some effective g values that are constant in the microwave frequency. This effect appears to be a direct consequence of the non-Kramers' nature of the disturbing spin (107).

A signal similar to that of Fig. 11 has been observed for the [3Fe-4S]⁰ cluster in *D. gigas* ferredoxin II (105), probably for the *D. gigas* Ni-Fe hydrogenase (173), and possibly also for aconitase (quoted in Ref. 169).

The determination of zero-field splitting parameters for non-Kramers' systems is more difficult than for Kramers' systems. The ambiguity introduced by the extra terms in the spin Hamiltonian, Eq. (44), especially the a term (cf. Fig. 10), makes it impossible to read a rhombicity directly from the spectrum. Unambiguous assignment requires the detection of resonances from *both* non-Kramers' doublets of an $S = 2$ system (144). This notion is still not generally appreciated (105, 169). Also, the determination of the intradoublet splitting in terms of the dominant D quantity [or its effective substitute in accordance with Eq. (44), $D' \approx D + 2F/15 + a/5$] is apparently not trivial. For the *T. thermophilus* ferredoxin, a positive D was indicated by EPR, whereas MCD spectroscopy clearly indicated a negative D (107). It was then suggested that the EPR was complicated by relaxation phenomena (107). Except for an early, naive attempt by the present author (162), spin lattice relaxation in biological non-Kramers' systems has not been explored.

We have very recently identified two new iron-sulfur non-Kramers' systems (57, 59). The EPR differs from that of hitherto reported biological $S = 2$ systems in two respects: (1) the line width is reduced by an order of magnitude and (2) the ratio of parallel-mode over normal-mode intensity has increased by an order of magnitude compared to the ratio of ≈ 2 , predicted by Eq. (43) and thus far found in practice (cf. Ref. 169). The bimodal spectrum for one of the systems is given in Fig. 12. The signal is from an intermediate redox state of the putative iron-sulfur supercluster, the P-cluster in the *A. vinelandii* Mo-Fe nitrogenase. The effective g value is ≈ 12 , and this is unusual because thus far determined—by spectral simulation— g_{eff} values for biological non-Kramers' systems are usually close to 8 (162). Note that some previously reported (cf. Refs. 173–175) g values close to 12 are only *apparent* values corresponding to the zero crossing of the asymmetrical spec-

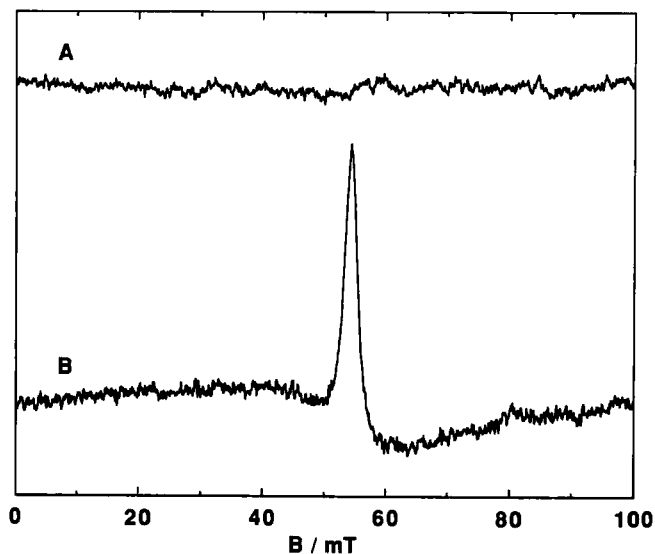


FIG. 12. Dual-mode $S = 3$ X-band EPR from the P-cluster in *Azobacter vinelandii* nitrogenase Mo-Fe protein poised at a potential of -188 mV at pH 7.5. Trace A is the normal-mode spectrum, i.e., with B perpendicular to B_1 ; trace B is the parallel-mode spectrum, i.e., with B parallel to B_1 . The two spectra were taken with the same bimodal cavity, all conditions, other than the frequency mode, being identical (57).

tral feature of the “ $|\Delta m| = 4$ ” transition at X-band. These values have no physical meaning.

A simple model to explain the spectrum of Fig. 12 is to assume that the system is $S = 3$, and the resonance is from the highest doublet, i.e., “ $|\Delta m| = 6$ ” with $g_{\text{eff}} = 12$ (57). No serious attempts have been made yet to support this view with simulations based on the $S = 3$ equivalent of the spin Hamiltonian in Eq. (44) (which should now also encompass sixth-order terms in S , i.e., of the form S^6).

The second novel system is the putative prismane protein, which in one of its intermediate redox states exhibits a sharp parallel-mode signal with $g_{\text{eff}} \approx 16$ (59). By the same token, this signal is identified with a “ $|\Delta m| = 8$ ” transition within the highest doublet of an $S = 4$ system (59).

These intuitive interpretations may perhaps soon prove to be premature. They do, however, make it clear that in the field of iron-sulfur EPR there is a considerable need for theoretical development regarding non-Kramers’ spins and super spins.

VI. Epilogue

EPR spectroscopy of iron-sulfur complexes and proteins is in its fourth decade. It was suggested in Section I that the field is experiencing its third renaissance; the body of this article gives support to this view. In conjunction with the opening up of the area of superclusters we expect to see important developments in our understanding of high-spin EPR, both for half-integer and integer systems. Data on these novel clusters and on the well-characterized "classical" two-, three-, and four-iron clusters will inspire us to further assess the relevance of mechanisms of double-exchange interactions. Also, it is hoped that work on the *g*-strain concept will gain impetus as new experimental data become available. Because of these progressions the iron-sulfur protein has by far long outdone the hemoprotein as the pet object of those interested in the development of metalloprotein EPR.

For various reasons, certain subjects have not explicitly been treated in this article. The mechanisms used by the $[2\text{Fe}-2\text{S}]^{1+}$ cluster for spin lattice relaxation have been shown to be standard (176), and with no other data available we have nothing to add but to assume that this is true also for other clusters. Similarly, the mixed-metal clusters were not a separate theme. The Mo-Fe and V-Fe clusters in nitrogenases were referred to for their $S = \frac{3}{2}$ EPR; however, the Co-, Zn-, and Cd-substituted cubanes (154, 177, 178) and a putative W-Fe-S cluster (179) were not treated, as there appears to be nothing fundamentally new in their EPR properties. The EPR-related double-resonance and pulsed techniques were left out partly because of limitations of size, but also because recent reviews of metalloproteins are available (180, 181).

One subject, that of the mixed spins, was swept under the rug because of a complete lack of theorization on its physical and biochemical nature. In recent times it has become increasingly evident that many iron-sulfur systems exist as a mixture of two or more spin states. This has been found for cubane structures (83, 84, 91, 125, 126, 151, 160, 182-184) and for superclusters (51, 52, 56, 57, 59). The term "physical mixture" has been proposed (184) to indicate that these states appear not to mix thermodynamically or quantum mechanically. One would hope that it will not take until the next renaissance of iron-sulfur EPR before it will dawn on us what a physical mixture of spin states means.

ACKNOWLEDGMENTS

S. P. J. Albracht introduced me to the Fe-S field some 15 years ago, and he continues to help me with the bimodal EPR. W. R. Dunham taught me the QM and a lot more; he

is now a key collaborator on the supercluster project. A. J. Pierik did most of the recent superspin EPR for his PhD thesis; he also made some of the figures for this article. I have had invaluable support from R. H. Sands and from C. Veege. Support is acknowledged from the Netherlands Foundation for Chemical Research (SON), with financial aid from the Netherlands Organization for Scientific Research (NWO).

REFERENCES

1. Zavoisky, E., *Fiz. Zh.* **9**, 211 (1945).
2. Abragam, A., and Bleaney, B., "Electron Paramagnetic Resonance of Transition Ions." Oxford Univ. Press (Clarendon), Oxford, 1970.
3. Bennett, J. E., Ingram, D. J. E., George, P., and Griffith, J. S., *Nature (London)* **176**, 394 (1955).
4. Bennett, J. E., and Ingram, D. J. E., *Nature (London)* **177**, 275 (1956).
5. Sands, R. H., *Phys. Rev.* **99**, 1222 (1955).
6. Sands, R. H., and Beinert, H., *Biochem. Biophys. Res. Commun.* **1**, 175 (1959).
7. Beinert, H., and Sands, R. H., *Biochem. Biophys. Res. Commun.* **3**, 41 (1960).
8. Sands, R. H., and Beinert, H., *Biochem. Biophys. Res. Commun.* **3**, 47 (1960).
9. Blumberg, W. E., and Peisach, J., in "Non-Heme Iron Proteins: Role in Energy Conservation" (A. San Pietro, ed.), p. 101. Antioch Press, Yellow Springs, Ohio, 1965.
10. Brintzinger, H., Palmer, G., and Sands, R. H., *Proc. Natl. Acad. Sci. U.S.A.* **55**, 397 (1966).
11. Van Voorst, J. D. W., and Hemmerich, P., in "Magnetic Resonance in Biological Systems" (A. Ehrenberg, B. G. Malmström, and T. Vänngård, eds.), p. 183. Pergamon, Oxford, 1967.
12. Johnson, C. E., Bray, R. C., Cammack, R., and Hall, D. O., *Proc. Natl. Acad. Sci. U.S.A.* **63**, 1234 (1969).
13. Gibson, J. F., Hall, D. O., Thornley, J. H. M., and Whatley, F. R., *Proc. Natl. Acad. Sci. U.S.A.* **56**, 987 (1966).
14. Thornley, J. H. M., Gibson, J. F., Whatley, F. R., and Hall, D. O., *Biochem. Biophys. Res. Commun.* **24**, 877 (1966).
15. Palmer, G., Dunham, W. R., Fee, J. A., Sands, R. H., Iizuka, T., and Yonetani, T., *Biochim. Biophys. Acta* **245**, 201 (1971).
16. Fritz, J., Anderson, R., Fee, J., Palmer, G., Sands, R. H., Tsibris, J. C. M., Gunsalus, I. C., Orme-Johnson, W. H., and Beinert, H., *Biochim. Biophys. Acta* **253**, 110 (1971).
17. Dunham, W. R., Bearden, A. J., Salmeen, I. T., Palmer, G., Sands, R. H., Orme-Johnson, W. H., and Beinert, H., *Biochim. Biophys. Acta* **253**, 134 (1971).
18. Eaton, W., Palmer, G., Fee, J. A., Kimura, T., and Lovenberg, W., *Proc. Natl. Acad. Sci. U.S.A.* **68**, 3015 (1971).
19. Dunham, W. R., Palmer, G., Sands, R. H., and Bearden, A. J., *Biochim. Biophys. Acta* **253**, 373 (1971).
20. Bertrand, P., and Gayda, J.-P., *Biochim. Biophys. Acta* **597**, 107 (1979).
21. Bertrand, P., and Gayda, J.-P., *Biochim. Biophys. Acta* **625**, 337 (1980).
22. Gayda, J.-P., Bertrand, P., More, C., and Cammack, R., *Biochimie* **63**, 847 (1981).
23. Bertrand, P., Guigliarelli, B., Gayda, J.-P., Bearwood, P., and Gibson, J. F., *Biochim. Biophys. Acta* **831**, 261 (1985).
24. Guigliarelli, B., Bertrand, P., and Gayda, J.-P., *J. Chem. Phys.* **85**, 1689 (1986).

25. Hearshen, D. O., Hagen, W. R., Sands, R. H., Grande, H. J., Crespi, H. L., Gunsalus, I. C., and Dunham, W. R., *J. Magn. Reson.* **69**, 440 (1986).
26. Emptage, M. H., *Am. Chem. Soc. Symp. Ser.* **372**, 343 (1988).
27. Beinert, H., and Kennedy, M. C., *Eur. J. Biochem.* **186**, 5 (1989).
28. Switzer, R. L., *BioFactors* **2**, 77 (1989).
29. Orme-Johnson, N. R., Orme-Johnson, W. H., Hansen, R. E., Beinert, H., and Hatefi, Y., *Biochem. Biophys. Res. Commun.* **44**, 446 (1971).
30. DerVartanian, D. V., Morgan, T. V., and Brantner, R. V., *Biochim. Biophys. Acta* **347**, 497 (1974).
31. Forget, P., and DerVartanian, D. V., *Biochim. Biophys. Acta* **256**, 600 (1972).
32. Beinert, H., Ackrell, B. A. C., Kearney, E. B., and Singer, T. P., *Biochem. Biophys. Res. Commun.* **58**, 564 (1974).
33. Ruzicka, F. J., and Beinert, H., *Biochem. Biophys. Res. Commun.* **58**, 556 (1974).
34. Ruzicka, F. J., and Beinert, H., *J. Biol. Chem.* **253**, 2514 (1978).
35. Sweeney, W. V., Rabinowitz, J. C., and Yoch, D. C., *J. Biol. Chem.* **250**, 7842 (1975).
36. Beinert, H., in "Iron-Sulfur Proteins" (W. Lovenberg, ed.), Vol. 3, p. 84. Academic Press, New York, 1977.
37. Emptage, M. H., Kent, T. A., Huynh, B. H., Rawlings, J., Orme-Johnson, W. H., and Münck, E., *J. Biol. Chem.* **255**, 1793 (1980).
38. Beinert, H., and Thomson, A. J., *Arch. Biochem. Biophys.* **222**, 333 (1983).
39. Beinert, H., Emptage, M. H., Dreyer, J.-L., Scott, R. A., Hahn, J. E., Hodgson, K. O., and Thomson, A. J., *Proc. Natl. Acad. Sci. U.S.A.* **80**, 393 (1983).
40. Kent, T. A., Dreyer, J.-L., Kennedy, M. C., Huynh, B. H., Emptage, M. H., Beinert, H., and Münck, E., *Proc. Natl. Acad. Sci. U.S.A.* **79**, 1096 (1982).
41. Kennedy, M. C., Kent, T. A., Emptage, M. H., Merkle, H., Beinert, H., and Münck, E., *J. Biol. Chem.* **259**, 14463 (1984).
42. Emptage, M. H., Kent, T. A., Kennedy, M. C., Beinert, H., and Münck, E., *Proc. Natl. Acad. Sci. U.S.A.* **80**, 4674 (1983).
43. Kent, T. A., Emptage, M. H., Merkle, H., Kennedy, M. C., Beinert, H., and Münck, E., *J. Biol. Chem.* **260**, 6871 (1985).
44. Stout, C. D., Ghosh, D., Patthabi, B., and Robbins, A. H., *J. Biol. Chem.* **255**, 1797 (1980).
45. Stout, G. H., Turley, S., Sieker, L. C., and Jensen, L. H., *Proc. Natl. Acad. Sci. U.S.A.* **85**, 1020 (1988).
46. Stout, C. D., *J. Biol. Chem.* **263**, 9256 (1988).
47. Kanatzidis, M. G., Hagen, W. R., Dunham, W. R., Lester, R. K., and Coucouvanis, D., *J. Am. Chem. Soc.* **107**, 953 (1985).
48. Hagen, W. R., van Berkel-Arts, A., Krüse-Wolters, K. M., Voordouw, G., and Veeger, C., *FEBS Lett.* **203**, 59 (1986).
49. Hagen, W. R., Wassink, H., Eady, R. R., Smith, B. E., and Haaker, H., *Eur. J. Biochem.* **169**, 457 (1987).
50. Hagen, W. R., Pierik, A. J., and Veeger, C., *J. Chem. Soc., Faraday Trans. 1* **85**, 4083 (1989).
51. Pierik, A. J., Hagen, W. R., and Veeger, C., *EBEC Rep.* **6**, 16 (1990).
52. Hagen, W. R., Pierik, A. J., and Veeger, C., *Ital. Biochem. Soc. Trans.* **1**, 85 (1990).
53. Jetten, M. S. M., Hagen, W. R., Pierik, A. J., Stams, A. J. M., and Zehnder, A. J. B., *Eur. J. Biochem.* **195**, 385 (1991).
54. Pierik, A. J., and Hagen, W. R., *Eur. J. Biochem.* **195**, 505 (1991).
55. Hagen, W. R., Pierik, A. J., Wolbert, R. B. G., Wassink, H., Haaker, H., Veeger, C.,

- Jetten, M. K., Stams, A. J. M., and Zehnder, A. J. B., *J. Inorg. Biochem.* **43**, 237 (1991).
56. Jetten, M. S. M., Pierik, A. J., and Hagen, W. R., *Eur. J. Biochem.* **202**, 1291 (1991).
57. Pierik, A. J., Wassink, H., Haaker, H., and Hagen, W. R., *Eur. J. Biochem.* (submitted for publication).
58. Pierik, A. J., Wolbert, R. B. G., Hagen, W. R., and Veeger, C., *Eur. J. Biochem.* (submitted for publication).
59. Pierik, A. J., Hagen, W. R., Dunham, W. R., and Sands, R. H., *Eur. J. Biochem.* (submitted for publication).
60. Adams, M. W. W., Eccleston, E., and Howard, J. B., *Proc. Natl. Acad. Sci. U.S.A.* **86**, 4932 (1989).
61. George, G. N., Prince, R. C., Stokley, K. E., and Adams, M. W. W., *Biochem. J.* **259**, 597 (1989).
62. Adams, M. W. W., *Biochim. Biophys. Acta* **1020**, 115 (1990).
63. Ravi, N., Moura, I., Tavares, P., LeGall, J., Huynh, B. H., and Moura, J. J. G., *J. Inorg. Biochem.* **43**, 252 (1991).
64. Bolin, J. T., Ronco, A. E., Mortenson, L. E., Morgan, T. V., Williamson, M., and Xuong, N.-H., in "Nitrogen Fixation: Achievements and Objectives" (P. M. Gresshoff, L. E. Roth, G. Stacey, and W. E. Newton, eds.), p. 117. Chapman & Hall, New York, 1990.
65. Bolin, J. T., Campobasso, N., Muchmore, S. W., Minor, W., Mortenson, L. E., and Morgan, T. V., *J. Inorg. Biochem.* **43**, 447 (1991).
66. Nomenclature Committee of the International Union of Biochemistry. Recommendations 1978, *Biochim. Biophys. Acta* **549**, 101 (1979); Recommendations 1989, *Eur. J. Biochem.* **200**, 599 (1991).
67. Orme-Johnson, W. H., and Sands, R. H., in "Iron-Sulfur Proteins" (W. Lovenberg, ed.), Vol. 2, Chap. 5. Academic Press, New York, 1973.
68. Orme-Johnson, W. H., and Orme-Johnson, N. R., in "Iron-Sulfur Proteins" (T. G. Spiro, ed.), Chap. 2. Wiley, New York, 1982.
69. Moura, I., Macedo, A., and Moura, J. J. G., in "Advanced EPR. Applications in Biology and Biochemistry" (A. J. Hoff, ed.), Chap. 23. Elsevier, Amsterdam, 1989.
70. Eaton, W. A., and Lovenberg, W., in "Iron-Sulfur Proteins" (W. Lovenberg, ed.), Vol. 2, p. 131. Academic Press, New York, 1973.
71. Hagen, W. R., *Eur. J. Biochem.* **182**, 523 (1989).
72. Moura, I., Xavier, A. V., Cammack, R., Bruschi, M., and LeGall, J., *Biochim. Biophys. Acta* **533**, 156 (1978).
73. Tavares, P., Ravi, N., Liu, M. Y., LeGall, J., Huynh, B. H., Moura, J. J. G., and Moura, I., *J. Inorg. Chem.* **43**, 264 (1991).
74. LeGall, J., Prickril, B. C., Moura, I., Xavier, A. V., Moura, J. J. G., and Huynh, B.-H., *Biochemistry* **27**, 1636 (1988).
75. Maltempo, M. M., and Moss, T. H., *Q. Rev. Biophys.* **9**, 181 (1976).
76. Palmer, G., and Brintzinger, H., *Nature (London)* **211**, 189 (1966).
77. Moura, I., Tavares, P., Moura, J. J. G., Ravi, N., Huynh, B. H., Liu, M.-Y., and LeGall, J., *J. Biol. Chem.* **265**, 21596 (1990).
78. Yost, F. J., and Fridovich, I., *J. Biol. Chem.* **248**, 4905 (1973).
79. Coucouvanis, D., Salisoglou, A., Kanatzidis, M. G., Dunham, W. R., Simopoulos, A., and Kostikas, A., *Inorg. Chem.* **27**, 4066 (1988).
80. Weigel, J. A., Holm, R. H., Surerus, K. K., and Münck, E., *J. Am. Chem. Soc.* **111**, 9246 (1989).
81. Norland, B., Sjöberg, V. B. M., and Eklund, H., *Nature (London)* **345**, 593 (1990).

82. Orme-Johnson, W. H., Hansen, R. E., Beinert, H., Tsibris, J. C. M., Bartolomaus, R. C., and Gunsalus, I. C., *Proc. Natl. Acad. Sci. U.S.A.* **60**, 368 (1968).
83. Moulis, J.-M., Auric, P., Gaillard, J., and Meyer, J., *J. Biol. Chem.* **259**, 11396 (1984).
84. Gaillard, J., Moulis, J.-M., Auric, P., and Meyer, J., *Biochemistry* **25**, 464 (1986).
85. Cline, J. F., Hoffman, B. M., Mims, W. B., LaHaie, E., Ballou, D. P., and Fee, J. A., *J. Biol. Chem.* **260**, 3251 (1985).
86. Telser, J., Hoffman, B. M., LoBrutto, R., Ohnishi, T., Tsai, A. L., Simpkin, D., and Palmer, G., *FEBS Lett.* **214**, 117 (1987).
87. Gurbiel, R. J., Batie, C. J., Sivaraja, M., True, A. E., Fee, J. A., Hoffman, B. M., and Ballou, D. P., *Biochemistry* **28**, 4861 (1989).
88. Britt, R. D., Sauer, K., Klein, M. P., Knaff, D. B., Kriauciunas, A., Yu, C.-A., Yu, L., and Malkin, R., *Biochemistry* **30**, 1892 (1991).
89. George, S. J., Armstrong, F. A., Hatchikian, E. C., and Thomson, A. J., *Biochem. J.* **264**, 275 (1989).
90. Armstrong, F. A., *Struct. Bonding* **72**, 137 (1990).
91. Conover, R. C., Kowal, A. T., Fu, W., Park, J.-B., Aono, S., Adams, M. W. W., and Johnson, M. K., *J. Biol. Chem.* **265**, 8533 (1990).
92. Münck, E., Debrunner, P. G., Tsibris, J. C. M., and Gunsalus, I. C., *Biochemistry* **11**, 855 (1972).
92. Hille, R., Hagen, W. R., and Dunham, W. R., *J. Biol. Chem.* **260**, 10569 (1985).
94. Varret, F., *J. Phys. (Paris)* **37**, C6, 437 (1976).
95. Coffman, R. E., and Stavens, B. W., *Biochem. Biophys. Res. Commun.* **41**, 163 (1970).
96. Tsukihara, T., Fukuyama, K., Tahara, H., Katsube, Y., Matsuura, Y., Tanaka, N., Kakudo, M., Wada, K., and Matsubara, H., *J. Biochem. (Tokyo)* **84**, 1645 (1978).
97. Hearshen, D. O., Dunham, W. R., Sands, R. H., and Grande, H. J., in "Electron Transport and Oxygen Utilization" (C. Ho, ed.), p. 395. Elsevier, New York, 1982.
98. Noodleman, L., and Baerends, E. J., *J. Am. Chem. Soc.* **106**, 2316 (1984).
99. Anderson, P. W., and Hasegawa, H., *Phys. Rev.* **100**, 675 (1955).
100. Middleton, P., Dickson, D. P. E., Johnson, C. E., and Rush, J. D., *Eur. J. Biochem.* **88**, 135 (1978).
101. Day, E. P., Peterson, J., Bonvoisin, J. J., Moura, I., and Moura, J. J. G., *J. Biol. Chem.* **263**, 3684 (1988).
102. Snyder, B. S., Patterson, G. S., Abrahamson, A. J., and Holm, R. H., *J. Am. Chem. Soc.* **111**, 5214 (1989).
103. Surerus, K. K., Münck, E., Snyder, B. S., and Holm, R. H., *J. Am. Chem. Soc.* **111**, 5501 (1989).
104. Ding, X.-Q., Bominaar, E. L., Bill, E., Winkler, H., Trautwein, A. X., Drüeke, S., Chaudhuri, P., and Wieghart, K., *J. Chem. Phys.* **92**, 178 (1990).
105. Papaefthymiou, V., Girerd, J.-J., Moura, I., Moura, J. J. G., and Münck, E., *J. Am. Chem. Soc.* **109**, 4703 (1987).
106. Münck, E., and Kent, T. A., *Hyperfine Interact.* **27**, 161 (1986).
107. Hagen, W. R., Dunham, W. R., Johnson, M. K., and Fee, J. A., *Biochim. Biophys. Acta* **828**, 369 (1985).
108. Sands, R. H., and Dunham, W. R., *Q. Rev. Biophys.* **7**, 443 (1975).
109. Girerd, J.-J., Papaefthymiou, V., Surerus, K. K., and Münck, E., *Pure Appl. Chem.* **61**, 805 (1989).
110. Kent, T. A., Huynh, B. H., and Münck, E., *Proc. Natl. Acad. Sci. U.S.A.* **77**, 6574 (1980).

111. Gayda, J. P., Bertrand, P., Theodule, F.-X., and Moura, J. J. G., *J. Chem. Phys.* **77**, 3387 (1982).
112. Münck, E., in "Iron-Sulfur Proteins" (T. G. Spiro, ed.), Chap. 4. Wiley, New York, 1982.
113. Gayda, J. P., Bertrand, P., Guigliarelli, B., and Meyer, J., *J. Chem. Phys.* **79**, 5732 (1983).
114. Bertrand, P., Guigliarelli, B., Meyer, J., and Gayda, J. P., *Biochimie* **66**, 43 (1984).
115. Guigliarelli, B., Gayda, J. P., Bertrand, J., and More, C., *Biochim. Biophys. Acta* **871**, 149 (1986).
116. Guigliarelli, B., More, C., Bertrand, P., and Gayda, J. P., *J. Chem. Phys.* **85**, 2774 (1986).
117. Evans, M. C. W., Hall, D. O., and Johnson, C. E., *Biochem. J.* **119**, 289 (1970).
118. Dickson, D. P. E., Johnson, C. E., Cammack, R., Evans, M. C. W., Hall, D. O., and Rao, K. K., *Biochem. J.* **139**, 105 (1974).
119. Middleton, P., Dickson, D. P. E., Johnson, C. E., and Rush, J. D., *Eur. J. Biochem.* **104**, 289 (1980).
120. Noodleman, L., *Inorg. Chem.* **27**, 3677 (1988).
121. Jordanov, J., Roth, E. K. H., Fries, P. H., and Noodleman, L., *Inorg. Chem.* **29**, 4288 (1990).
122. Banci, L., Bertini, I., and Luchinat, C., *Struct. Bonding* **72**, 113 (1990).
123. Luchinat, C., *J. Inorg. Biochem.* **43**, 239 (1991).
124. Antanaitis, B. C., and Moss, T. H., *Biochim. Biophys. Acta* **405**, 262 (1975).
125. Dunham, W. R., Hagen, W. R., Fee, J. A., Sands, R. H., Dunbar, J. B., and Humblet, C., *Biochim. Biophys. Acta* **1079**, 253 (1991).
126. Hagen, W. R., in "Advanced EPR. Applications in Biology and Biochemistry" (A. J. Hoff, ed.), Chap. 22. Elsevier, Amsterdam, 1989.
127. Beinert, H., and Albracht, S. P. J., *Biochim. Biophys. Acta* **683**, 245 (1982).
128. Aasa, R., and Vänngård, T., *J. Magn. Reson.* **19**, 308 (1975).
129. Isomoto, A., Watari, H., and Kotani, M., *J. Phys. Soc. Jpn.* **29**, 1571 (1970).
130. Johnston, T. S., and Hecht, H. G., *J. Mol. Spectrosc.* **17**, 98 (1965).
131. Venable, J. H., in "Magnetic Resonance in Biological Systems" (A. Ehrenberg, B. G. Malmström, and T. Vänngård, eds.), p. 373. Pergamon, Oxford, 1967.
132. Hagen, W. R., and Albracht, S. P. J., *Biochim. Biophys. Acta* **702**, 61 (1982).
133. Guigliarelli, B., Gayda, J.-P., Bertrand, P., and More, C., *Biochim. Biophys. Acta* **871**, 149 (1986).
134. Hagen, W. R., *J. Magn. Reson.* **44**, 447 (1981).
135. Strong, L. H., Ph.D. Thesis, The University of Michigan, Ann Arbor, Michigan (1976).
136. Hagen, W. R., Hearshen, D. O., Sands, R. H., and Dunham, W. R., *J. Magn. Reson.* **61**, 220 (1985).
137. Hearshen, D. O., Ph.D. Thesis, The University of Michigan, Ann Arbor, Michigan (1983).
138. Hagen, W. R., in "Cytochrome Systems. Molecular Biology and Bioenergetics" (S. Papa, B. Chance, and L. Ernster, eds.), p. 459. Plenum, New York, 1987.
139. Hagen, W. R., Hearshen, D. O., Harding, L. J., and Dunham, W. R., *J. Magn. Reson.* **61**, 233 (1985).
140. Salerno, J. C., and Siedow, J. N., *Biochim. Biophys. Acta* **579**, 246 (1979).
141. Cockle, S., Lindskog, S., and Grell, E., *Biochem. J.* **143**, 703 (1974).
142. Pake, G. E., and Estle, T. L., "The Physical Principles of Electron Paramagnetic Resonance," 2nd Ed., Chap. 4. Benjamin, Reading, Massachusetts, 1973.

143. Oosterhuis, W. T., *Struct. Bonding* **20**, 59 (1974).
144. Hagen, W. R., Dunham, W. R., Sands, R. H., Shaw, R. W., and Beinert, H., *Biochim. Biophys. Acta* **765**, 399 (1984).
145. Von Waldkirch, Th., Müller, K. A., and Berlinger, W. *Phys. Rev. B* **5**, 4324 (1972).
146. Troup, G. J., and Hutton, D. R., *Br. J. Appl. Phys.* **15**, 1493 (1964).
147. Blumberg, W. E., in "Magnetic Resonance in Biological Systems" (A. Ehrenberg, B. G. Malmström, and T. Vänngård, eds.), p. 119. Pergamon, Oxford, 1967.
148. Münck, E., Rhodes, H., Orme-Johnson, W. H., Davis, L. C., Brill, W. J., and Shah, V. K., *Biochim. Biophys. Acta* **400**, 32 (1975).
149. Hagen, W. R., in "Cytochrome Systems. Molecular Biology and Bioenergetics" (S. Papa, B. Chance, and L. Ernster, eds.), p. 459. Plenum, New York, 1987.
150. Morningstar, J. E., and Hales, B. J., *J. Am. Chem. Soc.* **109**, 6854 (1987).
151. Lindahl, P. A., Day, E. P., Kent, T. A., Orme-Johnson, W. H., and Münck, E., *J. Biol. Chem.* **260**, 11160 (1985).
152. Hagen, W. R., 1991. The DOS-program "RHOMBO" computes effective g -values for $S = \frac{1}{2}$ through $\frac{5}{2}$ as a function of rhombicity and real g -value. Available freely upon request.
153. Rawlings, J., Shah, V. K., Chisnell, J. R., Brill, W. R., Zimmermann, R., Münck, E., and Orme-Johnson, W. H., *J. Biol. Chem.* **253**, 1001 (1978).
154. Surerus, K., Münck, E., Moura, I., Moura, J. J. G., and LeGall, J., *J. Am. Chem. Soc.* **109**, 3805 (1987).
155. Verhagen, M. F. J. M., and Hagen, W. R., unpublished results, 1991.
156. Smith, B. E., Lowe, D. J., and Bray, R. C., *Biochem. J.* **130**, 641 (1972).
157. Zimmermann, R., Münck, E., Brill, W. J., Shah, V. K., Henzl, M. T., Rawlings, J., and Orme-Johnson, W. H., *Biochim. Biophys. Acta* **537**, 185 (1978).
158. Watt, G. D., Burns, A., Laough, S., and Tennent, D. L., *Biochemistry* **21**, 4926 (1980).
159. Johnson, M. K., Thomson, A. J., Robinson, A. E., and Smith, B. E., *Biochim. Biophys. Acta* **671**, 61 (1981).
160. Hagen, W. R., Eady, R. R., Dunham, W. R., and Haaker, H., *FEBS Lett.* **189**, 250 (1985).
161. Zambrano, I. C., Kowal, A. T., Mortenson, L. E., Adams, M. W. W., and Johnson, M. K., *J. Biol. Chem.* **264**, 20974 (1989).
162. Hagen, W. R., *Biochim. Biophys. Acta* **708**, 82 (1982).
163. Aasa, R., *J. Chem. Phys.* **52**, 3919 (1970).
164. Dunham, W. R., Hagen, W. R. L., Braaksma, A., Haaker, H., Gheller, S., Newton, W. E., and Smith, B., in "Nitrogen Fixation Research Progress" (H. J. Evans, P. J. Bottomley, and W. E. Newton, eds.), p. 591. Martinus Nijhoff, Dordrecht, The Netherlands, 1985.
165. Bleaney, B., and Scovil, H. E. D., *Philos. Mag.* **43**, 999 (1952).
166. Baker, J. M., and Bleaney, B., *Proc. R. Soc. London A* **245**, 156 (1958).
167. De Groot, M. S., and van der Waals, J. H., *Mol. Phys.* **3**, 190 (1960).
168. Bleaney, B., Llewellyn, P. M., Price, M. H. L., and Hall, G. R., *Philos. Mag.* **45**, 991 (1954).
169. Hendrich, M. P., and Debrunner, P. G., *Biophys. J.* **56**, 489 (1989).
170. Jabłoński, R., Krukowska-Fulde, B., and Niemyski, T., *Mater. Res. Bull.* **8**, 53 (1973).
171. Jabłoński, R., Domańska, M., Krukowska-Fulde, B., and Niemyski, T., *Mater. Res. Bull.* **8**, 749 (1973).
172. Mathews, R., Charlton, S., Sands, R. H., and Palmer, G., *J. Biol. Chem.* **249**, 4326 (1974).

173. LeGall, J., Ljungdahl, P. O., Moura, I., Peck, H. D., Xavier, A. V., Moura, J. J. G., Teixeira, M., Huynh, B. H., and DerVartanian, D. V., *Biochem. Biophys. Res. Commun.* **106**, 610 (1982).
174. Greenaway, F. T., Chan, S. H. P., and Vincow, G., *Biochim. Biophys. Acta* **490**, 62 (1977).
175. Brudvig, G. W., Stevens, T. H., Morse, R. H., and Chan, S. I., *Biochemistry* **20**, 3912 (1981).
176. Gayda, J.-P., Bertrand, P., Deville, A., More, C., Roger, G., Gibson, J. F., and Cammack, R., *Biochim. Biophys. Acta* **581**, 15 (1979).
177. Moura, I., Moura, J. J. G., Münck, E., Papaefthymiou, V., and LeGall, J., *J. Am. Chem. Soc.* **108**, 349 (1986).
178. Butt, J., Armstrong, F. A., Breton, J., George, S. J., Thomson, A. J., and Hatchikian, E. C., *J. Am. Chem. Soc.* **113**, 6663 (1991).
179. Mukund, S., and Adams, M. W. W., *J. Biol. Chem.* **265**, 11508 (1990).
180. Hoffman, B. M., Gurbiel, R. J., Werst, M. M., and Sivaraja, M., in "Advanced EPR. Applications in Biology and Biochemistry" (A. J. Hoff, ed.), Chap. 14. Elsevier, Amsterdam, 1989.
181. Mims, W. B., and Peisach, J., in "Advanced EPR. Applications in Biology and Biochemistry" (A. J. Hoff, ed.), Chap. 1. Elsevier, Amsterdam, 1989.
182. Watt, G. D., and McDonald, J. W., *Biochemistry* **24**, 7226 (1985).
183. Lindahl, P. A., Gorelick, N. J., Münck, E., and Orme-Johnson, W. H., *J. Biol. Chem.* **262**, 14945 (1987).
184. Carney, M. J., Papaefthymiou, G. C., Spartalian, K., Frankel, R. B., and Holm, R. H., *J. Am. Chem. Soc.* **110**, 6084 (1988).

STRUCTURAL AND FUNCTIONAL DIVERSITY OF FERREDOXINS AND RELATED PROTEINS

HIROSHI MATSUBARA and KAZUHIKO SAEKI

Department of Biology, Faculty of Science, Osaka University, Toyonaka, Osaka 560, Japan

- I. Introduction
- II. [2Fe-2S] Ferredoxins and Related Proteins
 - A. Ferredoxins in Oxygenic Photosynthetic Organisms
 - B. Reduction Potential Differences of Ferredoxin Iso-Forms
 - C. Ferredoxins and Related Proteins in Organisms Other Than Oxygenic Photosynthesizers
- III. [4Fe-4S] and [3Fe-4S] Ferredoxins and Related Proteins
 - A. Low-Potential Ferredoxins with a Single [4Fe-4S] or [3Fe-4S] Cluster
 - B. Ferredoxin-Like Proteins in Symbiotic Nitrogen-Fixing Bacteria
 - C. A Highly Thermostable [4Fe-4S] Ferredoxin
 - D. High-Potential Iron-Sulfur Proteins
 - E. Ferredoxins with a Single [3Fe-4S] Cluster in Oxygenase Systems
 - F. Proteins with a Single [4Fe-4S] Cluster Bridging Two Subunits
 - G. Succinate-Fumarate Oxidoreductases
- IV. 2[4Fe-4S] or [4Fe-4S][3Fe-4S] Ferredoxins and Related Proteins
 - A. Photosynthetic Bacterial and *nif*-Related Ferredoxins
 - B. *Azotobacter*-Type [4Fe-4S][3Fe-4S] Ferredoxins
 - C. *Desulfovibrio*-Type [4Fe-4S][3Fe-4S] Ferredoxins
 - D. Functional Differences of Distinct Ferredoxins in a Single Bacterium
 - E. Other Ferredoxins
 - F. F_A/F_B Proteins in Photosystem I Complexes
 - G. Ferredoxin-Like Proteins Encoded by Chloroplast and Cyanobacterial Genes: *frxB*, *orf167*, and *orf178*
- V. Polyferredoxins
- VI. Conclusions
- References

I. Introduction

The term "ferredoxin" was coined by D. C. Wharton (1) and applied to a nonheme iron protein isolated from nonphotosynthetic anaerobic bacteria, *Clostridium pasteurianum* (2, 3). The protein served as an

electron-transferring factor in the phosphoroclastic reaction of pyruvate oxidation linked with nitrogen fixation in this organism. Immediately afterward, another protein isolated from spinach chloroplasts was similarly named ferredoxin on the basis of the exchangeability of the proteins from different organisms in supporting photoreduction of NADP^+ by spinach chloroplasts (4). The presence of inorganic sulfides in these ferredoxins was recognized (5, 6), and these two classes of ferredoxins became the first representatives of iron-sulfur (Fe-S) proteins. However, as further studies have progressed, other ferredoxins of different types and related proteins similar to ferredoxins have been recognized (7-10). There are now five classes of ferredoxins defined in terms of their Fe-S cluster(s): $[2\text{Fe}-2\text{S}]$, $[4\text{Fe}-4\text{S}]$, $[3\text{Fe}-4\text{S}]$, $2[4\text{Fe}-4\text{S}]$, and $[4\text{Fe}-4\text{S}][3\text{Fe}-4\text{S}]$. In each class, however, we see further diverse structures and functions of these proteins, which have been isolated from organisms ranging from higher plants and animals to diverse microorganisms. For some, only the gene structures have been elucidated, and as a consequence of recent rapid progress in gene isolation and sequencing, the functions of their putative proteins can only be speculated. The present review will focus on ferredoxins and related proteins that have been relatively recently reported and that are of interest to the authors. In particular, the diverse structural and functional features of these proteins in one organism are emphasized. For earlier work readers should consult review articles that have appeared previously (7-14).

II. $[2\text{Fe}-2\text{S}]$ Ferredoxins and Related Proteins

A. FERREDOXINS IN OXYGENIC PHOTOSYNTHETIC ORGANISMS

Many, but not necessarily all, oxygenic photosynthetic plants and algae, including cyanobacteria (or blue-green algae), contain at least two molecular species of $[2\text{Fe}-2\text{S}]$ ferredoxin (11-15). These iso-forms function as electron carriers in diverse metabolic pathways, such as the photosynthetic electron transfer chain, nitrite reduction, sulfite reduction, glutamate synthesis, nitrogen fixation, thioredoxin oxidoreduction, and lipid desaturation (16-19), but the distinction between the iso-forms on the basis of their functions has been unclear (20), except for the heterocyst ferredoxin of the nitrogen-fixing cyanobacterium, *Anabaena* (21-25). In general, $[2\text{Fe}-2\text{S}]$ ferredoxins in plants and algae are very acidic (pI values from 3 to 4). They have absorption maxima in the visible region at about 330, 420, and 465 nm in the oxidized state,

with some slight variations depending upon source. On reduction, the absorbances decrease about 50% with no defined absorption maximum. The reduction potentials of these ferredoxins are very low, centered at around -400 mV.

So far, we have complete amino acid sequences of over 75 ferredoxins isolated from land plants (26–50), eukaryotic algae (51–60), and prokaryotic algae (61–85), including those deduced from DNA sequences in several cases (29, 40, 42–44, 70, 72–74, 79, 84, 85). The number of amino acid residues ranges from 93 to 99, giving a molecular mass of about 11 kDa, and they are all homologous, indicating that the molecules have been well conserved over 1.5 billion years, particularly the residues around the $[2\text{Fe}-2\text{S}]$ cluster (11, 86).

Three-dimensional structures of three cyanobacterial ferredoxins are now known (87–89) and show essentially the same polypeptide chain folding motif (Fig. 1). When their sequences are aligned they are representative of two types of this class of ferredoxin (12). The *Spirulina* and *Aphanothece* ferredoxin molecules have a β -barrel-like structure and the $[2\text{Fe}-2\text{S}]$ cluster is held in the polypeptide chain through four Fe–S bonds. Three of these Fe–S bonds are in a loop segment from positions 40 to 49 (*Spirulina* ferredoxin numbering). A hydrophobic core with several conserved residues is present inside the β -barrel-like structure. One of the two iron atoms should be more easily reduced than the other, indicated by the differences in the hydrogen bonding and hydrophobicity around the iron atoms (87, 88). A horsetail (*Equisetum arvens*) ferredoxin I (46) has recently been crystallized and analyzed at 1.8 Å, indicating the presence of small helical structures near positions 65–70 and the C-terminal portion (T. Tsukihara, personal communication, 1991) in addition to those found in the previous analyses (86–88). A crystallographic analysis of *Anabaena* PCC7120 ferredoxin has recently shown some secondary structural differences (89) compared to those previously reported for *Spirulina* ferredoxin (87). The refined analysis revealed four strands of β -pleated sheet and three α -helical segments.

The amino acid sequence of one of the two ferredoxins from *Aphanothece sacrum* (a unicellular cyanobacterium), ferredoxin I (82), has two gaps at positions 10 and 14 in the alignment given in Fig. 1. Ferredoxins of this type include those of all land plants, exemplified by spinach ferredoxin I (27) (Fig. 2a), except for ferredoxins of some tissues or organs as described below, and most of the eukaryotic algae (12); a red alga, *Rhodymenia palmata* (59), in the family Florideophyceae; and a unicellular cyanobacterium, *Synechocystis* 6714 (80). The sequence of *Spirulina platensis* (a filamentous cyanobacterium) ferredoxin (63) has

- (a) -AA-YKVT[.]LT[.]VT-PTG-NVEFQCPDDVYILDAAEEEGIDLPYSC[.]RAGSC[.]SSC[.]
 (b) -SAVKV[.]KLIG-PD[.]QGENEFDV[.]PDDQYILDAAEEAGVDLPYSC[.]RAGAC[.]SSC[.]
 (c) -AT-YKVT[.]LITKESG-TET[.]FDCPDDVYVLDQAE[.]EEGIDLPYSC[.]RAGSC[.]SSC[.]
 (d) -AT-YKVTLINEEEGINAOLEVADDQTILDAGEEAGLDLPSSCRAGSC[.]STC[.]
 (e) -AT-FKVTLINEAEGTKHEIEVPDDEYILDAAEEQGYDLPFSC[.]RAGAC[.]STC[.]
 (f) -AS-YQVRLINKKQDIDTTIEIDEETTIL[.]DGAENGIELPFSC[.]HSGSC[.]SSC[.]
 (g) -AT-YQVEVIY--QGQSQTFTADSDQSVLDSAQAAGVDLPASCLTGVCTTC[.]
 (h) .DDLFEKAADAGLDGEDYGTMEVAEGEYILEAAEAQGYDWPFS[.]CRAGAC[.]ANC[.]
 (i) ---MDKATLTF--TDVSITVNVPTGTRIEMSEKVGSGITYGCREGECGTC[.]
 (j) .GLFVPPPESTVSVRGQGFQFVPRGQTILESALHQGIAP[.]FDCKVGS[.]CGTC[.]
- (a) AGKLTGSL-NQDDQSFLDDDDQIDE-----GWV-LTCAAYPVSDVTIETHKEEELTA
 (b) AGKIEKGQV-DQSEGSFLEDHHFEK-----GYV-LTCVAYPQSDLVITHKEEELF
 (c) AGKV[.]VAGSV-DQSDQSFLDDDDQIEA-----GWV-LTCAAYPSADVTIETHKEEELTA
 (d) AGKLVS[.]GAA[.]PNQDDQAF[.]FLDDDDQLAA-----GWV-MTCVAYPTGDCITMTHQESEVL
 (e) AGKLVS[.]GT[.]V-DQSDQSFLDDDDQIEA-----GYV-LTCVAYPTSDVVIQTHKEEDLY
 (f) VGKVVEGEV-DQSDQIFLDDEQMGK-----GFA-LLCVTYPRSNCTIKTHQEPYLA
 (g) AARILSGEV-DQPDAMGVGPEPAKQ-----GYT-LLCVAYPRSDLKIETHKEDELYALQFGQPG
 (h) ASIVKEGEI-DMDMQQILSDEEVEE-----KDVR[.]LTCIGSPA[.]AEVKIVYNAKHL[.]DYLN[.]
 (i) MTHILEGSE-NLSEPTALEMRVLEENLGGKDDR-LACQCRVLGGAVKVRPA
 (j) KYKLISGRV-NELTSSAM---GLSGDLYQSGYR-LGCQCIPKEDLEIELD[.]TVLGQALVP[.] IET. .

FIG. 2. Amino acid sequences of [2Fe-2S] ferredoxins and ferredoxin-like proteins. Gaps are inserted to align the sequences for maximum homology. Italics show the residues emphasized in the text. (a) Spinach ferredoxin I (27), (b) radish root ferredoxin B-1 (41), (c) *Silene platensis* ferredoxin (40), (d) *Aphanothece sacrum* ferredoxin II (83), (e) *Anabaena* PCC7120 ferredoxin I (70), (f) *Anabaena* PCC7120 heterocyst ferredoxin (73), (g) *Synechococcus* 6301 putative ferredoxin (79), (h) *Halobacterium halobium* ferredoxin (135) (the N-terminal 20 residues are omitted), (i) *Rhodobacter capsulatus* ferredoxin-like protein (139), and (j) *Pseudomonas* XylA protein (161), the sequence of which starts from residue 5 and lacks the C-terminal portion.

no gap at these positions, as also is true of *A. sacrum* ferredoxin II (83) (Fig. 2d) as well as the ferredoxins of many other cyanobacteria, including heterocystous cyanobacteria (73); red algae in the Protofloridaephyceae; and the yellow-green alga, *Bumilleriopsis filiformis* (12, 58). An intermediate form is seen in the ferredoxins of a marine, unicellular green alga, *Bryopsis maxima* (51); three cyanobacteria, *Synechococcus* sp. (76), *Aphanizomenon flos-aquae* (67), and *Nostoc* MAC I (69); and higher plant nonphotosynthetic tissues (41, 42); these have only one gap at position 12 in the alignment given in Fig. 2, as exemplified by radish root ferredoxin I (41) (Fig. 2b). Another intermediate form is found in *Silene platensis* ferredoxin (40) with the gap at position 16 (Fig. 2c). These two positions are located near the corner of the first turn from the N terminus of the polypeptide chain (Fig. 1). Ferredoxins with deletions at both of the two positions always have a proline residue at position 13 (12), which emphasizes the turn at the corner (88). These

two events, the deletions and introduction of proline, probably occurred in concert during evolution (50). *Aphanothece sacrum* has two representative ferredoxins, I and II; the evolutionary implication of this has been discussed elsewhere (50, 83).

Many organisms have iso-forms of ferredoxin; the comparisons of the sequences in phylogenetic trees have revealed the relationships among ferredoxins (11, 12, 56, 90–92) and have led to the interpretation that gene duplications occurred long before speciations (11, 12, 46, 83, 92). Further, it has been suggested that [2Fe–2S] ferredoxins were derived from an ancestral form of clostridial-type 2[4Fe–4S] ferredoxin through unequal crossing-over of genes, differentiation, and translocation (93). Arguments for a common origin for the two different types (27, 31, 90, 94, 95) and counterarguments (see Ref. 8 and references therein) have been given.

The question as to whether the iso-forms of ferredoxin have different functions has not yet been answered by comparisons using various enzymatic assay systems (20, 96, 97), although amino acid compositions and reduction potentials of the iso-forms can be significantly different (13, 14, 69, 98–100). However, a distinct functional difference was found for the ferredoxins of vegetative cells and heterocysts of a nitrogen-fixing filamentous cyanobacterium, *Anabaena variabilis* (21–24).

Most cyanobacteria that fix nitrogen aerobically do so in specialized cells called heterocysts, which develop when the organism is grown in a medium deficient in nitrogen sources (101). Reduced heterocyst ferredoxin donated electrons to both *A. variabilis* nitrogenase and the NADP⁺ photoreduction system, but the vegetative cell ferredoxin was almost inactive in the nitrogenase system, suggesting a unique protein conformation of the heterocyst ferredoxin enabling its interaction with nitrogenase (21). The two ferredoxins showed some differences in their molecular masses, visible absorption spectra, pI values, and electron paramagnetic resonance (EPR) spectra, but their amino acid compositions, immunological properties, and midpoint reduction potentials were significantly different (23). Heterocyst ferredoxin had a reduction potential of –405 mV and vegetative cell ferredoxin had a reduction potential of –433 mV. Heterocysts contained another ferredoxin as a minor component; this was identical to vegetative cell ferredoxin and its function was assumed to be in cyclic photophosphorylation, supplying energy for nitrogen fixation (23, 73).

A related heterocystous cyanobacterium, *Anabaena sphaeria*, was shown to have two ferredoxins with biochemical properties and amino acid compositions that were nearly identical. They differed in molecular mass, 33,600 Da for ferredoxin I and 11,500 Da for ferredoxin II, and

only the latter was an effective electron donor to nitrogenase and hydrogenase (25).

Recently, the structural gene, *fdxH*, for *Anabaena* PCC7120 heterocyst ferredoxin was isolated and sequenced to deduce the encoded amino acid sequence (73) shown in Fig. 2f; for comparison, the amino acid sequence of the vegetative cell ferredoxin is shown in Fig. 2e (70). Both have 98 residues, which is typical for cyanobacterial ferredoxins (12), but 47 out of 98 residues in the aligned sequences are different, with a lesser number of acidic residues in heterocyst ferredoxin giving a higher *pI* value, 3.0, than that (below 2.7) of the vegetative ferredoxin (23). Although only a partial sequence of the N-terminal 40 residues of another heterocyst ferredoxin of *Anabaena* ATCC29413 is available, it is apparent that the number of amino acid differences between heterocyst ferredoxins in different strains of *Anabaena* is much smaller than that between heterocyst ferredoxin and vegetative cell ferredoxin in the same strain (73). This phenomenon is the same as those found for ferredoxin iso-forms in other cyanobacteria (11, 12, 92), but in particular the heterocyst ferredoxins seem to be developed to function specifically in nitrogen fixation. The alterations in amino acids around the Fe-S cluster, a loop region, from Arg 44 of vegetative ferredoxin (in the alignment of Fig. 2) to His of heterocyst ferredoxin, from Ala 45 and 47 to Ser, and from Thr 50 to Ser, might be responsible for the change of reduction potential and for critical interaction with nitrogenase (73). However, in contrast with similar changes at the loop area found between *Nostoc* strain MAC ferredoxins I and II, the reduction potential of a heterocyst ferredoxin appears to be higher than that of the vegetative ferredoxin.

Heterocyst ferredoxin is less acidic than vegetative ferredoxin and the distribution of the sites giving this charge difference was examined using the three-dimensional structural model of *Spirulina platensis* ferredoxin (73). They are positions 68, 12–15, 17–19, 23, 26, 57, 59, 75, 76, 87, 89, 93, 98, and 99. One notable difference was Ser in the vegetative cell ferredoxin and Ile in the heterocyst ferredoxin, at position 67, which is located near the cluster, where other ferredoxins except a putative second ferredoxin from *Synechococcus* (described later) have Ala, Thr, Ser, Asn, Gln, or Ala (Fig. 2). This region was suggested to interact with ferredoxin-NADP⁺ reductase (102, 103). The hydrophobic nature of this area may also be necessary to interact with nitrogenase. However, it is improbable that exchange of comparatively few amino acids would produce the large functional difference of ferredoxins derived by trial and error during evolution; therefore, elucidation of the structure–function relationship of the nitrogenase-specific ferredoxin

must await availability of the three-dimensional structure of the heterocyst ferredoxin. Site-directed mutagenesis experiments may also be useful to study the relationship (104).

Two iso-forms (I and II) of ferredoxin exist in mature spinach leaves (105) as well as in etiolated cotyledons (30). The two spinach ferredoxin sequences have 25 amino acid differences out of 97 residues, reflecting microenvironmental difference at the Fe-S clusters (106, 107).

A ferredoxin in bean sprouts (108) proved to have properties similar to those of spinach ferredoxin. Another ferredoxin was found in bean stems (109). The ratio of these ferredoxins varied during seedling development (30), with the relative content of ferredoxin II compared to ferredoxin I being higher in spinach etiolated tissues. Synthesis of ferredoxin II occurred in contrast with ferredoxin I was light independent. A multifunctional electron carrier encoded by the ferredoxin II gene was present before gene duplication, and was involved with non-photosynthetic electron pathways such as nitrite reduction, glutamate synthesis, etc., in early evolutionary time. The second ferredoxin, I, was produced by gene duplication with functions equivalent to ferredoxin II. These two ferredoxins subsequently became differentiated by accumulating mutations in association with the development of complicated metabolic systems, with the expression of the ferredoxin genes becoming divergent (30). The different expressions of the genes for ferredoxin iso-forms have been observed under variable growth conditions (13, 20, 110, 111). With this likelihood of distinct functions of ferredoxin iso-forms, the tissue- or organ-specific expression of ferredoxin genes in higher plants has become a target of recent research (41, 42, 96, 112-115).

Maize, a C_4 plant that evolved relatively recently, has a CO_2 fixation pathway modified from C_3 plants such as spinach. In maize, cell differentiation has occurred such that the bundle sheath cells have chloroplast thylakoids that differ morphologically from those of C_3 plants, whereas mesophyll cells retain thylakoids similar to those of C_3 plants but have a changed chloroplast enzymology (116). Four ferredoxin iso-forms [and possibly one more (42)] were isolated from maize seedlings. All four iso-forms, I-IV, were present in green and etiolated leaves, but only ferredoxins III and IV were detected in nonphotosynthetic organs such as mesocotyl and root. Ferredoxins I and II, the leaf-specific iso-forms, were light dependent, suggesting that they were involved in photosynthesis, but the non-organ-specific ferredoxins III and IV were light independent (115). Ferredoxin I was found in mesophyll and bundle sheath cells, but ferredoxin II was found only in bundle sheath cells. Although distinct functions of these four ferredoxins are still

obscure, the occurrence of a specific iso-form of ferredoxin, ferredoxin II in this case, in bundle sheath chloroplasts suggested this was adapted to a specific metabolic role in these chloroplasts (115).

Three maize ferredoxin cDNAs were cloned and sequenced to deduce the amino acid sequences of these iso-forms (42). The transit peptide of ferredoxin III was different from those of the other two leaf-specific ferredoxins (40, 43, 44, 117). The control of gene transcription was light independent. This ferredoxin was found in all tissues as described earlier, but the others were found only in leaves. The amino acid sequences of these three ferredoxins were compared (42) and the homology between ferredoxins I and III was about 64% compared with 70–80% among leaf-specific ferredoxins from maize and other plants (42). Similar differences were previously reported for radish and spinach ferredoxins isolated from leaves and roots (41, 114). Thus, ferredoxins of the same tissues (leaf or root) in different plant species (maize and radish) are more similar to each other than those of leaf and root of the same plant species.

It is interesting to note that the N-terminal region of maize ferredoxin III (115) shows only one gap in the alignment, at position 12 (Fig. 2), as is found for radish root ferredoxin B-1 (41) (Fig. 2b). Other ferredoxins were in this respect similar to spinach leaf ferredoxin (Fig. 2a), indicating that the root and light-independent ferredoxins are structurally intermediate between those of light-dependent (or phototrophic) ferredoxins, which might have evolved later, and the cyanobacterial ferredoxins, probably the most primitive ones.

The unique structural characteristics described for radish white root ferredoxins (R-Fds) B-1 and B-2 suggested that such root- (or nonphotosynthetic tissue)-specific ferredoxins might exist in all other angiosperms (41). Although these iso-forms of ferredoxin could not clearly be distinguished in terms of electron-donating function to the ferredoxin-dependent enzymes so far examined, they may differ in electron-accepting function from NADPH via a ferredoxin-dependent oxidoreductase in nonphotosynthetic tissues (41, 97). An enzyme similar to ferredoxin-NADP⁺ reductase was actually found in roots (118). This line of investigation was extended to spinach roots (114). Spinach root ferredoxin showed exactly the same structural characteristics at the N-terminal region as those of radish and maize root ferredoxins, as mentioned earlier; spinach root ferredoxin-NADP⁺ reductase also showed a unique N-terminal sequence, having a shorter sequence at, and an insertion near, the N terminus, compared with the spinach leaf enzyme. What, then, is the functional difference between these iso-forms? As discussed above, functional difference is closely linked to tissue develop-

ment. Specific tissues have their specific functions; the possible roles of root ferredoxins have been proposed (114).

A ferredoxin-like electron carrier was also isolated from nongreen cultured tobacco callus cells, and donated electrons to nitrite reductase but it did not function in an NADP^+ photoreduction system (119). The absorption spectrum and molecular size were somewhat different from those usual for ferredoxins, and the N-terminal sequence was quite different (K. Wada, personal communication).

Several ferredoxin sequences are known for strains of *Synechococcus* (74, 76–79), a unicellular cyanobacterium. Unexpectedly, *Synechococcus* 6301 (*Anacystis nidulans*) ferredoxin resembled most closely ferredoxins of filamentous heterocystous cyanobacteria (61, 62, 67, 72). Moreover, another ferredoxin sequence identified in the same organism (120), based on its gene sequence, showed a marked difference, more than 54 residues, from the soluble ferredoxin in cell extracts, with an eight-amino acid extension at the C terminus compared with all others (79) (Fig. 2g). Furthermore, from the alignment given in Fig. 2, it shows consecutive gaps at positions 12 and 13 not found in other cyanobacterial ferredoxins. The C-terminal extensions, though only three or four residues, are present in *Halobacteria* ferredoxins as described below, but the sequences show little similarity. A hydropathy plot of the ferredoxin deduced from the gene sequence was significantly different from those of other ferredoxins, particularly at the region contributing to iron chelation, although major structural features in the three-dimensional structure of *S. platensis* ferredoxin (87) are probably preserved with some difference in surface charge distribution (78).

A functional difference of this ferredoxin was suggested (79), but detailed experimental evidence to support this are lacking since efforts to isolate the gene product were unsuccessful (78). Trace amounts of minor ferredoxins were reported for some cyanobacteria—*Spirulina maxima* (100), *Microcystis aeruginosa* (121), and *Aphanizomenon flos-aquae* (121)—and growth conditions affected the ratio of the iso-forms. The latter two cyanobacteria contained membrane-bound ferredoxins (121), and the hydropathy profile of the *Synechococcus* gene product suggests this might also be the case (78), but it cannot be excluded that this gene was a pseudogene. The N-terminal sequence of a membrane-bound ferredoxin isolated from *M. aeruginosa* was determined to be A-K-K-I-K-T-T-T- (121), which is unusual and suggests it might be an extension at the N terminus. Its absorption spectrum was also unusual (121), but in the absence of more detail the function and structure of this membrane-bound form remain enigmatic. Another membrane-bound ferredoxin, solubilized by detergent, was found in small quantity

in *A. flos-aquae*, but this ferredoxin showed similarity to those of the usual cyanobacterial ferredoxins. The physiological significance of this ferredoxin is unclear.

B. REDUCTION POTENTIAL DIFFERENCES OF FERREDOXIN ISO-FORMS

Two ferredoxins, I and II, isolated from a cyanobacterium, *Nostoc* strain MAC, showed a marked difference in midpoint reduction potential, -350 mV for ferredoxin I and -455 mV for ferredoxin II (99, 100), and also in their activities in NADP^+ photoreduction and the phosphoroclastic reaction system (98, 122). They have 34 amino acid differences, probably reflecting the different biophysical properties of the two ferredoxins (69). *Chlorogloeopsis fritschii* ferredoxin (62) and *Synechocystis* 6714 ferredoxin (80) showed very similar reduction potentials and enzymatic activities compared to those of *Nostoc* MAC ferredoxin I (123). Further, in amino acid sequence, *Chlorogloeopsis* and *Synechocystis* ferredoxins showed 18 and 25 amino acid differences from *Nostoc* ferredoxin I and 25 and 35 differences from *Nostoc* ferredoxin II, respectively, indicating the latter ferredoxin to be markedly different from the others. These distinctions were visualized on the three-dimensional structure model based on *S. platensis* ferredoxin (69) as shown in Fig. 3. Unique amino acid changes in each ferredoxin, when compared with the others, were identified and most of the unique changes found in *Nostoc* ferredoxin II were located near the Fe-S cluster within 10 \AA of the cluster center. The low reduction potential of *Nostoc* ferredoxin II presumably results from the distribution of unique amino acid residues near the cluster, conferring its distinct biological properties (69).

C. FERREDOXINS AND RELATED PROTEINS IN ORGANISMS OTHER THAN OXYGENIC PHOTOSYNTHESIZERS

1. Halobacterial Ferredoxins

Two ferredoxins with a $[2\text{Fe}-2\text{S}]$ cluster were isolated from *Halobacterium halobium* (124, 125) and *Halobacterium* of the Dead Sea (126), extremely halophilic bacteria. Spectroscopic properties, the acidic nature of proteins, reduction potentials (-340 to -345 mV), and the contents of nonheme iron and inorganic sulfur atoms indicated that the proteins closely resembled those of chloroplast ferredoxins except that the molecular masses were larger, about 15 kDa (compared to 11 kDa (124–126). Immunological studies suggested the halophilic bacterial ferredoxins and chloroplast ferredoxins differed, but the bacterial ferre-

doxins themselves showed 80% antigenic cross-reactivity (127). *Halobacteria* do not perform photosynthesis, nitrogen fixation, or hydroxylation reactions, and these ferredoxins would not mediate electron transfer reactions in NADP^+ photoreduction by chloroplasts (125, 126) or ferredoxin-dependent cytochrome *c* reduction mediated by ferredoxin- NADP^+ reductase (126). *Halobacteria halobium* ferredoxin would function as an electron carrier in α -ketoacid decarboxylation of α -ketoglutarate, pyruvate, and α -ketobutyrate, as would a cyanobacterial ferredoxin (see Ref. 128 and references therein). Another ferredoxin from *Halobacteria* of the Dead Sea functioned in nitrite reduction (129), as would algal and plant ferredoxins. An interesting finding with the ferredoxin from *Halobacteria* of the Dead Sea was that it accepted electrons from the photosystem on illumination, but would not participate *in vitro* in further transfer of electrons to ferredoxin- NADP^+ reductase (130). This was also observed for the *H. halobium* ferredoxin (T. Hase, personal communication, 1980). This observation implies that halobacterial ferredoxins have a conformation different from those of chloroplast ferredoxins and that they probably failed to interact with the ferredoxin- NADP^+ reductase in forming the ternary complex of ferredoxin, reductase, and NADP^+ , as observed for chloroplast-type ferredoxins (131–134).

The amino acid sequences of these two halobacterial ferredoxins are known (135, 136) and that for *H. halobium* ferredoxin is given in Fig. 2h. Both ferredoxins have extensions of about 20 residues at their N termini and of 3 to 4 residues at their C termini, compared with those of chloroplast ferredoxins, making a total of 128 amino acid residues. The four cysteines essential for $[2\text{Fe}-2\text{S}]$ cluster formation are arranged just as in chloroplast ferredoxins. There is a high degree of homology between halobacterial ferredoxins and chloroplast ferredoxins (135, 136). Halobacterial and chloroplast-type ferredoxin residues either identical to or similar to each other are mainly located near the functionally important cysteine residues (135, 137). The lysine residue at position 118 in both ferredoxins was acetylated; the biological significance of this is unclear. The N-terminal region contains many acidic residues (36–41% of the 22 residues) and no basic residues. This might be a consequence of the adaptation of the organism to life in high salt concentrations (135, 137), or these structural features might imply some specific function for the halobacterial ferredoxins.

The three-dimensional structure of ferredoxin of *Halobacterium* of the Dead Sea (137, 138) was elucidated to see whether the tertiary fold of the *Spirulina* ferredoxin (87) could be discerned in the electron density map of the halobacterial ferredoxin. Most of the electron density

profile, as expected from the sequence comparison (102), fitted well except an unusual feature interpreted as belonging to the N-terminal region of the halobacterial ferredoxin, which seemed to form a separate domain remote from the cluster (137). The [2Fe-2S] cluster region was quite similar to that of *Spirulina* ferredoxin and was not protected by any acidic residues (137). Refinement of these data is now in progress and preliminary analysis suggests that one of the β strands at the extreme N-terminal region found in *Spirulina* ferredoxin (87) is missing in the halobacterial ferredoxin, and that the acidic N-terminal region projects toward the Fe-S cluster region, although other regions are likely to be in a folding configuration similar to that of *Spirulina* ferredoxin (K. Fukuyama, personal communication, 1991). More detailed analysis will enable correlation of the unique structural features with the specific functions of halobacterial ferredoxins.

Comparison of the amino acid sequences of *Spirulina* ferredoxin (or any one of the other plant-type ferredoxins) and the halobacterial ferredoxins showed a marked difference at position 85, which is Tyr for *Spirulina* ferredoxin, Phe or Ile for the others, and Ser for the halobacterial ferredoxins. The side chain at this position is oriented toward the outside of the molecule; therefore, this region of the chloroplast ferredoxins would interact readily with residues on adjacent proteins (87), and probably with ferredoxin-NADP⁺ reductase (88, 95, 102, 103), whereas halobacterial ferredoxin cannot interact with the reductase.

2. *Rhodobacter Ferredoxin*

A gene (*fdxC*) coding for a protein similar to the chloroplast-type [2Fe-2S] ferredoxins has recently been found in the nitrogen fixation gene (*nif* gene) clusters of *Rhodobacter capsulatus* SB1003, a photosynthetic purple nonsulfur bacterium (139). It was located just upstream of *fdxN* (Section IV,A), which encodes ferredoxin I, and the amino acid sequence deduced from its nucleotide sequence is given in Fig. 2i. A similar observation was also reported for a partial sequence of the corresponding *R. capsulatus* B10 gene (140), but with some differences. The sequence showed the four conserved cysteine residues, which would be able to chelate two iron atoms as in chloroplast-type ferredoxins. A comparison of this sequence and the sequence of horsetail or spinach ferredoxin showed that they had low but significant similarities to 24 or 18 corresponding residues, respectively (see Fig. 2). This sequence is also similar to those of [2Fe-2S] ferredoxin-like proteins that function in oxygenase systems (Fig. 2j), as described later. Aerobic nitrogen-fixing bacteria such as *Azotobacter vinelandii* must have mechanisms to protect the oxygen-sensitive nitrogenase when fixing nitrogen. Azo-

tobacter [2Fe–2S] ferredoxin (ferredoxin II), which is coinduced with the nitrogenase, has been assumed to function in protecting the oxygen inactivation of nitrogenase (141); we may speculate that any trace amount of oxygen is trapped by the oxygenase system to keep the environment of the nitrogenase oxygen free.

A mutant of *R. capsulatus* SB1003 with the *fdxC* gene engineered to eliminate the region near the Fe–S center with three cysteines would not grow on a medium containing no fixed nitrogen under illuminated anaerobic conditions; the wild-type bacteria grew rapidly under these conditions (142). The mutant grew on media with fixed nitrogen under either illuminated anaerobic or dark aerobic conditions. In conjunction with data from a complementation experiment, it was concluded that the *fdxC* gene product, a chloroplast-type [2Fe–2S] ferredoxin, is required for nitrogen fixation in *R. capsulatus* (142). A flavodoxin-like gene was found upstream of *fdxC* (143). A recent paper has reported that the *fdxC* gene was coexpressed with the ferredoxin I gene (*fdxN*) in *Escherichia coli* and that the product contained a [2Fe–2S] cluster (144), confirming a previously reported result (142). The protein was suggested to be involved in nitrogen fixation, which was in accord with the data obtained by the gene modification experiments mentioned above.

Other ferredoxin groups with a [2Fe–2S] cluster are found in several bacteria and also function in oxygenation and other reaction systems. These have been reviewed in detail elsewhere (8, 9), thus only a few groups are discussed in the following sections.

3. *Clostridium Ferredoxin*

A [2Fe–2S] ferredoxin was found in *Clostridium pasteurianum*, when it was grown with N₂, in addition to the typical 2[4Fe–4S] ferredoxin (see Refs. 8, 145, and 146 and references therein). The magnetic properties and amino acid sequence (102 residues) of the [2Fe–2S] ferredoxin were different from those of other [2Fe–2S] ferredoxins. Figure 4 compares the sequences of several ferredoxins, emphasizing the distribution of the cysteine residues, some or all of which will chelate the two iron atoms, depending on the particular ferredoxin. The fact that the *C. pasteurianum* ferredoxin (Fig. 4a) was a dimer and contained two [2Fe–2S] clusters is rather unique (146). Although its function is not definitely assigned, it will transfer electrons in the hydrogenase system (147) and may show relatedness to nitrogen fixation genes (146). From the sequence the secondary structure could be predicted, providing a basis for suggesting that there were several ferredoxin groups that originated from different ancestors (8, 9). Another [2Fe–2S] ferredoxin

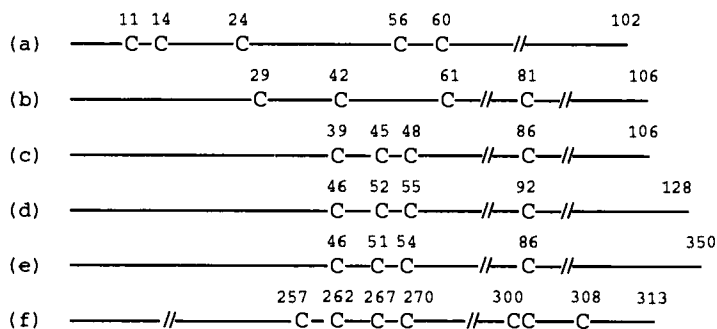


FIG. 4. Distribution of cysteine residues of various [2Fe-2S] ferredoxins and ferredoxin-like proteins. Cysteine residues (denoted by C) are the candidates for chelating the two iron atoms. (a) *Clostridium pasteurianum* [2Fe-2S] ferredoxin (146), (b) *Pseudomonas putida* ML2 protein B (155), (c) *P. putida* [2Fe-2S] ferredoxin (putidaredoxin) (150) (the four cysteine residues being assigned) (151), (d) bovine adrenodoxin (157, 170-172) (the four cysteine residues being assigned) (158), (e) *Pseudomonas* XylA protein (161), and (f) *Pseudomonas* VanB protein (164).

was isolated from a photosynthetic bacterium, *Rhodopseudomonas marina* (148), and proved similar to that of *Rhodopseudomonas palustris* (149) but was without marked resemblance to the clostridial [2Fe-2S] ferredoxin.

4. Ferredoxins in Oxygenase Systems

Pseudomonas putida, an aerobe, produces a [2Fe-2S] ferredoxin, putidaredoxin, which functions in the camphor methylene hydroxylase system (150). However, when the bacterium was grown on a medium containing various aromatic substrates, corresponding multicomponent oxygenating enzyme systems were induced with [2Fe-2S] ferredoxins of the putidaredoxin type (see Refs. 9 and 152 and references therein). Among them, a [2Fe-2S] ferredoxin, isolated as protein B from *P. putida* utilizing benzene as its sole carbon source, was found to function as an electron carrier in the benzene dioxygenase system (153, 154). The amino acid sequences of the ferredoxin from *P. putida* strain ML2 (106 residues) (155) and strain BE-81 (91 residues deduced from DNA sequencing) (156) showed that the former (Fig. 4b) has 15 additional residues at the N terminus compared to the latter, but there were only five amino acid differences throughout the rest of the polypeptide chain. Since the distribution of cysteine residues in the ML2 strain ferredoxin is completely different compared to putidaredoxin (150) (Fig. 4c) and adrenodoxin (157) (Fig. 4d), this ferredoxin comprises a new class. The

location of histidine near a cysteine was assumed to be responsible for the somewhat higher reduction potential of this ferredoxin (155).

A putidaredoxin-type [2Fe-2S] ferredoxin isolated from an anaerobic protozoan, *Trichomonas vaginalis*, was found to function in the pyruvate oxidation system (159); the sequence of this ferredoxin was closest to that of putidaredoxin (160).

Pseudomonas putida xylene monooxygenase consists of two nonidentical subunits and catalyzes the oxidation of toluene and xylene. The nucleotide sequences of the corresponding genes revealed that the deduced amino acid sequence of the XylA product (350 residues) showed a very high similarity, at the N-terminal 90 residues, to plant [2Fe-2S] ferredoxin sequences (161) (Figs. 2j and 4e). A further interesting fact is that the rest of the sequence was very similar to those of ferredoxin-NADP⁺ reductases (162, 163). Therefore, this subunit, which supplies electrons to a second subunit that participates in hydroxylation of the substrate carbon side chain, was formed by the fusion of a plant ferredoxin gene and a ferredoxin-NADP⁺ reductase gene (161). Similarly, the C-terminal region of the VanB component of vanillate demethylase (313 residues) (Fig. 4f) (164) and the N-terminal regions of the MmoC component (protein C) of methane monooxygenase (347 residues) (165) and a polypeptide-5 of phenol hydroxylase (353 residues) (166) have sequences similar to those of plant-type ferredoxins.

Mitochondrial adrenodoxin-type [2Fe-2S] ferredoxins functioning in cytochrome *P*-450-linked monooxygenase systems have been isolated from animal tissues: adrenocortex (adrenodoxin), ovary, thyroid, placenta, kidney (renodoxin), liver (hepatoredoxin), brain, and others (see Ref. 167 and references therein, 168).

The amino acid sequence of adrenodoxin was different from those of hepatoredoxin (167) and reno(re)doxin (169). In addition to adrenodoxin and reno(re)doxin, larger molecular species of about 1.5 kDa have been found in both porcine kidney and bovine adrenal mitochondria (169); these species were named Trp-ferredoxin because of the presence of tryptophan, not usually found in these proteins. Trp-ferredoxins isolated from both tissues were structurally similar to each other, but different from ferredoxins, adrenodoxin, and reno(re)doxin, of the same tissues. Further, Trp-ferredoxin was the major component in kidney, but the minor one in adrenal gland, indicating some functional distinction in different tissues, as discussed earlier for plant ferredoxins.

The amino acid sequence of bovine adrenodoxin (114 residues) as established initially (157) was later shown, when the encoding nucleotide sequence was established (170-172), to be of a partially degraded protein lacking 14 amino acids at the C-terminal region of the original

protein (Fig. 4d). A nondegraded adrenodoxin was later isolated (173), confirming that the mature adrenodoxin was composed of 128 residues. The amino acid sequence of porcine adrenodoxin is known from protein sequencing (174); the amino acid sequences of chicken (175) and human (168, 176) adrenodoxin have been determined from nucleotide sequencing. Two [3Fe-4S] ferredoxins functioning in an oxygenation reaction are also known and are mentioned in Section III,E.

5. Proteins in Respiratory Chain Complexes

Bovine heart mitochondrial complex II, succinate-ubiquinone oxidoreductase, is composed of four subunits; the larger two, 70 and 27 kDa, respectively, are the subunits of succinate dehydrogenase (SDH) (177). The 70-kDa subunit contains a covalently bound flavin. The enzyme has three Fe-S clusters, S-1, S-2, and S-3, distributed equally between the two subunits. Clusters S-1 and S-2 are of the [2Fe-2S] and [4Fe-4S] type and S-3 is of the [3Fe-4S] type, with these cluster structures having originally been assigned by mainly spectroscopic analyses (178). The enzymes were also isolated from several microorganisms: *Neurospora crassa* (179), *Bacillus subtilis* (180), *Micrococcus luteus* (181), *E. coli* (182, 183), and *Paracoccus denitrificans* (184). Amino acid sequence analyses of the subunits added further information about those amino acid residues, most probably cysteine residues, that held the Fe-S clusters, by comparing the cysteine distributions on the sequences (Fig. 5). Complete amino acid sequences deduced from DNA sequencing of the SDH genes of *E. coli* (182, 183), *B. subtilis* (185), and yeast (186), and partial sequences of SDH of several species, including mammals,

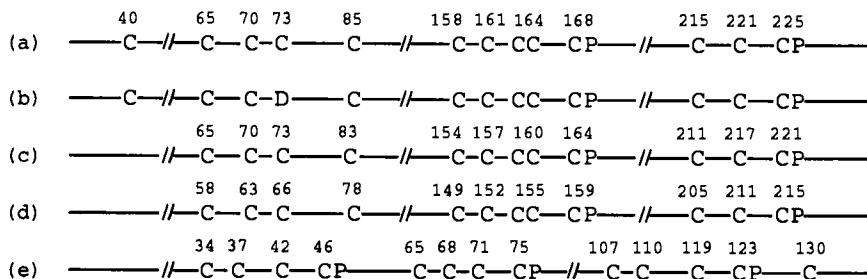


FIG. 5. Cysteine distributions of succinate dehydrogenase and fumarate reductase. Succinate dehydrogenase: (a) bovine (188) [yeast (186) shows essentially the same cysteine distribution as that of the bovine enzyme]; (b) *E. coli* (183) and (c) *Bacillus subtilis* (185). Those of human, rat, *Drosophila melanogaster*, *Arabidopsis thaliana*, and yeasts have been partially sequenced (187). Fumarate reductase: (d) *E. coli* (190) [*P. vulgaris* (192) shows essentially the same cysteine distribution as that of the *E. coli* enzyme] and (e) *P. vulgaris orfA*-encoded product (192).

insects, plants, and yeasts (187), as well as the results from direct protein sequencing of the bovine enzyme (188), are now available. The structure of fumarate reductase (FRD), the terminal reductase of an anaerobic respiration system, from *E. coli* (189–191), *Proteus vulgaris* (192), and *Wolinella succinogenes* (193) is similar in composition and cluster form to the structure of SDH (see Ref. 194 and references therein), and FRD and SDH sequences are also known to be similar.

Flavin-containing subunits of both SDH and FRD showed no apparent structural similarity to ferredoxins in terms of cysteine distribution; rather the cysteines were scattered along the whole sequences, leading to the suggestion that the three clusters in these enzymes may be held exclusively by the iron protein subunit (178, 195), since these showed very similar structural characteristics to those of ferredoxins in terms of cysteine distribution (Fig. 5). There are apparently three groups of cysteines, I to III. The arrangement of cysteines in group I is similar to those of the plant [2Fe–2S] ferredoxins (105), but *E. coli* SDH iron protein subunit has aspartic acid at the position corresponding to the third cysteine of cluster I. Therefore, the [2Fe–2S] cluster may be held by Cys 65, Cys 70, and two other cysteines, possibly Cys 85 and either another Cys from the iron protein subunit or one from the flavoprotein subunit. However, based on gene mutation analysis, the [2Fe–2S] cluster of *B. subtilis* SDH (196) is probably in the first cysteine group, I. For FRD, the [2Fe–2S] and [3Fe–4S] clusters are suggested to be entirely in the iron–protein subunit based on site-directed mutagenesis of the gene from *E. coli*, and the [4Fe–4S] cluster is probably in the flavoprotein subunit or bridges the two subunits (197). The [2Fe–2S] clusters of these two enzymes have reduction potentials and spectroscopic properties different from those of plant ferredoxins (178, 197). Another mutation experiment of *E. coli* FRD indicated that the four cysteine residues in group I are essential for the formation of a functional center 1, [2Fe–2S] cluster, but a noncysteinylligand cannot be excluded (198). Therefore, a final conclusion concerning the cluster awaits further results.

There are further proteins with [2Fe–2S] cluster(s) in respiratory and photosynthetic electron transfer systems, such as the Rieske Fe–S proteins of cytochrome *bc*₁ and *b₆f* complexes and the Fe–S proteins of complex I, NADH dehydrogenase (177, 199), but these are not reviewed here.

III. [4Fe–4S] and [3Fe–4S] Ferredoxins and Related Proteins

In this section we shall deal with a range of proteins with [4Fe–4S] or [3Fe–4S] clusters; a number of these, including aconitase (7), nitrite

reductase (200), sulfite reductase (200), trimethylamine dehydrogenase (201) and some others, are beyond the scope of this review, and some of the bacterial ferredoxins have been previously reviewed (9, 10).

A. LOW-POTENTIAL FERREDOXINS WITH A SINGLE [4Fe-4S] OR [3Fe-4S] CLUSTER

Several bacteria produce ferredoxins with only a single [4Fe-4S] or [3Fe-4S] cluster. These cluster types are interconvertible under certain conditions and the biological significance of the presence of a [3Fe-4S] cluster remains to be clarified (9), whether it occurs singly or in the [4Fe-4S][3Fe-4S] ferredoxins described later.

Bacteria with a single cluster include *Bacillus polymyxa* (9), several species of sulfate-reducing bacteria, *Desulfovibrio* (9, 202), the thermophile *Clostridium thermoaceticum* (203), *Clostridium formicoaceticum* (204), probably *Methanosarcina thermophila* (205), *Spirochaeta aurantia* (206), *Rhodopseudomonas marina* (148), the thermophiles *Bacillus stearothermophilus* (207) and *Bacillus thermoproteolyticus* (208), and a hyperthermophilic bacterium, *Pyrococcus furiosus* (209), which will be described in Section III,C. Their ferredoxins are variously involved in oxidoreduction reactions of bacterial nitrate reduction, sulfite reduction, CO₂ reduction, and pyruvate oxidation (9). Amino acid sequences of some of these ferredoxins are known: *Desulfovibrio gigas* [4Fe-4S] ferredoxin I, which is a trimer (210), and [3Fe-4S] ferredoxin II, which is a tetramer (9 and references therein); *Desulfovibrio africanus* [4Fe-4S] ferredoxin I (211); *Desulfovibrio desulfuricans* Norway [4Fe-4S] ferredoxin I (212); *D. vulgaris* Miyazaki [4Fe-4S] ferredoxin II (202); *B. stearothermophilus* (213) and *B. thermoproteolyticus* [4Fe-4S] ferredoxins (214); and *C. thermoaceticum* [4Fe-4S] ferredoxin (215).

Figure 6 compares the sequences of ferredoxins with a single [4Fe-4S] cluster. Among them the three-dimensional structures of *D. gigas* ferredoxin (216) and *B. thermoproteolyticus* ferredoxin (214, 217) are known.

The two closely related thermophilic bacterial ferredoxins have 81 amino acid residues, but the others have about 60 residues. They have only four common cysteine residues chelating four iron atoms, which conform to one [4Fe-4S] cluster out of the two found in clostridial-type 2[4Fe-4S] ferredoxins, as shown in the three-dimensional structure of *Peptococcus aerogenes* ferredoxin (218, 218a). The apparent sequence homology observed in these [4Fe-4S] ferredoxins indicated that they must have a common tertiary structure, and also they might in part

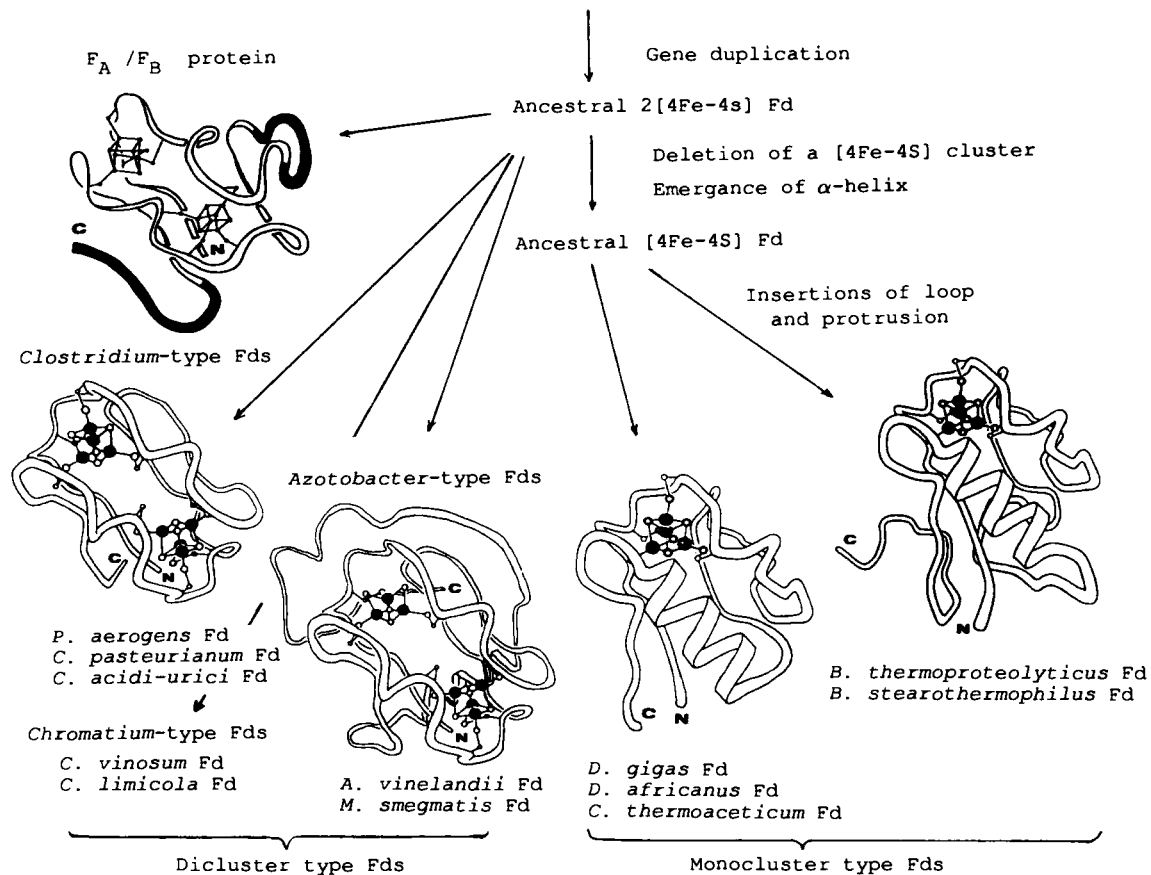
	10*	*	*	20	30	40	50	60*	70	80
(a)	PKYTIVDKETCIACGACGAAAPDIYDYDEDGI	-	AYVTLDDNQGIVEVP	-	DILIDDMDAFEGCPTESIKVADEPF	GDGDPNKF				
(b)	PKYTIVDKETCIACGACGAAAPDIYDYDEDGI	-	AYVTLDDNQGIVEVP	-	DILIDDMDAFEGCPTDSIKVADEPF	GDGDPNKF				
(c)	ARKFYVDQDECIACESCVEIAPGAFAMDPEIEKAYVKD	-	-	-	-	-	-	V-EGASQEEVEEAMDTCPVQSIEE		
(d)	PIEVNDD-CMACEACVEICPDVFEMNEEGDKAVVIN	-	-	-	-	-	-	P-DSDLDCVEEAIDSCPAEAI		
(e)	TIVIDHEECIGCESCVELCPEVFAMIDGEEKAMVTA	-	-	-	-	-	-	P-DSTAECAQDAIDACPVEAISKE		
(f)	AKYLYLDQDECMACESCVELCPEAFRMSAGEYAEVID	-	-	-	-	-	-	P-NTTAECVEDAISTCPVECIEWREE		
(g)	MKVTVDDQLCIACGTCIDLCPSVFDWDEGLSHVIVD	-	-	-	-	-	-	EVPEGAEDSCARESVMNECPTEAIKEV		
(h)	TMRVSADRTVCVGAGLCALTAPGVFDQDDGIVTVLTA	-	-	-	-	-	-	EPAADDDRRTAREAGHLCPSGAVRVVEDTE		
(i)	MRIHVDQDKCCGAGSCVLAAPDVFDQREEDGIVVLLD	-	-	-	-	-	-	TAPPAALHDAVREAATICPAAAITVTD		
(j)	AYVINDSCIACGACKPECP-VN--IQQG-SIY							ADSCIDCGSCASV-CPVGAPNPED		
		*	*	*					*	

FIG. 6. Amino acid sequences of [4Fe-4S] and [3Fe-4S] ferredoxins. Position number is for the *Bacillus* ferredoxins. Gaps are inserted to align the sequences for maximum homology. Positions for cluster-binding cysteine residues are indicated by asterisks. (a) *Bacillus stearothermophilus* (213), (b) *Bacillus thermoproteolyticus* (214), (c) *Desulfovibrio africanus* I (211), (d) *Desulfovibrio gigas* I (210), (e) *Desulfovibrio desulfuricans* Norway I (212), (f) *Desulfovibrio vulgaris* Miyazaki II (202), (g) *Clostridium thermoaceticum* (215), (h) *Streptomyces griseolus* [3Fe-4S] ferredoxin 1 (265), (i) *S. griseolus* [3Fe-4S] ferredoxin 2 (265), and (j) *Peptococcus aerogenes* (i.e., *Peptostreptococcus asaccharolyticus*) 2[4Fe-4S] ferredoxin (218a).

have a folding similar to that of *P. aerogenes* ferredoxin, although the primary structures of these two classes are diverse except for the region around the first cluster of *P. aerogenes* ferredoxin. Figure 7 suggests evolutionary trends with model drawings of the tertiary structures of four of the bacterial ferredoxins (adapted from Refs. 214 and 219) and one ferredoxin-like protein isolated from the photosynthetic reaction center (see Section IV,F). The [4Fe-4S] cluster of *B. thermoproteolyticus* ferredoxin is located at the top surface of the molecule and is geometrically identical to those of *P. aerogenes* ferredoxin (218). Hydrophobic residues surround the Fe-S cluster and the Ile 66, which is close to the cluster, is conserved in all [4Fe-4S] ferredoxins (Fig. 6).

The main chain topology of *B. thermoproteolyticus* ferredoxin with 81 residues is remarkably similar to that of *P. aerogenes* ferredoxin with 54 residues and the 2[4Fe-4S] clusters, and the conformations around the Fe-S clusters of *B. thermoproteolyticus* and the first cluster in *P. aerogenes* ferredoxin are superimposable. The NH-S hydrogen bonds and other segments of the upper half of the molecule are very similar to each other (214). The lower half of *B. thermoproteolyticus* ferredoxin molecule shows differences in topology and sequence from those of *P. aerogenes* ferredoxin, as seen in Fig. 7. The sequence Ile 51 to Gly 60 of *B. thermoproteolyticus* ferredoxin forms an α -helix, which corresponds to the second cluster of *P. aerogenes* ferredoxin, including Cys 53 and 56. A total of about 10 residues is inserted in *B. thermoproteolyticus* ferredoxin compared with the others and forms a loop structure, which can be deleted with three remaining residues without affecting helix formation (214). The C-terminal region of *B. thermoproteolyticus* ferredoxin has an extension of about 10 residues compared with the others. The other localized twofold symmetry observed in *P. aerogenes* ferredoxin (218) is not seen in *B. thermoproteolyt-*

FIG. 7. Evolutionary processes in bacterial ferredoxins and a chloroplast protein. Ferredoxins of the *Peptococcus* type (218) have two halves of a highly homologous sequence, each with a -C-X-X-C-X-X-C-X-X-C-P- sequence. *Chromatium* and *Chlorobium* ferredoxins have five to six residues instead of the two between the second and third Cys in the C-terminal half and have an extension at the C terminus (see also Fig. 9). Ferredoxins of the *Azotobacter* type (310, 311) have insertions similar to those of the *Chromatium* type and a large C-terminal extension. These have [4Fe-4S][3Fe-4S] clusters. Ferredoxins of the monocluster type have lost the second binding site in the sequence, which does not show any detectable internal duplication. The F_A/F_B protein isolated from the photosystem I complex (see Fig. 11 and Section IV,F) was simulated on the basis of the structure of *P. aerogenes* ferredoxin (218). This protein conserves the duplicated sequence with an insertion and C-terminal extension (349). Ferredoxins of the *Desulfovibrio* type (216) have a conformation similar to that of *B. thermoproteolyticus* ferredoxin (214).



icus ferredoxin (214). That the aromatic residues are not essential for electron transfer but rather are, with the hydrophobic amino acid residues, crucial for stabilization of the Fe-S cluster has been discussed in detail (214, 219).

On the basis of sequence comparison and secondary structure prediction, the α -helix found in *B. thermoproteolyticus* ferredoxin was predicted to be present in other [4Fe-4S] ferredoxins (214). The four other ferredoxins were suggested to fold in a manner similar to that of *B. thermoproteolyticus* ferredoxin except for the loop and the C-terminal extension (214). This prediction proved correct for *D. gigas* ferredoxin II (216). Both ferredoxins I and II of *D. gigas* have different oligomeric forms. Ferredoxin I is in a trimeric state and II is in a tetrameric state, with a [4Fe-4S] and a [3Fe-4S] cluster per monomeric unit, respectively, although the amino acid sequences of both ferredoxins are identical (9). The physiological significance of an interconversion between ferredoxins I and II, with reduction potentials of -450 mV for I and -130 mV for II (220), has been discussed (9).

The three-dimensional structure of *D. gigas* ferredoxin II (216) revealed that its main chain fold was similar to that of *P. aerogenes* 2[4Fe-4S] ferredoxin (218), with a helical segment as predicted in the structural study of *B. thermoproteolyticus* ferredoxin (214) as given in Fig. 7. The presence of the α -helix in *D. sulfuricans* Norway ferredoxin was also predicted by NMR spectroscopy (221). The [3Fe-4S] cluster was similar to the one found in aconitase (7) and the three irons were chelated by Cys 8, 14, and 50, but not by Cys 11, forming a cluster just like a [4Fe-4S] structure but lacking one iron atom. Cys 11 was rotated and the side chain extended toward the solvent and was interestingly modified by $S(CH_3)_{1-2}$, this perhaps having some physiological significance (216). A simple rotation of the Cys 11 side chain so as to chelate the fourth iron necessary to form a [4Fe-4S] cluster would require a readjustment of the polypeptide chain around this region (216).

Bacillus stearothermophilus and *B. thermoproteolyticus* ferredoxins and *D. africanus* ferredoxin I have only the four cysteine residues necessary to construct a [4Fe-4S] cluster, but ferredoxins from *D. gigas*, *D. desulfuricans* Norway, and *C. thermoaceticum* have six cysteine residues. In place of the extra two cysteine residues the former three ferredoxins have alanine and an acidic residue, respectively. Side chains at these positions are close together, leading to the likelihood of disulfide bond formation between Cys 18 and Cys 42 in the case of *D. gigas* ferredoxin (217, 222), as confirmed by the X-ray analysis (216). An earlier chemical study of *D. gigas* ferredoxin had suggested a disul-

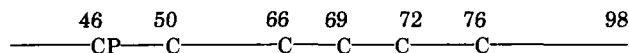
fide bond might be present in this molecule (223). The significance of the disulfide bridge is uncertain.

In their tertiary structure, *C. pasteurianum* ferredoxin and closely related 2[4Fe-4S] ferredoxins conserve the duplicated form of an ancestral half molecule in a twofold symmetry (Fig. 7). Other structures are variations of this basic form. The deletion of the second [4Fe-4S] cluster that is present in 2[4Fe-4S] ferredoxins was followed by the proximal peptide segment changing in conformation to an α -helix, maintaining a stable tertiary structure. Once it was introduced, the helix remained during evolution and only the N-terminal half segment has been conserved as the sequence holding an Fe-S cluster, corresponding to that present in the ferredoxins of more primitive fermentative bacteria such as *Clostridium*. As revealed by the comparison of *B. thermoproteolyticus* ferredoxin and *D. gigas* ferredoxin, the loop and protruding region found in the former were probably introduced after divergence of *B. thermoproteolyticus* ferredoxin and other [4Fe-4S] ferredoxins (214, 219).

Papers dealing in more detail with the evolutionary aspects of bacterial ferredoxins have appeared previously (224-227).

B. FERREDOXIN-LIKE PROTEINS IN SYMBIOTIC NITROGEN-FIXING BACTERIA

Genes coding for ferredoxin-like proteins, designated as *fixX*, have been found through molecular genetic studies of the root nodule symbiotic nitrogen-fixing bacteria, *Rhizobium meliloti* (228-230), *Rhizobium trifolii* (231), *Rhizobium leguminosarum* biovar *viciae* (232), *Bradyrhizobium japonicum* (233), and *Azorhizobium caulinodans* (234). Their products are composed of 98 residues, except the protein from *A. caulinodans* (97 residues), which lacks the N-terminal residue. As an example the sequence of *R. trifolii fixX*-encoded protein showing the cysteine distribution is

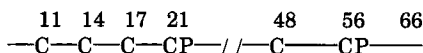


This protein has a single [4Fe-4S] cluster probably chelated by Cys 46, 66, 69, and 72, corresponding to the cysteine clusters of clostridial 2[4Fe-4S] ferredoxin but lacking the three cysteines near the N terminus, which, with one cysteine near the C terminus corresponding to Cys 76 in this sequence, forms one Fe-S cluster. They have the considerably longer N-terminal sequences than those of the common bacterial ferre-

doxins. To date, genes of this type have been only found in symbiotic nitrogen-fixing bacteria. The *R. meliloti* *fixX*-encoded product was reported to be essential for nitrogen fixation, a conclusion based upon transposon mutagenesis (229) and complementation (228) studies. All *fixX* genes except that in *B. japonicum* are located downstream of *fixABC*, which are required for symbiotic nitrogen fixation, and are cotranscribed from a promoter upstream of *fixA*. In *B. japonicum*, *fixX* is downstream of *fixBC*, and *fixA* is separate.

C. A HIGHLY THERMOSTABLE [4Fe-4S] FERREDOXIN

Several thermostable ferredoxins have been isolated from thermophilic bacteria (9, 235, 236) and cyanobacteria (61, 237). The major participation of external salt bridges linking residues near the N terminus to others near the C terminus was suggested to be responsible for the thermal stability of these bacterial ferredoxins (238); these ferredoxins also had increased hydrophobic interactions and hydrogen bond networks (235, 239) compared to other ferredoxins, which were less thermostable. Crucial salt bridges were also suggested to be responsible for the thermal stability of a cyanobacterial ferredoxin (76). A remarkably thermostable ferredoxin has been isolated from the hyperthermophilic, anaerobic archaebacterium, *Pyrococcus furiosus*, which grows optimally at over 100°C in submarine volcanic areas (209, 240). The ferredoxin, which donates electrons to hydrogenase, was purified under anaerobic conditions and was stable in 20% sodium dodecyl sulfate (SDS) or after incubation at 95°C for 12 hr. The reduction potential was -345 mV at pH 8.0. The molecular weight of this ferredoxin was about 7500, with four iron and four inorganic sulfur atoms and five cysteines, indicative of the presence of a [4Fe-4S] cluster. However, one of the four iron atoms was chelated by an aspartic acid and not a cysteine. The cysteine cluster was shown to be

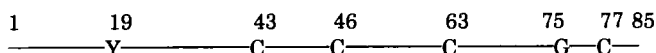


The interconversion between a [4Fe-4S] and [3Fe-4S] cluster was observed, but only the [4Fe-4S] with an aspartic acid coordinate cluster was thought to be present *in vivo*. A very recent report has shown that one of the four iron atoms in the native state of this ferredoxin is reactive with cyanide as an exogenous ligand (241).

D. HIGH-POTENTIAL IRON-SULFUR PROTEINS

A group of proteins with a single [4Fe-4S] cluster showing a high reduction potential at around +340 mV was found in various photosyn-

thetic bacteria, including *Chromatium vinosum* (242), *Rhodospirillum salinarum* (243), *Thiocapsa roseopersicina* (244), *Rhodopseudomonas marina* (148), and others, except for *Ectothiorhodospira halophila* (245) and the denitrification bacterium, *Paracoccus* sp. (246, 247); these proteins are called high-potential iron-sulfur proteins (HiPIPs). The molecular weights are less than 10,000 and they are thought to function as electron carriers in photosynthesis (248, 249), anaerobic metabolism (250), and thiosulfate oxidation (251), although definite functions remain to be clarified. Amino acid sequences of 10 HiPIPs are known (245, 247, 252–257), and they are quite different from those of other ferredoxins (Fig. 8). The sequences currently available are summarized elsewhere (245 and 257), but the *Chromatium* HiPIP sequence (254) is given below to illustrate the distribution of the cysteine residues and of other amino acid residues conserved in 10 HiPIPs.



Except for the four cysteine residues, which are necessary for chelating the four iron atoms, there are not so many conserved residues among HiPIPs as for low-potential ferredoxins. The four cysteines are distributed differently compared with those of low-potential ferredoxins. The evolutionary implications of the sequence anomaly of the HiPIPs have been described (257). Among the 10 HiPIPs, two isoforms, I (120 mV) and II (50 mV), from an extremely halophilic purple phototrophic bacteria, *Ectothiorhodospira halophila*, were isolated and sequenced (245). There is 72% identity between the two isoforms, and the four cysteines (Cys 43, 46, 63, and 77 using the *C. vinosum* HiPIP numbering) and two other residues (Tyr 19 and Gly 75) are conserved. The importance of these residues with particular regard to the reduction potential and hydrogen bonding in the three-dimensional structure is of interest. The sequence comparison suggested that *E. halophila* HiPIP iso-forms were most remote from the others (about 30% identity), indicating the divergence of these two at equal rates after gene duplication without evident change in function (245). This phenomenon may be different from those observed in various photosynthetic [2Fe–2S] ferredoxins (Section II,A). As they become available the sequences of HiPIP iso-forms found in other closely related bacteria should clarify the relationship between gene duplication and speciation (245). The three-dimensional structure of *C. vinosum* HiPIP is known (258–260) and the cluster geometry was shown to be essentially the same as those of the 2[4Fe–4S] from *P. aerogenes* ferredoxin (261, 262). Two

preliminary crystallographic analyses have been carried out for *Rhodospirillum tenue* (263) and *E. halophila* (264) HiPIPs.

E. FERREDOXINS WITH A SINGLE [3Fe-4S] CLUSTER IN OXYGENASE SYSTEMS

In general, ferredoxins functioning in oxygenase systems are of the [2Fe-2S] form with sequences similar either to those of plant-type ferredoxins or to putidaredoxin, as described in Section II,C,4. In contrast, two new types of ferredoxins having a [3Fe-4S] cluster were found to be components of the *Streptomyces griseolus* monooxygenase system induced by a sulfonylurea herbicide (265). The corresponding genes encoding ferredoxin 1 and 2 were sequenced and the deduced amino acid sequences, 68 and 64 residues, respectively, showed 52% identity to each other (Fig. 6h and 6i, respectively). The spectral properties and iron and sulfur contents of both ferredoxins suggested that they each contained a single [3Fe-4S] cluster. Ferredoxin 1 has only three cysteines with the motif -C-X-X-A-X-X-C---CP-, and ferredoxin 2 has four cysteines with the motif -C-C-X-A-X-X-C---CP-, compared with [4Fe-4S] ferredoxins (Section III,A).

F. PROTEINS WITH A SINGLE [4Fe-4S] CLUSTER BRIDGING TWO SUBUNITS

1. Photosystem I Reaction Center X Proteins

Oxygenic photosynthetic organisms have two photosystems (PSs), I and II. The oxidation of water with evolution of oxygen is achieved by PS II to produce a weak reductant whereas PS I produces a strong reductant able to reduce NADP^+ . The two systems are linked by an electron transfer complex, the cytochrome b_6/f complex that translocates protons (266, 267). The PS I complex is a multisubunit complex in the thylakoid membranes, which has six intrinsic electron transfer components enabling a series of oxidation-reduction transfers from plastocyanin to the [2Fe-2S] ferredoxin. Among them there are three Fe-S centers, X, A, and B. The Fe-S center X has a very low midpoint reduction potential, -705 mV , and transfers electrons from the chlorophyll primary electron donor, P-700, through A_0 and A_1 to the Fe-S center F_A/F_B protein (see Section IV,F). Various lines of evidence suggest that center X is a [4Fe-4S] cluster (268) bridged by two nonidentical but homologous proteins with the leucine zipper motif (269); these proteins are called core proteins I and II and have molecular masses of

about 64 kDa. The amino acid sequences of the two proteins of several organisms, ranging from higher plants to cyanobacteria, were deduced from the sequences of the corresponding genes (*psaA* and *psaB*) (266). The distribution of the four cysteine residues necessary for chelating the four iron atoms are completely different from those in other Fe-S proteins and were located in homologous positions in each subunit (266).

2. Fe Proteins in Nitrogenase and Related Proteins of Chloroplasts and Cyanobacteria

Nitrogenase is found only in prokaryotes and catalyzes the reduction of N_2 to NH_3 . It consists of two components, the iron(Fe) protein and molybdenum-iron (Mo-Fe) protein (270). The enzyme requires ATP and a low-potential reductant, such as ferredoxin or flavodoxin, to reduce N_2 . The Fe proteins have molecular masses of about 58–73 kDa, depending on source, and exist as homodimers. They function as a reductase with a reduction potential upon binding ATP of about -400 mV during electron transfer to the Mo-Fe protein. This has a $[4Fe-4S]$ cluster per dimer, forming a V shape with the Fe-S cluster at the junction highly exposed to solvent (271). The cysteine residues chelating four iron atoms are thought to be located at positions 97 and 132 in both subunits of the protein from *A. vinelandii*. The distribution is completely different from those of other Fe-S proteins, including ferredoxins (270).

When the complete nucleotide sequences of chloroplast DNAs from liverwort, *Marchantia polymorpha* (272), and tobacco, *Nicotiana tabacum* (273), were established in 1986, a notable difference was found between the two in the gene organization and the amino acid sequences of the putative Fe-S proteins. Liverwort chloroplast DNA has three genes, *frxA*, *frxB*, and *frxC*, but tobacco has only two: *psaC*, corresponding to *frxA*, and *orf167*, corresponding to *frxB*. The *frxA* and *frxB* genes have cysteine distributions similar to those of $2[4Fe-4S]$ ferredoxins, but the *frxC* gene has a cysteine distribution similar to those of the nitrogenase Fe protein encoded by the *nifH* gene (274), which codes for a polypeptide composed of 289 amino acid residues. Nitrogen fixation is a feature found only in prokaryotes such as bacteria and cyanobacteria, and it was therefore suspected that the *frxC* gene product might have a function in a system other than nitrogen fixation (275). Incidentally, the *frxC* gene does not form an operon with the other structural genes (*nifD* and *nifK*) for nitrogenase, as is the case for the *nifH* gene (276), and no nitrogenase activity was detected in either the whole cells or intact chloroplasts of liverwort (275). The *frxC* gene product was

immunochemically detected in the soluble fraction of liverwort chloroplasts and found to be present as a dimer (molecular weight of about 67,000) (275) analogous to the Fe protein of nitrogenase (274). Further, the protein had a consensus ATP-binding sequence, Gly-X-X-X-X-Gly-Lys-Thr(Ser)- (277) at the N-terminal region and would bind to an affinity column of Cibacron Blue. The distribution of cysteine residues necessary to form a [4Fe-4S] cluster (274, 278) were conserved in the sequence. All these lines of evidence indicate that the *frxC* gene product may function, like the Fe protein in nitrogen fixation.

The *nifH* genes are highly conserved among nitrogen-fixing organisms generally, with about 60% homology or more in amino acid sequence (279), though the *frxC* gene products of liverwort and *Plectonema boryanum*, a filamentous cyanobacterium fixing nitrogen, showed only about 35% homology with any of the Fe proteins (274, 280). Interestingly, the *frxC* protein showed about 44% homology with a putative protein encoded by the *F202* gene (281, 282) located in the photosynthetic gene cluster (282) of *Rhodobacter capsulatus*. Also, the *F202* gene showed a low homology with the *nifH* genes (281). Later, the authentic *nifH* gene of the same bacteria was sequenced and was found to be highly homologous with other *nifH* genes (283). Taken in conjunction, this circumstantial evidence suggests that the proteins encoded by the two genes (*frxC* and *F202*) function in a common novel manner other than in nitrogen fixation.

Plectonema boryanum has genes corresponding to both *frxC* and *nifH*, and their putative proteins showed about 83% homology with the *frxC*-encoded protein of liverwort and about 84% with the *nifH*-encoded Fe protein of *Anabaena* PCC7120, yet these two genes in *P. boryanum* showed only 34% homology (280). The *P. boryanum frxC*-encoded putative protein product also has the ATP-binding sequence motif and the cysteine residues necessary to form a [4Fe-4S] cluster. After duplication of an ancestral gene, it seems that the *frxC* and *nifH* genes diverged into two separate groups and evolved independently to function in different metabolic systems. Figure 9 compares the distributions of cysteine residues implicated in forming the [4Fe-4S] cluster and the ATP-binding sequences deduced from consideration of the *frxC* and *nifH* gene sequences.

The function of the *frxC* gene product was unknown and it was anticipated that it might be concerned with a specialized metabolic role in lower plants and algae. A mutant of *P. boryanum* lacking the *frxC* gene has recently been obtained by targeted gene disruption mutagenesis, and another mutant lacking the *nifHD* genes necessary for nitrogen fixation has also been prepared (289). As expected, the latter mutant

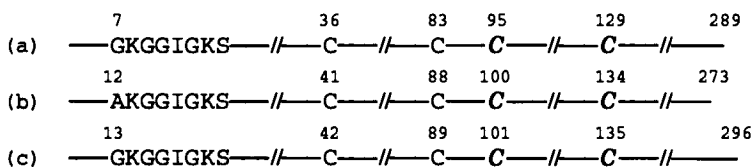


FIG. 9. Distributions of cysteine residues and ATP-binding motif in the sequences of *frxC*- and *nifH*-encoded proteins. Cysteine residues suggested to chelate iron atoms are italicized. Cysteine residues commonly found in all sequences are also given. (a) *Marchantia polymorpha* (liverwort) *frxC*-encoded protein (289 residues) (284) and *P. boryanum frxC*-encoded protein (286 residues) (280); (b) *R. capsulatus F202*-encoded protein (281); (c) *P. boryanum nifH*-encoded protein (296 residues) (280) and *Anabaena 7120 nifH*-encoded protein (299 residues) (285).

could not grow on a nitrogen-free agar plate but the former grew normally, regardless of the presence or absence of nitrogen sources, indicating the *frxC*-encoded protein is probably not essential for photosynthesis or nitrogen fixation. The *frxC* mutant grew almost at the same rate as the wild-type alga under dark conditions, but the chlorophyll content was greatly decreased. This finding is in agreement with the observations that cyanobacteria contain significant amounts of chlorophyll even when they are grown in the dark, in contrast to higher plants and algae, which have only the light-dependent chlorophyll biosynthetic system (286, 287). Liverwort similarly possessed chlorophyll even in a dark-grown culture. The light-independent reduction of protochlorophyllide *a* to chlorophyllide *a* has been demonstrated in a *Synechococcus* strain (288). These observations suggest that the *frxC*-encoded protein functions in an electron transfer reaction between protochlorophyllide *a* and chlorophyllide *a* (280, 289).

G. SUCCINATE-FUMARATE OXIDOREDUCTASES

As mentioned in Section II,C,5, succinate-fumarate oxidoreductase contains both [4Fe-4S] and [3Fe-4S] clusters that are probably formed by the cysteine clusters of the sequence motifs: -C-X-X-C-X-X-C-X-X-X-C-P- for cluster S-2 and -C-X-X-X-X-C-X-X-X-C-P- for cluster S-3, respectively (178) (Fig. 5).

IV. 2[4Fe-4S] and [4Fe-4S][3Fe-4S] Ferredoxins and Related Proteins

Since the observations in 1962 regarding bacterial and plant ferredoxins, many 2[4Fe-4S] and several [4Fe-4S][3Fe-4S] ferredoxins and

related proteins have been isolated and characterized. Bacterial ferredoxins with these clusters have been critically reviewed (9, 10) and here we deal only with a few special cases—in particular, several ferredoxins with specialized functions in one organism are discussed in relation to their structures. (Hydrogenases are reviewed by Voordouw, this volume.)

A. PHOTOSYNTHETIC BACTERIAL AND *nif*-RELATED FERREDOXINS

Ferredoxins isolated from the photosynthetic bacteria *Chlorobium thiosulfatophilum*, *Chlorobium limicola* I and II, *Chromatium vinosum*, and *Rhodospseudomonas palustris* I were classified in a phylogenetic subgroup of the 2[4Fe–4S] ferredoxins (9). They have sequences with two Cys clusters. The first group has the sequence -C-X-X-C-X-X-C-X-X-X-C-P-, typical of clostridial ferredoxins, whereas the second Cys clusters have a longer spacing of seven to eight residues between the second and third Cys rather than the typical spacing of two residues. They have also an extra (fifth) Cys (Fig. 10). There are two exceptions to this “photosynthetic bacterial” classification. One recently characterized exception is *R. capsulatus* ferredoxin II, which is of the [4Fe–4S][3Fe–4S] type and very similar to ferredoxin I from *A. vinelandii* (142, 295–297). The occurrence of ferredoxins of this type should be common to other members of Rhodospirillaceae, as is suggested for *R. rubrum* ferredoxin II from its physicochemical properties (298) and N-terminal sequence (K. Saeki and N. Nagai, unpublished results, 1990). Another puzzling exception is an extracellular ferredoxin purified from the culture medium of *R. rubrum*, which has a sequence closely similar to those of the clostridial ferredoxins (299). Since no similar ferredoxin has been reported from any other photosynthetic bacteria, genetic evidence is necessary to ascertain whether this ferredoxin is really encoded by the *R. rubrum* genome.

Among the members of this subgroup, only the *R. capsulatus* ferredoxin I gene (*fdxN*) has been cloned and studied in terms of its molecular biology (140, 144, 295), and this work is summarized below.

As a consequence of molecular biological studies on genes related to nitrogen fixation, six ferredoxin-like genes have been identified. These encode products that possess structural features similar to those of the photosynthetic bacterial ferredoxins mentioned above (Fig. 10). Three of them, found in *R. meliloti* (*fdxN*) (300, 301), *B. japonicum* (*frxA*) (302), and *A. vinelandii* (303), were located just downstream of and probably cotranscribed with *nifB*, whose product is concerned in Mo–Fe protein maturation. The *B. japonicum* *frxA*-encoded product has Leu

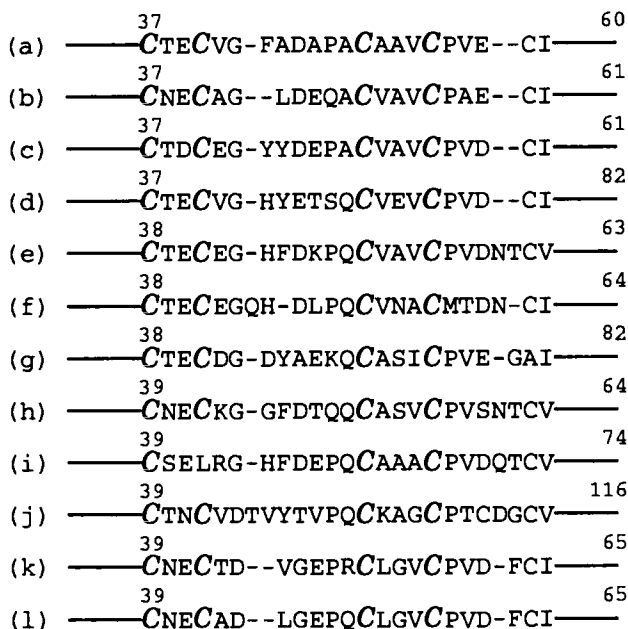


FIG. 10. Amino acid sequences of the second Cys clusters of photosynthetic and *nif* gene related ferredoxins. A gap is inserted to align the sequences for highest homology. Cysteine residues suggested to chelate the iron atoms are italicized. (a) *Chlorobium thiosulfatophilum* (290), (b) *Chlorobium limicola* I (291), (c) *C. limicola* II (292), (d) *Chromatium vinosum* (293), (e) *Rhodopseudomonas palustris* I (294), (f) *Rhodobacter capsulatus* (*fdxN*-encoded Fd I) (140, 144, 295), (g) *A. vinelandii* (*nifB* related) (303), (h) *Rhizobium meliloti* (*fdxN*) (300, 301), (i) *Bradyrhizobium japonicum* (*frxA*) (302), (j) *Anabaena* PCC7120 (300), (k) *A. vinelandii* (*vnfH* related) (305), and (l) *A. chroococcum* *nifH** related (304).

at the position, whereas its counterparts have the sixth Cys residue (302) (Fig. 10i) and an *A. vinelandii* *orf*-encoded product lacks the ninth Cys residue (303) (Fig. 10g). Another gene, *Anabaena* PCC7120 *fdxN*, is located upstream of *nifB* (300) (Fig. 10j). It is interesting that this gene in vegetative cells is split into two parts separated by 55 kbp of DNA, and becomes an entity only after excision of the DNA during genome rearrangement accompanying heterocyst formation (300). In addition, *R. capsulatus* *fdxN* is also located in one of the major *nif* gene clusters in the bacterium but not adjacent to *nifB* (140, 142). The other two genes were found as ORFs downstream of the *nifH* homologue (*vnfH*) of the alternative nitrogenase system in *A. chroococcum* (304) and *A. vinelandii* (305) (Fig. 10, l and k, respectively).

Gene-specific disruption experiments have been carried out on three of the ferredoxins mentioned above. Interposon mutation of *B. japonicum frxA* was reported to have little effect on symbiotic nitrogen fixation, but decreased the nitrogenase activity of free-living cells to approximately 50% (302). *Rhizobium meliloti fdxN* was demonstrated to be necessary for symbiotic nitrogen fixation by complementation experiments on mutants; *fdxN*-depleted mutants were unable to fix N₂, but the ability was restored by plasmids with *fdxN* (301). Such disruption following complementation also showed that *fdxN* of *R. capsulatus*, a nonsymbiotic bacterium, was an important component for nitrogen fixation (142).

Because most of the known photosynthetic bacteria fix nitrogen (306), it might be speculated that all the 12 ferredoxins of the group in Fig. 10 have some specific role in the nitrogen fixation system and the unique longer insertion between the sixth and seventh Cys residues might have some functional significance in interacting with other component(s) of the system.

B. *Azotobacter*-TYPE [4Fe-4S][3Fe-4S] FERREDOXINS

The [4Fe-4S][3Fe-4S] ferredoxins represented by *A. vinelandii* ferredoxin I have two unique structural features and have been classified into a distinct phylogenetic group (9). One of the features is that the first Cys cluster is unique, with the sequence -C-X-X-X-K-X-X-X-C-X-X-X-C-P-V-X-X-, where X is often but not necessarily always C; the second Cys group is the usual sequence -C-X-X-C-X-X-C-X-X-X-C-P-. The other notable feature is the long C-terminal extension of 30 to 50 residues compared to that of the typical clostridial ferredoxins. Since a previous review (9), three additional members, the ferredoxins from *Pseudomonas stutzeri* (307), *Streptomyces griseus* (308, 309), and *R. capsulatus* (142, 295-297), have been added to the group.

The three-dimensional structure of *A. vinelandii* ferredoxin I has been redetermined (310, 311) (see Fig. 7) and refinement to 1.9 Å resolution (312) has enabled revision of the previous model (313). The geometry of the 3Fe cluster is essentially the same as that of the [3Fe-4S] cluster for *D. gigas* ferredoxin (216) and aconitase (7, 314), i.e., as in a [4Fe-4S] cluster but with one Fe atom removed, and completely different from the previous [3Fe-3S] model. The ligands for the [3Fe-4S] cluster were Cys 8, 16, and 49, whereas those of the other accompanying [4Fe-4S] cluster were Cys 20, 39, 42, and 45. Cys residues corresponding to these positions are conserved in all the ferredoxins of this type. In this group, the residue corresponding to the nonli-

gand Cys 11 is Val in *Mycobacterium (Micrococcus) smegmatis* (315), *Thermus thermophilus* (316), and *S. griseus* (309) ferredoxins and Glu in *Bacillus acidocaldarius* (317) ferredoxin, and that corresponding to Cys 24 is Ala in *B. acidocaldarius* (317). Superposition of the main chain topologies of *A. vinelandii* ferredoxin with 106 residues and of *P. aerogenes* 2[4Fe-4S] ferredoxin with 54 residues showed a striking similarity within residues 1-58 of the former, except for the insertion of additional residues 9, 10, 29, and 30 (312). The extended C-terminal portion of the former ferredoxin, residues 59 to 106, is in contact with the expanded loops, which contain these four extra residues and contribute a significant feature in the tertiary structure.

Although it was known that the two clusters of ferredoxins of this type have considerably different reduction potentials, there were discrepancies among the actual values reported. Recently, a direct electrochemical characterization using pyrolytic graphite edge electrodes has revealed that *A. chroococcum* ferredoxin I, a close homologue of *A. vinelandii* ferredoxin I, has reduction potentials of -460 and -645 mV for the [3Fe-4S] and [4Fe-4S] clusters, respectively (318). The reduction potential of the [3Fe-4S] cluster of *M. smegmatis* ferredoxin was also estimated to be around -435 mV and that for the [4Fe-4S] cluster of *Pseudomonas ovalis* to be lower than -600 mV, these assessments being by EPR (319) and NMR (320) studies, respectively. Similar values were obtained for the centers of *S. griseus* ferredoxin, measured using EPR (309).

It was shown by site-directed mutagenesis and subsequent X-ray crystallographic analysis that the substitution of Cys 20, which was a ligand for the [4Fe-4S] cluster and remote from the other three ligands, by Ala resulted in structural rearrangement that enabled Cys 24, which was in van der Waals contact with the cluster in the authentic ferredoxin, to become an alternative ligand (321). The mutated protein showed various spectroscopic properties similar to those of the original protein, implying that both the [4Fe-4S] and [3Fe-4S] clusters were formed, although it showed a considerably different circular dichroism (CD) spectra, reflecting a substantial rearrangement around the [4Fe-4S] cluster. Interestingly, the modified protein was as stable to oxygen as the authentic ferredoxin.

Little is known about the physiological function of *Azotobacter*-type ferredoxins, despite these extensive structural and electrochemical studies. *Streptomyces griseus* ferredoxin is the only one of this group for which a specific function has been proposed (308). First, because it is not constitutively expressed but induced along with a cytochrome *P*-450 system by adding soybean flour to the medium, and, second, it can

react with the enzyme *in vitro*, its function may be as an electron donor to cytochrome *P*-450. Genetic studies on *A. vinelandii* ferredoxin I and *R. capsulatus* ferredoxin II are described later (Section IV,D).

C. *Desulfovibrio*-TYPE [4Fe-4S][3Fe-4S] FERREDOXINS

Analysis of aerobically prepared *Desulfovibrio africanus* ferredoxin III by combining direct electrochemical and spectroscopic methods demonstrated that it possessed a [3Fe-4S] cluster with a reduction potential of -140 mV and a [4Fe-4S] cluster of -410 mV (322). This ferredoxin has only seven Cys residues; thus the [4Fe-4S] cluster would be formed by Cys 21, 41, 44, and 47, as is usually observed, and the [3Fe-4S] cluster is predicted *in vitro* to be chelated by Cys 11, 17, and 51. The properties of this ferredoxin were the same as that of *D. gigas* ferredoxin II, the tetrameric form (9). However, it was also proposed that the cluster might be a [4Fe-4S] form, *in vivo*, with Asp 14 as the fourth ligand, because the reduced [3Fe-4S] cluster could be easily converted to the [4Fe-4S] cluster by the addition of Fe^{2+} ion to give a center with a reduction potential of -400 mV (323). This situation is similar to that observed for aconitase (7), but the fourth ligand of aconitase was a water molecule instead of the carboxyl side chain (324). It should be noted that the residue at position 52, next to Cys 51, is not Pro as usual, but Glu.

Desulfovibrio vulgaris Miyazaki ferredoxin I, which is the major isoform of the two ferredoxins present, was demonstrated to have two redox centers showing distinct behaviors (325). It has a sequence highly homologous to that of *D. africanus* ferredoxin III (326); 52 residues out of 61 residues are identical, including the sequences of the two Cys clusters with the unique Asp 14 and Glu 52. This ferredoxin was proposed to be the electron carrier in the phosphoroclastic reaction composed of pyruvate dehydrogenase and the hydrogenase-cytochrome c_3 system (325).

D. FUNCTIONAL DIFFERENCES OF DISTINCT FERREDOXINS IN A SINGLE BACTERIUM

A number of bacteria have been known to contain multiple ferredoxins that are structurally and phylogenetically distinct. However, it is not known if such multiple ferredoxins are really distinct in physiological function, because almost all of the bacterial ferredoxins are able to transfer electrons in the assays commonly used: NADP^+ photoreduction using plant chloroplasts, and some enzyme systems in extracts

from various organisms. Here, we focus on the functional differences of the ferredoxins from *A. vinelandii* and *R. capsulatus*; both organisms possess 2[4Fe-4S] and [4Fe-4S][3Fe-4S] ferredoxins.

Azotobacter vinelandii contains a [4Fe-4S][3Fe-4S] ferredoxin I that is well studied and two other possible 2[4Fe-4S] ferredoxins linked to either *nifB* or *vnfH* (303, 305) as described above. The gene for ferredoxin I, *fdxA*, was cloned and the single genomic copy was disrupted by homologous recombination to yield a mutant with essentially the same phenotype as that of the wild type (327). Such an event without any significant effect of the mutation was also observed for the flavodoxin gene *nifF* of this bacterium (328). The double mutant with both *fdxA* and *nifF* disrupted could grow at only one-third the rate of the wild type in medium replete in ammonium ion, but would grow as fast as the wild type with N₂ as the nitrogen source (329). These observations may indicate that the *nifB*-linked ferredoxin fulfills the need for either ferredoxin I or flavodoxin under nitrogen-fixing conditions but cannot compensate for their absence when a high concentration of ammonium ion represses its expression; another ferredoxin gene linked to *vnfH* might not be expressed in the presence of Mo. The disruption mutant of the *nifB*-linked ferredoxin gene, together with an unidentified ORF situated downstream, will still grow by nitrogen fixation at half the rate of that of the wild type (303), probably because either ferredoxin I or flavodoxin can compensate to some extent for its function. If these suppositions are correct, there may be no specific function for *A. vinelandii* [4Fe-4S][3Fe-4S] ferredoxin I.

Possession of two ferredoxins, I and II, by *R. capsulatus* has been observed at the protein level (330-332), and the genes *fdxN* and *fdxA* for these ferredoxins have recently been cloned and sequenced (140, 142, 297). Northern blotting, in-frame *lacZ* fusion, and Western blotting analyses indicated that *fdxN* is regulated similarly to the *nif* genes (140, 333, 333a). Furthermore, the mutants disrupted in *fdxN* scarcely grew on N₂ as the sole nitrogen source, and an *fdxN* nonpolar mutant could be induced to fix N₂ at the wild-type level by reintroducing the gene (142). This was good evidence that ferredoxin I was required for nitrogen fixation by the bacterium. Another ferredoxin gene was identified during studies on genes downstream of *nifENX* and this encoded a product of 101 residues with two Cys clusters of the typical -C-X-X-C-X-X-C-X-X-X-C-P- sequence. However, it had a longer insertion sequence between the two clusters of 42 residues compared to the usual 17 residues found in clostridial ferredoxins (334). The product is probably a 2[4Fe-4S] ferredoxin. Interestingly, it was pointed out that the insertion length was identical to that found in *nifJ*, which encodes

the pyruvate-flavodoxin oxidoreductase of *Klebsiella pneumoniae* (335). Disruption of this gene together with the partly overlapping *nifQ* rendered the bacterium unable to grow on N_2 , but the addition of a high concentration of Mo (1 mM) to the medium overcame this disability (334). Hence, the phenotype could be attributed to *nifQ* disruption. The fourth ferredoxin gene, *fdxC*, which encodes a protein homologous to plant [2Fe-2S] ferredoxins, was found just upstream of *fdxN* (142) and was shown also to be required to some extent for nitrogen fixation (Section II,C,2).

Therefore, three of the ferredoxin genes belonging to the *nif* gene family have been accounted for. The remaining [4Fe-4S][3Fe-4S] ferredoxin II encoded by *fdxA* was expressed constitutively under various growth conditions: photosynthesis, respiration, anaerobic respiration, or nitrogenase repressed or derepressed, as analyzed by transcriptional analysis using in-frame *lacZ* fusion (333a, b). In addition, *fdxA* cannot to date be disrupted, even by screening under the conditions that derepress the expression of the other three ferredoxin genes (142). These observations indicate that *R. capsulatus* [4Fe-4S][3Fe-4S] ferredoxin II has some specialized physiological function indispensable for the bacterium, unlike the case of the analogous protein from *A. vinelandii*. The biochemical significance in structure-function relationships in these ferredoxins remains to be elucidated.

Some nitrogen-fixing bacteria possess multiple ferredoxins apparently related to nitrogen fixation. *Rhizobium meliloti* *fdxN* and *fixX*, which encode possible 2[4Fe-4S] and [4Fe-4S] ferredoxins, respectively, appear to be essential for nitrogen fixation (224, 225, 301). The functional significance of an *Anabaena* PCC7120 ferredoxin, the *fdxN* product, remains to be elucidated, but is of great interest because of its uniqueness in bacterial cellular and genomic differentiation (300) and because of its relationship to the *fdxH*-encoded product, the heterocystous [2Fe-2S] ferredoxin (Section II,A).

E. OTHER FERREDOXINS

Clostridium perfringens ferredoxin was previously reported to have a single [4Fe-4S] cluster (336), but its sequence was highly homologous with that of *C. pasteurianum* ferredoxin (337), suggesting it might contain 2[4Fe-4S] clusters. It donates electrons to nitrate reductase (338).

Butyribacterium methylotrophicum, a methylotrophic heteroaceto-gen, has a ferredoxin whose physicochemical properties and sequence

are very similar to those of *C. pasteurianum* ferredoxin (339, 340). It interacts with hydrogenase but only poorly with the CO dehydrogenase of the bacterium. Ferredoxin and rubredoxin phylogenetic trees constructed for seven bacteria showed essentially the same topology (340).

Methanococcus thermolithotrophicum, a thermophilic methanogen, produces a thermostable ferredoxin that will withstand 88°C for 1 hr, but that is oxygen unstable (236). It has about 60 residues, including eight cysteines, and is thought to function as an electron acceptor for the CO dehydrogenase complex.

F. F_A/F_B PROTEINS IN PHOTOSYSTEM I COMPLEXES

As mentioned in Section III,F,1, the PS I complex has three Fe-S centers, X, A, and B. An 8- to 9-kDa polypeptide associated with the complex was suggested to be an Fe-S protein (341–343) and accepts electrons from the Fe-S center X and donates them to the [2Fe–2S] ferredoxin. The sequence analysis of the 9-kDa polypeptide proved it to be the apoprotein that carries centers A and B (344–346), i.e., F_A/F_B protein. Spinach protein was partially purified (347) and reconstituted with the PS I complex from which F_A/F_B protein was depleted (348). Thus, the 9-kDa F_A/F_B protein encoded by *psaC* (or *frxA* of liverwort) was identified to be an Fe-S protein with centers A and B. Spinach F_A/F_B protein isolated with partially degraded Fe-S clusters showed an amino acid sequence similar to those of ferredoxins of the clostridial 2[4Fe–4S] type (349) and the presence of two distinct Fe-S clusters was indicated by EPR spectroscopy (350). When the F_A/F_B protein was exposed to air, the cluster was rapidly destroyed (351), in contrast to most of the clostridial 2[4Fe–4S] ferredoxins. Results of treatments with alkali, chaotropic ions, trypsin, and cross-linking reagents indicated that the F_A/F_B protein was located peripherally on the stromal side of the thylakoid membranes, but was embedded under two other subunits situated closely to it (352). The protein was finally obtained from spinach leaves in a native state by isolation under anaerobic conditions (351). The iron and inorganic sulfur contents and the spectroscopic properties of the protein are nearly identical with those of the 2[4Fe–4S] ferredoxins of clostridial type. The reduction potentials of the two clusters were estimated to be –470 and –560 mV, respectively, although in complex I they were measured at –550 and –590 mV (353).

Amino acid sequences of several F_A/F_B proteins are known (272, 273, 349, 354–358), two of which (349, 354) were found by protein

sequencing. They are highly conserved with about 79% homology and are most closely related to *Chromatium* 2[4Fe-4S] ferredoxin (349). The cysteine residues at positions 10, 13, 16, 20, 47, 50, 53, and 57 are probably responsible for chelating the two [4Fe-4S] clusters in a manner similar to those of clostridial ferredoxins. Unlike the usual ferredoxins, these F_A/F_B proteins are weakly basic and rather hydrophilic in spite of their location as a component of a membrane protein complex (349). They are slightly larger than clostridial ferredoxins, with an insertion in the middle portion of the molecule and an extension at the C terminus. Figure 11. compares the sequence of spinach F_A/F_B protein with those of several bacterial ferredoxins. A three-dimensional structure was simulated (349) on the basis of the tertiary structure of *P. aerogenes* 2[4Fe-4S] ferredoxin (218), as given in Fig. 7.

G. FERREDOXIN-LIKE PROTEINS ENCODED BY THE CHLOROPLAST AND CYANOBACTERIAL GENES: *frxB*, *orf167*, AND *orf178*

Chloroplast DNAs of liverwort (272), tobacco (273), and rice (359) contained *frxB*, *orf167*, and *orf178*, respectively, which could encode putative ferredoxin sequences containing 2[4Fe-4S] clusters typical of clostridial 2[4Fe-4S] ferredoxins; their function is unknown. Corre-

```

(a) SHS-VKIYDTCIGCTQCVRACPTDVLLEMPWDGCKAK
(b)  A-YKIADSCVSCGACASECPVNAI-----SQG
(c)  ALY-ITEECTVCGACEPECPVTAI-----SAG
(d)  ALM-ITDQCINCNVCQPECPNGAI-----SQG

(a) QIASAPRTEDCVGCKRCESACPTDFLSVRVYLWHETT
(b) DSIFVIDADTCIDCGNCANVCPVGAPVQE
(c) DDIYVIDANTCNECAACVAVCPAECIVQG
      GLDEQ-
(d) DETYVIEPSLCTECVQCVEVCPVDCIIKDPS--HEET
      GHYETS

(a) -----RSMGLGY
(d) EDELRAKYERITGEG

```

FIG. 11. Comparison of the sequences of spinach 9-kDa F_A/F_B protein and bacterial 2[4Fe-4S] ferredoxins. Gaps are inserted to maximize homology in the alignment (349). Cysteine residues suggested to chelate iron atoms are italicized. (a) Spinach F_A/F_B protein (349), (b) *C. pasteurianum* ferredoxin (9), (c) *C. limicola* ferredoxin I (291), and (d) *C. vinosum* ferredoxin (293).

sponding genes were also identified in wheat (360) and *P. boryanum* (361). Their residue numbers ranged from 167 to 194 and they show substantial homology to each other, but are greatly divergent from bacterial ferredoxins (Fig. 12).

For *Chlamydomonas*, spinach, and tobacco (363, 364) the gene product was detected as an Fe-S protein (363) and located as a membrane-bound component on the peripheral portion of the thylakoid membranes. The *frxB* gene is in a gene cluster encoding four proteins homologous to mitochondrial complex I components. Several nuclear-encoded subunits of the mitochondrial complex I also have proteins homologous to those encoded by ORFs in chloroplast genomes, e.g., the 23-kDa subunit of bovine complex I is homologous to the *frxB* gene product (365–367), though to a lesser extent than seen in comparing *frxB* genes from chloroplasts. Another *frxB* homologue was found in the *E. coli hyc* operon encoding formate hydrogenlyase (368). These observations led to the suggestion that the *frxB*-encoded protein functions as a redox component of an NAD(P)H:plastoquinone reductase. A regulatory function in chloroplast DNA replication was also suggested (363). However, these are indirect bits of evidence and the real functional role of this protein in the thylakoid membranes is still unclear (361).

V. Polyferredoxins

Methanobacterium thermoautotrophicum, an archaebacterium, reduces CO₂ with H₂ to give CH₄, with hydrogenases being indispensable

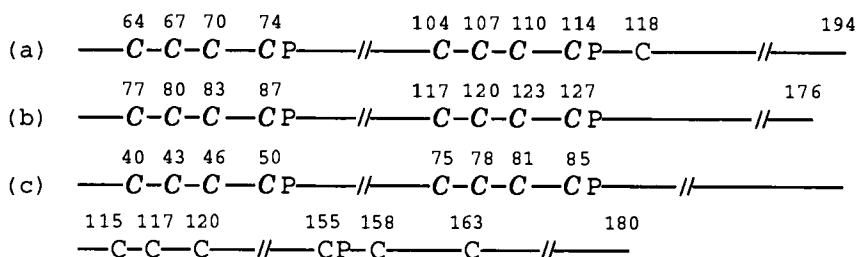


FIG. 12. Comparison of the sequences of *frxB*-encoded proteins and homologues. The positions of cysteine and proline residues are given. Cysteine residues suggested to chelate iron atoms are italicized. The *frxB*-encoded proteins of (a) *Plectonema boryanum* (194 residues) (361), liverwort (183 residues) (284), tobacco (167 residues) (362), rice (178 residues) (359), and wheat (176 residues) (360); (b) bovine mitochondrial complex I, 23-kDa subunit (367); and (c) *E. coli* formate hydrogenlyase *orf6* gene product (368).

enzymes for the reaction (369). The genes, *mvhDAG*, encode subunits of the methyl viologen-reducing hydrogenase of this bacterium. The organization and sequences of the genes indicated that they shared a common ancestor with eubacterial hydrogenase genes. The putative *mvhB* gene product contained six tandemly repeated domains corresponding to those of bacterial 2[4Fe-4S] ferredoxins, suggesting it was a polyferredoxin that contained 12[4Fe-4S] clusters. Another polyferredoxin sequence was also deduced from the DNA sequence of the *mvhB* gene of *Methanothermus fervidus*, which suggested the protein would have domains similar to the 2[4Fe-4S] ferredoxins and 64% identity to the *M. thermoautotrophicum* protein (370).

VI. Conclusions

Many ferredoxins and related (ferredoxin-like) proteins of different types have now been isolated from various organisms, and some of them have been well characterized in terms not only of physiological functions but also of chemical and physical aspects. With increasing emphasis on gene structural studies, a rapid accumulation of data on new ferredoxins and related proteins, in particular their primary structures, has resulted. The biosynthetic and regulatory mechanisms of these proteins have been the subject of recent interest. In particular, many iso-forms of ferredoxins have been detected in individual organisms ranging from higher plants to bacteria. The likelihood of distinct functions for the iso-forms in some organisms has been discussed, with the recent introduction of new approaches in genetic manipulations enabling more informed speculation on this. Table I gives some examples of iso-forms of ferredoxins and related proteins in some photosynthetic organisms. Nearly 20 years ago several investigators reported the presence of iso-forms of ferredoxins in various photosynthetic and nonphotosynthetic bacteria and oxygenic photosynthetic organisms (see Ref. 371 and references therein), but the significance of this multiplicity was far from clear. The first clear evidence of a distinct function for an iso-ferredoxin was the isolation of a ferredoxin from the heterocysts of the cyanobacterium, *Anabaena variabilis*. Only the heterocystous ferredoxin donated electrons to nitrogenase and the vegetative cell ferredoxin was ineffective in this reduction. Another ferredoxin in the heterocysts corresponded to the vegetative cell type and was assumed to function in the adapted photosynthetic system of this specialized cell to supply energy for nitrogen fixation. The [2Fe-2S] ferredoxins found in plant leaves and other oxygenic photosynthetic organisms function

TABLE I
NUMBER OF FERREDOXINS AND FERREDOXIN-LIKE PROTEINS IN
PHOTOSYNTHETIC ORGANISMS

Source	Ferredoxin and related protein			HiPIP [4Fe-4S]
	2[4Fe-4S]	[4Fe-4S] · [3Fe-4S]	[2Fe-2S]	
Spinach				
Leaves	2 ^{a,b}	—	2	—
Roots	—	—	1	—
<i>Anabaena</i> PCC7120				
Vegetative cells	(2) ^c	—	1	—
Heterocysts	1 + (2) ^c	—	2	—
<i>Chlorobium limicola</i>	2	—	—	—
<i>Chromatium vinosum</i>	1	—	—	1
<i>Rhodobacter capsulatus</i>	2	1	1	—

^a The reaction center F_A/F_B protein encoded by the *frxA* (liverwort) gene.

^b The membrane-bound protein encoded by the *frxB* (liverwort) gene.

^c The parentheses indicate the probable presence of proteins comparable to those indicated in footnotes *a* and *b*.

as the electron donors to $NADP^+$, but iso-forms of these have also been found in nonphotosynthetic tissues such as white roots. Tissue-specific ferredoxins have also been found in C_4 plants such as maize. Their functions other than in photosynthesis have been the subject of speculation and answers to this question can be anticipated in near future. Another differentiation of the function of iso-ferredoxins was first demonstrated in the photosynthetic purple nonsulfur bacteria, exemplified by *R. capsulatus*. They have at least four ferredoxins of three different types as listed in Table I. Gene inactivation experiments have revealed that two of them, the 2[4Fe-4S] and [2Fe-2S] ferredoxins, function in nitrogen-fixing systems and the [4Fe-4S][3Fe-4S] ferredoxin functions in some as-yet unidentified system that nevertheless has a critical role for the survival of this bacterium. *Chlorobium limicola* was shown to have two ferredoxins with sequences that differed at only a relatively few positions, and these may not have distinct functions. There is no indication whether these bacterial ferredoxins have a specific location in the cell or are associated with particular enzyme or protein complexes. Furthermore, it was surprising to locate in chloroplasts ferredoxin-like proteins very similar to the bacterial 2[4Fe-4S] ferredoxin. One of these functioned as the reaction center protein, F_A/F_B , in pho-

tosystem I of oxygenic photosynthesizers and the other was also found in photosynthetic organisms in a membrane-bound form, though at the moment there is no evidence of its function. Another Fe-S protein encoded by liverwort chloroplast DNA, but not by higher plant chloroplast DNA, is similar to the Fe protein of nitrogenase in prokaryotes. This product of the *frxC* gene has been shown to function in chlorophyll biosynthesis, and not in nitrogen fixation, of which the organism is incapable.

We have briefly reviewed in this article a number of aspects of the structure and functional diversity of ferredoxins and their homologues, but have not included the mechanism of Fe-S cluster formation *in vivo*, which is beyond the scope of the present review. However, recent studies conducted with spinach chloroplasts (372-374) are very interesting in demonstrating that ATP and NADPH are required to form the Fe-S cluster of spinach ferredoxin, when cysteine is used as the sulfur donor. This study is still in progress and we have no idea if the same mechanism as suggested for the spinach chloroplast system can be true also for other Fe-S proteins. There is no doubt that other important and interesting ferredoxins and related proteins will continue to be found and their physical and chemical characterizations, as well as studies of their physiological roles, will further broaden our insight into this important and diverse group of proteins.

ACKNOWLEDGMENTS

The authors express their thanks to Drs. K. Fukuyama, Y. Takahashi, H. Oh-oka, and Y. Fujita for their assistance and discussion in various phases of preparing this article. They are particularly indebted to Professor L. J. Rogers, The University of Wales, for critically reviewing and revising our manuscript.

REFERENCES

1. Valentine, R. C., *Bact. Rev.* **28**, 497 (1964).
2. Mortenson, L. E., Valentine, R. C., and Carnahan, J. E., *Biochem. Biophys. Res. Commun.* **7**, 448 (1962).
3. Mortenson, L. E., Valentine, R. C., and Carnahan, J. E., *J. Biol. Chem.* **238**, 794 (1963).
4. Tagawa, K., and Arnon, D. I., *Nature (London)* **195**, 537 (1962).
5. Fry, K. T., and San Pietro, A., *Biochem. Biophys. Res. Commun.* **9**, 218 (1962).
6. Mortenson, L. E., *Biochim. Biophys. Acta* **81**, 71 (1964).
7. Beinert, H., *FASEB J.* **4**, 2483 (1990).
8. Meyer, J., *Trends Evol. Ecol.* **3**, 222 (1988).

9. Bruschi, M., and Guerlesquin, F., *FEMS Microbiol. Rev.* **54**, 155 (1988).
10. Meyer, T. E., and Cusanovich, M. A., *Biochim. Biophys. Acta* **975**, 1 (1989).
11. Matsubara, H., Hase, T., Wakabayashi, S., and Wada, K., in "The Evolution of Protein Structure and Function" (D. S. Sigman and M. A. B. Brazier, eds.), p. 245. Academic Press, New York, 1980.
12. Matsubara, H., and Hase, T., in "Proteins and Nucleic Acids in Plant Systematics" (U. Jensen and D. E. Fairbrothers, eds.), p. 168. Springer-Verlag, Berlin, Heidelberg, New York, and Tokyo, 1983.
13. Rogers, L. J., in "The Cyanobacteria" (P. Fay and C. Van Baalen, eds.), p. 35. Elsevier, Amsterdam, New York, and Oxford, 1987.
14. Matsubara, H., and Wada, K., in "Methods in Enzymology" (L. Packer and A. N. Glazer, eds.), Vol. 167, p. 387. Academic Press, San Diego, California, 1988.
15. Sakihama, N., and Shin, M., *Arch. Biochem. Biophys.* **256**, 430 (1987).
16. Arnon, D. I., *Trends Biochem. Sci.* **13**, 30 (1988).
17. Arnon, D. I., in "Encyclopedia of Plant Physiology," Vol. 5, p. 8. Springer-Verlag, New York, 1977.
18. Crawford, N. A., Yee, B. C., Droux, M., Carlson, D. E., and Buchanan, B. B., in "Methods in Enzymology" (L. Packer and A. N. Glazer, eds.), Vol. 167, p. 415. Academic Press, San Diego, California, 1988.
19. Schmidt, H., and Heinz, E., *Plant Physiol.* **94**, 214 (1990).
20. Wada, K., Oh-oka, H., and Matsubara, H., *Physiol. Veg.* **23**, 679 (1985).
21. Schrautemeier, B., and Böhme, H., *FEBS Lett.* **184**, 304 (1985).
22. Schrautemeier, B., Böhme, H., and Böger, P., *Biochim. Biophys. Acta* **807**, 147 (1985).
23. Böhme, H., and Schrautemeier, B., *Biochim. Biophys. Acta* **891**, 1 (1987).
24. Böhme, H., and Schrautemeier, B., *Biochim. Biophys. Acta* **891**, 115 (1987).
25. Yakunin, A. F., Chan, K., Laurinavichene, T. U., and Gogotov, I. N., *Biokhimiya* **55**, 80 (1990).
26. Benson, A. M., and Yasunobu, K. T., *J. Biol. Chem.* **244**, 955 (1969).
27. Matsubara, H., Sasaki, R. M., and Chain, R. K., *Proc. Natl. Acad. Sci. U.S.A.* **57**, 439 (1967).
28. Matsubara, H., and Sasaki, R. M., *J. Biol. Chem.* **243**, 1732 (1968).
29. Wedel, N., Bartling, D., and Hermann, R. G., *Bot. Acta* **101**, 295 (1988).
30. Takahashi, Y., Hase, T., Wada, K., and Matsubara H., *Plant Cell Physiol.* **24**, 189 (1983).
31. Keresztes-Nagy, S., Perini, F., and Margoliash, E., *J. Biol. Chem.* **244**, 981 (1969).
32. Takruri, I., and Boulter, D., *Phytochemistry* **18**, 1481 (1979).
33. Nakano, T., Hase, T., and Matsubara, H., *J. Biochem. (Tokyo)* **90**, 1725 (1981).
34. Takruri, I., and Boulter, D., *Biochem. J.* **185**, 239 (1980).
35. Takruri, I., Gilroy, J., and Boulter, D., *Phytochemistry* **21**, 325 (1982).
36. Takruri, I., and Boulter, D., *Biochem. J.* **179**, 373 (1979).
37. Rao, K. K., and Matsubara, H., *Biochem. Biophys. Res. Commun.* **38**, 500 (1970).
38. Wakabayashi, S., Hase, T., Wada, K., Matsubara, H., Suzuki, K., and Takaichi, S., *J. Biochem. (Tokyo)* **83**, 1305 (1978).
39. Wakabayashi, S., Hase, T., Wada, K., Matsubara, H., and Suzuki, K., *J. Biochem. (Tokyo)* **87**, 227 (1980).
40. Smeekens, S., Van Binsbergen, J., and Weisbeek, P. J., *Nucleic Acids Res.* **13**, 3179 (1985).
41. Wada, K., Onda, M., and Matsubara, H., *J. Biochem. (Tokyo)* **105**, 619 (1989).

42. Hase, T., Kimata, Y., Yonekura, K., Matsumura, T., and Sakakibara, H., *Plant Physiol.* **96**, 77 (1991).
43. Elliott, R. C., Pedersen, T. J., Fristensky, B., White, M. J., Dickey, L. F., and Thompson, W. F., *Plant Cell* **1**, 681 (1989).
44. Somers, D. E., Caspar, T., and Quail, P. H., *Plant Physiol.* **93**, 572 (1989).
45. Hase, T., Wada, K., and Matsubara, H., *J. Biochem. (Tokyo)* **82**, 267 (1977).
46. Hase, T., Wada, K., and Matsubara, H., *J. Biochem. (Tokyo)* **82**, 277 (1977).
47. Minami, Y., Wakabayashi, S., Imoto, S., Ohta, Y., and Matsubara, H., *J. Biochem. (Tokyo)*, **98**, 649 (1985).
48. Hase, T., Yamanashi, H., and Matsubara, H., *J. Biochem. (Tokyo)* **91**, 341 (1982).
49. Kamo, M., Kotani, N., Tsugita, A., He, Y.-K., and Nozu, Y., *Protein Seq. Data Anal.* **2**, 289 (1989).
50. Wada, K., in "Biological Approaches and Evolutionary Trends in Plants" (S. Kawano, ed.), p. 159. Academic Press, New York, 1990.
51. Minami, Y., Sugimura, Y., Wakabayashi, S., Wada, K., Takahashi, Y., and Matsubara, H., *Physiol. Veg.* **23**, 669 (1985).
52. Masui, R., Wada, K., Matsubara, H., Williams, M. M., and Rogers, L. J., *Phytochemistry* **27**, 2817 (1988).
53. Sugeno, K., and Matsubara, H., *J. Biol. Chem.* **244**, 2979 (1969).
54. Hase, T., Matsubara, H., Ben-Amotz, A., Rao, K. K., and Hall, D. O., *Phytochemistry* **19**, 2065 (1980).
55. Schmitter, J.-M., Jacquot, J.-P., de Lamotte-Juery, F., Beauvallet, C., Dutka, S., Gadal, P., and Decottignies, P., *Eur. J. Biochem. (Tokyo)* **172**, 405 (1988).
56. Uchida, A., Ebata, S., Wada, K., Matsubara, H., and Ishida, Y., *J. Biochem. (Tokyo)* **104**, 700 (1988).
57. Takruri, I., Haslett, B. G., Boulter, D., Andrew, P. W., and Rogers, L. J., *Biochem. J.* **173**, 459 (1978).
58. Inoue, K., Hase, T., Bögers, P., and Matsubara, H., *J. Biochem. (Tokyo)* **94**, 1451 (1983).
59. Inoue, K., Hase, T., Matsubara, H., Fitzgerald, M. P., and Rogers, L. J., *Phytochemistry* **23**, 773 (1984).
60. Hase, T., Wakabayashi, S., Wada, K., Matsubara, H., Jüttner, H., Rao, K. K., Fry, I., and Hall, D. O., *FEBS Lett.* **96**, 41 (1978).
61. Hase, T., Wakabayashi, S., Matsubara, H., Rao, K. K., Hall, D. O., Widmer, H., Gysi, J., and Zuber, H., *Phytochemistry* **17**, 1863 (1987).
62. Takahashi, Y., Hase, T., Matsubara, H., Hutber, G. N., and Rogers, L. J., *J. Biochem. (Tokyo)* **92**, 1363 (1981).
63. Wada, K., Hase, T., Tokunaga, H., and Matsubara, H., *FEBS Lett.* **55**, 102 (1975).
64. Matsubara, H., Wada, K., and Masaki, R., in "Iron and Copper Proteins" (K. T. Yasunobu, H. F. Mower, and O. Hayaishi, eds.), p. 1. Plenum, New York, 1976.
65. Tanaka, M., Haniu, M., Yasunobu, K. T., Rao, K. K., and Hall, D. O., *Biochem. Biophys. Res. Commun.* **69**, 759 (1976).
66. Tanaka, M., Haniu, M., Yasunobu, K. T., Rao, K. K., and Hall, D. O., *Biochemistry* **14**, 5535 (1975).
67. Lee, I. S., Hase, T., Matsubara, H., Ho, K. K., and Krogmann, D. W., *Biochim. Biophys. Acta* **744**, 53 (1983).
68. Hase, T., Wada, K., Ohmiya, M., and Matsubara, H., *J. Biochem. (Tokyo)* **80**, 993 (1976).
69. Hase, T., Matsubara, H., Hutber, G. N., and Rogers, L. J., *J. Biochem. (Tokyo)* **92**, 1347 (1982).

70. Alam, J., Whitaker, R. A., Krogmann, D. W., and Curtis, S. E., *J. Bacteriol.* **168**, 1265 (1986).
71. Chan, T.-M., Hermodson, M. A., Ulrich, E. L., and Markeley, J. L., *Biochemistry* **22**, 5988 (1983).
72. Van der Plas, J., de Groot, R. P., Weisbeek, P. J., and van Arkel, G. A., *Nucleic Acids Res.* **14**, 7803 (1986).
73. Böhme, H., and Haselkorn, R., *Mol. Gen. Genet.* **214**, 278 (1988).
74. Van der Plas, J., de Groot, R. P., Woortman, M. R., Weisbeek, R. J., and van Arkel, G. A., *Nucleic Acids Res.* **14**, 7804 (1986).
75. Reith, M. E., Laudenbach, D. E., and Strauss, N. A., *J. Bacteriol.* **168**, 1319 (1986).
76. Hase, T., Matsubara, H., Koike, H., and Katoh, S., *Biochim. Biophys. Acta* **744**, 46 (1983).
77. Masui, R., Wada, K., Matsubara, H., and Rogers, L. J., *Phytochemistry* **27**, 2821 (1988).
78. Wada, K., Masui, R., Matsubara, H., and Rogers, L. J., *Biochem. J.* **252**, 571 (1988).
79. Cozens, A. L., and Walker, J. E., *Biochem. J.* **252**, 563 (1988).
80. Hase, T., Inoue, K., Matsubara, H., Williams, M. M., and Rogers, L. J., *J. Biochem. (Tokyo)* **92**, 1357 (1982).
81. Hase, T., Inoue, K., Hagihara, N., Matsubara, H., Williams, M. M., and Rogers, L. J., *J. Biochem. (Tokyo)* **94**, 1457 (1983).
82. Hase, T., Wada, K., and Matsubara, H., *J. Biochem. (Tokyo)* **79**, 329 (1976).
83. Hase, T., Wakabayashi, S., Wada, K., and Matsubara, H., *J. Biochem. (Tokyo)* **83**, 761 (1978).
84. Neumann-Spallart, C., Brandtner, M., Kraus, M., Jakowitsch, J., Bayer, M. G., Maier, T. L., Schenk, H. E. A., and Löffelhardt, W., *FEBS Lett.* **268**, 55 (1990).
85. Van der Plas, J., De Groot, R., Woortman, M., Cremers, F., Borrias, M., Van Arkel, G., and Weisbeek, P., *Photosynth. Res.* **18**, 179 (1988).
86. Fukuyama, K., Hase, T., Matsumoto, S., Tsukihara, T., Katsube, Y., Tanaka, N., Kakudo, M., Wada, K., and Matsubara, H., *Nature (London)* **286**, 522 (1980).
87. Tsukihara, T., Fukuyama, K., Nakamura, M., Katsube, Y., Tanaka, N., Kakudo, M., Wada, K., Hase, T., and Matsubara, H., *J. Biochem. (Tokyo)* **90**, 1763 (1981).
88. Tsukihara, T., Fukuyama, K., Mizushima, M., Harioka, T., Kusunoki, M., Katsube, Y., Hase, T., and Matsubara, H., *J. Mol. Biol.* **216**, 399 (1990).
89. Rypniewski, W. R., Breiter, D. R., Benning, M. M., Wesenberg, G., Oh, B.-H., Markley, J. L., Rayment, I., and Holden, H. M., *Biochemistry* **30**, 4126 (1991).
90. Otaka, E., and Ooi, T., *J. Mol. Evol.* **29**, 246 (1989).
91. Hunt, L. T., George, D. G., and Barker, W. C., *BioSystems* **18**, 223 (1985).
92. Matsubara, H., Hase, T., Wakabayashi, S., and Wada, K., in "Evolution of Protein Molecules" (H. Matsubara and T. Yamanaka, eds.), p. 209. Japan Sci. Soc. Press Center for Acad. Publ. Japan, Tokyo, 1978.
93. Matsubara, H., Jukes, T. H., and Cantor, C. R., *Brookhaven Symp. Biol.* **21**, 201 (1968).
94. Schwartz, R. M., and Dayhoff, M. O., in "Atlas of Protein Sequence and Structure" (M. O. Dayhoff, ed.), Vol. 5, Suppl. 3, p. 45. Natl. Biomed. Res. Foundation, Washington, D.C., 1978.
95. Tsukihara, T., Katsube, Y., Hase, T., Wada, K., and Matsubara, H., in "Molecular Evolution, Protein Polymorphism, and the Neutral Theory" (M. Kimura, ed.), p. 299. Japan Sci. Soc. Press, Tokyo/Springer-Verlag, Berlin, 1982.
96. Wada, K., Matsubara, H., Chain, R. K., and Arnon, D. I., *Plant Cell Physiol.* **22**, 275 (1981).

97. Wada, K., Onda, M., and Matsubara, H., *Plant Cell Physiol* **27**, 407 (1986).
98. Hutson, K. G., Rogers, L. J., Haslett, B. G., Boulter, D., and Cammack, R., *Biochem. J.* **172**, 465 (1978).
99. Hutson, K. G., and Rogers, L. J., *Biochem. Soc. Trans.* **3**, 377 (1975).
100. Cammack, R., Rao, K. K., Barger, C. P., Hutson, K. G., Andrew, P. W., and Rogers, L. J., *Biochem. J.* **168**, 205 (1977).
101. Castenholz, R. W., in "Methods in Enzymology" (L. Packer and A. N. Glazer, eds.), Vol. 167, p. 68. Academic Press, San Diego, C.
102. Tsukihara, T., Kobayashi, M., Nakamura, M., Katsube, Y., Fukuyama, K., Hase, T., Wada, K., and Matsubara, H., *BioSystems* **15**, 243 (1982).
103. Tsukihara, T., Fukuyama, K., and Katsube, Y., in "Iron-Sulfur Protein Research" (H. Matsubara, Y. Katsube, and K. Wada, eds.), p. 59. Japan Sci. Soc. Press, Tokyo/Springer-Verlag, Berlin, 1987.
104. Böhme, H., and Haselkorn, R., *Plant Mol. Biol.* **12**, 667 (1989).
105. Takahashi, Y., Hase, T., Wada, K., and Matsubara, H., *J. Biochem. (Tokyo)* **90**, 1825 (1981).
106. Ohmori, D., Hasumi, H., Yamakura, F., Murakami, M., Fujisawa, K., Taneoka, Y., and Yamamura, T., *Biochim. Biophys. Acta* **996**, 166 (1989).
107. Hasumi, H., and Ohmori, D., *Biochim. Biophys. Acta* **996**, 173 (1989).
108. Hirasawa, M., Sung, J.-D., Malkin, R., Zilber, A., Droux, M., and Knaff, D. B., *Biochim. Biophys. Acta* **934**, 169 (1988).
109. Ishiyama, Y., Shinoda, I., and Tamura, G., *Agric. Biol. Chem.* **49**, 2223 (1985).
110. Shanmugam, K. T., Buchanan, B. B., and Arnon, D. I., *Biochim. Biophys. Acta* **256**, 477 (1972).
111. Dutton, J. E., Rogers, L. J., Haslett, B. G., Takruri, I. A. H., Gleaves, J. T., and Boulter, D., *J. Exp. Bot.* **31**, 379 (1980).
112. Suzuki, A., Oaks, A., Jacquot, J.-P., Vidal, J., and Gadal, P., *Plant Physiol.* **78**, 374 (1985).
113. Vorst, O., van Dam, F., Oosterhoff-Teertstra, R., Smeekens, S., and Weisbeek, P., *Plant Mol. Biol.* **14**, 491 (1990).
114. Morigasaki, S., Takata, K., Sanada, Y., Wada, K., Yee, B. C., Shin, S., and Buchanan, B. B., *Arch. Biochem. Biophys.* **283**, 75 (1990).
115. Kimata, I., and Hase, T., *Plant Physiol.* **89**, 1193 (1989).
116. Hooper, J. K., "Chloroplasts." Plenum, New York, 1984.
117. Dobres, M. S., Elliott, R. C., Watson, J. C., and Thompson, W. F., *Plant Mol. Biol.* **8**, 53 (1987).
118. Morigasaki, S., Takata, K., Suzuki, T., and Wada, K., *Plant Physiol.* **93**, 896 (1989).
119. Ninomiya, Y., and Sato, S., *Plant Cell Physiol.* **25**, 453 (1984).
120. Cozens, A. L., and Walker, J. E., *J. Mol. Biol.* **194**, 359 (1987).
121. Cohn, L. C., Alam, J., and Krogmann, D. W., *Physiol. Veg.* **23**, 659 (1985).
122. Hutber, G. N., Smith, A. J., and Rogers, L. J., *FEMS Microbiol. Lett.* **4**, 11 (1978).
123. Hutson, K. G., Rogers, L. J., Haslett, B. G., and Boulter, D., *FEMS Microbiol. Lett.* **7**, 279 (1980).
124. Kerscher, L., and Oesterheld, D., *FEBS Lett.* **67**, 320 (1976).
125. Kerscher, L., Oesterheld, D., Cammack, R., and Hall, D. O., *Eur. J. Biochem. (Tokyo)* **71**, 101 (1976).
126. Werber, M. M., and Mevarech, M., *Arch. Biochem. Biophys.* **187**, 447 (1978).
127. Geiger, B., Mevarech, M., and Werber, M. M., *Eur. J. Biochem.* **84**, 449 (1978).
128. Kerscher, L., and Oesterheld, D., *FEBS Lett.* **83**, 197 (1977).
129. Werber, M. M., and Mevarech, M., *Arch. Biochem. Biophys.* **186**, 60 (1978).

130. Werber, M. M., Shahak, Y., and Avron, M., *FEBS Lett.* **113**, 111 (1980).
131. Batie, C. J., and Kamin, H., *J. Biol. Chem.* **259**, 8832 (1984).
132. Batie, C. J., and Kamin, H., *J. Biol. Chem.* **259**, 11976 (1984).
133. Masaki, R., Yoshikawa, S., and Matsubara, H., *Biochim. Biophys. Acta* **700**, 101 (1982).
134. Yoshikawa, S., Ohnishi, N., Morigiwa, A., Takeshima, K., Matsumoto, M., Nishiyama, K., Matsubara, H., and Kodo, K., in "Flavins and Flavoproteins" (R. C. Bray, P. C. Engel, and S. G. Mayhew, eds.), p. 489. de Gruyter, Berlin and New York, 1984.
135. Hase, T., Wakabayashi, S., Matsubara, H., Kerscher, L., Oesterheld, D., Rao, K. K., and Hall, D. O., *FEBS Lett.* **77**, 308 (1977); Hase, T., Wakabayashi, S., Matsubara, H., Kerscher, L., Oesterheld, D., Rao, K. K., and Hall, D. O., *J. Biochem. (Tokyo)* **83**, 1657 (1978).
136. Hase, T., Wakabayashi, S., Matsubara, H., Mevarech, M., and Werber, M. M., *Biochim. Biophys. Acta* **623**, 139 (1980).
137. Sussman, J. L., Brown, J. H., and Shoham, M., in "Iron-Sulfur Protein Research" (H. Matsubara, Y. Katsube, and K. Wada, eds.), p. 69. Japan Sci. Soc. Press, Tokyo/Springer-Verlag, Berlin, Heidelberg, New York, London, Paris, and Tokyo, 1987.
138. Sussman, J. L., Zipori, P., Harel, M., Yonath, A., and Werber, M. M., *J. Mol. Biol.* **134**, 375 (1979).
139. Saeki, K., Miyatake, Y., Young, D. A., Marrs, B. L., and Matsubara, H., *Nucleic Acids Res.* **18**, 1060 (1990).
140. Schatt, E., Jouanneau, Y., and Vignais, P. M., *J. Bacteriol.* **171**, 6218 (1989).
141. Scherings, G., Haaker, H., and Veeger, C., *Eur. J. Biochem.* **77**, 621 (1977).
142. Saeki, K., Suetsugu, Y., Tokuda, K., Miyatake, Y., Young, D. A., Marrs, B. L., and Matsubara, H., *J. Biol. Chem.* **266**, 12889 (1991).
143. Jouanneau, Y., Richaud, P., and Grabau, C., *Nucleic Acids Res.* **18**, 5284 (1990).
144. Grabau, C., Shatt, E., Jouanneau, Y., and Vignais, P. M., *J. Biol. Chem.* **266**, 3294 (1991).
145. Meyer, J., Moulis, J. M., and Lutz, M., *Biochem. Biophys. Res. Commun.* **119**, 828 (1984).
146. Meyer, J., Bruschi, M. H., Bonicel, J. J., and Bovier-Lapierre, G. E., *Biochemistry* **25**, 6054 (1986).
147. Cardenas, J., Mortenson, L. E., and Yoch, D. C., *Biochim. Biophys. Acta* **434**, 244 (1976).
148. Meyer, T. E., Cannac, V., Fitch, J., Bartsch, R. G., Tollin, D., Tollin, G., and Cusanovich, M. A., *Biochim. Biophys. Acta* **1017**, 125 (1990).
149. Yamanaka, T., and Kamen, M. D., *Biochim. Biophys. Acta* **131**, 317 (1967).
150. Gunsalus, S. E., and Lipscomb, J. D., in "Iron-Sulfur Proteins" (W. Lovenberg, ed.), Vol. 1, p. 151. Academic Press, New York, 1973.
151. Gerber, N. C., Horiuchi, T., Koga, H., and Sligar, S. G., *Biochem. Biophys. Res. Commun.* **169**, 1016 (1990).
152. Haigler, B. E., and Gibson, D. T., *J. Bacteriol.* **172**, 465 (1990).
153. Crutcher, S. E., and Geary, P. J., *Biochem. J.* **177**, 393 (1979).
154. Geary, P. J., Saboowalla, F., Patel, D. S., and Cammack, R., *Biochem. J.* **217**, 667 (1984).
155. Morrice, N., Geary, P., Cammack, R., Harris, A., Beg, F., and Aitken, A., *FEBS Lett.* **231**, 336 (1988).
156. Irie, S., Doi, S., Yorifuji, T., Takagi, M., and Yano, K., *J. Bacteriol.* **169**, 5174 (1987).

157. Tanaka, M., Haniu, M., Yasunobu, K. T., and Kimura, T., *J. Biol. Chem.* **248**, 1141 (1973).
158. Cupp, J. R., and Vickery, L. E., *J. Biol. Chem.* **263**, 17418 (1988).
159. Gorrell, T. E., Yarlott, N., and Müller, M., *Carlsberg Res. Commun.* **49**, 259 (1984).
160. Johnson, P. J., D'Oliveira, C. E., Gorrell, T. E., and Müller, M., *Proc. Natl. Acad. Sci. U.S.A.* **87**, 6097 (1990).
161. Suzuki, M., Hayakawa, T., Shaw, J. P., Rekik, M., and Harayama, S., *J. Bacteriol.* **173**, 1690 (1991).
162. Yao, Y., Tamura, K., Wada, K., Matsubara, H., and Kodo, K., *J. Biochem.* **95**, 1513 (1984); with a correction in *J. Biochem.* **96**, 935 (1984).
163. Karplus, P. A., Walsh, K. A., and Herriott, J. R., *Biochemistry* **23**, 6576 (1984).
164. Brunel, F., and Davison, J., *J. Bacteriol.* **170**, 4924 (1988).
165. Stainthorpe, A. C., Lees, V., Salmond, G. P. C., Dalton, H., and Murell, J. C., *Gene* **9**, 27 (1990).
166. Nordlund, I., Powlowski, J., and Shingler, V., *J. Bacteriol.* **172**, 6826 (1990).
167. Ichikawa, Y., Hamamoto, I., Waki, N., Iwahashi, K., Hiwatashi, A., and Tsubaki, M., in "Iron-Sulfur Protein Research" (H. Matsubara, Y. Katsube, and K. Wada, eds.), p. 97. Japan Sci. Soc. Press, Tokyo/Springer-Verlag, Berlin, 1986.
168. Picado-Leonard, J., Voutilainen, R., Kao, L.-C., Chun, B.-C., Strauss III, J. F., and Miller, W. L., *J. Biol. Chem.* **263**, 3240 (1988).
169. Driscoll, W. J., and Omdahl, J. L., *Eur. J. Biochem.* **185**, 181 (1989).
170. Okamura, T., John, M. E., Zuber, M. X., Simpson, E. R., and Waterman, M. R., *Proc. Natl. Acad. Sci. U.S.A.* **82**, 5705 (1985).
171. Okamura, T., Kagimoto, M., Simpson, E. R., and Waterman, M., *J. Biol. Chem.* **262**, 10335 (1987).
172. Bhasker, C. R., Okamura, T., Simpson, E. R., and Waterman, M. R., *Eur. J. Biochem.* **164**, 21 (1987).
173. Sakihama, N., Hiwatashi, A., Miyatake, A., Shin, M., and Ichikawa, Y., *Arch. Biochem. Biophys.* **264**, 23 (1988).
174. Akhrem, A. A., Lapko, A. G., Lapko, V. N., Morozova, L. A., Repin, V. A., Tishchenko, I. V., and Chashchin, V. L., *Bioorg. Khim.* **4**, 462 (1978).
175. Kagimoto, K., McCarthy, J. L., Waterman, M. R., and Kagimoto, M., *Biochem. Biophys. Res. Commun.* **155**, 379 (1988).
176. Mittal, S., Zhu, Y.-Z., and Vickery, L. E., *Arch. Biochem. Biophys.* **264**, 383 (1988).
177. Hatefi, Y., Ragan, C. I., and Galante, Y. M., in "The Enzymes of Biological Membranes" (A. N. Martonosi, ed.), Vol. 4. p. 1. Plenum, New York, 1985.
178. Ohnishi, T., *Curr. Top. Bioenerg.* **15**, 37 (1987).
179. Weiss, H., and Kolb, H. J., *Eur. J. Biochem.* **99**, 139 (1979).
180. Hederstedt, L., and Rutberg, L., *Microbiol. Rev.* **45**, 542 (1981).
181. Crowe, B. A., Owen, P., Patil, D. S., and Cammack, R., *Eur. J. Biochem.* **137**, 191 (1983).
182. Wood, D., Darlison, M. G., Wilde, R. J., and Guest, J. R., *Biochem. J.* **222**, 519 (1984).
183. Darlison, M. G., and Guest, J. R., *Biochem. J.* **223**, 507 (1984).
184. Pennoyer, J. D., Ohnishi, T., and Trumpower, B. L., *Biochim. Biophys. Acta* **935**, 195 (1988).
185. Philips, M. K., Hederstedt, L., Hasnain, S., Rutberg, L., and Guest, J. R., *J. Bacteriol.* **169**, 864 (1987).
186. Lombardo, A., Carine, K., and Scheffler, I. E., *J. Biol. Chem.* **265**, 10419 (1990).

187. Gould, S. J., Subramani, S., and Scheffler, I. E., *Proc. Natl. Acad. Sci. U.S.A.* **86**, 1934 (1987).
188. Yao, Y., Wakabayashi, S., Matsuda, S., Matsubara, H., Yu, L., and Yu, C.-A., in "Iron-Sulfur Protein Research" (H. Matsubara, Y. Katsube, and K. Wada, eds.), p. 240. Japan Sci. Soc. Press, Tokyo/Springer-Verlag, Berlin, 1987.
189. Cole, S. T., *Eur. J. Biochem.* **122**, 479 (1982).
190. Cole, S. T., Grundström, T., Jaurin, B., Robinson, J. J., and Weiner, J. H., *Eur. J. Biochem.* **126**, 211 (1982).
191. Grundström, T., and Jaurin, B., *Proc. Natl. Acad. Sci. U.S.A.* **79**, 1111 (1982).
192. Cole, S. T., *Eur. J. Biochem.* **167**, 481 (1987).
193. Lauterbach, F., Körtner, C., Arbracht, S. P. J., Unden, G., and Kröger, A., *Arch. Microbiol.* **154**, 386 (1990).
194. Cammack, R., Patil, D. S., and Weiner, J. H., *Biochim. Biophys. Acta* **870**, 545 (1986).
195. Johnson, M. K., Morningstar, J. E., Cecchini, G., and Ackrell, B. A. C., *Biochem. Biophys. Res. Commun.* **131**, 653 (1985).
196. Åvarsson, A., and Hederstedt, L., *FEBS Lett.* **232**, 298 (1988).
197. Johnson, M. K., Kowal, A. T., Morningstar, J. E., Oliver, M. E., Whittaker, K., Gunsalus, R. P., Ackrell, B. A. C., and Cecchini, G., *J. Biol. Chem.* **263**, 14732 (1988).
198. Werth, M. T., Cecchini, G., Manodori, A., Ackrell, B. A. C., Schröder, I., Gunsalus, R. P., and Johnson, M. K., *Proc. Natl. Acad. Sci. U.S.A.* **87**, 8965 (1990).
199. Hauska, G., Nitschke, W., and Herrmann, R. G., *J. Bioenerg. Biomembr.* **20**, 211 (1988).
200. Tamura, G., in "Iron-Sulfur Protein Research" (H. Matsubara, Y. Katsube, and K. Wada, eds.), p. 210. Japan Sci. Soc. Press, Tokyo/Springer-Verlag, Berlin, 1987.
201. Lim, L. W., Shmala, N., and Mathews, F. S., *J. Biol. Chem.* **261**, 15140 (1986).
202. Okawara, N., Ogata, M., Yagi, T., Wakabayashi, S., and Matsubara, H., *Biochimie* **70**, 1815 (1988).
203. Yang, S.-S., Ljungdahl, L. G., and LeGall, J., *J. Bacteriol.* **130**, 1084 (1977).
204. Ragsdale, S. W., and Ljungdahl, L. G., *J. Bacteriol.* **157**, 1 (1984).
205. Terlesky, K. C., and Ferry, J. G., *J. Biol. Chem.* **263**, 4080 (1988).
206. Johnson, P. W., and Canale-Parola, E., *Arch. Mikrobiol.* **89**, 341 (1973).
207. Mullinger, R. N., Cammack, R., Rao, K. K., Hall, D. O., Dickson, D. P. E., Johnson, C. E., Rush, J. D., and Simopoulos, A., *Biochem. J.* **151**, 75 (1975).
208. Tsukihara, T., Homma, K., Fukuyama, K., Katsube, Y., Hase, T., Matsubara, H., Tanaka, N., and Kakudo, M., *J. Mol. Biol.* **152**, 821 (1981).
209. Aono, S., Bryant, F. O., and Adams, M. W. W., *J. Bacteriol.* **171**, 3433 (1989).
210. Bruschi, M., *Biochem. Biophys. Res. Commun.* **91**, 623 (1979).
211. Bruschi, M., and Hatchikian, E. C., *Biochimie* **64**, 503 (1982).
212. Bruschi, M., Guerlesquin, F. A., Bovier-Lapierre, G. E., Bonicel, J. J., and Couchoud, P. M., *J. Biol. Chem.* **260**, 8292 (1985).
213. Hase, T., Ohmiya, N., Matsubara, H., Mullinger, R. N., Rao, K. K., and Hall, D. O., *Biochem. J.* **159**, 55 (1976).
214. Fukuyama, K., Nagahara, Y., Tsukihara, T., Katsube, Y., Hase, T., and Matsubara, H., *J. Mol. Biol.* **199**, 183 (1988).
215. Elliott, J., Yang, S.-S., Ljungdahl, L. G., Travis, J., and Reilly, C. F., *Biochemistry* **21**, 3294 (1982).
216. Kissinger, C. R., Adman, E. T., Sieker, L. C., Jensen, L. H., and LeGall, J., *FEBS Lett.* **244**, 447 (1989).

217. Fukuyama, K., Matsubara, H., Tsukihara, T., and Katsube, Y., *J. Mol. Biol.* **210**, 383 (1989).
218. Adman, E. T., Sieker, L. C., and Jensen, L. H., *J. Biol. Chem.* **248**, 3987 (1973).
- 218a. Tsunoda, J. N., Yasunobu, K. T., and Whiteley, H. R., *J. Biol. Chem.* **243**, 6262 (1968).
219. Fukuyama, K., *New Lett. Res. Center Protein Eng.* (in Japanese) **3**, 19 (1989).
220. Moura, J. J. G., Xavier, A. V., Hatchikian, E. G., and LeGall, J., *FEBS Lett.* **89**, 177 (1978).
221. Marion, D., and Guerlesquin, F., *Biochem. Biophys. Res. Commun.* **159**, 592 (1989).
222. Fukuyama, K., and Matsubara, H., *Seikagaku* **60**, 541 (1988).
223. Bruschi, M., and Couchoud, P., *Biochem. Biophys. Res. Commun.* **91**, 623 (1979).
224. George, D. G., Hunt, L. T., Yeh, L.-S. L., and Barker, W. C., *J. Mol. Evol.* **22**, 20 (1985).
225. Meyer, T. E., Cusanovich, M. A., and Kamen, M. D., *Proc. Natl. Acad. Sci. U.S.A.* **83**, 217 (1986).
226. Fitch, W. M., and Bruschi, M., *J. Mol. Evol.* **4**, 381 (1987).
227. Otaka, E., and Ooi, T., *J. Mol. Evol.* **26**, 257 (1987).
228. Earl, C. D., Ronson, C. W., and Ausubel, F. M., *J. Bacteriol.* **169**, 1127 (1987).
229. Dusha, I., Kovalenko, S., Banfalvi, Z., and Kondrosi, A., *J. Bacteriol.* **169**, 1403 (1987).
230. Buikema, W. J., Szeto, W. W., Lemley, P. V., Orme-Johnson, W. H., and Ausubel, F. M., *Nucleic Acids. Res.* **13**, 4539 (1985).
231. Iismaa, S. E., and Watson, J. M., *Nucleic Acids Res.* **15**, 3180 (1987).
232. Grönger, P., Manian, S. S., Reilander, H., O'Connell, M., Priefer, U. B., and Pühler, A., *Nucleic Acids. Res.* **15**, 31 (1987).
233. Gubler, M., Zürcher, T., and Hennecke, H., *Mol. Microbiol.* **3**, 141 (1989).
234. Arigoni, F., Kaminski, P. A., Hennecke, H., and Elmerich, C., *Mol. Gen. Genet.* **225**, 514 (1991).
235. Bruschi, M., Cambillan, C., Bovier-Lapierre, G., Bonicel, J., and Forget, P., *Biochim. Biophys. Acta.* **873**, 31 (1986).
236. Hatchikian, E. C., Fardeau, M. L., Bruschi, M., Belaich, J. P., Chapman, A., and Cammack, R., *J. Bacteriol.* **171**, 2384 (1989).
237. Koike, H., and Katoh, S., *Plant Cell Physiol.* **20**, 1157 (1979).
238. Peutz, M. F., and Raidt, H., *Nature (London)* **255**, 256 (1975).
239. Bruschi, M., Bonicel, J., Hatchikian, E. C., Fardeau, M. L., Belaich, J. P., and Frey, M., *Biochim. Biophys. Acta* **1076**, 79 (1991).
240. Conover, R. C., Kowal, A. T., Fu, W., Park, J.-B., Aono, S., Adams, M. W. W., and Johnson, M. K., *J. Biol. Chem.* **265**, 8533 (1990).
241. Conover, R., Park, J.-B., Adams, M. W. W., and Johnson, M. K., *J. Am. Chem. Soc.* **113**, 2799 (1991).
242. Dus, K., DeKlerk, H., Sletten, K., and Bartsch, R. G., *Biochim. Biophys. Acta* **140**, 291 (1967).
243. Meyer, T. E., Fitch, J., Bartsch, R. G., Tollin, D., and Cusanovich, M. A., *Biochim. Biophys. Acta* **1017**, 118 (1990).
244. Ciszewska, H., Bagyinka, C., Tigyi, G., and Kovacs, K. L., *Acta Biochim. Biophys. Hung.* **24**, 361 (1989).
245. Tedro, S. M., Meyer, T. E., and Kamen, M. D., *Arch. Biochem. Biophys.* **241**, 656 (1985).
246. Hori, K., *J. Biochem. (Tokyo)* **50**, 481 (1961).
247. Tedro, S. M., Meyer, T. E., and Kamen, M. D., *J. Biol. Chem.* **252**, 7826 (1977).

248. Bartsch, R. G., in "Bacterial Photosynthesis" (H. Gest, A. San Pietro, and L. P. Vernon, eds.), p. 315. Antioch Press, Yellow Springs, Ohio, 1963.
249. Evans, M. C. W., Lord, A. V., and Reeves, S. G., *Biochem. J.* **138**, 177 (1974).
250. Bartsch, R. G., in "Methods in Enzymology" (S. Fleischer and L. Packer, eds.), Vol. 53, p. 329. Academic Press, New York, 1978.
251. Fukumori, Y., and Yamanaka, T., *Curr. Microbiol.* **3**, 117 (1979).
252. Tedro, S. M., Meyer, T. E., Bartsch, R. G., and Kamen, M. D., *J. Biol. Chem.* **256**, 731 (1981).
253. Tedro, S. M., Meyer, T. E., and Kamen, M. D., *J. Biol. Chem.* **254**, 1495 (1979).
254. Dus, K., Tedro, S. M., Bartsch, R. G., and Kamen, M. D., *J. Biol. Chem.* **248**, 7318 (1973).
255. Tedro, S. M., Meyer, T. E., and Kamen, M. D., *J. Biol. Chem.* **249**, 1182 (1974).
256. Tedro, S. M., Meyer, T. E., and Kamen, M. D., *J. Biol. Chem.* **251**, 129 (1976).
257. Tedro, S. M., Meyer, T. E., and Kamen, M., *Arch. Biochem. Biophys.* **239**, 94 (1985).
258. Carter, C. W., Jr., Kraut, J., Freer, S. T., Xuong, Ng.-H., Alder, R. A., and Bartsch, R. G., *J. Biol. Chem.* **249**, 4212 (1974).
259. Carter, C. W., Jr., Kraut, J., Freer, S. T., and Alden, R. A., *J. Biol. Chem.* **249**, 6339 (1974).
260. Freer, S. T., Alden, R. A., Carter, C. W., Jr., and Kraut, J., *J. Biol. Chem.* **250**, 46 (1975).
261. Carter, C. W., Jr., Kraut, J., Freer, S. T., Alden, R. A., Sieker, L. C., Adman, E., and Jensen, L. H., *Proc. Natl. Acad. Sci. U.S.A.* **69**, 3526 (1972).
262. Carter, C. W., Jr., *J. Biol. Chem.* **252**, 7802 (1977).
263. Holden, H. M., Meyer, T. E., Cusanovich, M. A., and Rayment, I., *J. Biol. Chem.* **261**, 4219 (1986).
264. Holden, H. M., Meyer, T. E., Cusanovich, M. A., and Rayment, I., *J. Biol. Chem.* **261**, 14746 (1986).
265. O'Keefe, D. P., Gibson, K. J., Emptage, M. H., Lenstra, R., Romesser, J. A., Litle, P. J., and Omer, C. A., *Biochemistry* **30**, 447 (1991).
266. Golbeck, J. H., *Biochim. Biophys. Acta* **895**, 167 (1989).
267. Lagoutte, B., and Mathis, P., *Photochem. Photobiol.* **49**, 833 (1989).
268. Scheller, H. V., Svendsen, I., and Møller, B. L., *J. Biol. Chem.* **264**, 6929 (1989).
269. Webber, A. N., and Malkin, R., *FEBS Lett.* **264**, 1 (1990).
270. Coyle, C. L., and Zumft, W. G., in "Iron-Sulfur Protein Research" (H. Matsubara, Y. Katsube, and K. Wada, eds.), p. 185. Japan Sci. Soc. Press, Tokyo/Springer-Verlag, Berlin, 1986.
271. Rees, D., Georgiadis, M., and Chakrabarti, P.; cited by Moffat, A. S., *Science* **250**, 1513 (1990).
272. Ohyama, K., Fukuzawa, H., Kohchi, T., Shirai, H., Sano, T., Sano, S., Umesono, K., Shiki, Y., Takeuchi, M., Chang, Z., Aota, S., Inokuchi, H., and Ozeki, H., *Nature (London)* **322**, 572 (1986).
273. Shinozaki, K., Ohme, M., Tanaka, M., Wakasugi, T., Hayashida, N., Matsubayashi, T., Zaita, N., Chunwongse, J., Obokata, J., Yamaguchi-Shinozaki, K., Ohto, C., Torazawa, K., Meng, B. Y., Sugita, M., Deno, H., Tamagashira, T., Yamada, K., Kushida, J., Takaiwa, F., Kato, A., Tohdoh, N., Shimada, H., and Sugiura, M., *EMBO J.* **5**, 2043 (1986).
274. Orme-Johnson, W. H., *Annu. Rev. Biophys. Biophys. Chem.* **14**, 419 (1985).
275. Fujita, Y., Takahashi, Y., Kohchi, T., Ozeki, H., Ohyama, K., and Matsubara, H., *Plant Mol. Biol.* **13**, 551 (1989).
276. Ausubel, F. M., and Cannon, F. C., *Cold Spring Harbor Symp. Quant. Biol.* **45**, 487 (1980).

277. Higgins, C. F., Hiles, I. D., Salmond, G. P. C., Gill, D. R., Downie, J. A., Evans, I. J., Holland, I. B., Gray, L., Buckel, S. D., Bell, A. W., and Hermodson, M. A., *Nature (London)* **323**, 448 (1986).
278. Hausinger, R. P., and Howard, J. B., *J. Biol. Chem.* **258**, 13486 (1983).
279. Hennecke, H., Kaluza, K., Thöny, B., Fukrmann, M., Ludwig, W., and Stackebrandt, E., *Arch. Microbiol.* **142**, 342 (1985).
280. Fujita, Y., Takahashi, Y., Shonai, F., Ogura, Y., and Matsubara, H., *Plant Cell Physiol.* **32**, 1093 (1991).
281. Hearst, J. E., Alberti, M., and Doolittle, R. F., *Cell (Cambridge, Mass.)* **40**, 219 (1985).
282. Youvan, D. C., Bylina, E. J., Alberti, M., Begusch, H., and Hearst, J. E., *Cell (Cambridge, Mass.)* **37**, 949 (1984).
283. Jones, R., and Haselkorn, R., *Nucleic Acids Res.* **16**, 8735 (1988).
284. Kohchi, T., Shirai, H., Fukuzawa, H., Sano, T., Komano, T., Umesono, K., Inokuchi, H., Ozeki, H., and Ohyama, K., *J. Mol. Biol.* **203**, 353 (1988).
285. Mevarech, M., Rice, D., and Haselkorn, R., *Proc. Natl. Acad. Sci. U.S.A.* **77**, 6476 (1980).
286. Griffiths, T. W., *Biochem. J.* **174**, 681 (1978).
287. Schulz, R., Steinmüller, K., Klaas, M., Forreiter, C., Rasmussen, S., Hiller, C., and Apel, K., *Mol. Gen. Genet.* **217**, 355 (1989).
288. Peschek, G. A., Hinterstoisser, B., Wastyn, M., Kuntner, O., Pineau, B., Misbichler, A., and Lang, J., *J. Biol. Chem.* **264**, 11827 (1989).
289. Fujita, Y., Takahashi, Y., Chuganji, M., and Matsubara, H., *Plant Cell Physiol.* **33**, 81 (1992).
290. Hase, T., Wakabayashi, S., Matsubara, H., Evans, M. C. W., and Jennings, J. V., *J. Biochem. (Tokyo)* **83**, 1321 (1978).
291. Tanaka, M., Nakashima, T., Benson, A., Mower, H., and Yasunobu, K. T., *Biochemistry* **5**, 1666 (1966).
292. Tanaka, M., Haniu, M., Yasunobu, K. T., Evans, M. C. W., and Rao, K. K., *Biochemistry* **13**, 2953 (1974).
293. Matsubara, H., Sasaki, R. M., Tsuchiya, D. K., and Evans, M. C. W., *J. Biol. Chem.* **245**, 2121 (1970); revised by Hase, T., Matsubara, H., and Evans, M. C. W., *J. Biochem. (Tokyo)* **81**, 1745 (1977).
294. Minami, Y., Wakabayashi, S., Yamada, F., Wada, K., Zumft, W. G., and Matsubara, H., *J. Biochem. (Tokyo)* **96**, 585 (1984).
295. Saeki, K., Suetsugu, Y., Yao, Y., Horio, T., Marrs, B. L., and Matsubara, H., *J. Biochem. (Tokyo)* **108**, 475 (1990).
296. Jouanneau, Y., Meyer, C., Gaillard, J., and Vignais, P. M., *Biochem. Biophys. Res. Commun.* **171**, 273 (1990).
297. Duport, C., Jouanneau, Y., and Vignais, P. M., *Nucleic Acids Res.* **18**, 4618 (1990).
298. Yoch, D. C., Arnon, D. I., and Sweeney, W. V., *J. Biol. Chem.* **250**, 8330 (1975).
299. Matsubara, H., Inoue, K., Hase, T., Hiura, H., Kakuno, T., Yamashita, J., and Horio, T., *J. Biochem. (Tokyo)* **93**, 1385 (1983).
300. Mulligan, M. E., Buikema, W. J., and Haselkorn, R., *J. Bacteriol.* **170**, 4406 (1988).
301. Klipp, W., Reiländer, H., Schlüter, A., Krey, R., and Pühler, A., *Mol. Gen. Genet.* **216**, 293 (1989).
302. Ebeling, S., Noti, J., and Hennecke, H., *J. Bacteriol.* **170**, 1999 (1988).
303. Joerger, R. D., and Bishop, P. E., *J. Bacteriol.* **170**, 1475 (1988).
304. Robson, R., Woodley, P., and Jones, R., *EMBO J.* **5**, 1159 (1986).
305. Joerger, R. D., Loveless, T. M., Pau, R. N., Mitchenall, L. A., Simon, B. H., and Bishop, P. E., *J. Bacteriol.* **172**, 3400 (1990).

306. Yoch, D. C., in "The Photosynthetic Bacteria" (R. K. Clayton and W. R. Sistrom, eds.), p. 657. Plenum, New York, 1978.
307. Saeki, K., Wakabayashi, S., Zumft, W. G., and Matsubara, H., *J. Biochem. (Tokyo)* **104**, 242 (1988).
308. Trower, M. K., Emptage, M. H., and Sariaslani, F. S., *Biochim. Biophys. Acta* **1037**, 281 (1990).
309. Trower, M. K., Marshall, J. E., Dolesman, M. S., Emptage, M. H., and Sariaslani, F. S., *Biochim. Biophys. Acta* **1037**, 290 (1990).
310. Stout, G. H., Turley, S., Sieker, L. C., and Jensen, L. H., *Proc. Natl. Acad. Sci. U.S.A.* **85**, 1020 (1988).
311. Stout, C. D., *J. Biol. Chem.* **263**, 9256 (1988).
312. Stout, C. D., *J. Mol. Biol.* **205**, 545 (1989).
313. Howard, J. B., Lorschach, T. W., Ghosh, D., Melis, K., and Stout, C. D., *J. Biol. Chem.* **258**, 508 (1983).
314. Robbins, A. H., and Stout, C. D., *Proteins: Struct. Funct. Genet.* **5**, 289 (1989).
315. Hase, T., Wakabayashi, S., Matsubara, H., Imai, T., Matsumoto, T., and Tobari, J., *FEBS Lett.* **103**, 224 (1979).
316. Sato, S., Nakazawa, K., Hon-Nami, K., and Oshima, T., *Biochim. Biophys. Acta* **668**, 277 (1981).
317. Schlatter, D., Waldvogel, S., Zülfi, F., Suter, F., Portmann, W., and Zuber, H., *Biol. Chem. Hoppe-Seyler* **366**, 223 (1985).
318. Armstrong, F. A., George, S. J., Thomson, A. J., and Yates, M. G., *FEBS Lett.* **234**, 107 (1988).
319. Ohmori, D., Yamakura, F., Suzuki, K., Imai, T., and Nagayama, K., in "Iron-Sulfur Protein Research" (H. Matsubara, Y. Katsube, and K. Wada, eds.), p. 116. Japan Sci. Soc. Press, Tokyo/Springer-Verlag, Berlin, 1987.
320. Nagayama, K., Ohmori, D., Imai, T., and Oshima, T., in "Iron-Sulfur Protein Research" (H. Matsubara, Y. Katsube, and K. Wada, eds.), p. 125. Japan Sci. Soc. Press, Tokyo/Springer-Verlag, Berlin, 1987.
321. Martin, A. E., Burgess, B. K., Stout, C. D., Cash, V. L., Dean, D. R., Jensen, G. M., and Stephens, P. J., *Proc. Natl. Acad. Sci. U.S.A.* **87**, 598 (1990).
322. Armstrong, F. A., George, S. J., Cammack, R., Hatchikian, E. C., and Thomson, A. J., *Biochem. J.* **264**, 265 (1989).
323. George, S. J., Armstrong, F. A., Hatchikian, E. C., and Thomson, A. J., *Biochem. J.* **264**, 275 (1989).
324. Robbins, A. H., and Stout, C. D., *Proc. Natl. Acad. Sci. U.S.A.* **86**, 3639 (1989).
325. Ogata, M., Kondo, S., Okawara, N., and Yagi, T., *J. Biochem. (Tokyo)* **103**, 121 (1988).
326. Okawara, N., Ogata, M., Yagi, T., Wakabayashi, S., and Matsubara, H., *J. Biochem. (Tokyo)* **104**, 196 (1988).
327. Morgan, T. V., Lundell, D. J., and Burgess, B. K., *J. Biol. Chem.* **263**, 1370 (1988).
328. Bennett, L. T., Jacobson, M. R., and Dean, D. R., *J. Biol. Chem.* **263**, 1364 (1988).
329. Martin, A. E., Burgess, B. K., Iismaa, S. E., Smartt, C. T., Jacobson, M. R., and Dean, D. R., *J. Bacteriol.* **171**, 3162 (1989).
330. Hallenbeck, P., Jouanneau, Y., and Vignais, P. M., *Biochim. Biophys. Acta* **681**, 168 (1982).
331. Yakunin, A. F., and Gogotov, I. N., *Biochim. Biophys. Acta* **725**, 298 (1983).
332. Yakunin, A. F., and Gogotov, I. N., *Biokhimiya (Moscow)* **52**, 1977 (1987).
333. Hallenbeck, P., *Biochim. Biophys. Acta* **1057**, 97 (1991).
- 333a. Suetsugu, Y., Saeki, K., and Matsubara, H., *FEBS Lett.* **292**, 13 (1991).

- 333b. Duport, C., Jouanneau, Y., and Vignais, P. M., *Mol. Gen. Genet.* **231**, 323 (1992).
334. Moreno-Vivian, C., Hennecke, S., Pühler, A., and Klipp, W., *J. Bacteriol.* **171**, 2591 (1989).
335. Arnold, W., Rump, A., Klipp, W., Priefer, U. B., and Pühler, A., *J. Mol. Biol.* **203**, 715 (1988).
336. Seki, S., Hagiwara, M., Kudo, K., and Ishimoto, M., *J. Biochem. (Tokyo)* **85**, 833 (1979).
337. Seki, Y., Seki, S., and Ishimoto, M., *J. Gen. Appl. Microbiol.* **35**, 167 (1989).
338. Seki-Chiba, S., and Ishimoto, M., *J. Biochem. (Tokyo)* **82**, 1663 (1977).
339. Saeki, K., Jain, M. K., Prince, R. J., Shen, G.-J., and Zeikus, J. G., *J. Bacteriol.* **171**, 4376 (1989).
340. Saeki, K., Yao, Y., Wakabayashi, S., Shen, G.-J., Zeikus, J. G., and Matsubara, H., *J. Biochem. (Tokyo)* **106**, 656 (1989).
341. Lagoutte, B., Setif, P., and Duranton, J., *FEBS Lett.* **174**, 24 (1984).
342. Sakurai, H., and San Pietro, A., *J. Biochem. (Tokyo)* **98**, 69 (1985).
343. Høj, P. B., and Møller, B. L., *J. Biol. Chem.* **261**, 14292 (1986).
344. Oh-oka, H., Takahashi, Y., Wada, K., Matsubara, H., Ohyama, K., and Ozeki, H., *FEBS Lett.* **218**, 52 (1987).
345. Hayashida, N., Matsubayashi, T., Shinozaki, K., Sugiura, M., Inoue, K., and Hiyama, T., *Curr. Genet.* **12**, 247 (1987).
346. Høj, P. B., Svendsen, I., Scheller, H. V., and Møller, B. L., *J. Biol. Chem.* **262**, 12676 (1987).
347. Wynn, R. M., and Malkin, R., *FEBS Lett.* **229**, 293 (1988).
348. Golbeck, J. H., Mehari, T., Parett, K., and Ikegami, I., *FEBS Lett.* **240**, 9 (1988).
349. Oh-oka, H., Takahashi, Y., Kuriyama, K., Saeki, K., and Matsubara, H., *J. Biochem. (Tokyo)* **103**, 962 (1988).
350. Oh-oka, H., Takahashi, Y., Matsubara, H., and Itoh, S., *FEBS Lett.* **234**, 291 (1988).
351. Oh-oka, H., Itoh, S., Saeki, K., Takahashi, Y., and Matsubara, H., *Plant Cell Physiol.* **32**, 11 (1991).
352. Oh-oka, H., Takahashi, Y., and Matsubara, H., *Plant Cell Physiol.* **30**, 869 (1989).
353. Evans, M. C. W., Reeves, S. G., and Cammack, R. **49**, 111 (1974).
354. Scheller, H. V., Svendsen, I., and Møller, B. L., *Carlsberg Res. Commun.* **54**, 11 (1989).
355. Schantz, R., and Bogorad, L., *Plant Mol. Biol.* **11**, 239 (1988).
356. Dunn, P. P. L., and Gray, J. C., *Plant Mol. Biol.* **11**, 311 (1988).
357. Koike, H., Ikeuchi, M., Hiyama, T., and Inoue, Y., *FEBS Lett.* **253**, 257 (1989).
358. Bryant, D. A., Rhiel, E., Lorimier, R., Zhou, J., Stirewalt, V. J., Gasparich, G. E., Dubbs, J. M., and Snyder, W., in "Current Research in Photosynthesis" (M. Baltscheffsky, ed.), Vol. 2, p. 1. Kluwer, Dordrecht, The Netherlands, 1989.
359. Hiratsuka, J., Shimada, H., Whittier, R., Ishibashi, T., Sakamoto, M., Mori, M., Kondo, C., Honji, Y., Sun, C.-R., Meng, B.-Y., Li, Y.-Q., Konno, A., Nishizawa, Y., Hirai, A., Shinozaki, K., and Sugiura, M., *Mol. Gen. Genet.* **217**, 185 (1989).
360. Dunn, P. P., and Gray, J. C., *Nucleic Acids Res.* **16**, 348 (1988).
361. Takahashi, Y., Shonai, F., Fujita, Y., Kohchi, T., Ohyama, K., and Matsubara, H., *Plant Cell Physiol.* **32**, 969 (1991).
362. Matsubayashi, T., Wakasugi, T., Shinozaki, K., Yamaguchi-Shinozaki, K., Zaita, N., Hidaka, T., Meng, B. Y., Ohto, C., Tanaka, M., Kato, A., Maruyama, T., and Sugiura, M., *Mol. Gen. Genet.* **210**, 385 (1987).
363. Wu, M., Nie, Z. Q., and Yang, J., *Plant Cell* **1**, 551 (1989).
364. Lin, C.-H., and Wu, M., *Plant Mol. Biol.* **15**, 449 (1990).

- 365. Fearnly, I. M., Runswick, M. J., and Walker, J. E., *EMBO J.* **8**, 665 (1989).
- 366. Pilkington, S. J., Skehel, J. M., and Walker, J. E., *Biochemistry* **30**, 1901 (1991).
- 367. Dupuis, A., Skehel, J. M., and Walker, J. E., *Biochemistry* **30**, 2954 (1991).
- 368. Böhm, R., Sauter, M., and Böck, A., *Mol. Microbiol.* **4**, 231 (1990).
- 369. Reeve, J. N., Beckler, G. S., Cram, D. S., Hamilton, P. T., Brown, J. W., Krzycki, J. A., Kolodziej, A. F., Alex, L., Ohme-Johnson, W. H., and Walsh, C. T., *Proc. Natl. Acad. Sci. U.S.A.* **86**, 3031 (1989).
- 370. Steigerwald, V. J., Beckler, G. S., and Reeve, J. N., *J. Bacteriol.* **172**, 4715 (1990).
- 371. Hase, T., Wada, K., and Matsubara, H., *J. Biochem. (Tokyo)* **78**, 605 (1975).
- 372. Takahashi, Y., Mitsui, A., Hase, T., and Matsubara, H., *Proc. Natl. Acad. Sci. U.S.A.* **83**, 2434 (1986).
- 373. Takahashi, Y., Mitsui, A., and Matsubara, H., *Plant Physiol.* **95**, 97 (1990).
- 374. Takahashi, Y., Mitsui, A., Fujita, Y., and Matsubara, H., *Plant Physiol.* **95**, 104 (1990).

IRON-SULFUR CLUSTERS IN ENZYMES: THEMES AND VARIATIONS

RICHARD CAMMACK

Division of Biomolecular Sciences, King's College, London W8 7AH, England

- I. Introduction
- II. Methods of Identifying Iron-Sulfur Clusters in Proteins
 - A. Chemical Composition
 - B. Protein Structures
 - C. Amino Acid Sequences
 - D. Site-Directed Mutagenesis Experiments
 - E. Spectroscopy
- III. Classification of Iron-Sulfur Proteins
 - Ferredoxins and Other Electron Transfer Proteins
- IV. Membrane-Bound Iron-Sulfur Enzymes of Bioenergetic Systems
 - A. Respiratory Chains
 - B. Photosystem I
- V. Soluble Proteins with Iron-Sulfur Clusters
 - A. Oxygenase Systems with Iron-Sulfur Clusters
 - B. Iron-Sulfur Proteins with Molybdenum and Tungsten
 - C. Nickel Hydrogenases
 - D. Siroheme Iron-Sulfur Proteins
 - E. Catalytic Iron-Sulfur Clusters and Mixed-Metal Clusters
 - F. Nonredox Enzymes
 - G. Iron-Sulfur Proteins in Gene Regulation
 - H. Iron-Sulfur Proteins of Uncertain Function
- VI. Concluding Remarks
- References

I. Introduction

It would be interesting to know how many different types of iron-sulfur proteins there are. From the inventory of about a dozen ferredoxins and enzymes in 1967 (*1*), the number is now well over 100, and rising steadily. This has come about as more enzymes containing iron and acid-labile sulfide have been isolated, as more types of

iron-sulfur clusters have been found, and as more spectroscopic signals have been observed in biological systems. The large amount of gene sequence information, now emerging, has also revealed many ferredoxin-like sequences in open reading frames.

An even more interesting question is regarding how many functions iron-sulfur clusters may have in nature. They have long been known to function as secondary electron carriers, within or between redox enzyme systems. Now iron-sulfur clusters, long suspected, have been found that have catalytic functions of their own. Different properties of the iron-sulfur clusters are exploited by these systems, including electron transfer, coordination chemistry, and the ability to undergo cluster interconversions.

This review considers the diversity of iron-sulfur proteins. Differences are exhibited at several levels: (1) in the different types of iron-sulfur clusters, which have been identified by structure determination and by spectroscopy; (2) in the proteins that bind these clusters (the same type of cluster may be coordinated to protein domains of different sequences and structure); (3) in the other prosthetic groups that are present; and (4) in the different catalytic activities of the clusters. If we classify the iron-sulfur proteins according to these criteria (Table I), it becomes apparent that there are a number of different distinct structural themes. Within these themes there are variations, in the number and types of iron-sulfur clusters and other prosthetic groups, and in the catalytic functions performed. These relationships have implications for the evolution of the iron-sulfur proteins, which have been discussed elsewhere (2-6).

II. Methods of Identifying Iron-Sulfur Clusters in Proteins

From studies of the ferredoxins and other small iron-sulfur proteins it is known that there is a variety of iron-sulfur cluster types. These clusters are usually, but not invariably, coordinated to cysteine residues of the protein in conserved arrangements (e.g., Figs. 1 and 2). The types of clusters that have been identified, and some of their properties, are summarized in Table II.

A. CHEMICAL COMPOSITION

The most obvious method of detecting iron-sulfur clusters is by the presence of nonheme iron in the isolated protein. The iron-sulfur proteins are distinguished from other nonheme iron proteins in that the

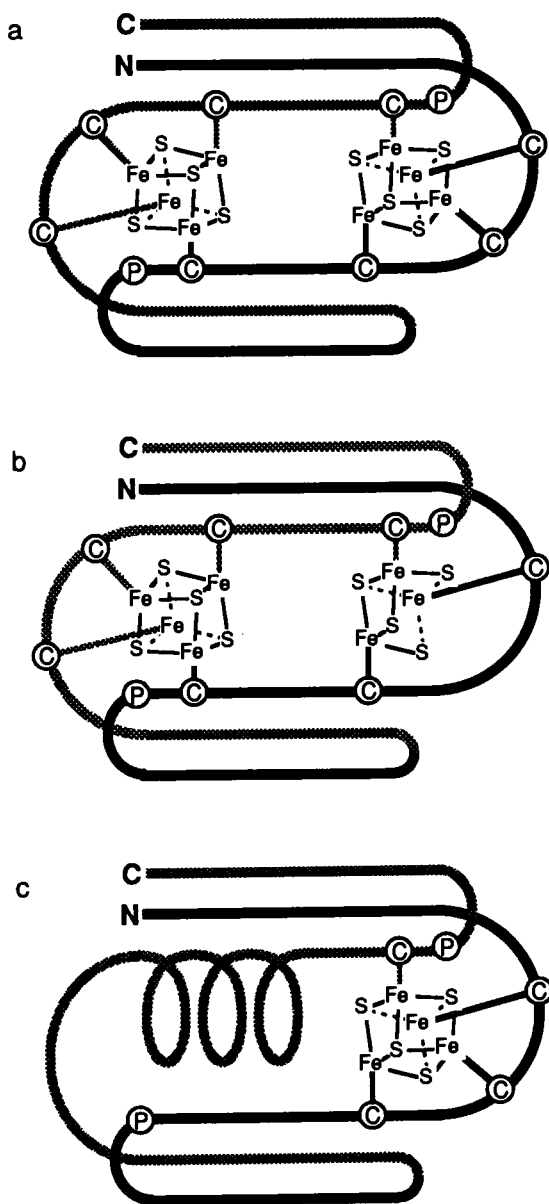


FIG. 1. (a) Outline of folding pattern of the 2[4Fe-4S] ferredoxins, showing the relevant cysteine residues (C) and prolines (P) (260). To emphasize the approximate twofold symmetry of the protein, the two halves are differently shaded. (b) The formation of a [3Fe-4S] cluster by omission of one of the cysteines (54, 55). (c) The fold for a [4Fe-4S] ferredoxin (52).

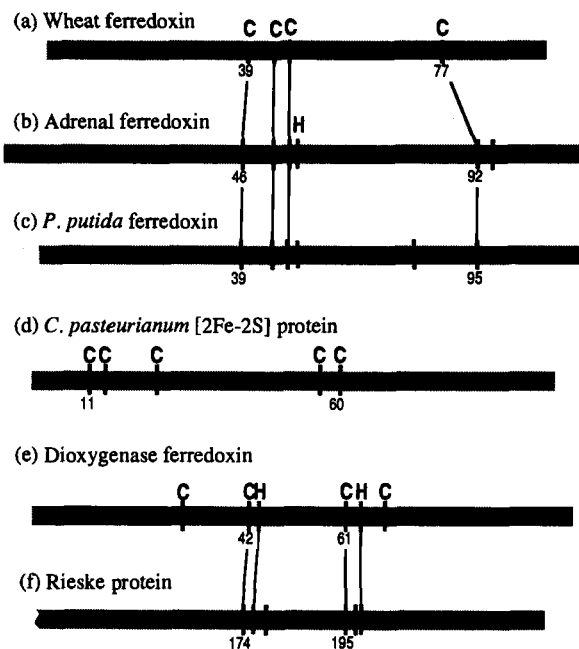


FIG. 2. Cysteine spacings for different types of [2Fe-2S] ferredoxins. (a) Wheat ferredoxin (266); (b) adrenal *P*-450-reducing ferredoxin (267); (c) *P. putida* *P*-450-reducing ferredoxin (268); (d) *C. pasteurianum* [2Fe-2S] ferredoxin (45); (e) *P. putida* strain ML2 benzene dioxygenase ferredoxin (104); (f) *Neurospora crassa* Rieske protein (269).

iron is coordinated to cysteine sulfurs from the protein, and, in all but the rubredoxins, by the presence of acid-labile sulfide. It must be said that the analytical values for iron and sulfide are rarely reliable on their own. There are cumulative uncertainties in the analyses for iron, sulfide, and protein, in the determination of the molecular mass, and in the purity and integrity of enzyme preparations. In most cases the number of iron and sulfide atoms per mole, originally estimated, has had to be revised as a result of spectroscopic or structural determinations. An honorable exception is the thorough study of aconitase and other proteins by Beinert and co-workers, where the values of $3\text{Fe} + 4\text{S}$, which were contrary to all structural and spectroscopic precedents, proved to be correct (7, 8).

B. PROTEIN STRUCTURES

The existence of the [2Fe-2S], [3Fe-4S], and [4Fe-4S] clusters in proteins has been established by high-resolution X-ray crystallography

TABLE I
EXAMPLES OF IRON-SULFUR PROTEINS^a

Protein	Typical source	Function	Subunit M_r ($\times 10^{-3}$)	Fe-S clusters	Other groups	Ref.
Simple iron-sulfur proteins						
[2Fe-2S] ferredoxin, plant type	Chloroplasts, cyanobacteria	Photosynthetic reduction of NADP, nitrite, thioredoxin, etc.	10.5	[2Fe-2S]	—	36
[3Fe-4S] ferredoxin	Bacteria, e.g., <i>D. gigas</i> , <i>S. griseolus</i>	Electron transfer	6-12	[3Fe-4S]	—	57, 58
[4Fe-4S] ferredoxin	Bacteria, e.g. <i>Bacillus</i> , <i>Desulfovibrio</i> spp.	Electron transfer	6-8	[4Fe-4S]	—	52
High-potential iron- sulfur protein (HiPIP)	Photosynthetic bacteria, e.g., <i>C. vinosum</i>	Not known	10	[4Fe-4S] ^{2+/3+}	—	171
7Fe ferredoxin	Bacteria, e.g., <i>A. vinelandii</i>	Not known	6-10	[4Fe-4S] + [3Fe-4S]	—	172
8Fe ferredoxin	Anaerobic bacteria, e.g., <i>C. pasteurianum</i>	Electron transfer	6-10	2[4Fe-4S]	—	173
Rubredoxin	Anaerobic bacteria, e.g., <i>Desulfovibrio</i> , <i>Clostridium</i>	Electron transfer	6	[Rd]	—	174
Desulforedoxin	<i>D. vulgaris</i>	Not known	2(7.9)	2[Rd]	—	175
Membrane-bound electron transfer proteins						
NADH ubiquinone oxidoreductase (complex I)	Mitochondria, aerobic bacteria	$\text{NADH} + \text{UQ} \leftrightarrow \text{NAD}^+ + \text{UQH}_2$	>30 subunits, depending on species	$n[2\text{Fe}-2\text{S}] + m[4\text{Fe}-4\text{S}]$	FMN	69
Succinate dehydrogenase (complex II)	Mitochondria, aerobic bacteria	$\text{Succinate} + \text{UQ} \rightarrow \text{fumarate} + \text{UQH}_2$	$70 + 27 + 13 + 15$	$[2\text{Fe}-2\text{S}] + [3\text{Fe}-4\text{S}] + [4\text{Fe}-4\text{S}]$	FAD + cyt <i>b</i>	176
Complex III-UQH ₂ : cyt <i>c</i> reductase	Mitochondria, aerobic bacteria	$\text{UQH}_2 + \text{cyt } c_{\text{ox}} \rightarrow \text{UQ} + \text{cyt } c_{\text{red}}$	22 (Rieske protein)	$[2\text{Fe}-2\text{S}]_{\text{R}}$	2 cyt <i>b</i> + cyt <i>c</i> ₁	177
Cytochrome <i>b₆f</i> complex	Chloroplasts	$\text{PQH}_2 + \text{PC}_{\text{ox}} \rightarrow \text{PQ} + \text{PC}_{\text{red}}$	20 (Rieske) + 33 + 23 + 17	$[2\text{Fe}-2\text{S}]_{\text{R}}$	2 cyt <i>b</i> + cyt <i>f</i>	178
ETF-UQ reductase	Mitochondria	$\text{ETF} \cdot \text{H}_2 + \text{UQ} \rightarrow \text{ETF} + \text{UQH}_2$	≈70	[4Fe-4S]	FAD	179, 180
Formate-hydrogen lyase	<i>E. coli</i>	$\text{H} \cdot \text{COO}^- + \text{H}^+ \rightarrow \text{H}_2 + \text{CO}_2$	110 + 32 + 20	$n[4\text{Fe}-4\text{S}]$	Mo-pterin, Se, Ni	181, 182
[NiFe] hydrogenase— (respiratory)	Bacteria, e.g., <i>E. coli</i> , <i>C. vinosum</i> ; <i>A. vinelandii</i>	$\text{H}_2 + \text{MK} \rightarrow \text{MKH}_2$	60 + 30 (+30)	$2[4\text{Fe}-4\text{S}] + [3\text{Fe}-4\text{S}]$	Nickel center (cyt <i>b</i>)	183

(Continued)

TABLE I (Continued)

Protein	Typical source	Function	Subunit M_r ($\times 10^{-3}$)	Fe-S clusters	Other groups	Ref.
Glycerol phosphate dehydrogenase (anaerobic)	<i>E. coli</i>	Glycerol phosphate + MK \rightarrow glyceraldehyde phosphate + MKH ₂	62 + 43 + 44	2[4Fe-4S] + [2Fe-2S] (predicted)	FAD, FMN?	64
Fumarate reductase	—	Fumarate + MKH ₂ \rightarrow succinate + MK	70 + 30 + 12 + 12	[2Fe-2S] + [3Fe-4S] + [4Fe-4S]	FAD	(14, 184, 185)
Nitrate reductase (respiratory)	Anaerobic bacteria, e.g., <i>E. coli</i>	NO ₃ ⁻ + MKH ₂ \rightarrow NO ₂ ⁻ + MK		3[4Fe-4S] + [3Fe-4S]	Mo-pterin	186
DMSO/TMAO reductase (respiratory)	Anaerobic bacteria, e.g., <i>E. coli</i>	DMSO + MKH ₂ \rightarrow DMS + MK + H ₂ O	87 + 23 + 31	4[4Fe-4S]	Mo-pterin	19
Methylenetetrahydrofolate reductase	<i>C. thermoaceticum</i>	CH ₂ =FH ₄ + D _{red} \rightarrow CH ₃ ·FH ₄ + D _{ox}	8(36)	2[4Fe-4S]	FAD, Zn	187
Photosystem I	Chloroplasts, cyanobacteria	Photosynthetic electron transfer from plastocyanin to ferredoxin	2(84), 22, 19, 9	3[4Fe-4S]	Chlorophyll, phaeophytin, vitamin K ₁	77
Soluble iron-sulfur enzymes						
NAD(P)H-glutamate synthase	Plants, <i>E. coli</i>	Glutamine + 2-oxoglutarate + NAD(P)H \rightarrow 2 glutamate + NAD(P) ⁺	166 + 52	[4Fe-4S]	FAD, FMN	188, 189
Ferredoxin-glutamate synthase	Plants	Glutamine + 2-oxoglutarate + 2Fd _{ox} \rightarrow 2 glutamate + 2Fd _{red}	140-160	[4Fe-4S] + ?[2Fe-2S]	FAD, FMN	190
Trimethylamine dehydrogenase	Bacterium W3A1	(CH ₃) ₃ NH ⁺ + [ETF] _{ox} \rightarrow (CH ₃) ₂ NH ₂ ⁺ + [ETF] _{red} + [C ₁]	2(83)	[4Fe-4S]	FMN, ADP	191
2-Enoate reductase	<i>C. kluyveri</i>	Reduction of 2-enoates R ₂ R ₃ =R ₁ COO ⁻ + NADH \rightarrow R ₂ R ₃ CH-CH·R ₁ ·COO ⁻	6(78)	4Fe + 4S	FAD	192
Adenylylsulfate reductase	Sulfate-reducing bacteria, e.g., <i>D. gigas</i>	AMP·SO ₄ + 2e ⁻ \leftrightarrow HSO ₃ ⁻ + AMP	4(70 + 23)	2[4Fe-4S] clusters per dimer	FAD	193
Dihydroorotate dehydrogenase	<i>Clostridium oroticum</i>	Dihydroorotate + NAD ⁺ \leftrightarrow orotate + NADH	115	2[2Fe-2S]	FAD, FMN	194
Pyruvate:NADP ⁺ oxidoreductase	<i>Euglena gracilis</i>	Pyruvate + CoA + NADP ⁺ \leftrightarrow acetyl-CoA + CO ₂ + NADPH	2(166)	4Fe, 4S	FAD	195
Pyruvate:ferredoxin oxidoreductase	Cyanobacteria, clostridia, protozoa	Pyruvate + CoA + Fd _{ox} \leftrightarrow acetyl-CoA + CO ₂ + Fd _{red}	123	2[4Fe-4S]	Thiamin diphosphate	196

Pyruvate : ferredoxin oxidoreductase	<i>Halobacterium halobium</i>	Pyruvate + CoA + Fd _{ox} ↔ acetyl-CoA + CO ₂ + Fd _{red}	2(86 + 42)	[4Fe-4S]	Thiamin diphosphate	91
Pyruvate : flavodoxin oxidoreductase	Bacteria, e.g., <i>K. pneumoniae</i>	Pyruvate + CoA + 2Fd _{ox} ↔ acetyl-CoA + CO ₂ + 2Fd _{red}	2(120)	2[4Fe-4S] per subunit	Thiamin diphosphate	89, 197
Oxoglutarate : ferredoxin oxidoreductase	<i>Halobacterium halobium</i>	Oxoglutarate + CoA + Fd _{ox} ↔ succinyl-CoA + CO ₂ + Fd _{red}	88 + 36; total 248	[4Fe-4S]	Thiamin diphosphate	91
[NiFe] hydrogenase (cytochrome c reducing)	<i>Desulfovibrio</i> spp.	H ₂ + cyt c _{ox} ↔ 2H ⁺ + cyt c _{red}	≈60 + ≈30	2[4Fe-4S] + [3Fe-4S]	Ni	29, 195
[NiFe] hydrogenase (NAD reducing)	Hydrogen bacteria, e.g., <i>A. eutrophus</i> , <i>Nocardia opaca</i>	H ₂ + NAD ⁺ → H ⁺ + NADH	63 + 56 + 30 + 26	3-4[4Fe-4S] + [2Fe-2S]	Ni, FMN	199
[NiFe] hydrogenase (MV reducing)	Methanogenic bacteria, e.g., <i>M. thermoautotrophicum</i>	H ₂ + A _{ox} ↔ 2H ⁺ + A _{red}	53 + 33 + 16	3-4[4Fe-4S] + [2Fe-2S]	Ni	165
[NiFe] hydrogenase (F ₄₂₀ reducing)	Methanogenic bacteria, e.g., <i>M. thermoautotrophicum</i>	H ₂ + F ₄₂₀ → F ₄₂₀ · H ₂	45 + 31 + 26 + 18	3-4[4Fe-4S] + [2Fe-2S]	Ni, FAD	200
[NiFeSe] hydrogenase	Sulfate-reducing and methanogenic bacteria	H ₂ + cyt c _{ox} ↔ 2H ⁺ + cyt c _{red}	≈60 + ≈30; total 90	2[4Fe-4S]	Ni, seleno-cysteine	201
[NiFeSe] hydrogenase (F ₄₂₀ reducing)-sulfur	Methanogenic bacteria, e.g., <i>Methanococcus voltae</i>	H ₂ + F ₄₂₀ → F ₄₂₀ · H ₂	55 + 45 + 37 + 27	3-4[4Fe-4S] + [2Fe-2S]	Ni, FAD	202
Corrinoid/iron-sulfur protein	Acetogenic and methanogenic bacteria	Transfer of methyl from CH ₃ · FH ₄ or CH ₃ · H ₄ MPT to acetyl-CoA synthase	88	[4Fe-4S]	Cobalamin	203
Hydroxylases and dioxygenases						
Ferredoxin (P-450 reducing)	Mitochondria, bacteria, e.g., <i>P. putida</i>	Electron transfer from flavoprotein reductase to cytochrome P-450	11.5	[2Fe-2S]	—	204, 205
Methane monooxygenase reductase	<i>Methylococcus capsulatus</i>	Reduction of methane monooxygenase (NADH)	38.5	[2Fe-2S]	FAD	206, 207
Rubredoxin	<i>P. oleovorans</i>	Electron transfer to ω-hydroxylase	—	2[Rd]	—	34
4-Methoxybenzoate monooxygenase (putidamonooxin)	<i>P. putida</i>	O-demethylation of 4-methoxybenzoate	3(41)	[2Fe-2S] _R	Fe	101
4-Methoxybenzoate monooxygenase reductase	<i>P. putida</i>	—	42	[2Fe-2S]	FMN	208
Benzene dioxygenase	<i>P. putida</i>	Benzene + NADH + O ₂ → cis-benzene glycol + NAD ⁺	2(54.5 + 23.5)	[2Fe-2S] _R	Fe	63, 103
Benzene dioxygenase ferredoxin	<i>P. putida</i>	—	11.9	[2Fe-2S]	—	63, 104
Toluene dioxygenase	<i>P. putida</i>	Dihydroxylation of toluene	2(529 + 21)	[2Fe-2S] _R	Fe	105
Toluene dioxygenase ferredoxin	<i>P. putida</i>	—	12	[2Fe-2S]	—	105
Naphthalene dioxygenase	<i>Pseudomonas</i> sp. strain NCIB-9816	Dihydroxylation of naphthalene	2(55 + 20)	[2Fe-2S] _R	Fe	208a, 271

(Continued)

TABLE I (Continued)

Protein	Typical source	Function	Subunit M_r ($\times 10^{-3}$)	Fe-S clusters	Other groups	Ref.
Naphthalene dioxygenase ferredoxin	<i>Pseudomonas</i> sp. strain NCIB-9816	—	15	[2Fe-2S]	—	209
Naphthalene dioxygenase reductase	<i>Pseudomonas</i> sp. strain NCIB-9816	—	36	[2Fe-2S]	FAD	210
Phthalate dioxygenase	<i>P. cepacia</i>	Dihydroxylation of phthalate	4(48)	[2Fe-2S] _R	Fe	211
Phthalate dioxygenase reductase	<i>P. cepacia</i>	—	34	[2Fe-2S]	FMN	98
Pyrazon dioxygenase	—	Dihydroxylation of pyrazon	180	[2Fe-2S] _R	Fe	212
Pyrazon dioxygenase ferredoxin	—	—	12	[2Fe-2S]	—	212
Benzoate dioxygenase	<i>P. arvilla</i>	Dihydroxylation of benzoate	3(50 + 20)	[2Fe-2S] _R	Fe	100, 102
Benzoate dioxygenase reductase	<i>P. arvilla</i>	—	37.5	[2Fe-2S]	FAD	100, 213
4-Chlorophenylacetate 3,4-Dioxygenase	—	Dihydroxylation of 4-chlorophenylacetate	3(46)	[2Fe-2S]	Fe	214
Enzymes with the molybdopterin cofactor						
Xanthine dehydrogenase	Liver, bacteria	Xanthine + NAD ⁺ \leftrightarrow urate + NADH	2(146)	2[2Fe-2S]	Mo-pterin, FAD	215, 216
Xanthine oxidase	Milk	Xanthine + O ₂ \rightarrow urate + H ₂ O ₂ + O ₂ ⁻	2(140)	2[2Fe-2S]	Mo-pterin, FAD	107
Aldehyde oxidase	Liver	Aldehyde + O ₂ \rightarrow carboxylate + H ₂ O ₂	2(140)	2[2Fe-2S]	Mo-pterin, FAD	217
Aldehyde dehydrogenase	<i>D. gigas</i> , <i>P. testosteroni</i>	R · CHO + D _{ox} \rightarrow R · COO ⁻ + D _{red}	2(92)	2[2Fe-2S]	Mo-pterin, FAD	218, 219
Aldehyde : ferredoxin oxidoreductase (tungsten containing)	<i>Pyrococcus furiosus</i>	R · CHO + Fd _{ox} \leftrightarrow R · COO ⁻ + Fd _{red}	85	\approx 7Fe, 5S	W	220
Purine hydroxylase II	<i>Anacystis nidulans</i>	Ring hydroxylation of purines	2(153)	2[2Fe-2S]	Mo, FAD	221
Carbon monoxide oxidoreductase	Carboxydovoric aerobic bacteria	CO + A _{ox} \rightarrow CO ₂ + A _{red}	230	2[2Fe-2S]	Mo-pterin, FAD	222
Furoyl-coenzyme-A dehydrogenase	<i>P. putida</i> Fu1	2-{furoyl-CoA + A _{ox} \rightarrow 5-hydroxy-2- furoyl-CoA + A _{red} }	2(55 + 25)	Fe, S	Mo, cyt b	223
Nicotinate dehydrogenase	<i>B. niacini</i>	Hydroxylation of nicotinate	2(85 + 34 + 20)	8.3Fe, 1.5S	2FAD, 2Mo	224

6-Hydroxynicotinate dehydrogenase	<i>B. niacini</i>	Hydroxylation of 6-hydroxynicotinate	85 + 34 + 20	Fe + S	FAD, Mo	224
Arsenite oxidase	<i>A. faecalis</i>	Arsenite + O ₂ → arsenate + H ₂ O ₂	85	2[2Fe-2S]	Mo-pterin	225
Ferredoxin-nitrate reductase	Cyanobacteria, e.g., <i>Plectonema boryanum</i>	NO ₃ ⁻ + Fd _{red} + 2H ⁺ → NO ₂ ⁻ + Fd _{ox} + H ₂ O	83	2[2Fe-2S]	Mo-pterin	226
Formate dehydrogenase (F ₄₂₀ reducing)	Methanogens, e.g., <i>M. formicicum</i>	H · COO ⁻ + H ⁺ + F ₄₂₀ → CO ₂ + F ₄₂₀ · H ₂	76 + 34	24Fe, 28S as [4Fe-4S] clusters	Mo-pterin	227
Formate dehydrogenase (NAD reducing)	Methanotrophs, e.g., <i>Methylosinus trichosporium</i>	H · COO ⁻ + NAD ⁺ → CO ₂ + NADH	2(98 + 56 + 19 + 11.5)	40Fe, 40S (~5 Fe-S clusters)	2 flavins/ dimer	228
Formate dehydrogenase (NAD reducing)	<i>P. oxalaticus</i>	H · COO ⁻ + NAD ⁺ → CO ₂ + NADH	320	17-20Fe, 17-20S	2FMN	229
Formate dehydrogenase (ferredoxin reducing)	<i>C. pasteurianum</i>	H · COO ⁻ + Fd _{ox} ↔ CO ₂ + Fd _{red}	76 + 34	3[4Fe-4S]	Mo-pterin	230, 231
Formate dehydrogenase (tungsten containing)	<i>C. thermoaceticum</i>	CO ₂ + Fd _{red} → H · COO ⁻ + Fd _{ox}	α ₂ β ₂ ; total 340	[4Fe-4S] + [2Fe-2S]	W-pterin, Se	117
Enzymes containing sirohaem						
Ferredoxin:sulfite reductase	Plants, bacteria	SO ₃ ²⁻ + 6Fd _{red} → S ²⁻ + 6Fd _{ox}	69	[4Fe-4S]	Siroheme	127
Sulfite reductase (assimilatory)	<i>E. coli</i>	HSO ₃ ⁻ + 3 NADPH + 3H ⁺ → HS ⁻ + 3 NADP ⁺ + 3H ₂ O	8(59 + 4 × 55)	[4Fe-4S]	Siroheme, FAD, FMN	88
Sulfite reductase (dissimilatory)	Sulfate-reducing bacteria, e.g., <i>D. vulgaris</i>	HSO ₃ ⁻ + 6D _{red} + 6H ⁺ → HS ⁻ + 6D _{ox} + 3H ₂ O	α ₂ β ₂ ; total 200	2[4Fe-4S]	Siroheme	232
Sulfite reductase (assimilatory)	Sulfate-reducing bacteria, e.g., <i>D. vulgaris</i>	HSO ₃ ⁻ + 6D _{red} + 6H ⁺ → HS ⁻ + 6D _{ox} 3H ₂ O	27	[4Fe-4S]	Siroheme (low spin)	233
Ferredoxin:nitrite reductase	Plants	NO ₂ ⁻ + 6Fd _{red} + 8H ⁺ → NH ₄ ⁺ + 6Fd _{ox} + 2H ₂ O	67	[4Fe-4S]	Siroheme	126
NADH:nitrite reductase	<i>E. coli</i>	NO ₂ ⁻ + 3NADH + 5H ⁺ → NH ₄ ⁺ + 3NAD ⁺ + 2H ₂ O	92	[2Fe-2S]	Siroheme, FAD	129
Proteins with catalytic Fe-S or mixed-metal clusters						
[Fe] hydrogenase	Anaerobic bacteria, e.g., <i>C. pasteurianum</i> , <i>D. gigas</i>	2H ⁺ + 2e ⁻ ↔ H ₂	≈60	H cluster + 2-4[4Fe-4S]	—	234
Carbon monoxide dehydrogenase	Photosynthetic bacteria, e.g., <i>Rhodospirillum rubrum</i>	CO + H ₂ O → CO ₂ + 2e ⁻ + 2H ⁺	61.8	≥2[4Fe-4S] + NiFe ₃₋₄ S _{≥4} + ?[6Fe-6S]	Zn	144
Carbon monoxide dehydrogenase (acetyl-CoA synthase)	Acetogenic and methanogenic bacteria, e.g., <i>C. thermoaceticum</i> , <i>Methanotherx soehngenii</i>	CH ₃ ·[CP] + CO + CoA ↔ CH ₃ CO-CoA + [CP]	Acetogens: 3(71 + 78) Methanogens: 90 + 21	≥2[4Fe-4S] + NiFe ₃₋₄ S _{≥4} + ?[6Fe-6S]		138,139 235, 236

(Continued)

TABLE I (Continued)

Protein	Typical source	Function	Subunit M_r ($\times 10^{-3}$)	Fe-S clusters	Other groups	Ref.
Mo nitrogenase	Nitrogen-fixing bacteria, e.g., <i>Rhizobium</i> , <i>Azotobacter</i> , <i>Klebsiella</i>	$N_2 + 8e^- + 10H^+ \rightarrow 2NH_4^+ + H_2$	2(50 + 60)	P clusters, Fe-Mo cofactor		131, 237
Vanadium nitrogenase	Nitrogen-fixing bacteria, e.g., <i>Rhizobium</i> , <i>Azotobacter</i>	$N_2 + 8e^- + 10H^+ \rightarrow 2NH_4^+ + H_2$	2(50 + 55 + 13)	VFe protein: P clusters + Fe-V cofactor		238
Iron nitrogenase	Nitrogen-fixing bacteria, e.g. <i>Azotobacter</i> , <i>Rhodobacter</i>	$N_2 + 8e^- + 10H^+ \rightarrow 2NH_4^+ + H_2$	2(58 + 51 + 15)	P clusters + Fe- Fe cofactor		239
Nitrogenase Fe protein (nitrogenase reductase)	Nitrogen-fixing bacteria, e.g. <i>Rhizobium</i> , <i>Azotobacter</i> , <i>Klebsiella</i>	$[MoFe\text{-protein}] + D_{red} + ATP$ $\rightarrow [MoFe\text{-protein}]_{red} +$ $D_{ox} + ADP + P_i$	2(68)	[4Fe-4S] per two subunits		237
Enzymes with nonredox Fe-S clusters						
Glutamine PRPP amidotransferase	Humans, <i>B. subtilis</i>	Glutamine + PRPP \rightarrow 5-phospho- ribosylamine + glutamine + PP _i	4(50)	[4Fe-4S]		148
Aconitase (aconitate hydratase)	Mitochondria, cytoplasm, bacteria	Citrate \leftrightarrow isocitrate	81	[4Fe-4S]		147
Maleate hydratase	Rabbit kidney	D-maleate \leftrightarrow maleate + H ₂ O	68	[4Fe-4S]		240
Lactyl-CoA dehydratase	<i>C. propionicum</i>	Lactyl-CoA \leftrightarrow acrylyl-CoA + H ₂ O	$n(48 + 41)$	[3Fe-4S], [4Fe-4S]		241
2-Hydroxyglutaryl-CoA dehydratase	<i>Acetaminococcus</i> <i>fermentans</i>	2-Hydroxyglutaryl-CoA \leftrightarrow glutanoyl-CoA + H ₂ O	2(55 + 42)	[4Fe-4S]		242
Dihydroxyacid dehydratase	Plants	$(CH_3)_2 \cdot C(OH) \cdot CH(OH) \cdot COO^- \leftrightarrow$ $(CH_3)_2 \cdot CH \cdot CO \cdot COO^- + H_2O$	$\approx 2(60)$	[2Fe-2S]		243
Dihydroxyacid dehydratase	<i>E. coli</i>	$(CH_3)_2 \cdot C(OH) \cdot CH(OH) \cdot COO^- \leftrightarrow$ $(CH_3)_2 \cdot CH \cdot CO \cdot COO^- + H_2O$	—	[4Fe-4S]		244
L(+)-Tartrate dehydratase	<i>P. putida</i>	L-tartrate \rightarrow oxaloacetate + H ₂ O	2(23 + 27)	[4Fe-4S]	—	245
L-Serine dehydratase	<i>Peptostreptococcus</i> <i>asaccharolyticus</i>	Serine \rightarrow pyruvate + NH ₄ ⁺	30 + 25; total 200	[4Fe-4S]	—	246
6-Phosphogluconate dehydratase	<i>Zymomonas mobilis</i>	—	126	6-8Fe, S/mole	—	247
Nitrile hydratase	<i>Brevibacterium</i> sp.	R · CN + H ₂ O \rightarrow R · CO · NH ₂	2(23 + 23.5)	2Fe	—	158
Fumarases A and B	<i>E. coli</i>	Fumarate + H ₂ O \leftrightarrow L-malate	60	[4Fe-4S]	—	149

DNA endonuclease III	<i>E. coli</i>	Apurinic and apyridimic endonuclease	24	[4Fe–4S]	—	157
Regulatory proteins						
Iron-responsive element binding protein	Humans	Regulation of translation of ferritin, etc., mRNA	89	[3Fe–4S]?	—	161
FNR protein	<i>E. coli</i>	Aerobic/anaerobic switch	30	1.1 Fe in isolated protein	—	163
Ferredoxin :thioredoxin reductase	Chloroplasts, cyanobacteria	Thioredoxin + $\text{Fd}_{\text{red}} \rightarrow$ thioredoxin _{red} + Fd_{ox}	13 + (7–16)	[4Fe–4S] cluster	Disulfide bridge	273
Miscellaneous iron–sulfur proteins of unknown function						
[6Fe–6S] protein	<i>D. vulgaris</i>	Not known	52	[6Fe–6S] cluster?	—	248
Rubrerythrin	<i>D. vulgaris</i>	Phosphatase?		Fe	[2Fe] _H	168
Desulfoferredoxin	<i>Desulfovibrio</i> spp.	Not known		[Rd]	Fe	169
Polyferredoxin	Methanogens, e.g., <i>M. thermoautotrophicum</i>	?-electron transfer to hydrogenase	48	12[4Fe–4S] predicted	—	165
Molybdenum iron–sulfur protein	<i>D. africanus</i>	Unknown	10(11.5)	20Fe, 20S	5–6Mo	249

^a Unless otherwise stated, [4Fe–4S] clusters are [4Fe–4S]^{2+/1+} type. Composition of iron–sulfur clusters and other groups is per minimum catalytic unit, e.g., where a protein is an ($\alpha_2\beta$)₃, the composition would be expressed per $\alpha_2\beta$ unit. Abbreviations: A_{ox}, A_{red}, oxidized and reduced electron acceptor; cyt, cytochrome; D_{red}, D_{ox}, reduced and oxidized electron donor; [Rd], rubredoxin-type Fe center; [2Fe–2S]_R, Rieske iron–sulfur cluster; [2Fe]_H, hemerythrin-like binuclear iron cluster; UQ, ubiquinone; UQH₂, ubiquinol.

TABLE II
TYPES OF IRON-SULFUR CLUSTERS

Type	Source	Typical E_m range (mV)
$[\text{Fe}]^{3+/2+}$	Rubredoxins	+ 20 to - 60
$[2\text{Fe}-2\text{S}]^{2+/1+}$	Ferredoxins	- 240 to - 460
$[\text{Fe}_2\text{S}_2(\text{RS})_2\text{N}_2]^{10/-1}$	Rieske proteins	+ 300 to - 155
$[3\text{Fe}-4\text{S}]^{1+/0}$	Ferredoxins	- 50 to - 420
$[4\text{Fe}-4\text{S}]^{2+/1+}$	Bacterial ferredoxins	0 to - 645
$[4\text{Fe}-4\text{S}]^{3+/2+}$	HiPIP	50 to 450
$[6\text{Fe}-6\text{S}]$	<i>D. vulgaris</i> protein	—
H-cluster	Hydrogenase	—
P-clusters	Nitrogenase protein 1	—
Fe-Mo cofactor	Mo Nitrogenase protein 1	—
Fe-V cofactor	V nitrogenase protein 1	—
Fe-Fe cofactor	Alternative nitrogenase protein 1	—
Fe-Ni cluster	CO dehydrogenase	—

of simple iron-sulfur proteins. Iron-sulfur proteins, for which the crystal structure has been determined crystallographically, are listed in Table III. These structures are extremely valuable for the information they provide about the environment and disposition of the clusters. It is also possible to investigate the binding sites for substrates and for other proteins, and the residues that influence the properties of the clusters. For future studies, two-dimensional nuclear magnetic resonance (NMR) is a promising technique for the determination of the structures of small proteins (up to 20 kDa) (9). In the region of the iron-sulfur clusters, contact-shifted resonances have been assigned, giving information about the paramagnetic states of the individual iron atoms and about their ligands (10a, 11).

C. AMINO ACID SEQUENCES

The sequences for genes encoding many iron-sulfur proteins from different species are emerging rapidly. From an analysis of sequences, consensus sequences may be derived for each type of iron-sulfur cluster. The most prominent features of the cluster-binding "motifs" are the cysteines that bind the clusters, with characteristic spacings in between (see Ref. 5).

TABLE III

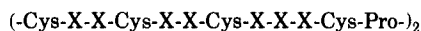
IRON-SULFUR PROTEINS OF WHICH THE STRUCTURE HAS BEEN DETERMINED

Protein	Source	Resolution (Å) ^a	Ref.
Rubredoxin	<i>Clostridium pasteurianum</i>	1.2	250
Rubredoxin	<i>Desulfovibrio vulgaris</i>	1.5	174
Rubredoxin	<i>Desulfovibrio desulfuricans</i>	1.5	251
Rubredoxin	<i>Desulfovibrio desulfuricans</i> strain 27774	1.5	252
Rubredoxin	<i>Desulfovibrio gigas</i>	1.4	253
[2Fe-2S] ferredoxin	<i>Anabaena</i> 7120	2.5	254
[2Fe-2S] ferredoxin	<i>Spirulina platensis</i>	2.5	255
[2Fe-2S] ferredoxin I	<i>Aphanothece sacrum</i>	2.2	256
[2Fe-2S] ferredoxin I	<i>Halobacterium</i> (Dead Sea)	2.5	257
[3Fe-4S] ferredoxin II	<i>Desulfovibrio gigas</i>	1.7	57
[4Fe-4S] ferredoxin	<i>Bacillus thermoproteolyticus</i>	2.3	52
[4Fe-4S] HiPIP	<i>Chromatium vinosum</i>	2.0	258
[4Fe-4S][3Fe-4S] ferredoxin I	<i>Azotobacter vinelandii</i>	1.9	259
2[4Fe-4S] ferredoxin	<i>Peptostreptococcus</i> <i>asaccharolyticus</i> ^b	2	260
2[4Fe-4S] ferredoxin	<i>Clostridium acidi-urici</i>	5	261
Trimethylamine dehydrogenase	Bacterium W3A1	2.4	262
Sulfite reductase hemoprotein subunit	<i>Escherichia coli</i>	3	124
Phthalate dioxygenase reductase	<i>P. cepacia</i>		98
Aconitase	Beef heart: [3Fe-4S] form	2.1 2.5	162
	[4Fe-4S] form		
Nitrogenase Fe-Mo protein	<i>Clostridium pasteurianum</i>	3.5	136
Nitrogenase Fe protein	<i>Clostridium pasteurianum</i>	3.0	137

^a Resolution given is that of the electron density map, or of the refined structure if available.

^b Formerly *Peptococcus aerogenes*, formerly *Micrococcus aerogenes*.

An example of a motif is the consensus sequence for the 2[4Fe-4S] ferredoxins, which contain two groups of cysteines of the following form:



As illustrated in Fig. 1a, each cluster is coordinated by three cysteine sulfurs from one group and one from the other. Thus, in the [4Fe-4S] ferredoxins, the cluster is bound by three closely spaced cysteines and one distant cysteine (Fig. 1c) (12). If the second cysteine of the group is missing, the result is usually a [3Fe-4S] cluster (Fig. 1b). Such

arrangements have been found in a number of complex iron-sulfur proteins.

Not all sequences that bind iron-sulfur clusters will conform to these motifs. There may be many ways to fold a polypeptide around a particular type of cluster. In other words, the same type of cluster may arise in different proteins by convergent evolution. For example, there are at least four different arrangements of cysteines in the [2Fe-2S] proteins (Fig. 2). Thus sequence information can help to identify different families of iron-sulfur proteins.

By examination of the sequence of an iron-sulfur protein it is sometimes possible to identify the iron-sulfur-binding motifs. This will determine the types of iron-sulfur clusters present, and their location. An example is the iron-sulfur protein subunit of fumarate reductase/succinate dehydrogenase, in which homologies to the 2Fe and 7Fe ferredoxins were observed (3, 13) before the presence of [2Fe-2S], [3Fe-4S], and [4Fe-4S] clusters was confirmed spectroscopically (14). Some examples of ferredoxin-like sequences in complex iron-sulfur proteins, which almost certainly bind equivalent clusters, are listed in Table IV.

It is possible for an iron-sulfur cluster to be coordinated by cysteine ligands from different protein domains or even different subunits. Examples are the iron protein of nitrogenase, and cluster X in photosystem I (see below). With such an arrangement it is difficult to identify the binding site by examination of an individual sequence, but in these cases the specific cysteines were found by comparison of sequences from diverse species and by site-directed mutagenesis.

With the accumulation of genomic libraries from different species, it is possible to search for new types of iron-sulfur proteins. Some interesting potential proteins of unknown function have already been found, such as the ferredoxin-like proteins associated with nitrogenase genes (15, 16), and an operon resembling a membrane-bound iron-sulfur protein in *Escherichia coli* (17). However, it should be remembered that such searches cannot be exhaustive, and some iron-sulfur proteins will be missed. None of the features of a motif is invariant. For example, in the [4Fe-4S] cluster motif in Fig. 1, cases are known where the spacings of the cysteines are different, where the terminal proline is absent, and even where one of the cysteines is replaced by another amino acid.

D. SITE-DIRECTED MUTAGENESIS EXPERIMENTS

The predictions about iron-sulfur cluster composition may be tested by site-directed mutagenesis experiments, wherein cysteines or other

TABLE IV

SEQUENCES IN ENZYMES THAT ARE HOMOLOGOUS TO FERREDOXIN SEQUENCES

Protein	Source	Homologous to	Ref.
Pyruvate:flavodoxin reductase	<i>Klebsiella pneumoniae</i>	2[4Fe-4S] ferredoxins	197
[Fe] hydrogenase	<i>Desulfovibrio vulgaris</i>	2[4Fe-4S] ferredoxins	263
F ₄₂₀ -reducing hydrogenase	<i>Methanobacterium thermoautotrophicum</i>	2[4Fe-4S] ferredoxins	200
Acetyl-CoA synthase	<i>Methanotherx soehngeni</i>	2[4Fe-4S] ferredoxins	236
Formate dehydrogenase	<i>Methanobacterium formicicum</i>	2[4Fe-4S] ferredoxins	231
DMSO reductase DmsB	<i>Escherichia coli</i>	4[4Fe-4S]	264
Nitrate reductase NarH	<i>Escherichia coli</i>	3[4Fe-4S], [3Fe-4S]	20
NAD-reducing [Ni] hydrogenase	<i>Alcaligenes eutrophus</i>	[2Fe-2S], [4Fe-4S]	265
Succinate dehydrogenase	Beef heart	[2Fe-2S], [3Fe-4S], [4Fe-4S]	[265a]
Fumarate reductase	<i>Escherichia coli</i>	[2Fe-2S], [3Fe-4S], [4Fe-4S]	184
Xanthine dehydrogenase	<i>Drosophila melanogaster</i>	Plant-type [2Fe-2S]	112
Xanthine dehydrogenase	Rat liver	Plant-type [2Fe-2S]	114
Benzene dioxygenase	<i>Pseudomonas putida</i>	Rieske proteins	99
Benzoate dioxygenase	<i>Acinetobacter calcoaceticus</i>	Rieske proteins	100
Benzoate dioxygenase reductase	<i>Acinetobacter calcoaceticus</i>	Plant-type [2Fe-2S]	100
Methane monooxygenase reductase	<i>Methylococcus capsulatus</i>	Plant-type [2Fe-2S]	94

putative ligands to the cluster may be substituted by other amino acids. In some cases this causes the loss of the cluster or failure of the protein to assemble; in other cases the protein retains its structure and function. Generally one would conclude that if the cluster is retained unchanged, the cysteine is not a ligand. However, the results of such experiments may be unpredictable and any conclusions require corroboration by other methods.

An instructive example is provided by the experiments (18) on the [4Fe-4S][3Fe-4S] ferredoxin I from *Azotobacter vinelandii*. A mutant protein, in which Cys 20 was substituted by alanine, retained both iron-sulfur clusters with properties apparently little changed. From this it might have been concluded that Cys 20 was not a ligand to a cluster. However X-ray crystallography demonstrated that Cys 20 is a ligand in the native protein, but that a structural rearrangement took place in the mutant, in which the missing cysteine was replaced by the free Cys 24.

In proteins that contain multiple iron-sulfur clusters, such as the membrane-bound electron transfer proteins, the functions of individual clusters may be studied by their removal or modification. For example, both the dissimilatory nitrate reductase and the dimethyl sulfoxide (DMSO) reductase of *E. coli* have similar structures, with an intermediate iron-sulfur protein containing four iron-sulfur clusters. In DMSO reductase the subunit contains four [4Fe-4S] clusters (19), whereas in nitrate reductase it contains three [4Fe-4S] clusters and one [3Fe-4S] cluster (20). The difference has been attributed to the replacement of a cysteine in the sequence of DMSO reductase, by a tryptophan in nitrate reductase. A DMSO reductase gene was constructed, in which the corresponding Cys 102 was substituted by Trp. Electron paramagnetic resonance (EPR) spectroscopy showed that the [4Fe-4S] cluster was converted to the predicted [3Fe-4S] cluster. In this case the capability to transfer electrons from quinols was lost (21).

The iron-sulfur protein subunits of *E. coli* fumarate reductase and succinate dehydrogenase, which each contain [2Fe-2S], [3Fe-4S], and [4Fe-4S] clusters, provide an ideal test system for the investigation of iron-sulfur cluster assembly and function. Cysteines 57, 62, 65, and 77 (numbering for fumarate reductase) were predicted to bind the [2Fe-2S] cluster, by analogy with the plant-type ferredoxins. These are invariant in all the fumarate reductases and succinate dehydrogenases, except that Cys 65 is replaced by aspartate in the succinate dehydrogenase of *E. coli* (13). Replacement of each of these cysteines by serines in fumarate reductase, replacing —SH groups by —OH, still permitted assembly of the [2Fe-2S] cluster, but with significantly modified redox potentials and EPR spectroscopic properties (22). An interesting conclusion from this is that the [2Fe-2S] cluster can accommodate at least one alternative nonsulfur ligand. However, substitution of cysteines by histidines, which are believed to be the ligands in the Rieske proteins, prevented assembly of the protein (23). The [3Fe-4S] cluster was converted into a [4Fe-4S] cluster by insertion of a cysteine. Surprisingly, the enzyme was still functional, despite a considerably more negative midpoint potential for the new cluster (24). There is clearly much scope for further experiments to determine the rules that govern the assembly of iron-sulfur clusters, and the pathways of electron transfer in these complex proteins.

E. SPECTROSCOPY

All iron-sulfur clusters are colored, and the visible absorption and circular dichroism spectra give indications of iron-sulfur cluster type.

However, the absorption bands are broad and featureless, so the presence of the clusters may go unnoticed in the presence of other chromophores such as heme or flavin. Numerous other forms of spectroscopy are available for examining the iron-sulfur clusters in isolated proteins. Low-temperature EPR spectroscopy, introduced by Beinert and Sands (25) for the study of the mitochondrial respiratory chain, remains the most versatile method for characterizing iron-sulfur clusters in complex systems. EPR can detect most iron-sulfur clusters in appropriate oxidation states and has the advantage that other groups such as flavin, molybdenum, or nickel may also be observed.

The identification of iron-sulfur clusters by EPR is not always straightforward. Both $[2\text{Fe}-2\text{S}]$ and $[4\text{Fe}-4\text{S}]$ clusters typically give $g = 1.94$ signals in the reduced states, though the temperature dependence is a rough indication of cluster type. Signals due to $[4\text{Fe}-4\text{S}]^{1+}$ clusters are undetectable or extremely broad at temperatures higher than 40 K; the high-potential iron-sulfur protein (HiPIP)-type $[4\text{Fe}-4\text{S}]^{3+}$ cluster signals are detectable (but broadened) up to 60 K, whereas the $[2\text{Fe}-2\text{S}]^{1+}$ clusters are often, though not always, detectable at temperatures above 60 K (26). The spectra of some clusters in proteins are unusual or very difficult to detect, due to the existence of paramagnetic states with $S > \frac{1}{2}$ (described by Hagen, this volume) and to the presence of weak spin-spin interactions between adjacent centers.

When two or more paramagnetic centers are present in the same protein, exchange and dipolar interactions between them cause the appearance of additional lines in the spectrum, which do not occur in the spectrum of either center alone. For example, in the spectra of $2[4\text{Fe}-4\text{S}]$ ferredoxins there are additional lines in the center of the spectrum and in the wings. These are not true g factors, as was demonstrated by multifrequency EPR (27). Similar spectral features have been observed in the EPR spectra of proteins with multiple iron-sulfur clusters, for example, DMSO reductase (19). Extremely broad EPR spectra attributed to $[4\text{Fe}-4\text{S}]$ clusters in succinate dehydrogenase, fumarate reductase (28), and $[\text{Ni}-\text{Fe}]$ hydrogenase of *Desulfovibrio gigas* (29) have been attributed to interactions with reduced $[3\text{Fe}-4\text{S}]$ clusters.

The spectra of oxidized $[4\text{Fe}-4\text{S}]^{3+}$ and $[3\text{Fe}-4\text{S}]^{+}$ clusters have average g factors greater than the free-electron g factor, $g_e = 2.0023$. The spectrum of HiPIP was the first of this type to be detected, and all spectra with $g > g_e$ were referred to as "HiPIP-type." In fact this was misleading. HiPIPs are unique types of soluble proteins, found so far only in a restricted range of bacteria (30). The other clusters that

give EPR signals in the oxidized state at $g = 2.01$ have proved to be $[3\text{Fe-4S}]^+$ clusters. In some proteins, such as succinate dehydrogenase and fumarate reductase, the $[3\text{Fe-4S}]^+$ clusters can be observed in intact cells by EPR spectroscopy and appear to be functional (31). However, many $[4\text{Fe-4S}]$ proteins undergo oxidative conversion to $[3\text{Fe-4S}]^+$ during isolation and yield substoichiometric signals around $g = 2.01$.

The reduced $[3\text{Fe-4S}]$ clusters have a spin-even state, e.g., $S = 2$. Since this is a non-Kramers' state the EPR spectrum may be undetectable, or, if detectable, very broad. In some proteins it is observed as a broad signal around $g = 12$, e.g., in the partially reduced Ni hydrogenase of *D. gigas* (32). When the protein is fully reduced, interactions of the cluster with reduced $[4\text{Fe-4S}]$ clusters cause the signal to disappear.

III. Classification of Iron-Sulfur Proteins

According to the International Union of Biochemistry (IUB) recommended nomenclature (33), iron-sulfur proteins have been classified into the following groups:

1. *Simple iron-sulfur proteins*, which have only iron-sulfur clusters. These include rubredoxins and ferredoxins, of which the only function is electron transfer, and other proteins, in which the iron-sulfur cluster(s) have a catalytic function.

2. *Complex iron-sulfur proteins*, which also contain other prosthetic groups and which generally have enzymatic activity. They are subdivided into iron-sulfur proteins containing flavin, molybdopterin, siroheme, and other prosthetic groups.

Table I includes a compilation, which is not exhaustive, of iron-sulfur proteins for which a function has been established or is strongly suggested. Comparisons of amino acid sequences help to identify families of proteins with similar structure but different enzymatic activities. The iron-sulfur proteins in Table I are loosely grouped in these families. It should be noted that there are also situations in which the same reaction is catalyzed by two different enzymes, coded by different genes, even in the same cell. In some cases, such as in fumarases and glycerol phosphate dehydrogenases from *E. coli*, there is one form, which is expressed under anaerobic conditions and which is an iron-sulfur protein, and another form, which is expressed under aerobic conditions and which is not an iron-sulfur protein. A possible reason is that the

iron-sulfur protein versions may be catalytically more efficient, but more sensitive to oxygen.

When describing the functions of enzymes, particularly in bacterial metabolism, it is often helpful to distinguish between *assimilatory* and *dissimilatory* electron transfer processes. Assimilatory processes are intended to synthesize nutrients for growth, such as the reduction of nitrate to ammonium for amino acid biosynthesis. Dissimilatory electron transport generates energy for growth, such as the reduction of nitrate to N_2 gas in the denitrifying bacteria. There are of course some enzymes with functions that do not fall into either category, such as degradative reactions for disposal of unwanted compounds. Generally the dissimilatory enzymes will have a greater activity within the cell than do the assimilatory enzymes, which has assisted their isolation. The enzymes of the assimilatory pathways tend to be present in a wider variety of cells, and present all the time, whereas the dissimilatory pathways are more specialized and are induced by growth substrates. This is another reason why an organism may express two or more isoenzymes catalyzing the same reaction. Different versions of the enzyme may be adapted for specific pathways.

FERREDOXINS AND OTHER ELECTRON TRANSFER PROTEINS

Ferredoxins and rubredoxins are electron transfer proteins containing iron-sulfur clusters, without enzymatic function. Their functions are to some extent interchangeable, as seen, for example, in the range of ferredoxins used by mono- and dioxygenase systems and by oxoacid:ferredoxin oxidoreductases (see below). The variations of the sequences of ferredoxins are discussed in detail by Matsubara *et al.*, this volume.

1. Rubredoxins

Rubredoxins are characterized by having single iron atoms without labile sulfide. They are classed as iron-sulfur proteins since the iron is ligated entirely by cysteine sulfurs, four per iron atom (designated [Rd]). One of the few known functions of this protein is as intermediate electron carrier in ω -hydroxylation of fatty acids, for which a unique rubredoxin with two rubredoxin domains is used (34). In *Clostridium perfringens*, a function in electron transfer to nitrate reductase has been suggested (35).

2. [2Fe-2S] Ferredoxins

The [2Fe-2S] ferredoxins were first identified as photosynthetic electron transfer proteins in chloroplasts of plants, such as spinach, and in

cyanobacteria. The chloroplast ferredoxins have been found to act as electron donors to several different enzymes, including nitrite reductase and glutamate synthase (36).

Other ferredoxins, which act as electron donors to cytochrome *P*-450, were isolated from animal tissues and bacteria. The naming of these proteins according to their source, such as adrenodoxin and putidaredoxin, has become established in the literature. The IUB Nomenclature Committee (33) prefers the terms "adrenal ferredoxin" and "*Pseudomonas putida* ferredoxin," and discourages the proliferation of further names. The homology of the sequences with the plant-type ferredoxins is very weak, but the [2Fe-2S] cluster-binding cysteines still occur in a similar arrangement. It is likely that these distantly related proteins have a similar folding pattern, as shown by recent two-dimensional NMR measurements (37, 38). The [2Fe-2S] ferredoxins of kidney and adrenal glands, like many eukaryotic proteins, undergo phosphorylation, which modulates their activity (39, 40).

A protein that is clearly homologous to the plant ferredoxins has been found in *Rhodobacter capsulatus*, although this organism does not have the type of photosynthetic NADP reduction that is found in plants (41). Its activity appears to be associated with nitrogen fixation. This purple photosynthetic bacterium has four ferredoxins, including two 2[4Fe-4S] ferredoxins and a [4Fe-4S][3Fe-4S] ferredoxin (42-44).

An unrelated [2Fe-2S] protein has been isolated from nitrogen-fixing *Clostridium pasteurianum* (45). The arrangement of cysteines in its sequence (Fig. 2) is so different from those in the plant-type ferredoxins (Fig. 2) that it probably has a completely different folding pattern (46). The function of this protein is unknown but it may resemble the [2Fe-2S] ferredoxin II from *A. vinelandii*, the function of which appears to be to bind to nitrogenase, protecting it from oxygen (47).

3. Rieske Proteins

Rieske proteins contain specialized [2Fe-2S] clusters with relatively high reduction potentials (0-300 mV). They were first isolated from mitochondrial complex III (48), but similar proteins were found in other types of membrane electron transfer chains. The [2Fe-2S] clusters of aromatic dioxygenases, which have somewhat more negative reduction potentials, appear to be similar (49). Spectroscopic studies have demonstrated that one of the iron atoms in the [2Fe-2S] cluster of the Rieske protein has two histidine nitrogen ligands instead of cysteines (50).

4. 2[4Fe-4S] Ferredoxins

The 2[4Fe-4S] ferredoxins are primarily found in bacteria, though a similar ferredoxin has been found in *Entamoeba histolytica* (51). Differ-

ent organisms use the 2[4Fe-4S] ferredoxins for different purposes, as low-potential electron carriers, particularly in anaerobic metabolism, and they have probably more different functions than any other iron-sulfur protein. The simple sequence of the 2[4Fe-4S] ferredoxins has almost twofold symmetry (Fig. 1), and may have been the evolutionary precursor of the [4Fe-4S][3Fe-4S], the [4Fe-4S], and the [3Fe-4S] ferredoxins (12), and similar sequences in many enzymes. Variations on the sequence are observed, such as insertion of a loop between the second and third cysteines, and the additional C-terminal extension in *A. vinelandii* ferredoxin I.

5. [4Fe-4S] Ferredoxins

The [4Fe-4S] ferredoxins can be considered as having evolved from the 2[4Fe-4S] type by the loss of two or more of the cysteines that bind the second cluster, Fig. 1c (52). The iron-sulfur clusters generally are similar in reduction potentials to those in the 2[4Fe-4S] ferredoxins and have a similar range of functions.

6. [4Fe-4S][3Fe-4S] Ferredoxins

The [4Fe-4S][3Fe-4S] ferredoxins require a minimum of seven cysteines for binding the clusters (Fig. 1b). This arrangement is found in ferredoxin from *Sulfolobus acidocaldarius* (53). Other 7Fe ferredoxins, such as the well-studied ferredoxin from *A. vinelandii*, contain more cysteines, in nonconserved positions, which do not bind the cluster (54, 55). Electrochemistry of *Desulfovibrio africanus* ferredoxin III indicated that on reduction it could incorporate an eighth iron ion to convert the [3Fe-4S] cluster to a [4Fe-4S] cluster. In this case, a noncysteine ligand is expected to bind the cluster, and an appropriately located aspartate was suggested (56) (see Armstrong, this volume).

7. [3Fe-4S] Ferredoxins

The [3Fe-4S] ferredoxins have been isolated and studied from a number of species. The most intensively studied is *D. gigas* ferredoxin II, for which the structure has been determined (57). The protein contains a total of six cysteines and appears to be an oxidized form of the *D. gigas* [4Fe-4S] ferredoxin I. The only proteins found to have the minimum three cysteines for the [3Fe-4S] cluster are the two ferredoxins of *Streptomyces griseolus*. Attempts to reconstitute the latter ferredoxins with [4Fe-4S] clusters were unsuccessful (58). *Desulfovibrio gigas* and *Pyrococcus furiosus* ferredoxins are prototypes for the [3Fe-4S] clusters, for which no chemical models have been synthesized.

Other metal ions, including zinc, cobalt, or nickel, may be incorporated into the reduced clusters, producing $[3\text{FeM-4S}]$ clusters (59–61).

8. High-Potential Iron–Sulfur Proteins

HiPIPs, found in purple sulfur bacteria and some other species, are unusual in that their $[4\text{Fe-4S}]$ cluster undergoes oxidation–reduction between the $[4\text{Fe-4S}]^{2+}$ and $[4\text{Fe-4S}]^{3+}$ oxidation states. As a result they have relatively high redox potentials and give EPR signals in the oxidized state. A long-standing anomaly in the EPR spectrum of the high-potential iron–sulfur protein of *Chromatium vinosum* was the appearance of several minor species that looked like other types of clusters or degraded forms. These occurred even in protein that was pure enough to be crystallized. These effects have now been explained (62) in terms of dimerized forms of the protein that occur in frozen EPR samples. This effect may also explain the EPR spectra of other ferredoxins that appear to contain more than one component, e.g., the ferredoxin of the benzene dioxygenase system (63).

IV. Membrane-Bound Iron–Sulfur Enzymes of Bioenergetic Systems

A. RESPIRATORY CHAINS

Membrane-bound electron transfer proteins that interact with quinones include hydrogenase, formate dehydrogenase, and succinate dehydrogenase, and, on the oxidizing side, nitrate reductase, fumarate reductase, and DMSO reductase. All of these proteins have a similar organization, consisting of a membrane anchor subunit or subunits that act as the binding site for quinone, and soluble subunits on the membrane surface that react with the soluble substrates. The iron–sulfur clusters, which act as intermediary electron carriers, are situated between these two components. In the structure of glycerol phosphate dehydrogenase from anaerobic *E. coli*, there are two $[4\text{Fe-4S}]$ clusters in the hydrophobic C subunit as deduced from the sequence of the *glpABC* operon (64).

Mitochondrial complex I (NADH:ubiquinone reductase), probably the most elaborate iron–sulfur protein, is encoded by more than 30 structural genes, many of which have been sequenced (65). Several of these subunits are encoded by the mitochondrial genome. Counterparts of complex I are found in bacterial respiratory chains. The protein not only transfers electrons, but pumps protons across the mitochondrial inner membrane (66). In purple photosynthetic bacteria, a similar en-

zyme operates in reverse for the energy-dependent reduction of NAD^+ . Proteins homologous with the sequences occur widely, for example, in chloroplasts (67, 68). The protein may be considered as being assembled from two parts—a flavoprotein and a membrane-bound iron-sulfur protein (69). The flavoprotein subunit of the soluble NAD-binding hydrogenase of *Alcaligenes eutrophus* is homologous with the flavin mononucleotide (FMN)-binding flavoprotein subunit (70, 71, 256). Complex I contains at least four EPR-detectable iron-sulfur clusters and there are probably more that are EPR silent. The sequences of subunits indicate that the 51-kDa subunit contains FMN and a [4Fe-4S] cluster, and the NADH-binding site. Iron-sulfur clusters are also found in the 75-, 24-, and 23-kDa subunits (M_r of the bovine heart enzyme).

Complex III of the mitochondrial respiratory chain (ubiquinol:cytochrome *c* reductase) contains one iron-sulfur cluster in the Rieske protein. Similar proteins have been identified in plant mitochondria (72), in the cytochrome b_6f complex of chloroplasts and cyanobacteria, and in respiratory and photosynthetic bacteria (73, 74). The [2Fe-2S] cluster of the protein appears to interact with quinones, as indicated by changes in the line shape of the EPR signal when quinone, quinol, or quinol-type inhibitors are added (75).

B. PHOTOSYSTEM I

In the photosynthetic electron transfer chain of plants and cyanobacteria, the primary electron acceptor complex of photosystem I comprises a large, membrane-bound complex in which electrons from the primary donor chlorophyll are transferred through iron-sulfur clusters to ferredoxin and ultimately NADP (76, 77). In this complex, three iron-sulfur clusters have been identified by EPR spectroscopy.

The iron-sulfur cluster X (78) is proposed to be a [4Fe-4S] cluster bound between the two subunits ps1A1 and ps1A2 (products of the *psaA* and *psaB* genes). Each of these 83-kDa proteins contains two cysteines that are conserved in all species and that are thought to bind to the cluster. Interestingly, the cysteines are closely preceded in the sequence by a leucine zipper motif (79). This motif, consisting of regularly spaced leucine residues, is found in DNA-binding proteins and other proteins, where it helps to stabilize heterodimers (80). In photosystem I it is proposed that a leucine zipper helps to orient the cysteines in order to bind the [4Fe-4S] cluster. Cluster X has an exceptionally negative redox potential, -705 mV (81).

The terminal electron acceptors of photosystem I are iron-sulfur clusters A and B. These clusters have recently been identified with a

9-kDa subunit, encoded by the *psaC* gene (82–84). This protein shows a strong homology with the bacterial 2[4Fe–4S] ferredoxins. A number of iron–sulfur clusters appear to be encoded by the chloroplast genome, which has been sequenced from several species of plants. In the liverwort *Marchantia polymorpha* three open reading frames were identified. The *frxA* (identified with *psaC*) and *frxB* genes also occur in the higher plant tobacco (*Nicotiana tabacum*) chloroplast DNA; both have the characteristic 2[4Fe–4S] sequence type (Fig. 1). The gene *frxC* of *M. polymorpha* exhibits a high degree of homology with the *nifH* gene of nitrogen-fixing bacteria (85) (see Matsubara, this volume).

V. Soluble Proteins with Iron–Sulfur Clusters

Iron–sulfur clusters are single-electron carriers and they interact with other electron-carrying centers, such as heme or nonheme iron, molybdenum, nickel, and corrinoids. Redox reactions of iron–sulfur clusters with organic cofactors, such as flavin, quinone, or thiamin diphosphate, generally involve the formation of free radicals. The iron–sulfur proteins that interact with pyridine nucleotides (NAD or NADP) do so through the intermediary of a flavoprotein (3). The classic example is the reduction of NADP by the [2Fe–2S] ferredoxin in plant photosynthesis. The structure of the intermediary flavoprotein, ferredoxin : NADP reductase, was recently determined (86) and provides the prototype for the flavin-binding domains of some iron–sulfur flavoproteins (87). Amino acid sequence homologies have been observed between ferredoxin : NADP reductase and the flavoprotein components of NADPH : sulfite reductases of *E. coli* and *Salmonella typhimurium* (88).

A group of enzymes, the oxoacid : ferredoxin oxidoreductases, catalyze the oxidative conversion of pyruvate and 2-oxoglutarate to acyl-CoA and succinyl-CoA, respectively, with the elimination of CO₂. The 2-oxoacid : ferredoxin oxidoreductases of anaerobic bacteria contain [4Fe–4S] clusters and thiamin diphosphate (89). In methanogens, acetogens, and some photosynthetic bacteria, the enzyme operates in reverse for the fixation of CO₂ (90). Various types of ferredoxins or flavodoxins are used as electron acceptors or donors: the 2[4Fe–4S] in *Clostridium*; flavodoxin in *Klebsiella*; and [2Fe–2S] ferredoxins in *Halobacterium* (91), in cyanobacteria, and in the protozoon *Trichomonas vaginalis* (92, 93).

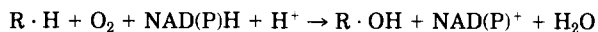
A. OXYGENASE SYSTEMS WITH IRON–SULFUR CLUSTERS

Many hydroxylation reactions in biology use the insertion of one or both atoms of the dioxygen molecule into a substrate, with a concomi-

tant oxidation of NAD(P)H. Examples of different types of such oxygenases, of which many are now known, are given in Table I.

1. Monooxygenases

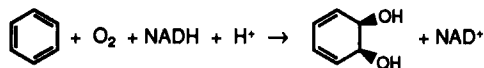
The monooxygenases catalyze the following reaction:



$R \cdot H$ may represent many types of aliphatic or aromatic molecules. These so-called mixed-function oxidases consist of a hydroxylase center, such as cytochrome *P*-450 or nonheme iron, and a short electron transfer chain that brings reducing equivalents from NAD(P)H. The electron transfer chain includes a flavin and often one or more iron-sulfur clusters of the [2Fe-2S] type. The iron-sulfur cluster may be either a separate ferredoxin, as in the *P*-450 systems, or part of an iron-sulfur flavoprotein that interacts with NAD(P) directly. In some cases the amino acid sequences of the iron-sulfur flavoproteins betray an ancestral relationship to the plant-type ferredoxins (94). The ferredoxins are usually [2Fe-2S] proteins, like adrenal ferredoxin or *Pseudomonas putida* ferredoxin. However, there are examples of ferredoxins with [4Fe-4S] and [3Fe-4S] clusters with this function. Two ferredoxins of the [3Fe-4S] type have been identified in the sulfonylurea monooxygenase systems in *S. griseolus* (58). A ferredoxin with a [4Fe-4S] cluster acts as the intermediary electron carrier to the steroid monooxygenase of *Bacillus megaterium* (95). [4Fe-4S][3Fe-4S] ferredoxins participate in the cytochrome *P*-450 of *Saccharopolyspora erythraea* involved in erythromycin biosynthesis (96), and in cytochrome *P*-450_{soy} of *Streptomyces griseus* (97).

2. Dioxygenases

In the dioxygenases considered here, the substrate is aromatic and the product is a *cis*-dihydrodiol:



The structures of the bacterial aromatic dioxygenases have been reviewed recently (98, 99). Each has a large iron-sulfur dioxygenase component, in which the hydroxylation is carried out at a mononuclear nonheme iron site. The dioxygenase component also contains a [2Fe-2S] cluster that is similar in spectroscopic properties to those of the Rieske proteins (99, 100). The 4-methoxybenzoate-*O*-demethylase is usually a monooxygenase, but has some dioxygenase activities and structurally falls into this category (101).

The NADH-dependent reductase chains of these dioxygenases are heterogeneous in composition (Table I). They consist of either a flavo-protein or an iron-sulfur flavoprotein, and in some cases a ferredoxin. The EPR spectrum of the NADH-reduced iron-sulfur flavoprotein, phthalate dioxygenase reductase, shows a flavin radical and a rhombic signal resembling that of spinach ferredoxin (98). The structure of the protein has been determined (98). The iron-sulfur flavoproteins of the benzoate and toluate dioxygenases comprise an N-terminal sequence resembling the plant-type ferredoxins (102a), and a C-terminal sequence resembling other flavoproteins, including NADP:ferredoxin oxidoreductase (100). It is of interest that benzoate dioxygenase reductase is one of the few complex iron-sulfur proteins in which, like the simple ferredoxins, the iron-sulfur cluster has been assembled *in vitro* from iron salts and inorganic sulfide (102). The sequences of the ferredoxin components of benzene and toluene dioxygenases do not resemble the plant ferredoxins but show some similarities to the Rieske proteins (102a-105) (Fig. 2).

B. IRON-SULFUR PROTEINS WITH MOLYBDENUM AND TUNGSTEN

With the exception of Mo nitrogenase, all of the molybdenum-containing iron-sulfur proteins have their molybdenum in the form of the molybdopterin cofactor (106, 107). This cofactor contains a pterin, and in bacterial molybdo proteins it also contains a guanidine or cytidine nucleotide group (108, 109). The molybdo-iron-sulfur proteins include oxidoreductases such as nitrate, formate, and DMSO reductases (110), and the molybdenum hydroxylases, which include xanthine dehydrogenase and aldehyde oxidase (111). The former proteins have multiple [4Fe-4S] clusters whereas the latter have two [2Fe-2S] clusters.

In the molybdenum hydroxylases, the molybdenum serves to introduce the —OH into the substrate; the oxygen derives from water rather than dioxygen. The sequences have been determined of the xanthine dehydrogenases from *Drosophila* (112, 113) and from rat liver (114). They are unusual in that the two [2Fe-2S] clusters appear to be bound in a relatively short, cysteine-rich peptide sequence near the N terminus. One group of cysteines conforms to the plant-type ferredoxin cluster-binding motif, but the other has different spacings. The latter has been tentatively assigned to the second cluster, Fe-S II, which has anomalous EPR behavior (115).

The formate dehydrogenases of bacteria contain, in various combinations, iron-sulfur clusters, molybdenum, tungsten, selenium, and flavin (110). These differences reflect their diverse functions. In *E. coli*,

there are two alternative membrane-bound enzymes for the oxidation of formate to CO_2 , one operating in the formate-hydrogen lyase pathway and in other respiratory pathways to fumarate and nitrate. In clostridia, formate dehydrogenases are soluble proteins and operate in the reverse direction, as a ferredoxin: CO_2 reductase, for fixation of carbon dioxide (116). The enzyme of *Clostridium thermoaceticum* contains tungsten instead of molybdenum (117).

C. NICKEL HYDROGENASES

Hydrogenases are enzymes that catalyze the oxidation or production of hydrogen with various electron acceptors or donors. The enzymes isolated from many bacterial species contain nickel and iron-sulfur clusters. Another class (see below) contains a specialized iron-sulfur cluster instead of the nickel center. The nickel-containing hydrogenases have been reviewed (118–120). In these enzymes, the nickel appears to be in a separate site, coordinated by two to four cysteine sulfurs, plus oxygen and nitrogen ligands from the protein. It is probably at this site that the hydrogen reacts. In some cases, selenium is also present in the enzyme, which changes some of the catalytic properties. It has been demonstrated in some enzymes that the selenium is present as selenocysteine and is a ligand to the nickel site (121, 122). The iron-sulfur clusters in the enzymes, and in some cases flavin or heme, serve to transfer electrons between the nickel site and donors or acceptors such as ferredoxin, NAD, deazaflavin, quinone, or cytochrome *c*. This leads to a considerable variety in the composition of the hydrogenases, though they all have a common basic structure with large and small subunits (see Voordouw, this volume).

D. SIROHEME IRON-SULFUR PROTEINS

Sulfite and nitrite reductases of plants and bacteria contain a specialized chlorin group known as siroheme and an iron-sulfur cluster. The NADPH-dependent assimilatory sulfite reductase of *E. coli* also has a flavoprotein subunit. Mössbauer and EPR spectra have been interpreted in terms of a heme iron antiferromagnetically coupled to a $[4\text{Fe}-4\text{S}]$ cluster (123). A low-resolution electron density map indicated the presence of an iron-sulfur cluster at a distance of 0.44 nm from the heme iron (124).

The ferredoxin:nitrite reductase of plants is also a siroheme-containing iron-sulfur protein (125, 126). The sequence of the protein shows homologies with the *E. coli* sulfite reductase iron-sulfur siro-

heme subunit. The two proteins are also similar in their spectroscopic properties (127).

The assimilatory nitrite reductase from *E. coli* appears to be different. The sequence of this protein contains a cysteine-rich region and a flavin-binding motif, but does not show homologies to other nitrite and sulfite reductases (128). It was found to contain flavin and about four iron atoms/mole. Only a [2Fe-2S] cluster was detected by EPR (129), though the possibility of other clusters with high-spin states cannot be ruled out.

E. CATALYTIC IRON-SULFUR CLUSTERS AND MIXED-METAL CLUSTERS

1. Nitrogenases

Nitrogenases catalyze the reduction of dinitrogen to ammonium. They comprise a specialized group of proteins with unique types of iron-sulfur clusters. The biochemistry of nitrogenases has been extensively reviewed elsewhere (130-134). The molybdenum-iron protein of nitrogenase has been known for many years. Recently, "alternative" nitrogenases, one containing vanadium and iron, the other only iron, have been found. Comparison of these alternative nitrogenases with the Mo nitrogenase provides some informative insights (135). They all contain a specialized metal cluster that is probably the site of reduction of N_2 to ammonium. In the Mo nitrogenase, the Fe-Mo cofactor can be extracted and analysis has indicated a composition of $Fe_{5-7}MoS_{4-8}$ (131, 133). In the V nitrogenase the composition is $Fe_{5-7}VS_{4-6}$.

The structures of all three nitrogenases are similar, and all require a similar set of genes for cofactor biosynthesis. Probably all of the nitrogen-reducing cofactors involve the organic component homocitrate, although the structures have not yet been resolved. Spectroscopic measurements and consideration of the amino acid sequences of a variety of nitrogenases have indicated that only one cysteine is involved in binding the cofactor to the protein, the other ligands being oxygen and nitrogen. Three to four invariant cysteines in the α subunit and three in the β subunit are available for binding the P-cluster(s).

The nitrogenase $\alpha\beta$ components contain iron-sulfur clusters of unique properties, known as the P-clusters, comprising six to eight iron and labile sulfide atoms. The P-clusters were originally considered to be two [4Fe-4S] clusters with unusual redox behavior, but now it seems possible that they represent a single cluster with six to eight iron atoms. A low-resolution structure of the molybdenum-iron protein shows the

P-clusters as an elongated region of electron density, located about 1.9 nm from the Mo-Fe cofactor (136).

Nitrogenase reductase, or the iron protein, is the second essential component of the nitrogenase system. It acts as a low-potential, ATP-dependent electron donor to the dinitrogen-reducing protein. Analyses have indicated the presence of one [4Fe-4S] cluster per dimer of two identical subunits. Furthermore, site-directed mutagenesis experiments have suggested that two cysteines from each subunit are required to bind the cluster. The location of this cluster between the subunits has been confirmed by crystallographic studies of Rees, Georgiadis, and Chakrabarti (see Ref. 137). A possible ATP-binding site has been located in a cleft between the two subunits. This type of electron transfer protein may have a wider application, as indicated by the homologous sequence of the *frxC* gene in the chloroplast genome of *M. polymorpha* (85). It seems likely that such an ATP-driven electron donor would be useful in other enzyme systems.

2. Iron Hydrogenases

The so-called [Fe] hydrogenases, which catalyze the production and consumption of hydrogen gas, also contain a specialized iron-sulfur cluster known as the H-cluster. (Their sequences and structure are discussed by Voordouw, this volume.) The relationship of the H-cluster to the active site clusters in nitrogenases, which are also capable of producing hydrogen gas, is at present unknown.

3. Carbon Monoxide Dehydrogenases

A number of different types of enzyme are referred to as "carbon monoxide dehydrogenases" (which is a misnomer, as CO does not contain hydrogen; a better term would be carbon monoxide oxidoreductase). They all catalyze the reversible oxidation of CO to CO₂. In aerobic, carboxydovoric bacteria a molybdenum-containing iron-sulfur protein with [2Fe-2S] clusters catalyzes the oxidation of CO.

A second type of CO oxidoreductase, isolated from acetogenic and methanogenic bacteria (138, 139), is probably better described as acetyl-CoA synthase. It catalyzes the reductive assembly of acetyl-CoA from a methyl-corrinoid protein, CoA, and either CO or CO₂ (140). The reaction is reversible; in acetogenic and some methanogenic bacteria it is used for the synthesis of acetate (141), and in acetoclastic methanogenic bacteria it is used for the consumption of acetate, which ultimately is converted to methane (142). The anabolic and catabolic acetyl-CoA synthetases differ in their molecular properties but appear to have a similar group of cofactors. EPR has detected the presence of several

[4Fe-4S] clusters and other, more unusual, species. At least one of the iron-sulfur clusters appears to have a spin state $>\frac{1}{2}$, and it has been suggested to be a [6Fe-6S] cluster (142). A third EPR-detectable component, seen in the CO-reduced enzyme from *C. thermoaceticum*, shows hyperfine splittings from the isotopes ^{57}Fe , ^{61}Ni , and ^{13}C , known as the Fe-Ni-C cluster (143).

In anaerobic photosynthetic bacteria such as *Rhodospirillum rubrum*, there is a nickel-iron-sulfur enzyme that catalyzes the oxidation of CO (144) and is probably coupled to the production of H_2 , in a reaction analogous to formate-hydrogen lyase (144a). Like the acetyl-CoA synthases, the *R. rubrum* enzyme contains several regular [4Fe-4S] clusters, another cluster or clusters with spin states $>\frac{1}{2}$, and a species containing nickel and iron (145).

F. NONREDOX ENZYMES

Iron-sulfur proteins in which the iron-sulfur cluster has a nonredox function have recently been reviewed (146-148). The majority of them catalyze hydration/dehydration of double bonds. The first representative of this class to be recognized was aconitase. This isomerase was known to be activated by iron. Due to the efforts of Beinert, Kennedy, and co-workers, it was demonstrated that the inactive enzyme contains a [3Fe-4S] cluster that is converted to a catalytically active [4Fe-4S] cluster (147). Catalysis is believed to take place at the fourth iron atom, acting as a Lewis acid rather than a redox cluster.

Fumarase (fumarate hydratase) is a familiar enzyme of the citric acid cycle; its reaction is analogous to aconitase (aconitate hydratase). Recently two new fumarases, fumarases A and B, both of which are iron-sulfur proteins, have been recognized in *E. coli* (149, 150). They have been termed class I fumarases and bear little homology with the class II fumarase C of *E. coli* or those of aerobic organisms, plants, and animals. Fumarases A and B are thermolabile in comparison with the class II enzymes and are expressed under anaerobic conditions (149). They show some sequence homologies with aconitase, in the region of the cysteine residues (151).

Glutamine 5-phosphoribosyl-1-pyrophosphate (PRPP) amidotransferase, an enzyme involved in purine nucleotide biosynthesis, contains a [4Fe-4S] cluster. This cluster is very difficult to reduce (152) and no catalytic function has been established. The enzyme from *Bacillus subtilis* has been extensively studied. Since the [4Fe-4S] cluster is oxygen sensitive, like many iron-sulfur clusters of enzymes of anaerobic bacteria, it was suggested that a function of the cluster might be to

inactivate the enzyme under aerobic conditions (148). If this is so, the function of the comparable cluster in human glutamine PRPP amidotransferase (153) remains to be established.

Endonuclease III from *E. coli* is an enzyme involved in the repair of various types of damaged nucleotides in DNA. The enzyme also contains a [4Fe-4S] cluster that is readily converted to a [3Fe-4S] cluster by oxidation (154). A possible function of the cluster might be in the β -elimination reaction catalyzed by the enzyme (155, 156). However, it is not known if the cluster has an accessible iron site as in aconitase; the ligands to the [4Fe-4S] cluster have not been identified in the sequence of the protein (157).

Nitrile hydratase, which catalyzes the conversion of nitriles to amides, contains an iron center. The iron is low spin and probably six coordinate. Recent extended X-ray absorption fine structure (EXAFS) and resonance Raman spectroscopic measurements indicate that it is coordinated by two to three sulfurs, the other ligands being oxygen and/or nitrogen. An optical absorption maximum at 710 nm was assigned as a ligand-to-metal charge transfer band (158). Therefore, in a broader definition this can be considered an iron-sulfur protein.

G. IRON-SULFUR PROTEINS IN GENE REGULATION

A new type of iron-binding protein has recently been isolated from human cells; this iron-responsive element binding protein (IRE-BP) regulates the synthesis of the iron-storage protein ferritin, and the transferrin receptor. The method of regulation is unusual in that the protein binds to the messenger RNA, rather than the DNA, at a sequence/structure motif known as the iron-responsive element (159). Excess iron causes an increase in the translation of ferritin mRNA and a decrease in the stability of transferrin receptor mRNA. It is likely that human erythroid 5-aminolevulinate synthase, involved in heme biosynthesis, is regulated in a similar way (160). The amino acid sequence of the IRE-BP shows homologies with aconitase; in particular, the three cysteines that bind the [3Fe-4S] cluster are conserved (161). Rouault *et al.* (161) have proposed that the iron binds to a [3Fe-4S] cluster in the protein, converting it to a [4Fe-4S] cluster, by analogy with the activation of aconitase (162). The resulting conformational change would cause the IRE-BP to dissociate from the mRNA. This discovery opens up new possibilities for the functions of iron-sulfur proteins.

Green *et al.* (163) have proposed a role for iron in the action of the FNR (fumarate/nitrate reductase) regulatory protein in *E. coli*. This

protein acts at the DNA level and controls the anaerobic/aerobic switch of many enzymes (164). The sequence of the FNR protein comprises a DNA-binding domain at the C terminus and a cysteine-rich region at the N terminus. Specific mutagenesis has shown that cysteines 20, 23, 29, and 122 are necessary for its function. The form of iron binding to the protein, if any, is not known at present.

H. IRON-SULFUR PROTEINS OF UNCERTAIN FUNCTION

The "polyferredoxin" from methanogenic bacteria is a remarkable protein that was first identified from the sequence of an open reading frame, *mvhB*, in *M. thermoautotrophicum* (165). The sequence of polyferredoxin contains six tandem repeats of four cysteines, each resembling a bacterial 2[4Fe-4S] ferredoxin, and is predicted to contain 48 iron atoms in 12 clusters. The intervening sequence was predicted to be an amphipathic α -helix that could attach to a membrane or form a membrane pore. The observation that this gene is linked to the structural genes of the "methylviologen-reducing" hydrogenase, for which the acceptor has not been determined, suggests a function in electron transport in hydrogen-dependent formation of methane.

Two interesting nonheme iron proteins have been isolated from *Desulfovibrio* spp. One, named rubrerythrin by its discoverers, was isolated from *D. vulgaris* (166). It contains a rubredoxin-type iron center and a binuclear iron cluster that resembles the μ -oxo-bridged iron dimer in acid phosphatase (167). The protein has been recently found to have pyrophosphatase activity (168). The other, termed "desulfoferredoxin," contains both a rubredoxin-type iron center and another iron center (169).

VI. Concluding Remarks

From consideration of the primary and tertiary structure of the iron-sulfur proteins determined so far, it is possible to discern a number of distinct structural themes. Most of the complex proteins are constructed from domains, some of which are related to the ferredoxin-like sequences and Rieske iron-sulfur proteins. These classes are indicated in Table I. Other proteins appear to be unrelated, including HiPIP, rubredoxins, Fe-S clusters of dehydratases, the H-cluster domain, the [4Fe-4S] clusters of siroheme-containing proteins, nitrogenases, and the nitrogenase reductases.

The present draft nomenclature of iron-sulfur clusters as [4Fe-

$4S]^{2+/1+}$, etc., has proved valuable in specifying the cluster types, avoiding the confusion that has befallen the hemoproteins, for example. It has been sufficiently flexible to encompass new types of clusters, such as the $[3Fe-4S]$ cluster. It can cope with mixed-metal clusters such as $[3FeNi-4S]$, although the terminology for clusters with noncysteine ligands needs clarification. The attempt to divide the conjugated iron-sulfur proteins into iron-sulfur flavoproteins, iron-sulfur molybdoproteins, etc., is less successful, as it leads to artificial divisions. As can be seen from Table I, the possible combinations of iron-sulfur clusters and other centers are numerous, and the resulting groupings are often unrelated to structure or function. Iron hydrogenase and aconitase have little in common with each other, apart from containing $[4Fe-4S]$ clusters. The molybdenum nitrogenase has greater affinities with the vanadium and iron nitrogenases than with other molybdenum-containing proteins, such as xanthine dehydrogenase. In the latter protein it appears that the iron-sulfur clusters are acting as secondary electron carriers, whereas the flavin and molybdenum react with the actual substrates. Indeed, from recent experiments on mutants of *Drosophila* xanthine dehydrogenase, it seems that the enzyme can transfer electrons from xanthine to O_2 quite well without the iron-sulfur clusters (170). A more satisfactory classification would take into account (1) function, as in the Enzyme Commission (EC) classification of enzymes, (2) the protein family, and (3) the cofactor composition.

With new tools for detecting and characterizing iron-sulfur clusters, we are becoming more aware of the versatility of the iron-sulfur proteins. The iron-sulfur enzymes with specialized functions are especially prevalent among the bacteria, owing to their diverse metabolism. This is particularly the case for the strict anaerobes, wherein the sensitivity of iron-sulfur clusters to oxygen is not a disadvantage. Hence there are the iron-sulfur equivalents of enzymes such as fumarase, which in aerobes are not metalloproteins. These iron-sulfur proteins are especially difficult to isolate in the intact state. Gene sequences have revealed new ferredoxins and ferredoxin-like regions within larger proteins. Some of the cluster-binding regions are not readily detected from their cysteine motifs, and are only apparent when the tertiary and even quaternary structures of proteins are examined. Many new iron-sulfur proteins, and probably some surprising new functions, wait to be discovered.

REFERENCES

1. Malkin, R., and Rabinowitz, J. C., *Annu. Rev. Biochem.* **36**, 113 (1967).
2. Hall, D. O., Rao, K. K., and Cammack, R., *Sci. Prog. (Oxford)* **62**, 285 (1975).

3. Cammack, R., *Chem. Scri.* **21**, 87 (1983).
4. Cammack, R., Rao, K. K., and Hall, D. O., *Physiol. Veg.* **23**, 649 (1985).
5. Bruschi, M., and Guerlesquin, F., *FEMS Microbiol. Rev.* **54**, 155 (1988).
6. Otaka, E., and Ooi, T., *J. Mol. Evol.* **29**, 246 (1989).
7. Beinert, H., and Thomson, A. J., *Arch. Biochem. Biophys.* **222**, 333 (1983).
8. Ryden, L., Ofverseldt, L. C., Beinert, H., Emptage, M. H., and Kennedy, M. C., *J. Biol. Chem.* **259**, 3141 (1984).
9. Marion, D., and Guerlesquin, F., *Biochem. Biophys. Res. Commun.* **159**, 592 (1989).
10. Chan, T. M., and Markley, J. L., *Biochemistry* **22**, 6008 (1984).
- 10a. Dugad, L. B., Lamar, G. N., Banci, L., and Bertini, I., *Biochemistry* **29**, 2263 (1990).
11. Banci, L., Bertini, I., and Luchinat, C., *Struct. Bonding* **72**, 113 (1990).
12. Fukuyama, K., Nakahara, Y., Tsukihara, T., Katsube, Y., Hase, T., and Matsu-
bara, H., *J. Mol. Biol.* **199**, 183 (1988).
13. Darlison, M. G., and Guest, J. R., *Biochem. J.* **223**, 507 (1984).
14. Johnson, M. K., Kowal, A. T., Morningstar, J. E., Oliver, M. E., Whittaker, K.,
Gunsalus, R. P., Ackrell, B. A. C., and Cecchini, G., *J. Biol. Chem.* **263**, 14732
(1988).
15. Robson, R., Woodley, P., and Jones, R., *EMBO J.* **5**, 1159 (1986).
16. Mulligan, M. E., Buikema, W. J., and Haselkorn, R., *J. Bacteriol.* **170**, 4406 (1988).
17. Andrews, S. C., Harrison, P. M., and Guest, J. R., *J. Gen. Microbiol.* **137**, 361
(1991).
18. Martin, A. E., Burgess, B. K., Stout, C. D., Cash, V. L., Dean, D. R., Jensen, G. M.,
and Stephens, P. J., *Proc. Natl. Acad. Sci. U.S.A.* **87**, 598 (1990).
19. Cammack, R., and Weiner, J. H., *Biochemistry* **29**, 8410 (1990).
20. Blasco, F., Iobbi, C., Giordano, G., Chippaux, M., and Bonnefoy, V., *Mol. Gen.
Genet.* **218**, 249 (1989).
21. Rothery, R. A., and Weiner, J. H., *Biochemistry* **30**, 8296 (1991).
22. Werth, M. T., Cecchini, G., Manodori, A., Ackrell, B. A. C., Schroder, I., Gunsalus,
R. P., and Johnson, M. K., *Proc. Natl. Acad. Sci. U.S.A.* **87**, 8965 (1990).
23. Schroder, I., Gunsalus, R. P., Ackrell, B. A. C., Cochran, B., and Cecchini, G.,
J. Biol. Chem. **266**, 13572 (1991).
24. Werth, M. T., Manodori, A., Ackrell, B. A. C., Schröder, I., Gunsalus, R. P., and
Johnson, M. K., *J. Inorg. Biochem.* **43**, 270 (1991).
25. Beinert, H., and Sands, R. H., *Biochem. Biophys. Res. Commun.* **3**, 41 (1960).
26. Rupp, H., Rao, K. K., Hall, D. O., and Cammack, R., *Biochim. Biophys. Acta* **537**,
255 (1978).
27. Mathews, R., Charlton, S., Sands, R. H., and Palmer, G., *J. Biol. Chem.* **249**, 4326
(1974).
28. Cammack, R., Patil, D. S., and Weiner, J. H., *Biochim. Biophys. Acta* **870**, 545
(1986).
29. Cammack, R., Patil, D. S., Hatchikian, E. C., and Fernandez, V. M., *Biochim.
Biophys. Acta* **912**, 98 (1987).
30. Meyer, T. E., and Cusanovich, M. A., *Biochim. Biophys. Acta* **975**, 1 (1989).
31. Johnson, M. K., Morningstar, J. E., Cecchini, G., and Ackrell, B. A. C., *Biochem.
Biophys. Res. Commun.* **131**, 653 (1985).
32. Teixeira, M., Moura, I., Xavier, A. V., Moura, J. J. G., Legall, J., Dervartanian,
D. V., Peck, H. D., and Huynh, B. H., *J. Biol. Chem.* **264**, 16435 (1989).
33. Palmer, G., and Reedijk, J., *Eur. J. Biochem.* **200**, 599 (1991).
34. Lode, E. T., and Coon, M. J., *J. Biol. Chem.* **246**, 791 (1971).
35. Seki, Y., Seki, S., Satoh, M., Ikeda, A., and Ishimoto, M., *J. Biochem. (Tokyo)* **106**,
336 (1989).

36. Knaff, D. B., and Hirasawa, M., *Biochim. Biophys. Acta* **1056**, 93 (1991).
37. Greenfield, N. J., Wu, X. H., and Jordan, F., *Biochim. Biophys. Acta* **995**, 246 (1989).
38. Pochapsky, T. C., and Ye, X. M., *Biochemistry* **30**, 3850 (1991).
39. Monnier, N., Defaye, G., and Chambez, E. M., *Eur. J. Biochem.* **169**, 147 (1987).
40. Nemani, R., Ghazarian, J. G., Moorthy, B., Wongsurawat, N., Strong, R., and Armbrrecht, H. J., *J. Biol. Chem.* **264**, 15361 (1989).
41. Grabau, C., Schatt, E., Jouanneau, Y., and Vignais, P. M., *J. Biol. Chem.* **266**, 3294 (1991).
42. Yakunin, A. F., and Gogotov, I. N., *Biokhimiya* **48**(Engl. Transl.), 697 (1983).
43. Schatt, E., Jouanneau, Y., and Vignais, P. M., *J. Bacteriol.* **171**, 6218 (1989).
- 43a. Oh-Oka, H., Itoh, S., Saeki, K., Takahashi, Y., and Matsubara, H., *Plant and Cell Physiology* **32**, 11 (1991).
44. Duport, C., Jouanneau, Y., and Vignais, P. M., *Nucleic Acids Res.* **18**, 4618 (1990).
45. Meyer, J., Bruschi, M., Bonicel, J. J., and Bovier-Lapierre, G. E., *Biochemistry* **25**, 6054 (1986).
46. Meyer, J., *Trends Evol. Ecol.* **3**, 222 (1988).
47. Scherings, G., Haaker, H., and Veeger, C., *Eur. J. Biochem.* **77**, 621 (1977).
48. Rieske, J. S., Hansen, R. E., and Zaugg, W. S., *J. Biol. Chem.* **239**, 3017 (1964).
49. Kuila, D., Fee, J. A., Schoonover, J. R., Woodruff, W. H., Batie, C. J., and Ballou, D. P., *J. Am. Chem. Soc.* **109**, 1559 (1987).
50. Gurbiel, R. J., Batie, C. J., Sivaraja, M., True, A. E., Fee, J. A., Hoffman, B. M., and Ballou, D. P., *Biochemistry* **28**, 4861 (1989).
51. Reeves, R. E., Guthrie, J. D., and Lobelle-Rich, P., *Exp. Parasitol.* **49**, 83 (1980).
52. Fukuyama, K., Matsubara, H., Tsukihara, T., and Katsube, Y., *J. Mol. Biol.* **210**, 383 (1989).
53. Minami, Y., Wakabayashi, S., Wada, K., Matsubara, H., Kerscher, L., and Oesterhelt, D., *J. Biochem. (Tokyo)* **97**, 745 (1985).
54. Stout, G. H., Turley, S., Sieker, L. C., and Jensen, L. H., *Proc. Natl. Acad. Sci. U.S.A.* **85**, 1020 (1988).
55. Stout, C. D., *J. Biol. Chem.* **263**, 9256 (1988).
56. Armstrong, F. A., George, S. J., Cammack, R., Hatchikian, E. C., and Thomson, A. J., *Biochem. J.* **264**, 265 (1989).
57. Kissinger, C. R., Sieker, L. C., Adman, E. T., and Jensen, L. H., *J. Mol. Biol.* **219**, 693 (1991).
58. O'Keefe, D. P., Gibson, K. J., Emptage, M. H., Lenstra, R., Romesser, J. A., Litle, P. J., and Omer, C. A., *Biochemistry* **30**, 447 (1991).
59. Moura, I., Moura, J. J. G., Papaefthymiou, V., and LeGall, J., *J. Am. Chem. Soc.* **108**, 349 (1986).
60. Surerus, K. K., Münck, E., Moura, I., Moura, J. J. G., and LeGall, J., *J. Am. Chem. Soc.* **109**, 3805 (1987).
61. Conover, R. C., Park, J. B., Adams, M. W. W., and Johnson, M. K., *J. Am. Chem. Soc.* **112**, 4562 (1990).
62. Dunham, W. R., Hagen, W. R., Fee, J. A., Sands, R. H., Dunbar, J. B., and Humblet, C., *Biochim. Biophys. Acta* **1079**, 253 (1991).
63. Geary, P. J., Saboowalla, F., Patil, D. S., and Cammack, R., *Biochem. J.* **217**, 667 (1984).
64. Cole, S. T., Eiglmeier, K., Ahmed, S., Honore, N., Elmes, L., Anderson, W. F., and Weiner, J. H., *J. Bacteriol.* **170**, 2448 (1988).
65. Ragan, C. I., *Curr. Top. Bioenerg.* **15**, 1 (1987).
66. Brown, G. C., and Brand, M. D., *Biochem. J.* **252**, 473 (1988).

67. Fearnley, I. M., Runswick, M. J., and Walker, J. E., *EMBO J.* **8**, 665 (1989).
68. Pilkington, S. J., Skehel, J. M., and Walker, J. E., *Biochemistry* **30**, 1901 (1991).
69. Weiss, H., Friedrich, T., Hofhaus, G., and Preis, D., *Eur. J. Biochem.* **197**, 563 (1991).
70. Patel, S. D., Aebersold, R., and Attardi, G., *Proc. Natl. Acad. Sci. U.S.A.* **88**, 4225 (1991).
71. Pilkington, S. J., Skehel, J. M., Gennis, R. B., and Walker, J. E., *Biochemistry* **30**, 2166 (1991).
72. Bonner, W. D., and Prince, R. C., *FEBS Lett.* **117**, 47 (1984).
73. Trumpower, B. L., *Microbiol. Rev.* **54**, 101 (1990).
74. Davidson, E., and Daldal, F., *J. Mol. Biol.* **195**, 13 (1987).
75. von Jagow, G., and Ohnishi, T., *FEBS Lett.* **185**, 311 (1985).
76. Lagoutte, B., and Mathis, P., *Photochem. Photobiol.* **49**, 833 (1989).
77. Evans, M. C. W., Bredenkamp, G., *Physiol. Plant.* **79**, 415 (1990).
78. Golbeck, J. H., and Bryant, D. A., *Curr. Top. Bioenerg.* **16**, 83 (1991).
79. Webber, A. N., and Malkin, R., *Febs Lett.* **264**, 1 (1990).
80. McKnight, S. L., *Sci. Am.* 1991 **264**, 32 (1991).
81. Chamorovsky, S. K., and Cammack, R., *Photobiochem. Photobiophys.* **4**, 195 (1982).
82. Høj, P. D., Svendsen, I., Scheller, H. V., and Møller, B. L., *J. Biol. Chem.* **262**, 12676 (1987).
83. Wynn, R. M., and Malkin, R., *FEBS Lett.* **229**, 293 (1988).
84. Oh-oka, H., Itoh, S., Saeki, K., Takahashi, Y., and Matsubara, H., *Plant Cell Physiol.* **32**, 11 (1991).
85. Ohyama, K., Kohchi, T., Sano, T., and Yamada, Y., *Trends Biochem. Sci.* **13**, 19 (1988).
86. Karplus, P. A., Daniels, M. J., and Herriott, J. R., *Science* **251**, 60 (1991).
87. Correll, C. C., Batie, C. J., Ballou, D. P., and Ludwig, M. L., *J. Biol. Chem.* **260**, 14633 (1985).
88. Ostrowski, J., Wu, J. Y., Rueger, D. C., Miller, B. E., Siegel, L. M., and Kredich, N. M., *J. Biol. Chem.* **264**, 15726 (1989).
89. Wahl, R. C., and Orme-Johnson, W. H., *J. Biol. Chem.* **262**, 10489 (1987).
90. Buchanan, B. B., and Arnon, D. I., *Photosynth. Res.* **24**, 47 (1990).
91. Kerscher, L., and Oesterheld, D., *Eur. J. Biochem.* **116**, 587 (1981).
92. Williams, K., Lowe, P. N., and Leadlay, P. F., *Biochem. J.* **246**, 529 (1987).
93. Johnson, P. J., Doliveira, C. E., Gorrell, T. E., and Muller, M., *Proc. Natl. Acad. Sci. U.S.A.* **87**, 6097 (1990).
94. Stainthorpe, A. C., Lees, V., Salmond, G. P. C., Dalton, H., and Murrell, J. C., *Gene* **91**, 27 (1990).
95. Berg, A., Gustafsson, J.-Å., Ingelman-Sundberg, M., and Carlström, K., *J. Biol. Chem.* **251**, 2831 (1976).
96. Shafiee, A., and Hutchinson, C. R., *J. Bacteriol.* **170**, 1548 (1988).
97. Trower, M. K., Emptage, M. H., and Sariaslani, F. S., *Biochim. Biophys. Acta* **1037**, 281 (1990).
98. Batie, C. J., Ballou, D. P., and Correll, C. J., "Chemistry and Biochemistry of Flavoenzymes." CRC Press, Boca Raton, Florida, 1991.
99. Mason, J. R., and Cammack, R., *Ann. Rev. Microbiol.* in press (1992).
100. Neidle, E. L., Hartnett, C., Ornston, L. N., Bairoch, A., Rekik, M., and Harayama, S., *J. Bacteriol.* **173**, 5385 (1991).
101. Bernhardt, F.-H., Heymann, E., and Traylor, P. S., *Eur. J. Biochem.* **92**, 209 (1978).
102. Yamaguchi, M., and Fujisawa, H., *J. Biol. Chem.* **256**, 6783 (1981).
- 102a. Harayama, S., Polissi, A., and Rekik, M., *FEBS Lett.* **285**, 85 (1991).

103. Irie, S., Doi, S., Yorifuji, T., Takagi, M., and Yano, K., *J. Bacteriol.* **169**, 5174 (1987).
104. Morrice, M., Geary, P., Cammack, R., Harris, A., Beg, F., and Aitken, A., *FEBS Lett.* **231**, 336 (1988).
105. Zylstra, G. J., and Gibson, D. T., *J. Biol. Chem.* **264**, 14940 (1989).
106. Rajagopalan, K. V., *Biochem. Soc. Trans.* **13**, 401 (1985).
107. Bray, R. C., *Q. Rev. Biophys.* **21**, 299 (1988).
108. Johnson, J. L., Rajagopalan, K. V., and Meyer, O., *Arch. Biochem. Biophys.* **283**, 542 (1990).
109. Johnson, J. L., Bastian, N. R., Schauer, N. L., Ferry, J. G., and Rajagopalan, K. V., *FEMS Microbiol. Lett.* **77**, 213 (1991).
110. Adams, M. W. W., and Mortenson, L. E., "Molybdenum Enzymes," pp. 519-593. Wiley, New York, 1985.
111. Wootton, J. C., Nicolson, R. E., Cock, J. M., Walters, D. E., Burke, J. F., Doyle, W. A., and Bray, R. C., *Biochim. Biophys. Acta* **1057**, 157 (1991).
112. Lee, C. S., Curtis, D., McCarron, M., Love, C., Gray, M., Bender, W., and Chovnik, A., *Genetics* **116**, 55 (1987).
113. Keith, T. P., Riley, M. A., Kreitmen, M., Lewontin, R. C., Curtis, D., and Chambers, G., *Genetics* **116**, 67 (1987).
114. Amaya, Y., Yamazaki, K., Sato, M., Noda, K., Nishino, T., and Nishino, T., *J. Biol. Chem.* **265**, 14170 (1990).
115. Hille, R., Hagen, W. R., and Dunham, W. R., *J. Biol. Chem.* **260**, 10569 (1985).
116. Scherer, P. A., and Thauer, R. K., *Eur. J. Biochem.* **85**, 125 (1978).
117. Deaton, J. C., Solomon, E. I., Watt, G. D., Wetherbee, P. J., and Durfor, C. N., *Biochem. Biophys. Res. Commun.* **149**, 424 (1987).
118. Lancaster, J. R., Jr., "The Bioinorganic Chemistry of Nickel." VCH Publ., Weinheim, Germany, 1988.
119. Cammack, R., *Adv. Inorg. Chem.* **32**, 297 (1988).
120. Bélaich, J. P., Bruschi, M., and Garcia, J. L., "Microbiology and Biochemistry of Strict Anaerobes Involved in Interspecies Hydrogen Transfer." Plenum, New York and London, 1990.
121. Yamazaki, S., *J. Biol. Chem.* **257**, 7926 (1982).
122. He, S. H., Teixeira, M., Legall, J., Patil, D. S., Moura, I., Moura, J. J. G., Dervartanian, D. V., Huynh, B. H., and Peck, H. D., *J. Biol. Chem.* **264**, 2678 (1989).
123. Christner, J. A., Münck, E., Janick, P. A., and Siegel, L. M., *J. Biol. Chem.* **256**, 2098 (1986).
124. McRee, D. E., Richardson, D. C., Richardson, J. S., and Siegel, L. M., *J. Biol. Chem.* **261**, 10277 (1986).
125. Cammack, R., Hucklesby, D. P., and Hewitt, E. J., *Biochem. J.* **171**, 519 (1978).
126. Ida, S., and Mikami, B., *Biochim. Biophys. Acta* **871**, 167 (1986).
127. Krueger, R. J., and Siegel, L. M., *Biochemistry* **21**, 2905 (1982).
128. Peakman, T., Crouzet, J., Mayaux, J. F., Busby, S., Mohan, S., Harborne, N., Wootton, J., Nicolson, R., and Cole, J., *Eur. J. Biochem.* **191**, 315 (1990).
129. Cammack, R., Jackson, R. H., Cornish-Bowden, A., and Cole, J. A., *Biochem. J.* **207**, 333 (1982).
130. Gresshoff, P. M., Roth, L. E., Stacey, G., and Newton, W. E., "Nitrogen Fixation: Achievements and Objectives." Chapman & Hall, New York & London, 1990.
131. Burgess, B. K., *Chem. Rev.* **90**, 1377 (1990).
132. Dilworth, M. J., and Glenn, A. R., "Biology and Biochemistry of Nitrogen Fixation." Elsevier, Amsterdam, 1991.
133. Eady, R. R., *Adv. Inorg. Chem.* **36**, 77 (1991).

134. Burris, R. H., *J. Biol. Chem.* **266**, 9339 (1991).
135. Pau, R. N., *Trends Biochem. Sci.* **14**, 183 (1989).
136. Bolin, J. T., Ronco, A. E., Mortenson, L. E., Morgan, T. V., Williamson, M., and Xuong, N. H., "Nitrogen Fixation: Achievements and Objectives," p. 117. Chapman & Hall, New York and London, 1990.
137. Moffat, A. S., *Science* **250**, 1513 (1990).
138. Ragsdale, S. W., Bauer, J. R., Gorst, C. M., Harder, S. R., Lu, W. P., Roberts, D. L., Runquist, J. A., and Schiau, I., *FEMS Microbiol. Rev.* **87**, 397 (1990).
139. Abbanat, D. R., and Ferry, J. G., *J. Bacteriol.* **172**, 7145 (1990).
140. Lu, W. P., Harder, S. R., and Ragsdale, S. W., *J. Biol. Chem.* **265**, 3124 (1990).
141. Hugenholtz, J., and Ljungdahl, L. G., *FEMS Microbiol. Lett.* **87**, 383 (1990).
142. Jetten, M. S. M., Hagen, W. R., Pierik, A. J., Stams, A. J. M., and Zehnder, A. J. B., *Eur. J. Biochem.* **195**, 385 (1991).
143. Fan, C. L., Gorst, C. M., Ragsdale, S. W., and Hoffman, B. M., *Biochemistry* **30**, 431 (1991).
144. Bonam, D., and Ludden, P. W., *J. Biol. Chem.* **262**, 2980 (1987).
- 144a. Ensign, S. A., and Ludden, P. W., *J. Biol. Chem.* **266**, 18395 (1991).
145. Stephens, P. J., Mckenna, M. C., Ensign, S. A., Bonam, D., and Ludden, P. W., *J. Biol. Chem.* **264**, 16347 (1989).
146. Emptage, M. H., "Metal Clusters in Proteins," pp. 343–371. American Chemical Society, Washington, D.C., 1988.
147. Beinert, H., and Kennedy, M. C., *Eur. J. Biochem.* **186**, 5 (1989).
148. Switzer, R. L., *BioFactors* **2**, 77 (1989).
149. Woods, S. A., Schwartzbach, S. D., and Guest, J. R., *Biochim. Biophys. Acta* **954**, 14 (1988).
150. Yumoto, N., and Tikushige, M., *Biochem. Biophys. Res. Commun.* **153**, 1236 (1988).
151. Bell, P. J., Andrews, S. C., Sivak, M. N., and Guest, J. R., *J. Bacteriol.* **171**, 3494 (1989).
152. Vollmer, S. J., Switzer, R. L., and Debrunner, P. G., *J. Biol. Chem.* **258**, 14284 (1983).
153. Itakura, M., and Holmes, E. W., *J. Biol. Chem.* **254**, 333 (1979).
154. Cunningham, R. P., Asahara, H., Bank, J. F., Scholes, C. P., Salerno, J. C., Surerus, K., Munck, E., Mccracken, J., Peisach, J., and Emptage, M. H., *Biochemistry* **28**, 4450 (1989).
155. Kow, Y. W., and Wallace, S. S., *Biochemistry* **26**, 8200 (1987).
156. Bailly, V., and Verly, W. G., *Biochem. J.* **242**, 565 (1987).
157. Asahara, H., Wistort, P. M., Bank, J. F., Bakerian, R. H., and Cunningham, R. P., *Biochemistry* **28**, 4444 (1989).
158. Nelson, M. J., Jin, H., Turner, I. M., Grove, G., Scarrow, R. C., Brennan, B. A., and Que, L., *J. Am. Chem. Soc.* **113**, 7072 (1991).
159. Theil, E. C., *J. Biol. Chem.* **265**, 4771 (1990).
160. Cox, T. C., Bawden, M. J., Martin, A., and May, B. K., *EMBO J.* **10**, 1891 (1991).
161. Rouault, T. A., Stout, C. D., Kaptain, S., Harford, J. B., and Klausner, R. D., *Cell (Cambridge, Mass.)* **64**, 881 (1991).
162. Robbins, A. H., and Stout, C. D., *Proc. Natl. Acad. Sci. U.S.A.* **86**, 3639 (1989).
163. Green, J., Trageser, M., Six, S., Uden, G., and Guest, J. R., *Proc. R. Soc. London Ser. B* **244**, 137 (1991).
164. Spiro, S., and Guest, J. R., *FEMS Microbiol. Lett.* **75**, 399 (1990).
165. Reeve, J. N., Beckler, G. S., Cram, D. S., Hamilton, P. T., Brown, J. W., Krzycki,

- J. A., Kolodziej, A. F., Alex, L., Orme-Johnson, W. H., and Walsh, C. T., *Proc. Natl. Acad. Sci. U.S.A.* **86**, 3031 (1989).
166. LeGall, J., Prickril, B. C., Moura, I., Xavier, A. V., Moura, J. J. G., and Huynh, B. H., *Biochemistry* **27**, 1636 (1988).
167. Sage, J. T., Xia, Y. M., Debrunner, P. G., Keough, D. T., Dejersey, J., and Zerner, B., *J. Am. Chem. Soc.* **111**, 7239 (1989).
168. Liu, M. Y., and Legall, J., *Biochem. Biophys. Res. Commun.* **171**, 313 (1990).
169. Moura, I., Tavares, P., Moura, J. J. G., Ravi, N., Huynh, B. H., Liu, M. Y., and Legall, J., *J. Biol. Chem.* **265**, 21596 (1990).
170. Hughes, R. K., Bennett, B., Doyle, W., Burke, J. F. A. C., and Bray, R. C., *Biochem. Soc. Trans.* **19**, 260 (1991).
171. Przysiecki, C. T., Cheddar, G., Meyer, T. E., Tollin, G., and Cusanovitch, M. A., *Biochemistry* **24**, 5647 (1985).
172. Johnson, M. K., Bennett, D. E., Fee, J. A., and Sweeney, W. V., *Biochim. Biophys. Acta* **911**, 81 (1987).
173. Graves, M. G., Mullenbach, G. T., and Rabinowitz, J. C., *Proc. Natl. Acad. Sci. U.S.A.* **82**, 1653 (1985).
174. Adman, E. T., Sieker, L. C., and Jensen, L. H., *J. Mol. Biol.* **217**, 337 (1991).
175. Moura, I., Huynh, B. H., Hausinger, R. P., Le Gall, J., Xavier, A. V., and Münck, E., *J. Biol. Chem.* **255**, 2493 (1980).
176. Ohnishi, T., "Current Topics in Bioenergetics." Academic Press, New York, 1987.
177. Beckmann, J. D., Ljungdahl, P. O., Lopez, J. L., and Trumpower, B. L., *J. Biol. Chem.* **262**, 8901 (1987).
178. Adam, Z., and Malkin, R., *FEBS Lett.* **225**, 67 (1987).
179. Ruzicka, F. J., and Beinert, H., *J. Biol. Chem.* **252**, 8440 (1977).
180. Beckmann, J. D., and Frerman, F. E., *Biochemistry* **24**, 3913 (1985).
181. Böhm, R., Sauter, M., and Bock, A., *Mol. Microbiol.* **4**, 231 (1990).
182. Axley, M. J., Grahame, D. A., and Stadtman, T., *J. Biol. Chem.* **265**, 18213 (1990).
183. Arp, D. J., McCollum, L. C., and Seefeldt, L. C., *J. Bacteriol.* **163**, 15 (1985).
184. Cole, S. T., *Eur. J. Biochem.* **167**, 481 (1987).
185. Kortner, C., Lauterbach, F., Tripier, D., Unden, G., and Kroger, A., *Mol. Microbiol.* **4**, 855 (1990).
186. Johnson, M. K., Bennett, D. E., Morningstar, J. E., Adams, M. W. W., and Mortenson, L. E., *J. Biol. Chem.* **260**, 5456 (1985).
187. Park, E. Y., Clark, J. E., DerVartanian, D. V., and Ljungdahl, L. G., "Chemistry and Biochemistry of Flavoproteins," pp. 389–400. CRC Press, Boca Raton, Florida, 1990.
188. Miller, R. E., and Stadtman, E. R., *J. Biol. Chem.* **247**, 7407 (1972).
189. Oliver, G., Gosset, G., Sanchez-Pescador, R., Lozoya, E., Ku, L. M., Flores, N., Becerril, B., Valle, F., and Bolivar, F., *Gene* **60**, 1 (1987).
190. Sakakibara, H., Watanabe, M., Hase, T., and Sugiyama, T., *J. Biol. Chem.* **266**, 2028 (1991).
191. Bellamy, H. D., Lim, L. W., Mathews, F. S., and Dunham, W. R., *J. Biol. Chem.* **264**, 11887 (1989).
192. Tischer, W., Bader, J., and Simon, H., *Eur. J. Biochem.* **97**, 103 (1979).
193. Lampreia, J., Moura, I., Teixeira, M., Peck, H. D., Legall, J., Huynh, B. H., and Moura, J. J. G., *Eur. J. Biochem.* **188**, 653 (1990).
194. Aleman, V., Handler, P., Palmer, G., and Beinert, H., *J. Biol. Chem.* **243**, 2560 (1968).

195. Inui, H., Ono, K., Miyatake, K., Nakano, Y., and Kitaoka, S., *J. Biol. Chem.* **262**, 9130 (1987).
196. Meinecke, B., Bertram, J., and Gottschalk, G., *Arch. Microbiol.* **152**, 244 (1989).
197. Arnold, W., Rump, A., Klipp, W., Priefer, U. B., and Pühler, A., *J. Mol. Biol.* **203**, 715 (1988).
198. Huynh, B. H., Patil, D. S., Moura, I., Teixeira, M., Moura, J. J. G., DerVartanian, D. V., Czechowski, M. H., Prickril, B. C., Peck, H. D., and LeGall, J., *J. Biol. Chem.* **262**, 795 (1987).
199. Schneider, K., Cammack, R., and Schlegel, H. G., *Eur. J. Biochem.* **142**, 75 (1984).
200. Alex, L. A., Reeve, J. N., Ormejohnson, W. H., and Walsh, C. T., *Biochemistry* **29**, 7237 (1990).
201. Teixeira, M., Moura, I., Fauque, G., Dervartanian, D. V., Legall, J., Peck, H. D., Moura, J. J. G., and Huynh, B. H., *Eur. J. Biochem.* **189**, 381 (1990).
202. Muth, E., Mörschel, E., and Klein, A., *Eur. J. Biochem.* **169**, 571 (1987).
203. Harder, S. R., Lu, W. P., Feinberg, B. A., and Ragsdale, S. W., *Biochemistry* **28**, 9080 (1989).
204. Driscoll, W. J., and Omdahl, J. L., *Eur. J. Biochem.* **185**, 181 (1989).
205. Koga, H., Yamaguchi, E., Matsunaga, K., Aramaki, H., and Horiuchi, T., *J. Biochem. (Tokyo)* **106**, 831 (1989).
206. Lund, J., Woodland, M. P., and Dalton, H., *Eur. J. Biochem.* **147**, 297 (1985).
207. Prince, R. C., and Patel, R. N., *FEBS Lett.* **203**, 127 (1986).
208. Eich, F., Geary, P. J., and Berhardt, F. H., *Eur. J. Biochem.* **153**, 407 (1986).
209. Haigler, B. E., and Gibson, D. T., *J. Bacteriol.* **172**, 465 (1990).
210. Haigler, B. E., and Gibson, D. T., *J. Bacteriol.* **172**, 457 (1990).
211. Batie, C. J., LaHaie, E., and Ballou, D. P., *J. Biol. Chem.* **262**, 1510 (1987).
212. Sauber, K., Frohner, C., Rosenberg, G., Eberspacher, J., and Lingens, F., *Eur. J. Biochem.* **74**, 89 (1977).
213. Yamaguchi, M., and Fujisawa, H., *J. Biol. Chem.* **253**, 8848 (1978).
214. Markus, A., Krekell, D., and Lingens, F., *J. Biol. Chem.* **261**, 12883 (1986).
215. Barber, M. J., Bray, R. C., Lowe, D. J., and Coughlan, M. P., *Biochem. J.* **21**, 3561 (1976).
216. Dalton, H., Lowe, D. J., Pawlik, R. T., and Bray, R. C., *Biochem. J.* **153**, 287 (1976).
217. Barber, M. J., Coughlan, M. P., Rajagopalan, K. V., and Siegel, L. M., *Biochemistry* **21**, 3561 (1982).
218. Poels, P. A., Groen, B. W., and Duine, J. A., *Eur. J. Biochem.* **166**, 575 (1987).
219. Turner, N., Barata, B., Bray, R. C., Deistung, J., LeGall, J., and Moura, J. J. G., *Biochem. J.* **243**, 755 (1987).
220. Mukund, S., and Adams, M. W. W., *J. Biol. Chem.* **266**, 14208 (1991).
221. Coughlan, M. P., Mehra, R. K., Barber, M. J., and Siegel, L. M., *Photobiophys.* **7**, 596 (1984).
222. Meyer, O., Jacobitz, S., and Kruger, B., *Microbiol. Rev.* **39**, 161 (1986).
223. Koenig, K., and Andreesen, J. R., *J. Bacteriol.* **172**, 5999 (1990).
224. Nagel, M., and Andreesen, J. R., *Arch. Microbiol.* **154**, 605 (1990).
225. Anderson, G. L., and Hille, R., *J. Inorg. Biochem.* **43**, 577 (1991).
226. Mikami, B., and Ida, S., *Biochim. Biophys. Acta* **791**, 294 (1984).
227. Barber, M. J., Siegel, L. M., Schauer, N. L., May, H. D., and Ferry, J. G., *J. Biol. Chem.* **258**, 10839 (1983).
228. Jollie, D. R., and Lipscomb, J. D., *J. Biol. Chem.* **266**, 21853 (1991).

229. Müller, U., Willnow, P., Ruschig, U., and Höpner, T., *Eur. J. Biochem.* **83**, 485 (1978).
230. Prince, R. C., Liu, C.-L., Morgan, V., and Mortenson, L. E., *FEBS Lett.* **189**, 263 (1985).
231. Shuber, A. P., Orr, E. C., Recny, M. A., Schendel, P. F., May, H. D., and Schauer, N. L., *J. Biol. Chem.* **261**, 12942 (1986).
232. Moura, I., LeGall, J., Lino, A. R., Peck, H. D., Fauque, G., Xavier, A. V., Dervartanian, D. V., Moura, J. J. G., and Huynh, B. H., *J. Am. Chem. Soc.* **110**, 1075 (1988).
233. Moura, I., Lino, A. R., Moura, J. J. G., Xavier, A. V., Fauque, G., Peck, H. D., and LeGall, J., *Biochem. Biophys. Res. Commun.* **141**, 1032 (1986).
234. Adams, M. W. W., *Biochim. Biophys. Acta* **1020**, 115 (1990).
235. Lindahl, P. A., Ragsdale, S. W., and Münck, E., *J. Biol. Chem.* **265**, 3880 (1990).
236. Eggen, R. I. L., Geerling, A. C. M., Jetten, M. S. M., and Devos, W. M., *J. Biol. Chem.* **266**, 6883 (1991).
237. Lindahl, P., Day, E. P., Kent, T. A., Orme-Johnson, W. H., and Münck, E., *J. Biol. Chem.* **260**, 11160 (1985).
238. Eady, R. R., Robson, R. L., Richardson, T. H., Miller, R. W., and Hawkins, M., *Biochem. J.* **244**, 197 (1987).
239. Chisnell, J. R., Premakumar, R., and Bishop, P. E., *J. Bacteriol.* **170**, 27 (1988).
240. Dreyer, J. L., *Eur. J. Biochem.* **150**, 145 (1985).
241. Kuchta, R. D., Hanson, G. R., Holmquist, B., and Abeles, R. H., *Biochemistry* **25**, 7301 (1986).
242. Schweiger, G., Dutscho, R., and Buckel, W., *Eur. J. Biochem.* **169**, 441 (1987).
243. Flint, D. H., and Emptage, M. H., *J. Biol. Chem.* **263**, 3558 (1988).
244. Flint, D. H., and Emptage, M. H., *J. Inorg. Chem.* **36**, 326 (1989).
245. Kelly, J. M., and Scopes, R. K., *FEBS Lett.* **202**, 274 (1986).
246. Grabowski, R., and Buckel, W., *Eur. J. Biochem.* **199**, 89 (1991).
247. Scopes, R. K., and Griffiths-Smith, K., *Anal. Biochem.* **136**, 530 (1984).
248. Hagen, W. R., Pierik, A. J., and Veeger, C., *J. Chem. Soc., Faraday Trans.* **85**, 4083 (1989).
249. Hatchikian, E. C., and Bruschi, M., *Biochem. Biophys. Res. Commun.* **86**, 725 (1979).
250. Watenpugh, K. D., Sieker, L. C., and Jensen, L. H., *J. Mol. Biol.* **131**, 509 (1979).
251. Sieker, L. C., Stenkamp, R. E., Jensen, L. H., Prickril, B., and LeGall, J., *FEBS Lett.* **208**, 73 (1986).
252. Stenkamp, R. E., Sieker, L. C., and Jensen, L. H., *Proteins: Struct. Funct. Genet.* **8**, 352 (1990).
253. Frey, M., Sieker, L., Payan, F., Haser, R., Bruschi, M., Pepe, G., and LeGall, J., *J. Mol. Biol.* **197**, 525 (1987).
254. Rypniewski, W. R., Breiter, D. R., Benning, M. M., Wesenberg, G., Oh, B. H., Markley, J. L., Rayment, I., and Holden, H. M., *Biochemistry* **30**, 4126 (1991).
255. Fukuyama, K., Hase, T., Matsumoto, S., Tsukihara, T., Katsube, Y., Tanaka, N., Kakudo, M., Wada, K., and Matsubara, H., *Nature (London)* **286**, 522 (1980).
256. Tsukihara, T., Fukuyama, K., Mizushima, M., Harioka, T., Kusunoki, M., Katsube, Y., Hase, T., and Matsubara, H., *J. Mol. Biol.* **216**, 399 (1990).
257. Sussman, J. L., Brown, J. H., and Shoham, M., "Iron-Sulfur Protein Research," p. 69. Japan Sci. Soc. Press Tokyo/Springer-Verlag, Tokyo/Berlin, 1986.
258. Freer, S. T., Alden, R. A., Carter, C. W. J., and Kraut, J., *J. Biol. Chem.* **250**, 46 (1975).

259. Stout, C. D., *J. Mol. Biol.* **205**, 545 (1989).
260. Adman, E. T., Sieker, L. C., and Jensen, L. H., *J. Biol. Chem.* **251**, 3801 (1976).
261. KrishnaMurthy, H. M., Hendrickson, W. A., Orme-Johnson, W. H., Merritt, E. A., and Phizackerley, R. P., *J. Biol. Chem.* **263**, 18430 (1988).
262. Lim, L. W., Shamala, N., Mathews, F. S., Steenkamp, D. J., Hamlin, R., and Xuong, N. H., *J. Biol. Chem.* **261**, 15140 (1986).
263. Voordouw, G., Walker, J. E., and Brenner, S., *Eur. J. Biochem.* **148**, 509 (1985).
264. Bilous, P. T., Cole, S. T., Anderson, W. F., and Weiner, J. H., *Mol. Microbiol.* **2**, 785 (1988).
265. Tran-Betcke, A., Warnecke, U., Bocker, C., Zaborosch, C., and Friedrich, B., *J. Bacteriol.* **172**, 2920 (1990).
- 265a. Yao, Y., Wakabayashi, S., Matsuda, S., Matsubara, H., Yu, L., and Yu, C.-A., "Iron-Sulfur Protein Research," pp. 240-244. Japan Sci. Soc. Press/Springer-Verlag, Tokyo/Berlin, 1986.
266. Takruri, I., and Boulter, D., *Biochem. J.* **179**, 373 (1979).
267. Tanaka, M., Haniu, M., Yasunobu, K. T., and Kimura, T., *J. Biol. Chem.* **248**, 1141 (1973).
268. Tanaka, M., Haniu, M., Yasunobu, K. T., Dus, K., and Gunsalus, I. C., *J. Biol. Chem.* **249**, 3689 (1974).
269. Harnisch, U., Weiss, H., and Sebald, W., *Eur. J. Biochem.* **149**, 95 (1985).
270. Ensign, S. A., and Ludden, P. W., *J. Biol. Chem.* **266**, 18395 (1991).
271. Ensley, B. D., and Gibson, D. T., *J. Bacteriol.* **155**, 505 (1983).
272. Harayama, S., Polissi, A., and Rekik, M., *FEBS Lett.* **285**, 85 (1991).
273. Droux, M., Jacquot, J.-P., Miginac-Maslow, M., Gadal, P., Huet, J. C., Crawford, N. A., Yee, B. C., and Buchanan, B. B., *Arch. Biochem. Biophys.* **252**, 426 (1987).

ACONITASE: AN IRON-SULFUR ENZYME

MARY CLAIRE KENNEDY* and C. DAVID STOUT†

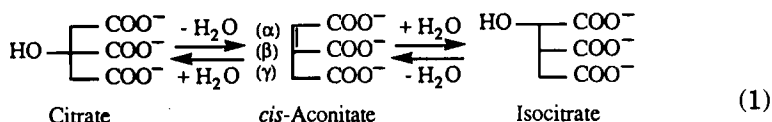
* Department of Biochemistry, Medical College of Wisconsin, Milwaukee, Wisconsin 53226

† Department of Molecular Biology, The Scripps Research Institute,
La Jolla, California 92037

- I. Introduction
- II. Properties of the Fe-S Cluster
- III. Interaction of Cluster and Substrate in the Enzymatic Reaction
- IV. Crystallographic Structure
- V. Studies on Mutants
- VI. Relationship of Cytoplasmic Aconitase to Iron-Responsive Element Binding Protein
- References

I. Introduction

Although the presence and function of the Krebs cycle enzyme aconitase [aconitate hydratase; citrate (isocitrate) hydro-lyase; EC 4.2.1.3] has been known for over 50 years (1), it is only recently that many of the unusual properties of this protein can be understood in molecular terms. The enzyme catalyzes the stereospecific conversion of citrate to threo-D₅-isocitrate via the obligatory intermediate *cis*-aconitate as illustrated in Eq. (1).



It was shown early on, particularly for the mitochondrial form of the enzyme, that activity lost during isolation could be restored upon addition of Fe²⁺ and reductant. It was only with the discovery that aconitase was an Fe-S protein (2) and after evidence had been obtained for the existence of 3Fe clusters (3, 4) that this phenomenon could be explained. Through the application of spectroscopy, especially Möss-

bauer (MB) spectroscopy in combination with electron paramagnetic resonance (EPR), in addition to chemical methods, it was established that the activation process involved the conversion of a $[3\text{Fe}-4\text{S}]$ cluster to a $[4\text{Fe}-4\text{S}]$ form (Fig. 1) (5, 6). Furthermore, these studies demonstrated that the iron added during this reaction, labeled Fe_a , was site specific. These discoveries in the early 1980s allowed for the subsequent design of a number of experiments to investigate details of the role of the cluster in the catalytic mechanism of the enzyme (7). A review by Emptage discusses in some detail how knowledge of aconitase has developed through the years (8).

II. Properties of the Fe-S Cluster

Aconitase and ferredoxin (Fd) II of *Desulfovibrio gigas* were among the first proteins that were shown to contain a 3Fe cluster (4). Because of its low molecular mass and its stability, Fd II of *D. gigas* became the prime example for spectroscopic characterization of proteins containing 3Fe clusters (9). Many of the properties originally found in studies on Fd II were later shown to occur also in aconitase. The $1e^-$ reduced $[3\text{Fe}-4\text{S}]^0$ state of Fd II was recognized as the simplest cluster state

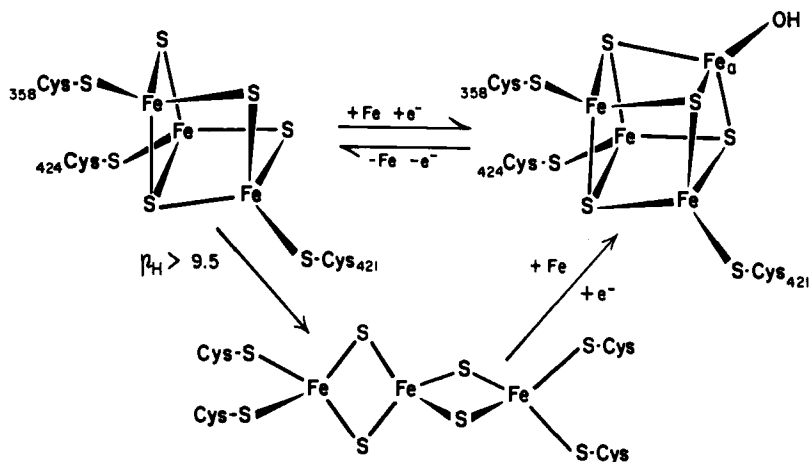


FIG. 1. Schematic description of the interconversions of the clusters in aconitase. The Cys residues bound to the linear cluster are those at positions 250, 257, 421, and 424. Their precise disposition at the cluster is not known (26). (Reproduced with permission from Ref. 7. Copyright 1989, Federation of European Biochemical Societies.)

that has a substructure with distinct localization of valence (10). Two Fe atoms share the extra electron added on reduction, and the third Fe remains ferric. The ferromagnetically coupled ($S = \frac{3}{2}$) ferric-ferrous pair containing the delocalized electron interacts antiferromagnetically with the ferric ion ($S = \frac{5}{2}$), resulting in a spin system of $S = 2$, in which the extra electron remains localized on two Fe ions. This coupling mode is thought to be due to what has become known as "double exchange" or "resonance splitting" (10, 11). This feature appears to be an intrinsic property of $[3\text{Fe}-4\text{S}]^0$ clusters. An analysis of this phenomenon has led to significant theoretical advances in our understanding of the electronic structure of the various Fe-S clusters. This has been considered and discussed in detail in recent literature (10, 12, 13). It has also been established for Fd II that the $[3\text{Fe}-4\text{S}]^0$ form is in fact not EPR silent, as previously thought (9), but has a broad signal at low field (<1000 G at X-band) now known to be typical of integer spin systems (14).

As mentioned above, the features originally described for Fd II have also been observed with aconitase, although usually at a lower signal-to-noise ratio. However, aconitase has a number of properties that make it more suitable for the detailed exploration of certain aspects. Because of the greater lability of the Fe-S cluster of aconitase, the Fe:S stoichiometry, namely $3\text{Fe}:4\text{S}$, could be determined much more convincingly for aconitase than for Fd II (15), and the conversion between the 3Fe and 4Fe forms could be readily followed (6). Because the Fe-S cluster in aconitase is more labile and because a reconstitutable apoprotein could be prepared (16), it was also possible to incorporate isotopes of Fe (6) or S (17) or even Se (18) instead of S in the cluster. This was a great advantage for spectroscopy. For aconitase it could be shown that Fe_a , the Fe that was removed by oxidation in the $4\text{Fe} \rightarrow 3\text{Fe}$ conversion, was returned to exactly the same position from which it had been removed (5, 6). This position is uniquely characterized by a MB doublet of $\delta = 0.45$ and $\Delta E_Q = 0.80$ mm/sec as compared to $\delta = 0.45$ and $\Delta E_Q = 1.30$ mm/sec for the other three Fe atoms (Fe_{b1-3}) of the cluster. These unique MB features of Fe_a , along with the fact that aconitase is an enzyme whose activity can be readily determined, have been very helpful in exploring the cluster properties of aconitase.

The native form of the active enzyme contains a diamagnetic $[4\text{Fe}-4\text{S}]^{2+}$ cluster that can be reduced to the EPR-detectable $[4\text{Fe}-4\text{S}]^+$ form with the enzyme still retaining 30% activity (19). The EPR spectra of this latter form in the absence and presence of substrate are dramatically different, thus establishing that there is direct interaction of the substrate with the cluster. This interaction was specifically

narrowed by MB spectroscopy to the ligation of substrate to Fe_a (20, 21). The MB spectrum of enzyme labeled with ^{57}Fe in Fe_a gives a single doublet with the parameters given above; the spectrum changes upon addition of substrate to give two new doublets, with substantially different characteristics (21). These new signals, labeled S_1 and S_2 , were interpreted as arising from a change in coordination of Fe_a from tetrahedral to five or six coordinate (20, 21). Formally, the $[\text{4Fe-4S}]^{2+}$ cluster has two Fe(III) and two Fe(II) atoms. Spectroscopy indicates that, generally in $[\text{4Fe-4S}]^{2+}$ clusters, the d electrons are delocalized over the whole cluster structure (12, 22). However, for the $[\text{4Fe-4S}]^{2+}$ cluster of aconitase, MB spectroscopy has shown that Fe_a acquires distinct ferrous character on addition of substrate to the +2 form, indicating a pronounced localization of valence at Fe_a . Electron-nuclear double-resonance spectroscopy (ENDOR) cannot give information on the diamagnetic +2 form. For the reduced $[\text{4Fe-4S}]^+$ cluster, however, both MB (21) and ENDOR (23) spectroscopies indicate a high degree of inequivalence among the Fe atoms, which becomes even more pronounced in the presence of substrate. The +1 cluster has formally one Fe(III) and three Fe(II) . Two pairs of Fe atoms can be distinguished in the +1 cluster: a mixed-valence delocalized ferric-ferrous pair (Fe_{b2} and Fe_{b3}), and a ferrous pair (Fe_a and Fe_{b1}), where the electron added on reduction largely resides. The observation of substructures consisting of two pairs of Fe atoms is in agreement with findings on other Fe-S proteins (24). However, a localization of valence of the magnitude found with aconitase has previously not been seen with Fe-S proteins. These results from the MB and ENDOR spectroscopic studies on aconitase together with theoretical work (13) have contributed to formation of the basis for present concepts of the substructure of multinuclear Fe-S clusters and are discussed in more detail in Refs. 10, 12, and 13. It might be mentioned that it was possible to deduce from ^{33}S ENDOR measurements that the sulfides in the $[\text{4Fe-4S}]^+$ cluster, with and without substrate bound, also occur in two distinct pairs, and the spatial arrangement between the individual Fe atoms and the sulfide pairs could be derived from the ^{57}Fe and ^{33}S ENDOR data (23). This is illustrated in Fig. 2. Finally, aconitase is able to accommodate a linear 3Fe cluster (Fig. 1) (25, 26). This cluster, which had been previously synthesized by Holm's group (27), occurs only in a partially unfolded form of aconitase and is not discussed further.

III. Interaction of Cluster and Substrate in the Enzymatic Reaction

Although the aforementioned studies clearly demonstrate the involvement of the iron-sulfur cluster in the enzymatic reaction, the

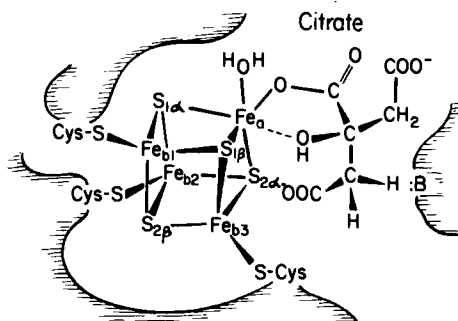


FIG. 2. Representation of ENDOR-derived information about the $[4\text{Fe}-4\text{S}]^+$ cluster of the aconitase enzyme-substrate complex, showing the two pairs of sulfur ($\text{S}_{1\alpha}$ and $\text{S}_{1\beta}$; $\text{S}_{2\alpha}$ and $\text{S}_{2\beta}$) in relationship to the four inequivalent iron sites, Fe_a , Fe_{b1} , Fe_{b2} , and Fe_{b3} , along with the bound substrate. (Reproduced with permission from Ref. 23. Copyright 1990, American Chemical Society.)

details of this involvement were obtained primarily by ENDOR studies at both X-band (9 GHz) (28) and Q-band (35 GHz) (29, 30). The feasibility of these studies was established when line broadening was observed in the EPR signal of the $[4\text{Fe}-4\text{S}]^+$ form of the enzyme in the presence of substrate in ^{17}O -labeled water (20). ENDOR measurements were made of enzyme in H_2O , D_2O , and ^{17}O -labeled water in the presence and absence of substrates or inhibitors (28, 30). Substrates and inhibitors were in turn specifically labeled with ^2H , ^{13}C , or ^{17}O . The data from these experiments yielded a wealth of information, leading to a detailed picture of the binding of substrate to cluster. The results of ^{17}O ENDOR spectroscopy of substrate labeled individually in each of the carboxyl groups (Table I) indicated binding to the β -carboxyl only (29). Similar information was obtained from ^{13}C ENDOR of labeled carboxylates. There was no evidence from these experiments for the binding of hydroxyl from substrate. This led to the interpretation that the predominant species of substrate bound to the $[4\text{Fe}-4\text{S}]^+$ cluster was *cis*-aconitate in the citrate mode (i.e., through the β -carboxyl). To establish binding in the isocitrate mode (i.e., through the α -carboxyl), the labeled inhibitor nitroisocitrate (1-hydroxy-2-nitro-1,3-propanedicarboxylate) was used. These experiments revealed binding not only to the α -carboxyl but also to the α -hydroxyl (Table I). From this it was concluded that the binding of substrate to cluster involves the formation of a five-membered ring of Fe_a with a carboxyl and hydroxyl of substrate (Fig. 2). This allows for the orientation of either citrate or isocitrate to enzyme such that the proton lost on reaction is in an identical position

TABLE I
ENDOR RESULTS ON ACONITASE WITH ^{17}O -LABELED
SUBSTRATES OR ANALOG

Added ^a	^{17}O labeling (●)	Hyperfine coupling constant A_v (MHz)
Citrate	HO — $\begin{array}{l} \text{C} \bullet \bullet \\ \text{COO}^- \\ \text{COO}^- \end{array}$	0
Citrate	HO — $\begin{array}{l} \text{COO}^- \\ \text{C} \bullet \bullet \\ \text{COO}^- \end{array}$	15
Isocitrate	HO — $\begin{array}{l} \text{COO}^- \\ \text{COO}^- \\ \text{C} \bullet \bullet \end{array}$	0
Nitroisocitrate	H● — $\begin{array}{l} \text{C} \bullet \bullet \\ \text{NO}_2 \\ \text{COO}^- \end{array}$	9,13
Nitroisocitrate	H● — $\begin{array}{l} \text{COO}^- \\ \text{NO}_2 \\ \text{COO}^- \end{array}$	9

^a Note that in the presence of active aconitase any substrate added is converted to an equilibrium mixture of the three substrates. (Reproduced with permission from Ref. 29. Copyright 1987.)

for both modes, a requirement established by earlier kinetic and stereochemical studies (31, 32).

In agreement with the X-ray structure, these studies also established that the fourth ligand to Fe_a is not a thiol but rather a hydroxyl from solvent. This is the first documented case in which the fourth ligand to iron in a cluster is not a Cys or Asp residue of the protein. Furthermore, a combination of ^1H , ^2H , and ^{17}O ENDOR demonstrated that this hydroxyl is converted to a water molecule upon the binding of substrate to cluster. These results indicate that Fe_a is six coordinate in the presence of substrate, thus corroborating the earlier conclusions from the MB data.

IV. Crystallographic Structure

The crystal structure of pig heart mitochondrial aconitase was solved and refined at 2.1 Å resolution using data collected aerobically and

crystals grown from ammonium sulfate in the presence of tricarballoylate, a weak binding inhibitor (33). The structure revealed a [3Fe-4S] cluster and bound sulfate, but no inhibitor, in the active site. Refinement of the structure relied on primary sequence data for pig heart aconitase, 754 residues, 83 kDa (34), and partial sequence data for the beef heart enzyme (35). The protein structure is arranged into four domains (Fig. 3). The first three from the N terminus are closely associated to create a shallow cavity at the Fe-S cluster and active site. Each of these domains contains a central β sheet with topology common to

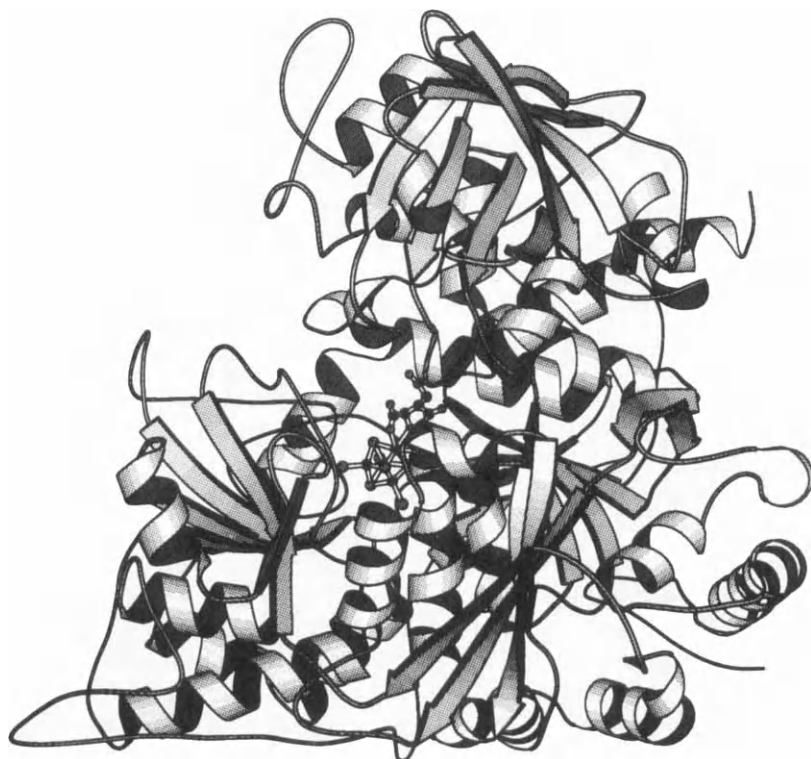


FIG. 3. The structure of heart mitochondrial aconitase showing the polypeptide chain, [4Fe-4S] cluster, and bound isocitrate. Water and three cysteine sulfurs also bonded to the cluster are shown. The protein secondary structure is represented by coils for helices and ribbons for strands within β sheets. The N terminus is at the lower right and the C terminus is at the upper right. In this view the fourth domain is at the top and the three N-terminal domains are arranged from right to left in the lower portion of the molecule. (This image was calculated by G. Gippert at Scripps Research Institute using the program Molscrip written by P. Kraulis.)

lactate dehydrogenase. The fourth and largest domain at the C terminus is tethered by an extended polypeptide chain termed the hinge/linker. This creates an extensive cleft running across the molecule between the fourth domain and the first three domains. The Fe-S cluster is at the bottom of this cleft. The fourth domain contains a mixed β sheet of novel topology. Details of the protein structure are described in Ref. 33.

To assess the [4Fe-4S] form of the enzyme in the crystalline state, the pig heart crystals were soaked anaerobically in ferrous ammonium sulfate and sodium dithionite. The refined structure at 2.5 Å resolution showed that a fourth Fe atom, i.e., Fe_a, was inserted into the [3Fe-4S] cluster isomorphously to create a [4Fe-4S] cluster (36). This result confirmed the 3Fe → 4Fe conversions observed in aconitase and *D. gigas* Fd II by MB and EPR spectroscopy as discussed above. The ligands of the Fe atoms in the [3Fe-4S] moiety in both the 3Fe and 4Fe forms are three cysteines; however, the ligand of Fe_a is not a cysteine but the oxygen atom from a hydroxyl, as observed in ENDOR experiments (a water molecule was modeled in the crystallographic refinement). Because the [4Fe-4S] cluster was formed by soaking crystals used for the original structure determination, a bound sulfate was again observed in the active site in place of inhibitor.

To obtain crystallographic information about the binding of substrates and inhibitors, pig heart aconitase crystals were used as seeds in anaerobic crystallization experiments in which either pig or beef heart enzyme was incubated in buffers containing the substrate or inhibitor of choice. A new crystal form was obtained that accommodates the binding of several compounds (37). (Crystals of the original form used for structure determination invariably cracked when soaked with substrates or tight-binding inhibitors.) Two structures have been reported for aconitase in the new crystal form, both refined at 2.0 Å resolution (37). Pig heart enzyme was used for determining the structure with isocitrate bound. The exclusive presence of isocitrate in the crystals was corroborated by MB spectroscopy on a sample consisting of many single crystals. Beef heart enzyme was used for determining the structure with the reaction intermediate analog, nitroisocitrate, bound. The inhibitor binds to the enzyme in a manner virtually identical to that of isocitrate. Both compounds bind to Fe_a of the [4Fe-4S] cluster via a hydroxyl oxygen and one carboxyl oxygen of the α -carboxyl group. A water molecule is also bound, making the Fe six coordinate. Thus, the crystal structures confirm the conclusions drawn from ENDOR experiments regarding the binding mode of isocitrate and nitroisocitrate and the coordination state of Fe_a.

All four domains of aconitase contribute residues to the active site (Fig. 4) (37). The residues participate in substrate recognition (Arg 447, Arg 452, Arg 580, Arg 644, Gln 72, Ser 166, and Ser 643), cluster ligation and interaction (Cys 358, Cys 421, Cys 424, Asn 258, and Asn 446), hydrogen bond support of active site side chains (Ala 74, Asp 568, Ser 571, and Thr 567), and catalysis (Ser 642). There are also three histidine-carboxylate pairs: Asp 100–His 101, Asp 165–His 147, and Glu 262–His 167.

The base necessary for proton abstraction from the β -carbon of isocitrate appears to be Ser 642; the oxygen atom is proximal to the calculated hydrogen position and the environment of this oxygen suggests stabilization of an alkoxide (an oxyanion hole formed by the amide and side chain of Arg 644). The histidine-carboxylate pairs appear to be required for proton transfer reactions involving two oxygen atoms bound to Fe_a , one derived from solvent (bound water) and one derived from substrate hydroxyl (Fig. 5). Each of these oxygens is in contact with a histidine and both oxygens through hydrogen bonding are in contact with the side chain of Asp 165, which bridges the two sites on the six-coordinate Fe. The proton transfers are expected to be required for the binding of substrate, as illustrated in Fig. 5, when Fe_a expands

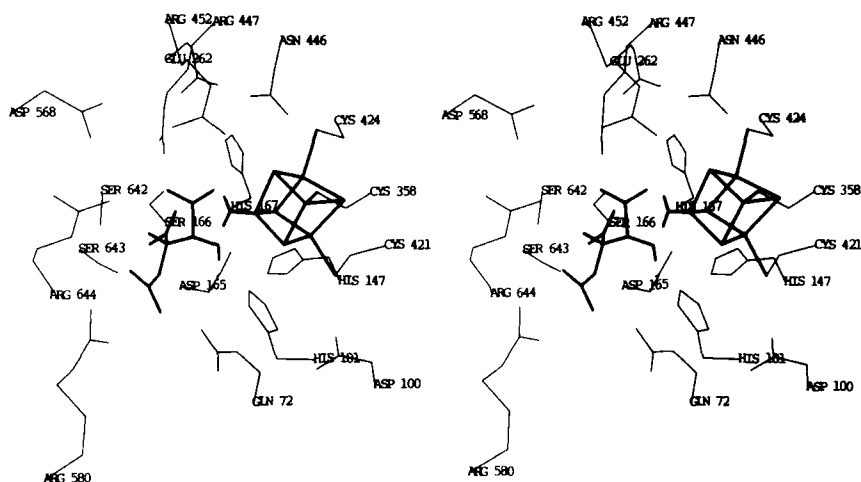


FIG. 4. Stereo view of the active site region in porcine mitochondrial aconitase. The α -carbon atoms and side chains of 19 adjacent residues are shown. The substrate isocitrate is shown in heavy lines along with the [4Fe-4S] cluster and bound H_2O with hydrogens included. (Reproduced with permission from Ref. 37. Copyright 1991, American Chemical Society.)

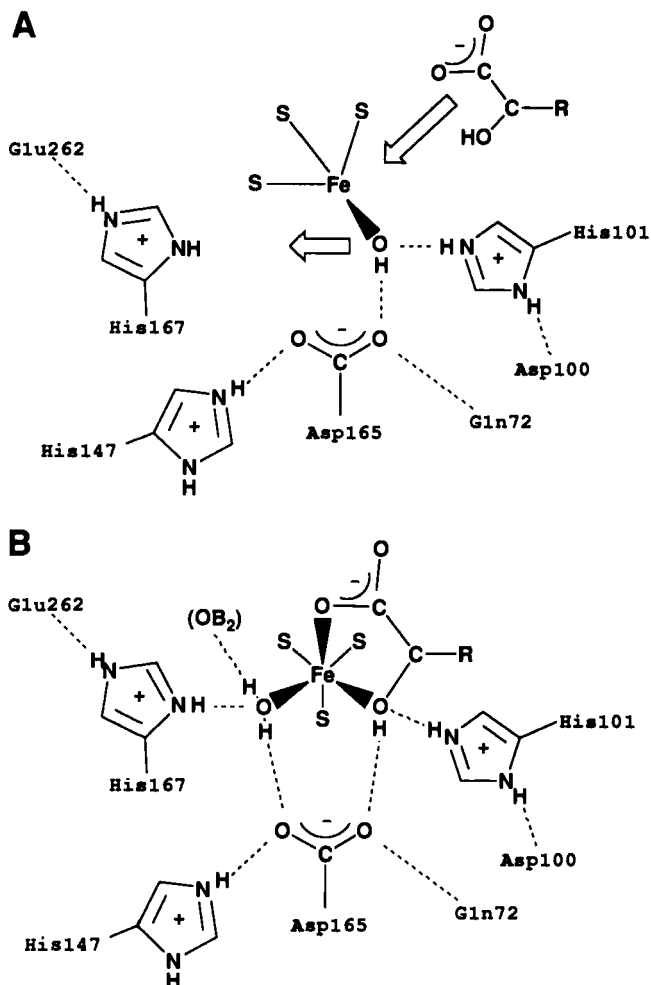


FIG. 5. Schematic representation of the transition from substrate-free aconitase (a) to the substrate-bound form (b). The proton derived from Ser 642 to form an alkoxide is formally equivalent to the proton added to Fe—OH to make Fe—OH₂. The contact of Fe—OH₂ to the β -carboxyl of substrate is shown separately for clarity. All three histidines are assumed to be protonated. (Reproduced with permission from Ref. 37. Copyright 1991, American Chemical Society.)

its coordination sphere from four to six and Fe—hydroxyl becomes Fe—water as observed by ENDOR (30). Further proton transfer involving His 101 is expected to be necessary for cleavage of the C—OH bond in the reaction isocitrate \rightarrow *cis*-aconitate, as illustrated in Fig. 6.

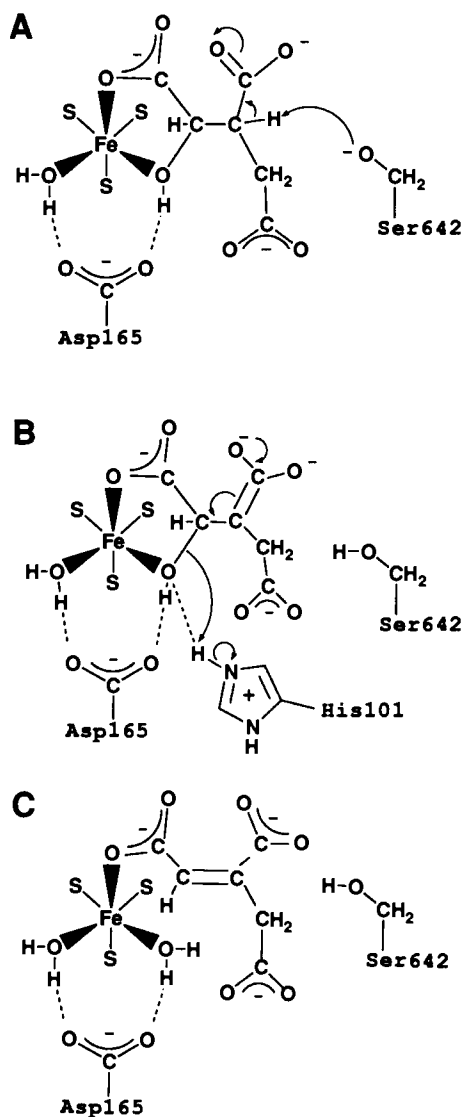


FIG. 6. Schematic representation of the reaction isocitrate \rightarrow *cis*-aconitate assuming deprotonation of Ser 642 when substrate binds and Fe—OH₂ is formed. Formation of an aci-acid intermediate (A) and collapse of this intermediate (B) forms the product (C). Electron density could also flow from the β -C—H bond to the α -C=C- β double bond, i.e., directly from step A to step C with concomitant cleavage of the α -C—OH bond. (Reproduced with permission from Ref. 37. Copyright 1991, American Chemical Society.)

Displacement of *cis*-aconitate by another *cis*-aconitate molecule binding to Fe_a via its β -carboxyl (rather than α -carboxyl) (8) and reversal of the steps in Fig. 6 would form citrate.

V. Studies on Mutants

With details of the X-ray structure known, and with the availability of the cDNA sequence for pig heart aconitase (34), it became possible to study the enzyme by site-directed mutagenesis. Of the 18 active site residues identified by X-ray crystallography, 9 have been individually changed to other amino acids (38). The mutations were designed to have a minimum effect on protein structure, and the codons most frequently used by *E. coli* were chosen to achieve high expression. The mutant proteins thus produced have been studied kinetically, examined by EPR, and tested for their ability to form tight complexes with substrate. Native enzyme, when incubated with radiolabeled substrate and rapidly desalted on a gel column anaerobically by centrifugation, will retain bound substrate. Since all the mutants exhibited essentially normal EPR spectra for both the [3Fe-4S]⁺, $g = 2.02$, and for the [4Fe-4S]⁺ substrate-free forms, only those changes observed upon addition of substrate to the latter will be discussed. The results of these studies are summarized in Table II.

TABLE II
SUMMARY OF EPR, TIGHT-BINDING, AND KINETIC MEASUREMENTS ON
ACONITASE MUTANTS

Mutant	Substrate EPR signal ^a	Tight binding ^b	Relative K_m (isocitrate) ^c	Relative V_{max} isocitrate \rightarrow aconitate ^c
Beef heart	+	+	1.0	1.0
His 101-Asn	-	-	3-4	1.3×10^{-3}
Asp 165-Ser	-	+	3-4	3×10^{-5}
Arg 452-Gln	\pm	-	~ 1	2.1×10^{-3}
Arg 580-Lys	-	-	≥ 30	1.2×10^{-3}
Ser 642-Ala	+	+	2-3	2.6×10^{-5}
Ser 642-Thr	-	\pm	1-2	1.7×10^{-4}

^a (+), Refers to a shift of g values from 2.06, 1.93, and 1.86 to 2.04, 1.85, and 1.78 upon addition of substrate.

^b (+), Indicates tight binding as described in text.

^c Ratio of values measured on mutant versus native enzyme under identical conditions. (Adapted from Ref. 38.)

Of particular interest are the mutants for Ser 642. Before the crystal structure of the enzyme with bound substrate was solved, this residue was not considered a likely candidate for being the base involved in the proton abstraction from substrate. However, analysis of both the Ser 642-Ala and Ser 642-Thr enzymes substantiates the conclusion that this is indeed its function (Figs. 4 and 6). Activity for both of these mutants drops four to five orders of magnitude, depending on substrate. Although according to Bordo and Argos (39) both of these substitutions could be considered "safe," there are obvious differences in the EPR and binding properties for these proteins. For the Ser 642-Thr mutant it appears that the added methyl group perturbs the active site such that tight binding and interaction of substrate with cluster, as determined by EPR, are substantially lower than for the alanine mutant.

Another key residue implicated in the catalytic mechanism is Asp 165. Analysis of the X-ray model of enzyme with bound substrate shows that the carboxylate of this amino acid can form hydrogen bonds to both the hydroxyl of substrate as well as to the H_2O ligated to Fe_a (Figs. 5 and 6). Thus this group appears to be essential for the proper orientation of substrate to Fe_a . Analysis of the aspartate-to-serine mutant at this position supports this conclusion. The activity of this enzyme decreases similarly to that of the Ser 642 mutants, and all interactions of substrate with cluster as detected by EPR are abolished. The enzyme, however, still exhibits tight binding.

Arg 580 has been identified as a key binding residue for the γ -carboxyl of substrate (Fig. 4). In keeping with the results deduced from the X-ray structure are results of the examination of the Arg 580-Lys protein. This mutant has a K_m for isocitrate ≥ 30 -times that of the wild type and has lost the ability to bind substrate tightly (Table II). The EPR spectrum in the presence of substrate is identical to that of the substrate free form. The increase in K_m may account for the 1000-fold loss of activity for this mutation. The kinetic data also show that the citrate \rightarrow aconitate and citrate \rightarrow isocitrate reactions were decreased 10-fold and 100-fold, respectively, when compared to the isocitrate \rightarrow aconitate reaction. This may suggest that citrate is bound less tightly than isocitrate. Another interesting feature of this mutant is that, in contrast to the native enzyme, it is inhibited by the threo- L_8 isomer of isocitrate. Beef or pig heart enzyme give identical activities when assayed with either threo- D_8 -isocitrate, the native substrate, or the racemic mixture threo- D_8L_8 -isocitrate (40). The ratio of the rate of the D_8 isomer to the racemic D_8L_8 mixture for the Arg 580-Lys enzyme is 2.2. This phenomenon was observed for only two other mutations,

His 147-Asn and Arg 447-Lys, for which the above ratio for the velocities was 13 and 2.7, respectively. Alteration of the active site caused by these mutations obviously allows for the binding of, and subsequent inhibition by, the L_s isomer. The reason for this, particularly in regard to the His 147-Asn mutant, which has over 30% of the activity of the wild type, is unclear at this time.

The only mutant thus far to give an abnormal EPR signal, i.e., a signal not observed with the native enzyme, is Arg 452-Gln in the presence of substrate. Arg 452 is in contact with the α -carboxyl of isocitrate bound to Fe_a (Fig. 4). The K_d for substrate binding to beef heart enzyme as measured by EPR is $1 \mu M$ (19) whereas the new signal was barely discernible at a substrate:enzyme ratio of 10:1. At a ratio of 80:1, this new signal, $g = 2.02, 1.91$, and 1.76 , accounted for only 50% of the total. Although tight binding was lost for this mutant, the K_m for isocitrate was essentially normal. The 1000-fold decrease in activity and the abnormal interaction of substrate with the cluster demonstrated by EPR imply that Arg 452 is critical for the proper orientation of the carboxyl bound to Fe_a .

As mentioned previously, His 101 most likely plays a critical role in the loss of substrate hydroxyl by its ability to protonate this group (Figs. 5 and 6B). His 101 is itself within hydrogen bonding distance of Asp 100, thus forming an ion pair with this group (Figs. 4 and 5). The mutant enzymes His 101-Asn and Asp 100-Ser both show a 100-fold decrease in activity and slight increases in their K_m values with isocitrate. They differ, however, in that His 101-Asn shows neither tight binding of substrate nor an EPR signal indicative of substrate bound to the cluster. The opposite is true for Asp 100-Ser. These effects again illustrate the importance of those residues in close proximity to the cluster for properly orienting the substrate with respect to Fe_a and for allowing the necessary interactions to occur for the reaction to proceed at a normal rate. It is interesting to note that all the mutations made thus far, of residues identified as being part of the active site, have significantly altered the catalytic properties of the enzyme.

Although the above discussion has focused on the effects of changes within the protein structure, one should not forget the essential role of the cluster in the function of aconitase. The loss of Fe_a results in an enzyme with 0.3% activity, and to date no other metal replacement has been found that will restore full activity (41). However, substitution of Se^{2-} for S^{2-} results in a viable enzyme that not only has activity comparable to the sulfur enzyme but in fact has 1.5 and 2.0 times more activity for the aconitate \rightarrow isocitrate and reverse reactions, respectively (18).

VI. Relationship of Cytoplasmic Aconitase to Iron-Responsive Element Binding Protein

Recent developments in the field of iron regulation in cells has focused attention on the cytoplasmic form of aconitase. Although its occurrence has been known for some time, this form of the enzyme has been less well characterized than its mitochondrial counterpart (42). The functional significance for its presence in the cytoplasm has never been clearly established. It now appears that cytoplasmic aconitase may be one and the same as the iron-responsive element binding protein (IRE-BP) (43, 44), which is expressed ubiquitously in various tissues and species (45).

IREs are stem-loop structures (46) with a well-defined nucleotide sequence; they were first identified in the mRNAs of ferritin (47, 48) and transferrin receptor (49). In iron-starved cells, a protein of approximate M_r 90,000 binds to these regulatory elements, and thus affects translation or stability of the mRNA. A computer search was carried out for sequences similar to the sequence for the human liver IRE-BP as determined from its cDNA. This search revealed that there is remarkable homology of this protein with pig heart mitochondrial aconitase (50, 51) and yeast isopropyl malate isomerase (51). Of the 18 residues identified in the active site of aconitase, all are conserved in the IRE-BP.

Interestingly, IREs have also been found in the mRNA of murine and human δ -aminolevulinic acid synthase (52, 53), an enzyme of the heme biosynthetic pathway, and surprisingly in the mRNA of mitochondrial aconitase from pig heart (53). Using a partially purified (40%) preparation of beef liver cytoplasmic aconitase, Zheng *et al.* were able to show the binding of this protein to the IRE of mitochondrial aconitase (44). This adds to the evidence that cytoplasmic aconitase and IRE-BP are identical (43). It also raises the interesting possibility that the synthesis of mitochondrial aconitase is itself regulated by its cytoplasmic counterpart! This new development will undoubtedly attract a whole new audience of researchers, previously working outside the area, to the field of iron-sulfur proteins.

ACKNOWLEDGMENTS

The authors gratefully acknowledge the advice and support of Helmut Beinert in the writing of this article, as well as his contributions to the field in general.

REFERENCES

1. Glusker, J. P., in "The Enzymes" (P. D. Boyer, ed.), Vol. 5, pp. 413-439. Academic Press, New York, 1971.
2. Kennedy, C., Rauner, R., and Gawron, O., *Biochem. Biophys. Res. Commun.* **47**, 740 (1972).
3. Emptage, M. H., Kent, T. A., Huynh, B. H., Rawlings, J., Orme-Johnson, W. H., and Münck, E., *J. Biol. Chem.* **255**, 1793 (1980).
4. Kent, T. A., Dreyer, J.-L., Emptage, M. H., Moura, I., Moura, J. J. G., Huynh, B. H., Xavier, A. V., LeGall, J., Beinert, H., Orme-Johnson, W. H., and Münck, E., in "Electron Transport and Oxygen Utilization" (C. Ho, ed.), pp. 371-374. Elsevier, New York, 1982.
5. Kent, T. A., Dreyer, J.-L., Kennedy, M. C., Huynh, B. H., Emptage, M. H., Beinert, H., and Münck, E., *Proc. Natl. Acad. Sci. U.S.A.* **79**, 1096 (1982).
6. Kennedy, M. C., Emptage, M. H., Dreyer, J.-L., and Beinert, H., *J. Biol. Chem.* **258**, 11,098 (1983).
7. Beinert, H., and Kennedy, M. C., *Eur. J. Biochem.* **186**, 5 (1989).
8. Emptage, M. H., in "Metal Clusters in Proteins" (L. Que, Jr., ed.), ACS Symp. Series 372, pp. 343-371. Am. Chem. Soc., Washington, D.C., 1988.
9. Beinert, H., and Thomson, A. J., *Arch. Biochem. Biophys.* **222**, 333 (1983).
10. Papaefthymiou, V., Girerd, J.-J., Moura, I., Moura, J. J. G., and Münck, E., *J. Am. Chem. Soc.* **109**, 4703 (1987).
11. Noodleman, L., and Baerends, E. J., *J. Am. Chem. Soc.* **106**, 2316 (1984).
12. Münck, E., and Kent, T. A., *Hyperfine Interactions* **27**, 161 (1986).
13. Noodleman, L., and Case, D. A., this volume.
14. Hendrich, M. P., and Debrunner, P. G., *Biophys. J.* **56**, 489 (1989).
15. Beinert, H., Emptage, M. H., Dreyer, J.-L., Scott, R. A., Hahn, J. E., Hodgson, K. O., and Thomson, A. J., *Proc. Natl. Acad. Sci. U.S.A.* **80**, 393 (1983).
16. Kennedy, M. C., and Beinert, H., *J. Biol. Chem.* **263**, 8194 (1988).
17. Kennedy, M. C., Emptage, M. H., and Beinert, H., *J. Biol. Chem.* **259**, 3145 (1984).
18. Surerus, K. K., Kennedy, M. C., Beinert, H., and Münck, E., *Proc. Natl. Acad. Sci. U.S.A.* **86**, 9846 (1989).
19. Emptage, M. H., Dreyer, J.-L., Kennedy, M. C., and Beinert, H., *J. Biol. Chem.* **258**, 11,106 (1983).
20. Emptage, M. H., Kent, T. A., Kennedy, M. C., Beinert, H., and Münck, E., *Proc. Natl. Acad. Sci. U.S.A.* **80**, 4674 (1983).
21. Kent, T. A., Emptage, M. H., Merkle, H., Kennedy, M. C., Beinert, H., and Münck, E., *J. Biol. Chem.* **260**, 6871 (1985).
22. Cammack, R., Dickson, D. P. E., and Johnson, C. E., in "Iron Sulfur Proteins" (W. Lovenberg, ed.), Vol. III, pp. 283-330. Academic Press, New York, 1977.
23. Werst, M. M., Kennedy, M. C., Houseman, A. L. P., Beinert, H., and Hoffman, B. M., *Biochemistry* **29**, 10,533 (1990).
24. Middleton, P., Dickson, D. P. E., Johnson, C. E., and Rush, J. D., *Eur. J. Biochem.* **88**, 135 (1978).
25. Kennedy, M. C., Kent, T. A., Emptage, M. H., Merkle, H., Beinert, H., and Münck, E., *J. Biol. Chem.* **259**, 14,463 (1984).
26. Plank, D. W., Kennedy, M. C., Beinert, H., and Howard, J. B., *J. Biol. Chem.* **264**, 20,385 (1989).
27. Hagen, K. S., Watson, A. D., and Holm, R. H., *J. Am. Chem. Soc.* **105**, 3965 (1983).
28. Telser, J., Emptage, M. H., Merkle, H., Kennedy, M. C., Beinert, H., and Hoffman, B. M., *J. Biol. Chem.* **261**, 4840 (1986).

29. Kennedy, M. C., Werst, M., Telser, J., Emptage, M. H., Beinert, H., and Hoffman, B. M., *Proc. Natl. Acad. Sci. U.S.A.* **84**, 8854 (1987).
30. Werst, M. M., Kennedy, M. C., Beinert, H., and Hoffman, B. M. *Biochemistry* **29**, 10,526 (1990).
31. Rose, I. A., and O'Connell, E. L., *J. Biol. Chem.* **242**, 1870 (1967).
32. Gawron, O., Glaid III, A. J., and Fondy, T. P., *J. Am. Chem. Soc.* **80**, 5856 (1958).
33. Robbins, A. H., and Stout, C. D., *Proteins* **5**, 289 (1989).
34. Zheng, L., Andrews, P. C., Hermodson, M. A., Dixon, J. E., and Zalkin, H., *J. Biol. Chem.* **265**, 2814 (1990).
35. Plank, D. W., and Howard, J. B., *J. Biol. Chem.* **263**, 8184 (1988).
36. Robbins, A. H., and Stout, C. D., *Proc. Natl. Acad. Sci. U.S.A.* **86**, 3639 (1989).
37. Lauble, H., Kennedy, M. C., Beinert, H., and Stout, C. D., *Biochemistry* (in press).
38. Zheng, L., Kennedy, M. C., Beinert, H., and Zalkin, H., *J. Biol. Chem.* (in press).
39. Bordo, D., and Argos, P., *J. Mol. Biol.* **217**, 721 (1991).
40. Thomson, J. F., Nance, S. L., Bush, K. J., and Szczepanik, P. A., *Arch. Biochem. Biophys.* **117**, 65 (1966).
41. Villafranca, J. J., and Mildvan, A. S., *J. Biol. Chem.* **246**, 5791 (1971).
42. Dickman, S. R., and Speyer, J. F., *J. Biol. Chem.* **206**, 62 (1954).
43. Kaptain, S., Downey, W. E., Tang, C., Philpott, C., Haile, D., Orloff, D. G., Harford, J. B., Rouault, T. A., and Klausner, R. D., *Proc. Natl. Acad. Sci. U.S.A.* **88**, 10109 (1991).
44. Zheng, L., Kennedy, M. C., Blondin, G. A., Beinert, H., and Zalkin, H., *Mol. Cell. Biol.* (submitted).
45. Neupert, B., Müllner, E. W., Rothenberger, S., Seiser, C., Thompson, N. A., Emery-Goodman, A., and Kühn, L., *J. Inorg. Chem.* **43**, 504 (1991).
46. Leibold, E. A., and Guo, B., *Annu. Rev. Nutr.* **12**, 325 (1992).
47. Hentze, M. W., Rouault, T. A., Caughman, S. W., Dancis, A., Harford, J. B., and Klausner, R. D., *Proc. Natl. Acad. Sci. U.S.A.* **84**, 6730 (1987).
48. Aziz, N., and Munro, H. N., *Proc. Natl. Acad. Sci. U.S.A.* **84**, 8478 (1987).
49. Casey, J. L., Hentze, M. W., Koeller, D. M., Caughman, S. W., Rouault, T. A., Klausner, R. D., and Harford, J. B., *Science* **240**, 924 (1988).
50. Rouault, T. A., Stout, C. D., Kaptain, S., Harford, J. B., and Klausner, R. D., *Cell* **64**, 881 (1991).
51. Hentze, M. W., and Argos, P., *Nucl. Acids Res.* **19**, 1739 (1991).
52. Cox, T. C., Bawden, M. J., Martin, A., and May, B. K., *EMBO J.* **10**, 1891 (1991).
53. Dandekar, T., Stripecke, R., Gray, N. K., Goossen, B., Constable, A., Johansson, H. E., and Hentze, M. W., *EMBO J.* **10**, 1903 (1991).

NOVEL IRON-SULFUR CENTERS IN METALLOENZYMES AND REDOX PROTEINS FROM EXTREMELY THERMOPHILIC BACTERIA

MICHAEL W. W. ADAMS

Department of Biochemistry and Center for Metalloenzyme Studies, University of Georgia,
Athens, Georgia 30602

- I. Introduction
- II. Extremely Thermophilic Bacteria
- III. *Pyrococcus furiosus*
 - A. Hydrogenase (Ni-Fe-S)
 - B. Ferredoxin (Fe-S)
 - C. Rubredoxin (Fe)
 - D. Aldehyde Ferredoxin Oxidoreductase (W-Fe-S)
 - E. Role of Fe-S Proteins in H₂ Production
- IV. *Thermotoga maritima*
 - A. Hydrogenase (Fe-S)
 - B. Role of Tungsten
- V. Summary
- References

I. Introduction

The aim of this article is to summarize the properties of a variety of Fe-S-containing proteins that have been purified from extremely thermophilic bacteria. Extreme thermophiles are defined as organisms that grow optimally at temperatures of 80°C and above. They are a relatively recent discovery in the microbial world. At the time we began this research in 1988, no metalloenzyme had been isolated from these bacteria. Since most of the extreme thermophiles metabolize molecular hydrogen (H₂), our initial objective was to characterize their hydrogenases, the enzymes responsible for catalyzing H₂ oxidation and H₂ production. Hydrogenases have been purified from several mesophilic organisms. All are thermolabile proteins containing Fe-S or Ni-Fe-S

centers. It was therefore of considerable interest to investigate the properties of enzymes capable of activating H_2 at temperatures near and above $100^\circ C$. Our initial research also led to the discovery that the growth of several extremely thermophilic bacteria is dependent upon tungsten (W), an element seldom used in biological systems. A new W-Fe-S-containing enzyme was subsequently purified, and its properties and proposed physiological role will also be described. The extreme thermophiles have also proved to be a rich source of more conventional Fe-S proteins, such as ferredoxin and rubredoxin. The properties of their Fe-S centers will also be discussed, both to emphasize their uniqueness and to demonstrate how they appear to be adapted to catalyze reactions and/or transfer electrons at temperatures near $100^\circ C$. As will become evident, extremely thermophilic Fe-S-containing proteins have distinct advantages over their mesophilic cousins. I begin with a brief description of the extremely thermophilic bacteria known at the present time.

II. Extremely Thermophilic Bacteria

As illustrated in Fig. 1 (1-5), that bacteria are able to grow optimally above $80^\circ C$ is a recently discovered phenomenon. In 1982, Stetter (6)

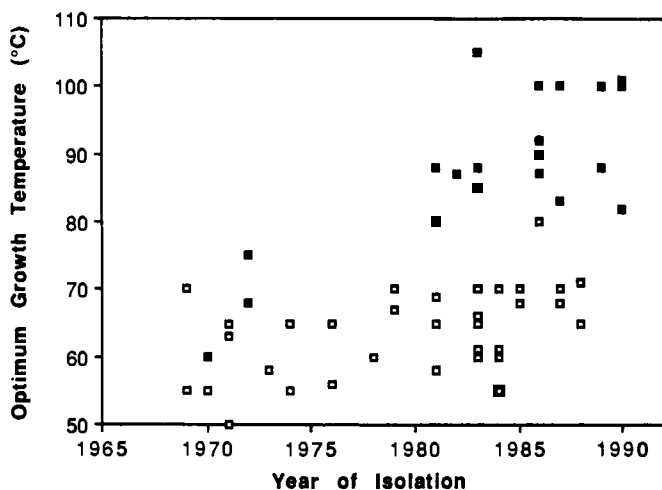


FIG. 1. The isolation of "thermophilic" bacteria over the last 20 years. Open symbols denote eubacteria in general; closed symbols are archaeobacteria. Data taken from Refs. 1-5.

first isolated a bacterium from shallow marine volcanic vents, his isolates grew at temperatures above 100°C. Since then, and due largely to the pioneering work of Stetter, almost 20 genera of bacteria able to grow near and above the normal boiling point of water have been isolated (2–4). All but one of these extremely thermophilic organisms are classified as archaeobacteria; these are in contrast to the numerous thermophilic eubacteria that have been isolated over the years, most of which have growth temperature optima (T_{opt}) below 70°C (5). The one exception is the novel eubacterial genus, *Thermotoga* (7), which, in addition to being the most thermophilic, is also the most ancient eubacterium currently known (7, 8). Recent phylogenetic analyses (9) have also indicated that the extremely thermophilic archaeobacteria and the eukaryotes have a common ancestor, suggesting that extremely thermophilic organisms are the remnant of some form of universal ancestor to all extant life, having evolved when the earth was much hotter than it is at present (8). Phylogenetic implications of the metal dependence of bacterial growth will be considered in Section IV,B.

The majority of the extremely thermophilic organisms depicted in Fig. 1 have been found in geothermally heated marine environments, in both shallow (several meters below sea level) and deep water (several kilometers below sea level). Most of the extremely thermophilic archaeobacteria are termed sulfur-dependent organisms, since, to a greater or lesser extent, they obtain energy for growth by the reduction or oxidation of elemental sulfur (S^0). Most grow anaerobically and reduce S^0 to H_2S , i.e., S^0 respiration, using either organic substrates or H_2 as the electron donor. They include the genera *Thermoproteus* (10), *Staphylothermus* (11), *Desulfurococcus* (12), *Thermofilum* (13), *Pyrobaculum* (14), *Acidianus* (15), *Desulfurolobus* (16), *Pyrodictium* (17, 18), *Thermoplasma* (1), *Pyrococcus* (19, 20), *Thermococcus* (21, 22), *Hyperthermus* (23), and the as-yet unclassified “ES-1” (24) and “ES-4” (25). Only species of *Desulfurolobus* and *Acidianus* are able to grow aerobically, and they do so by oxidizing S^0 to sulfuric acid. The remaining extremely thermophilic archaeobacteria are strict anaerobes, and they comprise three methanogenic genera, *Methanopyrus* (26), *Methanococcus* (27), and *Methanothermus* (28, 29), and a unique sulfate-reducing genus, *Archaeoglobus* (30). Species of the genera *Pyrococcus*, *Pyrobaculum*, *Pyrodictium*, *Hyperthermus*, and *Methanopyrus*, together with ES-4, grow optimally at or above 100°C, and the term “hyperthermophile” is usually used to refer to such organisms.

The dependence upon S^0 for optimal growth of most of the S^0 -dependent, extremely thermophilic anaerobes means that they cannot be readily grown in large-scale stainless-steel fermentors because of the

corrosive nature of the H_2S that is generated. This problem is exacerbated by the high salt requirement of many of these marine organisms. However, some species are able to grow by fermentation: they are not obligately dependent upon S^0 respiration. They include the archaeobacterium, *Pyrococcus furiosus*, and the extremely thermophilic eubacterium, *Thermotoga maritima*. Since these organisms also produce H_2 during growth, they were the obvious candidates with which to attempt the purification and characterization of metalloenzymes involved in H_2 metabolism. We now routinely grow each of these bacteria in 400-liter cultures and obtain cell yields of more than 600 g (wet weight) (31, 32). Purification procedures are routinely carried out using at least 1 kg of cells, which gives sufficient quantities of the Fe-S-containing enzymes and proteins described below for various biochemical and spectroscopic analyses. All procedures are also performed under strictly anaerobic conditions and the procedures have been optimized to obtain all of the Fe-S proteins of one organism from the same batch of cells. The O_2 sensitivity (half-life in air) of the enzymes that have been purified varies from a few seconds for the hydrogenase of *T. maritima* to several hours for *P. furiosus* hydrogenase. The following descriptions of the various Fe-S proteins are organized based on their source. This permits a summary of their proposed physiological roles in *P. furiosus*, and how this differs in *T. maritima*.

III. *Pyrococcus furiosus*

Pyrococcus furiosus was isolated from a shallow marine volcanic vent by Fiala and Stetter in 1986 (19). It is a strictly anaerobic heterotroph that grows up to 105°C by the fermentation of carbohydrates such as starch and maltose to organic acids, CO_2 , and H_2 . The doubling time at its optimal growth temperature, 100°C , is around 40 min. As with most fermentative organisms, the H_2 produced inhibits growth, but this can be relieved either by sparging cultures with an inert gas to remove the H_2 , or by adding S^0 , which is reduced to H_2S . The latter reaction does not appear to conserve energy. Our initial studies with *P. furiosus* (31) showed that cell yields could be increased almost 10-fold by the presence of tungstate ($10\ \mu\text{M}$) and of additional Fe in the growth medium. The role of W is discussed in Section III,D. The growth of *P. furiosus* was unaffected by the addition of salts of V, Cs, F, Pb, Rb, or Si, or by increased amounts ($>10\ \mu\text{M}$) of Ni, Mo, Se, Co, or Mn.

A. HYDROGENASE (Ni-Fe-S)

Pyrococcus furiosus hydrogenase, the enzyme responsible for catalyzing the production of H_2 during the fermentative growth of this organism, is located in the cytoplasm and is routinely purified from cells grown in the absence of S^0 (31). It has a M_r value of around 185,000 and comprises three dissimilar subunits. It is one of the most thermostable enzymes known at present, having a half-life at 80°C of about 24 hr and an optimal temperature for catalysis above 95°C. This hydrogenase contains approximately 1 Ni, 30 Fe, and 24 acid-labile sulfide (S^{2-}) atoms/mole. Other metals, including W (and also Se), are not detected. The *P. furiosus* enzyme is different from the hydrogenases found in mesophilic bacteria that grow by fermentation and produce H_2 , e.g., *Clostridium pasteurianum*, as these organisms contain a hydrogenase that lacks Ni (see Section IV,A). Ni-Fe hydrogenases are typically found in H_2 -oxidizing bacteria, in which they are usually membrane bound and associated with an electron transport system that serves to couple H_2 oxidation with the reduction of a substrate, e.g., O_2 . Most of the mesophilic Ni-Fe enzymes contain only two subunits ($\alpha\beta$) and immunological and DNA sequence analyses show extensive similarities between the enzymes from different bacterial genera (33–35). Some soluble Ni-Fe hydrogenases are known, and these usually have additional subunits that appear to function in the reduction of endogenous electron carriers, such as F_{420} in the methanogenic bacteria and NAD in the aerobic H_2 -oxidizing bacteria (36, 37). The *P. furiosus* enzyme is similar in this respect, as it appears to contain an additional subunit that interacts with its physiological electron donor, which is a ferredoxin (see Section III,B). *Pyrococcus furiosus* hydrogenase does not use NAD(P)H as an electron carrier (31).

Mesophilic Ni-Fe hydrogenases are usually referred to as "uptake" hydrogenases, as their physiological role is H_2 oxidation and they catalyze only low rates of H_2 evolution in the standard *in vitro* assay system using dithionite-reduced methyl viologen as the electron donor. In contrast, mesophilic Fe hydrogenases are much more active enzymes, often by orders of magnitude. It was therefore surprising to find that the *in vitro* H_2 evolution activity of the *P. furiosus* enzyme ($V_m = 2900 \mu\text{mol evolved/min/mg}$ or units/mg, at 80°C; Ref. 31) was comparable to that obtained with Fe hydrogenases, e.g., $V_m = 5500 \text{ units/mg}$ at 30°C for *C. pasteurianum* hydrogenase I (38), rather than the Ni-Fe enzymes (V_m values typically $< 100 \text{ units/mg}$ at 30°C; Refs. 33 and 39). In addition, all mesophilic hydrogenases (both Fe and Ni-Fe) preferentially catalyze H_2 oxidation when one compares the catalytic rates

of H_2 production with those obtained in H_2 oxidation assays using methylene blue or benzyl viologen as electron acceptors. The activity ratios (H_2 evolution/ H_2 oxidation) are less than unity and typically 0.2–0.3 (see Ref. 4). In contrast, the activity ratio for *P. furiosus* hydrogenase is approximately 4.0 between 45 and 80°C, and at 80°C remains more or less unchanged over the pH range 5–10. Moreover, above 80°C the activity ratio dramatically increases to around 12 at 95°C (4, 31). This change in catalytic activity at 80°C coincides with a transition point at 80°C in Arrhenius plots of enzyme activity, independent of the mode of assay. The *P. furiosus* enzyme therefore appears to be a new type of “evolution” hydrogenase. It is also well suited to its metabolic role, as it preferentially catalyzes H_2 evolution, the physiological reaction, at all temperatures, but especially above 80°C, at the growth temperature of *P. furiosus*.

Pyrococcus furiosus hydrogenase is purified anaerobically using buffers containing sodium dithionite (31). The electron paramagnetic resonance (EPR) spectra of the enzyme as isolated in its reduced state are shown in Fig. 2. The spectrum recorded at 70 K represents ~1 spin/mole and is typical of a single, reduced, and magnetically isolated $[2Fe-2S]^{1+}$ cluster. Below 15 K, the spectrum becomes more complex, indicating the presence of at least two interacting $[4Fe-4S]^{1+}$ -type clusters with extremely rapid spin relaxation rates. The complete spectrum seen at 10 K represents approximately 2 spins/mole, suggesting that the 4Fe-type centers are not completely reduced under these conditions. There is no significant EPR absorption at lower magnetic fields (<3.0 T) so the reduced protein appears to contain only $S = \frac{1}{2}$ centers. These analyses therefore indicate that reduced *P. furiosus* hydrogenase contains one $[2Fe-2S]^{1+}$ cluster and at least one $[4Fe-4S]^{1+}$ cluster. All mesophilic Ni-Fe hydrogenases that have been examined to date contain at least two $[4Fe-4S]^{1+}$ centers (33, 39, 40–42), but 2Fe clusters have been detected only in the hydrogenases of some aerobic H_2 -oxidizing bacteria, such as *Nocardia opaca* (43).

Pyrococcus furiosus hydrogenase is EPR silent upon anaerobic oxidation with thionine ($E_m = +11$ mV; Refs. 4 and 31). Thus, the majority of the Fe in this enzyme is not detected by EPR, as the 2Fe- and 4Fe-type centers account for at most 10 of its 30 Fe atoms. To investigate the possibility that the enzyme contained some unusual Fe-S center that was paramagnetic only at intermediate potentials, redox titrations were carried out using samples poised between –500 and +100 mV (at pH 8.0 and 20°C). However, no additional EPR signals were observed. The E_m value of the 2Fe cluster is estimated at –410 mV, whereas that of the 4Fe cluster(s) is –210 mV (Fig. 3), which is unusu-

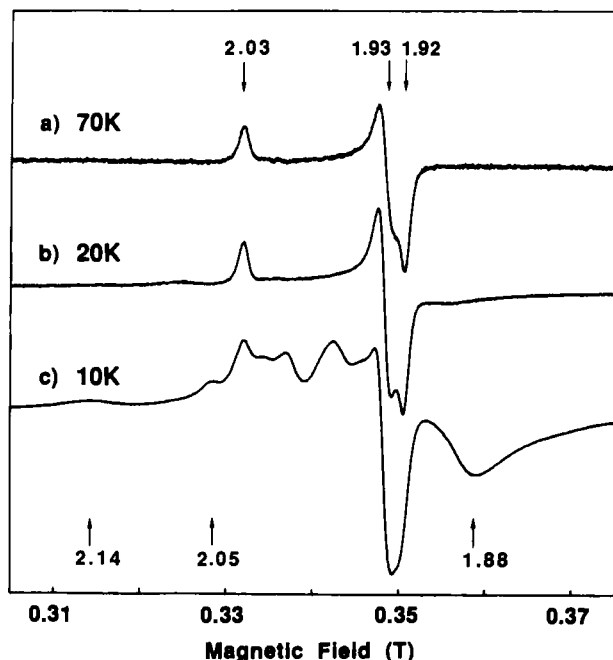


FIG. 2. EPR spectra of reduced *P. furiosus* hydrogenase. The hydrogenase (7.5 mg/ml) was under H_2 (1 atm) in 50 mM Tris/HCl buffer, pH 8.0, containing 1 mM sodium dithionite. The spectrometer microwave and power settings were (a and b) 2 mW and 5×10^5 ; (c) 50 mW and 4×10^4 . The spectra were recorded at the indicated temperatures. Taken from Ref. 31.

ally high for a ferredoxin-type center. These data also show that the 4Fe cluster(s) is completely reduced in the fully reduced protein: the intensity of the EPR signal remains constant between -300 and -500 mV (Fig. 3). The low-spin quantitation from the fully reduced enzyme is therefore not due to incomplete reduction of the 4Fe cluster(s).

Mesophilic Ni-Fe hydrogenases are purified aerobically and in this oxidized state they exhibit a characteristic EPR signal from the Ni center. Known as the Ni-A signal, this has g values of approximately 2.31, 2.23, and 2.02, and probably arises from a Ni(III) species (33, 39, 40, 44). This state is usually unable to catalyze H_2 oxidation without some form of reductive activation. The Ni-A EPR signal is lost during this process, and a transient EPR signal, termed Ni-C, is observed ($g = 2.19, 2.16$, and 2.02). The Ni-C signal is thought to arise from either a Ni(I) or Ni(III) species that has an E_m value of approximately

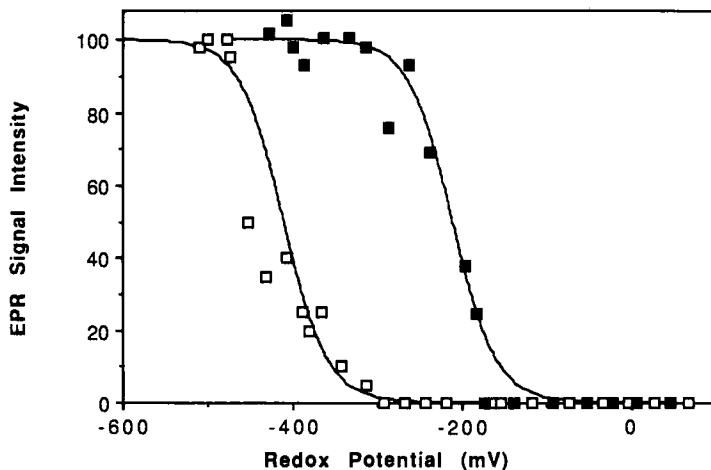


FIG. 3. Determination of the midpoint potentials of the 2Fe and 4Fe clusters in *P. furiosus* hydrogenase. The redox titration was carried out at 20°C and pH 8.0. The extent of reduction of the 4Fe cluster (closed symbols) and the 2Fe cluster (open symbols) was determined by the amplitudes of the $g = 1.88$ and $g = 2.03$ resonances (see Fig. 2), respectively (J.-B. Park and M. W. W. Adams, unpublished data, 1991).

–300 mV (44–46). In contrast, *P. furiosus* hydrogenase is purified anaerobically in a fully active state and remains active after oxidation with thionine, so it may not be expected to exhibit the Ni-A-type EPR signal. However, the mesophilic hydrogenases exhibit the Ni-C signal in the activated state, and it is therefore puzzling why a similar signal is not seen with the *P. furiosus* enzyme. Since this hydrogenase is virtually inactive at 20°C (see Fig. 4) (47), the temperature at which EPR samples are routinely prepared, it is possible that the Ni center can only be oxidized at higher temperatures. Our preliminary results suggest that this is indeed the case. An EPR signal reminiscent of the Ni-C signal is observed at approximately –300 mV when redox titrations are carried out at 80°C and samples are rapidly frozen for EPR analyses (J.-B. Park and M. W. W. Adams, unpublished data, 1991). The Ni site in this enzyme therefore appears to be inaccessible to redox mediators at ambient temperature, conditions under which its Fe–S centers are redox active. In contrast, a similar series of titrations focusing on the Fe–S clusters in this enzyme showed (1) that additional EPR signals are not apparent from samples prepared at high temperature, and (2) that the apparent E_m values of the 2Fe and 4Fe centers at 70°C are the same (± 20 mV) as those measured from samples prepared

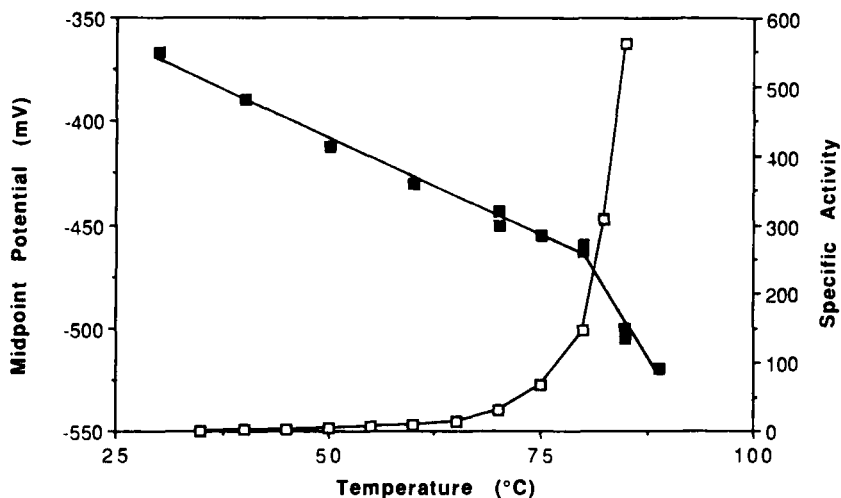


FIG. 4. Effect of temperature on the midpoint potential of *P. furiosus* ferredoxin and on the H_2 evolution activity catalyzed by *P. furiosus* hydrogenase using the ferredoxin as the electron donor. The midpoint potential data (closed symbols) are taken from Ref. 47. The hydrogenase activity (open symbols) is expressed as micromoles H_2 evolved/min/mg of hydrogenase using dithionite-reduced ferredoxin at the indicated temperature. Taken from Ref. 31.

at 20°C (Fig. 3). This is a very surprising result in view of the strong temperature dependence of the E_m values of Fe centers in other extremely thermophilic proteins (see Sections III,C–III,E).

It is therefore possible that the lack of significant catalytic activity of *P. furiosus* hydrogenase at low (ambient) temperature is because the Ni site is not accessible to the substrate (H^+ or H_2). It is assumed that the Fe–S clusters mediate electron transfer between the Ni site and the external electron carrier for the enzyme, so it is also likely that the Ni and Fe–S centers are not free to interact at low temperature, even though the Fe–S centers are accessible to redox mediators. It should be noted that the Ni site in the *P. furiosus* enzyme seems to be very different from that in the mesophilic enzymes. Not only does it preferentially catalyze H_2 evolution, it also has a unique response to the classical inhibitors of the mesophilic hydrogenases. For example, CO is a potent inhibitor of both Fe and Ni–Fe hydrogenases ($K_i \leq 30 \mu M$; Ref. 33) and the Ni–Fe, but not the Fe, enzymes, are also inhibited by acetylene (4, 48). Conversely, nitrite inhibits mesophilic Fe hydrogenases but it has little effect on the Ni–Fe enzymes (Ref. 33; see also Section IV,A). In complete contrast, *P. furiosus* hydrogenase is insensitive to inhibition

by CO, nitrite, and acetylene (4). Since the Ni site appears inaccessible to both redox dyes and H_2/H^+ at 30°C, this might be expected, but the enzyme is also insensitive to all of these inhibitors at 80°C, conditions under which the properties of the Ni site more resemble those of the mesophilic enzymes.

Both the Fe-S and Ni centers in *P. furiosus* hydrogenase therefore have unusual properties when compared to their mesophilic counterparts. Of particular interest are the mechanisms by which the protein stabilizes the Ni site in the reduced state at low temperature (20°) and also maintains the midpoint potentials of the Fe-S centers independent of temperature (20–70°C). As described below, some of the redox proteins that have been isolated from *P. furiosus* promise to give some insight into the nature of the metal centers of the more complex enzymes such as *P. furiosus* hydrogenase.

B. FERREDOXIN (Fe-S)

The physiological electron donor to the hydrogenase of *P. furiosus* hydrogenase is a ferredoxin (49). That is, *P. furiosus* ferredoxin acts as an electron carrier between sodium dithionite and *P. furiosus* hydrogenase in *in vitro* H_2 evolution assays. The hydrogenase has a high affinity for the ferredoxin: the apparent K_m value is 44 μM (49). However, as shown in Fig. 4, significant rates of H_2 production are observed only above 80°C, at the growth temperature of the organism. The ferredoxin also acts as an electron acceptor for the oxidation of pyruvate, glucose, and glyceraldehyde in *P. furiosus*, reactions catalyzed by three different oxidoreductases (see Sections III,D and III,E). Reduced *P. furiosus* ferredoxin also functions as an electron donor *in vitro* for H_2 evolution by the hydrogenase of the mesophile, *C. pasteurianum* (49). Although the apparent K_m value is very low (11 μM), the rate of H_2 evolution (V_m) is only 20% of that supported by *C. pasteurianum* ferredoxin.

Pyrococcus furiosus ferredoxin purified under anaerobic conditions (49) has an apparent molecular weight of ~7500 as determined by sedimentation analysis, which agrees with the value calculated from its amino acid sequence ($M_r = 7148$; J. B. Howard, J.-B. Park, and M. W. W. Adams, unpublished data, 1991). The protein contains a single $[4Fe-4S]^{1+/2+}$ cluster, and its UV-visible absorption spectrum is typical for a ferredoxin with a A_{390}/A_{280} ratio of 0.58 for the air-oxidized form. The molar absorbance coefficient at 390 nm is 15,400 $M^{-1} cm^{-1}$, and this decreases by 55% upon reduction with sodium dithionite. Interestingly, and in contrast to other ferredoxins, the reduction of *P. furio-*

sus ferredoxin by sodium dithionite is a time-dependent process at 23°C (taking ~20 min), although the reaction is immediate at 80°C. It is a remarkably thermostable protein: there are no changes in its spectroscopic properties (UV-visible and EPR) or in its electron carrier activity after a 12-hr incubation at 95°C (49). These data were obtained using the pure ferredoxin (0.5 mg/ml) in aqueous buffered solutions in the absence of any stabilizing agent. For comparison, the most "thermostable" ferredoxins previously reported are rapidly denatured (within minutes) at 85°C (50–52). *Pyrococcus furiosus* ferredoxin is also resistant to denaturants. There was no change in its spectroscopic properties and none of its iron became accessible to chelation after 3 hr at 23°C in the presence of sodium dodecyl sulfate (SDS) (20%, w/v). Similarly, a sample maintained in 6.0 M guanidinium hydrochloride containing 50 mM EDTA for 60 days at 4°C lost none of its iron. Iron is removed from the ferredoxin by prolonged acid treatment, but the apoprotein can be readily reconstituted by Fe^{2+} and S^{2-} to give a protein that was indistinguishable from the native protein in its stability and spectroscopic properties (49). The unusual stability of this protein is therefore an intrinsic property, and the novel spectroscopic properties of its cluster, described below, are not a purification artifact.

Ferredoxins containing [4Fe–4S] clusters have been purified from a wide range of bacteria, and over 30 amino acid sequences have been reported (53–55). Most of these proteins are of the 8Fe type and contain two [4Fe–4S] clusters. They have a consensus sequence of eight cysteinyl residues that binds the two clusters, invariably $-\text{CX}_2\text{CX}_2\text{CX}_3\text{CP}-$, in both halves of the molecule (53). As shown in Fig. 5, each cluster is coordinated by three cysteines of one-half of the molecule and by one cysteine (adjacent to the proline) in the other half. The few 4Fe ferredoxins known usually lack the fourth cysteine in one-half and up to three cysteines in the second half, but all maintain the 3 : 1 cysteine coordination to the cluster between the two halves of the molecule (Fig. 5). Alignment of the sequence of *P. furiosus* ferredoxin, however, shows that the second cysteine in the $-\text{CX}_2\text{CX}_2\text{CX}_3\text{CP}-$ sequence is replaced by aspartate (corresponding to position 14 in the *P. furiosus* protein). The replacement of one coordinating cysteine by an aspartate is found in only four other ferredoxins (Fd), from *Desulfovibrio vulgaris* (56), *Desulfovibrio africanus* (Fd III; Ref. 57), *Thermoplasma acidophilum* (58), and *Sulfolobus acidocaldarius* (59). However, all of these are 8Fe ferredoxins, leaving the *P. furiosus* protein as the only example of a 4Fe ferredoxin with incomplete cysteinyl coordination to its single [4Fe–4S] cluster. The likely ligand to the fourth iron atom of the cluster is discussed below.

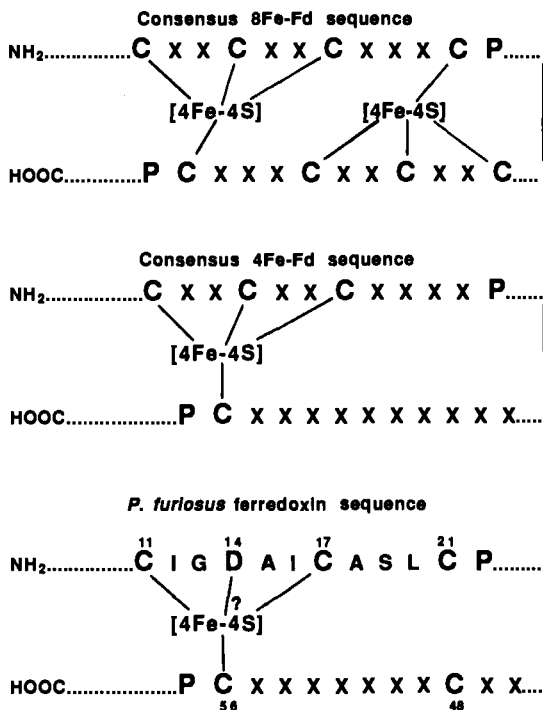


FIG. 5. Diagrammatic representation of the binding of [4Fe-4S] clusters to the consensus sequence of cysteinyl residues found in ferredoxins.

1. Spectroscopic Characterization of the [4Fe-4S] Cluster

a. Electron Paramagnetic Resonance Spectroscopy. Ferredoxins containing a single [4Fe-4S]^{1+/2+} cluster give rise in their reduced states to a characteristic rhombic EPR signal below 30 K with typical g values of 2.08, 1.94, and 1.90 (60). A more complex spectrum arising from spin-interacting clusters is observed from the 8Fe proteins (61). Although reduced *P. furiosus* ferredoxin as prepared under anaerobic conditions exhibited a comparable EPR signal (Fig. 6) (62), the spectrum is much broader ($g = 2.10, 1.87, \text{ and } 1.80$), it undergoes more rapid spin relaxation such that it is not observed above 15 K, and it represents only ~ 0.2 rather than 1 spin/molecule (49, 62). Furthermore, the reduced protein gives rise to additional EPR resonances at low field ($g = 4.96 \text{ and } 5.55$; Fig. 6). The relative intensities of these resonances are strongly temperature dependent and arise from the upper and lower zero-field doublets of an $S = \frac{3}{2}$ ground state as interpre-

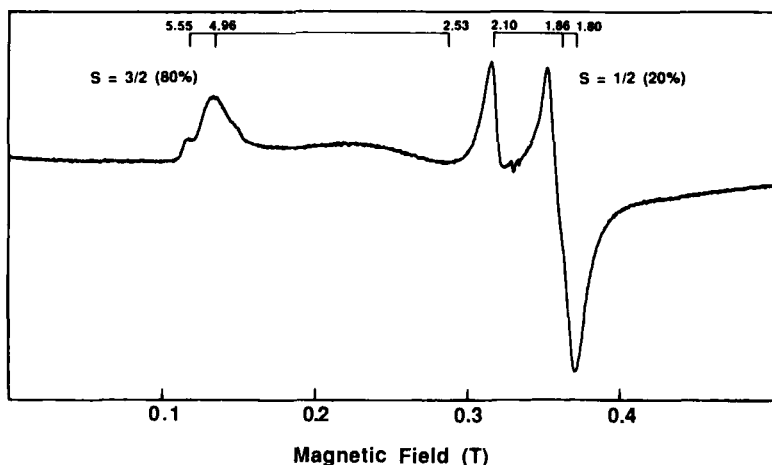


FIG. 6. EPR spectrum of reduced *P. furiosus* ferredoxin. The sample contained the ferredoxin (7 mg/ml) in 50 mM Tris/HCl buffer, pH 8.0, containing 2 mM sodium dithionite. The spectrum was recorded at 7 K using 10-mW microwave power. Modified from Ref. 62.

ted by a conventional spin Hamiltonian ($E/D = 0.22$, $D = +3.3 \pm 0.2$ cm⁻¹; Ref. 62). Spin determinations give a value of ~ 0.8 spin/mole for these low-field resonances. Q band EPR spectroscopy (at 35 GHz) of reduced *P. furiosus* ferredoxin showed resonances at the same g values as X band (at 9.3 GHz), confirming that the observed EPR absorption arises from a single magnetically isolated $[4\text{Fe-4S}]^{1+}$ cluster (47).

The $[4\text{Fe-4S}]^{1+}$ cluster in *P. furiosus* ferredoxin therefore exists with a spin mixture of $S = \frac{1}{2}$ (20%) and $S = \frac{3}{2}$ (80%) forms. Interestingly, comparable EPR properties were recently reported for the 8Fe ferredoxin of *D. africanus* (Fd III) in which one of the cysteine residues to one of its clusters is also replaced by aspartate (Ref. 63; see also Armstrong, this volume). Although 4Fe clusters with a $S = \frac{3}{2}$ ground state have not been reported for any other ferredoxin, they are found in nitrogenase Fe protein (64–66), *C. pasteurianum* hydrogenase I (67), and glutamine phosphoribosylpyrophosphate amidotransferase (68). The coordinating ligands to the cluster in the hydrogenase are not known, but for the Fe protein and the amidotransferase there is substantial evidence for complete cysteinyl coordination (68–71). On the other hand, elegant studies by Beinert and co-workers have shown that one of the iron atoms of the $[4\text{Fe-4S}]^{1+}$ cluster of aconitase has noncysteinyl ligation and is coordinated by either H₂O or OH⁻, but

this cluster exists in only a $S = \frac{1}{2}$ state (72, 73). Thus, noncysteinyll coordination of a specific iron atom of a $[4\text{Fe}-4\text{S}]^{1+}$ cluster is neither a prerequisite for, nor does not always lead to, an $S = \frac{3}{2}$ ground state. However, distinct differences do exist between the various $S = \frac{3}{2}$ clusters in their zero-field splitting parameters and in the ease with which they can be converted to the $S = \frac{1}{2}$ state. That of *P. furiosus* ferredoxin is so far unique in both aspects (62). For example, the two states of the cluster in this protein are very stable and are not interconverted by changes in the solvent media (47).

The E_m value of the $[4\text{Fe}-4\text{S}]$ cluster in *P. furiosus* ferredoxin is -345 mV at 20°C and pH 8, as determined by redox titrations using EPR spectroscopy to monitor the extent of cluster reduction (49). This is comparable to but slightly more positive than the midpoint potentials of mesophilic ferredoxins (typically around -420 mV). There is no detectable difference between the redox properties of the $S = \frac{1}{2}$ and $S = \frac{3}{2}$ states of the 4Fe cluster in *P. furiosus* ferredoxin (47). Moreover, the E_m values of both states decrease linearly with increasing temperature, by -1.7 mV/ $^\circ\text{C}$ over the range 20 – 80°C . As shown in Fig. 4, there appears to be a transition point at 80°C in the temperature dependence of the E_m value, with a change of approximately -6 mV/ $^\circ\text{C}$ between 80 and 89°C (47). The E_m values and the relative amounts of the $S = \frac{1}{2}$ and $S = \frac{3}{2}$ forms of the cluster are also unaffected by pH (6.8 – 10.5), even at 85°C , and are unchanged in the presence of NaCl (1.0 M), sodium dodecyl sulfate (10% , w/v), or ethylene glycol (50% , v/v), even at 80°C (47). These results are quite remarkable for a biological system, as the redox potential and spin state of a $[4\text{Fe}-4\text{S}]$ cluster are extremely sensitive monitors of the cluster environment, yet these appear to be unperturbed when the *P. furiosus* protein is subjected to extreme conditions.

In the redox titrations of *P. furiosus* ferredoxin, mediators were found to be superfluous at temperatures above 60°C (47), indicating that a mechanism exists for direct electron transfer between the Fe–S cluster of this relatively small protein and a platinum electrode. In contrast, the direct and preparative electrochemistry of mesophilic Fe–S proteins typically require the addition of “promoters,” which modify the electrode surface and facilitate cluster–electrode interaction (63, 74). This temperature effect is so far unique to *P. furiosus* ferredoxin as *P. furiosus* rubredoxin does not interact directly with a platinum electrode, even at 90°C (see Section III,C). The results shown in Fig. 4 also allow an estimation of the E_m value of *P. furiosus* ferredoxin at 100°C , at the growth temperature of the organism. By extrapolation, it is less than -550 mV, and possibly as low as -600 mV. Notably, the change in

the temperature dependence of the E_m value of the ferredoxin at 80°C corresponds with the tremendous increase in the rate of H_2 evolution above 80°C catalyzed by *P. furiosus* hydrogenase when the ferredoxin is the electron carrier (Fig. 4). A similar temperature effect on H_2 production is not observed with artificial electron carriers, e.g., methyl viologen, and the hydrogenase (31). Therefore, the redox potential of the ferredoxin may in some way limit the rate of electron transfer to the hydrogenase (and thus H_2 production) at temperatures below 80°C.

b. Electron-Nuclear Double Resonance. The question arises as to what differentiates the two spin states ($S = \frac{1}{2}$ and $S = \frac{3}{2}$) of the $[4Fe-4S]^{1+}$ cluster in *P. furiosus* ferredoxin. One explanation is that the two states are in thermodynamic equilibrium at the temperature at which the EPR spectra are recorded. This is not the case, however, as one would expect the relative intensities of the EPR signals of the two states to change between 4 and 15 K, but they remain constant over this temperature range (62). The two spin states must therefore reflect different conformations of a $[4Fe-4S]$ cluster, which themselves must be maintained by different structures of the protein. Electron-nuclear double-resonance (ENDOR) spectroscopy was used to determine if these structural differences were manifested by an inequivalence between the two forms of magnetically coupled protons. ENDOR is a double-resonance technique that provides information on the type and number of nuclei (where $I \neq 0$) that are part of or interact with an EPR-active paramagnetic center, e.g., Ref. 72. As shown in Fig. 7, multiple 1H ENDOR resonances were detected at the $g = 1.84$ EPR resonance ($S = \frac{1}{2}$) of *P. furiosus* ferredoxin (47). These correspond to hyperfine coupling constants of 4–6 MHz. Similar resonances have been observed with other reduced ferredoxins and they are assigned to the methylene protons of the cysteinyl residues that bind the $[4Fe-4S]^{1+}$ cluster. However, the *P. furiosus* protein also exhibited a 1H ENDOR resonance corresponding to a coupling constant of ~ 22 MHz (Fig. 7). Such a strongly coupled proton has not been reported for any other Fe-S protein. Moreover, when the ferredoxin is in D_2O , the weakly coupled protons remain unchanged, as expected, but the 22-MHz resonance is not observed (Fig. 7). Instead, a single 2H ENDOR resonance is seen showing that D_2O interacts directly with the paramagnetic center (47). A surprising result was obtained upon examination of the $g = 3.60$ EPR absorption ($S = \frac{3}{2}$) from *P. furiosus* ferredoxin. This showed similar although not identical ENDOR resonances from weakly coupled protons and also a strongly coupled resonance ($A \leq 20$ MHz), but the latter was unaffected when the ferredoxin was examined in D_2O (47). The

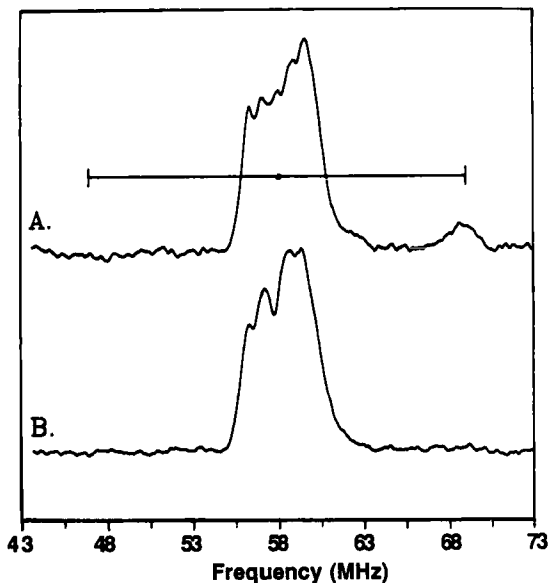


FIG. 7. Q band ^1H ENDOR of the $S = \frac{1}{2}$ form of the $[\text{4Fe-4S}]^{1+}$ cluster of *P. furiosus* ferredoxin. Samples of the ferredoxin (10.7 mM) were prepared in H_2O (A) and in D_2O (B). Spectra were recorded using a microwave frequency of 35.39 GHz and power of 0.05 mW at 2 K. The magnetic field was set at 1.375 T ($g = 1.84$). Taken from Ref. 47.

solvent accessibility of the $[\text{4Fe-4S}]^{1+}$ cluster therefore appears to be very different in the $S = \frac{1}{2}$ and $S = \frac{3}{2}$ ground states.

The two spin forms of the $[\text{4Fe-4S}]^{1+}$ cluster in *P. furiosus* ferredoxin can therefore be differentiated by the exchangeability (in the $S = \frac{1}{2}$ form) or nonexchangeability (in the $S = \frac{3}{2}$ form) of a water-derived hydrogen atom that directly interacts with the 4Fe cluster, an interaction not seen in other 4Fe ferredoxins. This hydrogen atom appears to be derived from OH^- rather than H_2O , as the EPR and redox properties of the protein were unchanged over the pH range 6.8–10.5 (47). The obvious conclusion is that these unique properties are associated with the lack of complete cysteinyl ligation to the $[\text{4Fe-4S}]^{1+}$ cluster of this protein, and suggest that an OH^- molecule directly coordinates to the unique fourth Fe atom. This is shown diagrammatically in Fig. 8. The coordination of OH^- (or H_2O) to a unique Fe site of the $[\text{4Fe-4S}]^{1+}$ cluster of aconitase has been established by crystallographic studies (75). However, as well as exclusively exhibiting an $S = \frac{1}{2}$ ground state (72), the D_2O -exchangeable ^1H ENDOR resonances associated with this cluster have A values ≤ 8 MHz, much less than that observed with *P.*

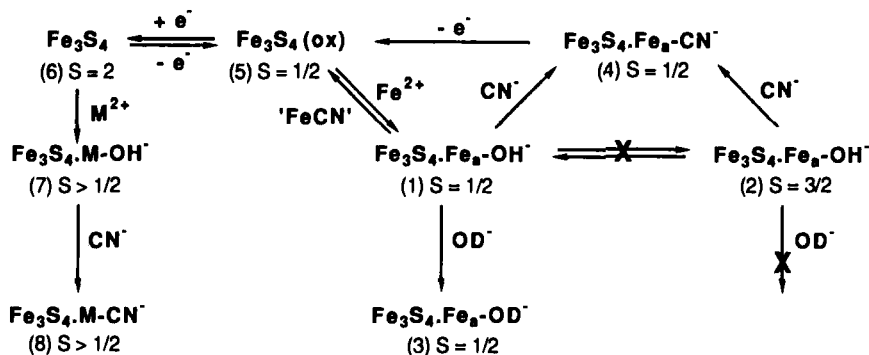


FIG. 8. Proposed reactions of the unique noncysteiny l Fe atom (Fe_a) in the $[4\text{Fe}-4\text{S}]$ cluster of *P. furiosus* ferredoxin. In the native protein the cluster (1 and 2) has OH^- bound, but only in the $S = \frac{1}{2}$ state (1) can this exchange with OD^- (3). Both spin states react with cyanide (4). The 3Fe cluster (5) is generated by ferricyanide (" FeCN^- ") treatment of (1) and (2) or by oxidation (> -100 mV) of (4). The Fe_a atom can be substituted by the addition to (6) of a metal ion, M (Ni, Co, or Zn). This is assumed also to bind OH^- (7) and M can also bind cyanide (8). All clusters except (5) are in their reduced forms and the spin state of each is indicated.

furiosus ferredoxin (76, 77). The differences between the 4Fe clusters of aconitase and *P. furiosus* ferredoxin may lie with the role of the amino acid side chain that replaces the expected cysteinyl group. In aconitase, which lacks the consensus sequence of cysteinyl residues found in the ferredoxins, there is no residue in the immediate vicinity of the unique Fe atom (75, 76). This may not be the case with the aspartyl group that replaces the cysteinyl residue in *P. furiosus* ferredoxin, although as yet there is no information as to whether this aspartyl residue interacts with the fourth Fe atom of the cluster.

A question then remains: why is the OH^- molecule bound to the $[4\text{Fe}-4\text{S}]^{1+}$ cluster in *P. furiosus* ferredoxin exchangeable in the $S = \frac{1}{2}$ form but not in the $S = \frac{3}{2}$ form? This would suggest that significant structural changes exist between the two ground states involving the adjacent amino acid residues, whereby the cluster is shielded from the solvent in the $S = \frac{3}{2}$ but not in the $S = \frac{1}{2}$ form. This then raises the question of what aspects of the protein structure determines which of the two forms predominate. Obviously this is an intrinsic property of the protein, since the reconstituted ferredoxin (after acid precipitation) has the same $S = \frac{1}{2}$ to $S = \frac{3}{2}$ ratio as the native protein (49). Similarly, the factors that contribute to one form or the other are exceedingly stable, unaffected by high temperature, pH extremes, and denaturants. As yet there is no information as to what these factors might be. Since

synthetic clusters of the $[4\text{Fe}-4\text{S}-4(\text{SR})]$ type have been shown to exist in mixtures of $S = \frac{1}{2}$ and $S = \frac{3}{2}$ spin states (in frozen dimethylformamide solution; Ref. 78, see also Holm, this volume), detailed structural studies of *P. furiosus* ferredoxin using, for example, NMR and crystallography, may yield information on this unsolved aspect of Fe-S cluster chemistry.

c. Magnetic Circular Dichroism and Resonance Raman Spectroscopy. Variable-temperature magnetic circular dichroism (MCD) is a particularly powerful spectroscopic technique in discriminating paramagnetic Fe-S clusters and in providing information on their electronic properties (see Refs. 67, 79, and 80). Thus, the MCD data of reduced *P. furiosus* ferredoxin were in accord with its EPR properties and showed that its cluster is of the 4Fe type with a predominant $S = \frac{3}{2}$ ground state (62). In resonance Raman spectroscopy, the bands observed correspond to stretching vibrations of bridging and terminal Fe-S bonds within an Fe-S cluster, the frequencies and intensities of which are very diagnostic of cluster type. Hence, the bands observed with oxidized *P. furiosus* ferredoxin (62) were very similar to those seen from $[4\text{Fe}-4\text{S}]^{2+}$ clusters in other ferredoxins (81, 82). The latter have been rigorously assigned to predominantly terminal (Fe-cysteinyl) or bridging Fe-S stretching by extensive studies using synthetic analogs, isotope shifts (with ^{54}Fe and ^{34}S), and normal mode calculations. The most significant difference in the Raman spectrum of *P. furiosus* ferredoxin is in the totally symmetric bridging vibration, which is the dominant feature in the Raman spectrum. In proteins and also in synthetic clusters that contain a $[4\text{Fe}-4\text{S}]^{2+}$ cluster with complete cysteinyl (or thiolate) coordination, the totally symmetric bridging frequencies range between 333 and 338 cm^{-1} (62, 81, 82). That of *P. furiosus* ferredoxin is shifted to higher energy and is seen at 342 cm^{-1} . Interestingly, a similar shift is also seen with the $[4\text{Fe}-4\text{S}]^{2+}$ clusters of aconitase (340 cm^{-1}) and sulfite reductase (342 cm^{-1}), both of which have a unique Fe site that arises because of atypical coordination. As noted above, this is $\text{H}_2\text{O}/\text{OH}^-$ in the case of aconitase (76), but an unknown ligand bridges between the siroheme and the 4Fe cluster in sulfite reductase (83). This site differentiation appears to lower the cluster symmetry (from D_{2d} to C_{3v}) and shift the totally symmetric bridging frequencies closer to those seen from $[3\text{Fe}-4\text{S}]^{1+}$ clusters, which are typically 347–348 cm^{-1} (82). The frequency of the totally symmetric bridging vibration may therefore prove to be a useful indicator of site differentiation in 4Fe clusters, arising from anomalous coordination to one Fe atom.

2. Spectroscopic Characterization of the [3Fe-4S] Cluster

Oxidation of anaerobically purified *P. furiosus* ferredoxin (with O₂, thionine, or 2,6-dichlorophenolindophenol) does not result in degradation of its cluster, but oxidation with a fivefold excess of potassium ferricyanide shows quantitative conversion of the [4Fe-4S]¹⁺ cluster to a [3Fe-4S]¹⁺ cluster (Fig. 8; Refs. 49 and 62). The EPR (Fig. 9), variable-temperature MCD, and resonance Raman spectra of the fer-

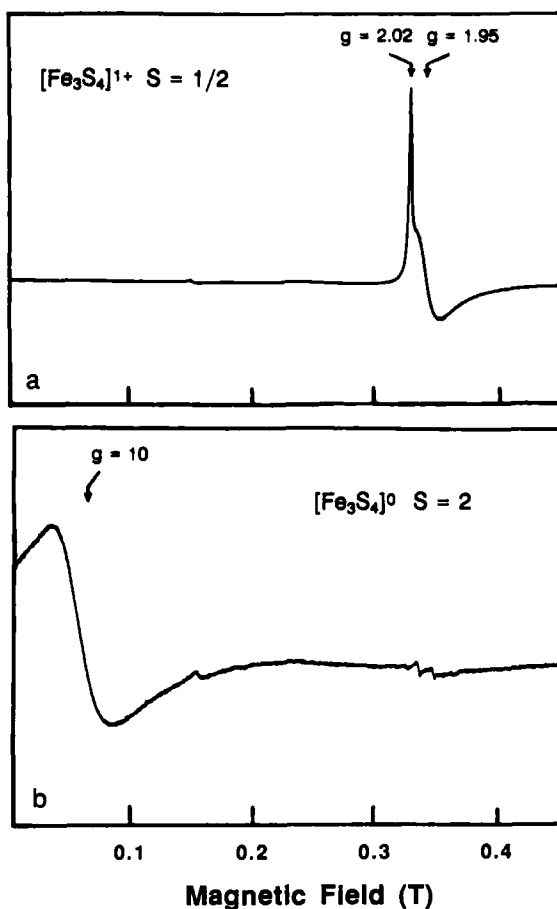


FIG. 9. EPR spectra of the oxidized (a) and reduced (b) states of the [3Fe-4S] cluster in *P. furiosus* ferredoxin. The sample concentration was 3 mg/ml and spectra were recorded at 8 K. The microwave power used was 1 mW (oxidized) and 50 mW (reduced). Modified from Ref. 62.

ricyanide-treated protein are all very similar to those of $S = \frac{1}{2}$ $[3\text{Fe}-4\text{S}]^{1+}$ clusters in other bacterial ferredoxins (62). EPR-monitored redox titrations indicate an E_m value of -160 mV (at pH 8.0 and 23°C) for the 3Fe center in *P. furiosus* ferredoxin (49). Upon reduction of the 3Fe ferredoxin with sodium dithionite, the only feature in its EPR spectrum is a broad derivative-shaped feature at $g = 10$ arising from transitions within a $M_s = \pm 2$ doublet of an $S = 2$ ground state (Fig. 9). In addition, MCD magnetization studies of the reduced 3Fe protein were only interpretable in terms of an $S = 2$ ground state with a negative axial zero-field splitting parameter, $D < 0$ (62). The intensity and form of the low-temperature MCD spectrum also indicates the presence of one $[3\text{Fe}-4\text{S}]^0$ cluster (62). Moreover, recent data from a saturation magnetization study are also consistent with one reduced 3Fe cluster per protein molecule. The fit parameters were $S = 2$, $D = -3 \text{ cm}^{-1}$, $E/D = 0.23$, and $g = 2.10$ (E. P. Day, J.-B. Park, and M. W. W. Adams, unpublished data, 1991). The $[3\text{Fe}-4\text{S}]^{0/1+}$ cluster in *P. furiosus* ferredoxin therefore has structural, electronic, and magnetic properties analogous to those in mesophilic 3Fe ferredoxins in both the oxidized and reduced states. Since the 4Fe cluster in this protein has unusual spectroscopic properties, it would seem likely that the Fe atom that is removed on formation of the $[3\text{Fe}-4\text{S}]$ cluster is the one that has noncysteinyll coordination. This is further supported by comparisons with the 3Fe form of the ferredoxin from *D. gigas*. This has the consensus sequence of cysteinyll residues and the one that is equivalent to the aspartyl residue in *P. furiosus* ferredoxin is the one that is not involved in coordinating the 3Fe cluster (84, 85).

A stoichiometric amount of a conventional $[3\text{Fe}-4\text{S}]$ cluster can therefore be readily generated in *P. furiosus* ferredoxin by a facile procedure, and all of the spectroscopic data indicate that there is no residual $[4\text{Fe}-4\text{S}]$ cluster (62). Indeed, even after incubating the 3Fe ferredoxin at 80°C for 4 days, there was no evidence of cluster destruction or conversion to the 4Fe form. However, as noted above, quantitative cluster conversion is easily accomplished by adding stoichiometric amounts of Fe(II) under reducing conditions to yield $[4\text{Fe}-4\text{S}]$ clusters with spectroscopic characteristics identical to those of the anaerobically purified protein (47, 62). This ease of cluster interconversion (both 4Fe to 3Fe and vice versa) is comparable to what has been found with aconitase (86), which, as discussed above, also has noncysteinyll ligation to the removable Fe atom (76). On the other hand, cluster conversion is much more difficult with mesophilic ferredoxins having total cysteinyll coordination. For example, the 4Fe clusters of *C. pasteurianum* ferredoxin tend to degrade rather than form 3Fe clusters (87). Similarly, *D.*

gigas ferredoxin can be purified as either the 3Fe or 4Fe form, and although the two can be interconverted, there is evidence for some cluster degradation and the presence of apoprotein (88). The presence of a single 4Fe cluster and quantitative cluster interconversion, coupled with extreme stability, makes *P. furiosus* ferredoxin an attractive model system with which to not only investigate the electronic and magnetic properties of Fe-S centers, but also their reactivity. This includes both to small molecules and to the incorporation of other metal ions to generate mixed-metal clusters.

3. Ferredoxin as a Model of Enzymatic Fe-S Clusters

Before considering the potential of *P. furiosus* ferredoxin as an analog of the active sites of Fe-S enzymes, it is necessary to summarize what is known about "catalytic" Fe-S clusters. Indeed, the notion that Fe-S clusters fulfill functions other than simple electron transfer is a fairly recent development in the Fe-S protein field. Although some Fe-S-containing enzymes contain a [4Fe-4S] cluster of no known function, e.g., endonuclease III (89) and glutamine phosphoribosylpyrophosphate amidotransferase (90), in some others, Fe-S clusters bind small molecule substrates and appear to participate in catalyzing chemical reactions. Since ferredoxin-type [4Fe-4S] (and [2Fe-2S]) clusters do not bind small molecules or catalyze any known chemical reaction (91, 91a), the question arises as to how such clusters have been "activated" or "functionalized" in Fe-S-containing enzymes such that they can bind and activate substrates. Two mechanisms appear to exist from the Fe-S enzymes studies so far. The first is by replacing one or more of the cysteinyl sulfur ligands that bind the Fe-S cluster to the protein. Into this group fall the hydratases, of which the tricarboxylic acid cycle enzyme, aconitase, is the prototypical example. Beinert and co-workers (75, 76) have shown that in addition to $\text{OH}^-/\text{H}_2\text{O}$, the non-sulfur-ligated Fe atom of its single [4Fe-4S] cluster can bind the substrates citrate or *cis*-aconitate. Several other hydratases (or hydrolases) have also been shown to contain Fe-S clusters and presumably these function in a similar fashion (92-96). Besides hydratases, there are so far only two examples of enzymes containing Fe-S clusters with partial nonsulfur ligation, and both are involved in catalyzing redox reactions. One is nitrogenase, which is discussed below, and the other example is Fe hydrogenases. As described in Section IV,A, the H_2 -activating center of the Fe hydrogenases is thought to be a novel Fe-S cluster, termed the H cluster (see Ref. 38 for review). A recent study showed that the H cluster of hydrogenases I from *C. pasteurianum* contains two distinct types of nitrogenous ligands (97), although the extent to which these

ligands participate in or enable catalysis by the H cluster is as yet unknown.

The second mechanism by which [4Fe-4S]-type clusters could be modified so that they can catalyze chemical reactions is by the replacement of one of the Fe atoms by a second type of metal. There are two enzymes that may fit into this category. The first is nitrogenase, which contains a dissociable Mo-Fe-S cluster at the site of N₂ reduction. Of stoichiometry Fe₆₋₈S₈₋₁₀Mo (98, 99), this appears to contain a [Mo-3Fe] unit (100, 101), and similar [V-3Fe] and ["Fe"-3Fe] cores are thought to be present in the alternative vanadium- and iron-containing nitrogenases (102-104). As noted above, nonsulfur ligands to these Fe-S clusters may also play a role in their catalytic abilities, since ESEEM spectroscopy has been used to show that the Mo-Fe-S cluster of the molybdenum nitrogenase has a degree of N coordination (105). The second enzyme that may contain a mixed-metal Fe-S cluster is the CO dehydrogenase of acetogenic, methanogenic, and photosynthetic bacteria (106-111). For example, a recent ENDOR study (112) concluded that when *Clostridium thermoaceticum* CO dehydrogenase is reacted with CO, a mixed metal-carbon complex of stoichiometry NiFe₃₋₄S_{≥4}C is generated. The data were consistent with either a [Ni-3Fe-4S] cluster or a mononuclear Ni bridged by a ligand to a [4Fe-4S]¹⁺ cluster as the source of the novel $S = \frac{1}{2}$ EPR resonance ($g_{\parallel} = 2.03$, $g_{\perp} = 2.07$) induced by CO treatment. Mössbauer data from the same enzyme (113) rule out a 3Fe-type center at the active site of this enzyme, unless another metal (M)—and Ni or Fe are the obvious choices—is incorporated into the site to give an M-3Fe-4S-type structure.

Enormous insight into the properties of biological Fe-S clusters and potential models of them have come from purely synthetic approaches. Largely through the work of Holm and co-workers, their synthesis and characterization has opened up a new area of inorganic chemistry (for example, see Refs. 91, 114-118). However, synthetic analogs are characterized in nonaqueous media, which does not easily allow one to mimic the chemical environment of a protein, and their redox properties, an essential parameter for comparisons with biological clusters, are frequently ill-defined and hard to translate to aqueous media. Also, no synthetic Fe-S cluster catalyzes a chemical reaction (some will generate H₂ and reduce C₂H₂, but in less than stoichiometric amounts; Ref. 119). In contrast to the synthetic analogs, Fe-S clusters in proteins afford a totally aqueous system and offer enormous potential for varying both ligands to specific sites of the cluster and the chemical environment of the cluster. In addition, functional amino acid groups likely to

participate in catalysis can be added at strategic points adjacent to the cluster (although a major disadvantage with proteins is that crystal structures cannot be as readily obtained as they can with synthetic analogs). The diversity in properties of enzymatic [4Fe-4S]-type clusters and their apparent catalytic potential make 4Fe ferredoxins the obvious choice for a model system, with the added prerequisite of facile 4Fe to 3Fe conversion. For example, the fourth site of the [3Fe-4S] cluster in *D. gigas* ferredoxin can be occupied by other divalent metals, namely, zinc or cobalt (120, 121). Although of no known biological relevance, spectroscopic data show that these $[M-3Fe-4S]^{1+}$ clusters (where $M = Co$ or Zn) are extremely useful in understanding intracluster magnetic interactions. However, the presence of a cysteinyl residue adjacent to the "vacant" site of the 3Fe cluster might be expected to hinder attempts at incorporating other metals, and cysteinyl coordination to the fourth Fe atom in a [4Fe-4S] cluster would preclude binding of exogenous ligands. In the following discussion it is shown that these difficulties do not arise with *P. furiosus* ferredoxin, owing to the presence of partial noncysteinyl ligation to its Fe-S cluster.

a. Formation and Properties of the [Ni-3Fe-4S] Cluster. The [Ni-3Fe-4S] cluster was generated in *P. furiosus* ferredoxin using procedures similar to those used by Münck and co-workers for incorporating Zn(II) and Co(II) into the [3Fe-4S] core of *D. gigas* ferredoxin to give [Zn-3Fe-4S] and [Co-3Fe-4S] clusters (120, 121). It is prepared by incubating dithionite-reduced 3Fe ferredoxin in 100 mM Mes buffer, pH 6.0, with a 20-fold excess of $NiCl_2$ under anaerobic conditions for 15 min at 23°C (122). Excess Ni(II) can be removed by treatment with EDTA and subsequent gel filtration under anaerobic conditions. As shown in Fig. 10b, incorporation of Ni(II) into the $S = 2$ [3Fe-4S]⁰ cluster yields a ground state with half-integer spin. This is analogous to the incorporation of Fe(II) into the 3Fe core, as this gives the $S = \frac{1}{2}$ and $S = \frac{3}{2}$ mixture of the $[4Fe-4S]^{1+}$ cluster (Fig. 10a). Thus, the binding of an M^{2+} ion ($M = Fe, Ni$) is accompanied by a one-electron reduction of the 3Fe cluster to the $[M-3Fe-4S]^{1+}$ state. However, in contrast to the $[Zn-3Fe-4S]^{1+}$ of *D. gigas* ferredoxin, which has an $S = \frac{5}{2}$ ground state (121), the Ni analog is an $S = \frac{3}{2}$ species. Its spectrum comprises positive maxima at $g = 5.7$ and 4.9 , a broad derivative centered at $g = 2.9$, and a weak negative feature at $g = 1.8$. These resonances can be rationalized using a spin Hamiltonian with an isotropic Zeeman interaction. For example, with $E/D = 0.18$, $D < 0$, and $g_0 = 2$, the $S = \frac{3}{2}$ spin Hamiltonian predicts $g(x, y, z) = 2.88, 4.95$, and 1.84 and $1.12, 0.94$, and 5.82 for the upper and lower doublets,

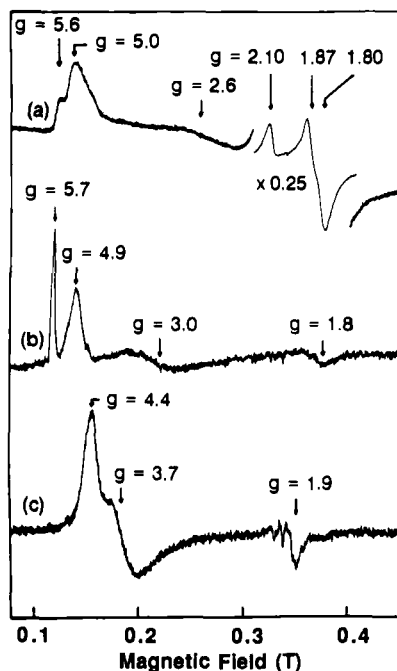


FIG. 10. EPR spectra of the $[\text{Ni-3Fe-4S}]^{1+}$ cluster in *P. furiosus* ferredoxin and the cyanide-bound form. The samples were as follows: (a) reduced ferredoxin (3.5 mg/ml) containing a $[\text{4Fe-4S}]^{1+}$ cluster; (b) reduced ferredoxin (2.5 mg/ml) containing a $[\text{Ni-3Fe-4S}]^{1+}$ cluster; (c) after treatment of sample b with a 50-fold excess of potassium cyanide. Temperatures and microwave powers used: (a) 8 K, 10 mW; (b) 4.5 K, 50 mW; (c) 7 K, 1 mW. Taken from Ref. 122.

respectively. The temperature dependence of the low-field EPR signals shows that the $g = 5.7$ and 4.9 components originate from the lower and upper doublets, respectively. Therefore, the zero-field splitting is opposite in sign compared to the $S = \frac{3}{2}$ $[\text{4Fe-4S}]^{1+}$ center (Fig. 10a). Analysis of the intensity ratio of the $g = 5.8$ and $g = 4.9$ features as a function of $1/T$ indicates $D = -2.2 \pm 0.2 \text{ cm}^{-1}$ (122). Preliminary variable-temperature MCD analyses of the $[\text{Ni-3Fe-4S}]^{1+}$ cluster of *P. furiosus* ferredoxin show a temperature-dependent spectrum that is distinct from the dithionite-reduced native 4Fe form (62), and the magnetization data are consistent with the EPR-determined ground state properties (R. C. Conover, J.-B. Park, M. W. W. Adams, and M. K. Johnson, unpublished data, 1991). It should be noted that Münck and co-workers (123) observed EPR resonances similar to those shown

in Fig. 10b during studies of the reaction of Ni(II) with the 3Fe form of *D. gigas* ferredoxin.

Evidence for the presence of a $[\text{Ni-3Fe-4S}]^{1+}$ cluster in *P. furiosus* ferredoxin comes from two sources. First, the $g = 5.7$ shown in Fig. 10b is broadened when ^{61}Ni ($I = \frac{3}{2}$) is used (122), showing that the observed spectroscopic changes involve the incorporation of Ni into the paramagnetic center. Second, a $[\text{Ni-3Fe-4S}]^{1+}$ cluster was recently synthesized and characterized by Holm, Münck, and co-workers (Ref. 124; see Holm, this volume). The cuboidal nature of the cluster was evident from crystallographic analysis that showed a Ni-Fe distance of 2.69 Å, analogous to the Fe-Fe distances (~ 2.7 Å) in both synthetic and biological $[\text{4Fe-4S}]$ clusters. The synthetic $[\text{Ni-3Fe-4S}]^{1+}$ cluster also has a $S = \frac{3}{2}$ ground state and exhibits EPR properties similar to those of the Ni-incorporated 3Fe form of *P. furiosus* ferredoxin. These data clearly show that the synthetic and protein-bound Ni-Fe clusters are structurally similar.

So, do the spectroscopic properties of the $[\text{Ni-3Fe-4S}]$ cluster in *P. furiosus* ferredoxin in any way resemble those reported for the Ni-Fe site in CO dehydrogenase? As noted above, the Ni-Fe complex in CO-treated *C. thermoaceticum* CO dehydrogenase exhibits a novel $S = \frac{1}{2}$ EPR resonance, but this is only observed upon CO reduction and it is a relatively minor component, typically accounting for only 0.15 spin/Ni (113). Furthermore, ill-defined $S = \frac{3}{2}$ EPR signals centered around $g = 5$ are apparent from both the dithionite- and CO-reduced enzyme. Similarly, EPR signals near $g = 4.3$ from a $S > \frac{1}{2}$ center as well as a $S = \frac{1}{2}$ resonance ($g = 2.04, 1.90, \text{ and } 1.71$) have been assigned to the Ni-Fe center in the CO dehydrogenase from *Rhodospirillum rubrum* (110). It is therefore possible that the majority of the active sites in these enzymes have a Ni-Fe complex with an $S = \frac{3}{2}$ ground state, although it remains to be seen if this has a structure analogous to the Ni-3Fe cluster in *P. furiosus* ferredoxin.

b. Exogenous Ligand Binding to the $[\text{M-3Fe-4S}]$ Clusters. Cyanide is a potent competitive inhibitor of all known CO dehydrogenases (125), so it was of great interest to investigate the possibility of cyanide binding to the $[\text{Ni-3Fe-4S}]^{1+}$ center in *P. furiosus* ferredoxin. As shown in Fig. 10, the addition of a 50-fold excess of cyanide to the Ni-substituted protein results in the complete conversion of the $S = \frac{3}{2}$ $[\text{Ni-3Fe-4S}]^{1+}$ EPR spectrum (Fig. 10b) to a new EPR signal (Fig. 10c; see Ref. 103). The g values (4.4, 3.7, and 1.9) indicate an axial $S = \frac{3}{2}$ species ($E/D = 0.06$), and temperature-dependence studies (4–15 K) show that this resonance arises exclusively from the lower Kramers'

doublet, i.e., $D > 0$ (122). Further studies to conclusively establish that Ni is the cyanide-binding site and the spectroscopic consequences of binding other ligands to the $[\text{Ni-3Fe-4S}]^{1+}$ cluster in *P. furiosus* ferredoxin are in progress. Interestingly, it may be of relevance to note that synthetic mixed-metal clusters containing $[\text{V-3Fe-4S}]^{2+}$, $[\text{Mo-3Fe-4S}]^{3+}$, and $[\text{W-3Fe-4S}]^{3+}$ cores, and the nitrogenase Fe-Mo cofactor (91, 126), all exhibit $S = \frac{3}{2}$ ground states with EPR characteristics remarkably similar to those of the cyanide-bound $[\text{Ni-3Fe-4S}]^{1+}$ ferredoxin (122).

We now return to the notion that reactivity (and catalytic activity) in biological Fe-S clusters can also be imparted by the presence of nonsulfur ligation to one of the Fe sites of a 4Fe cluster. The results described in Section III,B,1 indicate that the unique Fe atom of *P. furiosus* ferredoxin has an OH^- ligand, and that this can be displaced by OD^- (D_2O) in the $S = \frac{1}{2}$ state of the cluster, but not in the $S = \frac{3}{2}$ form. Thus there are questions: would the unique Fe site of the $[\text{4Fe-4S}]$ cluster (which we will now refer to as Fe_a) bind other ligands by displacing OH^- , and do the two spin states of the cluster show different reactivities? Cyanide is again the ligand of choice, as this is a potent inhibitor of many Fe-S-containing enzymes, as well as a substrate of nitrogenase. As shown in Fig. 11 (127) cyanide has a dramatic effect on the EPR properties of the $[\text{4Fe-4S}]^{1+}$ cluster of *P. furiosus* ferredoxin. Incubation of the reduced protein with a 250-fold excess of cyanide for 2 hr (pH 7.5–10.5) results in the complete conversion of the EPR resonances from both the $S = \frac{1}{2}$ and $S = \frac{3}{2}$ forms to a new $S = \frac{1}{2}$ resonance, $g = 2.09, 1.95$, and 1.92 (127). The latter represents 1 spin/mole, and can still be seen at 60 K, which is in contrast to the EPR absorption from the native cluster, as this is observed only below 15 K. Substantial broadening is observed using the ^{57}Fe -enriched protein (Fig. 11c), showing that the EPR signal induced by cyanide does arise from an Fe-containing center. However, its EPR properties are unlike those of any other biological 4Fe center; indeed, they are more reminiscent of reduced ferredoxin-type 2Fe clusters.

Evidence for the binding of cyanide to only Fe_a and without destruction or rearrangement of the $[\text{4Fe-4S}]^{1+}$ cluster is provided by the following. First, cyanide showed no reaction with the 4Fe clusters of *C. pasteurianum* ferredoxin (which have complete cysteinyl coordination) nor with the 3Fe form of *P. furiosus* ferredoxin (which lacks Fe_a). Second, the MCD of the cyanide-treated protein was characteristic of $S = \frac{1}{2}$ 4Fe-type rather than 2Fe-type centers. Third, simply removing the cyanide completely regenerates the characteristic $S = \frac{1}{2}$ and $S = \frac{3}{2}$ resonances of native protein. Fourth, as described above, the ferre-

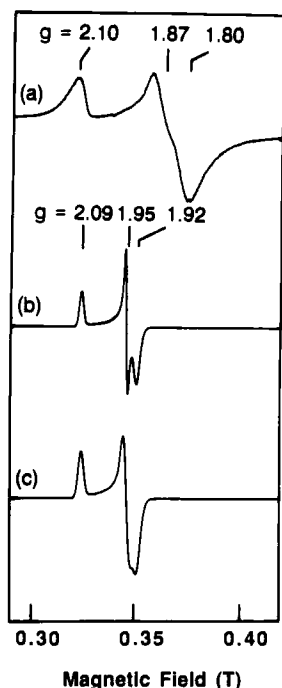


FIG. 11. EPR spectra of the cyanide-treated ferredoxin from *P. furiosus*. (a) Reduced ferredoxin (6 mg/ml); (b) after the addition of a 250-fold excess of potassium cyanide; (c) ^{57}Fe -reconstituted ferredoxin after cyanide treatment. The spectra were recorded at 20 K using 1-mW microwave power. Taken from Ref. 127.

doxin is exceptionally resistant to denaturation, therefore, the cyanide effect is unlikely to arise from cyanide-induced conformational changes of the protein. Fifth, anaerobic oxidation of the cyanide-treated protein by thionine generates the 3Fe form, indicating loss of Fe_a from an intact 4Fe cluster (127). Presumably, this is related to the fact that ferricyanide, and not other high potential oxidants such as thionine or 2,6-dichlororphenolindophenol, can effectively remove a single Fe atom from $[4\text{Fe}-4\text{S}]$ clusters. Sixth, preliminary data indicate that a ^{13}C ENDOR resonance is observed from the ^{13}CN -treated protein (C. Fan, R. Conover, J.-B. Park, M. W. W. Adams, M. K. Johnson, and B. M. Hoffman, unpublished, 1991). These results therefore provide the first evidence for exogenous ligand binding to a noncysteinylligated Fe atom of a $[4\text{Fe}-4\text{S}]^{1+}$ cluster in a bacterial ferredoxin (127). In contrast to the binding of OH^-/OD^- , cyanide reacts with the $S = \frac{3}{2}$ form of the

4Fe cluster in *P. furiosus* ferredoxin. Preliminary results using lower cyanide concentrations indicate that cyanide preferentially reacts with the $S = \frac{1}{2}$ ground state, but as yet conditions for exclusive reactivity have not been obtained.

The presence of a noncysteinyl ligand to one Fe atom (Fe_a) of the $[\text{4Fe-4S}]$ cluster in *P. furiosus* ferredoxin therefore has very useful consequences. These are discussed with reference to Fig. 8. Fe_a is able to bind exogenous ligands, such as OD^- and cyanide, and because of the reactivity of Fe_a , its removal is greatly facilitated (by ferricyanide). When cyanide is bound, facile removal of Fe_a occurs upon oxidation. The binding of ligands to Fe_a appears to be directly analogous to the reaction of the catalytic Fe-S center in aconitase with its substrates, and possibly to the reactions catalyzed by enzymes such as hydrogenase and nitrogenase. Moreover, the degree of reactivity of Fe_a seems to be related to the spin state ($S = \frac{1}{2}$ or $S = \frac{3}{2}$) of the cluster. In addition, replacement of Fe_a with other metal ions readily takes place, presumably because of the absence of the reactive thiol of the substituted cysteinyl residue. In fact, our preliminary experiments indicate that Co^{2+} or Zn^{2+} are incorporated into the 3Fe center even more readily than Ni^{2+} . It is assumed in Fig. 8 that OH^- binds to the M site. Although there is no direct evidence for this, the M site appears to bind ligands (cyanide) in the same fashion as Fe_a . Indeed, we have recently shown that cyanide dramatically changes the EPR and MCD properties of the Zn and Co clusters (R. C. Conover, M. Finnegan, J.-B. Park, M. W. W. Adams, and M. K. Johnson, unpublished, 1991). In other words, exogenous ligands such as cyanide appear to interact only with the unique, noncysteinyl and exchangeable metal site of the cubane cluster of *P. furiosus* ferredoxin, whether the metal be Fe, Zn, Ni, or Co. Although it remains to be seen if Fe-S-containing enzymes such as CO dehydrogenase (where $M = \text{Ni}$), nitrogenase (where $M = \text{Mo}$, V , or Fe), and Fe hydrogenase (where $M = \text{Fe}$) utilize the reactivity of such cubane clusters, further studies of the properties of this structure in *P. furiosus* ferredoxin should yield useful information on the chemical diversity of the $[\text{M-3Fe-4S}]$ unit in an extremely stable biological environment.

C. RUBREDOXIN (Fe)

Rubredoxins are a class of bacterial electron transfer proteins that contain a single iron atom coordinated by the sulfur atoms of four cysteinyl residues (128). All are monomeric proteins of molecular weight approximately 6000. The complete amino acid sequences of 11

rubredoxins are known (129–140) and four crystal structures have been reported (141, 142). As the simplest known class of redox protein, comparative studies of rubredoxins isolated from divergent species have the potential to provide insight into both the minimum structural requirements for this protein and the residues that influence electron transfer and the redox properties of the iron site, as well as phylogenetic relationships. In addition, the study of thermostable rubredoxins could provide information on the mechanisms of stabilizing proteins at extreme temperatures. To date, the only structural information available on rubredoxins comes from those purified from eubacteria, and all but one of them are from mesophilic species, the exception being *Clostridium thermosaccharolyticum* (131), which grows optimally at 55°C. *Pyrococcus furiosus* rubredoxin is the first to be purified from a hyperthermophilic bacterium, and also the first from an archaeobacterium.

The molecular properties of *P. furiosus* rubredoxin are similar to those of the mesophilic proteins (144). Its molecular weight, estimated by gel filtration, was 6800 ± 1000 , which is in reasonable agreement with the value calculated (5397; see below) from the amino acid sequence. The UV-visible spectrum of the oxidized protein is also typical of other rubredoxins: the absorption coefficients at the maxima are 25.6 (280 nm), 10.7 (390 nm), and 9.22 (494 nm) $\text{mM}^{-1} \text{cm}^{-1}$, and the A_{494}/A_{280} ratio is 0.36. In accordance, the protein contains 1.2 ± 0.2 g-atoms of Fe/5282 g of protein, but no acid-labile sulfide (144). Oxidized *P. furiosus* rubredoxin also exhibits the characteristic rubredoxin EPR spectrum ($g = 4.3$ and 9.4), which arises from the high-spin Fe(III) site. The midpoint potential of the Fe site at 25°C and pH 8.0 is 0 ± 15 mV (J.-B. Park and M. W. W. Adams, unpublished data, 1991). The effect on the E_m value of *P. furiosus* rubredoxin of temperature and of increasing the pH to 10 is shown in Fig. 12. Surprisingly, the E_m value at pH 10 is approximately 60 mV lower than that at pH 8.0 (at 25°C), suggesting that an ionizable protein residue has a direct influence on the redox properties of the Fe site (see, for example, Ref. 145). Whether this effect is unique to the *P. furiosus* protein is not known, as the pH dependence of the E_m value of a mesophilic rubredoxin has not been reported. Only a slight decrease (~ 0.3 mV/°C) in the E_m value is seen at both pH values upon raising the temperature to 50°C, but between 50 and 90°C, rather dramatic changes are observed. The E_m value decreases fairly linearly by 2.7 mV/°C at pH 10.0, and by 3.5 mV/°C at pH 8.0. These changes are greater than those found with *P. furiosus* ferredoxin (-1.7 mV/°C, 20–80°C; Section III,B,1) and with *P. furiosus* aldehyde ferredoxin oxidoreductase (~ -2.0 mV/°C, 20–70°C; Section III,D). All of these values are greater than those reported for the mesophilic redox protein, cytochrome *c* (-0.5 to -1.4 mV/°C, 5–60°C; Ref.

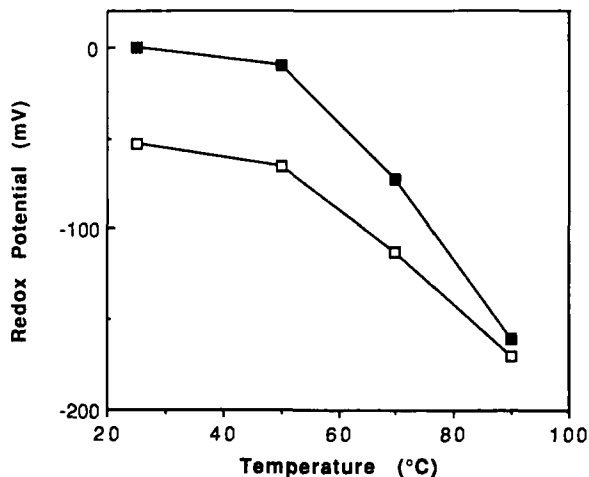


FIG. 12. The effect of temperature and pH on the midpoint potential of rubredoxin from *P. furiosus*. Redox titrations were monitored using EPR spectroscopy and were carried out at pH 8.0 (closed symbols) or 10.0 (open symbols) at the indicated temperature (J. B. Park and M. W. W. Adams, unpublished data, 1991).

146). In addition, the E_m value of *P. furiosus* rubredoxin showed a transition at 50°C, while *P. furiosus* ferredoxin showed a sharp transition at 80°C and a temperature-dependent transition was not evident for the aldehyde ferredoxin oxidoreductase (Section III,D). Each of these proteins therefore has a different dependence on temperature, indicating that the temperature-dependent data are not an electrode artifact or due to pH changes, and it is assumed that they reflect the actual E_m value of a redox center at a particular temperature. At 100°C, the optimum growth temperature for *P. furiosus*, the redox potential of the rubredoxin is estimated at approximately -200 mV (Fig. 12).

As might be expected, *P. furiosus* rubredoxin is considerably more thermostable than its mesophilic counterparts. For example, the UV-visible and EPR properties of the protein (1.0 mg/ml in 50 mM EPBS buffer, pH 8.4) are unaffected after a 24-hr incubation at 95°C. For comparison, the rubredoxin from *C. pasteurianum* is rapidly denatured at 80°C (147), whereas the protein from *D. gigas* loses 50% of its visible absorption ($t_{50\%}$) after approximately 2 hr at 80°C (148). The rubredoxin from the moderately thermophilic sulfate-reducing bacterium, *Thermodesulfobacterium commune*, which grows optimally at 70°C, is slightly more stable, having a $t_{50\%}$ value of about 6 hr at 80°C (148). Unfortunately, there is little indication of the mechanisms responsible

for the enhanced thermostability of the *P. furiosus* protein from its amino acid sequence. For example, the sequence of *P. furiosus* rubredoxin (144) is aligned with those of the rubredoxins from mesophilic organisms (Fig. 13). The overall sequence homology (identity) of *P. furiosus* rubredoxin with the others ranges from 42 to 67%, which is similar to the homologies (41–90%) found between the mesophilic rubredoxins. A previous study (131) of the amino acid sequences of 10 mesophilic rubredoxins noted 15 conserved residues. As indicated in Fig. 13, 14 of these residues, which include the four cysteinyl residues that bind the Fe atom together with an adjacent prolyl residue, are also conserved in *P. furiosus* rubredoxin. The exception, which may be of some significance (see below), is the N-terminal methionine residue. In addition, four unique residues previously identified in the rubredoxin of the moderate thermophile, *C. thermosaccharolyticum*, might confer stability to this protein (131). Of these, though, only one (Trp 4) is present in the *P. furiosus* protein. Also indicated in Fig. 13 are the seven residues that are present in *P. furiosus* rubredoxin but not in any of the others (excluding the absence of the N-terminal methionine).

The complete amino acid sequence of only one hyperthermophilic enzyme is known—that of glyceraldehyde-3-phosphate dehydrogenase (GAPD) from *Pyrococcus woessii* (149). Compared to mesophilic GAPDs, this shows a striking preference for phenylalanine and discrimination against aspartate, methionine, and cysteine (149). However, similar characteristics are not evident when one compares the sequence of the hyperthermophilic *P. furiosus* rubredoxin with the others listed in Fig. 13. Indeed, systematic comparisons show no obvious preference for any amino acid in *P. furiosus* rubredoxin compared with the others listed in Fig. 13. Perhaps the exception is isoleucine (four residues in *P. furiosus* rubredoxin, three in the *C. thermosaccharolyticum* protein, and two or less in the others), but the significance of this is hard to rationalize. Obviously, three-dimensional structures rather than amino acid sequence comparisons are required to determine the differences in protein structures that result in mesophilic rubredoxins rapidly denaturing at 80°C and *P. furiosus* rubredoxin being stable for 24 hr at 95°C.

NMR provides a particularly powerful approach to investigate the structural properties of low-molecular-weight proteins such as rubredoxins. Unfortunately, one- and two-dimensional ¹H NMR of the oxidized and reduced *P. furiosus* protein showed substantial paramagnetic line broadening, and this prevented a detailed structural study of the native protein. High-quality spectra were obtained though for the Zn-substituted protein (144). In addition, the intensities and the chemi-

																																																																																																																																																																																																																																																																																																																																																																																																																																																																																																																																																																																																																																																																																																																																																																																																																																																																																																																																																																																																																																																																																																																																																																																																																																																																																																																																																																																																																																																																</
--	--	--	--	--	--	--	--	--	--	--	--	--	--	--	--	--	--	--	--	--	--	--	--	--	--	--	--	--	--	--	--	--	--	--	--	--	--	--	--	--	--	--	--	--	--	--	--	--	--	--	--	--	--	--	--	--	--	--	--	--	--	--	--	--	--	--	--	--	--	--	--	--	--	--	--	--	--	--	--	--	--	--	--	--	--	--	--	--	--	--	--	--	--	--	--	--	--	--	--	--	--	--	--	--	--	--	--	--	--	--	--	--	--	--	--	--	--	--	--	--	--	--	--	--	--	--	--	--	--	--	--	--	--	--	--	--	--	--	--	--	--	--	--	--	--	--	--	--	--	--	--	--	--	--	--	--	--	--	--	--	--	--	--	--	--	--	--	--	--	--	--	--	--	--	--	--	--	--	--	--	--	--	--	--	--	--	--	--	--	--	--	--	--	--	--	--	--	--	--	--	--	--	--	--	--	--	--	--	--	--	--	--	--	--	--	--	--	--	--	--	--	--	--	--	--	--	--	--	--	--	--	--	--	--	--	--	--	--	--	--	--	--	--	--	--	--	--	--	--	--	--	--	--	--	--	--	--	--	--	--	--	--	--	--	--	--	--	--	--	--	--	--	--	--	--	--	--	--	--	--	--	--	--	--	--	--	--	--	--	--	--	--	--	--	--	--	--	--	--	--	--	--	--	--	--	--	--	--	--	--	--	--	--	--	--	--	--	--	--	--	--	--	--	--	--	--	--	--	--	--	--	--	--	--	--	--	--	--	--	--	--	--	--	--	--	--	--	--	--	--	--	--	--	--	--	--	--	--	--	--	--	--	--	--	--	--	--	--	--	--	--	--	--	--	--	--	--	--	--	--	--	--	--	--	--	--	--	--	--	--	--	--	--	--	--	--	--	--	--	--	--	--	--	--	--	--	--	--	--	--	--	--	--	--	--	--	--	--	--	--	--	--	--	--	--	--	--	--	--	--	--	--	--	--	--	--	--	--	--	--	--	--	--	--	--	--	--	--	--	--	--	--	--	--	--	--	--	--	--	--	--	--	--	--	--	--	--	--	--	--	--	--	--	--	--	--	--	--	--	--	--	--	--	--	--	--	--	--	--	--	--	--	--	--	--	--	--	--	--	--	--	--	--	--	--	--	--	--	--	--	--	--	--	--	--	--	--	--	--	--	--	--	--	--	--	--	--	--	--	--	--	--	--	--	--	--	--	--	--	--	--	--	--	--	--	--	--	--	--	--	--	--	--	--	--	--	--	--	--	--	--	--	--	--	--	--	--	--	--	--	--	--	--	--	--	--	--	--	--	--	--	--	--	--	--	--	--	--	--	--	--	--	--	--	--	--	--	--	--	--	--	--	--	--	--	--	--	--	--	--	--	--	--	--	--	--	--	--	--	--	--	--	--	--	--	--	--	--	--	--	--	--	--	--	--	--	--	--	--	--	--	--	--	--	--	--	--	--	--	--	--	--	--	--	--	--	--	--	--	--	--	--	--	--	--	--	--	--	--	--	--	--	--	--	--	--	--	--	--	--	--	--	--	--	--	--	--	--	--	--	--	--	--	--	--	--	--	--	--	--	--	--	--	--	--	--	--	--	--	--	--	--	--	--	--	--	--	--	--	--	--	--	--	--	--	--	--	--	--	--	--	--	--	--	--	--	--	--	--	--	--	--	--	--	--	--	--	--	--	--	--	--	--	--	--	--	--	--	--	--	--	--	--	--	--	--	--	--	--	--	--	--	--	--	--	--	--	--	--	--	--	--	--	--	--	--	--	--	--	--	--	--	--	--	--	--	--	--	--	--	--	--	--	--	--	--	--	--	--	--	--	--	--	--	--	--	--	--	--	--	--	--	--	--	--	--	--	--	--	--	--	--	--	--	--	--	--	--	--	--	--	--	--	--	--	--	--	--	--	--	--	--	--	--	--	--	--	--	--	--	--	--	--	--	--	--	--	--	--	--	--	--	--	--	--	--	--	--	--	--	--	--	--	--	--	--	--	--	--	--	--	--	--	--	--	--	--	--	--	--	--	--	--	--	--	--	--	--	--	--	--	--	--	--	--	--	--	--	--	--	--	--	--	--	--	--	--	--	--	--	--	--	--	--	--	--	--	--	--	--	--	--	--	--	--	--	--	--	--	--	--	--	--	--	--	--	--	--	--	--	--	--	--	--	--	--	--	--	--	--	--	--	--	--	--	--	--	--	--	--	--	--	--	--	--	--	--	--	--	--	--	--	--	--	--	--	--	--	--	--	--	--	--	--	--	--	--	--	--	--	--	--	--	--	--	--	--	--	--	--	--	--	--	--	--	--	--	--	--	--	--	--	--	--	--	--	--	--	--	--	--	--	--	--	--	--	--	--	--	--	--	--	--	--	--	--	--	--	--	--	--	--	--	--	--	--	--	--	--	--	--	--	--	--	--	--	--	--	--	--	--	--	--	--	--	--	--	--	--	--	--	--	--	--	--	--	--	--	--	--	--	--	--	--	--	--	--	--	--	--	--	--	--	--	--	--	--	--	--	--	--	--	--	--	--	--	--	--	--	--	--	--	--	--	--	--	--	--	--	--	--	--	--	--	--	--	--	--	--	--	--	--	--	--	--	--	--	--	--	--	--	--	--	--	--	--	--	--	--	--	--	--	--	--	--	--	--	--	--	--	--	--	--	--	--	--	--	--	--	--	--	--	--	--	--	--	--	--	--	--	--	--	--	--	--	--	--	--	--	--	--	--	--	--	--	--	--	--	--	--	--	--	--	--	--	--	--	--	--	--	--	--	--	--	--	--	--	--	--	--	--	--	--	--	--	--	--	--	--	--	--	--	--	--	--	--	--	--	--	--	--	--	--	--	--	--	--	--	--	--	--	--	--	--	--	--	--	--	--	--	--	--	--	--	--	--	--	--	--	--	--	--	--	--	--	--	--	--	--	--	--	--	--	--	--	--	--	--	--	--	--	--	--	--	--	--	--	--	--	--	--	--	--	--	--	--	--	--	--	--	--	--	--	--	--	--	--	--	--	--	--	--	--	--	--	--	--	--	--	--	--	--	--	--	--	--	--	--	--	--	--	--	--	--	--	--	--	--	--	--	--	--	--	--	--	--	--	--	--	--	--	--	--	--	--	--	--	--	--	--	--	--	--	--	--	--	--	--	--	--	--	--	--	--	--	--	--	----

FIG. 13. A comparison of the amino acid sequence of the rubredoxin from *P. furiosus* and those from anaerobic eubacteria. Abbreviations and sources of the data: Pf, *Pyrococcus furiosus* (144); Cpt, *Clostridium pasteurianum* (128, 129); Cpf, *Clostridium perfringens* (130); Cts, *Clostridium thermosaccharolyticum* (131); Cbt, *Chlorobium thiosulfatophilum* (132); DvH, *Desulfovibrio vulgaris* strain Hildenborough (133, 134); DvM, *Desulfovibrio vulgaris* strain Miyazaki (135); Dg, *Desulfovibrio gigas* (136); Dd, *Desulfovibrio desulfuricans* (137); Me, *Megasphaera elsdenii* (138); Pa, *Peptococcus aerogenes* (139); Bm, *Butyrivibacterium methylotrophicum* (140). Conserved cysteines are given in boldface letters; ↓ indicates residues (or lack of) unique to *P. furiosus* rubredoxin and ↑ indicates residues conserved in all known rubredoxins.

cal shifts of the cross-peaks in the two-dimensional NOESY (nuclear Overhauser effect) data that could be observed from the native protein matched those in the spectrum from the Zn protein, suggesting that Fe replacement by Zn produced minimal structural changes at the metal-binding site. This was expected since the backbone conformation of C-X-X-C-G sequence in the Zn domain of retroviral zinc finger proteins is virtually identical to the structure of the analogous residues in the Fe domain in mesophilic rubredoxins (150). Moreover, the preliminary NMR data of the Zn rubredoxin showed that its secondary structure is essentially the same as that of the rubredoxin from the mesophile, *C. pasteurianum*. These proteins have 60% sequence identity. Thus, both of these rubredoxins contain a similarly packed hydrophobic core, and a three-stranded antiparallel β sheet with several tight turns. Although the determination of the complete three-dimensional structure of *P. furiosus* rubredoxin is still underway, one potentially significant finding concerns the N terminus of the protein. As shown in Fig. 13, in contrast to all the other rubredoxins, the *P. furiosus* protein lacks an N-terminal methionine residue. The NMR data from *P. furiosus* Zn rubredoxin clearly show (144) that Ala 2 (which is the N terminus in the numbering system of Fig. 13) is part of the β sheet and its amino group interacts with the carboxyl groups of Glu 15 and Glu 53. Since, with one exception, the mesophilic rubredoxins have Pro at position 15, and all of them have an N-terminal methionine, the *P. furiosus* protein is uniquely able to generate such interactions. These may significantly stabilize one end of the β sheet and prevent its "unraveling" at extreme temperatures. Such an effect should be observed in variable high-temperature NMR studies of the *P. furiosus* protein, and these are in progress.

Finally, a word on the physiological role of rubredoxin in *P. furiosus*. Mesophilic rubredoxins have been suggested to function as electron carriers in the primary metabolic pathways of such diverse organisms as acetogenic (151, 152), methylotrophic (153), sulfate-reducing (135, 154), and nitrate-reducing (130) bacteria. On the other hand, a role for this protein has yet to be postulated in saccharolytic organisms, such as *C. pasteurianum*, *C. thermosaccharolyticum*, and *Megasphaera elsdenii*. This is of some relevance, since *P. furiosus* appears to grow by the fermentation of certain simple and complex carbohydrates to organic acids, CO₂, and H₂ (Ref. 19; see Section III,E). However, it is somewhat curious that the rubredoxins that have been purified are a remarkably homologous group of proteins, especially considering the range of metabolisms exhibited by the bacteria listed in Fig. 13. Moreover, they all have E_m values near 0 mV (at ambient temperature), and for the various

electron acceptor roles that have been suggested for this protein, it is far from clear what oxidizes reduced rubredoxin. Furthermore, in widely divergent species such as *P. furiosus* (a hyperthermophilic archaeobacterium) and, for example, *C. pasteurianum* (a mesophilic eubacterium), both of which are obligately dependent on the reduction of protons to H_2 for growth ($E_m = -420$ mV, 25°C), the role or even necessity of a rubredoxin ($E_m \sim 0$ mV, 25°C) is hard to rationalize. It may therefore be hypothesized that rubredoxin has the same physiological role in all of the anaerobic organisms listed in Fig. 13: that is, the fact that this protein is redox active may be merely fortuitous. For example, rubredoxin may be a storage form of Fe(II) with complete S ligation that is readily available for Fe-S cluster synthesis, or it may be a sensor of the availability of Fe(II) and play some regulatory role in anaerobic organisms. As yet, however, there is no evidence for these suggestions, although it should be mentioned that a ferredoxin has been postulated to regulate gene expression in response to cellular Fe(II) concentrations in the aerobic bacterium, *Azotobacter vinelandii* (155). In any event, the role of rubredoxin in *P. furiosus* is at present a mystery.

D. ALDEHYDE FERREDOXIN OXIDOREDUCTASE (W-Fe-S)

During our preliminary growth studies of *P. furiosus* it was found that the addition to the growth medium of W (in the form of tungstate) significantly stimulated cell growth (31). A red-colored, W-containing protein, abbreviated RTP for "red tungsten protein," was subsequently identified during the purification of *P. furiosus* hydrogenase and was purified under strictly anaerobic conditions to homogeneity (156). RTP is a monomeric protein of M_r 85,000 and contains approximately 1W, 7Fe, and $5S^{2-}$ atoms/mole. W is an element seldom used in biological systems; indeed, only one W-containing enzyme was previously known—a formate dehydrogenase purified from the acetogen, *C. thermoacetum*, by Ljungdahl and co-workers (157). However, *P. furiosus* RTP did not catalyze the oxidation of formate. Thus, there were obvious questions: what is the nature of the Fe and W in RTP, and what reaction does it catalyze? The following discussion shows how at least partial answers to these questions came from studies using electrochemistry and EPR spectroscopy.

RTP as isolated in dithionite-containing buffer has absorption throughout the visible region of the spectrum ($\Sigma_{425} = 8800 M^{-1} \text{cm}^{-1}$), with a broad feature near 540 nm (156). The protein turns green-brown in color when it is exposed to air or oxidized by ferricyanide. This is

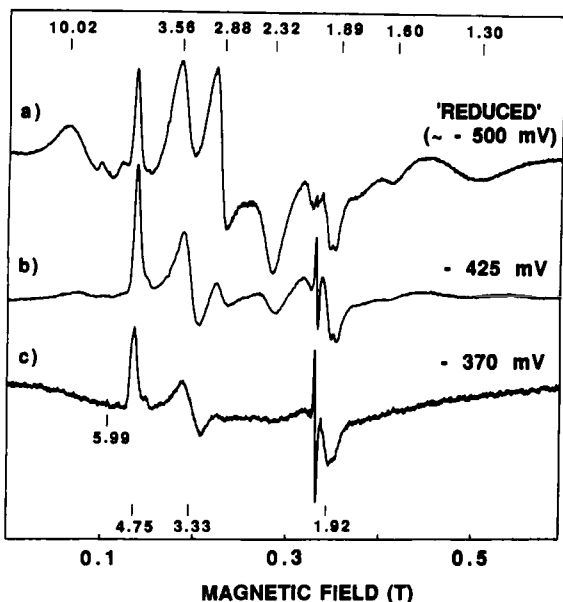


FIG. 14. EPR spectra of the red tungsten protein (RTP) of *P. furiosus*. The sample contained RTP (14 mg/ml) in 50 mM Tris/HCl buffer, pH 8.0, containing sodium dithionite (a) or poised at the indicated potential (b and c). The spectra were recorded at 6 K using 100-mW microwave power. The sharp isotropic signal at $g = 2$ in spectra b and c originates from redox mediators. Taken from Ref. 156.

accompanied by the loss of the 540-nm absorption and a large increase in the absorption near 400 nm ($\Sigma_{425} = 17,600 \text{ M}^{-1} \text{ cm}^{-1}$). Titrations show that the ferricyanide-oxidized protein is reduced by the equivalent of approximately 1.5 electrons/mole using sodium dithionite as the reductant (pH 8, 25°C), indicating that the protein contains two redox-active centers that are not completely reduced by sodium dithionite. The dithionite-reduced protein exhibits a remarkable EPR spectrum with g values ranging from 10.0 to 1.3 (Fig. 14), unlike that of any other biological or synthetic Fe-S system. The thionine-oxidized protein is EPR silent. Upon partial oxidation (to -370 mV , pH 8) of the dithionite-reduced protein ($\sim -500 \text{ mV}$), EPR from a single paramagnetic species with $S > \frac{1}{2}$ is observed (Fig. 14). These resonances can be interpreted using a spin Hamiltonian with an isotropic Zeeman interaction. For example, with $E/D = 0.135$, $D > 0$, and $g_0 = 2$, the $S = \frac{3}{2}$ spin Hamiltonian predicts $g(x, y, z) = 3.13, 4.75$, and 1.89 for the ground state doublet, values that are in reasonable agreement with the observed g

values of 3.33, 4.75, and 1.92. Theory also predicts $g(x, y, z) = 0.84$, 0.74, and 5.90 for the upper doublet. A minor resonance is observed at $g = 5.99$, and this is assigned to the excited doublet as its intensity increases with increasing temperature (≤ 10 K). Analysis of the temperature dependence of the intensity ratio of the $g = 4.75$ (lower) and $g = 5.99$ (upper) resonances indicated that $D = 4.3 \pm 0.5 \text{ cm}^{-1}$ (156).

One of the redox centers in RTP, which will be termed center A, therefore has a well-defined $S = \frac{3}{2}$ ground state. So, how does the complex spectrum of the dithionite-reduced protein arise? As shown in Fig. 14, upon reduction of partially oxidized RTP, the intensity of the EPR signal from reduced center A (A_{red}) increases in intensity before decreasing to that seen in the reduced sample. This suggests that the complex spectrum of the reduced protein is a result of the spin-spin interaction of A_{red} with a second but nonidentical paramagnetic species (center B). Center B has a slightly lower E_m value than center A, so that upon reduction of the oxidized protein, the spectrum of A_{red} is observed first. The EPR spectrum of B_{red} is not seen because as soon as this center is reduced, it interacts with A_{red} to give a complex EPR spectrum of the spin-coupled system. This spectrum dominates the EPR absorption of the dithionite-reduced protein, but this redox state of RTP also exhibits the EPR spectrum of the remaining A_{red} , i.e., that which is not interacting with B_{red} , as evidenced by the $g = 4.75$ resonance. Center A and the resultant spin-coupled system can therefore be differentiated potentiometrically. As will now be described, this enables the redox properties of center B to be evaluated, in spite of the fact that its EPR spectrum is not apparent.

The relative amounts of the oxidized and reduced forms of redox centers A and B can be calculated at a given potential using the Nernst equation [Eq. (1)], where n is the number of electron transfers (see, for example, Refs. 158 and 159). This simplifies to Eq. (2) for a one-electron

$$E_h = E_m + \frac{RT}{nF} \ln \frac{[\text{oxidized}]}{[\text{reduced}]} \quad (1)$$

$$E_h = E_m + 58.1 \log \frac{[\text{oxidized}]}{[\text{reduced}]} \quad (2)$$

transfer at 20°C (note that in temperature-dependent studies, the temperature term in the Nernst equation affects only the slope of the redox curve). The fractions of the centers in their reduced forms ($F_{A_{\text{red}}}$ and $F_{B_{\text{red}}}$) when the protein (P) is at a potential of E_h can be calculated by Eqs. (4) and (5), where E_{mA} and E_{mB} are their respective

$$F_{A_{\text{red}}} = [10^{(E_h - E_{mA})/\gamma} + 1]^{-1} \quad (4)$$

$$F_{B_{\text{red}}} = [10^{(E_h - E_{mB})/y} + 1]^{-1} \quad (5)$$

midpoint potentials (see Ref. 160). Let the fraction of the protein in the oxidized state, i.e., with neither center reduced, be P^0 , that with only one of the two centers reduced be P^- , and that with both reduced be P^{2-} . The fractions of the total protein in these two redox states at a given potential can be calculated by Eqs. (6) and (7). The singly reduced

$$[P^0] = (1 - F_{A_{\text{red}}})(1 - F_{B_{\text{red}}}) \quad (6)$$

$$[P^{2-}] = F_{A_{\text{red}}} F_{B_{\text{red}}} \quad (7)$$

protein (P^-) can exist in two different redox states, where each has only one of the two centers reduced ($A_{\text{red}} \cdot B_{\text{ox}}$ and $A_{\text{ox}} \cdot B_{\text{red}}$). Let the fraction of the protein that has only center A reduced be P_A^- ($A_{\text{red}} \cdot B_{\text{ox}}$), and that with only center B reduced be P_B^- ($A_{\text{ox}} \cdot B_{\text{red}}$). Equations (8) and (9) show how their concentrations may be determined.

$$[P_A^-] = 1 - (F_{A_{\text{red}}} F_{B_{\text{red}}}) - (1 - F_{A_{\text{red}}}) = F_{A_{\text{red}}}(1 - F_{B_{\text{red}}}) \quad (8)$$

$$[P_B^-] = 1 - (F_{A_{\text{red}}} F_{B_{\text{red}}}) - (1 - F_{B_{\text{red}}}) = F_{B_{\text{red}}}(1 - F_{A_{\text{red}}}) \quad (9)$$

With *P. furiosus* RTP, the concentration $[P^{2-}]$ of the doubly reduced protein can be measured by the amplitude of the $g = 2.88$ EPR signal (Fig. 14), whereas the fraction of the protein with only center A reduced, $[P_A^-]$, is proportional to the intensity of the $g = 4.75$ resonance. Figure 15 shows the results of a redox titration performed at 20°C and pH 8.0. The theoretical plots are calculated using E_m values for center A and center B of -410 mV and -500 mV, respectively. The data clearly correspond to the predicted redox behavior for two interacting centers, with the intensity of the $g = 4.75$ resonance rising and falling as the potential decreases. This type of theoretical analysis predicts that a maximum of only 2.1% of the protein has only center B reduced (at -455 mV), hence, it is unlikely that its EPR signal would be observed. Figure 15 also shows that the apparent E_m value (at pH 8.0) of the doubly reduced protein ($A_{\text{red}} \cdot B_{\text{red}}$) is -505 mV, and at this potential most of the remaining protein has only center A reduced (47%). Thus, at the potential usually obtained using sodium dithionite as the reductant (~ -500 mV at pH 8.0), the protein is reduced by 1.5 electrons/mole, in agreement with the visible absorption data described above (156). The effective reducing potential of sodium dithionite decreases with increasing pH (161) so that at pH 9.0 the protein is reduced to a greater extent than it is at pH 8.0 (Fig. 15). However, the E_m values of center

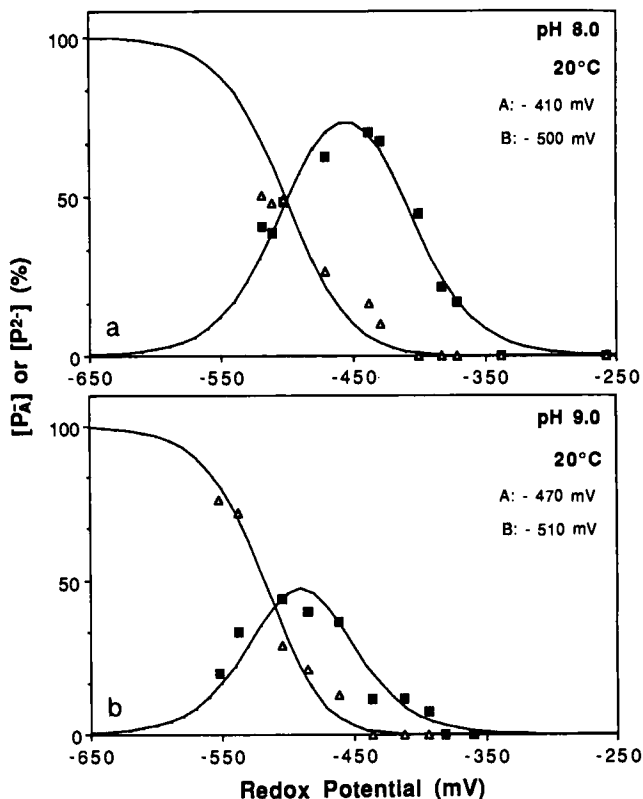
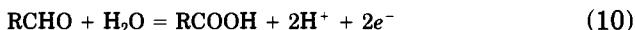


FIG. 15. Determination of the redox behavior of center A and center B in the tungsten protein (RTP) of *P. furiosus*. Redox titrations of RTP were carried out at 20°C at pH 8.0 (a) and pH 9.0 (b). [P²⁻] (open triangles) is the concentration of the doubly reduced protein ($A_{\text{red}} \cdot B_{\text{red}}$) as measured by the amplitude of the $g = 2.88$ signal shown in Fig. 14. [P_A⁻] (closed squares) is the concentration of the protein with only center A reduced ($A_{\text{red}} \cdot B_{\text{ox}}$) as measured by the amplitude of the $g = 4.75$ resonance (Fig. 14). The theoretical curves were calculated as described in the text using the indicated E_m values for the two redox centers. Modified from Ref. 156.

A and center B also decrease with increasing pH (>8.0), so the protein cannot be fully reduced with sodium dithionite even at pH 10. Such a pH dependence also indicates that a proton is involved in the reduction and oxidation of each center. In addition, the E_m values of centers A and B decrease with increasing temperature ($\Delta E_m/\Delta T \sim -2 \text{ mV}/^\circ\text{C}$ at pH 8.0 for both centers). At 100°C, the optimum growth temperature of *P. furiosus*, the E_m values are estimated at -590 mV (A) and -650

mV (B), values that are more than 150 mV lower than those determined at ambient temperature (156).

Analyses using visible absorption spectroscopy show that reduced RTP transfers electrons to *P. furiosus* ferredoxin ($E_m \leq -550$ mV at 100°C) but not to NAD(P) (156). It was therefore postulated (156) that RTP catalyzes an oxidoreductase-type reaction of extremely low potential (≤ -500 mV), in which the mechanism involves the transfer of two protons and two electrons, and ferredoxin serves as the electron donor. The problem is that few biochemical reactions take place at such low potentials, and RTP did not catalyze the oxidation of obvious substrates such as (the potentials are quoted at 20°C, pH 7, taken from Ref. 162) CO (to CO₂, $E_m = -510$ mV), pyruvate (to acetyl-CoA, $E_m = -520$ mV), or 2-ketoglutarate (to succinyl-CoA, $E_m = -520$ mV). However, RTP does catalyze a rather unusual reaction: the oxidation of aldehydes to the corresponding acid [Eq. (10)]. The aldehyde/acid redox couple has a midpoint of around -560 mV (163), so this reaction is consistent with the conclusions from the spectroscopic analyses. RTP is therefore now termed aldehyde ferredoxin oxidoreductase, or AOR (164). The likely physiological substrate for AOR is discussed in Section III.E.



We now turn to the nature of the redox centers in AOR and the source of the novel EPR signals shown in Fig. 14. The striking similarity of the EPR properties of reduced center A to those of synthetic [W-3Fe-4S] and [Mo-3Fe-4S] clusters (91, 126), all of which have $S = \frac{3}{2}$ ground states, led to the proposal that center A might be a [W-3Fe-4S] cluster (156). However, a recent study of dithionite-reduced AOR by extended X-ray absorption fine structure (EXAFS) spectroscopy (165) showed that this is not the case: no W-Fe interactions were observed in the W L_{III} edge EXAFS. AOR therefore contains a monomeric W site. The best fits for the data were obtained using two W=O at 1.74 Å, three W-S at 2.41 Å, and one W-O/N at 2.16 Å. The presence of the two oxo ligands and nature of the absorption edge spectrum showed that the W is present as W(VI), even though the sample contained sodium dithionite (165). The potential of the W(VI)/W(V) couple is therefore likely to be much less than -500 mV (at 25°C), which would be consistent with the aldehyde/acid redox couple. A mononuclear Mo(VI) center has been identified in a variety of molybdenum enzymes, in which it is bound to a pterin cofactor (see Refs. 166 and 167 and references therein). Indeed, the number and distances of the ligands to the Mo in, for example, sulfite oxidase (168), one of the best studied of the molybdopterin enzymes, are virtually identical to

those just described for W in AOR. Moreover, fluorescence spectroscopy of AOR after acid treatment shows that it contains a pterin-type cofactor that is similar, although not identical, to molybdopterin (164). A proposed structure of the W site in AOR is given in Fig. 16. By analogy with the molybdopterin-containing enzymes, the W site in AOR is probably reduced to the V and IV states during the catalytic cycle. It should therefore be possible to induce a transient W(V) EPR signal from AOR upon treatment with substrates. Since AOR is unaffected by a 6-hr incubation at 80°C, is virtually inactive at ambient temperature, and the optimum temperature for catalytic activity is $\geq 95^\circ\text{C}$ (164), it is well suited for the isolation of transient intermediates. Such "cryoenzymological" studies at 4–20°C, which approach 100°C below the optimum temperature for both catalysis and cell growth, are underway.

Since the III and V valence states of W are paramagnetic, the identification of a mononuclear W(VI) site in dithionite-reduced AOR rules out the possibility of W contributing to the EPR absorption. The EPR spectra shown in Fig. 14 must therefore arise from Fe–S centers. Several biological $[4\text{Fe}-4\text{S}]^{1+}$ clusters, including that in *P. furiosus* ferredoxin, are now known to exist in an $S = \frac{3}{2}$ spin state (although all are as mixtures of $S = \frac{1}{2}$ and $S = \frac{3}{2}$; see Section III,2,a,1). Considering the metal content of AOR (~ 7 Fe atoms/mole), it is not unreasonable to suggest that center A ($S = \frac{3}{2}$) is a $[4\text{Fe}-4\text{S}]^{1+}$ cluster. This would be the first example of a biological 4Fe cluster with a ground state spin of exclusively $S = \frac{3}{2}$. As for center B in AOR, the EPR analyses show only that it is paramagnetic in the reduced state ($S \geq \frac{1}{2}$), and the Fe content of the enzyme is consistent with it being either a 2Fe- or a 4Fe-type center. However, preliminary data from resonance Raman indicate that AOR contains only 4Fe-type centers (W. Fu and M. K. Johnson, unpublished data, 1991). The unusual EPR properties of reduced AOR are therefore proposed to arise from two spin-coupled 4Fe centers, one $S = \frac{3}{2}$ and one $S \geq \frac{1}{2}$, that have different midpoint potentials. As shown

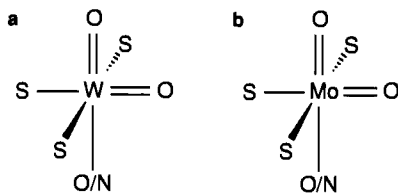


FIG. 16. Proposed structure of (a) the W site in dithionite-reduced aldehyde ferredoxin oxidoreductase of *P. furiosus* (165) and (b) the Mo site in oxidized mammalian sulfite oxidase (168).

Pyrococcus furiosus AOR is therefore a unique type of Fe-S-containing enzyme, although some fundamental properties of its Fe-S clusters, such as the spin state and EPR spectrum of center B, are not known at present. AOR is also the first aldehyde-oxidizing enzyme to be isolated from any archaeobacterium or any extreme thermophile, and is the first CoA-independent aldehyde oxidoreductase from a nonacetogenic anaerobe.

Pyrococcus furiosus AOR catalyzes the oxidation of a wide range of aldehydes, e.g., acetaldehyde, propionaldehyde, crotonaldehyde and glyceraldehyde, to the corresponding acid, using either methyl viologens or *P. furiosus* ferredoxin, but not NAD(P), as the electron acceptor. It does not oxidize glucose, glyoxylate, or glyceraldehyde-3-phosphate (164). So, why does *P. furiosus* need an enzyme that oxidizes aldehydes, and need it at very high cellular concentrations (at least five times that of the hydrogenase)? The organism obtains energy for growth by the fermentation of carbohydrates to organic acids, CO₂, and H₂. One would expect the organism to use the Embden–Meyerhof pathway for converting glucose ultimately to acetate, as do saccharolytic, anaerobic eubacteria (162). However, this pathway does not require an enzyme that oxidizes aldehydes, and the activities of key enzymes such as glyceraldehyde-3-phosphate dehydrogenase and phosphoglycerate ki-

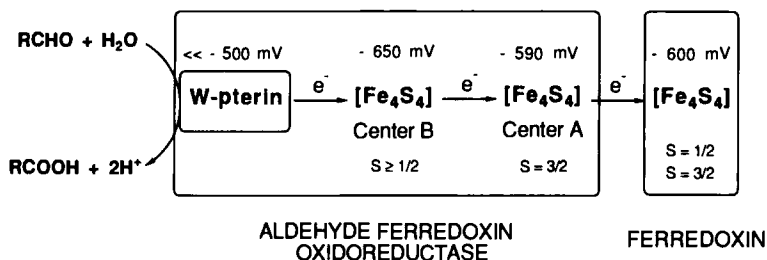


FIG. 17. Proposed redox centers and pathway of electron transfer at 100°C during aldehyde oxidation by aldehyde ferredoxin oxidoreductase of *P. furiosus*. The spin states of the 4Fe clusters in aldehyde ferredoxin oxidoreductase and ferredoxin and the redox potentials of all redox centers (estimated at 100°C) are indicated.

nase are present in *P. furiosus* at relatively low levels (164). We therefore proposed (164) that *P. furiosus* has a novel pathway for oxidizing glucose. It is analogous to the NAD(P)-dependent pathway thought to occur in some aerobic archaebacteria (169–171), but differs in that all the oxidation steps needed to convert glucose to acetate are catalyzed by ferredoxin-linked oxidoreductases. As shown in Fig. 18, AOR is

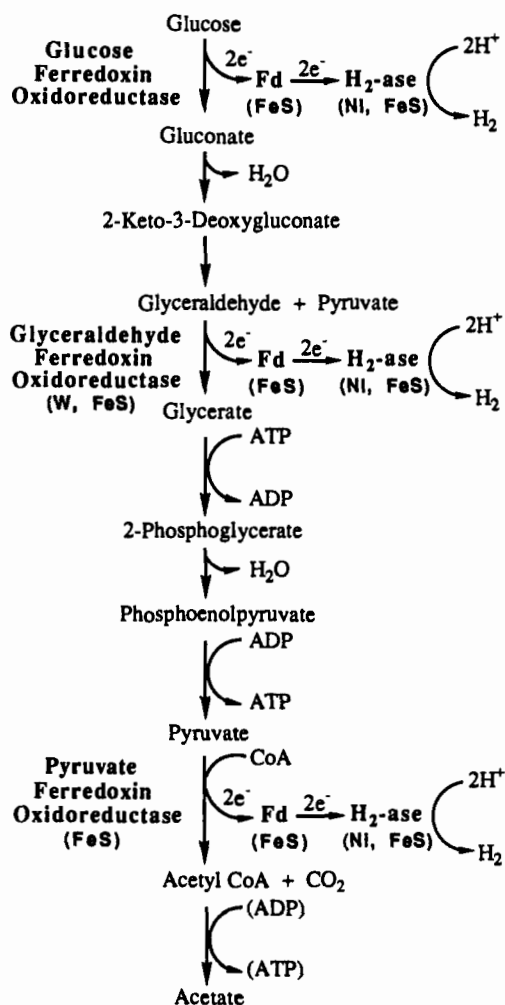


FIG. 18. Proposed "pyroglycolytic" pathway in *P. furiosus* and the role of Fe-S-containing proteins. Modified from Ref. 164.

proposed to catalyze a key step in the "pyroglycolytic" pathway—it functions as a glyceraldehyde ferredoxin oxidoreductase and converts glyceraldehyde to glycerate. The first step in the pathway is catalyzed by another new enzyme, glucose ferredoxin oxidoreductase (GOR), which generates gluconate from glucose. The final oxidation step is catalyzed by a more conventional pyruvate ferredoxin oxidoreductase (POR), yielding acetyl-CoA. Since ferredoxin is the physiological electron donor for *P. furiosus* hydrogenase, its use as an electron acceptor for each of these oxidoreductases enables the reductant generated from glucose oxidation to be directly removed as H_2 , via the hydrogenase.

A unique consequence of the proposed pyroglycolytic pathway for H_2 production is that *P. furiosus* could generate acetyl-CoA from glucose without the participation of NAD(P)H. These cofactors are particularly thermolabile (172), and their replacement in a primary metabolic pathway by a thermostable ferredoxin may be one of the key adaptations that enables this organism to grow at temperatures in excess of 100°C. In addition, the proposed pathway may not be limited to *P. furiosus*. We have found that the growth of two other heterotrophic and extremely thermophilic archaeobacteria, ES-4 (25), which grows up to 100°C, and *Thermococcus litoralis* (22), which grows up to 98°C, is also stimulated by tungsten. Moreover, cell extracts of these organisms contain high aldehyde oxidoreductase activity (S. Mukund and M. W. W. Adams, unpublished data, 1991). It will be of interest to characterize these enzymes and see how they compare with the AOR of *P. furiosus*.

As indicated in Fig. 18, all but one of the proteins involved in redox reactions in the proposed "pyroglycolytic" pathway of *P. furiosus* have been shown to contain Fe-S clusters. The properties of the hydrogenase, ferredoxin, and AOR have been described. In addition, POR has recently been purified from *P. furiosus* under strictly anaerobic conditions (J. Blamey and M. W. W. Adams, unpublished data, 1991). It is a trimeric protein ($\alpha\beta\gamma$, M_r 93,000) and contains approximately 8Fe atoms/mole. No other metals, including W, could be detected. EPR analysis of reduced POR indicates the presence of two $[4Fe-4S]^{1+}$ clusters, one of which has an $S = \frac{3}{2}$ ground state. The enzyme has half-life in air of about 15 min, and its optimum temperature for catalysis is above 90°C. POR has also been purified from several mesophilic organisms (173–178). In contrast to *P. furiosus* POR, these all have molecular weights of near 250,000 (usually as an α_2 dimer) and contain two or four $S = \frac{1}{2} [4Fe-4S]^{1+}$ clusters. Whether the other oxidoreductase in the glycolytic pathway shown in Fig. 17, GOR, is also an Fe-S enzyme is not known at present.

IV. *Thermotoga maritima*

Thermotoga maritima is the most thermophilic eubacterium currently known. It was isolated by Stetter and co-workers from geothermally heated marine sediments in 1986 (7). The genus represents the oldest and most slowly evolving branch within the eubacterial kingdom (8, 9). The organism is a strict anaerobe and grows at temperatures up to 90°C by the fermentation of both simple and complex carbohydrates. It produces organic acids, CO₂, and H₂, and, like *P. furiosus*, appears to use the reduction of S⁰ to H₂S as a means of removing H₂ rather than as a means of energy conservation. In our initial studies with this bacterium, we found that cell yields were increased twofold by the presence of additional Fe and of tungstate (10 μM) in the growth medium (32). The addition of salts of V, Cs, F, Pb, Rb, or Si, and increased amounts (>10 μM) of Ni, Mo, Se, Co, or Mn do not stimulate growth. In other words, W and Fe appear to have a similar effect on the growth of *T. maritima* as they do on *P. furiosus*. However, as will now be discussed, the role of these elements in the production of H₂ by *T. maritima* is quite different from what has been described in previous sections for *P. furiosus*.

A. HYDROGENASE (Fe-S)

Thermotoga maritima contains a single hydrogenase located in the cytoplasm. It is routinely purified from cells grown in the presence of W (see Section IV,B) and absence of S⁰ (32). The enzyme is very unstable in cell-free extracts at both 4 and 23°C, even under anaerobic and reducing conditions, and must be purified using buffers containing glycerol (10%, v/v) and dithiothreitol (2 mM) to prevent substantial losses in catalytic activity. The pure enzyme is a homotetramer (α₄) with a molecular weight of about 280,000. It is extremely sensitive to inactivation by O₂, having a half-life in air of 10 sec. It contains approximately 20 Fe and 18 S²⁻ atoms per monomer (M_r 68,000). Other metals, including Ni (and also Se), are present in only trace amounts. To date, hydrogenases lacking Ni have been purified and well characterized only from some mesophilic anaerobic bacteria. They are from the fermentative organisms, *C. pasteurianum*, in which two different Fe hydrogenases (termed I and II) are present (179–183), and *M. elsdenii* (184–187), and from the mesophilic sulfate reducer, *Desulfovibrio vulgaris* (33, 188–192). These are also soluble enzymes with molecular weights around 60,000, comparable to that of the monomer of the *T. maritima* enzyme, and in their active states they are also extremely

TABLE I
PROPERTIES OF Fe HYDROGENASES

	Source of hydrogenase ^a				
	Tm	Cp I	Cp II	Me	Dv
Molecular weight	280,000	62,000	54,000	58,000	55,820
Subunits:	4 × 68,000	—	—	—	1 × 45,820, 1 × 10,000
V_m , H ₂ evolution ^b	164 (80°C)	5500	10	7000	10,400
V_m , H ₂ oxidation ^c	180 (80°C)	24,000	34,000	9,000	50,000
Fe/mole ^d	20	20	14	13–18	9–15
S ²⁻ /mole ^d	18	18	11	16	13
Fe-S clusters ^d					
4Fe type					
($S = \frac{1}{2}$)	1	3	2	2	2
($S \geq \frac{3}{2}$)	1	1	—	—	—
2Fe type	2	—	—	—	—
Fe/mole available for the H cluster ^d	8	4	6	5–10	1–7
Ref.	32	67, 179, 181, 183	180–183	184–184	188–192

^a Abbreviations: Tm, *T. maritima*; Cp I, hydrogenase I from *C. pasteurianum*; Cp II, hydrogenase II from *C. pasteurianum*; Me, *Megasphaera elsdenii*; Dv, *Desulfovibrio vulgaris* (strain Hildenborough).

^b Expressed as micromoles of H₂ evolved/min/mg using dithionite-reduced methyl viologen as electron donor.

^c Expressed as micromoles of H₂ oxidized/min/mg using methylene blue or benzyl viologen as the electron acceptor.

^d Expressed per monomer for the *T. maritima* enzyme.

sensitive to inactivation by O₂. However, as might be expected, *T. maritima* Fe hydrogenase is much more thermostable. Its optimum temperature for H₂ production is above 95°C and it has a half-life at 90°C of about 1 hr. In contrast, the mesophilic enzymes denature in minutes at 70°C.

As shown in Table I, a major difference between the *T. maritima* and mesophilic Fe enzymes lies in their catalytic activities. The latter exhibit extremely high rates of H₂ oxidation and H₂ evolution in *in vitro* assays (the exception is H₂ evolution by *C. pasteurianum* hydrogenase II), and these are one to two orders of magnitude greater than those of the *T. maritima* enzyme, even at 80°C. In fact, the catalytic activities of *T. maritima* hydrogenase more resemble those of a Ni-Fe hydrogenase. In addition, the *T. maritima* enzyme shows "mixed" inhibition properties. It is as sensitive to inhibition by CO as the other Fe

hydrogenases ($K_i \leq 1 \mu M$), but like Ni-Fe hydrogenases, *T. maritima* hydrogenase is insensitive to inhibition by nitrite (10 mM) but is inhibited by acetylene ($t_{1/2} \sim 20$ min under 1 atm C_2H_2). The mesophilic Fe enzymes are inhibited by nitrite ($K_i = 3 \mu M$) but are unaffected by acetylene. A further difference between the *T. maritima* and mesophilic Fe hydrogenases lies in their physiological electron carriers. The hydrogenases of *C. pasteurianum* (I) and *M. elsdenii* evolve H_2 during cell growth and accept electrons from reduced ferredoxin *in vivo* (179, 185). In light of this, we recently purified a ferredoxin from *T. maritima* (J. Blamey and M. W. W. Adams, unpublished, 1991). Preliminary data indicate that it has a molecular weight of around 6000 and contains a single cluster. However, it did not serve as an electron donor to *T. maritima* hydrogenase in *in vitro* H_2 evolution assays, and the natural electron carrier for the enzyme is unknown.

As indicated in Table I, the Fe-S content of *T. maritima* hydrogenase (per monomer) is comparable to what has been reported for the other Fe hydrogenases. However, in contrast to the mesophilic enzymes, *T. maritima* hydrogenase in its reduced state exhibits EPR signals at high temperatures (60 K; see Fig. 19). A power saturation study showed that these resonances arise from two different species (32), and from their spin content, g values, and relaxation properties, they are assigned to two different $S = \frac{1}{2}$ $[2Fe-2S]^{1+}$ clusters. Additional resonances are observed when the temperature is reduced to 10 K (Fig. 19) and these arise from at least one $S = \frac{1}{2}$ $[4Fe-4S]^{1+}$ cluster. EPR is also observed from reduced *T. maritima* hydrogenase at low field and low temperature (Fig. 19). The major feature at $g = 5.7$ most likely originates from an $S = \frac{3}{2}$ $[4Fe-4S]^{1+}$ cluster, but the g values and temperature dependence of other resonances are inconsistent with an isolated $S = \frac{3}{2}$ system (for discussion, see Ref. 32). The EPR data therefore indicate that *T. maritima* hydrogenase contains two 4Fe centers, one $S = \frac{1}{2}$ and one in two or more spin states ($S \geq \frac{3}{2}$), in addition to two 2Fe centers. The E_m values (pH 8.0, 20°C) of the 2Fe- and 4Fe-type clusters are -440 and -390 mV, respectively. Ferredoxin-type 2Fe clusters are not present in the mesophilic Fe hydrogenases: they all contain $S = \frac{1}{2}$ $[4Fe-4S]$ clusters (*C. pasteurianum* hydrogenase I also has one $S = \frac{3}{2}$ 4Fe cluster; Ref. 67).

As mentioned in Section III,A, the site of H_2 oxidation and H_2 evolution in the mesophilic Fe hydrogenases is thought to be a novel Fe-S cluster, termed the H cluster (for review, see Ref. 38). Of unknown structure, it contains at least three and possibly six Fe atoms (38, 183). It has an E_m value of -400 mV (pH 8.0), is diamagnetic ($S = 0$) in the reduced state, and in the oxidized state ($S = \frac{1}{2}$) exhibits a characteristic

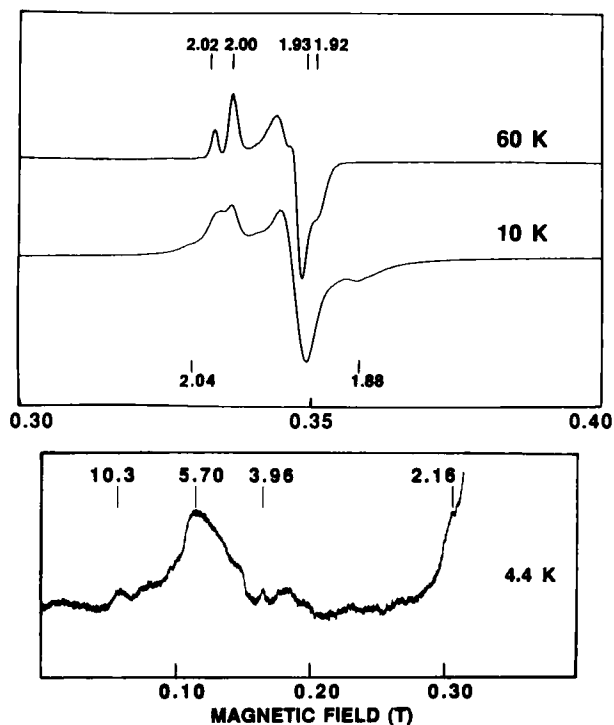


FIG. 19. EPR spectra of the Fe hydrogenase of *T. maritima*. The hydrogenase (10 mg/ml) was reduced with sodium dithionite (2 mM). Spectra were recorded at 4.4, 10, and 60 K as indicated using microwave power of 10 mW (upper panel) and 50 mW (lower panel: relative gain, times 40). Modified from Ref. 32.

rhombic EPR signal with $g_{av} > 2$. However, *T. maritima* hydrogenase in its oxidized state is EPR silent, and no EPR signals in addition to those of the ferredoxin-type centers are apparent during a redox titration (32). This was very surprising considering that the 4Fe and 2Fe centers in this enzyme account for only 12 iron atoms/monomer. This leaves up to 8 iron atoms/mole for an H cluster, but the remaining iron in *T. maritima* hydrogenase is not detectable by EPR spectroscopy. When one also considers the differences between the *T. maritima* enzyme and the mesophilic Fe hydrogenases in their catalytic activities and sensitivity to inhibitors (Table I), these data suggest that *T. maritima* hydrogenase has a catalytic Fe-S cluster that is different from the H cluster of the mesophilic enzymes. Why this site is EPR silent, however, remains to be established. It is relevant to mention that a

puzzling property of the mesophilic Fe enzymes is that, when oxidized, they give rise to paramagnetic MCD bands that arise from a center with an $S > \frac{1}{2}$ ground state, even though the only paramagnet detectable by EPR and Mössbauer spectroscopy is the $S = \frac{1}{2}$ oxidized H cluster (38, 67). Preliminary MCD studies of the oxidized *T. maritima* enzyme show that it also exhibits paramagnetic MCD (R. C. Conover, A. Juszczak, M. W. W. Adams, and M. K. Johnson, unpublished data, 1991). This suggests a possible relationship between its H_2 -activating center and the H cluster of the mesophilic enzymes. In addition, as already discussed (Section III,B,3), the H cluster of *C. pasteurianum* hydrogenase I has substantial noncysteinyll (nitrogenous) coordination (97). The finding of much less cysteine (12 per monomer) than iron in *T. maritima* hydrogenase suggests that this may also be the case for the H cluster of this enzyme.

B. ROLE OF TUNGSTEN

The presence of W in the growth medium of *T. maritima* was found to increase both the cellular concentration of the hydrogenase in cell-free extracts, and also its catalytic activity *in vitro* (32). For example, cells from W-supplemented media yield approximately 200 mg of pure hydrogenase/kg (wet weight), and the enzyme has a specific activity in the standard H_2 evolution assay of ≥ 50 units/mg. If W is omitted, the yield drops to around 100 mg/kg, and the specific activity of the final preparation is at least an order of magnitude lower, usually around 4 units/mg. However, there are no detectable differences in the physical properties of the two types of hydrogenases (from cells with and without W). That is, the EPR properties (both oxidized and reduced) and the Fe and S^{2-} content of the hydrogenase from cells grown without added W are the same as those of the enzyme described in Section III,A. It is possible that the H_2 -activating Fe-S center is quite different in these two forms of *T. maritima* hydrogenase, but since this cluster is not detectable by EPR spectroscopy, other techniques such as Mössbauer spectroscopy will be needed to determine if this is the case.

These results suggest that W directly influences both the amount of hydrogenase in *T. maritima* cells and the integrity of its catalytic Fe-S cluster, and lead to the obvious question: why, and what is the role of W in this organism? Like *P. furiosus*, *T. maritima* grows by fermenting carbohydrates and evolving H_2 , and the likely answer is that it contains a W-dependent glycolytic pathway analogous to that shown in Fig. 18. However, this is not the case, as *T. maritima* does not contain detectable aldehyde (or glucose) oxidoreductase activity (32). W could well be a

component of a key enzyme in yet another version of an H_2 -evolving glycolytic pathway, and its effect on *T. maritima* hydrogenase would be consistent with this. At present though, the function of W in the metabolism of *T. maritima* is a mystery.

Finally we turn to the question of why extremely thermophilic archaeobacteria, such as *P. furiosus*, *T. litoralis*, and "ES-4," and the most thermophilic eubacterium currently known, *T. maritima*, depend upon W for optimal growth, when the rest of the microbial world, indeed, the rest of biology, uses Mo as a key component of the active sites of a wide variety of important enzymes (e.g., Refs. 166, 167, and 193). In fact, since extreme thermophily is regarded as an ancient phenotype (8, 9), one could speculate that the earliest life forms were not only extremely thermophilic, they were also W-dependent organisms. Presumably, they then evolved into the mesophilic, Mo-dependent species that now overwhelmingly predominate. As to the W requirement, it is possible that W but not Mo is present in the environments in which extreme thermophilic organisms are found, such as near deep-sea hydrothermal vents. Alternatively, W may be easier to stabilize at extreme temperatures in the oxidation states and at the redox potentials required to catalyze biologically relevant reactions. However, as yet there is no experimental evidence to support either of these possibilities.

V. Summary

In this article the properties of some of the Fe-S enzymes and proteins involved in the production of H_2 by some extremely thermophilic bacteria have been described. The hyperthermophilic archaeobacterium, *P. furiosus*, which grows optimally at 100°C, contains an extremely thermostable Ni-Fe hydrogenase that is uniquely primed to catalyze the physiological reaction, H_2 production. Its active site Ni appears to be redox active only at high temperatures, whereas the redox properties of its 2Fe and 4Fe clusters seem insensitive to temperature. The physiological electron donor for this hydrogenase is an extremely thermostable 4Fe ferredoxin. The lack of complete cysteinyl coordination to its cluster enables other ligands to bind to the unique Fe site, the facile removal of this Fe atom, and its replacement with other metal ions, in particular Ni. Such [M-3Fe-4S] clusters in an extremely stable protein may prove to be useful models for the catalytic sites of several Fe-S enzymes. Tungsten, an element seldom used in biology, stimulates the growth of *P. furiosus*, and from it a novel tungstopterin-containing Fe-S enzyme has been characterized. The enzyme exhibits unique EPR

properties that arise from the spin coupling of two nonidentical Fe-S centers, and it is proposed to function as a glyceraldehyde ferredoxin oxidoreductase in a new glycolytic pathway. A unique aspect of this pathway, which appears also to be present in other extremely thermophilic archaebacteria, is that glucose can be oxidized to acetate without the participation of thermolabile nicotinamide nucleotides. An extremely thermostable rubredoxin has also been purified from *P. furiosus*. Preliminary NMR studies of the Zn-substituted protein is currently providing the first insights into the mechanisms of protein "hyperthermostability." The production of H_2 by the most thermophilic eubacterium currently known, *T. maritima*, is catalyzed by a new type of "Fe-only" hydrogenase. This differs from mesophilic Fe hydrogenases in its low catalytic activity, its sensitivity to inhibitors, its physiological electron carrier, and in the presence of 2Fe centers. It appears to contain a new type of Fe-S center for catalyzing H_2 production. The activity and cellular concentration of the hydrogenase in *T. maritima* is increased by the presence of W in the growth medium. However, this organism lacks the W-dependent "pyroglycolytic" pathway found in *P. furiosus*, and the role of W in its metabolism is unknown.

ACKNOWLEDGMENTS

I am indebted to the following persons for their contributions to much of the work described here and for many helpful discussions: Drs. M. K. Johnson, M. F. Summers, G. N. George, R. C. Prince, E. P. Day, J. B. Howard, B. M. Hoffman, and E. Münck. Research carried out in the author's laboratory was supported by grants from the Department of Energy, the Office of Naval Research, and the National Science Foundation.

REFERENCES

1. Stetter, K. O., in "The Thermophiles" (T. D. Brock, ed.), p. 39. Wiley, New York, 1986.
2. Kelly, R. M., and Deming, J. W., *Biotech. Prog.* **4**, 47 (1988).
3. Stetter, K. O., Fiala, G., Huber, G., Huber, R., and Segerer, G., *FEMS Microbiol. Rev.* **75**, 117 (1990).
4. Adams, M. W. W., *FEMS Microbiol. Rev.* **75**, 219 (1990).
5. Wiegel, J. K. W., and Ljungdahl, L. G., *Crit. Rev. Biotechnol.* **3**, 39 (1986).
6. Stetter, K. O., *Nature (London)* **300**, 258 (1982).
7. Huber, R., Langworthy, T. A., König, H., Thomm, M., Woese, C. R., Sleytr, U. B., and Stetter, K. O., *Arch. Microbiol.* **144**, 324 (1986).
8. Woese, C. R., Kandler, O., and Wheelis, M. L., *Proc. Natl. Acad. Sci. U.S.A.* **87**, 4576 (1990).

9. Woese, C. R., *Microbiol. Rev.* **51**, 221 (1987).
10. Stetter, K. O., and Zillig, W., in "The Bacteria" (C. R. Woese and R. S. Wolfe, eds.), Vol. 8, p. 85. Academic Press, New York, 1985.
11. Fiala, G., Stetter, K. O., Jannasch, H. W., Langworthy, T. A., and Madon, J., *Syst. Appl. Microbiol.* **8**, 106 (1986).
12. Jannasch, H. W., Wirsén, C. O., Molyneaux, S. J., and Langworthy, T. A., *Appl. Environ. Microbiol.* **54**, 1203 (1988).
13. Zillig, W., Gierl, S., Schreiber, G., Wunderl, S., Janekovic, D., Stetter, K. O., and Klenk, H. P., *Syst. Appl. Microbiol.* **4**, 79 (1983).
14. Huber, R., Kristjansson, J. K., and Stetter, K. O., *Arch. Microbiol.* **149**, 95 (1987).
15. Segerer, A., Neuner, A., Kristjansson, J. K., and Stetter, K. O., *Int. J. Syst. Bacteriol.* **36**, 559 (1986).
16. Zillig, W., Yeats, S., Holz, I., Böck, A., Rettenberger, M., Gropp, F., and Simon, G., *Syst. Appl. Microbiol.* **8**, 197 (1986).
17. Stetter, K. O., König, H., and Stackebrandt, E., *Syst. Appl. Microbiol.* **4**, 535 (1983).
18. Pley, U., Schipka, J., Gambacorta, A., Jannasch, H. W., Fricke, H., Rachel, R., and Stetter, K. O., *Syst. Appl. Microbiol.* **14**, 245 (1991).
19. Fiala, G., and Stetter, K. O., *Arch. Microbiol.* **145**, 56 (1986).
20. Zillig, W., Holz, I., Klenk, H.-P., Trent, J., Wunderl, D., Janekovic, D., Imsel, E., and Hass, B., *Syst. Appl. Microbiol.* **9**, 62 (1987).
21. Zillig, W., Holtz, I., Janekovic, D., Schafer, W., and Reiter, W. D., *Syst. Appl. Microbiol.* **4**, 88 (1983).
22. Neuner, A., Jannasch, H., Belkin, S., and Stetter, K. O., *Arch. Microbiol.* **153**, 205 (1990).
23. Zillig, W., Holz, I., and Wunderl, S., *Int. J. Syst. Bacteriol.* **41**, 169 (1991).
24. Pledger, R. J., and Baross, J. A., *Syst. Appl. Microbiol.* **12**, 249 (1989).
25. Pledger, R. J., and Baross, J. A., *J. Gen. Microbiol.* **137**, 203 (1990).
26. Huber, R., Kurr, M., Jannasch, H. W., and Stetter, K. O., *Nature (London)* **342**, 833 (1989).
27. Jones, W. J., Leigh, J. A., Moyer, F., Woese, C. R., and Wolfe, R. S., *Arch. Microbiol.* **136**, 254 (1983).
28. Stetter, K. O., Thomm, M., Winter, J., Wildegruber, G., Huber, H., Zillig, W., Janekovic, D., König, H., Palm, P., and Wunderl, S., *Zbl. Bakt. Hyg., I Abt. Orig. C2*, 166 (1981).
29. Lauerer, G., Kristjansson, J. K., Langworthy, T. A., König, H., and Stetter, K. O., *Syst. Appl. Microbiol.* **8**, 100 (1986).
30. Stetter, K. O., Lauerer, G., Thomm, M., and Neuner, A., *Science* **236**, 822 (1987).
31. Bryant, F. O., and Adams, M. W. W., *J. Biol. Chem.* **264**, 5070 (1989).
32. Juszczak, A., Aono, S., and Adams, M. W. W., *J. Biol. Chem.* **266**, 13834 (1991).
33. Fauque, G., Peck, H. D., Jr., Moura, J. J. G., Huynh, B. H., Berlier, Y., DerVartanian, D. V., Teixeira, M., Przybyla, A., Lespinat, P. A., Moura, I., and LeGall, J., *FEMS Microbiol. Rev.* **54**, 299 (1989).
34. Tran-Betcke, A., Warnecke, U., Böcker, C., Zaborosch, C., and Friedrich, B., *J. Bacteriol.* **172**, 2920 (1990).
35. Kovacs, K. L., Seefeldt, L. C., Tigyi, G., Doyle, C. M., Mortenson, L. E., and Arp, D. J., *J. Bacteriol.* **171**, 430 (1989).
36. Kojima, N., Fox, J. A., Hausinger, R. P., Daniels, L., Orme-Johnson, W. H., and Walsh, C., *Proc. Natl. Acad. Sci. U.S.A.* **80**, 378 (1983).
37. Schneider, K., Cammack, R., and Schlegel, H. G., *Eur. J. Biochem.* **142**, 75 (1984).
38. Adams, M. W. W., *Biochim. Biophys. Acta* **1020**, 115 (1990).

39. Cammack, R., Fernandez, V. M., and Schneider, K., in "Bioinorganic Chemistry of Nickel" (J. R. Lancaster, Jr., ed.), p. 167. VCH Publ., Deerfield Beach, Florida, 1988.
40. Hausinger, R. P., *Microbiol. Rev.* **51**, 22 (1987).
41. Cammack, R., Bagyinka, C., and Kovacs, K. L., *Eur. J. Biochem.* **182**, 357 (1989).
42. Van der Zwaan, J. W., Albracht, S. P. J., Fontijn, R. D., and Mul, P., *Eur. J. Biochem.* **169**, 377 (1987).
43. Schneider, K., Cammack, R., and Schlegel, H. G., *Eur. J. Biochem.* **142**, 75 (1984).
44. Teixeira, M., Moura, I., Xavier, A. V., Moura, J. J. G., LeGall, J., DerVartanian, D. V., Peck, H. D., Jr., and Huynh, B. H., *J. Biol. Chem.* **264**, 16435 (1989).
45. Cammack, R., Patil, D. S., and Fernandez, V. M., *Biochem. Soc. Trans.* **13**, 572 (1985).
46. Coremans, J. M. C. C., Van der Zwaan, J. W., and Albracht, S. P. J., *Biochim. Biophys. Acta* **997**, 256 (1989).
47. Park, J.-B., Fan, C., Hoffman, B. M., and Adams, M. W. W., *J. Biol. Chem.* **266**, 19351 (1991).
48. Hyman, M. R., and Arp, D. J., *Anal. Biochem.* **173**, 207 (1988).
49. Aono, S., Bryant, F. O., and Adams, M. W. W., *J. Bacteriol.* **171**, 3433 (1989).
50. Sato, S., Nakazawa, K., Hon-nami, K., and Oshima, T., *Biochim. Biophys. Acta* **668**, 277 (1981).
51. Terlesky, K. C., and Ferry, J. G., *J. Biol. Chem.* **263**, 4080 (1988).
52. Yang, S.-S., Ljungdahl, L. G., and LeGall, J., *J. Bacteriol.* **130**, 1084 (1977).
53. Brushi, M., and Guerlesquin, F., *FEMS Microbiol. Rev.* **54**, 155 (1988).
54. Saeki, K., Yao, Y., Wakabayashi, S., Shen, G.-J., Zeikus, J. G., and Matsubara, H., *J. Biochem. (Tokyo)* **106**, 656 (1989).
55. Schatt, E., Jouanneau, Y., and Vignais, P. M., *J. Bacteriol.* **171**, 6218 (1989).
56. Okawara, N., Ogata, M., Yagi, T., Wakabayashi, S., and Matsubara, H., *J. Biochem. (Tokyo)* **104**, 196 (1988).
57. Bovier-Lapierre, G., Bruschi, M., Bonicel, J., and Hatchikian, E. C., *Biochim. Biophys. Acta* **913**, 20 (1987).
58. Wakabayashi, S., Fujimoto, N., Wada, K., Matsubara, H., Kerscher, L., and Oesterheld, D., *FEBS Lett.* **162**, 21 (1983).
59. Minami, Y., Wakabayashi, S., Wada, K., Matsubara, H., Kerscher, L., and Oesterheld, D., *J. Biochem. (Tokyo)* **97**, 745 (1983).
60. Orme-Johnson, W. H., and Sands, R. H., in "Iron-Sulfur Proteins" (W. Lovenberg, ed.), Vol. 2, p. 185. Academic Press, New York, 1977.
61. Matthews, R., Charlton, S., Sands, R. H., and Palmer, G., *J. Biol. Chem.* **249**, 4326 (1974).
62. Conover, R. C., Kowal, A. T., Fu, W., Park, J.-B., Aono, S., Adams, M. W. W., and Johnson, M. K., *J. Biol. Chem.* **265**, 8533 (1990).
63. Armstrong, F. A., George, S. J., Cammack, R., Hatchikian, E. C., and Thomson, A. J., *Biochem. J.* **264**, 265 (1989).
64. Lindahl, P. A., Day, E. P., Kent, T. A., Orme-Johnson, W. H., and Münck, E., *J. Biol. Chem.* **260**, 11160 (1985).
65. Hagen, W. R., Eady, R. R., Dunham, W. R., and Haaker, H., *FEBS Lett.* **189**, 250 (1985).
66. Watt, G. D., and McDonald, J. W., *Biochemistry* **24**, 7226 (1985).
67. Zambrano, I. C., Kowal, A. T., Mortenson, L. E., Adams, M. W. W., and Johnson, M. K., *J. Biol. Chem.* **264**, 20974 (1989).
68. Onate, Y. A., Vollmer, S. J., Switzer, R. L., and Johnson, M. K., *J. Biol. Chem.* **264**, 18386 (1989).

69. Makaroff, C. A., Zalkin, H., Switzer, R. L., and Vollmer, S. J., *J. Biol. Chem.* **258**, 10586 (1983).
70. Hausinger, R., and Howard, J. B., *J. Biol. Chem.* **258**, 13486 (1983).
71. Howard, J. B., Davis, R., Moldenhauer, B., Cash, V. L., and Dean, D., *J. Biol. Chem.* **264**, 11270 (1989).
72. Kennedy, M. C., Werst, M., Telser, J., Emptage, M. H., Beinert, H., and Hoffman, B. M., *Proc. Natl. Acad. Sci. U.S.A.* **84**, 8854 (1987).
73. Emptage, M. H., Dreyer, J.-L., Kennedy, M. C., and Beinert, H., *J. Biol. Chem.* **258**, 11106 (1983).
74. Armstrong, F. A., Hill, H. A. O., and Walton, N. J., *Q. Rev. Biophys.* **18**, 261 (1986).
75. Robbins, A. H., and Stout, C. D., *Proteins: Struct. Funct. Genet.* **5**, 289 (1989).
76. Beinert, H., and Kennedy, M. C., *Eur. J. Biochem.* **186**, 5 (1989).
77. Werst, M. M., Kennedy, M. C., Beinert, H., and Hoffman, B. M., *Biochemistry* **29**, 1026 (1990).
78. Carney, M. J., Papaefthymiou, G. C., Spartalian, K., Frankel, R. B., and Holm, R. H., *J. Am. Chem. Soc.* **110**, 6084 (1988).
79. Johnson, M. K., Robinson, A. E., and Thomson, A. J., in "Iron-Sulfur Proteins" (T. G. Spiro, ed.), Vol. 4, p. 367. Wiley, New York, 1982.
80. Finnegan, M. G., Onate, Y. A., Hales, B. J., Switzer, R. L., and Johnson, M. K., *J. Inorg. Biochem.* **36**, 251 (1989).
81. Czernuszewicz, R. S., Macor, K. A., Johnson, M. K., Gewirth, A., and Spiro, T. G., *J. Am. Chem. Soc.* **109**, 7178 (1987).
82. Spiro, T. G., Czernuszewicz, R. S., and Han, S., in "Biological Applications of Raman Spectroscopy" (T. G. Spiro, ed.), Vol. 3, p. 523. Wiley, New York, 1988.
83. Madden, J. F., Han, S., Siegel, L. M., and Spiro, T. G., *Biochemistry* **28**, 5471 (1989).
84. Kissinger, C. R., Adman, E. T., Sieker, L. C., Jensen, L. H., and LeGall, J., *FEBS Lett.* **244**, 447 (1989).
85. Kissinger, C. R., Sieker, L. C., Adman, E. T., and Jensen, L. H., *J. Mol. Biol.* **219**, 693 (1991).
86. Kent, T. A., Dreyer, J.-L., Kennedy, M. C., Huynh, B. H., Emptage, M. H., Beinert, H., and Münck, E., *Proc. Natl. Acad. Sci. U.S.A.* **79**, 1096 (1982).
87. Thomson, A. J., Robinson, A., Johnson, M. K., Cammack, R., Rao, K. K., and Hall, D. O., *Biochim. Biophys. Acta* **637**, 423 (1981).
88. Moura, J. J. G., Moura, I., Kent, T. A., Lipscomb, J. D., Huynh, B. H., LeGall, J., Xavier, A. V., and Münck, E., *J. Biol. Chem.* **257**, 6259 (1982).
89. Cunningham, R. P., Asahara, H., Bank, J. F., Scholes, C. P., Salerno, J. C., Surerus, K., Münck, E., McCracken, J., Pesiach, J., and Emptage, M. H., *Biochemistry* **28**, 4450 (1989).
90. Vollmer, S. J., Switzer, R. L., and Debrunner, P. G., *J. Biol. Chem.* **258**, 14284 (1983).
91. Holm, R. H., and Simhon, E. D., in "Molybdenum Enzymes" (T. G. Spiro, ed.), p. 1. Wiley, New York, 1985.
- 91a. Adams, M. W. W., Rao, K. K., Hall, D. O., Christou, G., and Garner, G., *Biochim. Biophys. Acta* **589**, 1 (1980).
92. Flint, D. H., and Emptage, M. H., *J. Biol. Chem.* **263**, 3558 (1988).
93. Scopes, R. K., and Griffiths-Smith, K., *Anal. Biochem.* **136**, 530 (1984).
94. Dreyer, J.-L., *Eur. J. Biochem.* **150**, 145 (1985).
95. Kuchta, R. D., Hanson, G. R., Holmquist, B., and Abeles, R. H., *Biochemistry* **25**, 7301 (1986).
96. Kelly, J. M., and Scopes, R. K., *FEBS Lett.* **202**, 274 (1986).

97. Thomann, H., Bernadino, M., and Adams, M. W. W., *J. Am. Chem. Soc.* **113**, 7044 (1991).
98. Nelson, M. J., Levy, M. A., and Orme-Johnson, W. H., *Proc. Natl. Acad. Sci. U.S.A.* **80**, 147 (1983).
99. Orme-Johnson, W. H., *Annu. Rev. Biophys. Chem.* **14**, 419 (1985).
100. Holm, R. H., and Simhon, E. D., in "Molybdenum Enzymes" (T. G. Spiro, ed.), p. 1. Wiley, New York, 1985.
101. Challen, P. R., Koo, S.-M., Kim, C. G., Dunham, W. R., and Coucouvanis, D., *J. Am. Chem. Soc.* **112**, 8606 (1990).
102. Smith, B. E., Eady, R. R., Lowe, D. J., and Gormal, C., *Biochem. J.* **250**, 299 (1988).
103. Ciurli, S., and Holm, R. S., *Inorg. Chem.* **28**, 1685 (1989).
104. Chisnell, J. R., Premakumar, R., and Bishop, P. E., *J. Bacteriol.* **170**, 27 (1988).
105. Thomann, H., Morgan, T. V., Jin, H., Burgmayer, S. J. N., Bare, R. E., and Stiefel, E. I., *J. Am. Chem. Soc.* **109**, 7913 (1987).
106. Ragsdale, S. W., Wood, H. G., and Antholine, W. E., *Proc. Natl. Acad. Sci. U.S.A.* **82**, 6811 (1985).
107. Terlesky, K. C., Barber, M. J., Aceti, D. J., and Ferry, J. G., *J. Biol. Chem.* **262**, 15392 (1987).
108. Cramer, S. P., Eidsness, M. K., Pan, W.-H., Morton, T. A., Ragsdale, S. W., DerVar-tanian, D. V., Ljungdahl, L. G., and Scott, R. A., *Inorg. Chem.* **26**, 2477 (1987).
109. Bastian, N. R., Diekert, G., Niederhoffer, E. C., Teo, B.-K., Walsh, C. T., and Orme-Johnson, W. H., *J. Am. Chem. Soc.* **110**, 5581 (1988).
110. Stephens, P. J., McKenna, M.-C., Ensign, S. A., Bonam, D., and Ludden, P. A., *J. Biol. Chem.* **264**, 16347 (1989).
111. Ensign, S. A., Campbell, M. J., and Ludden, P. W., *Biochemistry* **29**, 2162 (1990).
112. Fan, C., Gorst, C. M., Ragsdale, S. W., and Hoffman, B. M., *Biochemistry* **30**, 431 (1991).
113. Lindahl, P. A., Ragsdale, S. W., and Münck, E., *J. Biol. Chem.* **265**, 3880 (1990).
114. R. H. Holm, This volume.
115. Challen, P. R., Koo, S.-M., Kim, C. G., Dunham, W. R., and Coucouvanis, D., *J. Am. Chem. Soc.* **112**, 8606 (1990).
116. Stack, T. D. P., and Holm, R. H., *J. Am. Chem. Soc.* **110**, 2484 (1988).
117. Stack, T. D. P., Carney, M. J., and Holm, R. H., *Inorg. Chem.* **111**, 1670 (1989).
118. Weigel, J. A., Srivastava, K. K. P., Day, E. P., Münck, E., and Holm, R. H., *J. Am. Chem. Soc.* **112**, 8015 (1990).
119. Berg, J. M., and Holm, R. H., in "Iron Sulfur Proteins" (T. G. Spiro, ed.), p. 1. Wiley, New York, 1982.
120. Moura, I., Moura, J. J. G., Münck, E., Papaefthymiou, V., and LeGall, J., *J. Am. Chem. Soc.* **108**, 349 (1986).
121. Surerus, K. K., Münck, E., Moura, I., Moura, J. J. G., and LeGall, J., *J. Am. Chem. Soc.* **109**, 2805 (1987).
122. Conover, R. C., Park, J.-B., Adams, M. W. W., and Johnson, M. K., *J. Am. Chem. Soc.* **112**, 4562 (1990).
123. Surerus, K. K., Ph.D. Dissertation, University of Minnesota, Minneapolis, Minne-sota (1989).
124. Ciurli, S., Yu, S., Holm, R. H., Srivastava, K. K. P., and Münck, E., *J. Am. Chem. Soc.* **112**, 8169 (1990).
125. Ensign, S. A., Hyman, M. R., and Ludden, P. W., *Biochemistry* **28**, 4973 (1989).
126. Carney, M. J., Kovacs, J. A., Zhang, Y.-P., Papaefthymiou, G. C., Spartalian, K., Frankel, R. B., and Holm, R. H., *Inorg. Chem.* **26**, 719 (1987).

127. Conover, R. C., Park, J.-B., Adams, M. W. W., and Johnson, M. K., *J. Am. Chem. Soc.* **113**, 2799 (1991).
128. Yasunobu, K. T., and Tanaka, M., in "Iron-Sulfur Proteins" (W. Lovenberg, ed.), Vol. 2, p. 27. Academic Press, New York, 1973.
129. Watenpaugh, K. D., Sieker, L. C., Herriott, J. R., and Jensen, L. H., *Acta Crystallogr.* **B29**, 943 (1973).
130. Seki, Y., Seki, S., Satoh, M., Ikeda, A., and Ishimoto, M., *J. Biochem. (Tokyo)* **106**, 336 (1989).
131. Meyer, J., Gagnon, J., Sieker, L. C., van Dorsselaer, A., and Moulis, J.-M., *Biochem. J.* **271**, 839 (1990).
132. Woolley, K. J., and Meyer, T. E., *Eur. J. Biochem.* **163**, 161 (1987).
133. Bruschi, M., *Biochim. Biophys. Acta* **434**, 4 (1976).
134. Voordouw, G., *Gene* **69**, 75 (1988).
135. Shimizu, F., Ogata, M., Yagi, T., Wakabayashi, S., and Matsubara, H., *Biochimie* **71**, 1171 (1989).
136. Bruschi, M., *Biochem. Biophys. Res. Commun.* **70**, 615 (1976).
137. Hormel, S., Walsh, K. A., Prickril, B. C., Titani, K., LeGall, J., and Sieker, L. C., *FEBS Lett.* **201**, 147 (1986).
138. Bachmeyer, H., Yasunobu, K. T., Peel, J. L., and Mayhew, S., *J. Biol. Chem.* **243**, 1022 (1968).
139. Bachmeyer, H., Benson, A. M., Yasunobu, K. T., Garrard, W. T., and Whiteley, H. R., *Biochemistry* **7**, 986 (1968).
140. Saeki, K., Yao, Y., Wakabayashi, S., Shen, G.-J., Zeikus, J. G., and Matsubara, H., *J. Biochem. (Tokyo)* **106**, 336 (1989).
141. Adman, E. T., Sieker, L. C., Jensen, L. H., Bruschi, M., and LeGall, J., *J. Mol. Biol.* **112**, 113 (1977).
142. Watenpaugh, K. D., Sieker, L. C., and Jensen, L. H., *J. Mol. Biol.* **131**, 509 (1979).
143. Sieker, L. C., Stenkamp, R. E., Jensen, L. H., Prickril, B., and LeGall, J., *FEBS Lett.* **208**, 73 (1989).
144. Blake, P. R., Park, J.-B., Bryant, F. O., Aono, S., Magnuson, J. K., Eccleston, E., Howard, J. B., Summers, M. F., and Adams, M. W. W., *Biochemistry*, **30**, 10885 (1991).
145. Dutton, P. L., in "Methods in Enzymology" (S. Fleischer and L. Packer, eds.), Vol. 54, p. 411. Academic Press, New York, 1978.
146. Koller, K. B., and Hawkrige, F. M., *J. Electroanal. Chem.* **239**, 291 (1988).
147. Lovenberg, W., and Sobel, B. E., *Proc. Natl. Acad. Sci. U.S.A.* **54**, 193 (1965).
148. Papavassiliou, P., and Hatchikian, E. C., *Biochim. Biophys. Acta* **810**, 1 (1985).
149. Zwickl, P., Fabry, S., Bogedain, C., Haas, A., and Hensel, R., *J. Bacteriol.* **172**, 4329 (1990).
150. Summers, M. F., South, T. L., Kim, B., and Hare, D. R., *Biochemistry* **29**, 329 (1990).
151. Ragsdale, S. W., Ljungdahl, L. G., and DerVartanian, D. V., *J. Bacteriol.* **155**, 1224 (1983).
152. Hugenholtz, J., and Ljungdahl, L. G., *FEMS Microbiol. Rev.* **87**, 383 (1990).
153. Saeki, K., Jain, M. K., Shen, G.-J., Prince, R. C., and Zeikus, J. G., *J. Bacteriol.* **171**, 4736 (1989).
154. Stewart, D. E., LeGall, J., Moura, I., Moura, J. J. G., Peck, H. D., Jr., Xavier, A. V., Weiner, P. K., and Wampler, J. E., *Eur. J. Biochem.* **185**, 695 (1989).
155. Thomson, A. J., *FEBS Lett.* **286**, 230 (1991).
156. Mukund, S., and Adams, M. W. W., *J. Biol. Chem.* **265**, 11508 (1990).
157. Yamamoto, I., Saiki, T., Liu, S.-M., and Ljungdahl, L. G., *J. Biol. Chem.* **258**, 1826 (1983).

158. Clark, W. M., "Oxidation Reduction Potentials of Organic Systems." Kruger Publ., Huntingdon, New York, 1972.
159. Wood, P. M., *Trends Biochem. Sci.* **10**, 106 (1985).
160. Prince, R. C., and Adams, M. W. W., *J. Biol. Chem.* **262**, 5125 (1987).
161. Mayhew, S. G., *Eur. J. Biochem.* **85**, 535 (1978).
162. Thauer, R. K., Jungermann, K., and Decker, K., *Bacteriol. Rev.* **41**, 100 (1977).
163. Loach, P. A., in "Handbook of Biochemistry and Molecular Biology" (G. D. Fasman, ed.), Vol. 1, p. 122. CRC Press, Cleveland, Ohio, 1976.
164. Mukund, S., and Adams, M. W. W., *J. Biol. Chem.* **266**, 14208 (1991).
165. George, G. N., Prince, R. P., Mukund, S., and Adams, M. W. W., *J. Am. Chem. Soc.* in press (1991).
166. Coughlan, M. P., in "Molybdenum and Molybdenum-Containing Enzymes" (M. P. Coughlan, ed.), p. 119. Pergamon, New York, 1980.
167. Hille, R., and Massey, V., in "Molybdenum Enzymes" (T. G. Spiro, ed.), p. 443. Wiley, New York, 1985.
168. George, G. N., Kipke, C. A., Prince, R. C., Sunde, R. A., Enemark, J. H., and Cramer, S. P., *Biochemistry* **28**, 5075 (1989).
169. De Rosa, M., Gambacorta, R., Nicolaus, B., Giardina, P., Poerio, E., and Buonocore, V., *Biochem. J.* **224**, 407 (1984).
170. Budgen, N., and Danson, M. J., *FEBS Lett.* **196**, 207 (1986).
171. Danson, M. J., *Adv. Microbiol. Physiol.* **29**, 165 (1989).
172. Dawson, R. M. C., Elliott, D. C., Elliott, W. H., and Jones, K. M., eds., in "Data for Biochemical Research," 3rd Ed. Oxford Univ. Press (Clarendon) Oxford, 1986.
173. Uyeda, K., and Rabinowitz, J. C., *J. Biol. Chem.* **246**, 3111 (1971).
174. Kerscher, L., and Oesterheld, D., *Eur. J. Biochem.* **116**, 587 (1981).
175. Drake, H. L., Hu, S.-I., and Wood, H. G., *J. Biol. Chem.* **256**, 11137 (1981).
176. Wahl, R. C., and Orme-Johnson, W. H., *J. Biol. Chem.* **262**, 10489 (1987).
177. Williams, K., Lowe, P. N., and Leadlay, P. F., *Biochem. J.* **246**, 529 (1987).
178. Meinecke, B., Bertram, J., and Gottschalk, G., *Arch. Microbiol.* **152**, 244 (1989).
179. Chen, J.-S., and Mortenson, L. E., *Biochim. Biophys. Acta* **371**, 283 (1974).
180. Chen, J.-S., and Blanchard, D. K., *Biochem. Biophys. Res. Commun.* **84**, 1144 (1978).
181. Adams, M. W. W., and Mortenson, L. E., *J. Biol. Chem.* **259**, 7045 (1984).
182. Adams, M. W. W., and Mortenson, L. E., *Biochim. Biophys. Acta* **766**, 51 (1984).
183. Adams, M. W. W., Eccleston, E., and Howard, J. B., *Proc. Natl. Acad. Sci. U.S.A.* **86**, 4932 (1989).
184. Grande, H. J., Dunham, W. R., Averill, B. A., van Dijk, C., and Sands, R. H., *Eur. J. Biochem.* **136**, 201 (1983).
185. van Dijk, C., Mayhew, S. G., Grande, H. J., and Veeger, C., *Eur. J. Biochem.* **102**, 317 (1979).
186. van Dijk, C., Grande, H. J., Mayhew, S. G., and Veeger, C., *Eur. J. Biochem.* **107**, 251 (1980).
187. Filipiak, M., Hagen, W. R., and Veeger, C., *Eur. J. Biochem.* **185**, 547 (1989).
188. Huynh, B. H., Czechowski, M. H., Krüger, H.-J., DerVartanian, D. V., Peck, H. D., Jr., and LeGall, J., *Proc. Natl. Acad. Sci. U.S.A.* **81**, 3728 (1984).
189. Grande, H. J., van Berkel-Arts, A., Breghe, J., van Dijk, K., and Veeger, C., *Eur. J. Biochem.* **131**, 81 (1983).
190. van der Westen, H. M., Mayhew, S. G., and Veeger, C., *FEBS Lett.* **86**, 122 (1978).
191. Hagen, W. R., van Berkel-Arts, A., Kruse-Wolters, K. M., Voorduw, G., and Veeger, C., *FEBS Lett.* **203**, 59 (1986).
192. Patil, D. S., Moura, J. J. G., He, S. H., Teixeira, M., Prickril, B. C., DerVartanian, D. V., Peck, H. D., Jr., LeGall, J., and Huynh, B. H., *J. Biol. Chem.* **263**, 18732 (1988).
193. Spiro, T. G., ed., "Molybdenum Enzymes." Wiley, New York, 1985.

EVOLUTION OF HYDROGENASE GENES

GERRIT VOORDOUW

Division of Biochemistry, Department of Biological Sciences, The University of Calgary,
Calgary, Alberta, T2N 1N4 Canada

- I. Introduction
- II. Hydrogenase Operons
 - A. Iron-Only Hydrogenases
 - B. Nickel-Containing Hydrogenases
- III. Evolution of Hydrogenase Genes: "Redon Shuffling" and Hydrogenase Export
- IV. Functions of Hydrogenases
- V. Perspectives
- References

I. Introduction

Hydrogenases catalyze the reversible oxidation of hydrogen. The past 7 years have seen a surge in published nucleotide sequences of the structural genes encoding these enzymes (Table I) (1–24). As a result, translated primary structures from different families, the iron-only and nickel-containing hydrogenases (25), are now available: 16 published sequences for nickel-containing hydrogenases, both from eubacteria (*Desulfovibrio*, *Bradyrhizobium*, *Azotobacter*, *Rhodobacter*, *Rhodocyclus*, *Alcaligenes*, and *Rhizobium*) and archaebacteria (*Methanobacterium* and *Methanothermus*), and three different sequences for iron-only hydrogenases (all *Desulfovibrio vulgaris*). Comparison of these sequences allows conserved features to be identified, as will be discussed below. All hydrogenases studied with molecular biological techniques to date consist of at least two subunits. The structural genes encoding these subunits are organized in an operon with the gene order (5' → 3') as indicated in Table I. Nucleotide sequencing has indicated the presence of additional genes in the operon, e.g., hydrogenase 1 of *Escherichia coli* is encoded by an operon encoding six open reading frames (Table I). Two of these (*hyaA* and *hyaB*) encode the small and large subunits,

TABLE I
HYDROGENASES FOR WHICH THE PRIMARY STRUCTURE HAS BEEN DETERMINED BY NUCLEOTIDE SEQUENCING OF
THEIR STRUCTURAL GENES

<i>N</i> ^a	Organism	Type	Gene name ^b	Ref.
1	<i>Desulfovibrio vulgaris</i> Hildenborough	[Fe]	<u>hydA</u> , <u>hydB</u> 46.0 9.6	1
2	<i>Desulfovibrio vulgaris</i> Monticello	[Fe]	<u>hydA</u> , <u>hydB</u> 46.0 9.6	2
3	<i>Desulfovibrio vulgaris</i> Hildenborough	[Fe]	<u>hydC</u> 65.8	3 ^d
4	<i>Desulfovibrio gigas</i>	[Ni-Fe]	<u>hynB</u> , <u>hynA</u> 28.4 61.3	4-6
5	<i>Desulfovibrio vulgaris</i> Miyazaki F	[Ni-Fe]	<u>hynB</u> , <u>hynA</u> 28.8 62.5	7
6	<i>Desulfovibrio fructosovorans</i>	[Ni-Fe]	<u>hynB</u> , <u>hynA</u> 28.4 61.6	8
7	<i>Desulfovibrio baculatus</i>	[Ni-Fe-Se]	<u>hysB</u> , <u>hysA</u> 30.8 56.8	5, 9
8	<i>Bradyrhizobium japonicum</i>	[Ni-Fe]	<u>orf1</u> , <u>orf2</u> , <u>orf3</u> 34.5 65.9 ? ^d	10
9	<i>Rhizobium leguminosarum</i>	[Ni-Fe]	<u>hupS</u> , <u>hupL</u> 34.4 65.9	11, 12
10	<i>Azotobacter chroococcum</i>	[Ni-Fe]	<u>hupS</u> , <u>hupL</u> , <u>orf3</u> 34.2 66.4 ?	13

11	<i>Azotobacter vinelandii</i>	[Ni-Fe]	<u>hoxK</u> , <u>hoxG</u> , <i>orf3</i>	14
			34.2 66.8 27.7	
12	<i>Rhodobacter capsulatus</i>	[Ni-Fe]	<u>hupS</u> , <u>hupL</u> , <i>orfX</i>	15
			34.3 68.1 30.2	
13	<i>Rhodocyclus gelatinosus</i>	[Ni-Fe]	<u>hupS</u> , <u>hupL</u>	16, 17
			34.6 68.5	
14	<i>Escherichia coli</i> (hydrogenase-1)	[Ni-Fe]	<u>hyaA</u> , <u>hyaB</u> , <i>hyaC</i> , <i>hyaD</i> , <i>hyaE</i> , <i>hyaF</i>	18
			35.6 66.2 27.6 21.5 14.9 31.5	
15	<i>Escherichia coli</i> (hydrogenase-3)	[Ni-Fe]	<i>orf1</i> , <i>orf2</i> , <i>orf3</i> , <i>orf4</i> , <i>orf5</i> , <i>orf6</i> , <i>orf7</i> , <i>orf8</i>	19
			17.6 21.8 64.1 33.3 65.0 20.3 28.0 15.5	
16	<i>Alcaligenes eutrophus</i>	[Ni-Fe]	<u>hoxF</u> , <u>hoxU</u> , <u>hoxY</u> , <u>hoxH</u>	20
			66.8 26.0 22.9 54.7	
17	<i>Methanobacterium thermoautotrophicum</i> ΔH	[Ni-Fe]	<u>mvhD</u> , <u>mvhG</u> , <u>mvhA</u> , <u>mvhB</u>	21
			15.8 33.0 53.0 44.0	
18	<i>Methanobacterium thermoautotrophicum</i> ΔH	[Ni-Fe]	<u>frhA</u> , <u>frhD</u> , <u>frhG</u> , <u>frhB</u>	22
			44.7 17.6 25.7 30.7	
19	<i>Methanothermus fervidus</i>	[Ni-Fe]	<u>mvhD</u> , <u>mvhG</u> , <u>mvhA</u> , <u>mvhB</u>	23
			? ^d ? ^d 53.0 44.0	
20	<i>Anabaena cylindrica</i>	?	<u>texP</u> ^e	24
			41.1	

^a Number used to identify hydrogenases in Table III.

^b Gene names as given in the referenced publications. The size (kDa) of the putative gene product is indicated below its name. Suggested structural genes are underlined. The gene order is that in the operon.

^c It is not clear whether this gene product is expressed.

^d Gene was not completely sequenced.

^e Gene name given in this publication.

which constitute this hydrogenase as it is isolated from *E. coli* (26). The function of the products of the other four genes (*hyaC*–*hyaF*) has not yet been established. They could function in anchoring the two-subunit hydrogenase to the membrane and in conducting electrons to the membrane-bound electron transport chain (see below). Similarly, in the hydrogenase 3 operon of *E. coli*, *orf5* has been indicated as a structural gene because of its homology with other [NiFe] hydrogenase large-subunit genes (e.g., *hyaB*). Again, assignment of the roles of the other seven gene products is difficult in the absence of definitive biochemical data, although an electron transfer function is implicated for the products of *orf2* and *orf6*. Some or all can be expected to constitute the membrane-bound hydrogenase 3 complex (27). In view of these uncertainties, only *hyaA* and *hyaB*, and *orf2*, *orf5*, and *orf6*, have been indicated as possible structural genes for hydrogenase 1 and hydrogenase 3 in Table I.

The problem of gene nomenclature needs some consideration. The names for the hydrogenase genes of *Desulfovibrio* are as described elsewhere (6, 28). Those for hydrogenase genes of other organisms (Table I) are generally as in the references given, except where no names were provided by the authors. This creates the problem that multiple designations are used for genes encoding homologous proteins (e.g., the gene for the large subunit of [NiFe] hydrogenase has been named *hynA*, *orf2*, *hupL*, *hoxG*, *hyaB*, *hoxH*, *mvhA*, and *frhA*) and, more seriously, that the same gene name may refer to completely different proteins in different operons (e.g., *orf2* of *Bradyrhizobium japonicum* and of the hydrogenase 3 operon of *E. coli*). Introduction of a unifying gene nomenclature will not be attempted here (see Section V). The advantage of this diversity is that it is often not necessary to specify the organism (e.g., *hyaB* is an *E. coli* gene only). Ambiguous names will be fully specified.

II. Hydrogenase Operons

A. IRON-ONLY HYDROGENASES

Periplasmic [Fe] hydrogenases have so far only been isolated from sulfate-reducing bacteria of the genus *Desulfovibrio*. The *hydA*,*B* operon of *D. vulgaris* Hildenborough encodes a simple two-subunit hydrogenase (Ref. 1; reviewed in Refs. 6, 29–32). Its large α subunit ($M_r = 46K$, encoded by the *hydA* gene) contains 18 cysteine residues, whereas the mature small β subunit ($M_r = 9.6K$) lacks cysteine. The small

subunit is synthesized in precursor form ($M_r = 13.5K$ for unprocessed pro- β). The three iron-sulfur clusters known to be present in this hydrogenase (33) must thus all coordinate to large-subunit cysteine residues. The NH_2 -terminal amino acid sequence of α (residues 1–105) is homologous with 8Fe–8S ferredoxins: two groups of 4 cysteine residues are present in the characteristic pattern C-X-X-C-X-X-C-X-X-X-C-P (Table II, elements 1 and 2), which have been shown to bind two 4Fe–4S clusters in the ferredoxin of *Peptococcus aerogenes* (34). The $COOH$ -terminal part of the α sequence (residues 106–420) contains the remaining 10 cysteine residues. Comparison of the amino acid sequences of the subunits of periplasmic [Fe] hydrogenase from *D. vulgaris* and *D. vulgaris* ssp. *oxamicus* Monticello (1, 2) with that of the putative 65.8-kDa *hydC* gene product (3) has indicated that 5 of these 10 cysteine residues, located in elements 3, 4, and 7 (Table II), are conserved and these could therefore serve as ligands to the third active site cluster, which is thought to have an unusual composition (6Fe–6S; Ref. 33). This conclusion cannot be based on comparison of subunit sequences for the two [Fe] hydrogenases alone, since these are too homologous (~75% identity) to allow firm conclusions, with respect to critically conserved residues, to be drawn. The amino acid sequence of the putative *hydC* gene product is only 20–40% identical. Some caution should be exercised in making comparisons with the *hydC* gene product sequence: this gene has so far only been found in *D. vulgaris* Hildenborough and two closely related strains (28). The *hydC* gene, which can be regarded as an in-frame fusion of the *hydA* and *hydB* genes, is present

TABLE II

SOME SEQUENCE ELEMENTS IN THE α AND β SUBUNITS OF PERIPLASMIC HYDROGENASE FROM *D. vulgaris* HILDENBOROUGH THAT HAVE BEEN CONSERVED IN THE *hydC* GENE PRODUCT^a

Element	Subunit	Sequence ^b	Possible function
1	α	34-KCIgCdtCsqyCptaaif	Coordination 4Fe–4S cluster (F cluster)
2	α	66-aCinCGQCltHCPenaif	Coordination 4Fe–4S cluster (F cluster)
3	α	172-LPqFTSCCPGW	Coordination active site H cluster
4	α	229-VSiMPCiAKKyE	Coordination active site H cluster
5	α	291-GgAtIFGvTGGVMEAAALR	?
6	α	346-VKVAVVHGAK	?
7	α	372-FiEyMACPGGCvcGGGQP	Coordination active site H cluster
8	β	80-PlghkSHdLLHThwfDkskgV	?

^a Conserved residues are indicated by uppercase letters.

^b The number indicates the position of first residue in the amino acid sequence.

immediately downstream from the *hydA,B* operon. Expression of *hydC* in *D. vulgaris* Hildenborough has yet to be demonstrated and it has been suggested that this gene has been deleted from other *Desulfovibrio* strains (2). The *hydC* gene is transcribed convergently with respect to the direction of transcription of the *hydA,B* genes: both genes may share the same transcription terminator (2, 3). Recent data by van den Berg *et al.* (35) indicated a size of 1.9 kilobases (kb) for the *hydA,B* mRNA transcript in *D. vulgaris* Hildenborough. This size is sufficient to accommodate the *hydA* (1.27 kb) and *hydB* (0.37 kb) genes and confirms that the suggested terminator functions *in vivo*.

The amino acid sequences of the periplasmic [Fe] hydrogenase subunits should ideally be compared with those of the cytoplasmic [Fe] hydrogenases from gram-positive bacteria, such as *Clostridium* and *Megasphaera* (36, 37). *Clostridium pasteurianum* has two hydrogenases (I and II). Hydrogenase II is thought to contain three iron-sulfur clusters, two 4Fe-4S ferredoxin-like (F) clusters, and one hydrogenase (H) cluster, thought to contain six Fe. This composition is similar to that of periplasmic [Fe] hydrogenase from *Desulfovibrio*. Hydrogenase I is thought to contain one H-cluster and four F-clusters (36) and could thus contain an extra 8Fe-8S ferredoxin domain. Both of these hydrogenases consist of a single polypeptide, which must combine the essential features of both the α and β subunit sequences, e.g., as in the putative *hydC* gene product.

The function of the β subunit in periplasmic [Fe] hydrogenase from *Desulfovibrio* is twofold: (1) it functions in the export of this hydrogenase to the periplasm via its complex 34-amino acid signal sequence (see Section III), and (2) despite the fact that it does not participate in cluster coordination via cysteine residues, it must contribute some essential catalytic function, possibly via element 8 (Table II), which contains several conserved His residues. These could participate as proton conductors to or from the hydrogenase active site during hydrogen production or consumption. Such assignments are, of course, entirely speculative in the absence of an [Fe] hydrogenase structure or biochemical data obtained for mutants, generated by oligonucleotide-directed mutagenesis.

The structure of periplasmic [Fe] hydrogenase from *Desulfovibrio* can thus be interpreted in terms of a simple model. The NH₂-terminal domain functions as the electron conductor via its two F-clusters, whereas the larger COOH-terminal domain contains the H-cluster. The three clusters are spatially arranged to allow rapid flow of electrons from the H-cluster to the F-clusters during hydrogen consumption and vice versa during hydrogen production. The physiological redox partner

of [Fe] hydrogenase in *Desulfovibrio* is thought to be cytochrome c_3 , which is exclusively present in the periplasm (38) and has four c -type hemes in a polypeptide chain of 13 kDa. The structure of this cytochrome is known (39, 40). Expression of the *hydA,B* genes in a heterologous system has not yet been successful. Expression in *E. coli* gives rise to an $\alpha\beta$ dimer that does contain part of the F-clusters but lacks the H-cluster (41). However, even overexpression in the homologous host *D. vulgaris*, made possible by recently developed bacterial conjugation technology (42–44), is difficult: increasing the gene dosage by presenting the *hydA,B* genes on a multiple-copy broad-host-range vector in addition to the chromosomal copy of these genes leads to increased synthesis of α and β subunits but hardly to an increase in enzyme activity (35, 42). The conclusions drawn from these experiments are that insertion of the H-cluster and possibly the F-clusters is mediated by the activity of specific protein factors that become limiting when overexpression in *D. vulgaris* is attempted and that are absent from a heterologous host such as *E. coli*. Combined with the need to export periplasmic [Fe] hydrogenase via a specific mechanism (Section III), these features provide an unusually complex assembly mechanism. Structure–function studies by oligonucleotide-directed mutagenesis may not be easily achieved in this system.

B. NICKEL-CONTAINING HYDROGENASES

The nickel-containing [Ni–Fe] and [Ni–Fe–Se] hydrogenases contain 1 mol of Ni per mole of enzyme and have been characterized by gene cloning and sequencing from a wide variety of sources (Table I). Sequence elements with conserved features are compared in Tables III and IV for 16 different nickel-containing hydrogenases. The hydrogenases in groups I–III are two-subunit enzymes, consisting of a small β (28–35 kDa) and a large α (56–68 kDa) subunit. Those in groups I and II are encoded by simple, two-gene-containing (bicistronic) operons, whereas those in group III are encoded by more complex, polycistronic operons. The enzymes in groups IV and V have a more complex, or unknown, subunit composition: homology with the small subunit sequence of groups I–III is fading in these hydrogenases. It is therefore appropriate to discuss the hydrogenases in groups I–V first of all with reference to the sequences of the “large subunits,” since this polypeptide has been found in every nickel-containing hydrogenase sequenced to date. From the discussion below it will become clear that the “large subunit” binds the active site nickel, whereas the “small subunit” has an electron transfer function. Since the designation “small” and “large”

TABLE III

CONSERVED SEQUENCE ELEMENTS IN THE NICKEL-BINDING α SUBUNIT OF Ni-CONTAINING HYDROGENASES

Group	N ^a	Gene	Element 1	Element 2	Element 3	Element 4 ^b
I	7	<i>hysA</i>	44-FRGFEQILGRDPRDSSQ-IVQRICGVCTAHCN	110-YLQSHILHFYHLAALDYVK	417-GTGFTEAPRGALLHYL	491-RLVRSYDP*LGCAVHVLHAE
II	4	<i>hynA</i>	42-FRGLEMILKGRDPRDAQH-FTQRACGVCTYVHAL	80-YMHDHLVHFYHLHALDWVN	454-GVGEVNAPRGMLSHWI	522-RTVHSYDPCACGVHVIDPE
	5	<i>hynA</i>	58-FRGLEIILKGRDPRDAQH-FTQRTCGVCTYTHAL	120-YLHDHIVHFYHLHALDFVD	469-GVGEVNAPRGGLSHWI	538-RTVHSFDPACGVHVIDGH
	6	<i>hynA</i>	49-FRGLEIILKGRDPRDAQH-FTQRACGVCTYVHAL	111-YLHDHLVHFYHLHALDWVD	468-GVGLADAPRGSLSHWI	535-RTVHAFDPCACGVHVIEPE
III	8	<i>orf2</i>	52-WRGIEVILKNRDPRDAWA-FTERICGVCTGTHAL	114-QVHDHVHFYHLHALDWVD	500-GVGFTEAPRGALAHWI	567-RTIHSFDPCLACSTHVMSPD
	9	<i>hupL</i>	52-WRGIEVILKNRDPRDAWA-FTERICGVCTGTHAL	114-QVHDHVHFYHLHALDWVD	500-GVGFTEAPRGALAHWI	567-RTIHSFDPCLACSTHVMSPD
	10	<i>hupL</i>	51-WRGLEVILKGRDPRDAWA-FVERICGVCTGTtrw ^c	113-QVQDHIVpFYHL1rLDWVN	505-GVGINEAPRGSAHWI	572-RTLHSFDPCLACSTHVMSPD
	11	<i>hoxG</i>	51-WRGLEVILKGRDPRDAWA-FVERICGVCTGTHAL	113-QVHDHIVHFYHLHALDWVN	508-GVGINEAPRGALGHWI	573-RTLHSFDPCLACSTHVMSPD
	12	<i>hupL</i>	51-WRGLEVILKGRDPRDAWA-FTERICGVCTGTHAL	113-QIHDHIVHFYHLHALDWVN	500-GVGMTEAPRGALGHVW	567-RTLHSFDPCLACSTHVMSAE
	13	<i>hupL</i>	51-WRGLEVILKGRDPRDAWA-FVERICGVCTGCHAL	113-QVHDHAVHFYHLHALDWVD	521-GVGTVAAPRGMLGHWI	588-RTLHSFDPCLACSTHVMSD
	14	<i>hyaB</i>	53-FRGLEIILQGRDPRDARA-FVERICGVCTGVHAL	115-WCHDHLVHFYQLAGMDWID	501-GVGFTEAPRGALGHWA	568-RTLHSFDPCLACSTHVLGDD
IV	16	<i>hoxH</i>	38-FRGFEKFLQGHFWEAPM-FLQRICGICFVSHHL	106-MLQSHTTAYFYLIIVPEMLF	382-GVGVEAPRGTLTHHY	449-VGIRAYDPCLSATHALGQM
	17	<i>mvhA</i>	38-FRGFEKFLQGRPIEEAPR-IVPRICGICDVQHHL	103-YMHSGLHFYFLAAPDFIA	368-GVGIVEAPRGTLTHHY	434-MVIRAYDPCLSATHIDISQ
	18	<i>frhA</i>	40-VRGLEKIVTGKAPETAPV-IVQRICGVCP1PHTL	101-HVNSHAIH-HFLIAPDFVP	300-GVGAIEGPRGLDVHMA	372-HVIRAYDPCLSATHVMVVD
	19	<i>mvhA</i>	38-FRGFEKFLQGRRIEEAPR-IVPRICGICGVQHHL	103-YVSHSGLHFYFLAAPDFIG	367-GVGIVEAPRGTLTHHY	434-MVIRAYDPCLSATHVDGK
V	15	<i>orf5</i>	216-HRGMKLAETMRGYNEVTFLSDRVCGICGFAHST	279-RLHSHLLNLGLACHFTGFD	469-ALGFAEAPRGDDIHWS	522-LIIGSLDPCYSCTDRMTVVD
CONSENSUS			1 RG E R CG C H H G PRG H DPC C			

^a See Table I.

^b The asterisk in the *hysA* sequence indicates selenocysteine.

^c Sequences that could be in error are indicated in lowercase letters.

TABLE IV

CONSERVED CYSTEINE-CONTAINING SEQUENCE ELEMENTS IN THE ELECTRON-TRANSFERRING β SUBUNIT OF THE
Ni-CONTAINING HYDROGENASES

Group	N ^a	Gene	Element 5 ^b	Element 6	Element 7	Element 8	Element 9	Element 10
I	7	<i>hysB</i>	48-GCTGCSVSLNNAVHP	155-VGTCSAYGGIPAA	192-NVPGCPPHP	240-HENCPYLDKY	262-GCKAEL--GCKGPSTYADCA	294-AVCIGCPEPDPFDGKSPFY
II	4	<i>hynB</i>	66-ECTGCSESLRTVDP	159-IGTCATYGGVQAA	194-NIAGCPPNP	235-HDNCPLRKHf	262-YCLYEL--GCKGPDYNNCP	294-HPCIACSEPNFWDLYSPFY
	5	<i>hynB</i>	66-ECTGCSESVLRAFEP	161-YGTCATFGGVQAA	196-NIAGCPPNP	238-HEQCPLRPHf	265-WCLYEL--GCKGPVTMNNCP	297-HPCIGCSEPDFWDAMTPFY
	6	<i>hynB</i>	66-ECTGCTEAAIRTIKf	157-cirhlphGGVQKa	192-NIPGCPPNP	233-HDNCPLRPHf	260-FCLYEL--GCKGPVTYNNCP	292-HPCIGCSEPDFWDTMTPFY
III	8	<i>orf1</i>	62-ECTCCS--FIRSAHP	158-WGACASWGCVQAA	191-KVPGCPPIA	233-HDKCYRRPHf	260-YCLYKM--GCKGPTTYNACS	293-HGCIGCSEDGFWD-KGSFY
	9	<i>hupS</i>	61-ECTCCSESFIRSAHP	157-WGACASWGCVQAA	190-KVPGCPPIA	232-HDKCYRRPHf	259-YCLYKM--GCKGPTTYNACS	292-HGCIGCSEDGFWD-NGSFY
	10	<i>hupS</i>	52-ECTCCSESFIRSGDP	144-WGSCASWGCVQAA	176-KVPGCPPIA	218-HDKsYRRPHf	245-YCLYKV--GCKGPTSYNACS	278-HGCIGCSEDGFWD-KGSFY
	11	<i>hoxK</i>	61-ECTCCSESFIRSAHP	157-WGSCASWGCVQAA	190-KVPGCPPIA	232-HDKCYRRPHf	259-YCLYKV--GCKGPTSYNACS	292-HGCIGCSEDGFWD-KGSFY
	12	<i>hupS</i>	62-ECTCCSESFIRSAHP	158-WGACASYGCVQAA	191-KVPGCPPIA	233-HDKCYRRPHf	260-YCLYKM--GCKGPTTYNACS	293-HGCIGCSEDGFWD-QGSFY
	13	<i>hupS</i>	58-ECTCCSESFIRSAHP	153-WGSCASWGCVQAA	186-KVPGCPPIA	228-HDKCYRRPHf	255-FCLYKV--GCKGPTTYNACS	288-HGarr-SEDGFWD-KGSFY
	14	<i>hyaA</i>	61-ECTCTESFIRSAHP	157-WGTCASWGCVQAA	191-KVPGCPPIP	232-HDKCYRRAHf	259-YCLYKM--GCKGPTTYNACS	292-HGCLGCAENGFWd-RGSFY
	17	<i>mvhG</i>	14-GCSGCHLSIADFHGK	86-YGTCVAVYGIPGL	149-EVPGCPPRS	181-CEVCPREKPP	184-LCLIPQGLICMGPA TVSICG	238-IPCRGCGYPTARVEDQGAK
IV	19	<i>mvhG</i>	n.d. ^c	n.d.	n.d.	181-?EECEREKPP	184-LCLIAQGLVCMGPATTSICG	238-IPCQGCYGPTKAVEDQGAK
	CONSENSUS 2		C C	G C G	GCPP	C	C C GP C	C C
	16	<i>hoxY</i>	39-GCWGCTLSFLDMDER	109-VGACAVWGGVPAM	172-FIPGCPPDG	n.p. ^d	n.p.	n.p.
	CONSENSUS 3		C C	G C G	GCPP			
	18	<i>frhG</i>	(2 Cys)	90-FGSCAQGTGCFTRY	128-AIPGCPPSP	(8 Cys in 8Fe-8S ferredoxin sequence)		
V	CONSENSUS 4			G C G	GCPP			
	15	<i>orf2</i>	(16 Cys in 2 8Fe-8S ferredoxin motifs)					
	15	<i>orf6</i>	(8 Cys in 8Fe-8S ferredoxin motif; 6 additional Cys)					

^a See Table I.

^b Numbering continued from Table III.

^c n.d., Not determined.

^d n.p., Not present.

becomes meaningless in the multisubunit hydrogenases of groups IV and V, these polypeptides will be referred to as electron-transferring and nickel-binding (or simply β and α) subunits, respectively.

1. Enzyme Groups and Nickel-Binding Subunit Sequences

As is clear from Table III, the sequences for the α subunits form five groups, with a high degree of sequence homology within each group. Group I comprises only one sequence, that of the [Ni-Fe-Se] hydrogenase of *Desulfovibrio baculatus* (5, 9). It is distinct from the three sequences in group II, which represent the [Ni-Fe] hydrogenases of *Desulfovibrio gigas*, *D. vulgaris* Miyazaki F, and *Desulfovibrio fructosovorans* (4, 5, 7, 8). The sequences for both the α and β hydrogenase subunits in this group are highly homologous and have been found to share 65–70% overall sequence identity. This is reflected in the nearly identical sequences for elements 1–4 (Table III).

The genes for the [Ni-Fe] hydrogenase of *D. gigas* (4, 5) and the [Ni-Fe-Se] hydrogenase of *D. baculatus* (5, 9) were the first to be cloned and sequenced for the class of nickel-containing hydrogenases. The sequence of the [Ni-Fe-Se] enzyme from *D. baculatus* shares only 30–40% overall sequence identity with that of the group II [Ni-Fe] hydrogenases. The 3' end of *hysA* (Table III, element 4) was found to have an unusual codon, TGA, which normally signals translation termination, but has been shown to encode selenocysteine in formate dehydrogenase from *E. coli* (45) and glutathione peroxidase from mouse cells (46). The homologous codon in the group II *hynA* sequences is TGC, which codes for cysteine. Spectroscopic studies have indicated coordination of the selenocysteine residue to the active site nickel (47, 48). The sequence comparison of [Ni-Fe] and [Ni-Fe-Se] hydrogenases from *D. gigas* and *D. baculatus* did thus establish one of the ligands to Ni (5). The (seleno)cysteine is the first of a pair of cysteine residues in the strictly conserved sequence DPCXXC, present in all α subunits of nickel-containing hydrogenases sequenced to date (Table III, consensus 1).

Group III comprises seven [NiFe] hydrogenase sequences from *B. japonicum*, *Rhizobium leguminosarum*, *Azotobacter chroococcum*, *Azotobacter vinelandii*, *Rhodobacter capsulatus*, *Rhodocyclus gelatinosus*, and *E. coli*. The sequences for elements 1–4 in this group are again highly homologous (Table III) and strongly resemble those for the [Ni-Fe] hydrogenases in group II. At the DNA level the degree of sequence identity is sufficient to allow the *hya* operon of *E. coli* to be cloned with the use of a group II DNA probe, derived from the *hynB*, *A* operon of *D. vulgaris* (18). Despite these strong similarities there are

two major, related differences between group II and group III hydrogenases. First, the group III [Ni-Fe] hydrogenases are encoded by a polycistronic operon. The *hya* operon of *E. coli* comprises six genes, of which the first two (*hyaA* and *hyaB*) encode the electron-transferring and the nickel-binding subunits, respectively. Reading frame 3 (*hyaC*) encodes a hydrophobic integral membrane protein of 27.6 kDa, which may interact with the *hyaA* and *hyaB* gene products. Evidence that the other six hydrogenases in group III are encoded by a similar polycistronic operon is provided by the observation that a gene homologous to *hyaC* has been found immediately downstream from the hydrogenase structural genes in *B. japonicum* (*orf3*), *A. chroococcum* (*orf3*), *A. vinelandii* (*orf3*), and *R. capsulatus* (*orfX*). The presence of additional genes downstream from *hupS* and *hupL* has been reported for *R. leguminosarum* (12). At the time of writing of this article, the *hya* operon is the only one for which the complete sequence has been published, and it remains to be established whether these other operons also comprise six genes and whether genes 4–6 share homology with *hyaD*–*hyaF*. This structural difference with group II [Ni-Fe] hydrogenases is precipitated by a different mode of action: group III hydrogenases deliver the electrons derived from hydrogen directly to a membrane-bound electron transport chain, whereas group II hydrogenases donate their electrons to a soluble, nonmembrane-bound, periplasmic cytochrome.

The second difference between group II and III hydrogenases is that the COOH-terminus of the electron-transferring β subunit of group III hydrogenases has an extension of ~ 50 amino acids, when compared with the group II β subunit sequences. This extension is hydrophobic and serves to anchor the $\alpha\beta$ hydrogenase dimer to the membrane. Isolation of group III [Ni-Fe] hydrogenases therefore requires detergent (to disrupt the membrane) or protease (to cleave the hydrophobic extension) treatment. This structural feature is presumably related to the first and helps in the interaction of the $\alpha\beta$ dimer with the other, membrane-bound components encoded by the operon.

The group IV hydrogenases are isolated as three- or four-subunit enzymes. This group includes the methyl viologen-reducing hydrogenase from the archaeobacteria *Methanobacterium thermoautotrophicum* and *Methanothermobacter ferredoxianus*, a three-subunit enzyme encoded by the *mvhD*, *mvhG*, and *mvhA* genes. The operon encoding this enzyme includes a fourth gene (*mvhB*) that encodes a polyferredoxin (21, 23), which does not copurify with the methyl viologen-reducing hydrogenase. The F_{420} -reducing hydrogenase from *M. thermoautotrophicum* also belongs to this group and is encoded by three structural genes (*frhA*, *frhB*, and *frhG*). Finally, the NAD^+ -reducing hydrogenase of

the eubacterium *Alcaligenes eutrophus* belongs to group IV. Its four subunits are encoded by the *hoxF*, *hoxU*, *hoxY*, and *hoxH* genes, which are organized in the *hoxS* operon (20). The nickel-binding subunits in these operons, encoded by the *hoxH*, *mvhA*, and *frhA* genes, share extensive sequence homology as indicated by the sequences for elements 1–4 in Table III. In element 4, for instance, the sequence IRAY is unique to this group.

Finally, group V is represented by only a single sequence for the nickel-binding subunit of hydrogenase-3 from *E. coli* encoded by *orf5* (19). This hydrogenase is, like the hydrogenases in group IV, a cytoplasmic enzyme. Hydrogenase 3 functions in hydrogen production in the formate hydrogenlyase reaction. The functional difference is reflected in the sequence of the nickel-binding subunit of this hydrogenase, which differs appreciably from those in groups I–IV. Highest homologies are observed with the enzymes from group IV (Table III).

Comparison of the sequences for elements 1–4 for all five groups leads to the definition of 18 strictly conserved residues, identical in all 16 sequences (Table III, consensus 1). These will be indicated with Roman numerals (R-I to C-XVIII) in the discussion below. Although it may seem an oversimplification to consider only 18 residues in a chain of 500–600, it must be realized that the actual degree of homology is much higher, since (1) the 18 conserved residues are grouped in four sequences (elements 1–4) that are similarly spaced in all 16 chains, and (2) the other residues in these elements often show only limited variation, as can easily be verified by comparing the sequences in Table III.

Which of these conserved residues coordinate to redox prosthetic groups and which types of redox prosthetic groups are present in the nickel-binding subunits? As indicated above, sequence comparison and spectroscopic measurements have established C-XVI as a nickel ligand. Extended X-ray absorption fine structure (EXAFS) studies have established that the coordination sphere of [Ni–Fe] and [Ni–Fe–Se] hydrogenases is very similarly occupied by 3 ± 1 N,O donors and 2 ± 1 S donors (47, 49). As discussed elsewhere, another S (in addition to C-XVI) and one N (e.g., imidazole) are likely to coordinate to Ni (50). These could be provided by one of the three strictly conserved cysteine and histidine residues of the consensus 1 sequence. If a histidine residue coordinates to nickel, it is unlikely to be one of the two histidines present in element 4 in group II and group III hydrogenases, since these are not conserved in groups IV and V (Table III). The nickel-binding subunit may also coordinate one Fe–S cluster, in close proximity to Ni. The interpretation of recent EXAFS studies (49) indicated that the

active site Ni of [Ni-Fe] and [Ni-Fe-Se] hydrogenase may be present in a Ni, Fe, and S cluster in which the Ni shares sulfur ligands with the Fe-S cluster. The [Ni-Fe] hydrogenase from *D. gigas* has been shown to contain two 4Fe-4S clusters, one 3Fe-4S (or 3Fe- α S) cluster, and a nickel atom (51, 54). As reviewed elsewhere (50), the small β subunit of this two-subunit nickel-containing hydrogenase is likely to coordinate the two electron-transferring 4Fe-4S clusters, whereas the 3Fe-4S cluster is coordinated by the α subunit. Taken together, the data indicate the existence of a Ni, Fe, and S cluster at the active site in the nickel-binding subunit of nickel-containing hydrogenases that is coordinated by the four cysteine residues and some of the other conserved residues indicated in the consensus 1 sequence of Table III. The remaining conserved residues could function as proton conductors in the hydrogen evolution/consumption reaction as discussed in Section II,A for [Fe] hydrogenase. The exact arrangement will only become clear from X-ray crystallographic studies (55, 56) and/or from spectroscopic work (e.g., EXAFS) on site-directed mutants.

2. Electron-Transferring Subunit Sequences

The sequences of conserved elements 5-10 of the electron-transferring subunit of the nickel-containing hydrogenases are compared in Table IV. It appears that a single comparison for all hydrogenase groups I-V is not meaningful: the electron-transferring subunits of two of the enzymes in group IV lack some conserved elements, whereas hydrogenase 3 (group V) lacks all conserved elements 5-10. Focusing first on groups I-III and the *mvhG* gene products of group IV, it appears that the 13 sequences have 17 strictly conserved positions as indicated in the consensus 2 sequence. These will again be labeled with Roman numerals, C-I to C-XVII, and include 10 cysteine, 4 glycine, and 3 proline residues. Interestingly, there are with the possible exception of the cysteines no conserved proton-conducting residues (e.g., histidines), confirming that the active site of hydrogenase and its proton-conducting channels are located on the nickel binding α subunit: the β subunit has a strictly electron-transferring function. As discussed in Section II,B,1, the 10 conserved cysteine residues are likely to coordinate two 4Fe-4S clusters. Assignment of specific cysteines to these two clusters is difficult because they are spread out over the β subunit amino acid sequence. Although two pairs and a triplet are present (Table IV, elements 5, 9, and 10), an F-cluster binding motif C-X-X-C-X-X-C-X-X-X-C as in [Fe] hydrogenase (Section II,A) is not found. Nevertheless, an assignment can be made when the sequence of the *A. eutrophus* *hoxY* gene product is considered. This protein shares elements 5, 6, and

7 with the consensus 2 sequence but lacks elements 8, 9, and 10. The *hoxY* gene product (22.9 kDa) is considerably smaller than the 13 consensus 2 electron-transferring subunits (28–35 kDa). Its polypeptide chain terminates immediately following element 7. The *hoxY* gene product binds only a single 4Fe–4S cluster (20), which is likely coordinated by the four cysteine residues of the consensus 3 sequence (Table IV). This cluster, referred to as F1 from hereon, is therefore also likely to be coordinated by the four corresponding cysteine residues of the consensus 2 sequence: C-I, C-II, C-IV, and C-VII. The second 4Fe–4S cluster, F2, of the electron-transferring subunit of consensus 2 hydrogenases, could then be coordinated by four of the six remaining conserved cysteine residues of the consensus 2 sequence: C-X, C-XI, C-XII, C-XV, C-XVI, and C-XVII. The variability in sequence of electron-transferring subunits is further demonstrated by considering the 25.7-kDa protein of the F₄₂₀-reducing hydrogenase of *M. thermoautotrophicum*. It shares the two cysteines (C-IV and C-VII) of elements 6 and 7 with the consensus 3 sequence. However, C-I and C-II are lacking, although two other cysteine residues are present in a sequence that is not homologous to element 5. Nevertheless, these four cysteines could coordinate the F1-cluster. Interestingly, although the COOH-terminal portion of this protein lacks elements 8–10, it does contain eight cysteine residues in an 8Fe–8S ferredoxin motif, which are likely to coordinate two additional F-clusters. The *frhG* gene product may thus coordinate three rather than two electron-transferring clusters. The culmination of these changes is provided by hydrogenase-3, which does not share any of the elements 5–10 in the sequences of the *orf2* and *orf6* gene products, which clearly encode electron transfer proteins since both contain 8Fe–8S ferredoxin motifs (Table IV). It thus appears that though the sequence of the nickel-binding subunit is relatively conserved in nickel-containing hydrogenases, the electron transfer function can be accommodated by a variety of Fe–S cluster-containing redox proteins.

III. Evolution of Hydrogenase Genes: "Redon Shuffling" and Hydrogenase Export

Comparison of the 19 hydrogenase sequences in Section II clearly confirms the existence of two different families, the iron-only and the nickel-containing hydrogenases. There are no significant homologies between the polypeptides encoding the active sites of these enzymes, respectively, the COOH-terminal portion (residues 106–420) of the α and the β subunits (89 residues) of periplasmic iron-only hydrogenases

and the nickel-containing subunit (500–650 residues) of the nickel-containing hydrogenases. Members within a family are related, but the two families must have evolved independently. The hydrogenase from *Anabaena cylindrica* (24) is again completely different and forms a third family that will not be considered here.

The significant homology among the nickel-binding subunits of 16 nickel-containing enzymes (Table III, consensus 1), representing different bacterial genera and classified here in five distinct enzyme groups, suggests evolution from a common ancestor. This polypeptide coordinates a Ni, Fe, and S cluster and specifies possibly conserved proton conduction pathways, which are essential for the conversion of hydrogen into protons and electrons or vice versa. It associates generally with one electron-transferring subunit, which is not as strongly conserved and shows a variety of Fe–S cluster coordination patterns. The present data should not be interpreted as indicating that the consensus 2 sequence for this subunit is the most common, since the sample of sequences currently available may not be representative. With this reservation in mind, the data do indicate that the suggested F1-cluster, coordinated by the four cysteines of the consensus 3 sequence (Table III), is more conserved than the F2-cluster, coordinated by cysteine residues in the COOH-terminal domain of the consensus 2 sequence. This observation suggests the following path for the electrons during hydrogen uptake: (Ni, Fe, S) \rightarrow F1 \rightarrow F2. The functional equivalent of cluster F2 is likely to reside on one of the other two subunits of the NAD⁺-reducing hydrogenase of *A. eutrophus*. The γ subunit (30 kDa) is thought to contain two 4Fe–4S clusters, whereas the δ subunit (63 kDa) contains a 2Fe–2S cluster and a bound FAD. Electrons may thus flow from F1 in the β subunit to clusters in γ and δ subunits and FAD, which then reduces NAD⁺. (Note: since α and β denote hydrogenase subunits in this review, all subunit symbols used here have a different meaning from those in Ref. 20.)

The different forms of the electron-transferring subunits found in group IV and V hydrogenases encoded by *frhG*, *orf2*, and *orf6* may have resulted by shuffling and combining genes encoding smaller redox proteins. Several of these genes have now been cloned and sequenced, e.g., the *rub* gene (156 nucleotides) encoding rubredoxin from *D. vulgaris* Hildenborough encodes a protein of only 52 amino acids, with two pairs of cysteines C-X-X-C present at the NH₂ and COOH terminus (57). The *dsr* gene of *D. gigas* (108 nt) encodes desulfiredoxin, a protein of only 36 amino acids, which also coordinates one Fe per polypeptide (58b). The 8Fe–8S ferredoxins (50–60 amino acids) are widespread (see Ref. 58 for a review) and their genes (*frd*, 150–160 nt) have been

analyzed from a variety of sources. The mode of coordination of eight cysteine residues to two 4Fe–4S clusters in these small redox proteins has been elucidated by X-ray crystallography (34). These small units of DNA (100–200 nt), encoding the smallest possible polypeptide domain coordinating a defined redox prosthetic group, will be referred to as redons. Genes for larger redox proteins can be assembled from these basic units by “redon shuffling.” For instance, the *rbo* gene encoding a novel redox protein recently discovered in *D. vulgaris* Hildenborough has the *dsr* redon at its 5′ end (59). The *rbr* gene, encoding rubrerythrin from the same organism, has the *rub* redon at its 3′ end (60). Fusion of six *frd* redons has given rise to the polyferredoxin gene (*mvhB*) of archaebacteria. The sequence variability of the electron-transferring subunit genes of nickel-containing hydrogenases thus originates from redon shuffling, e.g., the *frhG* gene may have formed by replacing DNA encoding the F2 cluster region by a *frd* redon. The variability found so far is large when one considers the limited number of sequences examined and indicates that other sequences may yet be found.

The electron-transferring subunit of nickel-containing hydrogenases has one other sequence variability option of great consequence: the presence of a complex 30- to 50-amino acid residue signal sequence at its NH₂ terminus destines the enzyme for export to the periplasm. Lack of the signal sequence causes a cytoplasmic location. The enzymes of groups I–III all have signal sequences, which are compared in Table V, and are periplasmic with the possible exception of the [NiFeSe] hydrogenase (61). The enzymes of groups IV and V do not have signal sequences and are cytoplasmic. There are two intriguing aspects to the signal sequences in Table V:

1. All sequences contain a strictly conserved element (consensus 5). This is most unusual for signal sequences and suggests that all of these hydrogenases are exported via a unique, conserved mechanism.
2. The nickel-binding subunit (generally referred to in the literature as the large subunit, since all periplasmic hydrogenases are two-subunit enzymes) lacks a signal sequence.

The mechanism of export of hydrogenase has been investigated in some detail (6, 29, 62). It appears that a pro- β , α complex may be formed in the cytoplasm or at the cytoplasmic face of the inner membrane, which is then exported, resulting in cleavage of the signal peptide. Thus a single signal peptide operates in the export of both subunits. Recent studies by Niviere *et al.* (63), in which DNA encoding the signal peptide for [NiFe] hydrogenase of *D. vulgaris* Hildenborough was fused to the gene for β -lactamase, lacking its natural signal peptide, provided fur-

TABLE V
HYDROGENASE SIGNAL PEPTIDES

Group	N ^a	Gene	Signal sequence ^b									
[Fe]	1	<i>hydB</i>	MQIASIT	RR	G	F	L	K	VACVTTGAALIGIRMTGKAVA↓AVK	++	+	+ + +
[Fe]	2	<i>hydB</i>	MQIVNLT	RR	G	F	L	K	AACVVTAALISIRMTGKAVA↓AAK	++	+	+ + +
I	7	<i>hysB</i>	MSLS	RR	E	F	V	K	LCSAGVAGLGISQIYHFGIVHA↓MTE	++	-	+ -
II	4	<i>hynB</i>	MKCYIGRGKNQVEERLERRGVS	RR	D	F	M	K	FCTAVAVAMGMGPAFAFKVAEA↓LTA	++	+	+ + +
	5	<i>hynB</i>	MKISIGLGKEGVEERLAERGV	RR	D	F	L	K	FCTAIAVTMGMGPAFAPEVARA↓LMG	++	+	+ + +
	6	<i>hynB</i>	MNFSVGLGRMNAEKRLVQNGVS	RR	D	F	M	K	FCATVAAAMGMGPAFAFKVAEA↓LTA	++	+	+ + +
III	8	<i>orf1</i>	MGAATETFYSVIRRGGIT	RR	S	F	H	K	FCSLTATSLGLGPLAASRIANA↓LET	++	+	+ + +
	9	<i>hupS</i>	MATAETFDVIRRGGIT	RR	S	F	T	K	FCSLTAASLGFPGGAATAMAEA↓LET	++	+	+ + +
	10	<i>hupS</i>	MRRQGIT	RR	S	F	L	K	YCSLTGRPCLGPTFAPQIAHA↓MET	++	+	+ + +
	11	<i>hoxK</i>	MSRLETFDVMRRQGIT	RR	S	F	L	K	YCSLTAALGLGPAFAFRIAHA↓MET	++	+	+ + +
	12	<i>hupS</i>	MMSDIETFDVMRRQGIT	RR	S	F	M	K	SVRSPQHVGLGLGFSFVPKIGEA↓MET	++	+	+ + +
	13	<i>hupS</i>	METFYEVMRRGIS	RR	S	F	L	K	YCSLTATSLGLAPSFPVQIAHA↓MET	++	+	+ + +
	14	<i>hyaA</i>	MNNEETFYQAMRRQGV	RR	S	F	L	K	YCSLAATSLGLGAGMAPKIAWA↓LEN	++	+	+ + +
CONSENSUS 5				RR	F	K						

^a See Table I.

^b Positively (+) and negatively (-) charged residues as well as the signal peptidase cleavage site (↓) are indicated.

ther evidence for a highly specialized export mechanism. In *E. coli* [Ni-Fe], hydrogenases 1 and 3 are only expressed under anaerobic conditions. It appeared that the constructed fusion was only efficiently exported and processed under anaerobic conditions. The results supported the theory that under these conditions at least one protein was expressed that specifically facilitates hydrogenase export and processing.

Thus, assuming that a cytoplasmic, nickel-containing hydrogenase existed first, the evolutionary path toward a periplasmic enzyme left the nickel-binding subunit and its assembly locus relatively unchanged. Instead, the malleable electron-transferring subunit was equipped with

a unique signal peptide and a specific export mechanism evolved, accommodating its own export and that of the nickel-binding subunit following cytoplasmic assembly of the (Ni, Fe, S) cluster in the latter.

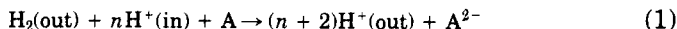
The limited number of [Fe] hydrogenase sequences makes it harder to speculate on their evolution. A gene for an H-cluster binding protein (encoding residues 200–606 of the putative *hydC* gene product; Ref. 3) may have fused with a *frd* redon to create a hydrogenase II-like gene. This gene encodes a simple cytoplasmic, single-subunit hydrogenase, which accommodates both the H-cluster and two F-clusters. The electron transfer function may also be less strictly conserved in cytoplasmic [Fe] hydrogenases, as observed for the nickel-containing enzymes (Section II,B and above). Fusion with a second *frd* redon at the 5' end of the hydrogenase II gene may have created the hydrogenase I gene, which encodes a cytoplasmic hydrogenase with four F-clusters (see Section V). Periplasmic localization was achieved, by fusing DNA encoding the specific signal peptide (Table V) near the 3' end of a hydrogenase II-like gene, such that a two-subunit enzyme was created. Assembly and export of this enzyme is through a similar mechanism as described for the group I–III nickel-containing hydrogenases: assembly of F- and H-clusters in the α subunit, binding of pro- β , and export and processing. It is indeed remarkable that the two classes of periplasmic hydrogenases do not share sequence homology, except the consensus 5 sequence (Table V).

IV. Functions of Hydrogenases

The main purpose of the speculations in Section III was to draw together, in an evolutionary model, the structures of the various hydrogenases that exist today. Such models, e.g., the evolution of genes for a periplasmic hydrogenase from those for a cytoplasmic hydrogenase, are generally hard to prove, and Section III will therefore remain largely speculative. Although it would appear that it must be easier to define the function of hydrogenases presently occurring in prokaryotes (Table I), this is actually difficult in cases in which multiple enzymes are present and/or when the organism lives both fermentatively (favoring hydrogen production) and respiratively (favoring hydrogen consumption).

The most straightforward case is that of the group III nickel-containing hydrogenases. These are membrane-bound, periplasmic-uptake hydrogenases that deliver the electrons from hydrogen to the membrane-bound electron transport chain, where they eventually reduce a

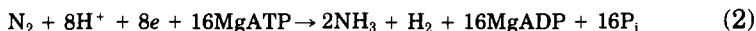
higher potential electron acceptor A (e.g., fumarate, nitrate, and oxygen). The overall reaction catalyzed by hydrogenase and the electron transport chain is thus:



Equation (1) indicates that the flow of two electrons from hydrogen to the electron acceptor A leads to free-energy conservation by coupled export of n protons to the periplasm, where n will increase with an increased difference in reduction potentials of the $2\text{H}^+/\text{H}_2$ and the A/A^{2-} couples. If these potentials are similar, then $n \approx 0$ and there may be no need for tight structural coupling of hydrogenase with the membrane-bound electron transport chain. This could be one of the main reasons for the structural differences of group II nickel-containing hydrogenases of sulfate-reducing bacteria and those of group III (Section II,B,1).

Since the hydrogenase uptake reaction releases two protons into the periplasm, the total number of protons released is $(n + 2)$, and assuming that m protons flow back via ATP synthase per ATP synthesized from ADP and P_i , a total of $(n + 2)/m$ moles of ATP can be formed per mole of hydrogen oxidized. From this discussion it would appear energetically advantageous to locate uptake hydrogenases in the periplasm. However, this may be an oversimplification: periplasmic and cytoplasmic compartments are kept at a different pH and potential, such that conversion of 1 mol of hydrogen to 2 mol of protons in the cytoplasm is accompanied by a larger decrease in free energy of the system (ΔG_c) than when this reaction is carried out in the periplasm (ΔG_p). A thermodynamic "cycle" in which cytoplasmic conversion is followed by export of 2 mol of protons (positive free energy, ΔG_e) could be energetically equivalent ($\Delta G_c + \Delta G_e = \Delta G_p$), but such a mechanism does of course require a proton pump. In conclusion, there may be no thermodynamic arguments against cytoplasmic uptake hydrogenases and these do indeed occur, e.g., those of archaebacteria (21–23, 64) and the enzyme of *Desulfotomaculum orientis* (65).

One of the functions of group III nickel-containing hydrogenases has been to trap hydrogen produced in the cytoplasm by another reaction, e.g., the fixation of nitrogen in *Azotobacter*, *Rhizobium*, and other species (66):



Azotobacter eutrophus appears to have a group III nickel-containing uptake hydrogenase, in addition to its NAD^+ -reducing hydrogenase (20, 67). The latter is not present in all members of the autotrophic

hydrogen-oxidizing bacteria (67). Of course, both NADH and ATP are needed in the fixation of CO₂ into carbohydrate and the combined action of these two hydrogenases may well provide a correct ratio of these two prerequisites, e.g., as provided by the combined action of photosystems I and II in plants.

The function of hydrogenase 3 has already been briefly mentioned in Section II,B,1. It is the only enzyme of Table I that has a firmly established function in hydrogen production [see Eq. (3)]. In addition to hydrogenase 1, *E. coli* has a second, nickel-containing uptake hydrogenase, hydrogenase 2. No structural information is available for this enzyme at present. The sequence of the hydrogenase 2 operon has not yet been reported. The enzyme is immunologically distinct from hydrogenase 1 (26, 68). Hydrogenase 1 is expressed under the same conditions that lead to expression of hydrogenase 3 and is, therefore, suggested to function in the uptake of hydrogen produced by hydrogenase 3 during the formate hydrogenlyase reaction:



Hydrogenase 2 is thought to couple hydrogen oxidation to, e.g., fumarate reduction under anaerobic conditions. Hydrogenase 2 is present but is believed to be inactive during fermentative growth in the presence of formate (69), and it has been suggested that, under these conditions, hydrogenase 1 recycles the fermentatively produced hydrogen by reducing endogenously generated electron acceptors (i.e., fumarate) (69). The rationale for having these two enzymes, which seem to share the same terminal electron acceptor(s), is thus not clear at present.

It is similarly difficult to prove definitively the roles of the various hydrogenases in the sulfate-reducing bacteria *Desulfovibrio*. As indicated in Table VI, the genes for periplasmic [Fe], periplasmic [Ni-Fe], and [Ni-Fe-Se] hydrogenase are distributed such that four classes arise (28). All contain the group II nickel-containing hydrogenase, which is the exclusive enzyme in the class 4 *Desulfovibrio* species. It has been proposed elsewhere that both the periplasmic [NiFe] and [Fe] hydrogenase of *Desulfovibrio* serve as hydrogen uptake enzymes (6), but that the [Fe] enzyme acts only at high hydrogen concentrations in view of its low H₂ affinity ($K_m \approx 100 \mu\text{M}$) compared to the [Ni-Fe] enzyme ($K_m \approx 1 \mu\text{M}$). The advantage of expressing periplasmic [Fe] hydrogenase for class 1 and 2 strains (Table VI) would then be that at high hydrogen concentration hydrogen can be taken up at a high rate, since the turnover number of [Fe] hydrogenase is ≈ 30 -fold higher than that of [Ni-Fe] hydrogenase. This proposal may apply to *D. vulgaris* Hildenborough, in which 95% of the periplasmic hydrogenase activity

TABLE VI

DISTRIBUTION OF HYDROGENASE GENES IN *Desulfovibrio*

Class 1:	[Fe], [Ni-Fe-Se], and [Ni-Fe] hydrogenase (9 species) <i>Desulfovibrio vulgaris</i> Hildenborough <i>Desulfovibrio vulgaris</i> Wandle <i>Desulfovibrio vulgaris</i> Brockhurst Hill <i>Desulfovibrio vulgaris</i> ssp. <i>oxamicus</i> Monticello 2 <i>Desulfovibrio desulfuricans</i> Berre Sol <i>Desulfovibrio desulfuricans</i> Canet 41 <i>Desulfovibrio desulfuricans</i> G200 <i>Desulfovibrio africanus</i> Walvis Bay <i>Desulfovibrio africanus</i> Bhengazi
Class 2:	[Fe] and [Ni-Fe] hydrogenase (4 species) <i>Desulfovibrio desulfuricans</i> El Agheila Z <i>Desulfovibrio desulfuricans</i> NCIMB 8307 <i>Desulfovibrio multispirans</i> <i>Desulfovibrio fructosovorans</i>
Class 3:	[Ni-Fe-Se] and [Ni-Fe] hydrogenase (6 species) <i>Desulfovibrio vulgaris</i> Miyazaki F <i>Desulfovibrio vulgaris</i> ssp. <i>oxamicus</i> UofA <i>Desulfovibrio desulfuricans</i> Norway 4 <i>Desulfovibrio salexigens</i> British Guiana <i>Desulfovibrio salexigens</i> California <i>Desulfovibrio salexigens</i> NCIMB 8365
Class 4:	[Ni-Fe] hydrogenase (3 species) <i>Desulfovibrio vulgaris</i> Groningen <i>Desulfovibrio desulfuricans</i> Teddington R <i>Desulfovibrio gigas</i>

(measured at high hydrogen concentration) is due to [Fe] hydrogenase (35) and the remaining 5% is due to the two nickel-containing hydrogenases. However, in *Desulfovibrio fructosovorans*, which contains only the [Fe] and [Ni-Fe] hydrogenase, the latter was found responsible for 90% of the total uptake hydrogenase activity (70). Inactivation of the *hynB,A* genes by marker exchange mutagenesis (Ref. 70; the first time directed gene inactivation has been achieved in this genus) caused a lag phase in the growth on hydrogen sulfate medium. However, the cells grew to the same density, indicating that hydrogen uptake through [Fe] hydrogenase was equally efficient thermodynamically. Repression of [Fe] hydrogenase in *D. vulgaris* Hildenborough by expression of *hydA,B* antisense mRNA slowed bacterial growth on lactate-sulfate medium and caused a reduced accumulation of H₂ in the

medium head space (35). *Desulfovibrio vulgaris* Hildenborough is a net hydrogen producer when grown in this medium. These results were interpreted as indicating that the function of [Fe] hydrogenase in *D. vulgaris* Hildenborough is hydrogen production, a function attributed to [Ni-Fe-Se] hydrogenase by others (61). It would be worthwhile to test growth of the [Fe] hydrogenase-repressed *D. vulgaris* Hildenborough on hydrogen-sulfate medium (71), on which *D. vulgaris* Hildenborough can also grow (R. K. Thauer, personal communication, 1991).

A final problem to be considered here in the function of hydrogenases in *Desulfovibrio* is how the electrons make their way to the cytoplasm, where the sulfate is reduced. As indicated in Section II,B,1, all three hydrogenase types are encoded by simple bicistronic operons that do not contain genes whose products could conduct the electrons through the membrane. The physiological electron carrier for hydrogenases in *Desulfovibrio* is thought to be cytochrome c_3 , a 13-kDa *c*-type cytochrome that binds four *c*-type hemes and is exclusively present in the periplasm. The problem is that the next electron carrier in the chain (hydrogenase \rightarrow cytochrome $c_3 \rightarrow ?$) is not known. The structure of the high-molecular-weight cytochrome (72), which is also a periplasmic protein, was recently determined by cloning and sequencing its gene (73). It appeared that the sequence of this protein, which binds 16 hemes covalently to a polypeptide chain of 58.9 kDa, can be described in terms of four cytochrome c_3 -like domains. Three complete domains, coordinating four *c*-type hemes similarly as cytochrome c_3 , and one incomplete domain, which may have a high-potential histidine-methionine coordinate heme. Although this more complex structure does not by itself solve the above problem, it was subsequently found (W. B. R. Pollock, 1992, unpublished) that Hmc is encoded by the first gene (*hmc*) in an operon that contains at least six open reading frames, encoding proteins Orf1-Orf6. Orf1 (Hmc) is the periplasmic high-molecular-weight cytochrome; Orf2 is a largely periplasmic iron-sulfur protein anchored to the membrane; Orf3, Orf4, and Orf5 are integral membrane proteins; and Orf6 is a cytoplasmic iron-sulfur protein. Thus the operon structure suggests that all proteins, Orf1-Orf6, may be physically interacting and that the *hmc* operon encodes the link between the periplasmic hydrogenases and the cytoplasmic redox chain in *D. vulgaris*.

V. Perspectives

Sections I-IV of this review were completed just prior to the Third International Conference on Molecular Biology of Hydrogenases in

Troia, Portugal, from July 29 to August 1, 1991. At this meeting, Thauer and co-workers reported on a novel family of hydrogenases in archaeobacteria in which the presence of a metal ion or other redox prosthetic group has yet to be demonstrated. Extensive nucleic acid sequencing of the [Ni-Fe] hydrogenase operons of *R. capsulatus* (Vignais and co-workers), *A. vinelandii* (Mortenson and co-workers), and *R. leguminosarum* (Ruiz-Argueso and co-workers) revealed that these comprise ~15 genes. In addition to the two hydrogenase structural genes and the equivalent of the *E. coli hyaC* gene, these include genes for nickel-processing proteins and genes homologous to open reading frames of the *E. coli hya*, *hyp*, and hydrogenase 3 operons. Possibly, these large operons specify all necessary functions to form an active periplasmic [NiFe] hydrogenase in these organisms. In *E. coli*, which likely requires additional genes to specify its three hydrogenases, these genes have been scattered over different genomic loci. The observation of widespread homology among the multitude of genes required for hydrogenase formation in different organisms makes a more uniform gene nomenclature desirable and a proposal in this direction is being prepared by P. Vignais. Kroger and co-workers reported the sequence of the [Ni-Fe] hydrogenase genes from *Wolinella succinogenes*, belonging to group III (Table III), and showed that the *E. coli hyaC* equivalent gene expresses a membrane-bound, *b*-type cytochrome. The sequence of hydrogenase I from *C. pasteurianum* was reported by Meyer and Gagnon (74). It showed striking homologies with the *hydC* and *hydA,B* gene products and confirmed the conserved elements listed in Table II. Hydrogenase I shares an additional seven conserved cysteine residues with the *hydC* gene product in a sequence located on the N-terminal side of elements 1 and 2 (Table II). These residues are not present in an 8Fe-8S ferredoxin motif, but must, in view of their conservation, contribute to the coordination of the two additional F-clusters of hydrogenase I. Site-directed mutagenesis of the *E. coli hyaB* gene (Przybyla and co-workers) confirmed several of the consensus-1 residues (Table III: R-IV, C-VII, D-XV, C-XVII, and C-XVIII) as essential. These and other presentations confirmed the great progress that has been made in the molecular biology of hydrogenases. What is still lacking is a three-dimensional structure and it must be hoped that current efforts (55, 56) to solve the structure of group II [Ni-Fe] hydrogenases will be successful soon. Lacking also is a firm understanding of the role of individual enzymes in organisms expressing multiple hydrogenases (e.g., *Desulfovibrio*). This understanding may be achieved by progress in directed mutagenesis studies and the achievement of a more thorough thermodynamic description of the metabolic energy transformations in these bacteria.

ACKNOWLEDGMENTS

Work in the author's laboratory was supported financially by the National Science and Engineering Research Council of Canada and intellectually by Michael Brumlik, Harm Deckers, Vincent Niviere, Brent Pollock, Hansje Voordouw, and Frankie Wilson.

REFERENCES

1. Voordouw, G., and Brenner, S., *Eur. J. Biochem.* **148**, 515 (1985).
2. Voordouw, G., Strang, J. D., and Wilson, F. R., *J. Bacteriol.* **171**, 3881 (1989).
3. Stokkermans, J., van Dongen, W., Kaan, A., van den Berg, W., and Veeger, C., *FEMS Microbiol. Lett.* **58**, 217 (1989).
4. Li, C., Peck, H. D., Jr., LeGall, J., and Przybyla, A. E., *DNA* **6**, 539 (1987).
5. Voordouw, G., Menon, N. K., LeGall, J., Choi, E.-S., Peck, H. D., Jr., and Przybyla, A. E., *J. Bacteriol.* **171**, 2894 (1989).
6. Voordouw, G., in "Microbiology and Biochemistry of Strict Anaerobes Involved in Interspecies Hydrogen Transfer" (J. P. Belaich, M. Bruschi, and J. L. Garcia, eds.), p. 37. Plenum, New York, 1990.
7. Deckers, H. M., Wilson, F. R., and Voordouw, G., *J. Gen. Microbiol.* **136**, 2021 (1990).
8. Rousset, M., Dermoun, Z., Hatchikian, C. E., and Belaich, J. P., *Gene* **94**, 95 (1990).
9. Menon, N. K., Peck, H. D., Jr., LeGall, J., and Przybyla, A. E., *J. Bacteriol.* **169**, 5401 (1987).
10. Sayavedra-Soto, L. A., Powell, G. K., Evans, H. J., and Morris, R. O., *Proc. Natl. Acad. Sci. U.S.A.* **85**, 8395 (1988).
11. Schneider, C. G., Schmitt, H. J., Schild, Ch., Tichy, H. V., and Lotz, W., *Nucleic Acids Res.* **18**, 5285 (1990).
12. Hidalgo, E., Levya, A., and Ruiz-Argueso, T., *Plant. Mol. Biol.* **15**, 371 (1990).
13. Ford, C. M., Garg, N., Garg, R. P., Tibelius, K. H., Yates, M. G., Arp, D. J., and Seefeldt, L. C., *Mol. Microbiol.* **4**, 999 (1990).
14. Menon, A. L., Stults, L. W., Robson, R. L., and Mortenson, L. E., *Gene* **96**, 67 (1990).
15. Leclerc, M., Colbeau, A., Cauvin, B., and Vignais, P. M., *Mol. Gen. Genet.* **214**, 97 (1988).
16. Richaud, P., Vignais, P. M., Colbeau, A., Uffen, R. L., and Cauvin, B., *FEMS Microbiol. Rev.* **87**, 413 (1990).
17. Uffen, R. L., Colbeau, A., Richaud, P., and Vignais, P. M., *Mol. Gen. Genet.* **221**, 49 (1990).
18. Menon, N. K., Robbins, J., Peck, H. D., Jr., Chatelus, C. Y., Choi, E.-S., and Przybyla, A. E., *J. Bacteriol.* **172**, 1969 (1990).
19. Bohm, R., Sauter, M., and Bock, A., *Mol. Microbiol.* **4**, 231 (1990).
20. Tran-Betcke, A., Warnecke, U., Bocker, C., Zaborosch, C., and Friedrich, B., *J. Bacteriol.* **172**, 2920 (1990).
21. Reeve, J. N., Beckler, G. S., Cram, D. S., Hamilton, P. T., Brown, J. W., Krzycki, J. A., Kolodziej, A. F., Alex, L., Orme-Johnson, W. H., and Walsh, C. T., *Proc. Natl. Acad. Sci. U.S.A.* **86**, 3031 (1989).
22. Alex, L. A., Reeve, J. N., Orme-Johnson, W. H., and Walsh, C. T., *Biochemistry* **29**, 7237 (1990).
23. Steigerwald, V. J., Beckler, G. S., and Reeve, J. N., *J. Bacteriol.* **172**, 4715 (1990).

24. Ewart, G. D., Reed, K. C., and Smith, G. D., *Eur. J. Biochem.* **187**, 215 (1990).
25. Prickril, B. C., He, S.-H., Li, C., Menon, N., Choi, E. S., Przybyla, A. E., DerVartanian, D. V., Peck, H. D., Jr., Fauque, G., LeGall, J., Texeira, M., Moura, I., Moura, J. J. G., Patil, D., and Huynh, B. J., *Biochem. Biophys. Res. Commun.* **149**, 369 (1987).
26. Sawers, R. G., and Boxer, D. H., *Eur. J. Biochem.* **156**, 265 (1986).
27. Stoker, K., Oltmann, L. F., and Stouthamer, A. H., *J. Bacteriol.* **170**, 1220 (1988).
28. Voordouw, G., Niviere, V., Ferris, F. G., Fedorak, P. M., and Westlake, D. W. S., *Appl. Environ. Microbiol.* **56**, 3748 (1990).
29. Voordouw, G., in "The Nitrogen and Sulphur Cycles" (J. A. Cole and S. Ferguson, eds.), p. 147. Soc. Gen. Microbiol. Symp. 42. Cambridge Univ. Press, Cambridge, 1988.
30. Voordouw, G., and Wall, J. D., in "Genetics and Molecular Biology of Anaerobic Bacteria" (M. Sebal, ed.), in press. Springer-Verlag, New York, 1991.
31. Fauque, G., Peck, H. D., Jr., Moura, J. G., Huynh, B. H., Berlier, Y., DerVartanian, D. V., Texeira, M., Przybyla, A. E., Lespinat, P. A., Moura, I., and LeGall, J., *FEMS Microbiol. Rev.* **54**, 299 (1988).
32. Reeve, J. N., and Beckler, G. S., *FEMS Microbiol. Rev.* **87**, 419 (1990).
33. Hagen, W. R., van Berkel-Arts, A., Kruse-Wolters, K. M., Voordouw, G., and Veeger, C., *FEBS Lett.* **203**, 59 (1986).
34. Adman, E. T., Sieker, L. C., and Jensen, L. H., *J. Biol. Chem.* **259**, 7045 (1973).
35. van den Berg, W. A. M., van Dongen, W. M. A. M., and Veeger, C., *J. Bacteriol.* **173**, 3688 (1991).
36. Adams, M. W. W., Eccleston, E., and Howard, J. B., *Proc. Natl. Acad. Sci. U.S.A.* **86**, 4932 (1989).
37. van Dijk, C., Mayhew, S. G., Grande, H. J., and Veeger, C., *Eur. J. Biochem.* **102**, 317 (1979).
38. Voordouw, G., and Brenner, S., *Eur. J. Biochem.* **159**, 347 (1986).
39. Pierrot, M., Haser, R., Frey, M., Payan, F., and Astier, J. P., *J. Biol. Chem.* **257**, 14341 (1982).
40. Higuchi, Y., Kusunoki, M., Matsuura, Y., Yasuoka, W., and Kakudo, M., *J. Mol. Biol.* **172**, 109 (1984).
41. Voordouw, G., Hagen, W. R., Kruse-Wolters, M., van Berkel-Arts, and Veeger, C., *Eur. J. Biochem.* **162**, 31 (1987).
42. Van den Berg, W. A. M., Stokkermans, J. P. W. G., and van Dongen, W. M. A. M., *J. Biotechnol.* **12**, 173 (1989).
43. Powell, B., Mergeay, M., and Christofi, N., *FEMS Microbiol. Lett.* **59**, 269 (1989).
44. Voordouw, G., Pollock, W. B. R., Bruschi, M., Guerlesquin, F., Rapp-Giles, B. J., and Wall, J. D., *J. Bacteriol.* **172**, 6122 (1990).
45. Zinoni, F., Birkman, A., Stadtman, T. C., and Bock, A., *Proc. Natl. Acad. Sci. U.S.A.* **83**, 4650 (1986).
46. Chambers, I., Frampton, J., Goldfarb, P., Affara, N., McBain, W., and Harrison, P. R., *EMBO J.* **5**, 1221 (1986).
47. Eidsness, M. K., Scott, R. A., Prickril, B., DerVartanian, D. V., LeGall, J., Moura, I., Moura, J. J. G., and Peck, H. D., Jr., *Proc. Natl. Acad. Sci. U.S.A.* **86**, 147 (1989).
48. He, S.-H., Texeira, M., LeGall, J., Patil, D. S., DerVartanian, D. V., Huynh, B. H., and Peck, H. D., Jr., *J. Biol. Chem.* **264**, 2678 (1989).
49. Maroney, M. J., Colpas, G. J., Bagyinka, N., and Mascharak, P. K., *J. Am. Chem. Soc.* **113**, 3962 (1991).
50. Hatchikian, E. C., Fernandez, V. M., and Cammack, R., in "Microbiology and

- Biochemistry of Strict Anaerobes Involved in Interspecies Hydrogen Transfer" (J. P. Belaich, M. Bruschi, and J. L. Garcia, eds.), p. 53. Plenum, New York, 1990.
51. Cammack, R., Patil, D. S., Hatchikian, E. C., and Fernandez, V. M., *Biochim. Biophys. Acta* **912**, 98 (1987).
52. Fernandez, V. M., Hatchikian, E. C., Patil, D. S., and Cammack, R., *Biochim. Biophys. Acta* **883**, 145 (1986).
53. Cammack, R., *Adv. Inorg. Chem.* **32**, 297 (1988).
54. Huynh, B. H., Patil, D. S., Moura, I., Texeira, M., Moura, J. J. G., Dervartanian, D. V., Czechowski, M. H., Peck, H. D., Jr., and LeGall, J., *J. Biol. Chem.* **262**, 795 (1987).
55. Higuchi, Y., Yasuoka, N., Kakudo, M., Katsube, Y., Yagi, T., and Inokuchi, H., *J. Biol. Chem.* **262**, 2823 (1987).
56. Niviere, V., Hatchikian, C., Cambilleau, C., and Frey, M., *J. Mol. Biol.* **195**, 969 (1987).
57. Voordouw, G., *Gene* **69**, 75 (1988).
58. Bruschi, M., and Guerlesquin, F., *FEMS Microbiol. Rev.* **54**, 155 (1988).
- 58b. Brumlik, M. J., LeRoy, G., Bruschi, M., and Voordouw, G., *J. Bacteriol.* **172**, 7289 (1990).
59. Brumlik, M. J., and Voordouw, G., *J. Bacteriol.* **171**, 4996 (1989).
60. Prickril, B. C., Kurtz, D. M., Jr., LeGall, J., and Voordouw, G., *Biochemistry* **30**, 11118 (1991).
61. Rohde, M., Furstenuau, U., Mayer, F., Przybyla, A. E., Peck, H. D., Jr., LeGall, J., Choi, E.-S., and Menon, E. K., *Eur. J. Biochem.* **191**, 389 (1990).
62. Van Dongen, W., Hagen, W., van den Berg, W., and Veeger, C., *FEMS Microbiol. Lett.* **50**, 5 (1988).
63. Niviere, V., Wong, S.-L., and Voordouw, G., submitted for publication (1992).
64. Thauer, R. K., Jungermann, K., and Decker, K., *Bacteriol. Rev.* **41**, 100 (1977).
65. Cypionka, H., and Dilling, W., *FEMS Microbiol. Lett.* **36**, 257 (1986).
66. Evans, H. J., Harker, A. R., Papen, H., Russell, S. A., Hanus, F. J., and Zuber, M., *Annu. Rev. Microbiol.* **41**, 335 (1987).
67. Bowien, B., and Schlegel, H. G., *Annu. Rev. Microbiol.* **35**, 405 (1981).
68. Ballantine, S. P., and Boxer, D. H., *Eur. J. Biochem.* **156**, 277 (1986).
69. Sawers, R. G., Jamieson, D. J., Higgins, C. F., and Boxer, D. H., *J. Bacteriol.* **168**, 398 (1986).
70. Rousset, M., Dermoun, Z., Chippaux, M., and Belaich, J. P., *Mol. Microbiol.* **5**, 1735 (1991).
71. Badziong, W., Thauer, R. K., and Zeikus, J. G., *Arch. Microbiol.* **116**, 41 (1978).
72. Higuchi, Y., Inaka, K., Yasuoka, N., and Yagi, T., *Biochim. Biophys. Acta* **911**, 341 (1987).
73. Pollock, W. B. R., Loutfi, M., Bruschi, M., Rapp-Giles, B. J., Wall, J. D., and Voordouw, G., *J. Bacteriol.* **173**, 220 (1991).
74. Meyer, J., and Gagnon, *Biochemistry* **30**, 9697 (1991).

DENSITY-FUNCTIONAL THEORY OF SPIN POLARIZATION AND SPIN COUPLING IN IRON-SULFUR CLUSTERS

LOUIS NOODLEMAN and DAVID A. CASE

Department of Molecular Biology, The Scripps Research Institute,
La Jolla, California 92037

- I. Introduction
 - II. Perturbation Formalism for Spin Coupling in Transition Metal Clusters
 - A. Overview
 - B. Singlet-Triplet Splittings for Two Unpaired Electrons
 - C. Nonorthogonal Orbitals
 - D. Interactions of More Than Two Electrons
 - E. Analysis of a Mixed-Valence Dimer
 - F. Summary
 - III. The Density-Functional and Broken Symmetry Methods
 - A. The Total Energy in Density-Functional Theory
 - B. Exchange Energy and the Fermi Hole
 - C. Correlation for Opposite Spins and the Coulomb Hole
 - IV. Monomeric Iron-Sulfur Complexes
 - V. Iron-Sulfur Dimers
 - A. Energy Level Structure
 - B. Density Differences and Spin Densities
 - C. Hyperfine, EPR, and Mössbauer Properties for Reduced Two-Iron Clusters
 - D. Heisenberg Coupling and Resonance Coupling
 - E. Electron Transfer and Optical Charge Transfer Spectra
 - VI. Three-Iron Clusters
 - A. Background
 - B. Broken Symmetry Analysis of Reduced Three-Iron Clusters
 - VII. Four-Iron Clusters
 - A. Energy Level Structure
 - B. Oxidized and Reduced Configurations
 - C. Relaxation Effects on Cluster Oxidation $+2 \rightarrow +3$
 - D. Relaxation Effects on Cluster Reduction $+2 \rightarrow +1$
 - E. Spin-Coupling Parameters
 - F. Stability of $S = \frac{1}{2}$ versus $S = \frac{3}{2}$ for Reduced (+1) Clusters
 - G. Phenomenological Modeling of Oxidized (+3) and Reduced (+1) Clusters
 - VIII. Conclusions and Prospects for Future Work
 - A. Summary
 - B. New Directions
- References

I. Introduction

A variety of metalloproteins have been characterized with active sites containing ligand-bridged transition metal centers that are used for electron transfer and catalysis (1). Iron-sulfur proteins provide excellent examples of these types of systems (2), as does nitrogenase (3), which contains both Fe-S and Mo-Fe-S clusters in a multiple-protein system. Other such electron transfer enzymes include cytochrome oxidase (4) and the oxygen-evolving complex of photosystem II (containing a polynuclear Mn-O cluster) (5, 6). In the category of substrate transformations, aconitase is a well-known member of a large class of dehydratases with an Fe-S cubane active site (7). From an electronic structure viewpoint, common features of all of these clusters include high-spin transition metal centers that are spin coupled via bridging and terminal ligands (1, 8, 9). The catalytic and electron transfer repertoires of these clusters can be quite broad, and often have important features that are not seen with single-metal sites. In this review we summarize recent progress toward the development of a unified picture of the electronic structures and spin interactions of iron-sulfur and related systems; these concepts provide a close connection between a spin Hamiltonian description and a more detailed orbital picture of the electron distribution.

The iron-sulfur proteins and synthetic analogs are challenging systems for quantum mechanical methods, both because they contain a large number of electrons and because spin polarization (10, 11) and spin coupling (8, 12-14) are essential features of the complexes. Standard approaches of *ab initio* quantum chemistry start from a spin-restricted picture, which is poorly adapted to problems involving high-spin transition metal centers (15). For this reason, we have developed a combination of broken symmetry and spin-unrestricted methods that is particularly well adapted to study spin-polarized and spin-coupled systems. Further, these ideas are well adapted for use with density-functional methods (12-14). In Section II, we develop the basic ideas of this approach, using a perturbation theory formalism to rationalize the spin Hamiltonian and energy-splitting formulas that should be appropriate for spin-coupled transition metal clusters. The basic approach parallels that of "textbook" explanations of superexchange (16) and double exchange (17, 18), but we consider aspects of the problem not often developed elsewhere.

The perturbation approach is useful in identifying the origins of ferromagnetic and antiferromagnetic interactions, and for developing interpolation formulas for calculating energy differences between spin

states. For relatively simple problems, such as the singlet–triplet splitting in dinuclear copper sites, it can also be useful in a computational sense (19–22). For coupling problems as complex as iron–sulfur clusters, however, the limitations of perturbation or configuration interaction approaches become severe. Our broken symmetry method, however, can be applied in *ab initio* (23–25) as well as in density-functional theory, although so far the computational complexity has constrained *ab initio* methods to smaller systems. In Section III, we outline an alternative, density-functional approach to this problem, which provides a tractable computational *ansatz* for quantitative studies of realistic clusters. In Section IV, spin polarization effects in monomeric iron–sulfur complexes are examined. In Section V, we provide a fair amount of detail for the “worked-out example” of dinuclear iron–sulfur clusters in both the Fe(III)–Fe(III) and Fe(III)–Fe(II) oxidation states. We intend Sections II–V to provide a reasonably self-contained outline of our basic theoretical goals and techniques.

Section VI reviews results of this approach for three-iron (3Fe) iron–sulfur clusters. Section VII contains a review of previous results on 4Fe iron–sulfur clusters, new results on relaxation effects on oxidation and reduction, and an examination of results on spin state equilibria, including some new ideas about $S = \frac{1}{2}$ versus $S = \frac{3}{2}$ ground states. In Section VIII, after a summary of important areas of progress, we look to the future and outline studies in progress on understanding the oxidation/reduction potentials and the ligand-exchange chemistry of these fascinating systems.

II. Perturbation Formalism for Spin Coupling in Transition Metal Clusters

A. OVERVIEW

It is typical to describe the coupling between high-spin transition metal centers in terms of a (phenomenological) Heisenberg Hamiltonian: for two coupled sites, we have $H = JS_1 \cdot S_2$ (22, 26, 27). As we show in this section, the Heisenberg, or isotropic, coupling model can be derived in a physically interesting way from second-order perturbation theory (19, 22, 26–29). One starts from noninteracting high-spin transition metal sites, and then allows for the mixing of “charge transfer” configurations in which the formal oxidation states of the metals are no longer equivalent. In this process, various terms make significant contributions, the most important of which are as follows (19, 26–29):

1. *Direct exchange*: this enters already in zeroth order, because there is an exchange interaction between sites even in the absence of charge transfer. The molecular version of Hund's rule ensures that orthogonal orbitals on different centers have the lowest energy in a parallel spin alignment. This interaction is thus ferromagnetic and of Heisenberg type.

2. *Superexchange*: here the metal sites interact by the overlap of opposite spins on neighboring sites. These mainly metal orbitals may contain a ligand part. In a configuration interaction language based on purely orthogonal orbitals, this is equivalent to mixing of charge transfer configurations with the principal configuration. These terms are antiferromagnetic and of Heisenberg type.

3. *Ligand spin polarization*: single-electron (or double-electron) transfers from the doubly occupied ligand orbitals to the high-spin metal sites produce a number of coupling terms of approximately Heisenberg type, which are usually antiferromagnetic (20, 21, 29). These terms have often been neglected, but can certainly be important for the types of complexes considered here.

4. *Resonance delocalization* (also called valence delocalization, or double exchange): this arises in mixed-valence situations from the degenerate mixing of equivalent (or nearly equivalent) ionic configurations. The original theory is due to Anderson and Hasegawa (30), following Zener (31), wherein it was applied to the apparent ferromagnetism of mixed-valence manganites of perovskite structure. The energy of delocalization of the itinerant electron of a mixed-valence pair in a spin-coupled system is given by $\pm|B|(S' + \frac{1}{2})$ for bonding (−) and antibonding (+) interactions, respectively, where S' is the spin quantum number for the coupled pair of sites (13, 17, 30, 32–36). In general, both Heisenberg terms and resonance coupling terms are present in mixed-valence complexes, and a key qualitative feature of iron–sulfur clusters is the competition between Heisenberg terms (which are predominantly antiferromagnetic and favor small values of the net spin) and resonance delocalization (which favors high spin values).

B. SINGLET–TRIPLET SPLITTINGS FOR TWO UNPAIRED ELECTRONS

Here we develop a picture of the basic interactions we expect in transition metal clusters, along the lines outlined above. The theory for a system with only two unpaired electrons is especially simple, and we begin with that (37, 38). Consider a single configuration wavefunction, defined as an antisymmetrized product of spin orbitals:

$$A[\psi_1(x_1)\psi_2(x_2)\cdots\psi_N(x_N)] = A[u_1(r_1)u_2(r_2)\cdots u_N(r_N)\Theta(s_1, s_2 \cdots s_N)] \quad (1)$$

where A is the antisymmetrizing operator. The factorization into space and spin parts is very convenient. Any single configuration wavefunction represents a state with a well-defined spin quantum number $M_S = \langle S_z \rangle$, the expectation value of the z component of total spin, given by $M_S = (N_\alpha - N_\beta)/2$. However, such a wavefunction is not necessarily an eigenfunction of the total spin S , that is, of the operator $\mathbf{S} \cdot \mathbf{S}$. In general, a pure-spin eigenfunction is obtained if all the spin parts of the orbitals are α or all are β outside a closed shell, but not otherwise. For example, consider an open shell composed of two orthogonal space orbitals a, b with opposite spins

$$\Psi_B = A(ab\alpha\beta) \equiv |ab\alpha\beta| \quad (3)$$

Following common practice, the coordinate labels can be omitted, with the convention that the labels increase from left to right. The function Ψ_B is not an eigenfunction of S . Proper spin eigenfunctions $\Psi(S, M_s)$ (37) are given by

$$\begin{aligned} \Psi(1, 1) &= |ab\alpha\alpha|, & \Psi(1, -1) &= |ab\beta\beta| \\ \Psi(1, 0) &= 1/\sqrt{2}(|ab\alpha\beta| + |ab\beta\alpha|) \\ \Psi(0, 0) &= 1/\sqrt{2}(|ab\alpha\beta| - |ab\beta\alpha|) \end{aligned} \quad (4)$$

from elementary spin algebra. Therefore,

$$\Psi_B = 1/\sqrt{2}[\Psi(1, 0) + \Psi(0, 0)] \quad (5)$$

The state Ψ_B has $M_S = 0$, but it is not an eigenstate of spin. Rather, it is a state of mixed spin (with both $S = 1$ and $S = 0$ contributing) and will be of broken spatial symmetry if $a(r) \neq b(r)$.

In general, a mixed-spin, broken symmetry state takes the form (15, 38)

$$\Psi_B = \sum_S C(S)\Psi_S \quad (6)$$

The "true" electron Hamiltonian of a many-electron system cannot mix eigenfunctions of different spin (in the absence of spin-orbit coupling), and since the total spin operator squared \mathbf{S}^2 commutes with this Hamiltonian, we have the energy equation for the broken symmetry state (15, 38):

$$E_B = \langle \Psi_B | H | \Psi_B \rangle = \sum_S [C(S)]^2 \langle \Psi_S | H | \Psi_S \rangle \quad (7)$$

There are no cross-terms here between states of different S .

To evaluate the energy of the singlet ($S = 0$) and triplet ($S = 1$)

states, we need also a separate equation for $S = 1$. Keeping always with energy evaluations involving only single configuration wavefunctions,

$$E(S = 1) = \langle \Psi(1, 1) | H | \Psi(1, 1) \rangle = \langle \Psi(1, -1) | H | \Psi(1, -1) \rangle \quad (8)$$

Note that we have chosen not to make use of $\Psi(1, 0)$ since this has more than one configuration. There is nothing "wrong" with multiconfigurational wavefunctions, but local density-functional theory (as we discuss below) is most easily given a concrete and well-defined form in terms of single configuration wavefunctions (15, 38).

The energy of the broken symmetry wavefunction in the present case is now easily found:

$$E_B = (\frac{1}{2})[E(S = 0) + E(S = 1)] \quad (9)$$

Of more interest is the singlet-triplet splitting:

$$E(S = 1) - E(S = 0) = 2[E(S = 1) - E_B] \equiv J \quad (10)$$

where J is the Heisenberg parameter in a Hamiltonian of the form $H = J\mathbf{S}_1 \cdot \mathbf{S}_2$. Equation (10) has been used for many years to estimate singlet-triplet splittings in molecular excited states using $X\alpha$ or local density-functional theory. The above derivation is of course a very simple one, but we will see that the basic concepts carry through to more complex situations; only the algebra becomes more complicated.

C. NONORTHOGONAL ORBITALS

So far, we have assumed that the space orbitals $a(r)$ and $b(r)$ are orthogonal, that is

$$\int a(r)b(r) dr \equiv S_{ab} = 0 \quad (11)$$

This will be true in many molecular excited states wherein the orbitals may be orthogonal by symmetry. For the case of coupling of two transition metal ions, it may be approximately true if the coupling is weak. Hund's rule implies that the coupling will be ferromagnetic ($J < 0$) when a and b are orthogonal, but it can be either ferromagnetic or antiferromagnetic when a and b are nonorthogonal. We now consider the more general situation for nonorthogonal orbitals (e.g., valence bond orbitals) a' , b' with overlap $S_{a'b'}$. Then it may be shown that the corresponding broken symmetry wavefunction is (15, 39)

$$\Psi_B = [(1 + S_{a'b'}^2)/2]^{1/2} \Psi(0, 0) + [(1 - S_{a'b'}^2)/2]^{1/2} \Psi(1, 0) \quad (12)$$

The corresponding energy equation is (15, 39)

$$E(S = 0) = [2/(1 + S_{a'b'}^2)]E_B - [(1 - S_{a'b'}^2)/(1 + S_{a'b'}^2)]E(S = 1) \quad (13)$$

For small $S_{a'b'}$, this reduces to Eq. (10); as $S_{a'b'} \rightarrow 1$, we have the strong bonding limit, in which the broken symmetry state approaches the singlet state [Eq. (12)]. The two-electron valence bond problem is thus solvable throughout the entire range of $S_{a'b'}$. Taking the difference $J = E(S = 1) - E(S = 0)$ from Eq. (13) gives the singlet-triplet splitting solely in terms of $E(S = 1)$, E_B , and the overlap $S_{a'b'}$. These results have been used effectively together with density-functional calculations to evaluate the singlet-triplet splitting and electronic structure in (d^9 - d^9) copper dimer and (d^9 - d^1) copper-vanadium dimer complexes in both the strong bonding and weak bonding regimes (40-43). Some of these are copper dimer peroxide complexes having structural relevance to the active sites of hemocyanin and tyrosinase (40).

D. INTERACTIONS OF MORE THAN TWO ELECTRONS

However, when more than two unpaired electrons are weakly coupled, the complete problem is not solvable; substantial progress can be made through recourse to perturbation theory (28, 29). Consider a single configuration wavefunction (determinant) in which both spin and space symmetry restrictions have been lifted. For a dinuclear metal cluster, this would have nonorthogonal "magnetic orbitals" d'_l, d'_r , mainly on the metal centers (where l and r denote the left and right transition metal centers), and nonorthogonal ligand orbitals $l^{k'}\alpha, l^{k''}\beta$, including both the bridging and terminal ligands. Typically, this single configuration wavefunction would be variationally optimized as a broken symmetry unrestricted Hartree-Fock or local density-functional wavefunction. This wavefunction can be expanded in terms of determinants built upon *orthogonal* orbitals (28, 29):

$$\Psi_B = |[d'_l][\alpha\alpha\alpha \cdots][l^{k'}l^{k''}][\alpha\beta][d'_r][\beta\beta\beta \cdots]| = D_0 + \sum_u a_u(B)D_u \quad (14)$$

The excited configurations D_u are created by excitations from the principal determinant D_0 , and the $a_u(B)$ are mixing coefficients in the expansion of the broken symmetry state Ψ_B . The principal determinant D_0 is built from orthogonalized metal and ligand orbitals:

$$D_0 = |[d_l][\alpha\alpha\alpha \cdots][l^k l^k][\alpha\beta][d_r][\beta\beta\beta \cdots]| \quad (15)$$

For simplicity, D_0 is assumed to be orbitally nondegenerate, and with n unpaired electrons on the left of spin α , n unpaired electrons on the right of spin β , and with doubly occupied ligand orbitals on the bridging and terminal ligands with space part l^k . (Formally, doubly occupied d orbitals can be treated in way analogous to doubly occupied ligand orbitals.)

Through a corresponding orbital transformation (44, 45) the nonorthogonal orbitals d' can be made to overlap only in pairs, so that $\langle d'_{lu} | d'_{ru} \rangle$ vanishes unless $u = v$. In terms of the normalized orthogonal orbitals d_l and d_r , we then have $d'_{lu} = d_{lu} + a_u(B)d_{ru}$, $d'_{ru} = d_{ru} + a_u(B)d_{lu}$, and $\langle d'_{lu} | d'_{ru} \rangle = 2a_u(B)$. This provides a relationship between the mixing coefficients in the orthogonal representation [Eq. (14)] and the magnetic orbital overlaps in the nonorthogonal representation (26, 28). Thus, interactions such as superexchange can often be described equally well in terms of orbital overlap or configurational mixing, and both descriptions are common in the literature. The magnetic orbitals are partly delocalized onto the bridging and terminal ligands, as well as onto the opposite metal center. The overlaps $\langle d'_{lu} | d'_{ru} \rangle$ often strongly involve the bridging ligands, so that their contribution to spin coupling is called superexchange (26, 27, 46). Similarly, the nonorthogonal ligand orbitals $l^{k'}$, $l^{k''}$ can be expanded as a doubly occupied set plus a small deviation due to delocalization onto the neighboring metal site(s) (20, 29). The contribution of the latter to spin coupling is called ligand spin polarization, or "hole" polarization. Each of these mechanisms can lead to spin transfer from the metal to the ligands.

To treat the states of pure spin, we recognize that each determinant in Eq. (14) is like an "outer product" of monomer spins. The Clebsch-Gordan algebra can be used to express this in terms of the spin eigenstates of the coupled system (47-49):

$$|S_1 M_1\rangle |S_2 M_2\rangle = \sum_S C(S_1 S_2 S; M_1 M_2) |SM\rangle \quad (16)$$

where C is a Clebsch-Gordan coefficient. In the principal determinant D_0 , there are n unpaired electrons on the left and right, and the two spin vectors $S_1 = S_2 = n/2$ are coupled to total spin S ; for superexchange, the relevant excited state configurations D_u arise from $d_l \rightarrow d_r$ or $d_r \rightarrow d_l$ excitations that leave $n - 1$ unpaired electrons per site, so that $S_1 = S_2 = \frac{1}{2}(n - 1)$; for ligand spin polarization, the excited configurations arise from $l^k \rightarrow d_l$ or $l^k \rightarrow d_r$ excitations, again with $S_1 = S_2 = n/2$. Hence, there are two important types of coupling coefficients, $C_1(S) \equiv [C(\frac{1}{2}n \frac{1}{2}n S; \frac{1}{2}n - \frac{1}{2}n)]$ and $C_2(S) \equiv \{C[\frac{1}{2}(n - 1) \frac{1}{2}(n - 1) S; \frac{1}{2}(n - 1) - \frac{1}{2}(n - 1)]\}$.

Combining Eqs. (14) and (16) then yields an expression for the broken symmetry state in terms of spin eigenstates:

$$\begin{aligned}\Psi_B &= \sum_S C_1(S) \Phi_0(S) + \sum_S \sum_u a_u(B) C_u(S) \Phi_u(S) \\ &= \sum_S C_1(S) \left\{ \Phi_0(S) + \sum_u [a_u(B) C_u(S) / C_1(S)] \Phi_u(S) \right\} \quad (17)\end{aligned}$$

where Φ represents the appropriate spin-coupled state $|SM\rangle$, and $C_u(S)$ will be $C_2(S)$ for determinants of the superexchange type and $C_1(S)$ for ligand spin polarization excitations. The quantity in brackets is nearly $\Psi(S)$, the wavefunction that would be generated by spin projection on Ψ_B , followed by variational optimization (28, 29). This equivalence is exact for excitations of the superexchange type, and is approximate (but expected to be fairly accurate) for ligand spin polarization (29). This has the fortunate consequence that a variational optimization of Ψ_B followed by spin projection [the construction followed for each term in brackets in Eq. (17)] yields results nearly as accurate as those obtained by constructing the proper spin states first, and then performing the variational optimization, a more accurate but difficult procedure. As with Eqs. (6) and (7), we can then write:

$$\Psi_B = \sum_S C_1(S) \Psi(S) \quad (18)$$

$$E_B \equiv \langle \Psi_B | H | \Psi_B \rangle = \sum_S C_1(S)^2 \langle \Psi(S) | H | \Psi(S) \rangle \equiv \sum_S C_1(S)^2 E_S \quad (19)$$

These expressions contain an important (and perhaps surprising) result: that both the broken symmetry wavefunction and its energy can be connected in a simple way to pure spin states. This forms the foundation for the application of the Wigner-Eckart theorem to the calculation of spin properties (to be discussed in Sections V and VII) and for the estimation of spin state energetics, which we discuss next.

The second main ingredient in our approach to spin coupling involves the development of an expression for E_S . Since we have already alluded to the use of a Heisenberg Hamiltonian, it may seem natural to expect E_S to be proportional to $S(S + 1)$, but it is important to note that this is a consequence of our theoretical picture of transitional metal clusters and not just a convenient assumption. A justification for the Heisenberg form for the pure spin states has been given in several earlier papers (13, 28, 29), and here we only have space for an outline of the argument.

The basic ideas can be illustrated by considering the effects of spin projection on the principal determinant D_0 , Eq. (15). Let O_S be the

projection operator onto the subspace of spin S ; then applying Eq. (16) as before, we can write:

$$O_S D_0 = C_1(S) \Phi_0(S) = [C_1(S)]^2 \sum_v X_v(S) D_v^0 \quad (20)$$

In the second equation, we recognize that spin projection will result in a mixture of determinants D_v^0 arising from interchanges of spin indices from the sets $[d_i]$ and $[d_r]$. The coefficient $X_v(S)$, where $v = (ij)$, represents the substitution ($d_i^j \alpha \rightarrow d_i^j \beta$, $d_r^i \beta \rightarrow d_r^i \alpha$) turns out to have the form (50–52)

$$X_{(ij)}(S) = -\{[n - S(S + 1)]/n^2\} \quad (21)$$

and the coefficient for the principal determinant, X_0 , is just unity. Then the energy of the spin-projected state is

$$\langle \Phi_0(S) | H | \Phi_0(S) \rangle = \langle D_0 | H | D_0 \rangle + E^{(1)}(S) \quad (22)$$

where

$$E^{(1)}(S) = \{[n - S(S + 1)]/n^2\} \sum_{ij} \langle d_i^j d_r^i | r_{12}^{-1} | d_r^i d_i^j \rangle = -[n - S(S + 1)] J_F / 2 \quad (23)$$

Since the spin-dependent portion goes like $S(S + 1)$, the result is of Heisenberg form, and the final equality in Eq. (23) defines J_F , the ferromagnetic Heisenberg parameter for a “direct exchange” interaction. Since the exchange integrals in Eq. (23) are positive definite, J_F must be negative (ferromagnetic) so that orthogonal orbitals on the two centers have the lowest energy for parallel spin alignment.

The effects of spin projection on the matrix elements for the excited determinants D_u follows a similar, although algebraically more complex, path. It turns out that for the superexchange excitations, the spin states also fit the Heisenberg form, but with an exchange parameter J_{AF} that is predominantly positive (antiferromagnetic) (28). The ligand spin polarization terms lead to energies that have a Heisenberg component plus terms of order $[S(S + 1)]^2$; the latter terms would correspond to a spin Hamiltonian $J_q(S_1 \cdot S_2)^2$, but are expected to be smaller than the Heisenberg contributions (29).

The above considerations motivate us to adopt the *ansatz* that the E_S values are of Heisenberg form with $E_S = S(S + 1)J/2$, where $J = J_F + J_{AF}$. The Clebsch–Gordan algebra also allows one to directly show that (28)

$$\sum_{S=0}^{S_{\max}} C_1(S)^2 S(S + 1) = n = S_{\max} \quad (24)$$

Combining Eqs. (19) and (24) yields an expression for the energy difference between two single configuration states, that of S_{\max} and the broken symmetry state:

$$E(S_{\max}) - E_B = (S_{\max}^2 J/2) \quad (25)$$

where $J = (J_F + J_{AF})$. This is the principal result of this section, since (as we discuss below) it is computationally tractable to estimate the energies of single configuration states. Note that Eq. (10) is a special case of this relation, with $S_{\max} = 1$.

E. ANALYSIS OF A MIXED-VALENCE DIMER

When an electron is added to form the reduced dimer, the resulting energy terms are of two types. First, there are Heisenberg terms that originate from direct exchange, superexchange, and ligand spin polarization, analogous to those in the preceding discussion. In addition, there are resonance delocalization interactions resulting from the mixing of the degenerate configurations created by the (arbitrary) assignment of the extra electron to the left or right side of the system (13, 30).

It is easiest to characterize the principal and excited functions by their vector coupling structure. Consider an outer product spin state of the form $|S_1 M_1\rangle_L |S_2 M_2\rangle_R$, where L and R are the left and right metal centers. The principal spin configuration is $|\frac{5}{2} \frac{5}{2}\rangle_L |2 - 2\rangle_R$, with the electron added to side R. Excited configurations of superexchange type can be included by methods analogous to those in the previous section. These terms lead to a Heisenberg Hamiltonian for the pure spin states and to the corresponding energy difference equation (13, 28)

$$E(S_{\max}) - E_B = n(n - 1)J/2 \quad (26)$$

for the broken symmetry state, compared with the pure spin state energy difference:

$$E(S_{\max}) - E(S = \frac{1}{2}) = (n + 1)(n - 1)J/2 \quad (27)$$

Resonance delocalization terms have a different character entirely (13). To see this, consider the principal determinant wherein an electron is added to the metal site on the right of the dimer. Then the normalized principal determinant is

$$D_{0R} = |[d_{1L} \cdots d_{5L}][\alpha^5][d_{1R}d_{1R}][\alpha\beta][d_{2R} \cdots d_{5R}][\beta^4]| \quad (28)$$

Now D_{0R} is the outer product state $|\frac{5}{2} \frac{5}{2}\rangle_L |2 -2\rangle_R$, so that we can use the Clebsch–Gordan algebra of Eq. (16) to write it in terms of spin eigenstates:

$$D_{0R} = \sum_S C(\frac{5}{2} 2S; \frac{5}{2} -2) \Phi_{0R}(S) \quad (29)$$

Applying the spin projection operator O_S to both sides, and rearranging,

$$\Phi_{0R}(S) = O_S D_{0R} / C_a(S) \quad (30)$$

where $C_a(S) \equiv C(\frac{5}{2} 2S; \frac{5}{2} -2)$. A similar equation holds for spin projection of D_{0L} . Then the resonance matrix element of the spin-projected states can be written:

$$\begin{aligned} \langle \Phi_{0L}(S) | H | \Phi_{0R}(S) \rangle &= [C_a(S)]^{-2} \langle O_S D_{0L} | H | O_S D_{0R} \rangle \\ &= [C_a(S)]^{-2} \langle D_{0L} | H | O_S D_{0R} \rangle \end{aligned} \quad (31)$$

In the second line, we have made use of the fact that O_S is idempotent (so that projection only needs to be done once).

Now we note [as in Eq. (20)] that the effect of spin projection on D_{0R} will again be to mix in other determinants D_{0R}^p in which spin indices have been interchanged:

$$O_S D_{0R} = C_a(S) \Phi_{0R}(S) = C_a(S) \sum_p z_p D_{0R}^p \quad (32)$$

There is only one non-vanishing term in the sum, so that

$$\langle \Phi_{0L}(S) | H | \Phi_{0R}(S) \rangle = [C_a(S)]^{-1} z_{p'} \langle D_{0L} | H | D_{0R}^{p'} \rangle \quad (33)$$

The important determinant is the one that nearly matches D_{0L} , except that one of the R orbitals, $d_{1R}\beta$, appears in the determinant where the matching L orbital, $d_{1L}\beta$, appears in D_{0L} :

$$D_{0R}^{p'} = |[d_{1R} \cdots d_{5R}][\alpha^5][d_{1L}d_{1R}][\alpha\beta][d_{2L} \cdots d_{5L}][\beta^4]| \quad (34)$$

$$D_{0L} = |[d_{1R} \cdots d_{5R}][\alpha^5][d_{1L}d_{1L}][\alpha\beta][d_{2L} \cdots d_{5L}][\beta^4]| \quad (35)$$

Note further that $D_{0R}^{p'}$ is a determinant in the expansion of the state function $|\frac{5}{2} -\frac{5}{2}\rangle_L |2 2\rangle_R$, so that the coefficient $z_{p'}$ will involve the Clebsch–Gordan coefficient $C(\frac{5}{2} 2S; -\frac{5}{2} 2) \equiv C_b(S)$; in fact, $z_{p'} = C_b(S)/(5)^{1/2}$. Thus the spin-dependent part of Eq. (33) becomes $C_b(S)/C_a(S)(5)^{1/2}$. By direct examination of the Clebsch–Gordan coefficients it can be shown that this ratio is $(S + 1/2)/(5)$. Hence we have finally that

$$\langle \Phi_{0L}(S) | H | \Phi_{0R}(S) \rangle = B(S + 1/2) \quad (36)$$

where B is a constant of proportionality. Equation (36) is the principal result of this analysis; we discuss below ways in which B can be estimated from single configuration wavefunctions.

F. SUMMARY

There is a lot of algebra in the above exposition, and it may be worthwhile here to summarize the most important results:

1. Most of the contributions (through second order in perturbation theory) to the energies of a transition metal dimer with the same number of d electrons on each site have a spin dependence like that of the Heisenberg spin Hamiltonian, $H = JS_1 \cdot S_2$. Some aspects of ligand spin polarization effects have a more complex spin dependence, but these terms are expected to be small.

2. Direct exchange between the magnetic orbitals on the two sites will lead to a ferromagnetic (negative) contribution to J , whereas superexchange interactions will make a contribution that is generally antiferromagnetic. Ligand spin polarization effects will also generally be antiferromagnetic. Each of these contributions can be identified with the mixing of particular sorts of excited configurations into a canonical single-determinant reference state.

3. A broken symmetry, spin-unrestricted wavefunction provides a simple wavefunction that also contains these physical interactions. The broken symmetry solution is not a spin eigenfunction, but can be written as a superposition of spin eigenfunctions, with relatively simple expressions for the weighting coefficients [see Eqs. (16)–(18)]. This implies that the energy of the broken symmetry function can be related to that of the spin eigenstates, Eq. (19), providing a convenient path for obtaining estimates of the Heisenberg coupling constants, Eq. (25). For the mixed-valence case, the Heisenberg coupling constants are found from Eq. (26).

4. For mixed-valence situations, an additional type of interaction arises from the resonance interaction between mirror-image configurations, in which the extra electron is assigned either to the left- or the right-hand metal site. These terms are also expected to have a relatively simple spin dependence, as the product of a "hopping interaction" times the factor $S + \frac{1}{2}$. Mixed-valence clusters also have Heisenberg terms analogous to those in the even-electron clusters, so that the appropriate spin Hamiltonian must contain both Heisenberg and resonance delocalization terms.

III. The Density-Functional and Broken Symmetry Methods

Density-functional methods are an alternative to *ab initio* methods for complex quantum chemical problems (53). Compared to *ab initio* methods, the distinctive feature of density-functional theory is that the exchange correlation part of the energy is approximated by terms that depend only on functionals of the electron density (54, 55). The use of this approximate form has the advantage of being more efficient than *ab initio* Hartree–Fock methods; for transition metal ions and related complexes, these are also often more accurate than Hartree–Fock calculations, as we discuss below (53). Spin-polarized density functional theory is analogous to unrestricted Hartree–Fock (UHF) theory (13, 15, 28). Unlike spin-restricted Hartree–Fock theory (RHF), this takes spin-polarized transition metal sites as its starting point. If the overall system is spin coupled to less than the maximal spin alignment, the simplest way to express this is to have different spatial orbitals for the different spin indices, giving a spin-polarized broken symmetry description of the molecule (12, 13, 28).

A. THE TOTAL ENERGY IN DENSITY-FUNCTIONAL THEORY

To have a language general enough to encompass both density-functional theory and the quantum mechanical theory of many-electron systems, we begin our analysis with some basic concepts from the theory of reduced density matrices. Our discussion basically follows that of McWeeny and Sutcliffe (37), and of Ziegler *et al.* (38), but at the end there is an interesting new twist. Let a general coordinate $x = (r, s)$ represent both independent space and spin variables. Let the electrons occupy orbitals $u_{i\alpha}(r)\alpha(s)$ and $u_{i\beta}(r)\beta(s)$ for α and β spins, respectively, with corresponding electron densities $\rho_\alpha(r)$, $\rho_\beta(r)$:

$$\begin{aligned}\rho_\alpha(r) &= \sum_{i\alpha} n_i u_i^*(r) u_i(r) \\ \rho_\beta(r) &= \sum_{i\beta} n_i u_i^*(r) u_i(r) \\ \rho(r) &= \rho_\alpha(r) + \rho_\beta(r)\end{aligned}\tag{37}$$

where the n_i are orbital occupation numbers.

To formulate the total energy expression in density functional theory, a generalized version of the electron density ρ is needed, called the first-order density matrix:

$$\rho_1(r; r') = \sum_{i=\alpha,\beta} n_i u_i(r) u_i^*(r')\tag{38}$$

The full first-order density matrix is needed so that the kinetic energy of the system can be defined entirely in terms of expectation values over density matrices. The following expression is then valid even for very complicated correlated wavefunctions:

$$\begin{aligned}
 E &= \int_{r'=r} [-\nabla^2/2] \rho_1(r; r') dr + \int_r \rho(r) V_N(r) dr \\
 &\quad + \frac{1}{2} \int_{x_1, x_2} \rho_2(x_1, x_2) r_{12}^{-1} dx_1 dx_2 + U_{NN} \\
 &= T + V_{Ne} + U_{ee} + U_{NN}
 \end{aligned} \tag{39}$$

Here the first term (T) is the total kinetic energy of the electronic system, the second term is the nuclear–electron attraction energy (V_{Ne}), the third term is the total electron–electron repulsion energy of the system (U_{ee}), and the last term is the nuclear–nuclear repulsion energy; $\rho_2(x_1, x_2)$ is the diagonal part of the second-order density matrix. The electron–electron repulsion is given by the expectation value of the electron–electron Coulomb repulsion operator r_{12}^{-1} with ρ_2 . The use of the generalized space-spin coordinates x_1, x_2 shows that this repulsion includes both that of α spin electrons among themselves, of β spin electrons among themselves, and of α electrons with β electrons. The diagonal part of the second-order density matrix can be separated into four terms involving only the two space variables (r_1, r_2), and spin indices α, β . These are $\rho_2^{\alpha\alpha}, \rho_2^{\beta\beta}, \rho_2^{\alpha\beta}$, and $\rho_2^{\beta\alpha}$.

For a system in which the total number of electrons is N , we have the following conservation equations

$$\int \rho(r) dr = N \tag{40}$$

$$\int \rho_2(r_1, r_2) dr_1 dr_2 = N(N - 1) \tag{41}$$

Since the conservation equation applies equally to α and β spin electrons, $N_\alpha + N_\beta = N$. The last equation can be interpreted as saying that every electron in the system interacts with all other electrons (but not with itself). The factor of $\frac{1}{2}$ in the U_{ee} equation is required so that every pairwise interaction of electrons is counted only once, giving the number of distinct pairwise interactions as $N(N - 1)/2$. We can expand $N(N - 1)$ in the following illuminating way:

$$\begin{aligned}
 N(N - 1) &= (N_\alpha + N_\beta)(N_\alpha + N_\beta - 1) \\
 &= N_\alpha(N_\alpha - 1) + N_\beta(N_\beta - 1) + N_\alpha N_\beta + N_\beta N_\alpha
 \end{aligned} \tag{42}$$

The individual terms on the right-hand side are the integrals of $\rho_2^{\alpha\alpha}(r_1, r_2)$, $\rho_2^{\beta\beta}(r_1, r_2)$, $\rho_2^{\alpha\beta}(r_1, r_2)$, and $\rho_2^{\beta\alpha}(r_1, r_2)$. All α electrons interact with all β electrons, and with the other $N_\alpha - 1$ electrons of the same spin. Further insight into electron-electron interactions comes from comparing correlated and uncorrelated forms of second-order density matrix. Specifically, $\rho_2(r_1, r_2)$ is the joint probability density for finding any electron at r_1 and another at r_2 . By contrast, a "classical" (uncorrelated) electron density would give a joint probability distribution

$$\rho_2^{\text{class}}(r_1, r_2) = \rho(r_1)\rho(r_2) \quad (43)$$

Similar relations apply for the α and β densities independently. In the next sections we consider separately the types of correlations expected for electrons of the same spin and of opposite spins.

B. EXCHANGE ENERGY AND THE FERMI HOLE

Clearly, for $\rho_2^{(\alpha\alpha)}$, the equations above dictate that the correct joint probability function deviates substantially from the classical uncorrelated form, since

$$\int \rho_2^{\text{class}(\alpha\alpha)}(r_1, r_2) dr_1 dr_2 = N_\alpha^2 \quad (44)$$

rather than $N_\alpha(N_\alpha - 1)$. The exact quantum mechanical $\rho_2^{(\alpha\alpha)}$ can be expressed in the following form (37):

$$\rho_2^{(\alpha\alpha)}(r_1, r_2) = \rho^\alpha(r_1)\rho^\alpha(r_2)[1 + f^{\alpha\alpha}(r_1, r_2)] \quad (45)$$

This result is the sum of an uncorrelated part plus an additional term describing "Fermi correlation." Dividing both sides by $\rho^\alpha(r_2)$ yields the conditional probability for finding an electron of spin α at r_1 given that there is another spin α electron at r_2 . Rearranging Eq. (45),

$$[\rho_2^{(\alpha\alpha)}/\rho^\alpha(r_2) - \rho^\alpha(r_1)] = \rho^\alpha(r_1)[f^{\alpha\alpha}(r_1, r_2)] \quad (46)$$

The right-hand side of the equation is the "Fermi hole" density. The integral of this density over r_1 is -1 for any r_2 . Further, the Pauli exclusion principle requires that as $r_1 \rightarrow r_2$, $f^{\alpha\alpha}(r_1, r_2) \rightarrow -1$, so that no two α spin electrons can be at the same place. Thus, electrons of the same spin exhibit "Fermi correlation" in their interactions. For a single configuration wavefunction (an antisymmetrized product of spin orbitals), a Fermi hole with the properties cited above is obtained by construction, leading to the exchange term in the total energy equation. In density-functional theory, the constraints above can be used to obtain a reasonable form for the exchange potential in terms of the electron

density. For a uniform electron gas with density ρ , this turns out to have the form $V_X^\sigma = (\frac{2}{3})U_X^\sigma$, where $U_X^\sigma = -(\frac{2}{3})\alpha[\frac{3}{4}\pi\rho^\sigma]^{1/3}$, where $\sigma = \alpha$ or β spin indices and the prefactor $\alpha = \frac{2}{3}$ for pure exchange and is variable in some other approaches (54, 56). The entire electron–electron repulsion energy (U_{ee}) of the system is approximated by

$$U_{ee} = \frac{1}{2} \int \rho(r_1)\rho(r_2) r_{12}^{-1} dr_1 dr_2 + \frac{1}{2} \int [\rho^\alpha(r_1)U_X^\alpha(r_1) + \rho^\beta(r_1)U_X^\beta(r_1)] dr_1 \quad (47)$$

The first integral is the “classical” electron–electron repulsion, and the second is the total exchange energy. A similar philosophy applies for the analysis of correlation effects. The goal is to find an approximate form for U_{XC} (where XC means exchange and correlation) for use in an equation similar to Eq. (47), based, for example, on the exchange and correlation energy of an electron gas (local spin density functional, or LSD) method (57–60), or on gradient corrections to the exchange energy (Becke’s energy) (61).

C. CORRELATION FOR OPPOSITE SPINS AND THE COULOMB HOLE

Consider now the joint distribution function for electrons of opposite spin. We can write this in a form similar to Eq. (45) (37):

$$\rho_2^{(\alpha\beta)}(r_1, r_2) = \rho^\alpha(r_1)\rho^\beta(r_2)[1 + f^{\alpha\beta}(r_1, r_2)] \quad (48)$$

but now the “Coulomb hole density” integrates to zero for any r_2 :

$$\int \rho^\alpha(r_1)f^{\alpha\beta}(r_1, r_2) dr_1 = 0 \quad (49)$$

This follows directly from the fact that the integral of $\rho_2^{(\alpha\beta)}$ is $N_\alpha N_\beta$. The Coulomb hole is not necessarily small, despite the fact that it must integrate to zero over all space. The important physical result is that as $r_1 \rightarrow r_2$, $\rho_2^{(\alpha\beta)}(r_1, r_2)$ becomes small so that electrons of opposite spin avoid each other so as to reduce their Coulomb repulsion. The Coulomb hole density is thus negative at short distances and positive at larger distances, to give a zero integral over all space.

As with exchange energies, these opposite-spin correlation effects could be approximated by using an $f^{\alpha\beta}$ function derived for a uniform electron gas, or from explicitly correlated wavefunctions. This is not, however, the only way. Unlike the Pauli principle, which is a precise symmetry requirement for fermions, the Coulomb hole is essentially a means by which a wavefunction can lower its electron–electron repulsion, and also its total energy. One way to achieve this is to remove

whatever constraints are keeping the electron–electron repulsion too high. In a standard spin-restricted framework, as, for example, in restricted Hartree–Fock theory, $\rho^\alpha(r) = \rho^\beta(r) = \rho/2$, and the electron repulsion between α and β electron densities is high. Our alternative is not to focus on $f^{\alpha\beta}(r_1, r_2)$, but instead to change the form of ρ^α, ρ^β from restricted to unrestricted form, allowing the electron densities for α and β spin to differ in space; how they differ precisely will be determined by the self-consistent field of the system in the density functional calculation. For the individual orbitals, this means removing the constraint that the orbitals be members of the irreducible representations of the molecular point group defined by the nuclear geometry. The orbitals are instead calculated in a subgroup compatible with the symmetries of ρ^α and ρ^β . By using unrestricted spin orbitals, all of the energy terms (kinetic energy, nuclear electron attraction, and electron–electron repulsion) will change in a variationally optimal way. Both the classical electron–electron repulsion and the exchange energy terms in U_{ee} are altered when passing from the spin-restricted to the spin-unrestricted case. In general, the α and β densities become more compact, and occupy different regions in space. These effects are quite strong when there are spin-polarized transition metal atoms, because the energetic cost on the kinetic energy of having compact α and β densities is outweighed by the advantageous lowering of the electron–electron repulsion and of the spin polarization (exchange) energies. Further, the broken symmetry state and its energy will differ significantly from the high-spin state and its energy, even though both will experience spin polarization, because the two states have different covalency and delocalization, affecting all the energy terms.

IV. Monomeric Iron–Sulfur Complexes

There have been two different types of first-principle calculations on single-iron Fe–S clusters: unrestricted Hartree–Fock plus configuration interaction [on models $\text{Fe}(\text{SH})_4^{1-/2-}$] (11) and spin-polarized (unrestricted) $X\alpha$ -scattered wave (sw) [on $\text{Fe}(\text{SH})_4^{1-/2-}$ and $\text{Fe}(\text{SCH})_3^{1-/2-}$] (10, 14). These are in good agreement. The ground state of the models and of oxidized rubredoxin is high-spin $S = \frac{5}{2}$; formally, simple orbital counting gives ferric d^5 for the oxidized complex and ferrous d^6 for the reduced complex. When the orbitals are optimized in the spin-polarized self-consistent field (SCF) procedure, there is extensive mixing of sulfur into the mainly Fe magnetic orbitals, and, conversely, mixing of Fe character into doubly occupied S levels. In the

oxidized complex (10, 14) there is about a 5-eV splitting between the occupied spin-up Fe(3*d*) orbitals (majority spin orbitals, lower energy) and the unoccupied spin-down Fe(3*d*) orbitals (minority spin orbitals, higher energy), indicative of a large intraatomic exchange splitting. The mainly S(3*p*) levels lie between the two sets of Fe(3*d*) in energy and are also spin split, but by a much smaller amount and in the opposite sense (spin-down below spin-up).

This general level pattern persists in polynuclear iron-sulfur clusters and has strong experimental support in model systems. This level structure, with the S(3*p*) band lying between the exchange-split Fe(3*d*) band, is not found in standard ligand field models (derived from low-spin systems), where all the ligand levels are expected to lie below all the metal levels, and seems to be a general feature of high-spin transition metals in the presence of weak-field ligands such as S. This "inverted bonding scheme" has been established experimentally by Solomon and co-workers (62–65) in the monomeric ferric complexes FeCl₄[−] and Fe(SR)₄[−] by a combination of spectroscopies, including photoelectron spectra (PES), polarized absorption, magnetic circular dichroism (MCD), and EPR. These show that the lowest lying spin-forbidden transitions in the oxidized system have substantial ligand → Fe character and are incompatible with ligand field Fe *d* → *d* transitions. Their energies are much lower in synthetic Fe(SR)₄[−] complexes than in FeCl₄[−], consistent with the stronger metal–ligand covalency in the thiolate complex. Resonance PES further establishes that the majority spin Fe(3*d*) lies below S(3*p*) in energy (62, 63).

V. Iron–Sulfur Dimers

A. ENERGY LEVEL STRUCTURE

In Fig. 1, we give the energy levels for the broken symmetry (BS) state (low spin, $M_S = 0$) of the dimeric cluster Fe₂S₂(SH)₄^{2−} in C_{2v} symmetry (13). The symmetry is lowered from the D_{2h} geometrical symmetry of the cluster by removing the mirror plane through the bridging S* atoms. The energy level structure and orbitals are consistent with antiparallel coupling of two high-spin subunits, each with spin vector $S = \frac{5}{2}$. On the diagram, the orbitals are arranged in columns according to their spatial distribution on the left, center, and right of the molecule, and according to the spin index [solid and dashed lines for spin-up (α) and spin-down (β) orbitals, respectively].

Because this is a homonuclear cluster with a geometrical equivalence

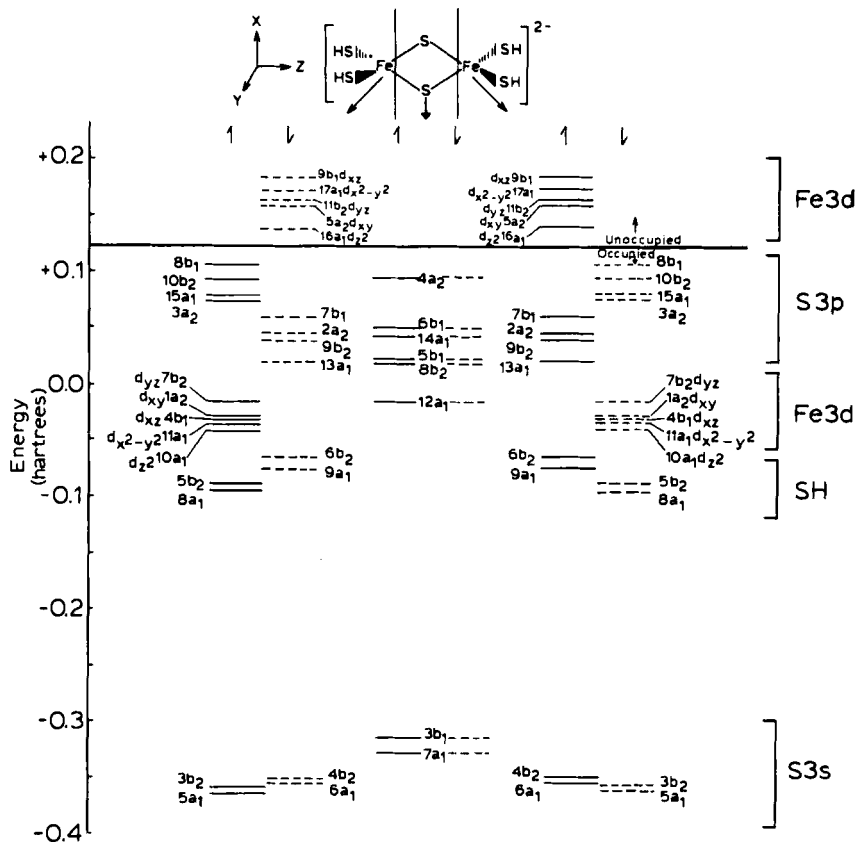


FIG. 1. $X\alpha$ -LCAO energy levels for $\text{Fe}_2\text{S}_2(\text{SH})_4^{2-}$; antiferromagnetic configuration. The orbitals are grouped according to their distribution on the left, center, or right of the molecule. Spin-up (α) levels are shown with solid lines, spin-down (β) levels are shown with dashed lines. See Ref. 13.

between the left and right halves, each spin-up level on the left is energetically degenerate with a mirror-image spin-down orbital on the right. Further, the orbitals can be grouped into a set of spin-up/spin-down pairs with large spatial overlap, mainly on the ligands, and into a set, mainly on the metal atoms where the spin-up/spin-down overlap between occupied orbital pairs is small. For example, $8a_1\alpha$, $9a_1\beta$ are SH bonding orbitals on the left, and $3a_2\alpha$, $2a_2\beta$ are terminal S orbitals. These are essentially "doubly occupied" ligand orbitals, and most of the orbitals in the system are of S, S^* , or SR type. In contrast to this are the mainly Fe(3d) orbitals, which experience a large intraatomic exchange splitting. The occupied or "magnetic" spin-up Fe(3d) orbitals

on the left (majority spin) are strongly stabilized by spin polarization and are metal–ligand bonding, whereas the corresponding spin-down $\text{Fe}(3d)$ orbitals on the left (minority spin) are destabilized and unoccupied. The magnetic orbitals exhibit weak spatial overlap between the occupied spin-up orbitals on the left, largely on Fe_L , and the occupied spin-down orbitals on the right, largely on Fe_R . The weak valence bond (VB) type of interaction between the metal centers can be thought of as a type of very weak M–M covalent bonding, distributed over the five valence bond pairs.

The high-lying $\text{S}(3p)$ orbitals obey the “inverted bonding scheme” lying between the two parts of the exchange-split $\text{Fe}(3d)$ band. The terminal $\text{S}(3p)$ spin splitting (about 1.5 eV) is considerably smaller than that for $\text{Fe}(3d)$ (about 5 eV), with the terminal S spin-down orbitals lying lower when the neighboring $\text{Fe}(3d)$ occupied orbitals are spin-up. Energetically, the bridging $\text{S}^*(3p)$ orbitals also appear between the majority-spin and the empty minority-spin $\text{Fe}(3d)$ levels, resembling the lower $\text{S}(3p)$ terminal orbitals in energy.

The majority-spin $\text{Fe}(3d)$ levels are metal–ligand (M–L) bonding. The adjacent terminal $\text{S}(3p)$ orbitals of opposite spin to the $\text{Fe}(3d)$ are also primarily of M–L bonding character, which is achieved by mixing with empty $\text{Fe}(3d)$ atomic orbitals. The $\text{S}^*(3p)$ orbitals behave similarly, while the highest terminal $\text{S}(3p)$ orbitals are pushed up by antibonding interactions with the adjacent filled $\text{Fe}(3d)$ levels of the same spin. The greatest Fe–S antibonding interactions occur in the empty ligand field levels; the reduction from tetrahedral Fe site symmetry to C_{2v} splits $e \rightarrow a_1, a_2$, and $t_2 \rightarrow a_1, b_1, b_2$. Overall, the exchange splitting of the $\text{Fe}(3d)$ band is further enhanced by bonding and antibonding interactions with $\text{S}(3p)$.

In Fig. 2, we show a contour map of the Fe magnetic orbital $7b_2\alpha$. There is considerable S radical character in $7b_2\alpha$, as well as a small $7b_2\alpha$ – $7b_2\beta$ superexchange interaction. Other magnetic orbitals displaying superexchange are shown in Ref. 13. For example, in the interaction of the magnetic orbitals $10a_1\alpha$ with $10a_1\beta$, superexchange interactions are clearly present since there is metal–ligand as well as metal–metal overlap. Figure 2 also includes a map of a high-lying occupied $\text{S}(3p)$ orbital, $10b_2\alpha$, and of two ligand field orbitals, $16a_1\alpha$ and $9b_1\alpha$; these are unoccupied $\text{Fe}(3d)$ orbitals in the oxidized model. On reduction, the added electron goes into $16a_1\alpha$, composed mainly of a localized $\text{Fe}(3d_{z^2})$ orbital.

B. DENSITY DIFFERENCES AND SPIN DENSITIES

Density difference maps for the difference between the molecular electron density of the BS state and that of the spin-restricted atoms

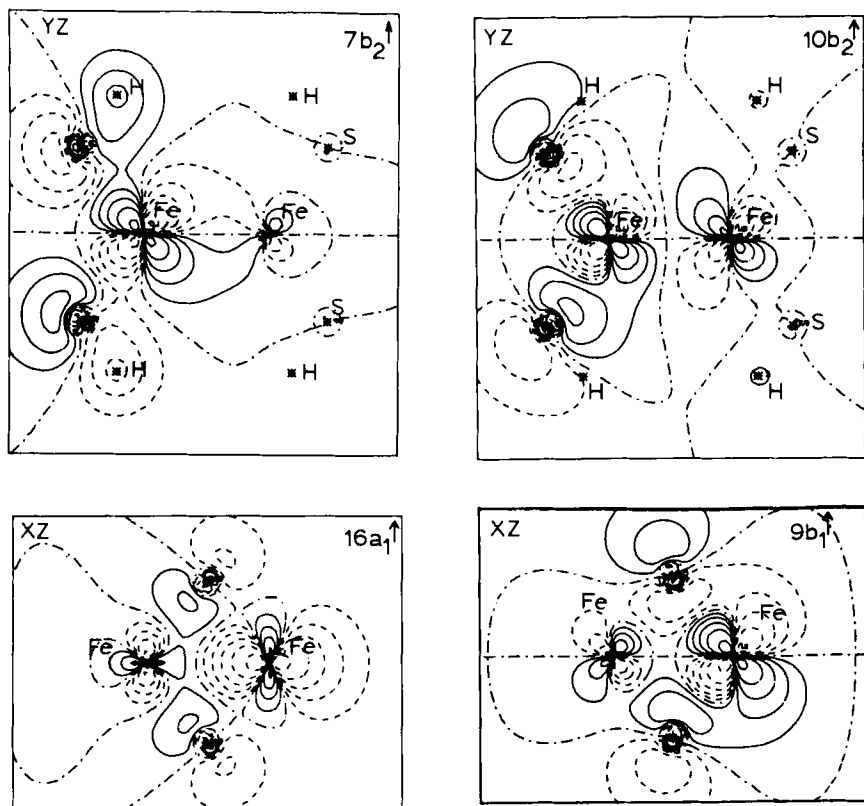


FIG. 2. Contour maps for the orbitals $7b_2$, $10b_2$, $16a_1$, and $9b_1$ spin-up (α) in the Fe-S* bridging (xz) or Fe-SR terminal (yz) plane as indicated for $\text{Fe}_2\text{S}_2(\text{SH})_4^{2-}$. See Ref. 13.

clearly show the accumulation of electrons in the bonding region between Fe and S, and in the SH bonds (see Ref. 13). When compared, the maps of the reduced and oxidized cluster show a complex rearrangement of charge. Occupation of $16a_1\alpha$ produces a substantial increase of axial electron density on the trapped Fe site (right), $0.64e^-$ in the reduced-site $\text{Fe}(3d_{z^2})$ population. However, electron relaxation through the other "passive" orbitals leads to a large backflow of electron density out of the other reduced-site Fe orbitals; the total $\text{Fe}(3d)$ population increases by only $0.11e^-$ compared with oxidized cluster. The increased electron population in the reduced form has thus gone almost entirely to the sulfurs. Further, the two SH groups (right) adjacent to the reduced Fe site have a larger electron population than two SH (left)

by $0.24e^-$. Hence the asymmetry and trapping are preserved at the level of net charge flow, as well as for the orbital occupied on reduction in Ψ_B . These results show the strong participation of the S, S* in the redox process, and demonstrate the importance of metal–ligand covalency.

Spin density maps for Ψ_B in both the oxidized and reduced forms of the cluster are also given in Ref. 13. For the oxidized cluster, the spin density maps show the strong spin polarization on Fe and the substantial spin transfer from Fe \rightarrow terminal S. The opposite spin alignment on the two Fe sites is also evident. Upon reduction, the same general picture holds, but with a reduction in the axial spin density on the reduced site (at the right). The relationship of these spin density maps to what is actually observed, for example, in the Fe or proton hyperfine tensors, contains some subtleties. When the $S = 0$ ground state is projected out of the broken symmetry state of the oxidized cluster, the spin density necessarily vanishes. However, the higher states of the spin ladder ($S > 0$) have nonvanishing spin density, which shows up, for example, as paramagnetic shifts in the nuclear magnetic resonance (NMR) of oxidized proteins at the cysteine methylene protons, and in related synthetic clusters (9, 66). This opposite spin alignment is also clearly seen in the Fe hyperfine tensors of reduced clusters.

C. HYPERFINE, EPR, AND MÖSSBAUER PROPERTIES FOR REDUCED TWO-IRON CLUSTERS

For the reduced dimer, spin projection of the $S = \frac{1}{2}$ ground state from Ψ_B leads to an effective spin density from which hyperfine properties can be determined (13). Let (S_1, M_{S_1}) and (S_2, M_{S_2}) be the monomer subunit spin quantum numbers; for Ψ_B , $M_{S_1} = S_1 = \frac{5}{2}$ and $M_{S_2} = -S_2 = -2$. Next, the properties of the proper $S = \frac{1}{2}$ ground state must be related to those in Ψ_B . From the Wigner–Eckart theorem for vector operators (49), the effective **A** tensors are then $\mathbf{A}_{i\text{eff}} = K_i \mathbf{a}_i$, where $K_i = \langle \mathbf{S} \cdot \mathbf{S}_i \rangle / S(S + 1)$ (so that $K_1 = \frac{7}{8}$, $K_2 = -\frac{3}{8}$), and the \mathbf{a}_i are “site tensors” determined as for monomeric metal complexes (9, 67). The analysis of the **g** tensor is similar, with $\mathbf{g} = K_1 \mathbf{g}_1 + K_2 \mathbf{g}_2$ (8). Griffith has shown that the **g** and \mathbf{A}_{eff} tensors for the total system can be constructed and diagonalized to give principal values and axes, independent of whether the site tensors have the same principal axis system (68).

Our **g** and **A** tensor calculations for the $\text{Fe}_2\text{S}_2^{1+}$ model cluster have been discussed in detail previously (13, 69–71). Here we emphasize a few important points. The calculated **g** tensor is rhombic in a principal

axis system, with $g_x = 1.87$, $g_y = 1.96$, $g_z = 2.01$, where z is the Fe–Fe axis, xz is the 2Fe–2S* bridge plane, and yz is the 2Fe–4(SR) terminal plane as in Fig. 1. These results are in rather good agreement with results for typical reduced plant ferredoxins (such as spinach), $g_x = 1.88$, $g_y = 1.96$, $g_z = 2.04$ (9), and not in agreement with the axial g tensors found in putidaredoxin or adrenal ferredoxins (67). The anisotropic parts of the Fe hyperfine tensors show the same behavior, with much better agreement for the plant ferredoxins (9, 72, 73). The largest value (magnitude) of the anisotropic part of the A tensor on the ferrous site is along the Fe–Fe axis from the theory, consistent with the filling of $16a_1\alpha$ (Fe d_{z^2}). The predicted Mössbauer quadrupole splitting for the reduced site is large and negative ($\Delta E_Q = -3.1$ mm/sec, with principal axis z) (14), which is similar to the values measured for reduced plant ferredoxins (9, 72, 74). Comparison of our theoretical results for g values with the phenomenological model of Bertrand and Gayda shows similar covalency: orbital reduction factor 76% for the spin–orbit coupling constant (67) versus 56 to 75% Fe(3d) character in the unoccupied orbitals $16a_1$ to $9b_1$. The mixing between Fe d_{z^2} and $d_{x^2-y^2}$ is small in $16a_1$ (13). When the mixing parameter θ is defined by $|16a_1\rangle = \cos \theta |d_{z^2}\rangle + \sin \theta |d_{x^2-y^2}\rangle$, we find $\theta = 8^\circ$ for the reduced system [$X\alpha$ –linear combination of atomic orbitals (LCAO)]. The extent of mixing depends, however, on the orientation of the SR groups; in general, the mixing is larger if the SR groups lie close to the Fe–Fe (z) axis, and smaller (as above) for SR away from the z axis (13). Further, the latter case corresponds to a large negative quadrupole splitting with the z principal axis on the ferrous site, whereas the former may have a positive value and/or another principal axis (14).

Utilizing the predicted Mössbauer trends above (negative ΔE_Q in algal ferredoxins), and the known X-ray structure of the algal ferredoxin *Spirulina platensis* (75), we predicted (14) that the reduced site in this ferredoxin should be at Fe Cys 46, Cys 41, since the z direction opposite to Fe–Fe is rather open here, in contrast to Fe Cys 79, Cys 49. This prediction has recently been confirmed by NMR nuclear Overhauser experiments of Dugad *et al.* (76).

D. HEISENBERG COUPLING AND RESONANCE COUPLING

To analyze spin coupling, the broken symmetry state Ψ_B with energy E_B must be compared with the high-spin state $\Psi(S_{\max})$ with energy $E(S_{\max})$. In the oxidized system, the broken symmetry state [also referred to as the low-spin and antiferromagnetic (AF) configuration] is described by the energy level structure in Fig. 1; the spin vectors for

the monomer subunits are oppositely aligned (12, 13). The oxidized high-spin state [or ferromagnetic (F) configuration] is constructed by parallel spin alignment of the monomer spin vectors. The oxidized F state thus has 10 spin- α magnetic electrons and none of spin β ; its energy level diagram is the result of an independent SCF calculation for $S = 5$, shown in Fig. 3. The F state has essentially the same D_{2h} symmetry as the nuclear framework, and both the V_α and V_β one-electron potentials have the same symmetry. In Fig. 3, notice that the unoccupied (minority or β) spin orbitals are symmetrically delocalized over both halves of the molecule. These are mainly Fe($3d$) in character. There is then no barrier to electron delocalization upon reduction for the F state, in contrast to a substantial barrier and localization that we find for the broken symmetry, AF configuration. This is depicted schematically in Fig. 4.

The Heisenberg exchange coupling constant for the oxidized system was evaluated using Eq. (25). In the X-ray structures of 2Fe-2S algal ferredoxins (75, 77), at least one axial site is rather open; in all cases, however, the protein structures give a much less symmetric cluster coordination geometry to cysteine S than in our theoretical models. Experimentally, $J_{\text{ox}} = 366$ and 298 cm^{-1} for oxidized spinach ferredoxin (78) and for a synthetic analog (79). The theoretical values are larger, X α -LCAO gives $J_{\text{ox}} = 620 \text{ cm}^{-1}$ for an open axial-site model geometry; see Table I (13).

For the reduced system, we must consider both the Heisenberg coupling parameter J_{red} and the resonance parameter B in our analysis. For the proper spin eigenstates, we begin with the Heisenberg spin ladder, which is then split by resonance delocalization into g , u components of the form

$$E(S)_{g,u} = JS(S + 1)/2 \pm B(S + \frac{1}{2}) \quad (50)$$

For the higher spin eigenstates, the resonance splitting is substantial, and we expect that local asymmetries will not be strong enough to quench the resonance. For the lowest spin states, the resonance splitting is much smaller, and (given that the J coupling is antiferromagnetic) the resonance can be quenched by environmental asymmetries, including the coordination environment, hydrogen bonding, solvation, and vibronic effects.

Our goal is to extract the J_{red} and B parameters from the density-functional calculations and to explore the implications of the results. Figure 5 is a schematic diagram of the Heisenberg plus resonance Hamiltonian. The Heisenberg spin ladder is at the left, and the resonance splitting is shown in the next column. At the right is the corre-

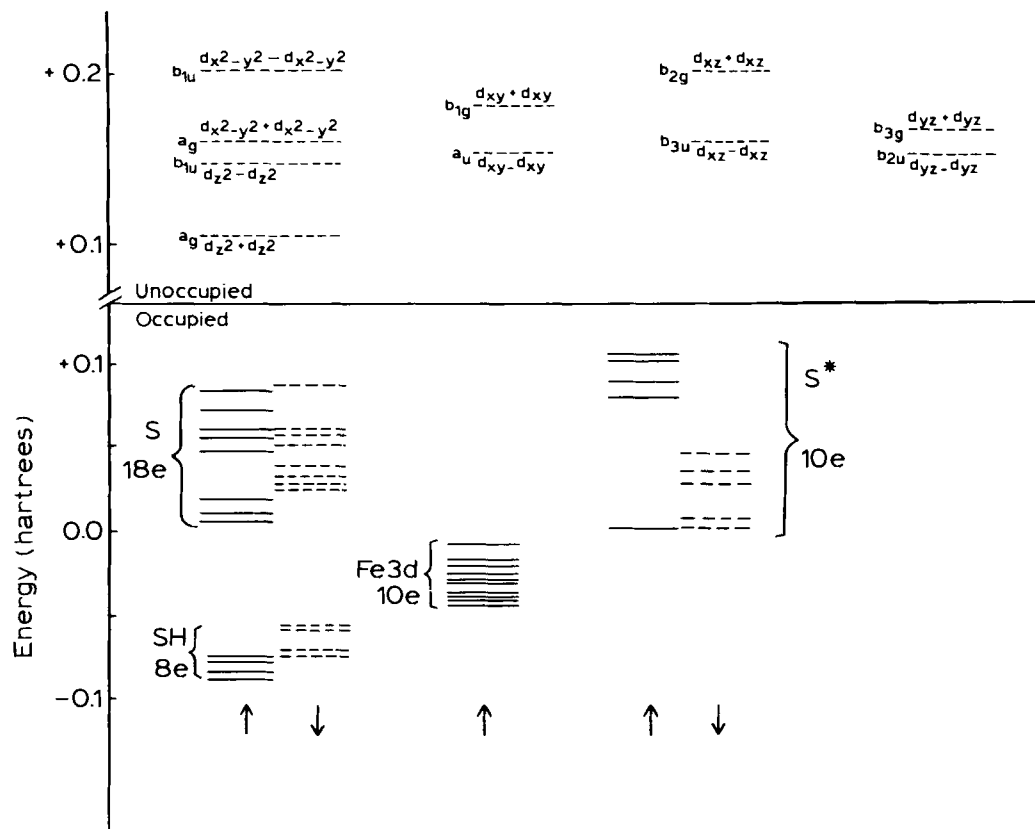


FIG. 3. X α -LCAO energy levels for high-spin ferromagnetic configuration, $\text{Fe}_2\text{S}_2(\text{SH})_4^{2-}$. There is an excess of 10 spin- α electrons. The occupied levels are grouped according to orbital character (S, Fe, etc.), and the unoccupied levels are specified by their symmetries in the D_{2h} group and Fe(3d) character. See Ref. 13.

TABLE I
SPIN HAMILTONIAN PARAMETERS^a

Compound	Geometry	J_{ox}	J_{red}	B'	B	$J_{\text{red}}/J_{\text{ox}}$	$ B/J_{\text{red}} $
$\text{Fe}_2\text{S}_2^{2+/1+}$		620	346		-516	0.56	1.5
$\text{Fe}_3\text{S}_4^{1+/0}$	Linear	544	407	—	-568	0.75	1.4
$\text{Fe}_3\text{S}_4^{1+/0}$	Cubane	369	297	-30	-406	0.81	1.4
$\text{ZnFe}_3\text{S}_4^{3+/2+}$	Cubane	360	282	-28	-407	0.78	1.4
$\text{ZnFe}_3\text{S}_4^{1+}$	Cubane	—	45	-64	-426	0.16 ^b	9.5
$\text{Fe}_4\text{S}_4^{3+}$	A	—	416	—	-722	1.09 ^c	1.7
			472	-297	-722	0.96 ^c	1.5
$\text{Fe}_4\text{S}_4^{2+}$	A	—	454 ^d	—	-740 ^d	—	1.6
$\text{Fe}_4\text{S}_4^{1+}$	A	—	231 ^e	—	-715 ^e	0.51 ^b	3.1
			379	-590	-715	0.83 ^b	1.9
	B		145	—	-696	0.32 ^b	4.8
			300	-622	-696	0.66 ^b	2.3

^a Values in cm^{-1} . Except as noted below, all values are determined from the $X\alpha$ potential; results for 3Fe clusters are from scattered-wave calculations (91, 92, 95), and those for 2Fe and 4Fe clusters are from LCAO expansions (13, 94). For the +1 and +3 oxidation states of Fe_4S_4 , the upper line gives results for a two-parameter fit in which the interlayer resonance B' is ignored; the lower line gives results for a three-parameter fit in which it is included. For Fe_4S_4 , the A geometry is taken from model complexes in the +2 oxidation states, and the B geometry is from model complexes in the +1 oxidation state; see Ref. 14 for details.

^b Ratio for the +1 and +2 oxidation states.

^c Ratio for the +2 and +3 oxidation states.

^d With the VSB potential (see text) J is 654 and B is -795 cm^{-1} .

^e With the VSB potential, J is 459 and B is -774 cm^{-1} .

sponding broken symmetry picture. The broken symmetry state is assumed to exhibit complete trapping, whereas the high-spin state has an $E(S_{\text{max}})_{\text{u}} - E(S_{\text{max}})_{\text{g}} = 10B$ splitting. The latter splitting is, in fact, similar to the orbital splitting between the lowest unoccupied $a_g\beta$ and $b_{1u}\beta$ seen in Fig. 3. The J_{red} value is determined from the equation,

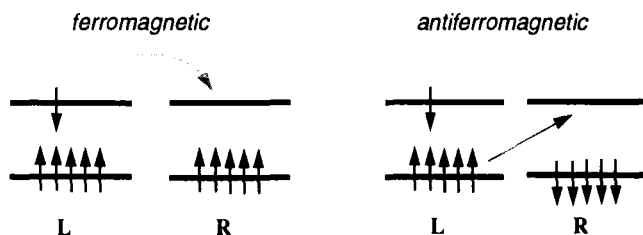


FIG. 4. Delocalization of the added electron in the reduced dimer is compared for the ferromagnetic (F) and antiferromagnetic (AF) configurations. There is loss of spin polarization energy for AF but no loss for F. See Ref. 13.

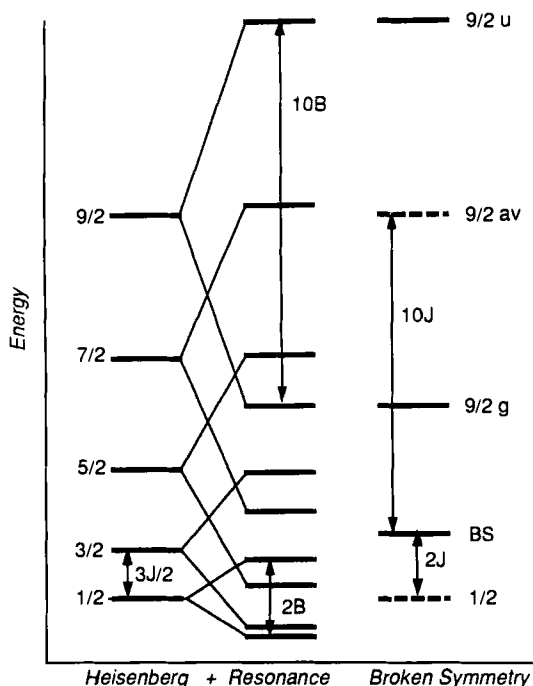


FIG. 5. Schematic spin state diagram for a reduced $\text{Fe}_2\text{S}_2^{1+}$ dimer. The spin states for a Heisenberg, Heisenberg plus resonance ladder, and within the broken symmetry picture are indicated, including the broken symmetry (BS), and high-spin $S = \frac{9}{2}$ states. $E(S = \frac{9}{2})_{\text{av}}$ is taken as the simple average of the $E(S = \frac{9}{2})_{\text{g,u}}$ states. See text and Ref. 13.

$E(S_{\text{max}})_{\text{av}} - E_B = n(n-1)J/2 = 10J$ [Eq. (26)], where $E(S_{\text{max}})_{\text{av}}$ is the average taken over the g, u energies.

The assumption of complete trapping implies that $E(S_{\text{max}})_{\text{av}}$ can be taken as a simple average of $E(S_{\text{max}})_{\text{g}}$ and $E(S_{\text{max}})_{\text{u}}$. This should be a fairly good assumption, but it is not exact. An argument can be made with reference to Figs. 1 and 4. In the state $\Psi_L(B)$ —where an electron has been added to $16a_1\beta$, Fe $d_{z^2}\beta$ localized on the left—this electron cannot delocalize, since the corresponding orbital of the same spin $10a_1\beta$, Fe $d_{z^2}\beta$ on the right is already occupied. Only a small amount of delocalization of $10a_1\alpha$ (left) to the right side is allowed with molecular orbital (MO) mixing coefficient c , because spin polarization energy is lost on $L \rightarrow R$ electron transfer (see Fig. 4). Further, only the resonance part of this, giving a further factor $1/\sqrt{5}$, leads to nonorthogonality between $\Psi_L(S)$ and $\Psi_R(S)$ for $S = S_{\text{max}}$, where $\Psi_L(S)$ and $\Psi_R(S)$ are obtained by projection from $\Psi_L(B)$ and $\Psi_R(B)$. It is this nonorthogonality that leads to the more general weighted average equation in Ref. 13 in

place of the simple average $E(S_{\max})_{\text{av}}$. In the present context, the simple average is well justified. [The proper coefficient for use in Eq. (7) of Ref. 13 is $c' = c/\sqrt{5}$, not c , so that $c' = 0.2$; moreover, c is difficult to calculate accurately.]

The calculated values for the J and B parameters are $J_{\text{red}} = 346 \text{ cm}^{-1}$ and $|B| = 516 \text{ cm}^{-1}$; the ratio $|B|/J_{\text{red}}$ is 1.49 (Table I). Experimental J_{red} values are 196 cm^{-1} from blue-green algal ferredoxin (80) and 220 cm^{-1} from spinach ferredoxin (81); these are all AF. As in the oxidized case, the theoretical prediction overestimates the J value. However, the reduced case is complicated by the presence of the B parameter, which does not appear at all in the Heisenberg Hamiltonian that was used in fitting the magnetic susceptibility data to the Heisenberg model to extract an "experimental J_{red} " value. If we take the Heisenberg plus resonance Hamiltonian seriously, we see that when B is substantial the higher spin states are closer to $S = \frac{1}{2}$ than for the corresponding Heisenberg Hamiltonian. In fact, a higher spin state can become the ground state for large enough B . By plotting the energy versus $|B|/J$, as in the work of Münck *et al.* (17), the $S = \frac{3}{2}$ becomes the ground state in place of $S = \frac{1}{2}$ for $1.5 \leq |B|/J \leq 2.5$, whereas for $|B|/J \geq 4.5$ the ground spin state is $S = \frac{5}{2}$. Our calculated $|B|/J_{\text{red}}$ value of 1.49 is nearly at the $S = \frac{1}{2}$, $S = \frac{3}{2}$ crossover point. If, however, a difference in the site energies of the left and right sites is introduced, a new situation is obtained. The higher spin states are less stabilized than with the Heisenberg plus resonance Hamiltonian. When the site energy difference is large, $|E_{\text{L}} - E_{\text{R}}| \gg |B|(S + \frac{1}{2})$, then the resonance term and the site energy difference together combine to give an effective J parameter, $J_{\text{eff}} = J - 2B^2/|E_{\text{L}} - E_{\text{R}}|$ (17). The resonance term in the presence of different site energies thus makes an effective ferromagnetic contribution to J_{eff} . Something like this must be happening in reduced 2Fe-2S proteins and clusters. Mössbauer spectroscopy clearly indicates trapped valence. With B of the order of 500 cm^{-1} , the site energy difference (or other mechanisms, such as vibronic coupling) should be sufficient to localize the $S = \frac{1}{2}$ ground state as originally proposed in our 1984 paper. However, there is no simple way to evaluate the separate terms in J_{eff} either theoretically or experimentally. The localization is that of a Robin-Day Class II complex (82). Direct evaluation of the B parameter by experimental methods would be quite difficult here; as we discuss below, the situation is more promising in polynuclear Fe-S systems where some dimer subunits have a large net spin.

E. ELECTRON TRANSFER AND OPTICAL CHARGE TRANSFER SPECTRA

The presence of the "inverted level scheme" with $S, S^*(3p)$ orbitals lying just below empty minority spin $\text{Fe}(3d)$ levels immediately sug-

gests a role for $S(3p)$ in mediating the rapid electron transfer observed between ferredoxins and other redox centers (13). We will consider direct transfer of an electron from a negatively charged donor to ferredoxin. Dipole and spin-allowed charge transfer bands (and also spin-forbidden charge transfer bands) of $S, S^*(3p) \rightarrow Fe(3d)$ appear at low energy in 2Fe-2S proteins (83-85). Since these are at low energy (10,000 to 25,000 cm^{-1}), charge transfer intermediate states with a hole in the $S(3p)$ band and internal electron transfer cysteine $S \rightarrow Fe d_{z^2}$ are very likely, the charge transfer (CT) being induced by polarization due to the electric field of the donor. These intermediates are closely analogous to the spin- and dipole-allowed CT excitations. (Whether these are real intermediates or virtual intermediates, essentially quantum mechanical resonances, is an interesting open question.) The electron from the donor can then fill the empty $S(3p)$ hole, completing the electron transfer. This mechanism clearly shows how reduction at Fe can occur without direct contact of the Fe center with the donor. Rapid, nearly diffusion-controlled electron transfer of aquated electrons to oxidized $Fe_2S_2^{2+}$ parsley ferredoxin has been measured with a second-order rate constant $k_2 = 9.7 \times 10^9 M^{-1} \text{sec}^{-1}$ (86). Electron transfer is also rapid between rubredoxin molecules, with an apparent self-exchange rate constant of 1.7×10^8 to $1 \times 10^9 M^{-1} \text{sec}^{-1}$ (87).

VI. Three-Iron Clusters

A. BACKGROUND

The extension of the ideas discussed above to three-iron clusters was pioneered by Münck, Huynh, Girerd, and their co-workers (17, 33, 88). Here we can consider both the total spin S and a "subdimer spin" S' . The initial motivation came from analysis of the reduced three-iron cluster in *Desulfovibrio gigas* ferredoxin, which showed clearly that one component of this cluster was a delocalized $Fe(II)/Fe(III)$ dimer with $S' = \frac{3}{2}$ (33). Later studies have confirmed that a spin Hamiltonian that contains both Heisenberg and resonance delocalization terms can explain many of the properties in a variety of clusters (89). Here we outline the way in which a very simple theory of reduced three-iron clusters can be constructed; the oxidized (all Fe^{3+}) clusters are also of interest, and for our theoretical work on this problem, see Ref. 90.

B. BROKEN SYMMETRY ANALYSIS OF REDUCED THREE-IRON CLUSTERS

Following the results found for two-iron clusters, we assume that the true electrostatic interactions that couple iron spins together can be replaced by an interaction of the Heisenberg type (90, 91):

$$\hat{H} = J(\mathbf{S}_1 \cdot \mathbf{S}_2 + \mathbf{S}_1 \cdot \mathbf{S}_3 + \mathbf{S}_2 \cdot \mathbf{S}_3) \quad (51)$$

and that the off-diagonal matrix elements connecting states where electron delocalization is "allowed" will be of the form $B(S' + \frac{1}{2})$, as discussed above. Consider first a three-iron cluster with three equivalent metal sites in the "singly reduced" Fe(II)/Fe(III)/Fe(III) formal oxidation state. In the high-spin configurations, the first five d electrons on each site are aligned in a parallel fashion, say spin-up. We can form three basis configurations by allowing the final d electron (which must be spin-down) to reside, in turn, on each of the three sites. Using the results cited above, the spin Hamiltonian matrix becomes

$$\mathbf{H}_{\text{hs}} = \begin{bmatrix} (\frac{65}{4})J & 5B' & 5B' \\ 5B' & (\frac{65}{4})J & 5B' \\ 5B' & 5B' & (\frac{65}{4})J \end{bmatrix} \quad (52)$$

Here and below, the diagonal elements represent the system energy in the absence of delocalization, and the off-diagonal elements give the specific resonance delocalization effects, recognizing that $(S' + 1/2) = 5$ for parallel-spin Fe(II)/Fe(III) dimers. The eigenvalues are $E_1 = (\frac{65}{4})J + 10B'$, and $E_{2,3} = (\frac{65}{4})J - 5B'$ (doubly degenerate). For these clusters we find $B' < 0$, and hence E_1 lies lowest.

For the broken symmetry state, the first five d electrons of one of the iron atoms (which we call "a") is of spin opposite to that of an equivalent pair "b." There are still three basis configurations, corresponding to the three possible locations of the last d electron. Following Papaefthymiou *et al.* (33), we will adopt the simplest delocalization hypothesis, that resonance interaction is important only between the two irons of the same spin, pair "b." Here the spin matrix is

$$\mathbf{H}_{\text{bs}} = \begin{bmatrix} -(\frac{25}{4})J & 0 & 5B \\ 0 & -(\frac{15}{4})J & 0 \\ 5B & 0 & -(\frac{25}{4})J \end{bmatrix} \quad (53)$$

Here we have allowed the delocalization parameter in the broken symmetry state, B , to differ from that in the high-spin state; the $X\alpha$ results reported below show that this indeed happens. Eigenvalues for the broken symmetry case are $E_{1,2} = -({}^{25}_4)J \pm 5B$ and $E_3 = -({}^{15}_4)J$.

The J and B values can thus be estimated by comparing the energy differences arising from these formulas with those computed from a broken symmetry molecular orbital approach, and estimates of the pure spin state energies (including the ground state energy and its spin value) are then made from the resulting parametrized spin Hamiltonian.

To apply these ideas, we have carried out scattered-wave calculations on models for Fe_3 and ZnFe_3 clusters, using the $X\alpha$ approximation for exchange and correlation effects (90–92). Structures of “cubane” 3Fe clusters are not known from high-resolution X-ray crystallography, and our assumptions about the structures are given elsewhere. For the singly reduced 3Fe cluster, a high-spin unrestricted self-consistent wavefunction (with 15 spin-up d electrons and one spin-down d electron) was determined. Then, the spin-up and spin-down potentials of one iron atom were interchanged, and the solution reconverged to a broken symmetry state with a large spin-up spin population on two irons and a large spin-down population on the third. As with the 2Fe clusters, significant spin populations are also found on sulfur centers. The highest occupied orbitals (except for the last one) are primarily of sulfur p character, and the majority-spin $\text{Fe } d$ orbitals are below these. For each wavefunction, the very highest occupied orbital is primarily of minority-spin $\text{Fe } d$ character. For the high-spin case, the two potential orbitals for this last electron (of a_1 and e symmetry) lead to total energies that are separated by 450 cm^{-1} , which can be identified with $15B'$ through Eq. (52). Hence the effective resonance interaction B' is fairly small, about -30 cm^{-1} . In the broken symmetry case, where delocalization can occur over only two centers (the “ b ” pair, which have the same spin alignment), we find g and u states (of a' and a'' symmetry) that are split by a much larger amount, 4060 cm^{-1} [which by Eq. (53) is $10B$], so that B is -406 cm^{-1} . The J value for this complex is determined primarily by the difference in the high-spin and broken symmetry energies; fitting the $X\alpha$ energies to the eigenvalues given above yields $J = 297 \text{ cm}^{-1}$.

Table I summarizes the results of our calculations, along with previous work on two- and three-iron clusters. As before, the general tendency of the $X\alpha$ scattered-wave method is to overestimate J : for example, the experimental estimate of J for the oxidized linear three-iron cluster is 300 cm^{-1} , about 45% lower than the value we estimate.

Several interesting features emerge from Table I. First, the magni-

tude of J decreases as the complexes are reduced. This happens even when the geometries are unchanged, as we have assumed here. It is likely that reduction of the complexes will in addition lead to slight expansions of the core, which would reinforce this drop in J as the complexes are reduced. The magnitudes of J appear to be correlated with geometry: the linear two- and three-iron complexes (with nearly identical bridging geometries) have higher values for J than do the cubanelike clusters. Second, the resonance parameters B are negative, indicating that the symmetric combination of atomic orbitals on the "b" irons lies below the antisymmetric combination. As with J , the magnitudes of B appear to be related to the geometry of the bridge, with larger absolute values for the linear than for the cubane geometry. Computed magnitudes of $|B|/J$ are around 1.5; since, however, we expect the computed J values to be too large, we likewise expect the true values of $|B|/J$ to be larger than those shown in Table I, probably in the range 2.0–3.0. For the cubanelike three-iron cluster, with all J values equal, the ground state is predicted to be $S = 2$ (as is observed) when $|B|/J > 2.0$ (17, 33).

VII. Four-Iron Clusters

A. ENERGY LEVEL STRUCTURE

4Fe–4S clusters commonly appear in three oxidation states (93). All the calculations we will describe are on the model system $[\text{Fe}_4\text{S}_4(\text{SCH}_3)_4]^{1-2-3-}$, with the equivalent cubane core oxidation states, $[\text{Fe}_4\text{S}_4]^{3+/2+/1+}$ (14, 94, 95). The calculations have typically been made with an assumed D_{2d} molecular geometry, and with the reduced electronic symmetry of C_{2v} after symmetry breaking. For details about the molecular geometries employed, and computational methodology, we refer to our published work (14, 94, 95).

Our basic reference point is the electronic structure of the $[\text{Fe}_4\text{S}_4]^{2+}$ cluster. In the broken C_{2v} electronic symmetry, the equivalence between the top and bottom halves of the cluster is removed and a spin-polarized calculation is done to determine Ψ_B . Qualitatively, the broken symmetry state is constructed by antiparallel alignment of the two $[\text{Fe}_2\text{S}_2]^{1+}$ subunits. Each subunit is high spin, so that $S_{12} = S_{34} = \frac{5}{2}$ aligned to give $M_S = 0$, where S_{12}, S_{34} are spin quantum numbers for the dimeric subunits, and M_S is the z component of total cluster spin S . The true spin ground state has both $S = 0$, and $M_S = 0$, and has an energy $E(S = 0)$ below E_B . In Ψ_B each dimeric subunit has 10 occupied

majority-spin [mainly $\text{Fe}(3d)$] levels at low energy, and one occupied minority-spin $\text{Fe}(3d)$ level at much higher energy. Between the two exchange-split $\text{Fe}(3d)$ sets lies the $\text{S}^*(3p)$ and $\text{S}(3p)$ bands, in accordance with the inverted level scheme. The formal metal oxidation state is $\text{Fe}^{2.5+}$, with a formal spin population of 4.5 per iron. Iron sulfur covalency leads to a much lower Fe charge, a smaller Fe spin population, and a higher total Fe d population than for these "formal" values.

The highest occupied molecular orbital (HOMO) $20a_1$ is a delocalized Fe–Fe σ bonding orbital $(d_{x^2-y^2})_a + (d_{x^2-y^2})_b$, largely confined to one dimeric subunit of the cluster (Plate 1). It is also weakly Fe–S antibonding (or possibly nonbonding), based on Plate 1. The minority-spin energy levels and various spectroscopic parameters are indicated in Fig. 6 (94). Of primary importance is $10B_\sigma$, which gives the splitting between the occupied Fe–Fe σ bonding orbital, $20a_1$, and the empty Fe–Fe σ^* antibonding orbital, $14b_2$. The J parameter is determined from the configuration energy difference between the high-spin state, $E(S_{\max})$ (all spin vectors aligned with $S_{12} = S_{34} = \frac{9}{2}$, $S_{\max} = 9$), and the broken symmetry energy E_B as

$$E(S_{\max}) - E_B = S_{\max}^2 J/2 = (n - 1)^2 J/2 = 81J/2 \quad (54)$$

The corresponding pure spin state energy separation for the highest and lowest states of the ladder is

$$E(S_{\max}) - E(S = 0) = S_{\max}(S_{\max} + 1)J/2 = 45J \quad (55)$$

so $E(S = 0)$ lies $9J/2$ below E_B .

B. OXIDIZED AND REDUCED CONFIGURATIONS

The ligand field levels $20a_1$, $9a_2$, and $14b_2$ (see Fig. 6) (94) are also the levels filled or emptied by $\text{Fe}_4\text{S}_4^{2+/1+}$ and $\text{Fe}_4\text{S}_4^{2+/3+}$ redox processes (14, 95). In the oxidized (+3) high-potential cluster (HP_{ox}), one of two $20a_1$ electrons is removed. In the reduced (+1) oxidation state, one electron is added either to Fe–Fe σ^* or δ^* so that the final orbital configuration (OC) is $\text{OC1} = (20a_1\alpha, 20a_1\beta, 14b_2\alpha)$ or $\text{OC2} = (20a_1\alpha, 20a_1\beta, 9a_2\alpha)$ (14, 96). These are nearly degenerate in energy, with OC2 slightly lower by about 0.1 eV (14, 95). Since the cluster geometry D_{2d} is rather idealized, and the cluster geometry and environment may provide distortions or asymmetries, we can expect a mixing and splitting of the two orbital configurations OC1 and OC2. The variability of the quadrupole splittings on the 2Fe^{2+} pair among different $\text{Fe}_4\text{S}_4^{1+}$ clusters and proteins is consistent with the large difference in the

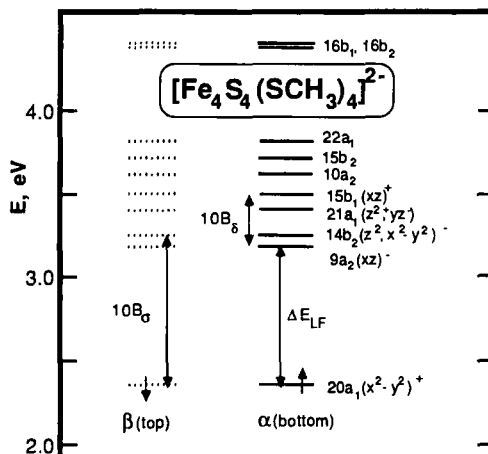


FIG. 6. $X\alpha$ -LCAO energies for the ligand field levels (highest occupied and lowest unoccupied levels) of $[\text{Fe}_4\text{S}_4(\text{SCH}_3)_4]^{2-}$. All these levels are mainly Fe(3d). Spin α and β levels are specified with solid and dotted lines, and their location on the top and bottom faces of the cluster is indicated. See Ref. 94.

calculated ΔE_Q on the 2Fe^{2+} reduced sites (14, 96). Further, the presence of these two nearly degenerate configurations, OC1 and OC2, is relevant to the relative stability of an $S = \frac{1}{2}$ versus $S = \frac{3}{2}$ ground state.

C. RELAXATION EFFECTS ON CLUSTER OXIDATION $+2 \rightarrow +3$

Plates 1 and 2 show the orbital amplitude in orbital $20a_1\alpha$ of the $+2$ cluster, and the total valence electron density difference between the reduced ($+2$) and oxidized ($+3$) states, respectively. Both calculations used the same ($+2$) geometry, so the differences are entirely electronic and contain no effects from geometry changes on oxidation (in contrast to experimental X-ray density difference maps, which give a composite of electronic and geometric effects) (93). (Further, the isovalue contour levels for the orbital map were set to the plus/minus square roots, gray/blue, of the positive contour level for the density difference map, so these are strictly comparable; isovalues for Plates 3 and 4 were set to the same values as for Plates 1 and 2, respectively.) The blue region on Plate 2 is the region of net electron depletion on oxidation, mainly on the two oxidized irons and on all sulfurs, and the green region shows the backflow of electron density, giving a compensating region of increased electron density. The blue region in Plate 2 resembles the $20a_1$ orbital

(Plate 1) around the oxidized iron centers, as one might expect. However, there are two major differences between the orbital density and the total electron density difference. First, the charge depletion region on Plate 2 is much larger and more diffuse than in the orbital map; it extends to all terminal and bridge sulfurs, and shows that the charge on sulfurs becomes considerably less negative on oxidation. Second, the backflow of electron density, which represents bonding density and $S \rightarrow Fe$ electron donation, is completely absent in the orbital map (Plate 1). Both of these effects are consequences of electron relaxation in the "passive" orbitals (all orbitals except $20a_1\alpha$).

Some physically important consequences follow from this electron density difference map: (1) the cluster oxidation is an electronically asymmetric process; (2) since the charge depletion occurs from the weakly Fe–S antibonding orbital $20a_1\alpha$, and backflow arises from bonding density via $S \rightarrow Fe$ electron donation to the $2Fe^{3+}$ oxidized centers, there should be asymmetric Fe–S bond strengthening confined largely to the "oxidized" layer of the cluster; (3) all sulfur centers become less negative on oxidation by about 0.1 electron per sulfur; (4) the net Fe($3d$) population decreases by only 0.05–0.07 electron per iron for the oxidized iron sites, but there is considerable charge rearrangement on these sites.

The electron density difference map lends further support to the analysis we have given of resonance Raman spectra for *Chromatium vinosum* $Fe_4S_4^{2+/3+}$ and $Fe_4Se_4^{2+/3+}$ high-potential proteins (97). The observed increase in Fe–S terminal stretch frequencies and the lower symmetry of the vibrations in the oxidized (+3) compared with the reduced (+2) form correspond to points 1 and 2 above. Higher Fe–S* stretch frequencies are not observed, although these are also implicated by our calculations. Both Fe–S terminal and Fe–S* bond strengthening on oxidation is also implied by the shorter Fe–S* and Fe–S terminal bond lengths as seen in the structure of a synthetic $Fe_4S_4^{3+}$ cluster, by about 0.02 and 0.04 Å, respectively, compared with synthetic +2 clusters (98). Longer NH–S hydrogen bonds (by about 0.1–0.4 Å) to many of the S_t , S^* atoms have been found from the protein X-ray structure of

PLATE. 1. Orbital $20a_1\alpha$ (+2) form of 4Fe–4S cluster, showing atoms of Fe (purple), S (yellow), C (green), and H (small, light-blue spheres). Positive/negative amplitudes are gray/blue, and isovalue levels are set as the plus/minus square roots of those in Plate 2. The top layer on all plates corresponds to the bottom layer in Fig. 6.

PLATE. 2. Total valence electron density difference +2 – +3. Blue shows net electron depletion on oxidation and green shows increased density.



PLATE 1.

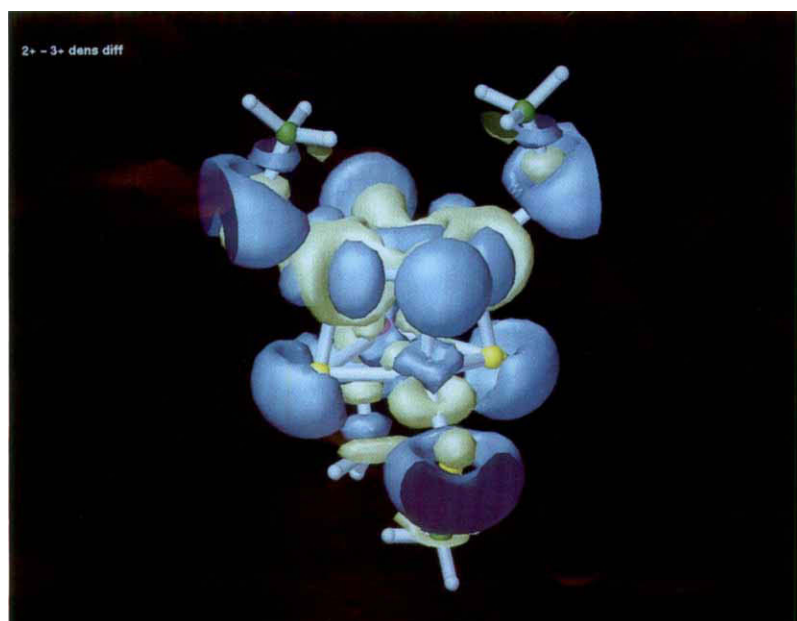


PLATE 2.

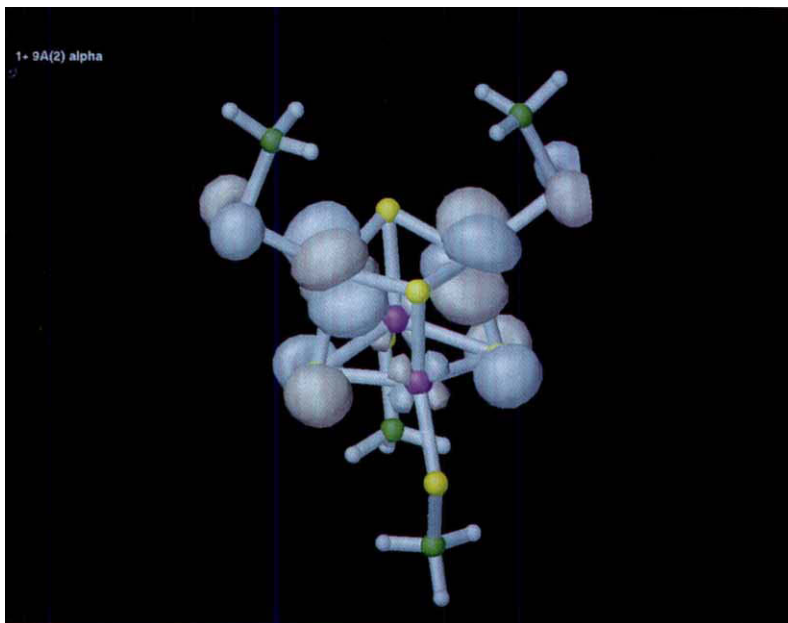


PLATE 3.

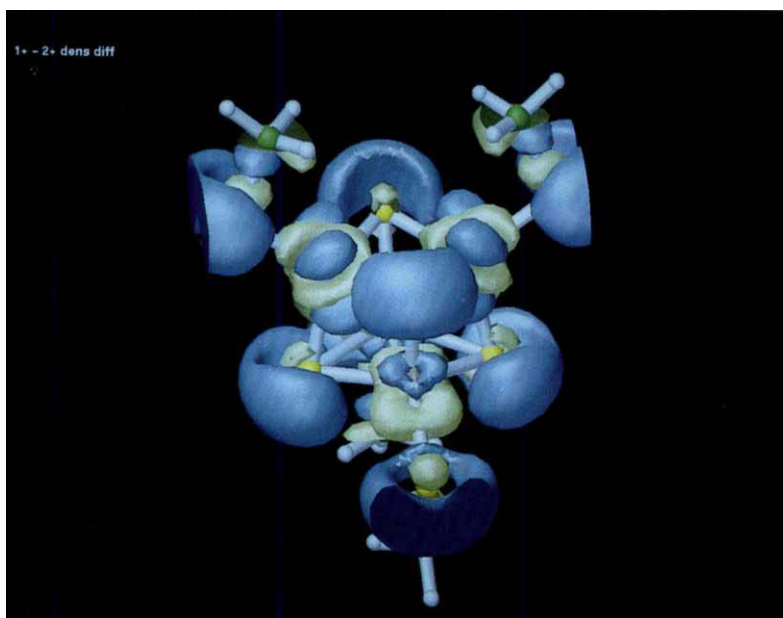


PLATE 4.

HP_{ox} compared to the reduced protein or to ferredoxins (93). These are consistent with the less negative charge on all S, S* in the oxidized form (point 3). The changes in electron density on oxidation are quite spread out, and modeling of redox effects on hydrogen bond strengths should take this into account. For example, the increase in hydrogen bond strength for (reduced minus oxidized) high-potential iron protein (HiPIP) is probably considerably less for each H bond than in the local model of Sheridan *et al.*, but most or all H bonds would be strengthened (99).

The modest difference in Mössbauer isomer shift observed when comparing the Fe_{ox} sites of +3 synthetic clusters and proteins to Fe sites in +2 clusters (100) is consistent with the small change calculated in net $Fe(3d)_{ox}$ population on oxidation (point 4).

D. RELAXATION EFFECTS ON CLUSTER REDUCTION $+2 \rightarrow +1$

Plate 3 shows the highest orbital of $Fe_4S_4^{1+}$, which resides largely on the reduced half of the cluster, $9a_2\alpha$ (HOMO) in configuration OC2. Again the total valence electron density difference (Plate 4) for +1 minus +2 includes substantial relaxation effects, and therefore differs from the HOMO $9a_2\alpha$. On Plate 4, blue represents increased electron density and yellow represents decreased density upon reduction. The net $Fe(3d)$ population on the reduced iron sites increases by only about 0.05–0.10 electron per iron on reduction, whereas all sulfur populations increase by about 0.1 per sulfur (with more than 0.8 electron going to all eight sulfurs). Sulfur as well as iron is thus involved in the changes in electron distribution on reduction.

E. SPIN-COUPLING PARAMETERS

Our spin Hamiltonian model for 4Fe clusters closely follows the ideas outlined above for smaller systems. The proposed spin Hamiltonian solution for the pure spin states of the +2 form is

$$E(S) = (J/2)S(S + 1) \pm B(S_{34} + \frac{1}{2}) \pm B(S_{12} + \frac{1}{2}) \quad (56)$$

PLATE. 3. Orbital $9a_2\alpha$ (+1) form of cluster. Labeling and isovalues as in Plate 1.

PLATE. 4. Total valence electron density difference +1 – +2. Blue shows increased electron density on reduction and green shows decreased density. Same isovalues as in Plate 2.

with S_{12} and S_{34} as the spin quantum numbers for the two mixed-valence pairs. Energies for the +1 and +3 states are

$$E(S) = (J/2)S(S+1) \pm B(S_{34} + \frac{1}{2}) \pm B'(S + \frac{1}{2}) + C_1 \quad (57)$$

where for +3, S_{12} is the spin quantum number for the 2Fe^{3+} pair, and for +1, S_{12} is the spin for 2Fe^{2+} . For all three oxidation states, S_{34} is the spin of the $\text{Fe}^{2+}-\text{Fe}^{3+}$, and S is the total spin quantum number. The first term in Eq. (57) is the Heisenberg coupling energy, the second is the resonance delocalization energy of the mixed-valence pair with parameter B , and the third represents the possibility of resonance of sites 1, 2 with 3, 4 ("interlayer resonance") involving the parameter B' . The last term is a spin-independent constant (C_1).

We will focus on the +1 cluster form, seeking the broken symmetry and high-spin energy equations necessary to determine the coupling parameters. The broken symmetry energy equation is

$$\begin{aligned} E_B &= J(\mathbf{S}_{12} \cdot \mathbf{S}_{34}) \pm B(S_{34} + 1/2) + C_2 \\ &= -J(n-1)(n-2)/4 \pm 10B + C_2 = -18J \pm 10B + C_2 \end{aligned} \quad (58)$$

where

$$C_2 = J(\mathbf{S}_1 \cdot \mathbf{S}_2) + J(\mathbf{S}_3 \cdot \mathbf{S}_4)$$

with $n-2 = 8$ being the maximum number of unpaired electrons for 2Fe^{2+} . Here C_2 is a constant for fixed quantum numbers S_{12} and S_{34} . The corresponding equation for the energies of the high-spin states is

$$\begin{aligned} E(S_{\max}) &= J(\mathbf{S}_{12} \cdot \mathbf{S}_{34}) \pm B(S_{34} + \frac{1}{2}) \pm B'(S + \frac{1}{2}) + C_2 \\ &= +J(n-1)(n-2)/4 \pm 10B \pm B'(S + \frac{1}{2}) + C_2 \\ &= +18J \pm 10B \pm 9B' + C_2 \end{aligned} \quad (59)$$

with $S_{\max} = \frac{1}{2}n$ for the +1 cluster. Equations (58) and (59) are sufficient to determine the J , B , and B' parameters from the density-functional energies. J is determined from the configuration energy difference between the high-spin and the broken symmetry SCF energies, while B and B' were determined from orbital energy differences. The parameters for the oxidized (+3) state are determined in a similar fashion.

Table I collects results for a number of our calculations (13, 14, 91, 92, 94, 95). The density-functional LCAO results for the $\text{Fe}_4\text{S}_4^{1+/3+}$ clusters have not been published previously; corresponding LCAO results for the +2 cluster are from Ref. 94. The general trend that $J_{\text{ox}} > J_{\text{red}}$ is seen in the comparison of $2\text{Fe}-2\text{S}$, $3\text{Fe}-4\text{S}$, and $4\text{Fe}-4\text{S}$ cluster oxidation states by either $X\alpha$ -SW or $X\alpha$ -LCAO (also VSB potential).

[The VSB potential is a local spin density (LSD) potential due to Vosko *et al.* with a correlation correction due to Stoll *et al.* and an exchange energy gradient term due to Becke] (57–61). Geometry *A* is based on the experimental synthetic model geometry for +2 clusters whereas geometry *B* is a typical expanded geometry for the +1 cluster. The interlayer resonance parameter is seen to be significant in the sense that the three-parameter model parameters differ from the two-parameter fits (*J* and *B*), where *B'* is ignored. This is particularly strong for the +1 state (OC2) and where the cluster is expanded so that the *B'/J* is larger.

A summary of spectroscopic and spin-coupling parameters for $[\text{Fe}_4\text{S}_4]^{2+}$ is given in Table II, which also compares values from $\text{X}\alpha\text{-LCAO}$ and $\text{X}\alpha\text{-SW}$ (94). The two methods give parameters that are quite close. For the *J* parameter, Holm's group has obtained values of about 450–550 cm^{-1} from magnetic susceptibility fits for an analogous synthetic cluster, which is rather close to our calculated values (101). However, a combined Heisenberg plus resonance Hamiltonian would give both *J* and *B* parameters from fits to Eq. (56), and *J* would be expected to change significantly from the fit using a Heisenberg Hamiltonian alone. Two other points are of significance. The resonance B_σ pathway is clearly much stronger than the B_δ pathway within each resonance pair. The ligand field splitting between $20a_1$ and $9a_2$ is fairly large, with a substantial contribution from the stronger B_σ than B_δ resonance (see also Fig. 6). Qualitatively, the low-lying character of $20a_1$ compared to the other ligand field levels makes an electronic contribution to the high positive redox potential of the HP cluster +2/+3 redox process. A more quantitative assessment requires a consideration of solvation and other effects.

TABLE II

SPECTROSCOPIC AND SPIN-COUPLING
PARAMETERS FOR $[\text{Fe}_4\text{S}_4(\text{SCH}_3)_4]^{2+}$ ^a

Parameter	$\text{X}\alpha\text{-LCAO}$	$\text{X}\alpha\text{-SW}$
<i>J</i>	454	401
B_σ	−740	−585
B_δ	248	239
ΔE_{LF}	6751	5243

^a Values in cm^{-1} . See Fig. 6 and the text for definitions of the parameters. See Ref. 94.

F. STABILITY OF $S = \frac{1}{2}$ VERSUS $S = \frac{3}{2}$ FOR REDUCED (+1) CLUSTERS

The experimental observation of a variety of spin ground states, $S = \frac{1}{2}$, $\frac{3}{2}$, or $\frac{7}{2}$, in reduced $\text{Fe}_4\text{S}_4^{1+}$ and $\text{Fe}_4\text{Se}_4^{1+}$ clusters and proteins, is an important discovery by a number of groups (102–107). From a theoretical perspective [see Blondin and Girerd (18) and Borshch and Chibotaru (108)] interlayer resonance has been considered as a mechanism of possible significance for spin equilibria in both Fe_3S_4^0 cubane and in $\text{Fe}_4\text{S}_4^{3+/1+}$ clusters. The question is where and under what circumstances this mechanism will alter the spin ground state, or the low-lying excited spin states. Our very recent $X\alpha$ -LCAO calculations cast some light on this problem. For the +1 cluster, Table I gives $J = 300 \text{ cm}^{-1}$, $|B'| = 622 \text{ cm}^{-1}$ with a ratio $|B'|/J = 2.1$ for the expanded geometry B of OC2, for which Eq. (57) yields an $S = \frac{3}{2}$ ground state with low-lying $S = \frac{5}{2}$ and $S = \frac{1}{2}$ excited states. The situation of interlayer resonance in reduced $\text{Fe}_4\text{S}_4^{1+}$ clusters bears a close analogy to the resonance problem in reduced $\text{Fe}_2\text{S}_2^{1+}$ [compare Eqs. (50) and (57); see also Münck *et al.* (17)]. By contrast to OC2 (which has δ^* interlayer resonance), the orbital configuration OC1 (with σ^* interlayer resonance) should have $B' = 0$ by symmetry, which gives an $S = \frac{1}{2}$ ground state. Of course, the D_{2d} geometric symmetry is not exact, and mixing and splitting of OC1 and OC2 are to be expected. We note as well that the 2Fe^{2+} reduced pair Mössbauer ΔE_Q is always considerably smaller experimentally in $S = \frac{3}{2}$ ground state clusters than in $S = \frac{1}{2}$ type clusters (102–107), consistent with the lower calculated ΔE_Q for OC2 than for OC1 (14, 96). This is true whether or not all 4Fe sites have the same ΔE_Q . This explanation for the presence of an $S = \frac{3}{2}$ ground state in some clusters is physically distinct from the one proposed in our recent phenomenology papers, based on an inequality between $J(\text{Fe}^{2+}-\text{Fe}^{2+})$ and $J(\text{Fe}^{3+}-\text{Fe}^{2+})$ (96, 109). Though both mechanisms may be present, the interlayer resonance mechanism appears to be more robust in yielding an $S = \frac{3}{2}$ ground state. The competition between the Heisenberg term and the B' term is rather delicate, yielding a stabilization of about 170 cm^{-1} for $S = \frac{3}{2}$ compared to $S = \frac{1}{2}$ in the absence of any localizing forces. A more detailed analysis of this problem will be presented elsewhere.

G. PHENOMENOLOGICAL MODELING OF OXIDIZED (+3) AND REDUCED (+1) CLUSTERS

We have previously noted the trend in Heisenberg coupling constants, $J(2\text{Fe}^{2+}) < J(\text{Fe}^{2+}-\text{Fe}^{3+}) < J(2\text{Fe}^{3+})$, which is verified both

from our calculations on 2Fe, 3Fe, 3Fe–Zn, and 4Fe complexes (13, 91, 92, 95) and from experimental Heisenberg parameters in these systems (101, 110). A combined Heisenberg plus resonance Hamiltonian can be constructed with unequal Heisenberg parameters, and having a single resonance interaction within a specific mixed-valence pair. The resonance interaction is of the form $\pm B(S_{34} + \frac{1}{2})$, and neglects any interlayer resonance ($B' = 0$). (We may contrast this with the preceding section, where all J parameters are assumed equal but where $B' \neq 0$.) We have explored the consequences of such phenomenological models for both HP + 3 clusters (111) and for reduced + 1 clusters where the core is $\text{Fe}_4\text{Se}_4^{1+}$ or $\text{Fe}_4\text{S}_4^{1+}$ (96, 109). Many important phenomena can be derived from these models, and the appropriate ranges of the Heisenberg parameters plus the resonance parameter can be estimated from our density-functional calculations.

In HP + 3 clusters, taking the trend in J values above, and with $B/J > 0.9$, $\Delta J_{12}/J < 0.25$, (110, 111), the model gives a ground state of the type $|S_{34} S_{12}\rangle = |\frac{7}{2} \frac{1}{2} 4\rangle$, which with reasonable assumptions about the intrinsic site g_i and hyperfine a_i values (33), yields observed effective isotropic hyperfine parameters A_i and average total g value g_{eff} in fairly good agreement with those obtained from magnetic Mössbauer, ENDOR, and EPR spectroscopies (100, 112). Here $\Delta J_{12} = J(2\text{Fe}^{3+}) - J$, where $J(2\text{Fe}^{3+})$ is the ferric pair and J (with no subscript) is the interlayer coupling parameter. The latter describes four equal interlayer site couplings (111, 110). Phenomenological fits to the magnetic susceptibility for a synthetic HP analog indicate the presence of a very low-lying spin state of the form $|\frac{7}{2} \frac{1}{2} 3\rangle$ nearly degenerate with the state above, one further low-lying $S = \frac{1}{2}$ state, and two $S = \frac{3}{2}$ states, $|\frac{9}{2} \frac{3}{2} 3\rangle$ and $|\frac{7}{2} \frac{3}{2} 2\rangle$ (110). Further, the susceptibility fits give an interlayer J coupling of 652 cm^{-1} , $|B| = 529 \text{ cm}^{-1}$, compared with the theoretical values $J = 416 \text{ cm}^{-1}$, $|B| = 722 \text{ cm}^{-1}$ (Table I).

Since the hyperfine and EPR properties of $|\frac{7}{2} \frac{1}{2} 3\rangle$ are predicted to be very close to those of $|\frac{9}{2} \frac{1}{2} 4\rangle$, it is difficult to distinguish these states, and either may be the ground state. We have calculated both the \mathbf{g} tensor and the anisotropic part of the \mathbf{A} tensors from density-functional methods, and using the vector model based on the Wigner–Eckart theorem. These results will be reported separately. For the present, we give the \mathbf{g} tensor principal values for the state $|\frac{9}{2} \frac{1}{2} 4\rangle$ as $g_x = 2.02$, $g_y = 2.02$, and $g_z = 2.07$ in C_{2v} symmetry. Here the z axis is the S_4 axis perpendicular to the Fe^{2+} – Fe^{3+} pair bond x axis, and to the Fe^{3+} – Fe^{3+} pair bond y axis. (The z axis is also the axis of compression for the cluster.) These results are in good agreement with experimental EPR g values on high-potential proteins and synthetic analogs (100, 112,

113). It may be feasible to distinguish between the two possible ground states by ENDOR of the proton hyperfine coupling. (121, 122).

For reduced +1 clusters, J values are typically lower than for +2 and +3 clusters, and a substantial inequality between the smaller $J_2(2\text{Fe}^{2+})$ and larger $J_1(\text{Fe}^{2+}-\text{Fe}^{3+})$ parameters is often expected. With three Fe-Fe Heisenberg pairwise couplings of each type and resonance delocalization as well, the modeling requires the use of Racah algebra. The implications of phenomenological models of this type with a single resonance-delocalized pair (with parameter B) have been explored (96, 109). In addition to providing a good general account of isotropic hyperfine and g values for various $S = \frac{1}{2}$ states, the model gives a clear analysis of the physical basis for the coexistence of a delocalized $S = \frac{1}{2}$ state and a localized $S = \frac{7}{2}$ state, as found in reduced Se clostridial ferredoxin. The presence of external localizing forces is also quite important in determining the spin ground state and degree of delocalization. Further, there is a simple proposed mechanism for the presence of two states with significantly different rhombic EPR tensors in the unusual cluster in *Desulfovibrio vulgaris* hydrogenase (114), provided that the later is, in fact, a reduced 4Fe-4S cluster.

VIII. Conclusions and Prospects for Future Work

A. SUMMARY

A brief summary of some of the important areas wherein theory has made a contribution follows: (1) there is an inverted level scheme in both mononuclear and polynuclear Fe-S complexes with empty Fe(3d) levels in close energetic proximity to filled S(3p) levels (14, 64); (2) spin polarization effects produce both a large intraatomic exchange splitting between majority spin and minority spin Fe(3d) levels and significant spin transfer to the ligands (9, 13); (3) orbital relaxation effects on oxidation or reduction are large, and implicate both S, S* and Fe in redox processes (13, 14, 97); (4) there is a close connection between valence delocalization (resonance delocalization or "double exchange") and spin coupling (13, 17); this produces a distinctive term in the spin Hamiltonian; (5) trapped valence in reduced 2Fe-2S systems is produced by competition between resonance and Heisenberg coupling terms in the presence of external localizing forces; by contrast, the pair delocalization observed in 3Fe-4S and 4Fe-4S systems results because some pair spin vectors can be large, facilitating delocalization while maintaining many other pair spin vectors antiparallel, this being re-

lated to the concept of "spin frustration" in Hamiltonians having only Heisenberg-type terms (17, 18); (6) the general trend $J_{\text{ox}} > J_{\text{red}}$ is found for most clusters both theoretically and experimentally (92, 101); (7) the complex spin state crossovers and equilibria found especially in reduced 4Fe-4S and 4Fe-4Se clusters arise from the interplay of different Heisenberg J parameters with resonance delocalization, and from the presence of localizing forces of various possible types (96, 109); resonance may either involve a specific mixed-valence pair, or there may be additional interlayer resonance; (8) density-functional calculations give numerical estimates of J and B parameters, providing a starting point for detailed comparisons with experiment.

In all of these areas, both quantitative density-functional calculations and phenomenological modeling have been valuable. The first is characterized by the ability to make concrete predictions about spectroscopy and energetics for structurally well-defined systems, and by the ability to picture electron densities and spin densities in three-dimensional space. Further, density-functional theory combined with the concept of broken symmetry has a hierarchical conceptual structure, passing from energy levels and orbitals to electron and spin densities. From here, a connection can be made to spin-dependent properties, and the energies of different electron orbital and spin configurations can be related to spin-coupling Hamiltonians and their solutions.

The phenomenological approach has its own advantages, being characterized by flexibility and the possibility for exploration. There is no requirement here for the system to be well-defined geometrically, and even the coordination geometry may not be completely defined (although both are helpful for determining reasonable parameter ranges). Certainly, phenomenological models are the natural meeting place for experiment and theory. Here one optimizes the fit of a chosen model to experimental data (110). Our experience in Fe-S systems indicates that a proper "physical" model of a system may require fitting different types of experiments, such as EPR, ENDOR, NMR, Mössbauer, optical, and magnetic susceptibility, to an individual model. For example, infrared measurements provide a potential means of directly determining the B parameter in 4Fe-4S complexes, whereas other measurements are sensitive to both B and J parameters. These results can also serve to exclude physically unacceptable models (96, 109, 111).

At present, both the fitting of data to models and quantitative density-functional calculations have been restrictive in the number of J and B parameters determined, but we can look forward to density-functional calculations that will determine unequal J parameters as well as B and B' parameters and to a variety of measurements and

fitting procedures that will experimentally determine these same parameters. Further improvements in our theoretical methods are to be expected. At the same time, there appears to be a better correspondence between theoretical and experimental J values in 4Fe than in 2Fe or 3Fe systems. This is possibly due either to the larger high-spin minus broken symmetry energy difference in the 4Fe case [also a larger multiple of J , comparing, for example, $81J/2$ with $25J/2$ from Eqs. (54) and (25)], or due to the more realistic thiolate ligand model used. In many cases, only a lower bound to the J value can be determined experimentally, because susceptibility measurements are only feasible within a limited temperature range (89). The experimental determination of B parameters has only begun (110). We note here the single case in which B has been measured by UV-visible spectroscopy in an iron-hydroxo dimer complex; this is the first delocalized $S = \frac{5}{2}$ Fe dimer complex ever found (115). This optical transition is relatively high in energy ($10B = 13,000 \text{ cm}^{-1}$) compared with corresponding transitions predicted theoretically ($10B = 4000\text{--}7000 \text{ cm}^{-1}$) in Fe-S polynuclear complexes, probably because of the short Fe-Fe bond distance (2.5 Å) in the iron-hydroxo dimer system. Of course, there may be more surprises in store in the area of spin coupling and electron delocalization than are presently anticipated.

B. NEW DIRECTIONS

There are many important areas for future development. We have begun work on the energetics of cluster bonding, starting with the evaluation of the mean energy of Fe-S bonds in 4Fe-4S clusters (94). We have new results on redox potentials for both $+2/+1$ and $+3/+2$ couples of model clusters in the presence of solvent. It will be interesting to extend these results to investigate the effects of protein-cluster interactions on redox potentials, and on the electronic structure of clusters. Protein-cluster interactions can be mediated through hydrogen bonding, longer range electrostatic interactions, and solvation. The effects of asymmetric ligation of the Fe sites (by hydroxyl or carboxylate, for example) should have significant effects on electronic structure (7), as will the presence of mixed-metal coordination (Mo, Ni, and Zn) in various enzymes (17, 116-119). The electron transfer pathways to and from the cluster should involve electronic polarization, but this is not well understood (13). Further, spin coupling and valence delocalization would be expected to play a significant role in tuning the redox potential (120), an area that deserves careful investigation. On all of

these problems, the interaction of experimental and theoretical approaches seems the best strategy for further advances.

ACKNOWLEDGMENTS

We thank E. Münck, B. H. Huynh, B. Lamotte, E. P. Day, J. M. Moulis, J. Gaillard, J. Jordanov, E. Roth, J. M. Mouesca, G. Rius, D. Stout, G. Blondin, and J. J. Girerd for valuable discussions, and H. Beinert and M. C. Kennedy for their encouragement and insights. We thank E. J. Baerends for the use of the Amsterdam LCAO density functional programs, and P. Vernooijs for technical assistance. We thank M. Pique for his work on the color graphics pictures using the Stardent AVS hardware and software. This work was supported by NIH Grant GM39914.

REFERENCES

1. Ibers, J. A., and Holm, R. H., *Science* **209**, 223 (1980).
2. Beinert, H., *FASEB J.* **4**, 2483 (1990).
3. Burgess, B. K., in "Molybdenum Enzymes" (T. G. Spiro, ed.), p. 161. Wiley, New York, 1985.
4. Scott, R. A., Li, P. M., and Chan, S. I., *Ann. N.Y. Acad. Sci.* **550**, 53 (1988).
5. Kim, D. H., Britt, R. D., Klein, M. P., and Sauer, K., *J. Am. Chem. Soc.* **112**, 9389 (1990).
6. Brudvig, G. W., Beck, W. F., and de Paula, J. C., *Annu. Rev. Biophys. Biophys. Chem.* **18**, 25 (1989).
7. Beinert, H., and Kennedy, M. C., *Eur. J. Biochem.* **186**, 5 (1989).
8. Gibson, J. F., Hall, D. O., Thornley, J. H. M., and Whatley, F. R., *Proc. Natl. Acad. Sci. U.S.A.* **56**, 987 (1966).
9. Sands, R. H., and Dunham, W. R., *Q. Rev. Biophys.* **7**, 443 (1975).
10. Norman, J. G., Jr., and Jackels, S. C., *J. Am. Chem. Soc.* **97**, 3833 (1975).
11. Bair, B. A., and Goddard, W. A., *J. Am. Chem. Soc.* **100**, 5669 (1978).
12. Norman, J. G., Jr., Ryan, P. B., and Noodleman, L., *J. Am. Chem. Soc.* **102**, 4279 (1980).
13. Noodleman, L., and Baerends, E. J., *J. Am. Chem. Soc.* **106**, 2316 (1984).
14. Noodleman, L., Norman, J. G., Jr., Osborne, J. H., Aizman, A., and Case, D. A., *J. Am. Chem. Soc.* **107**, 3418 (1985).
15. Noodleman, L., and Norman, J. G., Jr., *J. Chem. Phys.* **70**, 4903 (1979).
16. Ballhausen, C. J., "Molecular Electronic Structures of Transition Metal Complexes." McGraw-Hill, Chatham, U.K., 1979.
17. Münck, E., Papaefthymiou, V., Surerus, K. K., and Girerd, J. J., in "Metal Clusters in Proteins" (L. Que, Jr., ed.), ACS Symp. Ser. 372, p. 302. American Chemical Society, Washington, D.C., 1988.
18. Blondin, G., and Girerd, J. J., *Chem. Rev.* **90**, 1359 (1990).
19. Loth, P. de, Cassoux, P., Daudey, J. P., and Malrieu, J. P., *J. Am. Chem. Soc.* **103**, 4007 (1981).
20. Loth, P. de, Karafiloglou, P., Daudey, J. P., and Kahn, O., *J. Am. Chem. Soc.* **110**, 5676 (1988).

21. Astheimer, H., and Haase, W., *J. Chem. Phys.* **85**, 1427 (1986).
22. Kahn, O., *Angew. Chem., Int. Ed. Engl.* **24**, 834 (1985).
23. Yamaguchi, K., Tsunekawa, T., Toyoda, Y., and Fueno, T., *Chem. Phys. Lett.* **143**, 371 (1988).
24. Yamaguchi, K., Fueno, T., Ueyama, N., Nakamura, A., and Ozaki, M., *Chem. Phys. Lett.* **164**, 210 (1989).
25. Hart, J. R., Rappe, A. K., Gorun, S. M., and Upton, T. H., *Inorg. Chem.* (submitted).
26. Hay, P. J., Thibeault, J. C., and Hoffman, R., *J. Am. Chem. Soc.* **97**, 4884 (1975).
27. Anderson, P. W., in "Solid State Physics" (D. Turnbull, ed.), p. 99. Academic Press, New York, 1963.
28. Noodleman, L., *J. Chem. Phys.* **74**, 5737 (1981).
29. Noodleman, L., and Davidson, E. R., *Chem. Phys.* **109**, 131 (1986).
30. Anderson, P. W., and Hasegawa, H., *Phys. Rev.* **100**, 675 (1955).
31. Zener, C., *Phys. Rev.* **82**, 403 (1951).
32. Girerd, J. J., *J. Chem. Phys.* **79**, 1766 (1983).
33. Papaefthymiou, V., Girerd, J. J., Moura, I., Moura, J. J. G., and Münck, E., *J. Am. Chem. Soc.* **109**, 4703 (1987).
34. Borshch, S. A., Kotov, I. N., and Bersuker, I. B., *Sov. J. Chem. Phys.* **3**, 1009 (1985).
35. Belinskii, M. I., Tsurkerblat, B. S., and Gerbeleu, N. V., *Sov. Phys.-Solid State (Engl. Transl.)* **26**, 1142 (1983).
36. Karpenko, B. V., *J. Magn. Magnetic Mater.* **3**, 267 (1976).
37. McWeeney, R., and Sutcliffe, B. T., "Methods of Molecular Quantum Mechanics." Academic Press, New York, 1976.
38. Ziegler, T., Rauk, A., and Baerends, E. J., *Theor. Chim. Acta* **43**, 261 (1977).
39. Dunlap, B. I., *Phys. Rev. A* **29**, 2902 (1984).
40. Ross, P., and Solomon, E. I., *J. Am. Chem. Soc.* **113**, 3246 (1991).
41. Bencini, A., *J. Chim. Phys.* **86**, 763 (1989).
42. Albonico, C., and Bencini, A., *Inorg. Chem.* **27**, 1934 (1988).
43. Bencini, A., and Gatteschi, D., *J. Am. Chem. Soc.* **108**, 5763 (1986).
44. Amos, A. T., and Hall, G. G., *Proc. R. Soc. London, Ser. A* **263**, 483 (1961).
45. Martin, R. L., and Davidson, E. R., *Phys. Rev. A* **16**, 1341 (1977).
46. Anderson, P. W., *Phys. Rev.* **115**, 2 (1959).
47. Rose, M. E., "Elementary Theory of Angular Momentum." Wiley, New York, 1957.
48. Heine, V., "Group Theory in Quantum Mechanics." Pergamon, Oxford, 1960.
49. Merzbacher, E., "Quantum Mechanics," 2nd Ed. Wiley, New York, 1970.
50. Lowdin, P. O., *Phys. Rev.* **97**, 1509 (1955).
51. Nesbet, R. K., *Ann. Phys.* **3**, 397 (1958).
52. Nesbet, R. K., *Ann. Phys.* **4**, 87 (1958).
53. Ziegler, T., and Tschinke, V., in "Density Functional Methods in Chemistry" (J. K. Labanowski and J. W. Andzelm, eds.), p. 139. Springer-Verlag, New York, 1991.
54. Slater, J. C., *Adv. Quantum Chem.* **6**, 1 (1972).
55. Cook, M., and Karplus, M., *J. Phys. Chem.* **91**, 31 (1987).
56. Case, D. A., *Annu. Rev. Phys. Chem.* **33**, 151 (1982).
57. Vosko, S. H., Wilk, L., and Nusair, M., *Can. J. Phys.* **58**, 1200 (1980).
58. Painter, G. S., *Phys. Rev. B* **24**, 4264 (1981).
59. Stoll, H., Golka, E., and Preuss, H., *Theor. Chim. Acta* **55**, 29 (1980).
60. Stoll, H., Pavlidou, C. M. E., and Preuss, H., *Theor. Chim. Acta* **149**, 143 (1978).
61. Becke, A. D., *J. Chem. Phys.* **84**, 4524 (1986).
62. Butcher, K. D., Didziulis, S. V., Briat, B., and Solomon, E. I., *J. Am. Chem. Soc.* **112**, 2231 (1990).

63. Butcher, K. D., Gebhard, M. S., and Solomon, E. I., *Inorg. Chem.* **29**, 2067 (1990).
64. Gebhard, M. S., Deaton, J. C., Koch, S. A., Millar, M., and Solomon, E. I., *J. Am. Chem. Soc.* **112**, 2217 (1990).
65. Gebhard, M. S., Koch, S. A., Millar, M., Devlin, F. J., Stephens, P. J., and Solomon, E. I., *J. Am. Chem. Soc.* **113**, 1640 (1991).
66. Banci, L., Bertini, I., and Luchinat, C., *Struct. Bonding* **72**, 113 (1990).
67. Bertrand, P., and Gayda, J. P., *Biochim. Biophys. Acta* **579**, 107 (1979).
68. Griffith, J. S., *Struct. Bonding* **10**, 87 (1972).
69. McGarvey, B. R., in "Transition Metal Chemistry" (R. L. Carlin, ed.), p. 90. Dekker, New York, 1966.
70. Stone, A. J., *Proc. R. Soc. London, Ser. A* **271**, 424 (1964).
71. Geurts, P. J. M., Bouten, P. C. P., and Avoird, A. van der, *J. Chem. Phys.* **73**, 1306 (1980).
72. Dunham, W. R., Bearden, A. J., Salmeen, I. T., Palmer, G., Sands, R. H., Orme-Johnson, W. H., and Beinert, H., *Biochim. Biophys. Acta* **253**, 134 (1971).
73. Münck, E., Debrunner, P., Tsibris, J. C. M., and Gunsalus, I. C., *Biochemistry* **11**, 885 (1972).
74. Anderson, R. E., Dunham, W. R., Sands, R. H., Bearden, A. J., and Crespi, H. L., *Biochim. Biophys. Acta* **408**, 306 (1975).
75. Fukuyama, K., Hase, T., Matsumoto, S., Tsukihara, T., Katsube, Y., Tanaka, N., Kakudo, M., Wada, K., and Matsubara, H., *Nature (London)* **286**, 522 (1980).
76. Dugad, L. B., La Mar, G. N., Banci, L., and Bertini, I., *Biochemistry* **29**, 2263 (1990).
77. Tsukihara, T., Fukuyama, K., Mizushima, M., Harioka, T., Kusunoki, M., Katsube, Y., Hase, T., and Matsubara, H., *J. Mol. Biol.* **216**, 399 (1990).
78. Palmer, G., Dunham, W. R., Fee, J. A., Sands, R. H., Izuka, T., and Yonetani, T., *Biochim. Biophys. Acta* **245**, 201 (1971).
79. Gillum, W. O., Frankel, R. B., Foner, S., and Holm, R. H., *Inorg. Chem.* **15**, 1095 (1976).
80. Petersson, L., Cammack, R., and Rao, K. K., *Biochim. Biophys. Acta* **622**, 18 (1980).
81. Palmer, G., in "Iron-Sulfur Proteins" (W. Lovenberg, ed.), p. 285. Academic Press, New York, 1973.
82. Robin, M. B., and Day, P., *Adv. Inorg. Chem. Radiochem.* **10**, 247 (1967).
83. Eaton, W. A., Palmer, G., Fee, J. A., Kimura, T., and Lovenberg, W., *Proc. Natl. Acad. Sci. U.S.A.* **68**, 3015 (1971).
84. Gray, H. B., Siiman, O., and Rawlings, J., *Proc. Natl. Acad. Sci. U.S.A.* **71**, 125 (1974).
85. Mayerle, J. J., Denmark, S. E., Pamphilis, B. V. De, Ibers, J. A., and Holm, R. H., *J. Am. Chem. Soc.* **97**, 1032 (1975).
86. Adzhamli, I. K., Kim, H. O. W., Sykes, A. G., and Buxton, G. V., *J. Inorg. Biochem.* **16**, 311 (1982).
87. Jacks, C. A., Bennett, L. E., Raymond, W. N., and Lovenberg, W., *Proc. Natl. Acad. Sci. U.S.A.* **71**, 1118 (1974).
88. Huynh, B. H., Moura, J. J. G., Moura, I., Kent, T. A., LeGall, J., Xavier, A. V., and Münck, E., *J. Biol. Chem.* **255**, 3242 (1980).
89. Day, E. P., Peterson, J., Bonvoisin, J. J., Moura, I., and Moura, J. J. G., *J. Biol. Chem.* **263**, 3684 (1988).
90. Noodleman, L., Case, D. A., and Aizman, A. J., *J. Am. Chem. Soc.* **110**, 1001 (1988).
91. Sontum, S. F., Noodleman, L., and Case, D. A., in "The Challenge of d and f Electrons: Theory and Computation" (D. R. Salahub and M. C. Zerner, eds.), p. 366. American Chemical Society, Washington, D.C., 1989.

92. Noodleman, L., Case, D. A., and Sontum, S. F., *J. Chim. Phys.* **86**, 743 (1989).
93. Carter, C. W., in "Iron-Sulfur Proteins" (W. Lovenberg, ed.), p. 157. Academic Press, New York, 1977.
94. Noodleman, L., Case, D. A., and Baerends, E. J., in "Density Functional Methods in Chemistry" (J. K. Labanowski and J. W. Andzelm, eds.), p. 109. Springer-Verlag, New York, 1991.
95. Aizman, A., and Case, D. A., *J. Am. Chem. Soc.* **104**, 3269 (1982).
96. Noodleman, L., *Inorg. Chem.* **30**, 246 (1991).
97. Moulis, J. M., Lutz, J., Gaillard, J., and Noodleman, L., *Biochemistry* **27**, 8712 (1988).
98. O'Sullivan, T., and Millar, M. M., *J. Am. Chem. Soc.* **107**, 4096 (1985).
99. Sheridan, R. P., Allen, L. C., and Carter, C. W., *J. Biol. Chem.* **256**, 5052 (1981).
100. Papaefthymiou, V., Millar, M. M., and Münck, E., *Inorg. Chem.* **25**, 3010 (1986).
101. Papaefthymiou, G. C., Laskowski, E. J., Frota-Pessoa, S., Frankel, R. B., and Holm, R. H., *Inorg. Chem.* **21**, 1723 (1982).
102. Moulis, J. M., Auric, P., Gaillard, J., and Meyer, J., *J. Biol. Chem.* **259**, 11396 (1984).
103. Gaillard, J., Moulis, J. M., Auric, P., and Meyer, J., *Biochemistry* **25**, 464 (1986).
104. Auric, P., Gaillard, J., Meyer, J., and Moulis, J. M., *Biochemistry* **242**, 525 (1987).
105. Lindahl, P. A., Day, E. P., Kent, T. A., Orme-Johnson, W. H., and Münck, E. J., *Biol. Chem.* **260**, 11160 (1985).
106. Carney, M. J., Papaefthymiou, G. C., Spartalian, K., Frankel, R. B., and Holm, R. H., *J. Am. Chem. Soc.* **110**, 6084 (1988).
107. Collision, D., and Mabbs, F. E., *Chem. Soc., Dalton Trans.*, 1573 (1982).
108. Borshch, S. A., and Chibotaru, L. F., *Chem. Phys.* **135**, 375 (1989).
109. Noodleman, L., *Inorg. Chem.* **30**, 256 (1991).
110. Jordanov, J., Roth, E. K. H., Fries, P. H., and Noodleman, L., *Inorg. Chem.* **29**, 4288 (1990).
111. Noodleman, L., *Inorg. Chem.* **27**, 3677 (1988).
112. Rius, G., and Lamotte, B., *J. Am. Chem. Soc.* **111**, 2464 (1989).
113. Gloux, J., Gloux, P., Hendriks, H., and Rius, G., *J. Am. Chem. Soc.* **109**, 3220 (1987).
114. Patil, D. S., Moura, J. J. G., He, S. H., Teixeira, M., Prickil, B. C., DerVartanian, D. V., Peck, H. D., Jr., LeGall, J., and Huynh, B. H., *J. Biol. Chem.* **263**, 18732 (1988).
115. Ding, X. Q., Bominaar, E., Bill, E., Winkler, H., Trautwein, A. X., Drueke, S., Chaudhuri, P., and Wieghardt, K., *J. Chem. Phys.* **92**, 178 (1990).
116. Conover, R., Park, J.-B., Adams, M. W. W., and Johnson, M. K., *J. Am. Chem. Soc.* **112**, 4562 (1990).
117. Cook, M., and Karplus, M., *J. Chem. Phys.* **83**, 6344 (1985).
118. Coucouvanis, D., *Acc. Chem. Res.* **24**, 1 (1991).
119. Orme-Johnson, W. H., *Annu. Rev. Biophys. Biophys. Chem.* **14**, 419 (1985).
120. Bertrand, P., and Gayda, J. P., *Biochim. Biophys. Acta* **680**, 331 (1982).
121. Mouesca, J. M., Ph.D. thesis, University Joseph Fourier-Grenoble I, France (1991).
122. Mouesca, J. M., Rius, G., and Lamotte, B., in "Mixed Valency Systems: Applications in Chemistry, Physics, and Biology" (K. Prassides, ed.), p. 431, Kluwer, The Netherlands, 1991.

INDEX

A

- Acid denaturation, apoprotein
 - preparation, 81
- Aconitase, 323–337
 - cluster
 - interconversion, 324
 - substrate interaction in enzymatic reaction, 326–328
 - crystallographic structure, 328–334
 - active site, 331
 - anaerobic crystallization experiments, 330
 - crystalline state, 330
 - heart mitochondrial, 329–330
 - isocitrate → *cis*-aconitate reaction, 332–333
 - transition from substrate-free to substrate-bound form, 331–332
 - cytoplasmic, relation to iron-responsive element binding protein, 337
 - ENDOR studies, 326–328
 - [4Fe–4S]²⁺ cluster, 326–327
 - Fe–S cluster properties, 324–326
 - mutant studies, 334–336
 - Arg 452, 336
 - Arg 580, 335–336
 - Asp 165, 335
 - His 101, 336
 - Ser 642, 335
 - native form, 325–326
- Aconitate hydratase, *see* Aconitase
- Adrenodoxin, amino acid sequence, 239–240
- Adsorbed protein films, cluster
 - reactivities, 144–159
 - clusters
 - population ratio, 154
 - with extraneous ligands, 157–159
 - cyclic voltammetry, 144–147
 - at different scan rates, 157–158
 - E*° values, 149, 151
 - Fe(II) release, 151–152
 - [3Fe–4S] clusters, 146, 148
 - [3Fe–4S]⁰ clusters, 154
 - oxidative scans, 148, 150
 - reduced product of C', 146–147
 - reduction potentials as function of TI(I) concentration, 155–156
 - reversible binding of divalent metal ions, 153
- Aldehyde ferredoxin oxidoreductase, *P. furiosus*, 374–381
- Amino acid sequences
 - A. vinelandii* Fd I, 129
 - D. africanus* Fd III, 138, 140
- Anabaena*, heterocyst ferredoxin, 229
- Anabaena sphaeria*, ferredoxins, 228–229
- Anaerobic controlled potential
 - electrolysis, *Azotobacter*, 129
- Aphanothece sacrum*, ferredoxins, amino acid sequence, 225–227
- Apoproteins, selenium-substituted, preparation, 80–82
- Azotobacter* Fd I, redox properties, 128–138
 - anaerobic controlled potential electrolysis, 132
 - cyclic voltammetry, 130–131
 - [3Fe–4S]⁰ clusters, 129–130
 - [4Fe–4S] clusters, 130
 - physiologic function, 134, 138
 - protein structure effect, 134–136
 - protonation site, 134
 - square-wave voltammetry, 134–136
 - variation in [4Fe–S] clusters, 133
- Azotobacter chroococcum* Fd I, cyclic voltammetry, 130–131
- Azotobacter*-type [4Fe–4S] [3Fe–4S] ferredoxins, 257–259
- Azotobacter vinelandii*
 - ferredoxin, 5, 7, 18, 22, 255–257
 - amino acid sequences, 129
 - square-wave voltammetry, 134–136

- [4Fe—4S] [3Fe—4S], 260, 295
pH dependence of E° values, 134–135,
137

B

- Bacillus* ferredoxins, cysteine residues,
246
Bacillus thermoproteolyticus ferredoxins,
chain topology, 244, 246
Beans, [2Fe—2S] ferredoxins, 230
Bertrand–Gayda Model, 176–178
Biomolecules, selenium-containing,
75–76
Bradyrhizobium japonicum frxA,
255–257
Bridging ligand, Fe—S clusters, 172
Broken-symmetry analysis, reduced
three-iron clusters, 453–455
Broken symmetry energy equation,
427–428, 431
four-iron clusters, 460
Butyribacterium methylotrophicum
ferredoxin, 261–262

C

- Carbon monoxide dehydrogenases, Fe—S
clusters as electron carriers,
309–310
cDNA, maize ferredoxin, 231
Chloroplasts, Fe proteins, 252–254
Chromatium, HiPIP sequence, 249
Chromatium vinosum HiPIP, 108, 133
Citrate, stereospecific conversion, 323
Citrate hydrolyase, *see* Aconitase
Clebsch–Gordon algebra, 430, 432, 434
Clebsch–Gordon coefficient, 434
Clostridial 2[4Fe—4Se]⁺ ferredoxins,
ground spin state variability, 92–94,
96–97
proton NMR data, 100–101
 $S = 3/2$ spin state, 92–93
 $S = 7/2$ spin state, 93
Clostridium pasteurianum, 299–300
ferredoxin, 80, 84
[2Fe—2S], 105, 237–238
[4Fe—4Se], 106–108
2[4Fe—4S], redox properties,
126–127

- resonance Raman spectra, 85, 87
stability, 86
tertiary structure, 247
UV–visible absorption spectra,
85–86
hydrogenase, 345–346
nitrogenase iron protein
EPR spectra, 102–103
hydrogenases, 402
Clostridium perfringens ferredoxin, 261
Clostridium thermoaceticum, CO
dehydrogenase, 362
[CoFe₃S₄]²⁺, 48
[CoFe₃S₄] clusters, 46
Contour maps, Fe—S dimers, 443–444
Coulomb hole, 439–440
[Cp₃Mo₃S₄], 24
Cyanobacteria, Fe proteins, 252–254
Cyclic trithiolate ligand, 8–9
Cyclic voltammetry, *A. chroococcum* Fd
I, 130–131
Cys residues, Fe—S proteins, 3–7

D

- Delocalization, added electron, reduced
dimer, 447, 449
Density difference
Fe—S dimers, 443–445
map, four-iron clusters, 458
Density-functional theory, 423–467
 α and β densities, 440
broken symmetry method, 425
conservation equations, 437
correlation for opposite spins and
Coulomb hole, 439–440
electron densities, 436
exchange energy and Fermi hole,
438–439
Fe—S dimers, 441–452
four-iron clusters, 455–464
energy level structure, 455–456
oxidized and reduced configurations,
456–457
phenomenological modeling of
oxidized (+3) and reduced (+1)
clusters, 462–464
relaxation effects on cluster
oxidation +2 \rightarrow +3, 457–459

- relaxation effects on cluster reduction
 - + 2 \rightarrow + 1, 459
- spin-coupling parameters, 459–461
- stability of $S = \frac{1}{2}$ versus $S = \frac{3}{2}$ for
 - reduced (+ 1) cluster, 462
- future development, 466–467
- joint probability distribution, 438
- monomeric Fe—S complexes, 410–411
- perturbation formalism, 425–435
- phenomenological approach, 465
- summary, 464–466
- three-iron clusters, 452–455
- total energy, 436–438
- Desulfovibrio*
 - β subunit function, 402
 - ferredoxin structure, 246
 - hydrogenase gene distribution, 416–418
 - nickel-containing hydrogenases, 406
- Desulfovibrio africanus*, 6
- Desulfovibrio africanus* Fd III, 18, 22
 - amino acid sequence, 138, 140
 - chemistry of Fe—S clusters, 152–153
 - cyclic voltammetry, 144–147
 - reactions with Zn(II) or Cd(II), 149
- Fe—S clusters, 138–144
 - bulk electrolytic reduction, 142
 - controlled potential electrolysis, 140
 - cyclic voltammetry, 139–141
 - EGTA effect, 139–140
 - EPR and MCD spectroscopy, 143
- [3Fe—4S]
 - binding sites, 157
 - cluster, 148
 - ground spin state variability, 100
- Desulfovibrio gigas* Fd II, 17–18, 22–24, 324–325
- Desulfovibrio*-type [4Fe—4S] [3Fe—4S]
 - ferredoxins, 259
- Desulfovibrio vulgaris*, sulfite reductase, X-band EPR, 207
- Desulfovibrio vulgaris* Hildenborough, periplasmic hydrogenase, 400–402
- Dinuclear clusters
 - ferrous site distortion, 175
 - spin ladder, 182–183
- Dioxygenases, Fe—S
 - clusters as electron carriers, 305–306
 - proteins, 287–288
- Direct exchange, 426
 - magnetic orbitals, 435
- Dithiolate bridges, Fe—S proteins, 12–13
- Divalent metal ions, reversible binding, 153
- DMSO reductase, 296
- DNAs, chloroplast, nucleotide sequences, 252
- Double exchange, 426
- Dual-mode EPR spectroscopy, 208–211
- Dynamic electrochemistry, Fe—S
 - proteins, 117–160
 - advantages of absorbed molecules on electroactive monolayer/submonolayer, 123–125
 - applications, 128–159
 - Azotobacter* Fd I redox properties, 128–138
 - cluster reactivities in absorbed protein films, 144–159
 - D. africanus* Fd III containing reactive [3Fe—4S] cluster, 138–144
 - definition, 117
 - ferredoxins, 126–128
 - ideal case, 124
 - problems, 118, 120–121
 - recent developments, 119–120
 - sensitivity, 125
 - techniques, 125–126
 - underuse, 118
 - useful features, 121–126
 - useful potential range, 122
 - voltammetric response, 121
 - voltammetry of adsorbed protein molecules, 122–123

E

- Ectothiorhodospira halophila*, HiPIPs, 249
- Effective g values, calculation, 195–197
- Electrochemistry, *see* Dynamic electrochemistry, Fe—S proteins
- Electron densities, 436
 - difference map, four-iron clusters, 458
- Electron–electron repulsion energy, 437, 439
 - [4Fe—4S] cluster, 355–358

- Electron–nuclear double-resonance spectroscopy, *see* ENDOR studies
- Electron paramagnetic resonance, *see* EPR spectroscopy
- Electron-transferring subunit, nickel-containing hydrogenases, 409–410
- Electron transfer spectra, reduced Fe–S dimers, 451–452
- ELS classification, 170–171
- ENDOR studies
aconitase, 326–328
[4Fe–4S] cluster, 355–358
- ¹H ENDOR, [4Fe–4S]¹⁺ cluster, 355–356
- Energy, spin-projected state, 432
- Energy difference equation, 433
- Energy equation, broken symmetry state, 427–428, 431
- Energy level structure
Fe–S dimers, 441–443
four-iron clusters, 455–456
- Energy matrix, 196
- Enzymatic activity, iron–selenium proteins, 89
- Enzyme Fe–S clusters
containing selenium, 75
ferredoxin as model, 361–368
Fe replacement with metal, 362
H clusters, 361–362
[M–3Fe–4S] cluster, 365–368
[Ni–3Fe–4S] cluster, 363–365
nonsulfur-ligated Fe, 361
synthetic analogs, 362
- EPR spectroscopy, 165–215
assimilatory and dissimilatory electron transfer processes, 299
basic building blocks, 171–173
bridging ligand, 172
cyanide-treated ferredoxin from *P. furiosus*, 366–367
double exchange, 178–186
evaluation, 183–186
Liverpool model, 184–185
spin ladders, 180–183
valence delocalization, 178–180
- ELS classification, 170–171
- external ligation, 172–173
- Fe hydrogenase of *T. maritima*, 386–387
- Fe–S cluster, identification, 297–298
- [3Fe–4S] cluster, 359–360
- [4Fe–4S] cluster, 351–355
- Fe–S enzymes, 281–313
- Fe–S protein history, 167–170
free-electron *g* value, 167–168
grand concept, 168–169
multicenter proteins, 169
supercluster concept, 169–170
- four-iron clusters, 463–464
- g* strain in doublet systems, 186–193
g-strain equation, 190–193
inhomogeneous broadening, 186–190
integration over unit sphere, 188
- high-spin Kramers' systems, 194–208
effective *g* value calculation, 195–197
energy matrix, 196
multiple rhombicities, 207
practical aspects, 205–208
rhombogram reading, 197–205
rules of thumb relating to spectra intensity, 202–205
spin Hamiltonian, 194
spin multiplet inversion, 206
weak-field regime, 194–195
- history, 165–167
- membrane-bound in bioenergetic systems, 302–304
photosystem I, 303–304
respiratory chains, 302–303
- metalloproteins, 165–167
- with molybdopterin cofactor, 288–289
- [Ni–3Fe;4S]¹⁺ cluster, 363–364
- Non-Kramers' systems, 208–214
dual-mode principles, 208–211
Fe–S, 211–214
intradoublet splitting, 210
zero-field Hamiltonian, 211
zero-field splitting parameters, 213
- with nonredox Fe–S clusters, 290–291
- red tungsten protein, 375–376
- reduced *P. furiosus* hydrogenase, 346–347
- reduced two-iron clusters, 445–446
- single-crystal, 166
- with sirohaem, 289
- soluble, 286–287
- spin state of iron in Fe–S clusters, 171–172
- superexchange, 173–178

- Bertrand-Gayda model, 176–178
 Gibson model, 174–176
 Heisenberg exchange interaction, 173–174
 valency of iron in Fe—S clusters, 171
Escherichia coli
 fumarate reductase, Fe—S proteins
 subunits, 296
 hyaC gene, 419
 EXAFS studies
 Fe—S proteins, 52–54
 nickel-containing hydrogenases, 408–409
 Exchange energy, 438–439
 Exogenous ligand binding, [M—3Fe—4S] clusters, 365–368
 Extended x-ray absorption fine structure
 Fe—S proteins, 52–54
 nickel-containing hydrogenases, 408–409
 Extremely thermophilic bacteria, 341–390
 isolation, 342–343
 S⁰-dependent, 343–344
- F**
- F_A/F_B proteins, photosystem I complexes, 262–263
 Fe—Fe distance, 14–15
 Fe—Mo cofactor, 52–53
 bound distances, 53
 models, 55
 Mo/V sites, 53–54
 Fe—Mo—Fe angle, 54
 Fe(3d) orbitals, 442–443
 Fermi hole, 438–439
 Ferredoxin-like proteins, in symbiotic nitrogen-fixing bacteria, 247–248
 Ferredoxins, 223–267
 amino acid sequences, 225–227
 bacterial, 266–267
 cyanobacterial, structure, 225–226
 dynamic electrochemistry, Fe—S proteins, 126–128
 Fd I, Cys residues, 6
 Fd II, Cys residues, 6
 functional differences, in single bacterium, 259–261
 gene inactivation experiments, 266
 halobacterial, 233, 235–236
 iso-forms, reduction potential differences, 233–234
 photosynthetic organisms, 265–266
 polyferredoxins, 264–265
 Fe—S clusters
 assembly mechanisms, 84–87
 catalytic, 361
 as electron carriers, 304
 functions, 282
 identifying in proteins, 282–284, 292–298
 amino acid sequences, 292–294
 chemical composition, 282, 284
 protein structures, 284, 292–293
 site-directed mutagenesis experiments, 294–296
 spectroscopy, 296–298
 nomenclature, 312–313
 types, 292
 [2Fe—2S] clusters
 cysteines, 294
 P-band spectrum, 191–192
 X-band spectrum, 189
 [2Fe—2S]¹⁺ clusters
 EPR spectroscopy, 187
 excess electron localization, 179–180
 [Fe₃S₃] clusters, binding patterns, 4–5
 [3Fe—4S] clusters, 16–24, 119–120
 conversion reactions, 17–18
 D. africanus Fd III, 138–144
 electronic structure, 19
 electron transfer series, 18–19
 formation, oxidation and spin states, 17–22
 isomer shift data, 20, 50
 as ligand and cluster spin, 48–52
 Mössbauer parameters, 19–21
 oxidation levels, 47
 spectroscopic characterization, 359
 structures, 22–24
 [3Fe—4S]⁰ clusters, 325
 [3Fe—4S]¹⁺ cluster, double exchange, 183–184
 [4Fe—4S] clusters
 binding
 to consensus sequence of cysteinyl residues, 351–352
 patterns, 4–5

- cysteines, 293
- oxidation states, 455
- P. furiosus*, 351
- spectroscopic characterization, 352
- [4Fe—4S]²⁺ cluster, aconitase, 326–327
- 2[4Fe—4S] clusters, 254–264
 - consensus sequence, 293
 - F_A/F_B proteins, 262–263
 - functional differences in single
 - bacterium, 259–261
 - photosynthetic bacterial and *nif*-related ferredoxins, 255–257
 - proteins encoded by chloroplast, 263–264
- [Fe₄S₄]^{2+/1+} couple, potential shifts, 10
- Fe—S dimers, 441–452
 - density differences and spin densities, 443–445
 - electron transfer and optical charge transfer spectra, 451–452
 - energy level structures, 441–443
 - Heisenberg and resonance coupling, 446–451
 - hyperfine, EPR and Mössbauer properties, 445–446
- Fe—S distance, 15
- [4Fe—4Se]⁺ clusters, ground spin state variability, 91–104
 - clostridial 2[4Fe—4Se]⁺ ferredoxins, 92–94, 96–97
 - glutamine phosphoribosylpyrophosphate amidotransferase, 99–100
 - ground spin state variability, 104
 - nitrogenase
 - iron protein, 94–95
 - Mo—Fe protein, 98–99
 - room temperature data, proton NMR, 100–104
 - synthetic analogs, 95, 98
- [Fe₄Se₄(LS₃)Cl]²⁻, Ph₄P⁺ salt, 10
- Fe—Se proteins, 73–109
 - active sites, assembly, 82–83
 - enzymatic activity, 89
 - magnetic properties, 89–91
 - preparation, 80–83
 - active site assembly, 82–83
 - apoproteins, 80–82
 - history, 80
 - prospects, 108–109
 - redox potentials, 88–89
 - stability, 86–87
 - UV–visible absorption spectra, 87–88
- [2Fe—2Se] proteins
 - magnetic properties, 89–90
 - vibrational spectroscopy, 105–106
- [3Fe—4Se] proteins, magnetic properties, 91
- [4Fe—4Se] proteins
 - magnetic properties, 90–91
 - vibrational spectroscopy, 106–108
- [4Fe—4S] [3Fe—4S] ferredoxin I, *A. vinelandii*, 295
- [Fe₄S₄(LS₃)Cl]²⁻ subsite-specific substitution reactions, 10–11
- Fe₄S₄(NO)₄, 29
- [Fe₄S₄(SEt)₄]^{2-/3-}, 45–46
- Fe—S—Fe bridge, 55
- [2Fe—2S] ferredoxins, 224–241, 299–300
 - beans, 230
 - C. pasteurianum*, 237–238
 - cysteine spacings, 284
 - halobacterial, 236
 - heterocyst, 228–230
 - iso-forms, 224, 228, 230
 - maize, 230–231
 - mitochondrial adrenodoxin-type, 239
 - in oxygenase systems, 238–240
 - oxygenic photosynthetic organisms, 224–233
 - quasi-reversible electrochemistry, 127
 - Rhodobacter*, 236–237
- [3Fe—4S] ferredoxins, 241–254, 301–302
 - amino acid sequences, 242–243
 - oxygenase systems, single cluster, 251
 - single cluster, low-potential ferredoxins, 242–247
 - succinate–fumarate oxidoreductases, 254
- [4Fe—4S] ferredoxins, 241–254, 301
 - amino acid sequences, 242–243
 - cysteine residue distribution, 253
 - highly thermostable, 248
 - HiPIPs, 248–251
 - amino acid sequences, 249–250
 - cysteine residues, 249
 - R. trifolii*, 247–248
 - single cluster bridging two subunits, 251–254
 - Fe proteins in nitrogenase, 252–254

- photosystem I reaction center X
 - proteins, 251–252
- single cluster low-potential
 - ferredoxins, 242–247
- succinate–fumarate oxidoreductases, 254
- 2[Fe–4S] ferredoxins, 300–301
 - folding pattern, 283
 - quasi-reversible electrochemistry, 127
- [4Fe–4S] [3Fe–4S] ferredoxins, 254–264, 301
 - Azotobacter*-type, 257–259
 - Desulfovibrio*-type, 259
 - functional differences in single
 - bacterium, 259–261
 - photosynthetic bacterial and *nif*-related, 255–257
 - proteins encoded by chloroplast, 263–264
- [FeS₄]⁵⁻ ions, 32
- Fe–S proteins, 1–62, 282, 285–291
 - bond distances, 53–54
 - with catalytic Fe–S or mixed metal clusters, 289–290
 - classification, 298–302
 - complex, 298
 - [2Fe–2S] ferredoxins, 299–300
 - [3Fe–4S] ferredoxins, 301–302
 - [4Fe–4S] ferredoxins, 301
 - 2[4Fe–4S] ferredoxins, 300–301
 - [4Fe–4S] [3Fe–4S] ferredoxins, 301
 - HiPIPs, 302
 - Rieske proteins, 300
 - rubredoxins, 299
 - simple, 298
 - with determined structures, 293
- dioxygenases, 287–288
- heterometallic MFe₃S₄ cubane-type
 - clusters, 29–62
 - biological implications, 52–62
 - cluster as ligand and cluster spin, 48–52
 - [CoFe₃S₄] clusters, 46
 - linked cubane clusters, 55–56
 - [MoFe₃S₄] and [WFe₃S₄] clusters, 32–37
 - [NiFe₃S₄] clusters, 44–46
 - nonbiological M'M₃S₄ clusters, 56–61
 - prospectus, 6–62
 - protein bound clusters, 47–48
 - [ReFe₃S₄] clusters, 41–43
 - scope of cluster formation, 30–31
 - stability patterns, 43–44
 - structural models, 52–54
 - tetrathiometalates, 30–32
 - [VFe₃S₄] and [NbFe₃S₄] clusters, 37–41
- homometallic cubane-type clusters, 2–16, 5
 - circumstances leading to
 - unconventional binding patterns, 6
 - cluster binding patterns, 3–6
 - destabilization of cluster, 7
 - dithiolate bridges, 12–13
 - Fe–Fe distance, 14–15
 - Fe–S distance, 15
 - structural definition, 3
 - 2:2 subsite differentiation, 14–16
 - 3:1 subsite differentiation, 8–14
 - unconventional terminal ligation, 3–8
- homologous sequences, 294–295
- hydroxylases, 287–288
- membrane-bound electron transfer
 - proteins, 285–286
- nonredox, 290–291
- regulatory, 291
- simple, 285
- sulfur replacement by selenium, *see* Fe–Se proteins
- trinuclear cuboidal clusters, 16–29
 - clusters of related structure, 24–28
 - Fe₃S₄ clusters, 16–24
 - inverted (M₄S₃) clusters, 28–29
 - of unknown function, 291
- [Fe₆S₉(SR)₂]⁴⁻, 28
- Fe–Te clusters, active sites, assembly, 83
- [4Fe–4Te] clusters, 83
- Fe–V cofactor, 53–54
- [Fe₂X₂ (YR)₄]²⁻, resonance Raman spectra, 106
- Four-iron clusters, *see* Density-functional theory
- frd* redon, 412, 414
- frxB* gene, 263–264
- frxC* gene, 252–254
- Fumarate reductase, cysteine
 - distribution, 240–241

G

- Gene regulation, Fe—S proteins, 311–312
- Gibson model, 174–176
- Glutamine 5-phosphoribosyl-l-pyrophosphate amidotransferase, 310–311
- Glutamine phosphoribosylpyrophosphate amidotransferase, ground spin state variability, 99–100
- g* strain, *see* EPR spectroscopy
- g*-strain equation, 190–193
 - physical interpretation, 191
 - unrestricted form, 191–192
- g*-tensor equations, 176–177

H

- Halobacterial ferredoxins, 233, 235–236
- Halobacteria* of the Dead Sea, 233, 235–236
- Hamiltonian, double-exchange, 181
- Heisenberg coupling
 - constants, 462–463
 - Fe—S dimers, 446–451
- Heisenberg exchange coupling constant, 447
- Heisenberg exchange interaction, 173–174
- Heisenberg Hamiltonian, 425–426, 431–433, 435, 451
 - four-iron clusters, 461
- Heisenberg parameters, 463
- Heisenberg spin ladder, 447, 449–450
- Heterocysts, 228–230
- Highest occupied molecular orbital, four-iron clusters, 456
- High-potential iron—sulfur proteins, *see* HiPIPs
- High-spin Kramers' systems, *see* EPR spectroscopy
- High-spin state, 446–447
- HiPIPs, 133
 - C. vinosum*, 108
 - [4Fe—4S] ferredoxins, 248–251
- hoxY* gene product, 409–410
- HP proteins, sequence patterns, 5
- H₂ production, role of Fe—S proteins, 381–383

- hyaA* gene products, 407
- hyaB* gene products, 407
- hydC* gene, 401–402
- Hydrogenase 3, function, 416
- Hydrogenase genes, 410–414
 - distribution in *Desulfovibrio*, 416–418
- Hydrogenase operons, 400–410
 - iron-only hydrogenases, 400–403
 - nickel-containing hydrogenases, 403–410
- Hydrogenases, 397–419
 - electron-transferring subunits, 411–412
 - export, 410–414
 - functions, 414–418
 - in *Desulfovibrio*, 416–418
 - nickel-containing, 414–416
 - uptake reaction, 415–416
 - gene function, 400
 - iron-only, 410–411
 - nickel-containing, 411
 - nucleotide sequencing of structural genes, 397–99
 - perspectives, 418–419
 - signal peptides, 412–413
 - T. maritima*, 384–388
- Hydroxylases, Fe—S proteins, 287–288
- Hyperfine properties
 - four-iron clusters, 463–464
 - reduced two-iron clusters, 445–446

I

- Inhomogeneous broadening, Fe—S, 186–190
- Integration over unit sphere, 188
- Inverted bonding scheme, 441
- Iron hydrogenases, Fe—S clusters as electron carriers, 309
- Iron-only hydrogenases, 400–403
- Iron-responsive element binding protein, relation to cytoplasmic aconitase, 337
- Isomer shift data, Fe₃S₄ clusters, 20, 50

J

- Joint probability distribution, 438

L

- Lewis acids, Fe—S proteins acting as, 168
- Ligand spin polarization, 426
- Ligation, external, Fe—S clusters, 172–173
- Linked cubane clusters, Fe—S proteins, biological implications, 55–56
- Local density-functional wavefunction, 429
- Low-potential ferredoxins, with single [4Fe—4S] or [3Fe—4S] cluster, 242–247

M

- Magnetic circular dichroism, [4Fe—4S] cluster, 358
- Magnetic orbitals, 430
 - direct exchange, 435
- Maize, [2Fe—2S] ferredoxins, 230–231
- [MCu₃OS₃Cl₃]²⁻, 29
- [MCu₃OS₃Cl (PPh₃)₃], 29
- Metalloproteins, EPR spectroscopy, 165–167
- Methanobacterium thermoautotrophicum*, 264–265
- Methanococcus thermolithotrophicum* ferredoxins, 262
- [M—3Fe—4S] clusters
 - exogenous ligand binding, 365–368
 - oxidation and spin states, 20–22
 - structural properties, 48–49
- [MFe₃S₄(R₂dtc)₅]¹⁻, formation, 35
- [M₂Fe₇S₈(SR)₁₂]³⁻, 44
- Midpoint potential, rubredoxin, 369–370
- Mitochondrial complex, 302–303
- Mixed-metal clusters, Fe—S proteins, 289–290
- Mixed-valence dimer, analysis, 433–435
- M'Mo₃S₄ clusters, 57–59
 - schematic structures, 57–58
- M'M₃S₄ clusters, nonbiological, 56–61
 - Cu(I) presence, 60
 - heterometallic cubane-type, 56–57
- [MoFe₃S₄] clusters, 32–37, 379
 - self-assembly system, 32–34
 - terminal phosphine ligands, 36
- [MoFe₃S₄]³⁺, 51

- [Mo₂Fe₆S₈(SEt)₉]^{3-/4-}, 43
- Molybdenum, Fe—S clusters as electron carriers, 306–307
- Molybdopterin cofactor, in Fe—S enzymes, 288–289
- Monomeric Fe—S complexes, density-functional theory, 410–411
- Monooxygenases, Fe—S clusters as electron carriers, 305
- Mo—Fe cofactor, proteins necessary for synthesis, 85
- Mo—Fe protein, X-band spectrum, 205–206
- Mo—(OH)—Mo bridge, 56
- Mo₂O_{4-n}S_n complexes, reduction, 26
- Mo—S bridge, 55
- Mo—X—Mo angles, 55
- Mo₄S₄ clusters, preparation, 26–27
- [Mo₃S₄]²⁺ core, formation, 59
- [Mo₃S₄(edt)₃]²⁻, 26
- [Mo₃S₄(OH₂)₁₂]⁴⁺, 26
- Mössbauer properties
 - Fe₃S₄ clusters, 19–21
 - four-iron clusters, 463–464
 - reduced two-iron clusters, 446
- M₃S₄
 - cuboidal core, synthetics with, 25–26
 - preparation, 28
- (M₄S₃), inverted clusters, 28–29
- Mycobacterium smegmatis*, ferredoxin, 258

N

- [NbFe₃S₄] clusters, 37–41
 - self-assembly system, 40–41
- Nernst equation, 376
- Nickel-containing hydrogenases, 403–410
 - conserved residues, 408–409
 - conserved sequence elements, 403–405
 - electron-transferring subunits, 409–410
 - enzyme groups and nickel-binding subunit sequences, 406–409
 - evolution, 411–414
 - EXAFS studies, 408–409
 - function, 414–416
 - methyl viologen-reducing, 407–408

Nickel hydrogenases, Fe—S clusters as electron carriers, 307

Ni—Fe hydrogenases, mesophilic, 345–348

[Ni—3Fe—4S] cluster, 44–46
formation and properties, 363–365

nifF gene, 260

nifH gene, 252–254

nif-related ferredoxins, 255–257

Nitrogenase Fe protein, 252–254
ground spin state variability, 94–95
proton NMR data, 101–102

Nitrogenase Mo—Fe protein
ground spin state variability, 98–99
P-clusters, 91–92

Nitrogenases, Fe—S clusters as electron carriers, 308–309

Nitrogen-fixing bacteria, symbiotic, ferredoxin-like proteins, 247–248

Nitrogenase, cofactors, 30

NMR
P. furiosus rubredoxin, 371, 373
proton, Fe—Se proteins, 100–104

Non-Kramers' systems, EPR spectroscopy, 211–214

Nonorthogonal ligand orbitals, 430

Nonorthogonal orbitals, 428–429

Nonredox enzymes, Fe—S clusters, 310–311

Nuclear-electron attraction energy, 437

O

Opposite-spin correlation, 439–440

Optical charge transfer spectra, reduced Fe—S dimers, 451–452

orf167 gene, 263

orf178 gene, 263

Oxidation states
Fe₃S₄ clusters, 17–22
heterometal cluster formation, 51–52

Oxidized configuration, four-iron clusters, 456–457

Oxygenase systems, single [3Fe—4S] ferredoxins cluster, 251

Oxygenic photosynthetic organisms, [2Fe—2S] ferredoxins, 224–233

P

P-band spectrum, [2Fe—2S] cluster, 191–192

Peptides, artificial incorporation of selenium, 77–79

Peptococcus aerogenes ferredoxin, structure, 242, 244–245

Perturbation formalism, spin coupling in transition metal clusters, 425–435
electron interactions, 429–433
mixed-valence dimer, 433–435
nonorthogonal orbitals, 428–429
singlet-triplet splittings, 426–428
summary, 435

Phenomenological modeling
density-functional theory, 465
oxidized (+3) and reduced (+1) clusters, four-iron clusters, 462–464

Photosynthetic bacteria, 2[4Fe—4S] and [4Fe—4S] [3Fe—4S] ferredoxins, 255–257

Photosystem I, 303–304
F_A/F_B proteins, 262–263
reaction center X proteins, single [4Fe—4S] ferredoxins cluster bridging two subunits, 251–252

Plectonema boryanum, 253

Polyferredoxins, 264–265, 312

Probe, selenium, 77, 80

Proteins
artificial incorporation of selenium, 76–79
respiratory chain complexes, 240–241
soluble, with Fe—S clusters as electron carriers, 304–312
carbon monoxide dehydrogenases, 309–310
catalytic and mixed-metal clusters, 308–310
dioxygenases, 305–306
in gene regulation, 311–312
iron hydrogenases, 309
nickel hydrogenases, 307
nitrogenases, 308–309
nonredox enzymes, 310–311
oxygenase systems, 304–306
proteins with molybdenum and tungsten, 306–307

- sirohaem proteins, 307–308
 - of uncertain origins
 - monooxygenases, 305
- Proton NMR, room temperature data,
 - Fe–Se proteins, 100–104
- Pseudomonas putida*
 - [2Fe–2S] ferredoxins, 238–239
 - xylene monooxygenase, 239
- Pyrococcus furiosus*, 344–383
 - aldehyde ferredoxin oxidoreductase, 374–381
 - electron transfer pathway, 381
 - Nernst equation, 376
 - redox centers, 376–378
 - red tungsten protein, 374–379
 - W site structure, 380
- cyanide-treated, 366–367
- ferredoxin, 13–14, 350–368
 - cysteinyI and noncysteinyI
 - coordination, 353–354
 - direct electron transfer, 354
 - electron–nuclear double resonance, 355–358
- EPR of [4Fe–4S] cluster, 351–355
- [3Fe–4S] cluster characterization, 359–361
- [4Fe–4S] clusters, 351
 - ground spin state variability, 100
- magnetic circular dichroism and
 - resonance Raman spectroscopy, 358
- as model of enzymatic Fe–S
 - clusters, 361–368
- [Ni–3Fe–4S]¹⁺ cluster, 363–365
- resistance to denaturants, 351
- spin forms, 356
- Fe–S protein role in H₂ production, 381–383
- hydrogenase, 345–350
 - catalytic activity, 349
 - electron donor, 350
 - mesophilic, 345–348
 - midpoint potentials, 347–349
 - purification, 346
 - reduced, 346–347
- Ni–Fe hydrogenase, 389
- pyroglycolytic pathway, 382–383
- rubredoxin, 368–374
 - amino acid sequence, 371–372
 - midpoint potential, 369–370
 - molecular properties, 369
- NMR, 371, 373
 - physiological role, 373–374
 - thermostability, 370–371
- Pyroglycolytic pathway, H₂ production, 383

Q

Quantum mechanical methods, 424

R

- Radish white root ferredoxins, 231
- Redon shuffling, 410–414
- Redox potentials, Fe–Se proteins, 88–89
- Redox properties, *Azotobacter* Fd I, 128–138
- Red tungsten protein, *see* RTP
- Reduced configuration, four-iron clusters, 456–457
- Reduction potential differences,
 - ferredoxin iso-forms, 233–234
- ReFe₃S₄ cluster, 41–43
 - self-assembly system, 41–42
- Relaxation
 - effects on cluster oxidation + 2 → +3,
 - four-iron clusters, 457–459
 - effects on cluster reduction + 2 → +1,
 - four-iron clusters, 459
- Resonance coupling, Fe–S dimers, 446–451
- Resonance delocalization, 426
- Resonance Raman spectra
 - C. pasteurianum* ferredoxin, 85, 87
 - [4Fe–4S] cluster, 358
- Resonance splitting, 447
- Respiratory chains
 - complexes, proteins, 240–241
 - membrane-bound Fe–S enzymes, 302–303
- Restricted Hartree–Fock theory, 440
- Reversible binding, divalent metal ions, 153
- Rhizobium trifolii*, ferredoxin-like proteins, 247–248
- Rhodobacter capsulatus*
 - fdxN*, 255–257

ferredoxin I and II, 260
 [2Fe—2S] ferredoxins, 236–237
 Rhombograms, reading, 197–205
 Rieske proteins, 300
 RTP, 374–379
 as catalyst, 379
 redox centers, 376–378
 Rubredoxin, 299
P. furiosus, 368–374

S

Scattered-wave calculations, 454
 Selenide, production, 82
 Selenium
 in biology, 74–80
 artificial incorporation into proteins, 76–79
 beneficial effects, 76
 biomolecules, 75–76
 poisoning, 74–75
 as probe, 77, 80
 chemical properties, 74
 isotope, 77, 80
 Selenocysteine, 76
 Selenocysteinyl-tRNA, 75
 Selenomethionine, 76
⁷⁶Se → ⁸²Se isotopic substitution, 105–107
 Singlet–triplet splittings, unpaired electrons, 426–428
 Sirohaem Fe—S proteins, 289
 Fe—S clusters as electron carriers, 307–308
 Site-directed mutagenesis experiments, Fe—S proteins, amino acid sequences, 294–296
 Spectroscopy, Fe—S proteins, amino acid sequences, 296–298
 Spinach root ferredoxin, 231
 Spin coupling, *see also* Density-functional theory
 model, 51
 coupling parameters, four-iron clusters, 459–461
 Spin density, Fe—S dimers, 443–445
 Spin eigenfunctions, 427
 Spin Hamiltonian, 194
 four-iron clusters, 459–460

 matrix, 453
 parameters, 447, 449
 Spin ladders, 180–183
 Spin polarization, *see* Density-functional theory
 Spin projection, 431–432
 Spin states
 diagram, reduced Fe—S dimer, 447, 449–450
 energy separation, four-iron clusters, 456
 Fe₃S₄ clusters, 17–22
 heterometal cluster formation, 31, 51
 iron in Fe—S clusters, 171–172
Spirulina ferredoxin, amino acid sequences, 236
Spirulina platensis, ferredoxins, structure, 225–226, 233–234,
 S(3p) orbitals, 443
 Stability
 patterns, heterometallic MFe₃S₄
 cubane-type clusters, 43–44
 S = $\frac{1}{2}$ versus S = $\frac{3}{2}$ for reduced (+1)
 clusters, four-iron clusters, 462
Streptomyces griseolus, 6–7
 ferredoxin, 258–259
 monooxygenase system, 251
 Structural models, Fe—S proteins, 52–54
 Subsite differentiation
 3:1, 8
 2:2, 14–16
 Succinate dehydrogenase, cysteine distribution, 240–241
 μ -Sulfide, bridging ligand, 172
 Sulfide bridge, Fe—S proteins 13
 Superexchange, 426
 EPR spectroscopy, 173–178
Synechococcus, ferredoxin sequences, 232
 Synthetic analogs, Fe—Se proteins, ground spin state variability, 95, 98

T

Tetracysteinate binding, Fe—S proteins, 3
 Tetrathiometalates, 30–32
 Thermophilic bacteria, *see* Extremely thermophilic bacteria

Thermotoga maritima, 384–389

- hydrogenase, 384–388
 - catalytic activity, 385–386
 - EPR spectra, 386–387
 - Fe–S content, 386
 - inhibition, 385–386
 - molecular properties, 384
 - properties, 385
- tungsten role, 388–389

Thermus thermophilus ferredoxin,

- X-band EPR, 211–212

Three-iron clusters

- broken-symmetry analysis, 453–455
- density-functional theory, 452–455

Ti(I)

- biological target, 156
- concentration and *D. africanus* Fd(III)
 - reduction potential, 155–156

Total energy, density-functional theory,

436–438

Transition metal clusters, perturbation

- formalism for spin coupling, 425–435

Trithiol ligand, 8–9

tRNA, containing selenium, 75

Trp-ferredoxins, 239

Tungsten

- Fe–S clusters as electron carriers,
 - 306–307
- role in *T. maritima*, 388–389
- III and V valence states, 380

U

Unpaired electrons, singlet–triplet

- splittings, 426–428

UV–visible absorption spectra

- C. pasteurianum* ferredoxin, 85–86
- iron–selenium proteins, 87–88

V

Valence delocalization, 178–186, 426

[VFe₃S₄Cl₃(DMF)₃]¹⁻, 37[VFe₃S₄] clusters, 37–41

- self-assembly system, 37–38

W

Wavefunction

- local density-functional, 429

- single configuration, 426–427

[W–3Fe–4S] cluster, 32–37, 379

X

X α –LCAO energy levels

- Fe–S dimers, 441–442

- four-iron clusters, 456–457

- high-spin ferromagnetic configuration,
 - 447–448

X-band spectrum

- [2Fe–2S] cluster, 189

- Mo–Fe protein, 205–206

X-ray absorption near-edge structure,

- Fe–S proteins, 52

Xylene monooxygenase, *Pseudomonas putida*, 239

Z

Zeeman interaction, 195, 209

Zero-field Hamiltonian, 211

[Zn₃Fe–4S] clusters, 154

CONTENTS OF RECENT VOLUMES

VOLUME 28

Fast-Atom Bombardment Mass
Spectrometry and Related
Techniques

Jack Martin Miller

The Chemistry of Berkelium

J. R. Peterson and D. E. Hobart

Preparations and Reactions of Oxide
Fluorides of the Transition Metals,
the Lanthanides, and the Actinides

John H. Holloway and David Laycock

Chemical Effects of Nuclear
Transformations

G. A. Brinkman

Homocyclic Selenium Molecules and
Related Cations

Ralf Steudel and Eva-Maria Strauss

The Element Displacement Principle: A
New Guide in p-Block Element
Chemistry

A. Haas

Compounds of Pentacoordinated
Arsenic(V)

R. Bohra and H. W. Roesky

Perchlorate Ion Complexes

*N. M. N. Gowda, S. B. Naikar, and
G. K. N. Reddy*

INDEX

VOLUME 29

Inorganic Silylenes. Chemistry of
Silylene, Dichlorosilylene, and
Difluorosilylene

Chao-Shiuan Liu and Tsai-Lih Hwang

Trifluorophosphine Complexes of
Transition Metals

John F. Nixon

Solvent Extractions of Metal
Carboxylates

*Hiromichi Yamada and Motoharu
Tanaka*

Alkyne-Substituted Transition Metal
Clusters

Paul R. Raithby and Maria J. Rosales

Organic Superconductors: Synthesis,
Structure, Conductivity, and
Magnetic Properties

Jack M. Williams and Kim Carneiro

Where Are the Lone-Pair Electrons in
Subvalent Fourth-Group
Compounds?

S.-W. Ng and J. J. Zuckerman

INDEX

VOLUME 30

Catenated Nitrogen Ligands Part I.
Transition Metal Derivatives of
Triazenes, Tetrazenes,

Tetrazadienes, and Pentazadienes
*David S. Moore and Stephen D.
Robinson*

The Coordination Chemistry of
2,2':6',2"-Terpyridine and Higher
Oligopyridines

E. C. Constable

High-Nuclearity Carbonyl Clusters:
Their Synthesis and Reactivity

*Maria D. Vargas and J. Nicola
Nicholls*

Inorganic Chemistry of
Hexafluoroacetone

*M. Witt, K. S. Dhathathreyan, and
H. W. Roesky*

INDEX

VOLUME 31

Preparation and Purification of Actinide Metals

J. C. Spirlet, J. R. Peterson, and L. B. Asprey

Astatine: Its Organonuclear Chemistry and Biomedical Applications

I. Brown

Polysulfide Complexes of Metals

A. Müller and E. Diemann

Iminoboranes

Peter Paetzold

Synthesis and Reactions of Phosphorus-Rich Silylphosphanes

G. Fritz

INDEX

VOLUME 32

Dynamics of Spin Equilibria in Metal Complexes

James K. Beattie

Hydroxo-Bridged Complexes of Chromium(III), Cobalt(III), Rhodium(III), and Iridium(III)

Johan Springborg

Catenated Nitrogen Ligands Part II. Transition Metal Derivatives of Triazoles, Tetrazoles, Pentazoles, and Hexazine

David S. Moore and Stephen D. Robinson

The Redox Chemistry of Nickel

A. Graham Lappin and Alexander McAuley

Nickel in Metalloproteins

R. Cammack

Nitrosyl Complexes of Iron-Sulfur Clusters

Anthony R. Butler, Christopher Glidewell, and Min-Hsin Li

INDEX

VOLUME 33

1,6-Disubstituted Triptycenes

Alan G. Massey

Cysteine-Containing Oligopeptide Model Complexes of Iron-Sulfur Proteins

Akira Nakamura and Norikazu Ueyama

Reduction Potentials Involving Inorganic Free Radicals in Aqueous Solution

David M. Stanbury

The Nitrogen Fluorides and Some Related Compounds

H. J. Emeléus, Jean'ne M. Shreeve, and R. D. Verma

Higher Oxidation State Manganese Biomolecules

John B. Vincent and George Christou

Double Bonds between Phosphorus and Carbon

R. Appel and F. Knoll

INDEX

VOLUME 34

Homoleptic Complexes of 2,2'-Bipyridine

E. C. Constable

Compounds of Thorium and Uranium in Low (<IV) Oxidation States

Isabel Santos, A. Pires de Matos, and Alfred G. Maddock

Leaving Groups on Inert Metal Complexes with Inherent or Induced Lability

Geoffrey A. Lawrance

The Coordination of Metal Aquaions

G. W. Neilson and I. E. Enderby

An Appraisal of Square-Planar Substitution Reactions

R. J. Cross

Transition Metal Nitrosyl Complexes

D. Michael, P. Mingos, and Darren J. Sherman

INDEX

VOLUME 35

Chemistry of Thioether Macrocyclic Complexes

Alexander J. Blake and Martin Schröder

Vanadium: A Biologically Relevant Element

Ron Wever and Kenneth Kustin

Structure, Reactivity, Spectra, and Redox Properties of Cobalt(III) Hexaamines

Philip Hendry and Andreas Ludi

The Metallic Face of Boron

Thomas P. Fehlner

Developments in Chalcogen-Halide Chemistry

Bernt Krebs and Frank-Peter Ahlers

Interaction between Optical Centers and Their Surroundings: An Inorganic Chemist's Approach

G. Blasse

INDEX

VOLUME 36

Inorganic Chemistry and Drug Design

Peter J. Sadler

Lithium and Medicine: Inorganic Pharmacology

N. J. Birch and J. D. Phillips

The Mo-, V-, and Fe-Based Nitrogenase Systems of *Azotobacter*

Robert R. Eady

The Extraction of Metals from Ores Using Bacteria

D. Keith Ewart and Martin N. Hughes

Solid-State Bioinorganic Chemistry: Mechanisms and Models of Biomineralization

Stephen Mann and Carole C. Perry

Magnetic Circular Dichroism of Hemoproteins

M. R. Cheesman, C. Greenwood, and A. J. Thomson

Flavocytochrome b_2

Stephen K. Chapman, Scott A. White, and Graeme A. Reid

X-Ray Absorption Spectroscopy and the Structures of Transition Metal Centers in Proteins

C. David Garner

Direct Electrochemistry of Proteins and Enzymes

Liang-Hong Guo and H. Allen O. Hill

Active-Site Properties of the Blue Copper Proteins

A. G. Sykes

The Uptake, Storage, and Mobilization of Iron and Aluminum in Biology

S. Jemil A. Fatemi, Fahmi H. A. Kadir, David J. Williamson, and Geoffrey R. Moore

Probing Structure-Function Relations in Ferritin and Bacterioferritin

P. M. Harrison, S. C. Andrews, P. J. Artymiuk, G. C. Ford, J. R. Guest, J. Hirzmann, D. M. Lawson, J. C. Livingstone, J. M. A. Smith, A. Treffry, and S. J. Yewdall

INDEX

VOLUME 37

On the Coordination Number of the Metal in Crystalline Halogenocuprates(I) and Halogenoargentates(I)

Susan Jagner and Göran Helgesson

Structures of Organonitrogen-Lithium Compounds: Recent Patterns and Perspectives in Organolithium Chemistry

Karina Gregory, Paul von Ragué Schleyer, and Ronald Snaith

Cubane and Incomplete Cubane-Type Molybdenum and Tungsten Oxo/Sulfido Clusters

Takashi Shibahara

Interactions of Platinum Amine
Compounds with Sulfur-Containing
Biomolecules and DNA Fragments
Edwin L. M. Lempers and Jan Reedijk

Recent Advances in Osmium Chemistry
Peter A. Lay and W. Dean Harman

Oxidation of Coordinated Diimine
Ligands in Basic Solutions of
Tris(diimine)iron(III),
-ruthenium(III), and -osmium(III)
O. Mønsted and G. Nord

INDEX